Environmental Assessment of the Alaskan Continental Shelf

Annual Reports of Principal Investigators for the year ending March 1978

Volume XII. Hazards

U.S. DEPARTMENT OF COMMERCE
National Oceanic and Atmospheric Administration

U.S. DEPARTMENT OF INTERIOR
Bureau of Land Management

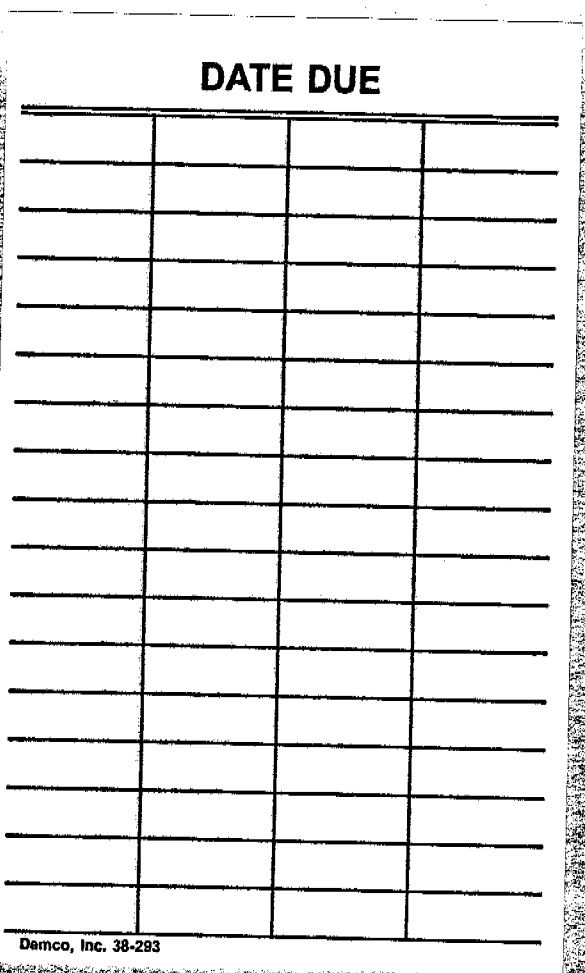

VOLUME I	RECEPTORS -- MAMMALS BIRDS
VOLUME II	RECEPTORS -- BIRDS
VOLUME III	RECEPTORS -- BIRDS
VOLUME IV	RECEPTORS -- FISH, LITTORAL, BENTHOS
VOLUME V	RECEPTORS -- FISH, LITTORAL, BENTHOS
VOLUME VI	RECEPTORS -- MICROBIOLOGY
VOLUME VII	EFFECTS
VOLUME VIII	CONTAMINANT BASELINES
VOLUME IX	TRANSPORT
VOLUME X	TRANSPORT
VOLUME XI	HAZARDS
VOLUME XII	HAZARDS
VOLUME XIII	DATA MANAGEMENT

Environmental Assessment of the Alaskan Continental Shelf

Annual Reports of Principal Investigators for the year ending March 1978

Volume XII. Hazards

Outer Continental Shelf Environmental Assessment Program
Boulder, Colorado

October 1978

U.S. DEPARTMENT OF COMMERCE
National Oceanic and Atmospheric Administration

U.S. DEPARTMENT OF INTERIOR
Bureau of Land Management

DISCLAIMER

The National Oceanic and Atmospheric Administration (NOAA) does not approve, recommend, or endorse any proprietary product or proprietary material mentioned in this publication. No reference shall be made to NOAA or to this publication furnished by NOAA in any advertising or sales promotion which would indicate or imply that NOAA approves, recommends, or endorses any proprietary product or proprietary material mentioned herein, or which has as its purpose an intent to cause directly or indirectly the advertised product to be used or purchased because of this publication.

ACKNOWLEDGMENT

These annual reports were submitted as part of contracts with the Outer Continental Shelf Environmental Assessment Program under major funding from the Bureau of Land Management.

HAZARDS

Contents

ANNUAL REPORT

Contract #03-5-022-56
Research Unit #290
Reporting Period 4/1/77 - 3/31/78
Number of Pages 57

BENTHOS - SEDIMENTARY SUBSTRATE INTERACTIONS

Dr. Charles M. Hoskin
Institute of Marine Science
University of Alaska
Fairbanks, Alaska 99701

March 31, 1978

The enclosed Summary Report for this project constitutes the Annual Report and a portion of the Final Report. Completion of this project awaites the completion of a Masters of Science Thesis currently being prepared by Ms. Gerd Tommos. This thesis will be finished by September 30, 1978, at which time it will be submitted as the second portion of the Final Report for this Task Order.

The attached Summary Report deals with all work undertaken by this task from inception through January 1978. This report was presented at the Synthesis Meeting held in Menlo Park, California earlier this year.

SUMMARY REPORT

Contract: #03-5-022-56

Research Unit: #290/291/292

Reporting Period: 10/75-1/78

Number of Pages: 57

BENTHOS-SEDIMENTARY SUBSTRATE INTERACTIONS

Dr. Charles M. Hoskin

Institute of Marine Science

University of Alaska

January 1978

I. BACKGROUND AND OBJECTIVES

Many macroscopic benthic organisms live on and in sediment substrates. They interact with the substrate by ingesting sediment through feeding. Sorption reactions occur between hydrocarbons, trace metals and sediment. As the fine-grained sediment fraction (< 62 μm) is particularly susceptible to sorption, it is necessary to determine the grain size composition of sediment to identify those places characterized by fine-grained deposits.

There have been two main objectives in this work: (1) to determine what relationships, if any, exist between the grain size modes of bottom sediment in the eastern Bering Sea and the distribution and abundance of the living macrobenthos, and (2) to provide grain size data for samples submitted by OCSEAP benthic biologists and chemists.

II. METHODS

Grain size analysis of sediments has been done in the laboratory following the procedures of Hoskin (1976).

III. RESULTS

Sediments have been analyzed from Kotzebue Sound in the Chukchi Sea, and Norton Sound and the eastern Bering Sea shelf, Alaska. Kotzebue Sound sediments contain an average of 48 percent mud (range 2.8 - 98.9, n = 32) and Norton Sound sediments contain an average of 47 percent mud (range 7.0 - 94.6, n = 32). Much more work has been done on eastern Bering Sea sediments. Silt and clay contents for 72 samples were found to be $\overline{X}$ = 18.9 (range 0.02 - 53.7) and $\overline{X}$ = 7.2 (range 0.0 - 23.8) respectively.

IV. LATEST SIGNIFICANT OBSERVATIONS

The geographic distribution of eastern Bering Sea samples is shown in Figure 1, and further data are given in Table 1. Duplicate analyses have been done for randomly-selected samples to determine the reproducibility of lab work. Results of these duplicate runs for the sand fraction are given in Table 2, and in only 1 of 8 samples was a shift in the grain size mode detected. For mud, duplicate runs on 11 samples were made, and the greatest deviation between runs 1 and 2 was found to be just over 3 percent, with the average deviation well under 1 percent (Table 3). For six stations, samples have been collected and analyzed for two different times (Table 4). It must be understood that "same station" is used in the ordinary operational sense, as can be seen by comparing longitudes and latitudes in Table 4. Descriptive grain size parameters for these size sample pairs are similar for all but stations 060 and 082. It is probable (but not certain) that the differences between samplings at these stations are due to the June and August samples coming from "different" stations, and are not due to changes in the sediment at the "same" station during the intervening 73 days.

The main objective of the Bering Sea work was to determine relationships between the grain size mode of bottom sediment and distribution and abundance of the macrobenthos. The original sampling grid for the eastern Bering Sea had stations centered in 45 mile squares. Due to the wide station spacing, frequency of storms, length of time for sampling (May-October) and lack of rigid controls to evaluate within versus between station variations, comparison of data in a map format is highly speculative. With the foregoing caveats in mind, a map is included (Fig. 2) showing the geographic distribution of grain size modes on the eastern Bering Sea Shelf. A line encloses the stations with a grain size mode of 149 μm, and it can be seen that 20 of the 27 stations

containing this grain size mode form a band paralleling the 25 fathom bathymetric contour. A histogram constructed for grain size modes shows a dominant mode of 149 μm, and a secondary mode at 74 μm. Grain size modes are coarsest in Bristol Bay (Sharma, 1975) and tend to be finer offshore, and to the northwest.

Using data for macrobenthos as provided by the Marine Sorting Center of the University of Alaska, relationships were sought between sediment and the benthos. Scatter diagrams for total number of individuals/m^2 and wet weight/m^2 for each of the 25 stations having paired benthos-sediment data showed a reciprocal pattern, Figures 3 and 4, respectively. Largest total number of individuals on a unit area basis occurred for stations having grain size modes of 125-149 μm (fine sand) with smaller numbers of individuals at stations having coarser or finer sediment. Lowest total wet weight/m^2 was found in these fine sand sediments, with larger weights of macrobenthos tending to occur at stations with coarser or finer sediment. One maverick data point (2420 g wet weight, grain size mode at 125 μm) marrs this pattern. As sediment particles between 100 and 200 μm are among the first to move under current stress (Sternberg, 1972) and tend to be well sorted as a consequence, it appears that the large number of small individuals at fine sand stations is the result of current action. Scatter plots of number and weights of the macrobenthos versus sand, silt and clay content revealed no finer structure in this relationship (Figs. 5, 6, 7 - numbers; Figs. 8, 9, 10 - weight).

Correlation coefficients (r) between numbers and weights per square meter of each species of macrobenthos occurring at 2.5 weight percent or greater and the sediment grain size mode were calculated using the University of Alaska's Honeywell 6600 series computer, and these data are given in Table 5. For the 16 of 138 species having a correlation coefficient of 0.5 or greater, the data were depicted in scatter diagrams (Figs. 11-32).

For convenience, these 16 taxa were categorized by feeding type. The scavengers *Paraphoxus* sp. (Figs. 11, 12) and *Echinarachnius parma* (Fig. 13) increase in abundance with increasing coarseness of grain size modes. There appears to be a threshold in substrate grain size for these two species as they were not found in substrates having grain size modes smaller than 149 µm.

For three predators, *Nephthys longasetosa* (Figs. 14, 15), *N. caeca* (Fig. 16) and *Polinices nanus* (Fig. 17), numbers and/or weight increased with increasing coarseness of grain size modes in their substrate. For one predator, *Cylichna alba* (Figs. 18, 19) numbers of individuals and total wet weight decreased with increasing coarseness of substrate.

The deposit feeders *Ophelia limacina* (Figs. 20, 21) and *Spio filicornis* (Fig. 22) increase in numbers and/or weight with increasing grain size modes of their substrate. There may be a particle size threshold for *O. limacina* as it was not found in this sampling in substrates having grain size modes smaller than 105 µm. There appears to be no relationship between substrate modal grain size and abundance of the deposit feeding polychaetes *Myriochele heeri* (Fig. 23) and the Terebellids (Fig. 24). For the deposit feeding polychaetes *Ampharete arctica* (Fig. 25) and *Travisia forbesii* (Fig. 26) the data are inconclusive.

The filter feeding amphipod *Houstorious eous* (Figs. 27, 28) was not found in substrates having grain size modes finer than 149 µm. Numbers of *H. eous* decrease with increasing coarseness of the substrate; the weight relationship to substrate grain size modes is not clear.

The feeding type of the snail *Solariella obscura* (Figs. 29, 30) is not known; it appears that numbers and weight decrease with increasing coarseness of the substrate. Feeding types are diverse for the taxa Polychaeta (Fig. 31)

and Nematoda (Fig. 32), and no clear-cut relationship between abundance and substrate grain size modes was found.

V. PROBLEMS ENCOUNTERED

None.

VI. RECOMMENDATIONS FOR FUTURE RESEARCH

Particle size is only one of many parameters that control the distribution and abundance of benthic organisms. Careful consideration should be given to obtaining data for total organic carbon and the main components - protein, carbohydrate and lipid, to aid in characterizing the quality of organic carbon as food for the benthos. As suggested by Bekman and Mizandrontsev (1971), large amounts of organic carbon as cellulose may not correlate well with the biomass of deposit feeders because cellulose is low quality food. Lie (1974) has shown positive correlations between percent nitrogen, fine-grained sediments and benthos in Puget Sound, Washington.

Measurements should be made from box core samples of sediment shear strength and bulk density, and sediment traps should be used to measure sediment flux. Engineering properties of the sedimentary substrate are very likely to be important to species of the infauna. Hoskin (1977) found that as sediment flux decreased from head-to-mouth in Blue Fjord, western Prince William Sound, Alaska, the number of individuals, the species diversity, percentage of filter feeders and average wet weight of the benthos increased. A similar pattern between sediment flux and benthos abundance was found in Queen Inlet, Glacier Bay, Alaska (Hoskin *et al.*, 1976). Mueller *et al.* (1976) found that the benthos biomass of Torch Bay, Alaska, was twice that of Dixon

Table III. Duplicate pipet analyses from separate aliquots of mud fraction

Station	Cumulative percent coarser at grain size Ø																				Difference between Run 1 and Run 2, %	
	4.5 Ø		5.0 Ø		5.5 Ø		6.0 Ø		6.5 Ø		7.0 Ø		7.5 Ø		8.0 Ø		9.0 Ø		10.0 Ø			
	Run 1	Run 2	Run 1	Run 2	Run 1	Run 2	Run 1	Run 2	Run 1	Run 2	Run 1	Run 2	Run 1	Run 2	Run 1	Run 2	Run 1	Run 2	Run 1	Run 2	Maximum	Average 4.5 through 10 Ø
1	95.23	95.12	96.44	96.20	98.02	96.74	97.21	97.10	97.57	97.38	97.67	97.66	97.93	97.86	98.07	98.18	98.48	98.44	98.82	98.83	1.28	.22
16	56.96	57.70	69.32	68.10	77.21	75.86	82.48	81.76	85.31	84.52	87.10	86.86	88.75	88.59	90.16	90.26	92.27	92.33	94.59	94.58	1.35	.54
19	70.13	71.43	81.41	81.87	87.03	87.33	90.07	89.96	91.67	91.79	92.82	92.85	93.55	93.68	94.16	94.42	95.45	95.45	96.76	-	.46	.19
31	88.16	88.08	90.44	90.46	92.26	92.40	93.61	93.72	94.48	94.74	95.20	95.16	95.62	95.69	96.08	96.30	96.96	97.02	97.66	-	.26	.11
32	83.50	83.29	89.91	89.65	92.39	92.18	93.66	93.56	94.66	94.37	95.39	95.07	95.84	95.76	96.41	96.03	96.98	97.10	98.06	97.99	.38	.20
37	85.41	86.06	88.56	89.16	89.55	90.68	91.73	92.00	92.60	93.02	93.61	93.84	94.29	94.32	95.15	95.00	96.08	96.42	97.12	97.25	1.13	.40
45	69.23	72.06	80.64	81.77	86.84	87.15	90.67	91.11	92.48	92.98	94.11	94.09	94.57	94.73	95.47	95.60	96.68	96.68	97.28	37.59	2.83	.58
54	42.79	42.63	57.25	57.15	67.71	68.03	76.80	75.88	81.46	81.55	85.49	85.64	87.84	87.50	89.62	89.58	95.68	92.40	92.88	93.93	3.28	.65
66	93.30	93.44	94.96	95.29	95.83	96.01	96.34	96.38	96.69	96.66	96.69	97.04	97.26	97.30	97.60	97.68	98.14	98.18	98.69	98.73	.35	.13
73	78.71	79.13	82.10	82.12	84.66	84.77	86.91	87.01	89.37	89.16	90.99	90.85	92.17	92.28	93.22	93.46	94.90	94.95	96.10	96.61	.51	.19
83	73.76	73.59	81.65	82.27	85.56	85.40	88.63	87.49	90.13	90.18	92.02	92.03	93.18	93.08	94.18	93.98	95.43	95.61	96.22	96.58	1.14	.30

Table IV. Grain size parameters from a station sampled at two different times.

Station	Sampling date 1975	N. Lat.	W. Long.	Depth m	Dry wt. of sample analyzed	Weight Percent				Mean ø M_z	Standard deviation ø σ_I	Skewness Sk_I	Normalized kurtosis K'_G	Grain size mode μm	Wt. % in modal class size
						gravel	sand	silt	clay						
010	10 May	57°19.5'	161°05.8'	65	67.82	0	80.90	8.68	10.42	3.15	2.08	+0.70	0.82	177	57
	9 June	57°19.5'	161°05.8'	65	79.24	0	88.47	5.32	6.22	2.50	1.65	+0.42	0.83	210	34
027	11 June	57°40.1'	164°16.3'	53	80.76	0	84.77	8.25	6.98	3.02	1.58	+0.54	0.83	149	40
	4 October	57°40.0'	164°23.0'	50	75.93	0	82.21	10.65	7.14	3.22	1.66	+0.61	0.83	149	37
057	13 June	58°36.3'	168°12.1'	53	82.97	0	80.81	12.47	6.72	3.41	1.80	+0.76	0.83	149	45
	29 August	58°36.0'	168°12.8'	55	72.08	0	77.02	16.41	6.56	3.34	1.70	+0.72	0.78	149	43
060	13 June	59°42.9'	166°24.5'	29	82.45	19.22	74.99	3.52	2.28	0.71	2.85	-0.70	0.90	210	35
	25 August	59°44.0'	166°27.5'	27	84.58	0	55.27	37.44	7.29	4.08	1.95	+0.70	0.67	88	40
062	14 June	59°05.9'	169°15.1'	55	89.72	0	74.72	18.45	6.84	3.43	1.77	+0.67	0.71	149	35
	28 August	59°04.8'	169°14.2'	55	92.33	0	71.69	20.74	7.58	3.58	1.93	+0.72	0.70	149	33
082	9 June	60°32.9'	170°29.9'	60	75.90	0	88.17	5.20	6.63	2.98	1.47	+0.46	0.86	149	44
	22 August	60°32.9'	170°29.9'	60	70.34	0	43.85	48.21	7.94	4.43	1.95	+0.57	0.71	63	47

Harbor on a unit area basis. Dixon Harbor received glacially-derived sediment through meltwater from Brady Glacier, which was lacking in Torch Bay.

VII. REFERENCES CITED

Bekman, M. Y., and Mizandrontsev, I. B. 1971. Connection between the distribution of the benthos and organic matter in sediments. *Trud. Limnologich Inst. Sib. Otdel* AN SSSR, 12:127-132.

Hoskin, C. M. 1976. Procedures and quality control for grain size analysis and data reduction of Bering Sea bottom sediments. Report to NOAA/OCSEAP, Inst. Mar. Sci., Univ. Alaska, Fairbanks. 9 p.

_____. 1977. Macrobenthos from three fjords in western Prince William Sound, Alaska. Report R77-1, Inst. Mar. Sci., Univ. Alaska, Fairbanks. 28 p.

Hoskin, C. M., D. C. Burrell, and G. R. Freitag. 1976. Suspended sediment dynamics in Queen Inlet, Glacier Bay, Alaska. *Mar. Sci. Comm.* 2:95-108.

Lie, U. 1974. Distribution and structure of benthic assemblages in Puget Sound, Washington, USA. Marine Biology. 26:203-223.

Mueller, G. J., A. S. Naidu, and D. Schamel. 1976. Background benthic studies of the Torch Bay-Dixon Harbor area of the Glacier Bay National Monument. Inst. Mar. Sci., Univ. Alaska, Fairbanks. 100 p.

Sharma, G. D. 1975. Contemporary epicontinental sedimentation and shelf grading in the southeast Bering Sea. p. 33-48. *In*: Forbes, R. B. (ed.), Contributions to the Geology of the Bering Sea Basin and adjacent regions. Geol. Soc. America, Special Paper 151. 214 p.

Sternberg, R. W. 1972. Predicting initial motion and bedload transport of sediment particles in the shallow marine environment. p. 61-82. *In*: Swift, D. J. P., D. B. Duane, and O. H. Pilkey (eds.), *Shelf sediment transport; process and pattern.* Dowden, Hutchinson & Ross, Stroudsburg, Pennsylvania. 656 p.

Table I. Samples used in this report.

Station number	Sampling date in 1975	N. Lat.	W. Long.	Water depth m	Macrobenthos data	Grain size mode, μm
1	22 or 24 Sept.	55°18.0'	163°19.0'	50	no	125
3	8 June	56°17.4'	161°02.3'	52	no	177
5	8 June	57°20.5'	158°58.0'	48	yes	2830, 300
6	6 October	57°43.4'	159°05.4'	48	no	300
7	8 June	58°58.0'	158°15.7'	35	yes	2380, 300
8	6 October	57°17.0'	159°31.7'	22	no	149
9	9 June	57°54.8'	160°08.5'	53	yes	210
10	10 May	57°19.5'	161°05.8'	65	yes	177
10	9 June	57°19.5'	161°05.8'	65	no	210
11	9 June	56°45.5'	161°59.7'	71	yes	149
13	2 September	55°05.5'	164°47.0'	102	no	125
14	7 June	54°38.7'	165°25.3'	163	yes	2380, 177
16	2 September	54°53.1'	165°48.0'	198	no	105
17	2 September	55°28.2'	165°49.2'	124	no	88
19	10 June	56°40.0'	163°57.6'	77	yes	125
20	4 October	57°15.0'	163°05.0'	54	no	149
21	5 October	57°32.1'	162°40.0'	48	no	149
22	7 October	57°50.1'	162°10.8'	46	no	177
23	7 October	58°20.0'	161°21.1'	33	no	300
24	8 October	58°46.1'	162°30.3'	48	no	2380, 300
25	8 October	58°19.7'	163°13.0'	33	no	177
26	4 October	57°44.4'	164°14.4'	51	no	149
27	11 June	57°40.1'	164°16.3'	53	no	149
27	4 October	57°40.0'	164°23.0'	50	yes	149
28	11 June	57°09.9'	165°04.3'	70	yes	125
29	1 September	56°36.2'	165°54.0'	84	no	125
31	6 June	55°21.9'	167°46.5'	166	yes	105
34	5 June	55°52.8'	168°44.1'	150	no	105
37	1 September	57°05.9'	167°00.1'	77	no	149
38	12 June	57°40.0'	166°05.9'	66	yes	74
39	12 June	58°02.7'	165°29.8'	52	no	105

Table I. Continued

Station number	Sampling date in 1975	N. Lat.	W. Long.	Water depth m	Macrobenthos data	Grain size mode, μm
40	12 June	58°08.5'	165°17.4'	47	yes	149
41	8 October	58°45.8'	164°12.2'	35	no	149
42	8 October	59°16.0'	165°20.0'	23	no	149
43	27 August	58°42.5'	166°16.3'	40	no	149
44	13 June	58°26.0'	166°43.0'	47	yes	149
45	14 October	58°09.8'	167°10.7'	62	no	125
46	19 August	57°34.8'	168°07.0'	75	no	149
47	18 August	56°59.0'	169°01.0'	84	yes	149
48	4 June	56°19.1'	169°42.0'	155	no	6800, 149
49	4 June	56°24.6'	169°56.7'	105	yes	74, 37, 13
50	4 June	59°06.9'	170°23.6'	135	no	149
54	4 June	56°58.2'	170°58.8'	110	no	88
55	20 August	57°31.0'	170°00.0'	73	yes	149
56	31 August	58°05.0'	169°02.0'	75	no	74
57	13 June	58°36.3'	168°12.1'	53	yes	149, 37
57	29 August	58°36.0'	168°12.8'	55	no	149, 53
58	29 August	58°49.2'	168°57.1'	46	no	149
59	25 August	59°11.7'	167°16.2'	38	no	149
60	13 June	59°42.9'	166°24.5'	29	yes	210
60	25 August	59°44.0'	166°27.5'	27	no	88
61	28 August	59°39.0'	168°21.8'	38	no	149
62	14 June	59°05.9'	169°15.1'	55	no	149
62	28 August	59°04.8'	169°14.2'	55	no	149
63	30 August	58°33.4'	170°10.0'	75	no	74
64	20 August	58°01.0'	171°08.5'	93	no	88
65	15 June	57°24.7'	172°05.5'	109	no	88
66	15 June	56°44.2'	173°11.5'	141	no	149
68	15 June	57°29.7'	173°05.7'	135	no	74
69	15 June	57°56.5'	173°05.2'	114	no	74
70	21 August	58°29.0'	172°13.0'	106	yes	88
71	21 August	59°03.9'	171°10.8'	82	yes	125

Table I. Continued

Station number	Sampling date in 1975	N. Lat.	W. Long.	Water depth m	Macrobenthos data	Grain size mode, μm
72	24 August	59°33.9'	170°19.0'	68	yes	74
73	23 August	60°02.4'	169°29.2'	48	yes	125
82	9 June	60°32.9'	170°29.9'	60	no	149
82	22 August	60°32.9'	170°29.9'	60	yes	63
83	23 August	60°02.0'	171°26.0'	73	yes	74
92	22 August	60°28.5'	172°27.0'	57	no	74
932	23 May	57°47.0'	167°43.0'	69	yes	74
933	23 May	57°53.0'	167°45.0'	67.5	no	53
935	24 May	58°51.0'	169°17.0'	68	no	2380, 210
936	24 May	58°46.0'	169°19.0'	65.5	no	53

Table II. Duplicate sieve analyses from separate aliquots of sand fraction.

Station	Grain size mode μm	
	Run 1	Run 2
044	149	149
045	125	88
049	74	74
056	74	74
059	149	149
062	149	149
066	149	149
070	74	74

Table III. Duplicate pipet analyses from separate aliquots of mud fraction

Station	Cumulative percent coarser at grain size ∅																				Difference between Run 1 and Run 2, %	
	4.5 ∅		5.0 ∅		5.5 ∅		6.0 ∅		6.5 ∅		7.0 ∅		7.5 ∅		8.0 ∅		9.0 ∅		10.0 ∅		Maximum	Average 4.5 through 10 ∅
	Run 1	Run 2	Run 1	Run 2	Run 1	Run 2	Run 1	Run 2	Run 1	Run 2	Run 1	Run 2	Run 1	Run 2	Run 1	Run 2	Run 1	Run 2	Run 1	Run 2		
1	95.23	95.12	96.44	96.20	98.02	96.74	97.21	97.10	97.57	97.38	97.67	97.66	97.93	97.86	98.07	98.18	98.48	98.44	98.82	98.83	1.28	.22
16	56.96	57.70	69.32	68.10	77.21	75.86	82.48	81.76	85.31	84.52	87.10	86.86	88.75	88.59	90.16	90.26	92.27	92.33	94.59	94.58	1.35	.54
19	70.13	71.43	81.41	81.87	87.03	87.33	90.07	89.96	91.67	91.79	92.82	92.85	93.55	93.68	94.16	94.42	95.45	95.45	96.76	-	.46	.19
31	88.16	88.08	90.44	90.46	92.26	92.40	93.61	93.72	94.48	94.74	95.20	95.16	95.62	95.69	96.08	96.30	96.96	97.02	97.66	-	.26	.11
32	83.50	83.20	89.91	89.65	92.39	92.18	93.66	93.56	94.66	94.37	95.39	95.07	95.84	95.76	96.41	96.03	96.98	97.10	98.06	97.99	.38	.20
37	85.41	86.06	88.56	89.16	89.55	90.68	91.73	92.00	92.60	93.02	93.61	93.84	94.29	94.32	95.15	95.00	96.08	96.42	97.12	97.25	1.13	.40
46	69.23	72.06	80.64	81.77	86.84	87.15	90.67	91.11	92.48	92.98	94.11	94.09	94.57	94.73	95.47	95.60	96.68	96.68	97.28	97.59	2.83	.58
54	42.79	42.63	57.25	57.15	67.71	68.03	76.80	75.88	81.46	81.55	85.49	85.64	87.84	87.50	89.62	89.58	95.68	92.40	92.88	93.93	3.28	.65
66	93.30	93.44	94.96	95.29	95.83	96.01	96.34	96.38	96.69	96.66	96.69	97.04	97.26	97.30	97.60	97.68	98.14	98.18	98.69	98.73	.36	.13
73	78.71	79.13	82.10	82.12	84.66	84.77	86.91	87.01	89.37	89.16	90.99	90.85	92.17	92.28	93.22	93.46	94.90	94.95	96.10	96.61	.51	.19
83	73.76	73.59	81.65	82.27	85.56	85.40	88.63	87.49	90.13	90.18	92.02	92.03	93.18	93.08	94.18	93.98	95.43	95.61	96.22	96.58	1.14	.30

Table IV. Grain size parameters from a station sampled at two different times.

Station	Sampling date 1975	N. Lat.	W. Long.	Depth m	Dry wt. of sample analyzed	Weight Percent gravel	sand	silt	clay	Mean ϕ M_z	Standard deviation ϕ σ_I	Skewness Sk_I	Normalized kurtosis K'_G	Grain size mode um	Wt. % in modal class size
010	10 May	57°19.5'	161°05.8'	65	67.82	0	80.90	8.68	10.42	3.15	2.08	+0.70	0.82	177	57
	9 June	57°19.5'	161°05.8'	65	79.24	0	88.47	5.32	6.22	2.50	1.65	+0.42	0.83	210	34
027	11 June	57°40.1'	164°16.3'	53	80.76	0	84.77	8.25	6.98	3.02	1.58	+0.54	0.83	149	40
	4 October	57°40.0'	164°23.0'	50	75.93	0	82.21	10.65	7.14	3.22	1.66	+0.61	0.83	149	37
057	13 June	58°36.3'	168°12.1'	53	82.97	0	80.81	12.47	6.72	3.41	1.80	+0.76	0.83	149	45
	29 August	58°36.0'	168°12.8'	55	72.08	0	77.02	16.41	6.56	3.34	1.70	+0.72	0.78	149	43
060	13 June	59°42.9'	166°24.5'	29	82.45	19.22	74.99	3.52	2.28	0.71	2.85	-0.70	0.90	210	35
	25 August	59°44.0'	166°27.5'	27	84.58	0	55.27	37.44	7.29	4.08	1.95	+0.70	0.67	88	40
062	14 June	59°05.9'	169°15.1'	55	89.72	0	74.72	18.45	6.84	3.43	1.77	+0.67	0.71	149	35
	28 August	59°04.8'	169°14.2'	55	92.33	0	71.69	20.74	7.58	3.58	1.93	+0.72	0.70	149	33
082	9 June	60°32.9'	170°29.9'	60	75.90	0	88.17	5.20	6.63	2.98	1.47	+0.46	0.86	149	44
	22 August	60°32.9'	170°29.9'	60	70.34	0	43.85	48.21	7.94	4.43	1.95	+0.57	0.71	63	47

Table V. Correlation coefficients between number and weight of taxa and grain size modes

Taxon name	Correlation coefficients (with grainsize) % by No.	% by wt	No./m^2	wt/m^2
Unidentified fragments	0.2158	0.2807	0.2080	0.2512
Porifera	0.1682	-	0.1675	-
Nematoda	0.4533	0.3523	0.4085	0.5342
Polychaeta	0.7608	0.4308	0.7243	0.4477
Polynof canadensis	0.1762	0.0951	0.1965	0.0964
Phloe minuta	0.4740	0.1949	0.4548	0.3259
Anaitides maculata	0.2936	0.2726	0.2473	0.2996
Nephtys ciliata	0.2244	0.3511	0.3650	0.3062
Nephtys caeca	0.2919	0.3976	0.3967	0.5977
Nephtys punctata	0.2385	0.3050	0.2751	0.3111
Nephtys longasetosa	0.5288	0.5906	0.5984	0.5440
Glycinde picta	0.3093	0.2733	0.4263	0.3244
Lumbrineris sp.	0.2590	0.2072	0.2597	0.2659
Lumbrinereis similabris	0.1238	0.2126	0.1585	0.2403
Lumbrinereis zonata	0.1375	0.1375	0.1375	0.1375
Ninoe gemmea	0.1375	0.1375	0.1375	0.1375
Haploscoloplos panamensis	0.5405	0.2908	0.3439	0.4143
Haploscoloplos elongatus	0.4027	0.3593	0.3324	0.2642
Scoloplos armiger	0.3662	0.3482	0.3329	0.3281
Aricidea uschakowi	0.3743	0.1610	0.3628	0.2069
Polydora socialis	0.1375	0.1375	0.1375	0.1375
Spio filicornis	0.4617	0.4202	0.4614	0.5057
Spiophanes bombyx	0.4715	0.2171	0.4772	0.4660
Spiophanes cirrata	0.4088	0.2136	0.4157	0.2373
Pygiospio sp.	0.3371	0.2786	0.3448	0.3353
Magelona japonica	0.2705	0.2684	0.3597	0.3350
Magelona pacifica	0.4775	0.3525	0.4624	0.4529
Tharyx sp.	0.4349	0.2785	0.3163	0.3138
Scalibregma inflatum	0.2062	0.2077	0.2016	0.1833
Ophelia limicina	0.6361	0.5573	0.6403	0.5697
Travisia brevis	0.3377	0.2783	0.3468	0.3031
Travisia forbesii	0.5736	0.2536	0.4780	0.5471
Sternaspis scutata	0.1793	0.1735	0.2536	0.2094
Capitellidae	0.1425	0.1398	0.1597	0.1177
Capitella capitata	0.3400	0.2238	0.3548	0.3046
Heteromastus filiformis	0.2516	0.2409	0.2469	0.1793
Maldane sarsi	0.1948	0.1258	0.2228	0.1216
Maldane glebifex	0.1637	0.1637	0.1637	0.1637
Nicomache personata	0.1637	0.1637	0.1637	0.1637

Table V. Continued

Taxon name	Correlation coefficients (with grainsize) % by No.	% by wt	No./m^2	wt/m^2
Notoproctus pacifica	0.1637	0.1637	0.1637	0.1637
Praxillella gracilis	0.2316	0.1868	0.2368	0.2225
Praxillella praetermissa	0.4846	0.3436	0.4799	0.2957
Rhodine sp.	0.2003	0.1979	0.2047	0.1992
Rhodine loveni	0.3788	0.2298	0.3264	0.2369
Owenia fusiformis	0.3048	0.1856	0.3124	0.2432
Myriochele heeri	0.5289	0.1690	0.6018	0.3553
Cistenides granulata	0.3339	0.2814	0.3324	0.2764
Cistenides hyperborea	0.2296	0.3310	0.2482	0.2130
Ampharete arctica	0.5549	0.3090	0.5152	0.4041
Ampharete acutifrons	0.3334	0.2121	0.3968	0.2434
Terebellidae	0.4595	0.1819	0.5333	0.2461
Artacama proboscidea	0.0932	0.1304	0.1216	0.2210
Proclea sp.	0.2974	0.2513	0.3017	0.2343
Terebellides stroemii	0.2857	0.2234	0.2868	0.2657
Chone cincta	0.1564	0.2133	0.2245	0.2212
Chone duneri	0.2631	0.1907	0.2341	0.2256
Euchone analis	0.3402	0.3973	0.4234	0.3970
Pelecypoda	0.4846	0.5089	0.4995	0.3235
Nucula tenuis	0.3552	0.2740	0.3387	0.3158
Nuculana pernula	0.3156	0.3174	0.3153	0.3216
Yoldia sp.	0.3714	0.2444	0.3478	0.3048
Yoldia amygdaiea	0.2622	0.2446	0.2466	0.2653
Yoldia hyperborea	0.2785	0.1654	0.3062	0.2001
Yoldia scissurata	0.3468	0.4085	0.3888	0.2856
Dacrydium pacificum	0.1951	0.1951	0.1951	0.1951
Cyclocardia ventricosa	0.2875	0.2622	0.2969	0.3053
Cyclocardia crebricostata	0.2221	0.3012	0.1797	0.1710
Axinopsida serricata	0.2343	0.2227	0.2483	0.2250
Thyasira flexuosa	0.2181	0.2350	0.1871	0.1762
Mysella sp.	0.4470	0.3880	0.4103	0.4486
Mysella tumida	0.4088	0.3319	0.4138	0.3376
Mysella aleutica	0.0969	0.0969	0.0969	0.0969
Odontogena borealis	0.1407	0.1423	0.1422	0.1449
Clinocardium ciliatum	0.1689	0.2202	0.2507	0.2158
Spisula polynyma	0.3165	0.2828	0.3391	0.2776
Macoma calcarea	0.2488	0.3071	0.1983	0.3126
Macoma brota	0.1152	0.1152	0.1152	0.1152
Macoma moesta alaskana	0.2972	0.2555	0.2879	0.2592
Macoma lama	0.2750	0.2750	0.2750	0.2750
Tellina lutea alternidentata	0.5002	0.5686	0.4699	0.4810

Table V. Continued

Taxon name	Correlation coefficients (with grainsize) % by No.	% by wt	No./m^2	wt/m^2
Gastropoda	0.4348	0.3467	0.4701	0.4234
Margarites olivaceus	0.4310	0.4487	0.4595	0.4067
Solariella obscura	0.7389	0.4327	0.5937	0.5276
Polinices nanus	0.5438	0.2926	0.5316	0.2480
Retusa obtusa	0.2324	0.2143	0.2704	0.2164
Cylichna alba	0.3903	0.3511	0.5032	0.5031
Balanidae	0.2750	-	0.2750	-
Balanus hesperius	0.1951	0.1951	0.1951	0.1951
Nebaliacea	0.3167	0.2709	0.2848	0.3232
Leucon sp.	0.3692	0.3386	0.3068	0.2843
Eudorella emarginata	0.2992	0.2177	0.3655	0.2784
Eudorella pacifica	0.3269	0.3283	0.3767	0.3903
Eudorellopsis integra	0.2446	0.2503	0.2817	0.2643
Eudorellopsis deformis	0.4158	0.2775	0.4095	0.4173
Diastylis alaskensis	0.2774	0.2985	0.3236	0.3191
Tanaidae	0.3232	0.3435	0.2980	0.3100
Amphipoda	0.3904	0.2774	0.3184	0.3714
Ampelisca macrocephala	0.5190	0.2898	0.4634	0.4108
Ampeliscidae birulai	0.2082	0.1434	0.2136	0.1469
Byblis gaimandi	0.3990	0.3062	0.3388	0.2734
Corophium sp.	0.1951	0.1951	0.1951	0.1951
Corophium crassicorne	0.2881	0.2229	0.2722	0.2903
Erichthonius hunteri	0.1375	0.1375	0.1375	0.1375
Melita formosa	0.2289	0.1410	0.2101	0.2273
Pontoporeia femorata	0.2206	0.2137	0.2158	0.2239
Haustorious eous	0.5271	0.4627	0.5319	0.5914
Isaeidae	0.2688	0.2183	0.2244	0.2362
Photis sp.	0.2894	0.2706	0.2446	0.2189
Photis spasskii	0.2952	0.2932	0.2722	0.2721
Photis ninogradovi	0.1951	0.1951	0.1951	0.1951
Protomedeia sp.	0.4900	0.2985	0.4445	0.2243
Protomedeia fascata	0.1951	0.1951	0.1951	0.1951
Protomedeia grandimana	0.2734	0.3002	0.3350	0.2692
Protomedeia chaelata	0.1637	0.1637	0.1637	0.1637
Ischyoceros sp.	0.3011	0.2708	0.2492	0.2565
Ischyrocerus anguipes	0.0969	0.0969	0.0969	0.0969
Hippomedon kurilious	0.5087	0.3924	0.4333	0.4495
Archomene sp.	0.2359	0.2372	0.2310	0.2314
Oedicerotidae	0.1338	0.1330	0.1624	0.1397
Bathymedon sp.	0.4228	0.2333	0.3851	0.3432
Bathymedon nanseni	0.2046	0.2145	0.1938	0.1948
Monoculodes martensi	0.4684	0.4794	0.4521	0.4775
Harpinia gurjanovae	0.3585	0.3828	0.4946	0.4670
Harpania tarasovi	0.1696	0.1453	0.1757	0.1801

Table V. Continued

Taxon name	Correlation coefficients (with grainsize) % by No.	% by wt	No./m^2	wt/m^2
Phoxocephalus	0.4629	0.4118	0.4669	0.3970
Paraphoxus sp.	0.6307	0.5409	0.6883	0.7710
Paraphoxus obtusidens	0.2817	0.1916	0.2320	0.2770
Sipunculida	0.1637	0.1637	0.1637	0.1637
Golfingia margaritacea	0.1979	0.1163	0.2281	0.1177
Phascolion strombi	0.1525	0.1441	0.1733	0.1796
Ectoprocta	0.1862	0.2447	0.1695	0.2536
Echinarachnius parma	0.5608	0.5942	0.4685	0.6188
Ophiuroidea	0.1312	0.1587	0.1249	0.1230
Amphipholis pugetana	0.0969	0.0969	0.0969	0.0969
Diamphiodia craterodmeta	0.2961	0.2795	0.2964	0.2752
Cucumaria calcigera	0.0973	0.1011	0.0994	0.0987
Molgula sp.	0.3493	0.2238	0.2898	0.2176

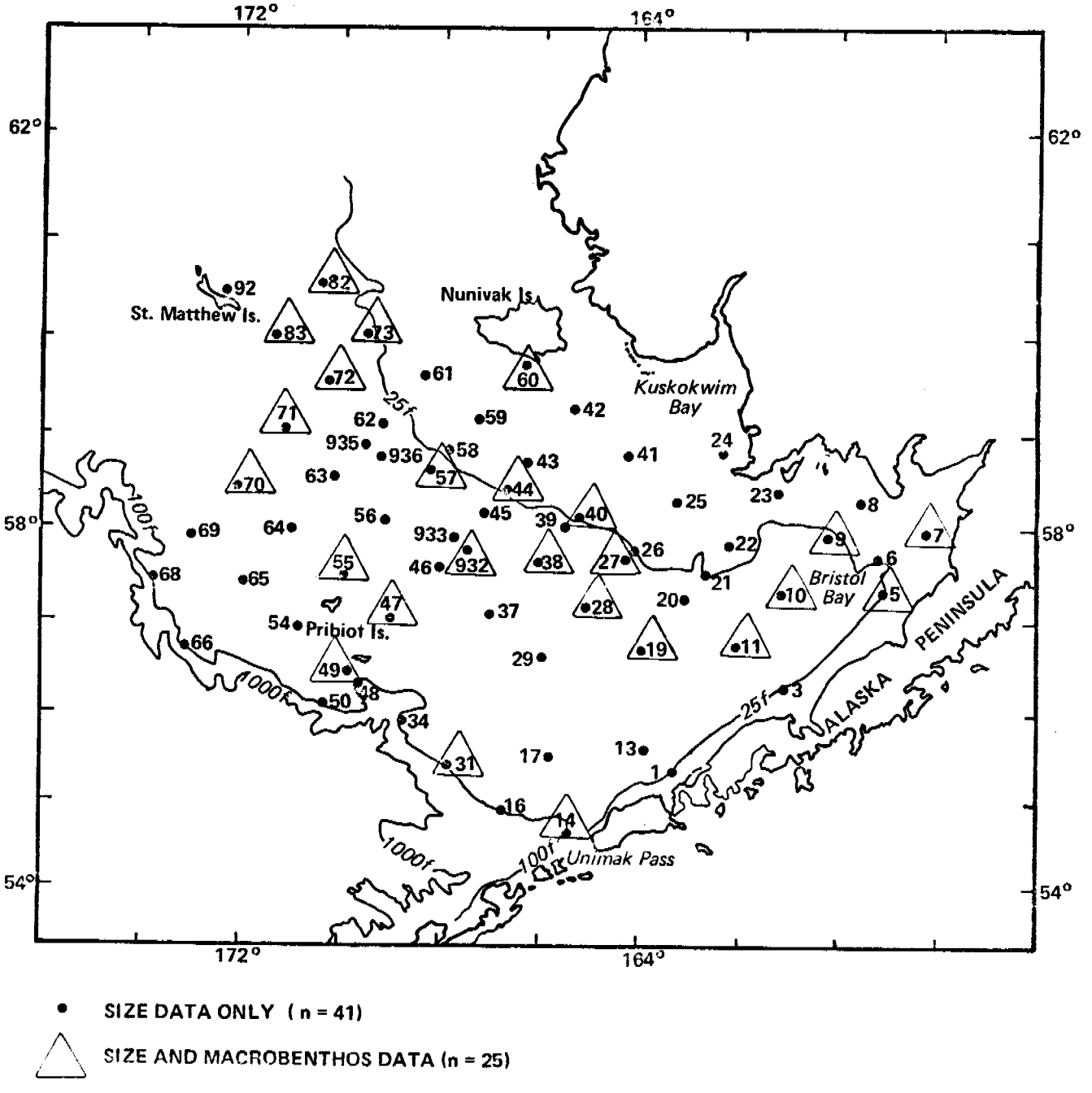

● SIZE DATA ONLY (n = 41)

△ SIZE AND MACROBENTHOS DATA (n = 25)

Figure 1. Index map of the southeastern Bering Sea, showing location of Van Veen grab stations.

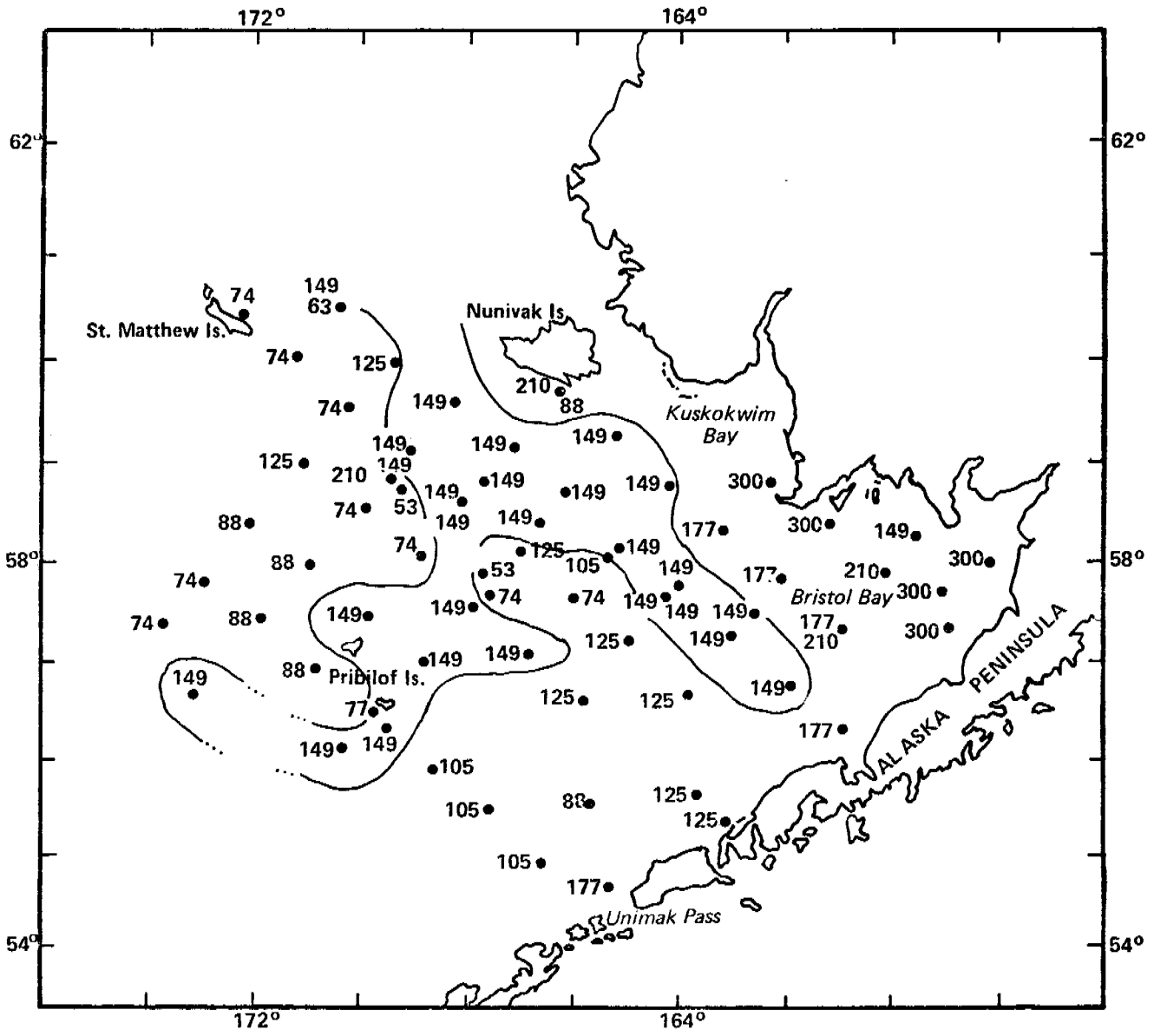

Figure 2. Map of grain size modes, μm, for the sand fraction. Number of samples = 66.

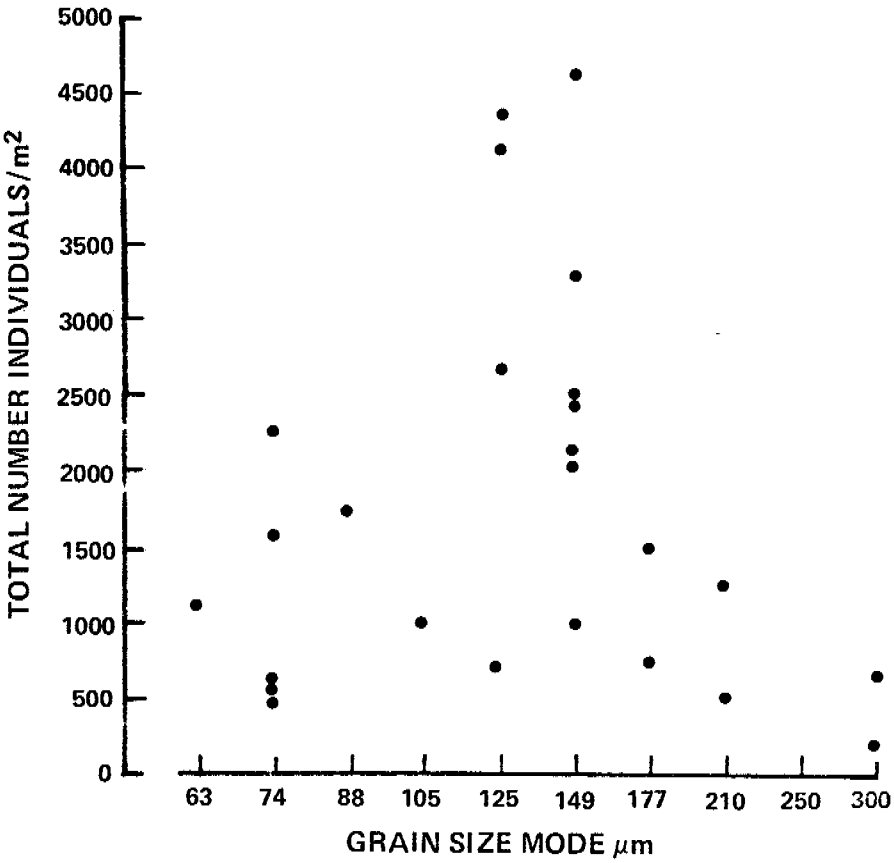

Figure 3. Scatter plot for total number of macrobenthos individuals/m^2 against grain size modes.

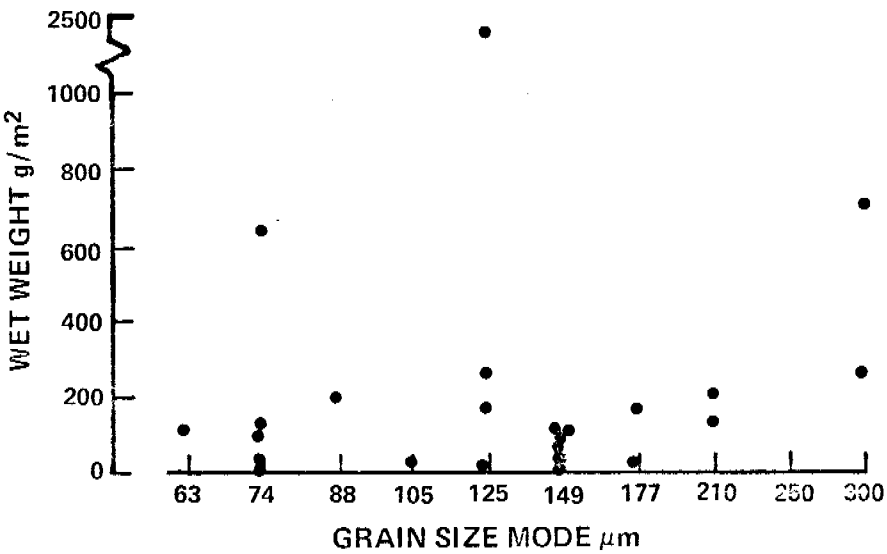

Figure 4. Scatter plot for total wet weight of macrobenthos/m^2 against grain size modes.

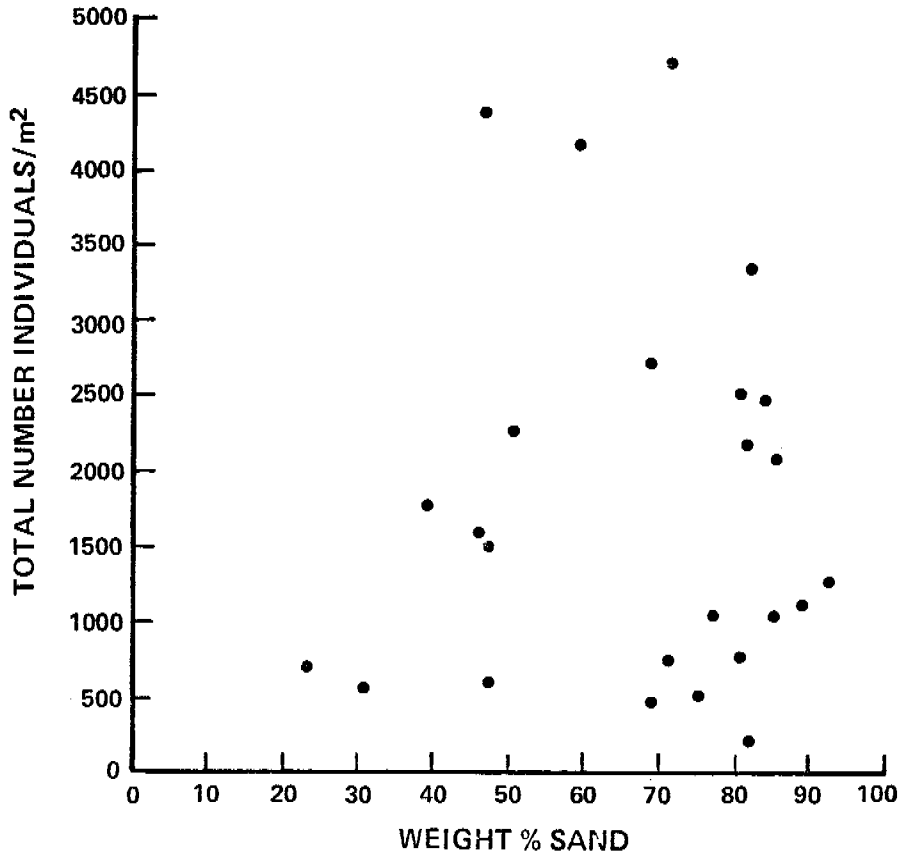

Figure 5. Scatter plot for total number of macrobenthos individuals/m^2 against weight percent sand.

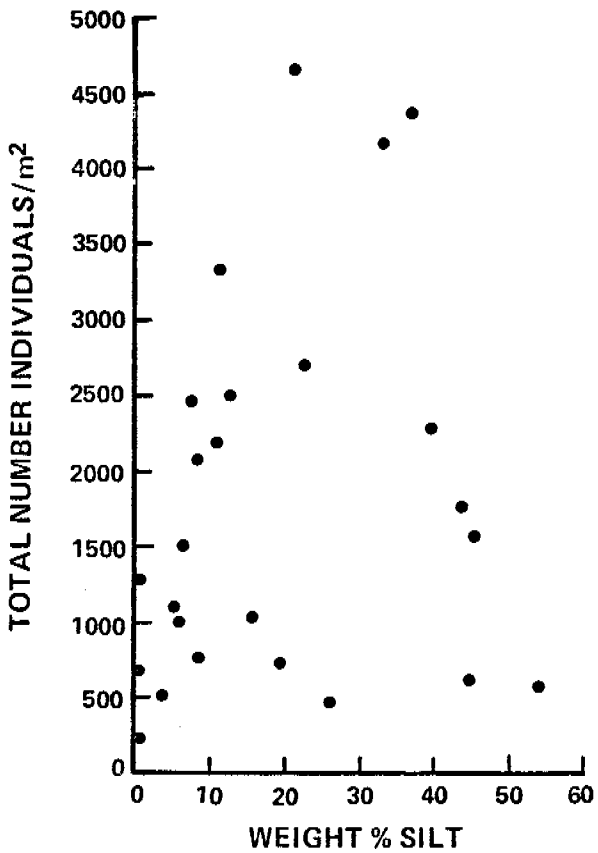

Figure 6. Scatter plot for total number of macrobenthos individuals/m^2 against weight percent silt.

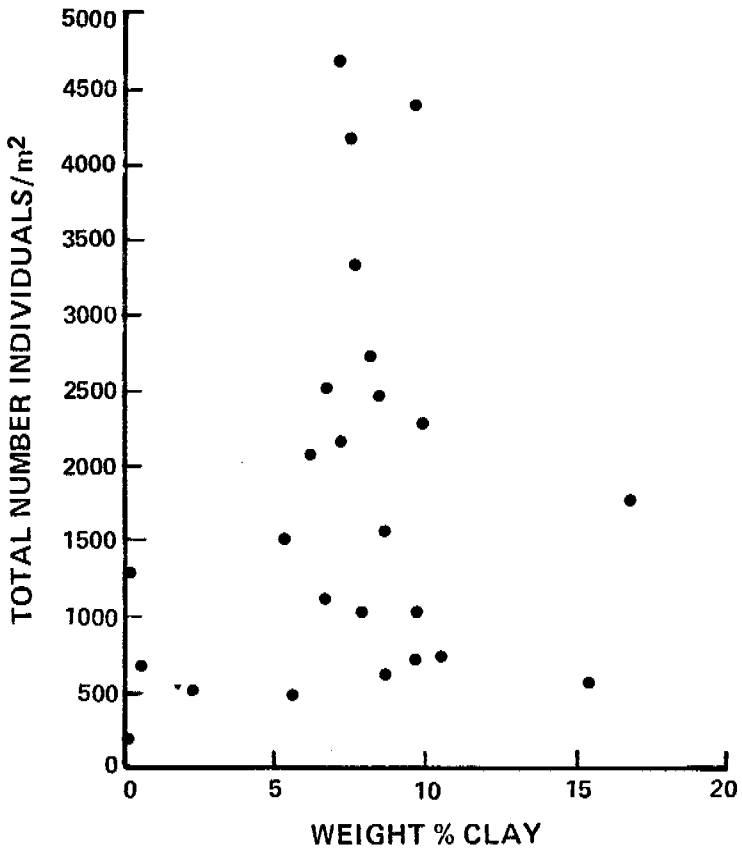

Figure 7. Scatter plot for total number of macrobenthos individuals/m^2 against weight percent clay.

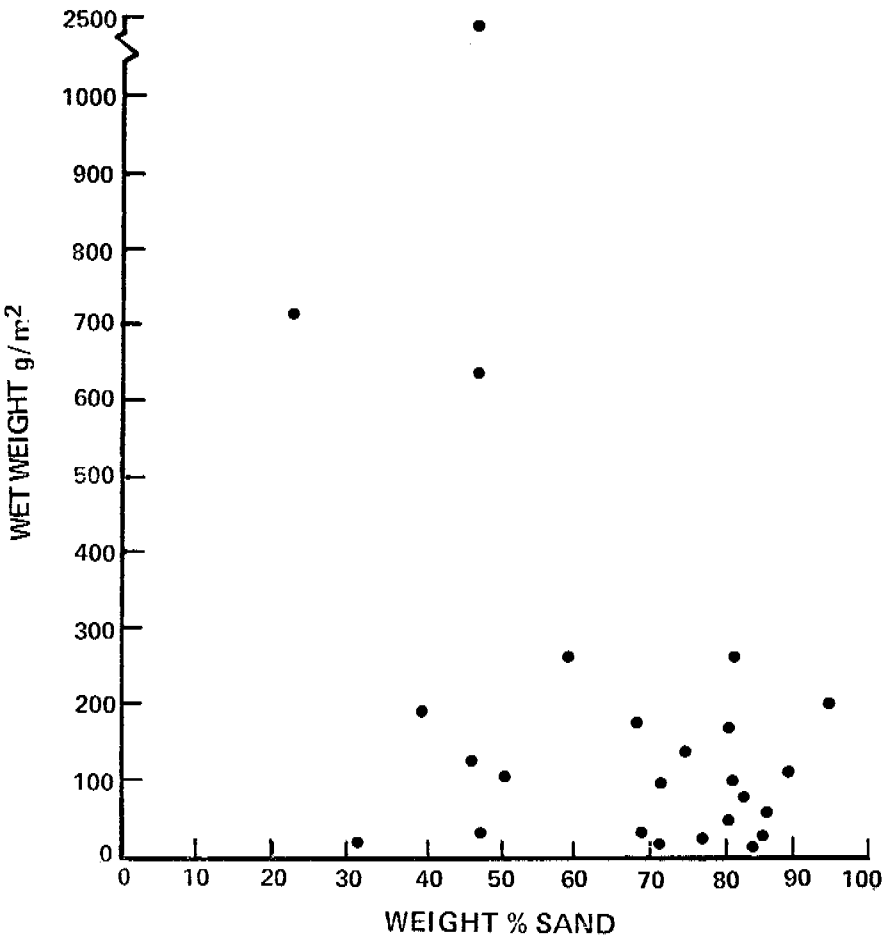

Figure 8. Scatter plot for total wet weight of macrobenthos/m^2 against weight percent sand.

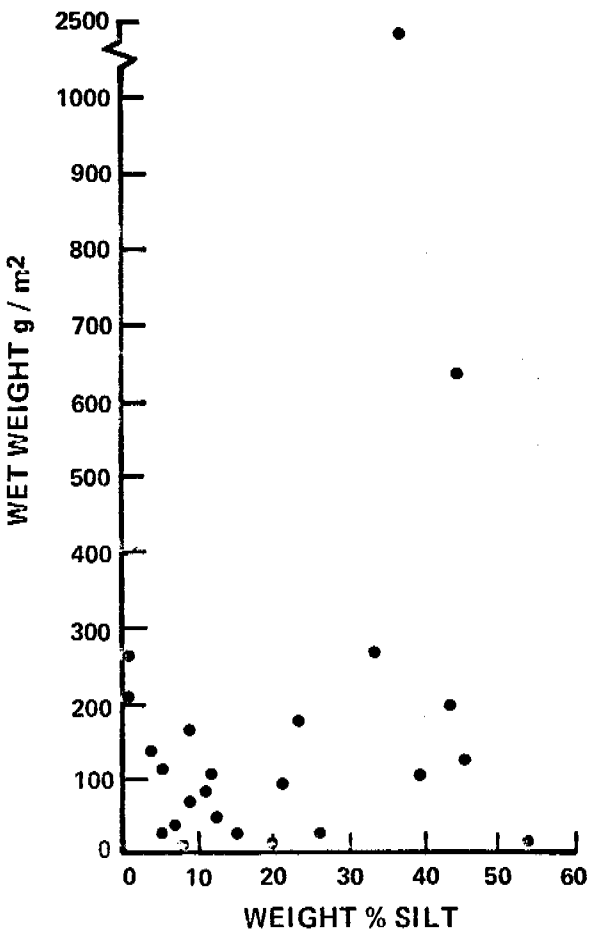

Figure 9. Scatter plot for total wet weight of macrobenthos/m^2 against weight percent silt.

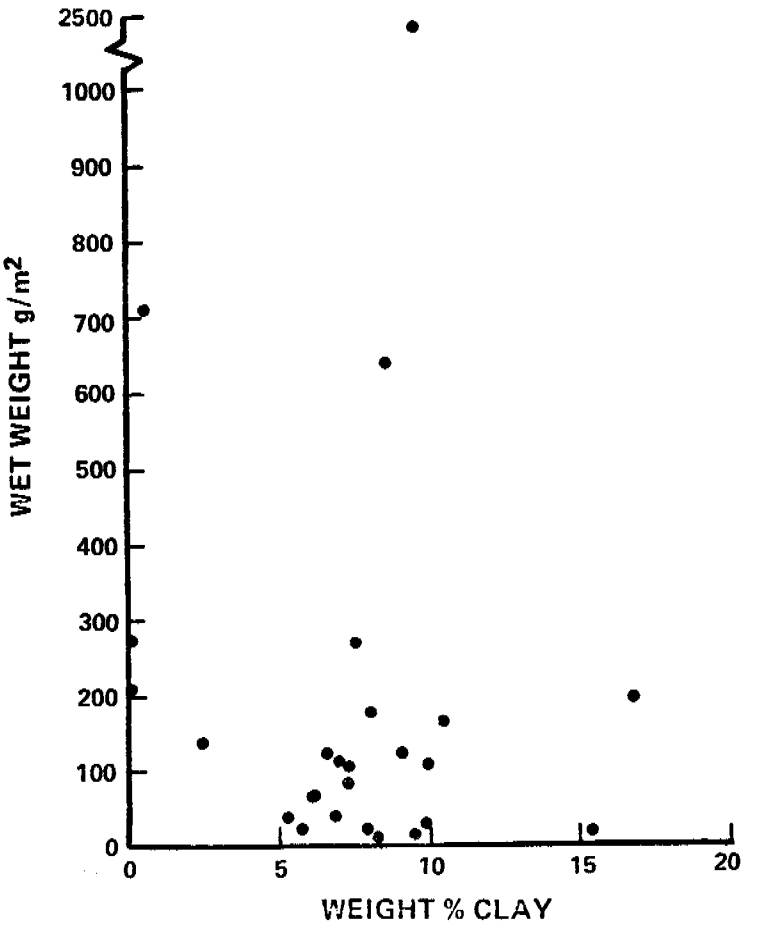

Figure 10. Scatter plot for total wet weight of macrobenthos/m^2 against weight percent clay.

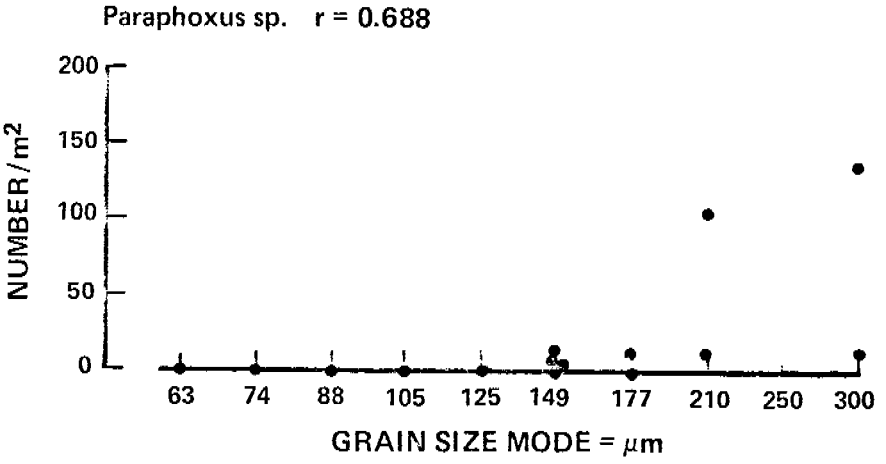

Figure 11. Scatter plot for number of individuals of the scavenger amphipod *Paraphoxus* sp./m^2 against grain size modes.

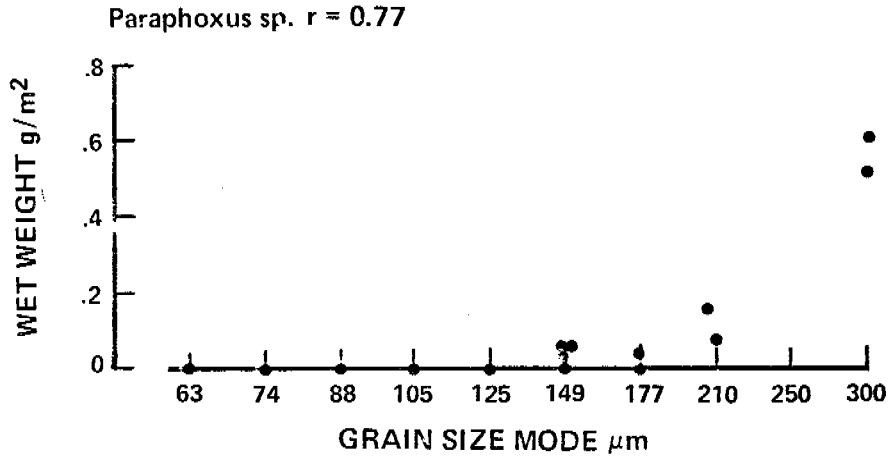

Figure 12. Scatter plot for wet weight of the scavenger amphipod *Paraphoxus* sp. against grain size modes.

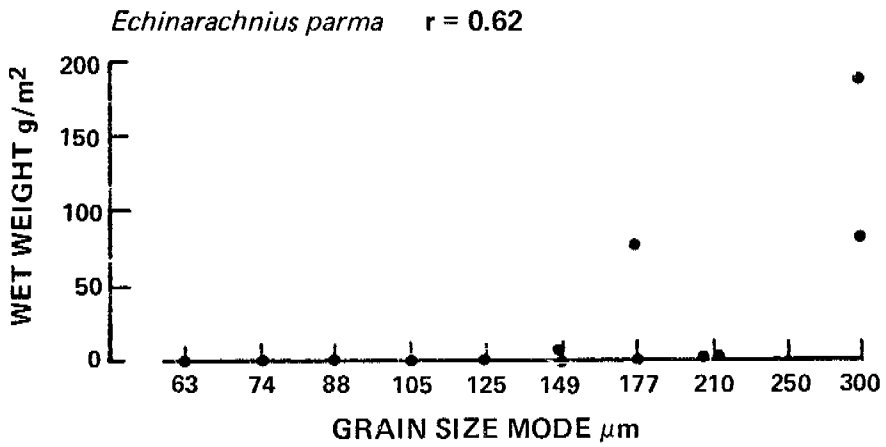

Figure 13. Scatter plot for wet weight of the scavenger sand dollar *Echinarachnius parma*/m² against grain size modes.

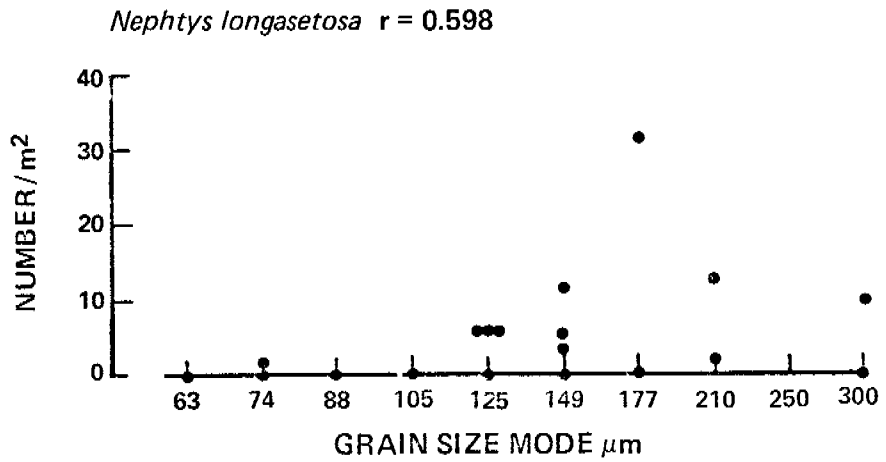

Figure 14. Scatter plot for number of individuals of the predaceous polychaete *Nephtys longasetosa*/m² against grain size modes.

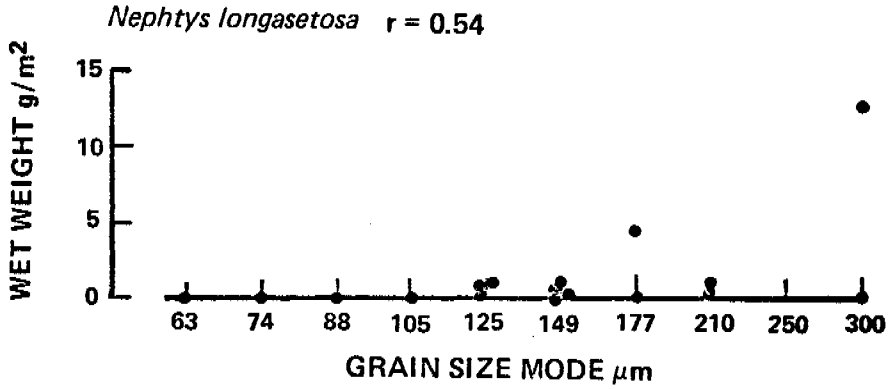

Figure 15. Scatter plot for wet weight of the predaceous polychaete *Nepthys longasetosa*/m² against grain size modes.

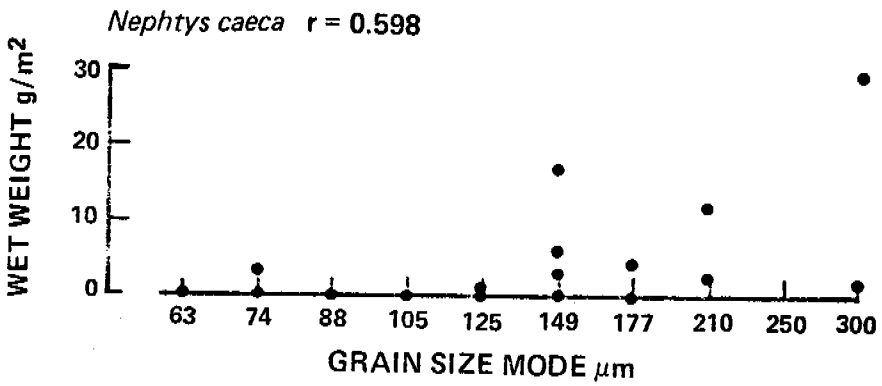

Figure 16. Scatter plot for wet weight of the predaceous polychaete *Nepthys caeca*/m² against grain size modes.

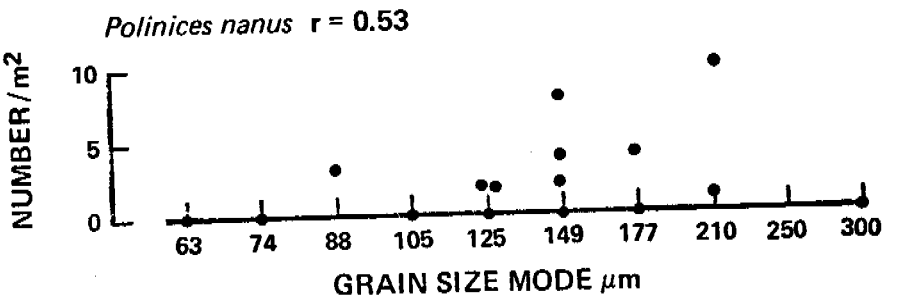

Figure 17. Scatter plot for number of individuals of the predaceous gastropod *Polinices nanus*/m² against grain size modes.

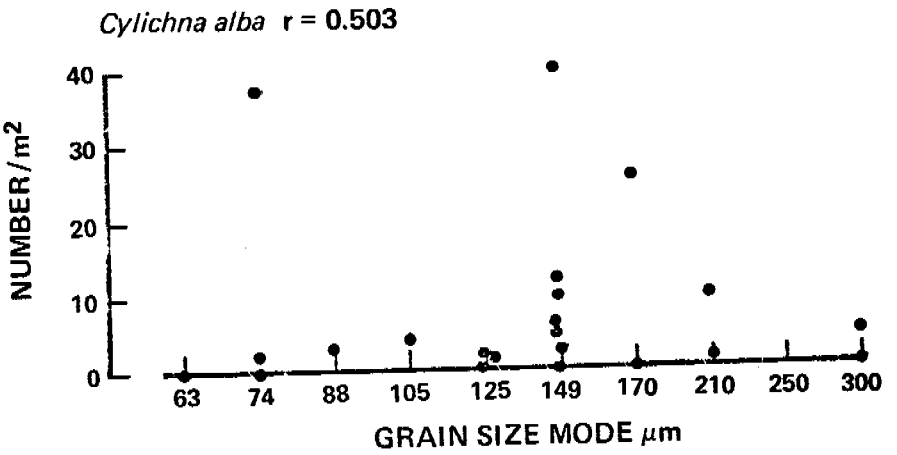

Figure 18. Scatter plot for number of individuals of the predaceous gastropod *Cylichna alba*/m² against grain size modes.

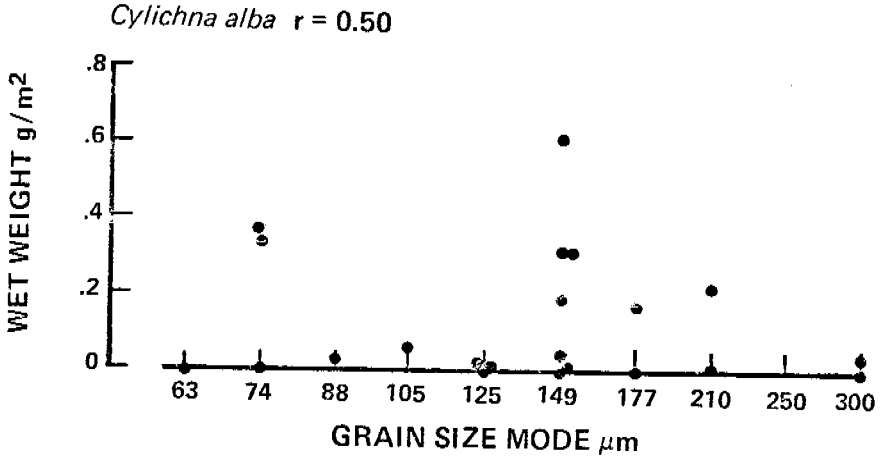

Figure 19. Scatter plot for wet weight of the predaceous gastropod *Cylichna alba*/m^2 against grain size modes.

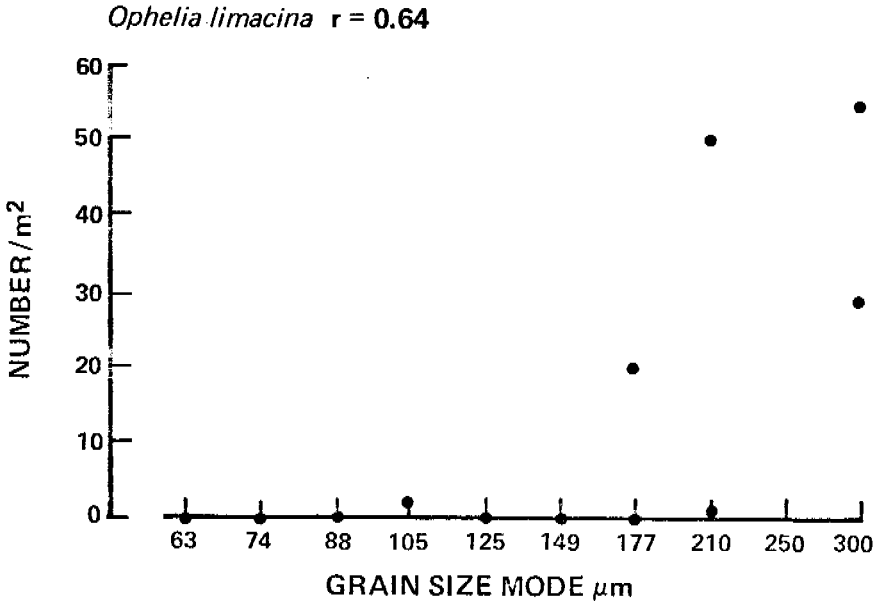

Figure 20. Scatter plot for the number of individuals of the deposit feeding polychaete *Ophelia limacina*/m^2 against grain size modes.

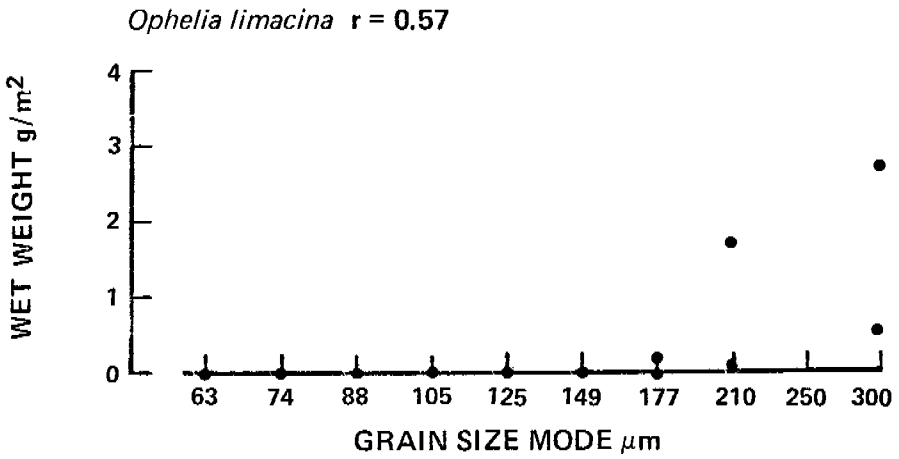

Figure 21. Scatter plot for wet weight of the deposit feeding polychaete *Ophelia limacina*/m^2 against grain size modes.

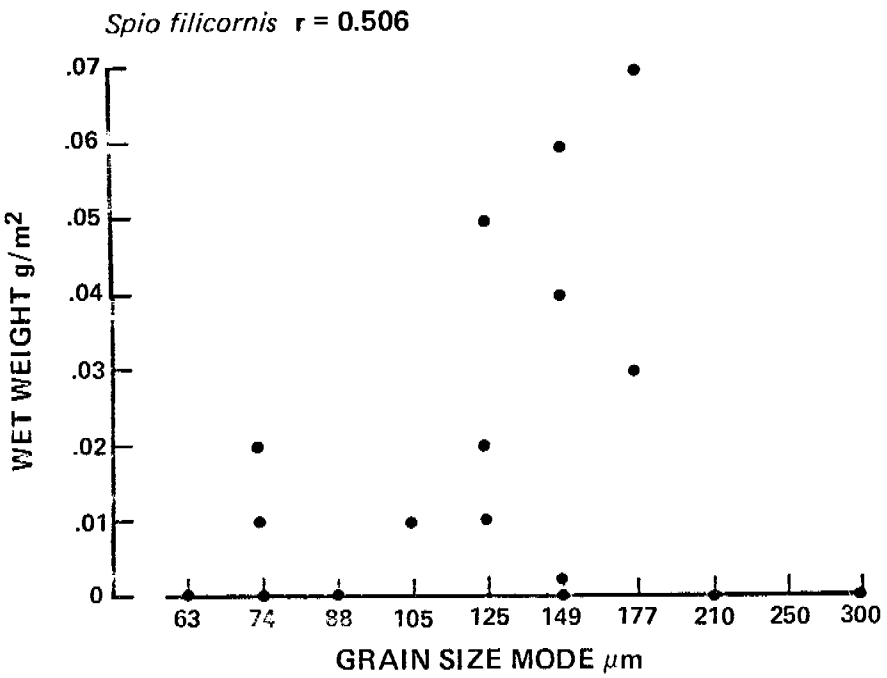

Figure 22. Scatter plot for wet weight of the deposit feeding polychaete *Spio filicornis*/m^2 against grain size modes.

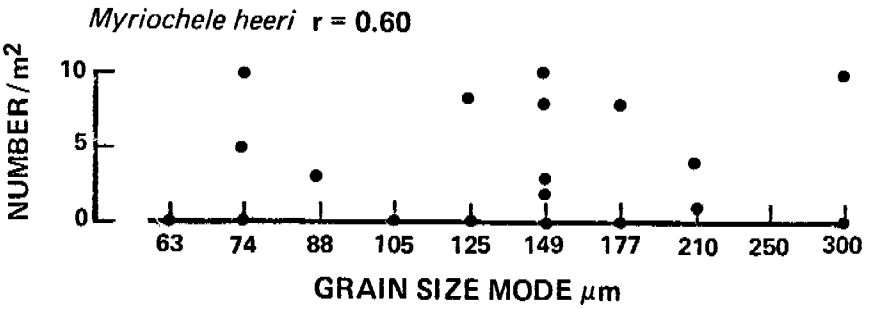

Figure 23. Scatter plot for number of individuals of the deposit feeding polychaete *Myriochele heeri*/m^2 against grain size modes.

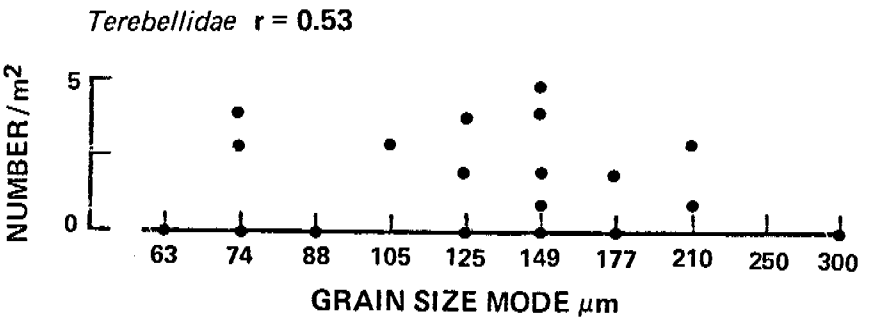

Figure 24. Scatter plot for the number of individuals of deposit feeding polychaetes *Terebellidae*/m^2 against grain size modes.

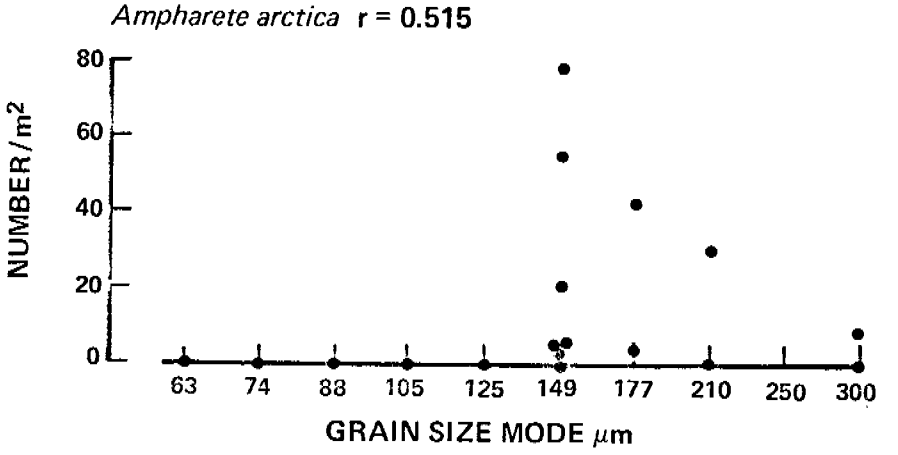

Figure 25. Scatter plot for the number of individuals of the deposit feeding polychaete *Ampharete arctica*/m² against grain size modes.

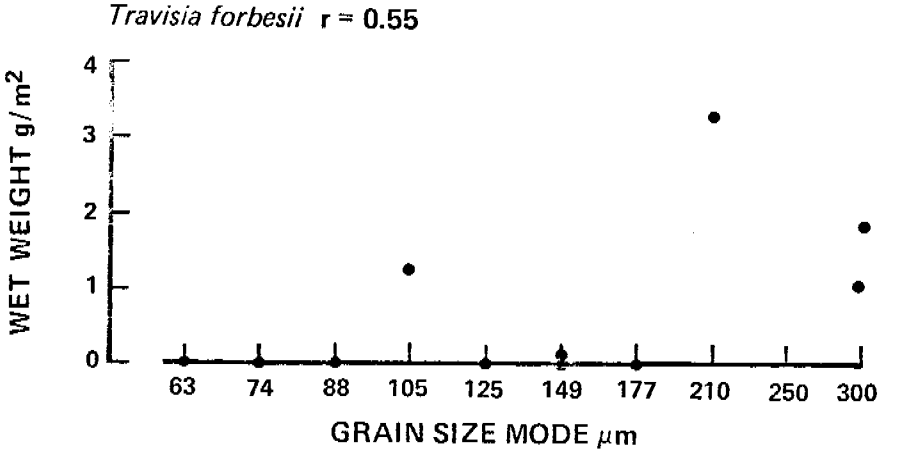

Figure 26. Scatter plot for wet weight of the deposit feeding polychaete *Travisia forbesii*/m² against grain size modes.

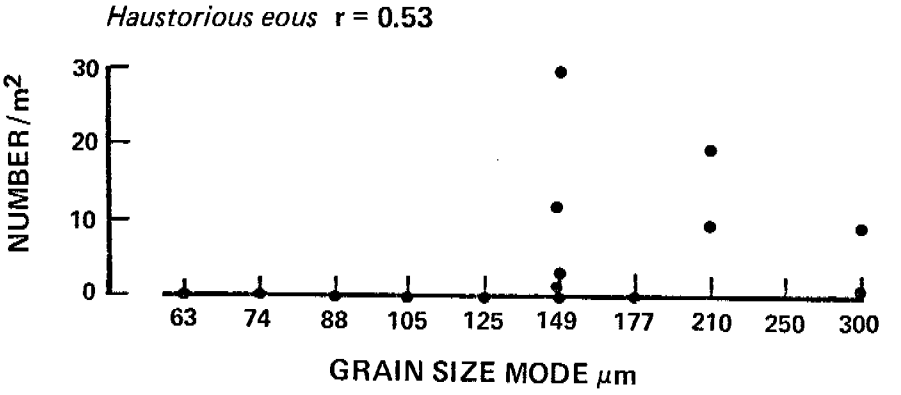

Figure 27. Scatter plot for the number of individuals of the filter feeding amphipod *Haustorious eous*/m² against grain size modes.

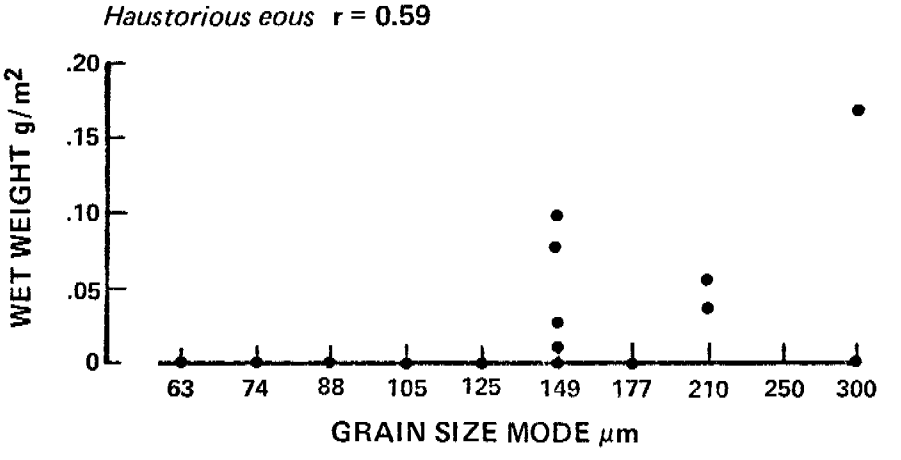

Figure 28. Scatter plot for wet weight of the filter feeding amphipod *Haustorious eous*/m² against grain size modes.

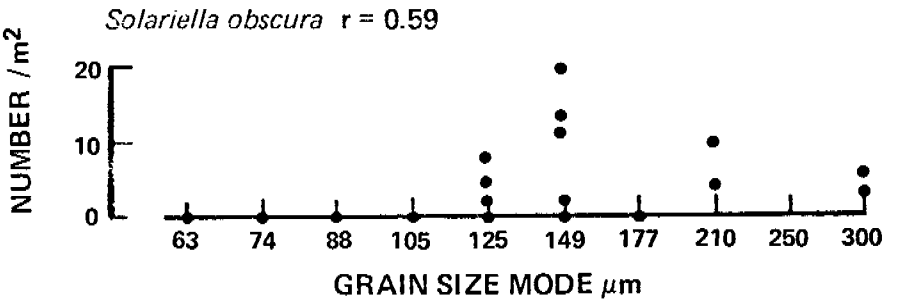

Figure 29. Scatter plot for the number of individuals of the gastropod *Solariella obscura*/m² against grain size modes; feeding type unknown.

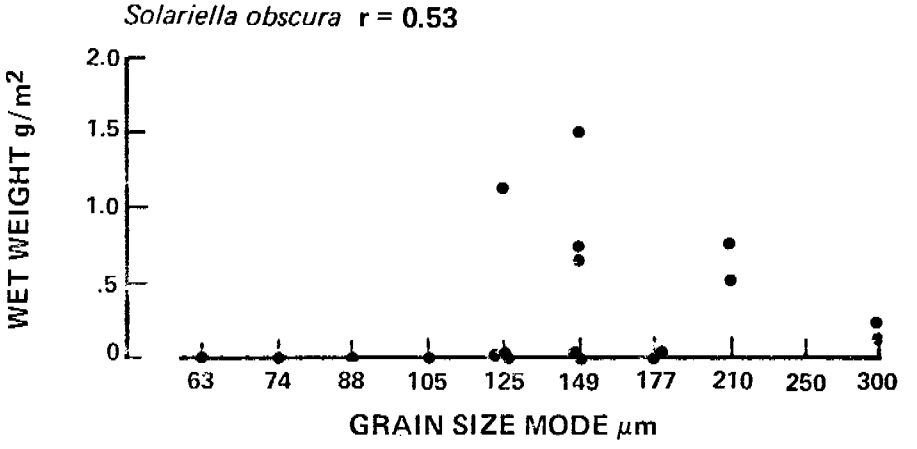

Figure 30. Scatter plot for wet weight of the gastropod *Solariella obscura*/m² against grain size modes.

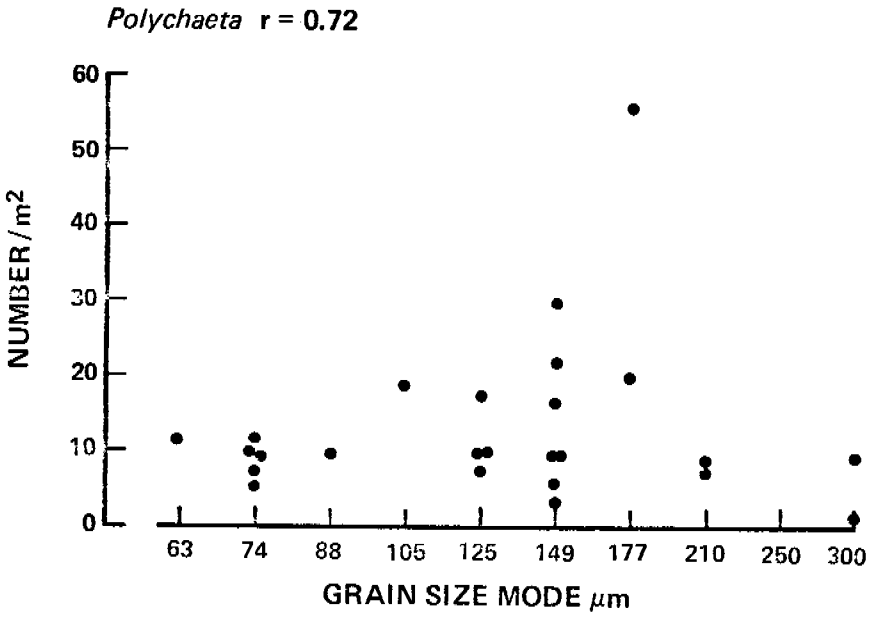

Figure 31. Scatter plot for numbers of individuals of *Polychaeta*/m² against grain size modes; diverse feeding types.

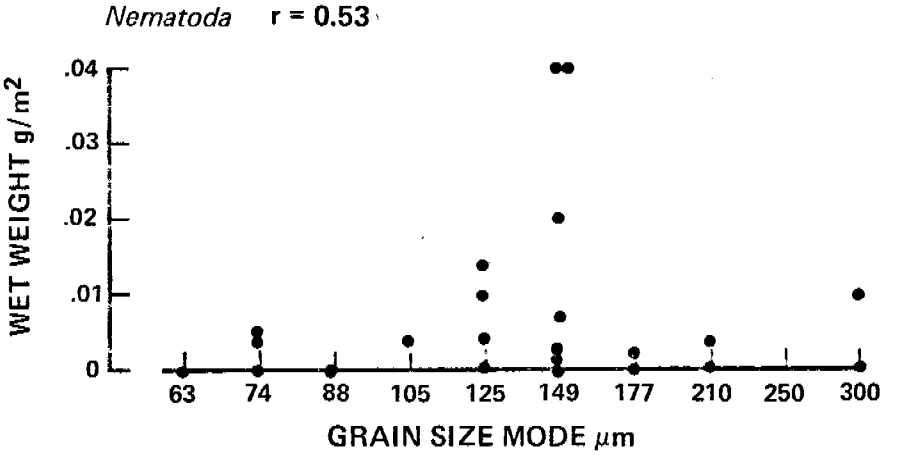

Figure 32. Scatter plot for wet weight of *Nematoda*/m² against grain size modes; diverse feeding types.

Table III. Duplicate pipet analyses from separate aliquots of mud fraction

Station	Cumulative percent coarser at grain size Ø																				Difference between Run 1 and Run 2, %	
	4.5 Ø		5.0 Ø		5.5 Ø		6.0 Ø		6.5 Ø		7.0 Ø		7.5 Ø		8.0 Ø		9.0 Ø		10.0 Ø			
	Run 1	Run 2	Run 1	Run 2	Run 1	Run 2	Run 1	Run 2	Run 1	Run 2	Run 1	Run 2	Run 1	Run 2	Run 1	Run 2	Run 1	Run 2	Run 1	Run 2	Maximum	Average 4.5 through 10 Ø
1	95.23	95.12	96.44	96.20	98.02	96.74	97.21	97.10	97.57	97.38	97.67	97.66	97.93	97.86	98.07	98.18	98.48	98.44	98.82	98.83	1.28	.22
16	56.96	57.70	69.32	68.10	77.21	75.86	82.48	81.76	85.31	84.52	87.10	86.86	88.75	88.59	90.16	90.26	92.27	92.33	94.59	94.58	1.35	.54
19	70.13	71.43	81.41	81.87	87.03	87.33	90.07	89.96	91.67	91.79	92.82	92.85	93.55	93.68	94.16	94.42	95.45	95.45	96.76	-	.46	.19
31	88.16	88.08	90.44	90.46	92.26	92.40	93.61	93.72	94.48	94.74	95.20	95.16	95.62	95.69	96.08	96.30	96.96	97.02	97.66	-	.26	.11
32	83.50	83.29	89.91	89.65	92.39	92.18	93.66	93.56	94.66	94.37	95.39	95.07	95.84	95.76	96.41	96.03	96.98	97.10	98.06	97.99	.38	.20
37	85.41	86.06	88.56	89.16	89.55	90.68	91.73	92.00	92.60	93.02	93.61	93.84	94.29	94.32	95.15	95.00	96.08	96.42	97.12	97.25	1.13	.40
45	69.23	72.06	80.64	81.77	86.84	87.15	90.67	91.11	92.48	92.98	94.11	94.09	94.57	94.73	95.47	95.60	96.68	96.68	97.28	97.59	2.83	.58
54	42.79	42.63	57.25	57.15	67.71	68.03	76.80	75.88	81.46	81.55	85.49	85.64	87.84	87.50	89.62	89.58	95.68	92.40	92.88	93.93	3.28	.65
66	93.30	93.44	94.96	95.29	95.83	96.01	96.34	96.38	96.69	96.66	96.69	97.04	97.26	97.30	97.60	97.68	98.14	98.18	98.69	98.73	.35	.13
73	78.71	79.13	82.10	82.12	84.66	84.77	86.91	87.01	89.37	89.16	90.99	90.85	92.17	92.28	93.22	93.46	94.90	94.95	96.10	96.61	.51	.19
83	73.76	73.59	81.65	82.27	85.56	85.40	88.63	87.49	90.13	90.18	92.02	92.03	93.18	93.08	94.18	93.98	95.43	95.61	96.22	96.58	1.14	.30

Table IV. Grain size parameters from a station sampled at two different times.

Station	Sampling date 1975	N. Lat.	W. Long.	Depth m	Dry wt. of sample analyzed	Weight Percent				Mean Ø M_z	Standard deviation Ø σ_I	Skewness Sk_I	Normalized kurtosis K'_G	Grain size mode µm	Wt. % in modal class size
						gravel	sand	silt	clay						
010	10 May	57°19.5'	161°05.8'	65	67.82	0	80.90	8.68	10.42	3.15	2.08	+0.70	0.82	177	57
	9 June	57°19.5'	161°05.8'	65	79.24	0	88.47	5.32	6.22	2.50	1.65	+0.42	0.83	210	34
027	11 June	57°40.1'	164°16.3'	53	80.76	0	84.77	8.25	6.98	3.02	1.58	+0.54	0.83	149	40
	4 October	57°40.0'	164°23.0'	50	75.93	0	82.21	10.65	7.14	3.22	1.66	+0.61	0.83	149	37
057	13 June	58°36.3'	168°12.1'	53	82.97	0	80.81	12.47	6.72	3.41	1.80	+0.76	0.83	149	45
	29 August	58°36.0'	168°12.8'	55	72.08	0	77.02	16.41	6.56	3.34	1.70	+0.72	0.78	149	43
060	13 June	59°42.9'	166°24.5'	29	82.45	19.22	74.99	3.52	2.28	0.71	2.85	-0.70	0.90	210	35
	25 August	59°44.0'	166°27.5'	27	84.58	0	55.27	37.44	7.29	4.08	1.95	+0.70	0.67	88	40
062	14 June	59°05.9'	169°15.1'	55	89.72	0	74.72	18.45	6.84	3.43	1.77	+0.67	0.71	149	35
	28 August	59°04.8'	169°14.2'	55	92.33	0	71.69	20.74	7.58	3.58	1.93	+0.72	0.70	149	33
082	9 June	60°32.9'	170°29.9'	60	75.90	0	88.17	5.20	6.63	2.98	1.47	+0.46	0.86	149	44
	22 August	60°32.9'	170°29.9'	60	70.34	0	43.85	48.21	7.94	4.43	1.95	+0.57	0.71	63	47

ANNUAL PRINCIPAL INVESTIGATORS' REPORT
OCSEAP Research Unit #327

Shallow faulting, bottom instability, and movement of sediments in lower Cook Inlet and western Gulf of Alaska

Principal Investigators: Monty A. Hampton
Arnold H. Bouma
U.S. Geological Survey, Menlo Park, California

I. Summary of Objectives, conclusions and implications with respect to OCS oil and gas development.

Environmental geologic investigations in lower Cook Inlet and the western Gulf of Alaska (Kodiak shelf) were continued in 1977 with a 3.5 week cruise aboard the R/V SEA SOUNDER. Seismic profiling, side scan sonar, bottom sampling and underwater TV and camera were the prime activities. Due to rough weather not all observations are of good quality.

Based on the 1976 reconnaissance study, we were able to concentrate on certain geologic phenomena that may pose a problem to development and need detailed studies before conclusions can be drawn.

In lower Cook Inlet we concentrated on two areas, one off Anchor Point and one around the semisubmersible OCEAN RANGER engaged in drilling a stratigraphic test hole. A dense trackline net of high resolution seismic reflection profiles and side-scan sonar provided information about types of bedforms, shape of bedforms fields and field boundary conditions. A correlation was observed between these parameters and water depth, showing linear regular boundaries in deeper water and irregular ones in shallow. Two reasons may be given for the irregular field boundaries: influence of Kachemak Bay circulation and storm-wave effects on the bottom. The regular boundaries reflect the principal influence of tidal currents. In addition to profiling we collected a number of cores around the semisubmersible. The distribution of drill cuttings show possible trough depths of ripples, and also that at least 13.5 cm of the sand was worked over by transport during the summer 1977.

A number of 1973 and 1974 industrial seismic lines were rerun under tight navigational control to study migration of large bedforms. The industrial data has not yet been released.

A number of samples, collected during the 1976 field season, that contained calcareous life forms were analyzed by Richard Rezak, Professor of Geological Oceanography at Texas A & M University. His results are given in Appendix VIII.

On the Kodiak shelf, the principal geo-environmental concerns are related to sediment distribution and movement, and to the structural-tectonic setting. Our objectives, based on this premise, have been to determine sediment dispersal patterns across the shelf, to enable prediction of pollutant transport routes and storage sites, and to study the movement history of seafloor faults to determine which ones have recently been active and which have not.

Sediment dispersal processes acting on the seafloor of the Kodiak shelf include winnowing of broad areas of Albatross and Portlock Banks, with some of the fine-grained winnowing products accumulating in local depressions on the banks but with most of it carried into the adjacent troughs. Kiliuda. Chiniak, and Amatuli Troughs are long-term storage areas for this winnowed material and probably for seafloor pollutants also. Relatively strong currents sweep Stevenson Trough and deliver bedload sediments to the continental slope through well-defined pathways.

Transfer of bedload sediments to the continental slope along the rest of the shelf appears to be restricted to areas where shoal physiographic barriers occur extensively along southern and middle Albatross Banks, as well as Portlock Bank, but are generally absent along northern Albatross Bank. Transfer of seafloor pollutants to the continental slopes should also be controlled by the distribution of the barriers.

Attempts to study the movement history of seafloor faults near Kodiak Island were prevented by bad weather. The study is rescheduled for the 1978 field season.

Keith Kvenvolden and George Redden collected a number of subsamples for hydrocarbon analyses. Their results are presented in Appendix VII.

II. Introduction

A. General Nature and Scope of Study: Assessment of the environmental geologic hazards, sediment types and sediment distribution of lower Cook Inlet and the Kodiak shelf, western Gulf of Alaska.

B. Specific Objectives: The identification of active surface faults, areas of sediment instability, the relationship of sediment types with regard to bottom morphology and circulation patterns, and types and movement of bedforms.

C. Relevance to Problems of Petroleum Development: The above-mentioned objectives have direct relevance to problems of offshore petroleum development. Active faulting and sediment instability might endanger emplacement of offshore structures. The relation between morphology and sediment characteristics will identify the presence of areas where erosion is more active than deposition and of areas that are sediment traps and consequently may act as sinks for nutrients as well as pollutants.

III. Current State of Knowledge

Lower Cook Inlet: Based on the 1976 field operations and the results from the Petty Ray Geophysical, Inc. work conducted for the USGS, Conservation Division, in Anchorage, we were able to delineate the potential geologic hazards that pertain to OCSEAP studies.

Within the lease area no surface faulting of any importance could be observed, which means that no fault could be correlated from one to the adjacent trackline. Locally active faults of minor extent may be present but if surface expressions would be occurring they would be eliminated by bottom erosional action. Outside the nomination area a large number of faults occur, specifically around the Barren Islands and on the backsides of Augustine Island (Bouma and Hampton, 1976; Hampton and Bouma, 1976).

Although some local steep slopes are present, no evidence of slumping and sliding of any significance has been observed. The nature of the bottom sediments, mainly of glacial origin, covered locally with a thin veneer of sand, does not lend itself to slumping and sliding on low slopes.

Seismicity and volcanism are two hazards that play an important role in lower Cook Inlet (see Pulpan and Kienle, R.U. 251). Presently not much is known about the offshore effects of volcanism related to Augustine, but a pilot study will be made during the 1978 summer cruise to investigate if a larger study should be proposed.

The major other geologic hazard in lower Cook Inlet is formed by the active motion of sand on the seafloor and by the migration of bedforms. The larger bedforms with wave lengths ranging from 500 to 1000 m, and wave heights ranging from 5 to 10 m, contain enormous quantities of sand and much material has to be moved before significant migration can be established. Movements in the order of 10 cm per day require a number of years before the amount of migration can be measured conclusively within the accuracy of high-precision navigation (mini-ranger). For this purpose we rerun some 1973 and 1974 industrial lines, using preplotting methods. The industrial data is still proprietory and we are trying to have the lines in question released. Preliminary results show

that large bedforms appear and disappear and that thickness of the sand sheet changes over the period of 4 years. However, those companies did not store their navigational data and enlarging their navigation plots does not improve accuracy. Their information will be very valuable but for accurate measurements we will resurvey those lines during this 1978 and the 1979 season.

Short-term measurements provide information about the movement and dependency of opposing tidal flows. Side-scan sonar, bottom television and bottom camera have given valuable information (Bouma and others, 1977, a,b, 1978 a,b). Scanning electron microscopy examinations give the impression that net transport of sand grains in and out of large bedform fields seems unlikely on a large scale, although the studies do not indicate the time frame such may be restricted to (Hampton and others, 1978 and Appendix I).

The effects of migration of sandwaves and other bedforms in areas with high tidal flows can have serious effects on large and small structures. Although examples of such effects on platforms and pipelines are known, very little information about this is available in the open literature. Erosion or deposition can influence the lateral capacity on an underwater structure (Palmer, 1969). Two types of scour in non-cohesive sediment have been observed around a group of pilings. The first forms a conical hole around each pile penetrating the bed, while the second results in a general lowering of the bottom under the whole structure, topping off at zero at a considerable distance. The second type is less common but more serious (Posey, 1971).

An artificial structure can influence the local bottom current to a large degree, and when dealing with non-cohesive sediment can influence the degree of erosion. Wilson and Abel (1973) conducted experiments about the effect of scour created by 80-ft diameter pontoons of a semi-submersible drilling rig to be placed in water 90 feet deep on the Nova Scotia shelf with tidal currents reaching a maximum velocity of about 1.5 knots (77 cm/s). They concluded that without scour protection, erosion would occur under and around the pontoons, which in turn would cause adverse settlement of the rig even at current velocities as low as 0.43 knots (21 cm/s).

Fluttering of pipelines can occur in areas where sand is moving causing parts of a pipeline to become suspended. Flutter is a phenomenon that occurs when the frequency of vortices shedding in the wake of a stationary long slender cylindrical object (e.g. floating drilling marine conductor, suspended pipeline) in a moving current approaches the natural frequency of the body, or about half of that when couplings are involved. The shedding of vortices must occur in a regular frequency on alternate sides of the body in order to establish alternating forces which induce motion at right angles to the current direction (Goepfert, 1969). The phenomenon of flutter has been described from upper Cook Inlet, Alaska (Geopfert, 1969) and from the North Sea.

In area with severe ice conditions, the engineer often designs a tapered section at the water line for the outer breasting platform piles and the mooring dolphin piles to provide less resistence to flow of ice. Variations in tidal heights are taken care off, but a change in the depth of water due to erosion or deposition in the time between the site survey and the emplantment of the rig may not be compensated for (Visser, 1969), which shows that these dynamic processes can have serious effects. This latter example pertains to upper Cook Inlet and not to lower Cook Inlet.

Industry has developed several methods to protect the area around platforms from scouring. However, pipe lines still pose a severe problem and although they have to be buried in these water depths where active bedforms are present, no guidelines have been made by the responsible agencies as to what procedures should be used due to lack of necessary information.

Very few samples have been collected during the 1977 season because the few weather windows were used for observations on the bedforms rather than for sampling stations. As far as lower Cook Inlet is concerned the best plot of grain size data is given in Bouma and Hampton (1976) and few additional detailed analyses in Bouma and others (1978a) (Appendix II). Contacts have been made with other investigators and industry to provide us with cuts of samples. The present density of data points does not warrant the making of a sediment distribution map (Fig. 1; Table I).

The incorporation of material within the sediment column was studied on a small number of cores collected near the D/V OCEAN RANGER, utilizing drill cuttings as tracers. The results indicate that vertical incorporation of material took place at least to a depth of 13.5 cm during a 100-day drilling period during June - September, 1977. We hope to be able to continue such studies making use of drilling rigs operational in the area and requesting the operators to collect samples prior to leaving the site. The preliminary results are given in Bouma and others (1978b) and Appendix III.

A detailed study on the bedforms was conducted off Anchor Point. The detailed survey provided sufficient trackline density to make a map of this area and to describe the bedforms, bedform fields and bedform field boundaries. Preliminary results are given in Bouma and others (1978b) and additional data are presented in Appendix IV.

The bathymetry of lower Cook Inlet is rather complicated. The bathymetry map of the lease sale area was constructed by Petty-Ray Geophysical, Inc., and we enlarged the area to cover all of lower Cook Inlet (Appendix V; Bouma and others, 1978a,b,). Presently we are studying the bathymetry as physiographic units related to depth zones and to bottom features. Additional track lines and sampling will be done this summer to finalize some of the critical boundaries.

Kodiak shelf: The original objectives of the 1977 cruise on the Kodiak shelf, with regard to OCSEAP studies, were to determine the recency of movement of some of the major shallow faults and to more precisely define sediment dispersal patterns.

Some of the major faults on the Kodiak shelf trend across young sediments. In particular, a set of major faults cuts across the head of Chiniak Trough, which is partially filled by laterally prograding sediment wedges that may have been deposited as recent as the last shoreline transgression (approximately 11-13,000 years ago). Lack of post-transgressional sediment accumulation has left these sediments exposed at the seafloor. By the use of minisparker, side-scanning sonar, underwater TV, and bottom camera, we hoped to determine if the faults had offset these young sediments at the seafloor, thereby placing a maximum age of activity. However, bad weather forced us to abandon this part of our program. It is rescheduled for the upcoming 1978 cruise.

Sediment dispersal patterns on the Kodiak shelf have been generally defined from data gathered during the 1976 field season. It was found that influx of Holocene sediment is low and that Pleistocene sediments are being reworked, with most Albatross and Portlock Banks sediments being winnowed whereas Kiluida, Chiniak and Amatuli Troughs are being filled with these winnowing products and with occasional inputs of volcanic ash. Stevenson Trough is being swept by relatively strong currents, with sediment being moved seaward and eventually to the continental slope. The implications regarding pollutant transport along the seafloor are that Kiliuda, Chiniak, and Amatuli Troughs would serve as long-term storage and concentration areas for pollutants, whereas other parts of the shelf would not.

Several questions remained after analysis of the 1976 data, and the sampling pattern of the 1977 cruise was designed to answer some of these. Three main aspects of shelf sediment disperal were addressed: 1) the interaction between dispersal processes on the Kodiak shelf, in lower Cook Inlet, and in Shelikof Strait; 2) the relation between sediment dispersal and small physiographic features on the banks and troughs; and 3) sediment dispersal across the shelf break, especially as controlled by the prominent tectonic-physiographic features that exist there.

We recovered samples at most of the desired stations, and although analyses of textures and compositions are still underway, some preliminary conclusions can be drawn. The locations of samples are shown in Figure 2, and descriptions are given in Table I. Descriptions of samples collected in 1976 are given in Table II.

The transition in textures from the Kodiak shelf into lower Cook Inlet is gradual, going from typical Kodiak shelf gravelly sand at station 52 (1976 data) to pebbly-muddy sands, muddy sands, and sandy muds into Cook Inlet. Station 203, which is located just within Shelikof Strait, yielded a soft mud, implying a rather abrupt fining of sediment into the trough.

The distribution of sediments implies a relatively gradual transition between the lower Cook Inlet and Kodiak shelf environments, with no obvious sinks for pollutants. However, Barren Deep to the northeast of station 200 needs to be sampled to determine if it is a possible sink.

The fine-grained nature of sediment at station 203 suggests that suspended sediment is deposited in significant quantities as water moves from lower Cook Inlet into Shelikof Strait. More sampling will be done to confirm this. Pollutants might also be concentrated in Shelikof Strait.

Linear sampling traverses have been run across middle and northern Albatross Bank and in Chiniak Trough, to determine the variability across the banks and within the troughs. Analysis of samples collected in 1976 implied that sediment distribution within the troughs is relatively uniform whereas sediment distribution on the banks is nonuniform and related to small physiographic variations (see Hampton, Bouma, Frost, and Colburn, in press, and 1977 Annual Report). The traverse across northern Albatross Bank (stations 61-67, 81-82) shows that sediments on the elevated, normal portions of the banks tend to be gravelly to bouldery sands, commonly with abundant shell material and low to moderate amounts

of volcanic ash. Within broad shallow depressions on the banks, the sediments are similar except with large amounts of volcanic ash, typically present as a surficial layer less than 3 cm thick (sample 66). Ash contents dominate and accumulations become much thicker in the adjacent troughs (sample 81). The traverse across middle Albatross Bank (stations 215-218, 115) shows similar variations, although the normal bank sediments tend to contain relatively little, if any, material coarser than sand. Bank sediments appear to be winnowed on the normal, elevated portions, whereas some of the winnowing products are deposited in the shallow depressions.

The traverse in Chiniak Trough (stations 68,87,88,229,231) yielded samples that were composed mostly or entirely of volcanic ash, both along the normal floor of the trough and within a depression just landward of the shelf break. Sedimentation conditions are uniform throughout the trough.

Along the shelf break, tectonic and erosional processes have produced variations in physiography, both along the banks and within the troughs. Uplifted ridges, commonly eroded to expose sedimentary bedrock, exist discontinuously along the outermost continental shelf. These "shelf-break highs" were suspected to be barriers to bedload transport across the shelf break, and a sampling program was carried out to verify this. The shelf-break high is well developed along middle Albatross Bank, and several samples were taken across it and out past the shelf break. Several samples taken on the high (stations 116-124, 220) show a layer less than a few centrimeters thick overlying bedrock. Sediments on the adjacent upper continental slope are fine grained, except within local basins, and from preliminary observations appear to be compositionally similar to the sedimentary bedrock in that their fine fraction is composed mostly of quartz rather than clay minerals. They do not appear similar to normal unconsolidated bank sediments, especially in their lack of volcanic ash. The nature of the sediment distribution implies that unconsolidated sediments of middle Albatross Bank are not transported across the shelf break high to the continental slope. That is, bedload transport across the shelf break does not appear to be taking place.

Sediments seaward of Chiniak Trough (stations 227,228), beyond the shelf-break high that apparently forms a continuous sill across the mouth of the trough, are distinctly different from the ash-rich sediments in the trough. They are composed of terrigeuous and biogenic debris rather than pyroclastic debris. Once again, the shelf-break high appears to block transfer of sediment from the shelf to the slope.

On northern Albatross Bank the situation changes. The shelf break high is absent along most of this bank, and the transition from shelf to slope is a smooth one. The sediments on the slope (stations 232,242) are different from those off middle Albatross Bank in that their fine fraction contains significant clay. Sediment from station 232 looks similar to nearby unconsolidated sediments of the shelf. The evidence tentatively suggests that transfer of bedload sediment across the shelf break is occurring where the shelf break high is subdued. Further comparison of sediments will be made to verify this.

The shelf-break high is discontinuous across the mouth of the Stevenson Trough, with a few channels breaching it. Sediments within Stevenson Trough typically are sands with low to moderate amounts of volcanic ash. Sediments from the channel breaches and from connecting channels on the upper continental slope (stations 59,60,236,241,244) are similar sands, some containing minor amounts of coarser material. Sediments from on top of the sill (staions 243,245),

on the other hand, are slightly pebbly and muddy sands with abundant forams, similar to samples from nearby northern Albatross and Portlock Banks (e.g., samples 61,141). The breaches through the sill appear to be conduits for present-day transfer of sediment (and possibly pollutants) to the continental slope. The high parts of the sill have relict sediments like those on the adjacent banks.

The distribution of sediment on the Kodiak shelf shows that sediment dispersal is influenced significantly by tectonic and closely related physiographic features. Also, a study of submarine sediment slides on the upper continental slope showed a relation between slope instability and tectonics (see Hampton and Bouma, 1977 and Appendix VI). The shelf-break high that is prominent along southern, middle Albatross and Portlock Banks reflects active tectonic deformation of the shelf-break area. Slope steepening, faulting, and seismic activity associated with this tectonic activity causes the submarine slides. Northern Albatross bank, where the shelf-break high is subdued or absent, apparently is not being actively deformed, at least with the intensity of the adjacent areas. Large sediment slides are absent from the slope in this area.

Therefore, an understanding of the regional tectonic processes in the Kodiak shelf area provides an understanding of sediment (pollutant) dispersal and slope instability. It is likely that other environmentally significant conditions are distributed in relation to the tectonic setting, especially seismicity (distribution of epicenters, strong ground motion, etc.).

Another objective of the 1977 cruise was to study the near-bottom currents in Stevenson Trough, which seem to be relatively strong compared to other areas on the banks. Two near-bottom current meters were to be moored; one within the trough and the other on northern Alabatross Bank. Using the data gathered with these meters, we hoped to verify the relatively strong current regime in Stevenson Trough. Loss of one of the current meters in lower Cook Inlet, prior to arrival to Kodiak shelf, disallowed this study. Bottom TV observations were made in the bedform area of Stevenson Trough. They showed no signs of bedload movement during the time we were there.

In addition to determinations of the textures and compositons of sediment samples from the Kodiak shelf, two other projects are underway. A structural map of the shelf, showing shallow faults, fold axes, and areas of bedrock outcrops is being prepared with Roland von Huene. An isopach map, showing the thickness of surficial unconsolidated sediments is also being prepared.

IV. Study Area

1) Lower Cook Inlet between Shelikof Strait at latitude 58°40'N and Cape Ninichik at latitude 60°00'N, mainly encompassing OCS lease-sale area CI.

2) Kodiak shelf between Amatuli Trough at latitude 59°00'N and the middle of southern Alabatross Bank at altitude 56°40'N, mainly encompassing OCS lease-sale area 46.

V. Sources, Methods and Rationale of Data Collection

The results presented come from data collected during a 6-week cruise in June and July, 1976, and 3.5 week cruise in September and October, 1977, both aboard the R/V SEA SOUNDER. Some additional data for lower Cook Inlet came from copies of a 1976 Petty-Ray Geophysical, Inc. survey made under contract to the U.S. Geological Survey, Conservation Division in Anchorage. Additional high-resolution seismic records were collected by R. von Huene aboard the research vessel S.P. LEE during his 1976 survey of Kodiak.

Seismic and sampling methods have been discussed in Bouma and Hampton (1976) and Hampton and Bouma (1976). The rationale for collecting data with the instruments and equipment, described in the above-mentioned U.S. Geological Survey Open-file Reports, is that such procedures are the only ones generally recognized to achieve the objectives of the proposed study.

VI, VII, VIII Results, Discussion, and Conclusions

It has to be kept in mind that the 1976 cruise aboard the R/V SEA SOUNDER was a reconnaissance due to lack of public information relating to environmental geohazards. Consequently no specific details could be studied in the field at that time. The field data were reported on by Bouma and Hampton (1976) and Hampton and Bouma (1976). During the 1977 field season we planned to study details pertaining to the geohazards but weather and sea state made many of the efforts impossible or reduced the quality of the geophysical high-resolution records to such a minumum that interpretation becomes impossible.

The high energy environment in lower Cook Inlet has a direct impact on the bottom. Where sufficient unconsolidated sand-sized material is available, the bottom is characterized by different types and sizes of bedforms, such as sand-waves, sand ridges and dunes. Where such unconsolidated material is scarce or absent one finds sand ribbons, sand tails, boulder fields, or a smooth bottom (see Appendices II and IV; Bouma and others, 1977a,b, 1978a,b; Hampton and others, 1978). The nature of this smooth bottom is variable according to seismic records. It is assumed to be of glacial origin and locally may contain fluvio-glacial deposits. However, no data on this smooth bottom material, that also underlies all mentioned bedforms, are available.

Although high velocities of sand moving over the crests of large bedforms were noted, we have the idea that net migration of the large sand bodies is only in the order of a few tens of meters per year. To move such bedforms over such short distances still requires enormous amounts of sand to be transported and the dynamics of the water column and the sand are such thay they pose a hazard to offshore installations and platforms (see under Pt. III). Our scanning electron microscopy investigations suggest that sand within the fields of large bedforms is in active motion, but that sand transport to and from such fields is minor (Hampton and others, 1978; Appendix I). Although industry has developed systems to cope with scouring around platforms in such areas, we feel that still little attention has been given to the migration of such large and the smaller bedforms to the best approach of laying pipelines in such a dynamic area, burial of the pipelines, and the preventing of scouring underneath that may result in flutter.

Preliminary studies on the incorporation of drill cuttings into the unconsolidated sand sheet indicate that at least 13.5 cm of sand was in motion during the 100-day observation period in the summer of 1977. The concentrations of drill cuttings within the sand column are low which indicates that large amounts of sand are moved during such period and that the low concentrations suggest a good dispersal which is a favorable condition when dealing with heavy pollutants although a large area may be involved (see also Appendix III; Bouma and others, 1978b).

The bathymetry of lower Cook Inlet is rather complicated. Additional research is needed to relate the physiography to the development of the area after the last retreat of the glaciers. It is obvious, however, that the bathymetry has a significant influence on the paths of bottom water and on the distribution of bedforms, the large ones basically being concentrated in the central depression in water deeper than 60 m, and on the asymmetric triangular apex in front of the southern terminus of this central depression (see Appendix V; Bouma and others, 1978a,b).

The principal geo-environmental concerns on the Kodiak shelf are related to sediment distribution and movement, and to the structural-tectonic setting. Shelf sediments are distributed in relation to physiography. Much of Albatross and Portlock Banks are covered with a thin veneer of coarse-grained sediments, generally sparse in clay sizes and locally containing abundant shells. The veneer is absent over large areas, yielding exposures of semi-lithified to lithified siltstones, silty sandstones, and pebbly mudstones. Within broad, shallow depression on the banks, the coarse debris is covered with a few cm of fine-grained sediment that is rich in volcanic ash. The banks appear to be formed of relatively stable foundation material, but the actual behavior during cyclic or static loading is unknown.

Kiliuda, Chiniak, and Amatuli Troughs contain surficial layers of fine-grained sediments up to 20 m thick. Surface samples of these sediments are composed almost entirely of volcanic ash from the 1912 eruption of Katmai volcano. These troughs appear to be quiet areas of sedimentation, receiving fine-grained material winnowed from the adjacent banks. They are likely to act as long-term storage sites for pollutants that reach the sea floor of the Kodiak shelf. The ash-rich sediments are weak, but their geotechnical properties and engineering behavior have not been studied in detail.

Stevenson Trough, which may connect with tidally dominated Cook Inlet to the north, contains relatively well sorted, sandy sediments that have been molded into seaward-facing sand waves in one locality within the trough and have been spread onto the adjacent continental slope. A relatively high-energy bottom current regime in Stevenson Trough transports sediment seaward past the shelf break to deeper parts of the ocean floor. Pollutants carried into the trough can be expected to experience a similar fate. Scour of sediments, due to movement by high-energy bottom currents, may affect structures located in the trough.

Transport of bottom sediments across the shelf break of the Kodiak shelf appears to be localized and does not occur in areas where physiographic barriers exist. Kiliuda and Chiniak Troughs, for example, have well defined sills near the shelf break that distinctly separate the ash-rich sediments within the troughs from fine-grained, ash-poor sediments on the adjacent upper continental slope. Although Stevenson Trough also has a sill, it is breached in a few places, and these breaches appear to be avenues of transport for the sandy trough sediments into deeper waters.

Shoaling of the sea floor due to tectonic action has occurred near the shelf break on many parts of the banks, commonly with a broad depression on the landward side. Preliminary data from sediment samples indicate that transfer of bottom sediments from the shelf to the continental slope may be restricted to areas where an effective barrier has not been produced by shoaling. Transfer of shelf pollutants to deeper parts of the sea floor might also be localized due to this physiographic control on sediment dispersal.

IX Needs for Further Study

Lower Cook Inlet: No specific studies have been conducted offshore Augustine Island on the significance that the lava flows have on the bottom in subaerial conditions during low sea level as well as at the present time as submarine events. Augustine is known to be a volcano that can release enormous amounts of energy during an eruptive phase, and its material is of such a petrologic composition that nuée ardentes are formed. We do not know anything about the distance the hot ash clouds can travel over water, where their solids will be deposited in this dynamic area, and how much farther the heat front may travel. A pilot program will be conducted this 1978 summer to see if a detailed study is warranted. This study aspect is in cooperation with Juergen Kienle (R.U. 251) and John Whitney (U.S.G.S., Cons. Div., Anchorage).

The migration of bedforms, influence of ebb and flood flows on non-cohesive material and bedforms, and the long and short distance transport of sand are very important study aspects, of which the results are of direct interest to the development activities, planning, and permitting of the area. We will continue our long-term observations on the large bedforms, using industrial and own data collected along the same track lines. Because industry did not store their navigational raw data it is necessary for us to continue this survey aspect for several more years. In addition to the normal R/V SEA SOUNDER approach we should at least once go out with a smaller vessel (positioning by mini-ranger, bathymetry-side scan sonar) just before the winter season sets in and then the same operation after the winter to delineate the influence of winter storm wave-induced bottom effects against the normal tidal flows during the period of high runoff.

In order to understand the dynamics of the system it is needed to do comprehensive studies from the R/V SEA SOUNDER utilizing, in addition to echo sounding and side scan sonar, the seismic high-resolution systems, bottom TV and camera, the BLASTER (Bottom Layer And Sediment Transport Evaluation Rack), sampling tools, and the Geoprobes (in conjunction with Caccione and Drake) to understand the flow dynamics and the transport of grains under ebb and flood conditions. The obtained data should provide data points that can be applied to other areas in lower Cook Inlet such as near-bottom current meter stations deployed by PMEL and by industry, as well as by hydrodynamisists and for flume experiments. It is anticipated that we can correlate these short -term observations with the long-term ones to address the problem what agents have most influence on the movement of sand and bedforms, and how stable the bedform fields and the locations of their boundaries are.

Kodiak shelf: The sediment distribution on the Kodiak shelf shows significant variations that probably have an important effect on the distribution of benthic organisms. Moreover, the potential for concentration of pollutants implies that certain animal types are more vunerable than others to contamination of shelf sediments. A cooperative effort between geologists and biologists is needed to determine the relation between animal and sediment types and to predict the effect of pollution incidents.

The wide-reaching implications of the tectonic setting on the Kodiak shelf and the high concern with seismic activity point to the need for a cooperative effort between marine geologists, seismologists, and seismic and geotechnical engineers to better define the tectonic segmentation of the shelf, determine its causes, and also determine its control on the distribution of epicenters and ground response.

Evidence for shallow gas has been noticed in seismic reflection records from the shelf. Suggestions of both biogenic and thermogenic sources are present. A closer look at potentially gas-charged areas should be taken, with a determination of the areal limits. Measurement of the levels of gas in the sediments should be made. Most important, though, a process-oriented study should be initiated to determine the engineering effect of gases in sediments. Questions to be adressed include the effects of gases on the strength of sediments, means for identifying sediments with critical levels of gas, and how to asses the blowout potential in gas-charged areas. In 1978, we will run high-resolution seismic - reflection surveys over suspected gas-charged areas on the Kodiak shelf, and sediment samples will be collected for gas analysis.

X Summary of January - March Quarter

No cruises or field projects were conducted. This period was utilized to continue our examinations of seismic and side-scan sonar records, to carry out grain size analyses in the laboratory, to study the physiography of lower Cook Inlet, and to continue microscopial analyses on the drill cutting distribution and on compositions of Kodiak shelf sediments.

XI Auxiliary Material: References Used, Papers, and Presentations

Bouma, A.H., and Hampton, M.A., 1976, Preliminary report on the surface and shallow subsurface geology of lower Cook Inlet and Kodiak Shelf, Alaska: U.S. Geol. Survey Open-File Report 76-695, 36 p., 9 maps.

Bouma, A.H., and Hampton, M.A., 1976, Large sandwaves and others bedforms in lower Cook Inlet, Alaska (abstract): Conference on Marine Slope Stability, Louisiana State University, Oct. 14 and 15, 1976.*

Bouma, A.H., and Hampton, M.A., Tidally influenced migration of sandwaves in lower Cook Inlet, Alaska: Tenth Intern. Congr. Sedimentology, Volume of Abstracts, in press (Abstr.).*

Bouma, A.H., and Hampton, M.A., High resolution seismic profiles, side scan records, and sampling locations from lower Cook Inlet and Kodiak Shelf, R/V SEA SOUNDER cruise S7-77-WG, September-October, 1977: U.S. Geol. Survey Open-File Report 78__ , in preparation.

Bouma, A.H., Hampton, M.A., Frost, T.P., Torresan, M.E., Orlando, R.C., and Whitney, J.W., 1978a, Bottom characteristics of lower Cook Inlet, Alaska: U.S. Geol. Survey Open-File Rept. 78-236, 90 p., 2 plates.

Bouma, A.H., Hampton, M.A., and Orlando, R.C., 1977b, Sandwaves and other bedforms in lower Cook Inlet, Alaska: Mar. Geotechnology, v. 2, p. 291-308.*

Bouma, A.H., Hampton, M.A., Rappeport, M.L., Whitney, J.W., Teleki, P.G., Orlando, R.C., and Torresan, M.E., 1978b, Movement of sand waves in lower Cook Inlet, Alaska: Preprints Offshore Technology Conference, OTC Paper 3311, in press.*

Bouma, A.H., Hampton, M.A., Wennekens, M.P., and Dygas, J.A., 1977a, Large dunes and other bedforms in lower Cook Inlet, Alaska: Preprints Offshore Technology Conference, OTC Paper 2737, p. 79-90.*

Goefert, B.L., 1969, An engineering challenge - Cook Inlet, Alaska: Offshore Technology Conf., Preprint OTC 1048, p. I 511-524.

Hampton, M.A., and Bouma, A.H., 1976, Seismic profiles of lower Cook Inlet and Kodiak Shelf, R/V SEA SOUNDER, June-July, 1976: U.S. Geol. Survey Open-File Report 76-848, 36 p., 4 maps, 9 rolls.

Hampton, M.A., and Bouma, A.H., 1977, Slope instabiltiy near the shelf break, western Gulf of Alaska: Mar. Geotechnology, v. 2, p. 309-331.*

Hampton, M.A., and Bouma, A.H., Quaternary sedimentation and environmental geology of the Kodiak Shelf, western Gulf of Alaska: Tenth Intern. Congr. Sedimentology, Volume of Abstracts, in press (Abstr.).*

Hampton, M.A., Bouma, A.H., and Frost, T.P., 1977, Volcanic ash in surficial sediments of the Kodiak shelf - an indicator of sediment dispersal patterns: in preparation.

Hampton, M.A., Bouma, A.H., Torresan, M.E., and Colburn, I.P., 1978, Analysis of micro textures on quartz sand grains from lower Cook Inlet: Geology, v. 6, p. 105-110.

Hein, J.R., Bouma, A.H., and Hampton, M.A., 1977, Distribution of clay minerals in lower Cook Inlet and Kodiak shelf sediment, Alaska: U.S. Geol. Survey Open-File Rept. 77-581, 17 p.

Palmer, H.D., 1969, Wave-induced scour on the sea floor: Proc. Civil Eng. in the Oceans - II. Miami Beach, Fla., ASCE, p. 703-716.

Posey, C.J., 1971, Protection of offshore structures against underscour: Journ. Hydraulics Division ASCE, No. HY7, Proc. Paper 8230, p. 1011-1016.

Visser, R.C., 1969, Platform design and construction in Cook Inlet, Alaska: J. Petrol. Techn., p. 411-420.

Wilson, N.D. and Abel, W., 1973, Seafloor scour protection for a semi-submarine drilling rig on the Nova Scotian shelf: Offshore Technology Conf., Preprint OTC 1891, p. II 631-646.

*Also presented orally.

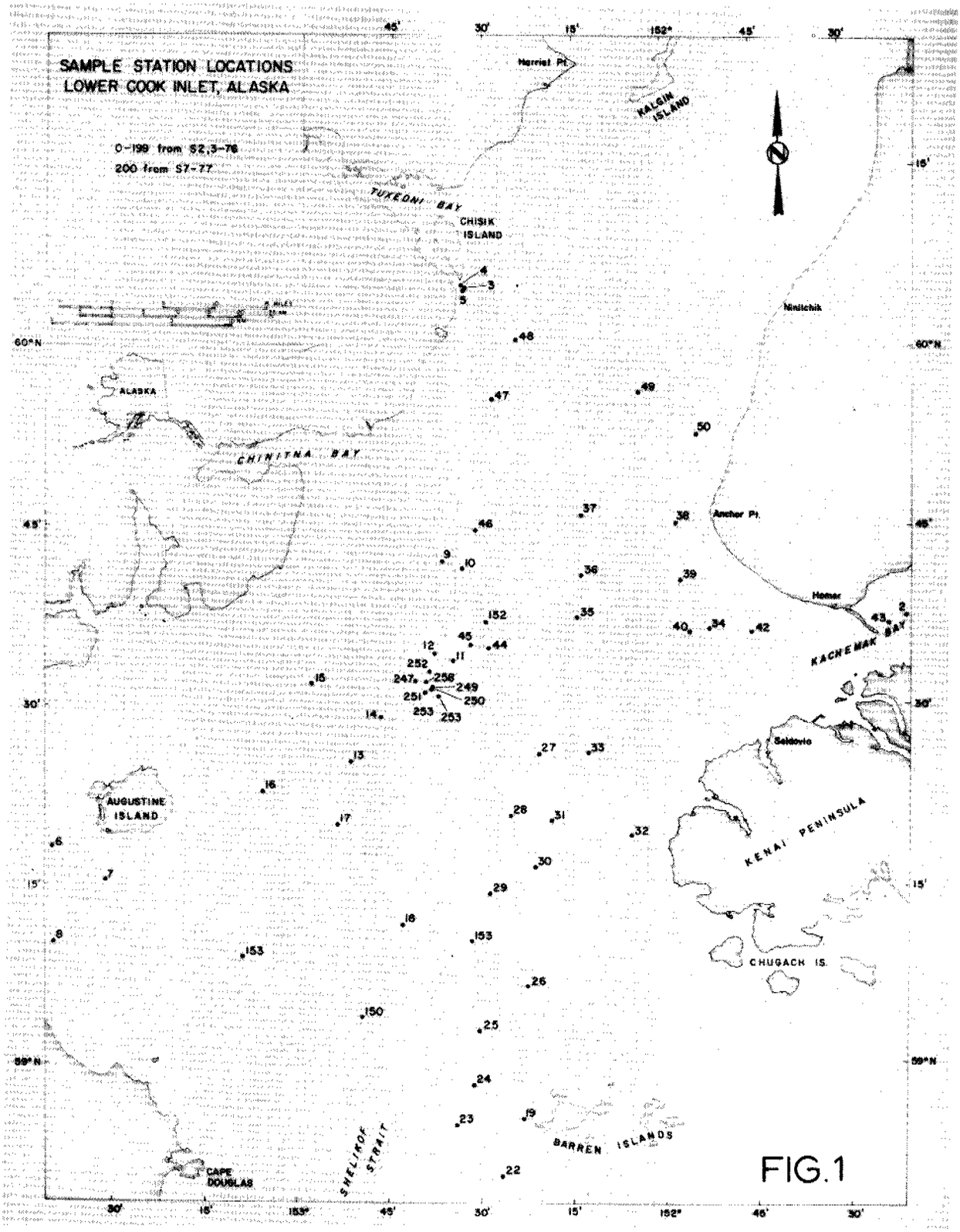
SAMPLE STATION LOCATIONS
LOWER COOK INLET, ALASKA
0-199 from S2,3-76
200 from S7-77
Harriet Pt.
KALGIN ISLAND
TUXEDNI BAY
CHISIK ISLAND
Nnilchik
ALASKA
CHINITNA BAY
Anchor Pt.
Homer
KACHEMAK BAY
Seldovia
KENAI PENINSULA
AUGUSTINE ISLAND
CHUGACH IS.
BARREN ISLANDS
SHELIKOF STRAIT
CAPE DOUGLAS
60°N
59°N
45'
30'
15'
152°
153°

FIG.1

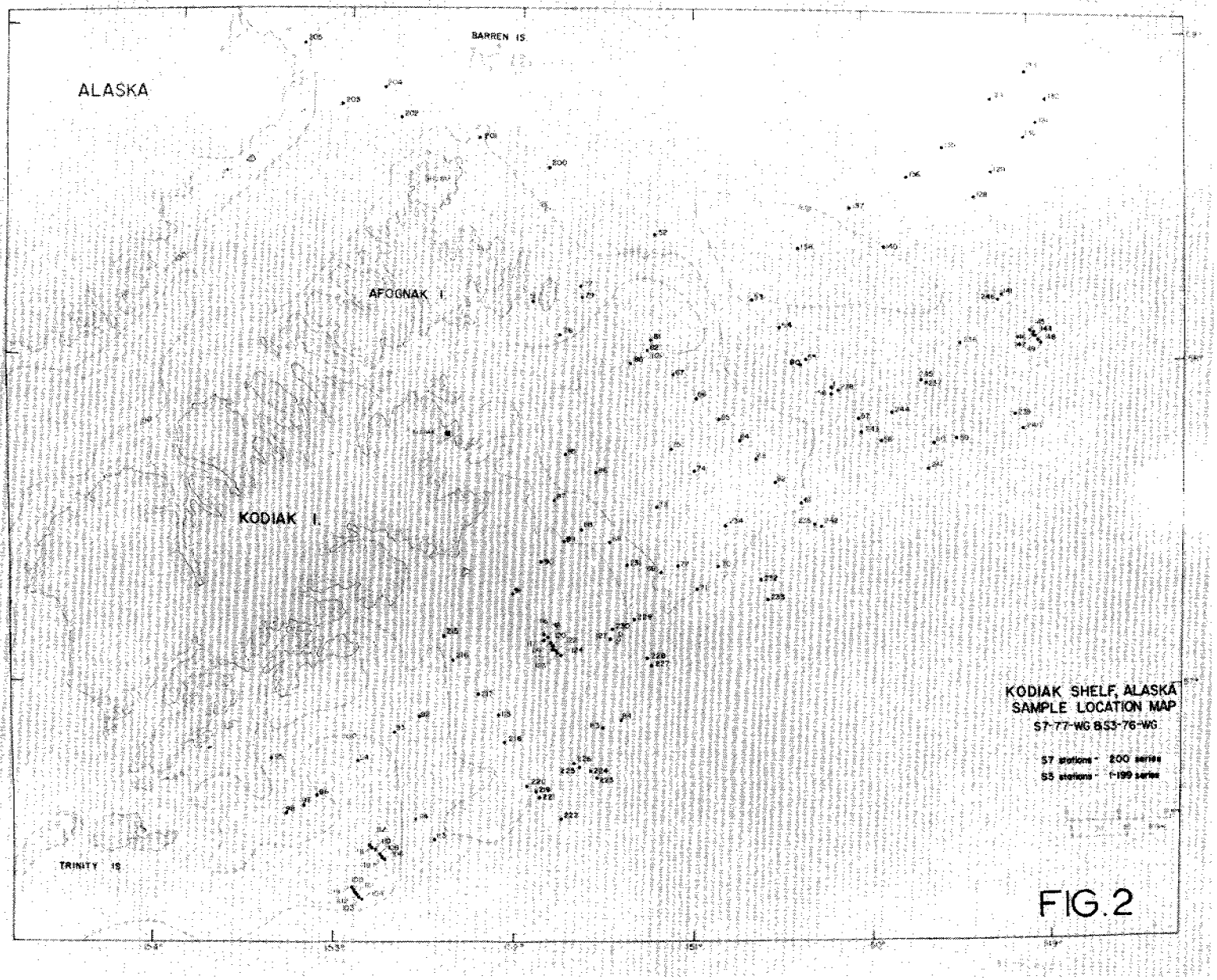
ALASKA
BARREN IS.
AFOGNAK I.
KODIAK I.
TRINITY IS.
KODIAK SHELF, ALASKA
SAMPLE LOCATION MAP
S7-77-WG BS3-76-WG
57 stations - 200 series
55 stations - 1-199 series

FIG.2

Table I. Data for surficial sediment samples, R/V SEA SOUNDER cruise S7-77, lower Cook Inlet and off Kodiak.

Station Number	Latitude Longitude	Water Depth (m)	Equipment Type	Comments	Physiographic Location
200	58° 36.8'N 151° 50.3'W	159	Soutar Van Veen	Pebbly muddy sand	Transition Kodiak Shelf to lower Cook Inlet
201	58° 41.4'N 152° 14.9'W	126	"	Pebbly sand layer over pebbly muddy sand.	"
202	58° 45.6'N 152° 42.5'W	190	"	Sandy mud	"
203	58° 46.4'N 153° 02.5'W	149	Gravity corer	Mud (100 cm)	"
204	58° 51.3'N 152° 54.2'W	164	Soutar Van Veen	Pebbly muddy sand	"
205	58° 58.8'N 153° 11.3'W	118	"	Muddy sand	"
206	59° 28.5'N 152° 41.7'W to 59° 32.3'N 152° 37.2'W	66 64	Bottom TV and 70 mm camera	Bedforms observations	medium-sized bedforms
207	59° 33.9'N 151° 56.3'W to 59° 33.9'N 151° 56.1'W	41 33	"	Station abandoned due to equipment malfunction.	small-sized bedforms
208	59° 33.4'N 152° 15.2'W	?	"	"	"
209	59° 31.3'N 151° 56.0'W to 59° 34.0'N 151° 58.3'W	41 46	"	Bedform observations	different types of bedforms, mainly small-sized ones
210	59° 33.2'N 152° 08.5'N to 59° 32.8'N 152° 11.0'W	45 45	" "	Bedform observations "	" "

Table I. Data for surficial sediment samples, R/V SEA SOUNDER cruise S7-77, lower Cook Inlet and off Kodiak.

Station Number	Latitude Longitude	Water Depth (m)	Equipment Type	Comments	Physiographic Location
211	59° 33.0'N 152° 16.3'W	71	"	Station abandoned due to equipment malfunction	small-medium sized bedforms
	to				
	59° 34.4'N 152° 15.6'W	69			
212	59° 31.0'N 152° 33.6'W	70	"	Bedform observations	small-sized bedforms
	to				
	59° 31.3'N 152° 30.9'W	58			
213	59° 29.6'N 152° 28.3'W	63	Soutar Van Veen	Sand	large-sized bedforms
214	59.° 27.6'N 152.° 25.7'W	63	"	Sand	medium-sized bedforms
215	57° 11.4'N 152° 25.9'W	115	Gravity corer	Shell and ash-bearing sand (19 cm)	Depression north of middle Albatross Bank
216	57° 06.0'N 152° 20.6'W	96	Soutar Van Veen	Ash-bearing sand	Shallow depression on middle Albatross Bank
217	57° 00.0'N 152° 12.9'W	75	"	Sandy mud	Middle Albatross Bank
218	56° 51.4'N 152° 03.5'W	97	Gravity corer	No recovery	Shelf-break trough, middle Albatross Bank
219	56° 42.6'N 151° 53.6'W	79	Soutar Van Veen	Sandy gravel	Seaward of bedrock high, middle Albatross Bank
220	56° 43.8'N 151° 55.9'W	62	"	One boulder recovered	Bedrock high, middle, Albatross Bank
221	56° 41.4'N 151° 51.9'W	191	Gravity corer	15cm sand overlying clayey, pebbly sand (57cm)	Shelf break, middle Albatross Bank
222	56° 36.9'N 151° 46.5'W	942	"	Muddy sandy gravel (10cm)	Continental slope, off middle Albatross Bank
223	56° 45.4'N 151° 33.0'W	1303	Soutar Van Veen	Mud (silt and clay)	Slope basin below. Slump, off middle Albatross Bank

Table I. Data for surficial sediment samples, R/V SEA SOUNDER cruise S7-77, lower Cook Inlet and off Kodiak.

Station Number	Latitude Longitude	Water Depth (m)	Equipment Type	Comments	Physiographic Location
224	56° 46.8'N 151° 34.8'W to 56° 46.5'N 151° 34.8'W	997	Gravity corer	Olive green mud (270cm)	Within slump, off middle Albatross Bank
		1034	Piston corer	" (415cm)	
225	56° 47.9'N 151° 37.5'W	601	Gravity corer	Slightly sandy mud (290cm)	Headwall scarp above Slump, off middle Albatross Bank
226	56° 48.1'N 151° 40.0'W	370	"	Muddy sand (101cm)	Undisturbed slope above slump, off middle Albatross Bank
227	57° 05.6'N 151° 40.0'W	358	Soutar Van Veen	Sandy, silty clay	Continental slope, off Chiniak Trough
228	57° 07.5'N 151° 15.2'W	185	"	Shell layer over gravelly sand	Shelf break, Chiniak Trough
229	57° 14.2'N 151° 20.0'W	172	"	Silty ash	Shelf-break trough, Chiniak Trough
230	57° 12.4'N 151° 27.2'W	102	"	Station abandoned due to rough weather	Progradational wedge, Chiniak Trough
231	57° 24.3'N 151° 22.4'W	182	Gravity corer	Ash (70cm)	Chiniak Trough
232	57° 22.0'N 150° 35.9'W	262	Soutar Van Veen	Sandy gravel	Shelf break, northern Albatross Bank
233	57° 17.4'N 150° 35.7'W	633	"	No recovery	Continenal slope of northern Albatross Bank
234	57° 31.3'N 150° 49.7'W	94	"	Gravelly sand	Northern Albatross Bank
235	57° 31.7'N 150° 18.0'W	258	"	No recovery	Continental slope, off northern Albatross Bank
236	57° 04.2'N 149° 28.2'W	230	"	Sandy mud layer over slightly muddy sand grading to sand (20cm)	Stevenson Trough, breach through sill
237	57° 57.3'N 149° 40.6'W	134	"	Station abandoned due to rough weather	Stevenson trough, on sill

Table I. Data for surficial sediment samples, R/V SEA SOUNDER cruise S7-77, lower Cook Inlet and off Kodiak.

Station Number	Latitude Longitude	Water Depth (m)	Equipment Type	Comments	Physiographic Location
238	57° 56.0'N 150° 10.0'W	191	Bottom TV and 70 mm camera	Bedform observations	Stevenson Trough, bedform field.
	to				
	57° 56.0'N 150° 10.1'W	200			
239	57° 51.0'N 149° 07.9'W	975	Gravity corer	Slightly gravelly and sandy mud (290 cm)	Headwall scarp above slump, off Portlock Bank.
240	57° 48.4'N 149° 05.4'W	1415	"	Slightly pebbly and sandy mud (70 cm)	Within slump, off Portlock Bank
241	57° 41.4'N 149° 39.0'W	572	"	Pebbly sand in core catcher	Continental slope off Stevenson Trough
	57° 41.3'N 149° 39.2'W	606	Soutar Van Veen	Sand	
242	57° 31.3'N 150° 16.6'W	300	"	Muddy sand	Continental slope, off northern Albatross Bank
243	57° 48.5'N 150° 01.2'W	190	"	Slightly muddy sand layer over sand	Stevenson Trough, on sill
244	57° 51.7'N 149° 50.9'W	257	"	Sand	Stevenson Trough, wide breach through sill
245	57° 57.6'N 149° 39.7'W	135	"	Gravel layer over muddy sand	Stevenson Trough, on sill
246	58° 12.8'N 149° 13.4'W	134	"	Sand	Portlock Bank
247	59° 32.3'N 152° 41.2'W	58	"	"	small-sized bedforms
248	59° 32.0'N 152° 39.5'W	62	"	"	"
249	59° 31.2'N 152° 38.6'W	69	"	"	"
250	59° 31.2'N 152° 38.5'W	69	"	"	"

Table I. Data for surficial sediment samples, R/V SEA SOUNDER cruise S7-77, lower Cook Inlet and off Kodiak.

Station Number	Latitude Longitude	Water Depth (m)	Equipment Type	Comments	Physiographic Location
251	59° 30.8'N 152° 38.9'W	62	Soutar Van Veen	Sand	small-sized bedforms
252	59° 36.7'N 152° 38.1'W	73	"	"	"
	59° 32.5'N 152° 38.1'W	73	"	"	"
253	59° 30.4'N 152° 36.9'W	60	Soutar Van Veen	Sand	small-sized bedforms

Table II. Data for surficial sediment samples, Kodiak Shelf: summer 1976.

Sample Number	Latitude Longitude	Water Depth(m)	Ash Content(%)	Estimated Grain Sizes of Epiclastic Material(%) >Sand	Sand	Silt	Clay	Physiographic Location
51	58°12.54'N 151°55.74'W	60	0	100	-	-	-	Between Marmot I. and Afognak I.
52	58°24.42'N 151°13.80'W	107	45	25	75	tr	tr	Stevenson Trough
53	58°12.70'N 150°39.94'W	86	12	73	27	tr	tr	Edge of Stevenson Trough
54	58°07.36'N 150°30.26'W	175	59	tr	99	tr	tr	Stevenson Trough
55	58°01.86'N 150°21.64'W	184	35	-	100	tr	tr	Stevenson Trough
56	57°55.22'N 150°12.77'W	190	24	-	100	-	-	Stevenson Trough - within sand wave field
57	57°55.22'N 150°03.74'W	194	35	-	100	-	-	Stevenson Trough
58	57°46.99'N 149°55.40'W	232	89	5	94	-	-	Stevenson Trough - in depression just landward of shelf break
59	57°46.60'N 149°29.66'W	495	51	3	97	tr	tr	Continental slope - seaward of Stevenson Trough
60	57°45.96'N 149°37.41'W	444	69	tr	99	tr	tr	" "
61	57°35.61'N 150°24.46'W	112	38	20	80	tr	tr	Northern Albatross Bank
62	57°39.05'N 150°32.48'W	102	29	27	73	tr	tr	" " "
63	57°43.96'N 150°39.25'W	90	22	38	62	tr	tr	" " "
65	57°51.50'N 150°51.50'W	77	44	64	36	tr	tr	" " "
66	57°55.10'N 150°59.30'W	81	89	25	75	tr	tr	Northern Albatross Bank on edge of very slight depression
67	57°59.70'N	82	59	25	75	tr	tr	Northern Albatross Bank
	151°06.40'W	82	59	25	75	tr	tr	
68	57°28.10'N 151°28.70'W	154	100	-	97	2	1	Chiniak Trough
69	57°23.25'N 151°10.95'W	80	51	2	98	tr	tr	Northern Albatross Bank
70	57°24.08'N 150°52.25'W	96	24	-	100	tr	tr	" " "
71	57°20.01'N 150°59.08'W	95	36	-	100	tr	tr	" " "

Table II. cont.

Sample Number	Latitude Longitude	Water Depth(m)	Ash Content(%)	Estimated Grain Sizes of Epiclastic Material(%) >Sand	Sand	Silt	Clay	Physiographic Location
72	57°24.20'N 151°05.10'W	92	92	-	100	tr	tr	Northern Albatross Bank, just seaward of the crest of the Bank
73	57°34.90'N 151°12.15'W	66	35	97	3	tr	tr	Northern Albatross Bank
74	57°41.10'N 151°00.40'W	75	36	93	7	tr	tr	Northern Albatross Bank
75	57°48.80'N 151°08.05'W	70	28	6	94	tr	tr	" " "
76	58°06.02'N 151°46.10'W	95	77	-	100	tr	tr	Chiniak Trough
77	58°11.60'N 151°37.00'W	38	0	96	4	tr	tr	Bank near Marmot I.
79	58°13.23'N 151°38.07'W	68	12	84	15	tr	tr	" " " "
81	58°05.21'N 151°14.55'W	143	90	-	90	10	tr	Stevenson Trough
82	58°03.60'N 151°15.90'W	103	49	63	36	1	tr	" "
83	56°53.73'N 151°29.84'W	706	1	-	-	-	-	Continental Slope
84	56°55.06'N 151°24.58'W	859	2	-	-	-	-	" "
85	57°45.00'N 151°44.00'W	55	29	-	100	tr	tr	Northern Albatross Bank
86	57°41.48'N 151°34.70'W	61	54	1	98	tr	tr	" " "
87	57°36.50'N 141°47.65'W	132	98	-	100	tr	tr	Chiniak Trough
88	57°31.2'N 151°38.00'W	167	100	-	76	23	1	" "
90	57°25.10'N 151°51.90'W	67	38	-	95	5	-	Middle Albatross Bank
91	57°19.29'N 152°04.82'W	73	89	-	100	tr	tr	Middle Albatross Bank in very broad, shallow basin
92	56°56.50'N 152°33.0'W	167	100	-	1	3	96	Kiliuda Trough
93	56°53.45'N 152°40.90'W	128	97	-	90	8	2	" "
94	56°48.15'N 152°52.60'W	63	47	58	41	tr	tr	Southern Albatross Bank

Table II. Cont.

Sample Number	Latitude Longitude	Water Depth(m)	Ash Content(%)	Estimated Grain Sizes of Epiclastic Material(%) >Sand	Sand	Silt	Clay	Physiographic Location
95	56°48.10'N 153°21.35'W	170	39	90	10	tr	tr	Kiliuda Trough
96	56°41.40'N 153°05.90'W	146	100	-	5	35	60	" "
97	56°40.10'N 153°10.02'W	150	100	-	4	26	70	" "
98	56°38.00'N 153°16.00'W	145	100	-	3	20	77	" "
113	56°33.5'N 152°27.2'W	197	32	8	89	2	tr	Kiliuda Trough - between double shelf break
114	56°37.60'N 152°34.00'W	160	81	40	55	2	3	Kiliuda Trough
115	56°57.02'N 152°06.28'W	80	83	-	100	tr	tr	Middle Albatross Bank in shallow basin landward of shelf break
127	57°11.24'N 151°29.59'W	69	54	18	81.1	tr	tr	Continental slope - near shelf break
128	58°31.47'N 149°21.90'W	121	82	5	79	11	5	Portlock Bank - in shallow faulted basin
129	58°35.85'N 149°14.91'W	97	32	90	10	tr	tr	Portlock Bank
130	58°42.23'N 149°03.38'W	145	36	tr	98	1	tr	Edge of Amatuli Trough
131	58°44.99'N 148°58.18'N	214	39	4	76	15	5	Amatuli Trough
132	58°49.24'N 148°54.71'W	236	95	11	81	4	4	" "
135	58°40.39'N 149°31.82'N	136	45	-	94	2	4	Edge of Amatuli Trough
136	58°34.90'N 149°45.19'W	125	29	-	97	2	1	Portlock Bank
137	58°29.46'N 150°05.25'W	93	41	34	56	9	1	" "
138	58°22.27'N 150°24.07'W	60	35	70	29	30	tr	" "
140	58°22.2'N 149°54.26'W	83	74	89	10	1	tr	Portlock Bank - in shallow graben
141	58°13.12'N 149°11.85'W	120 120	82 82	57 57	37 36	6 6	tr tr	Portlock bank in basin behind shelf break

APPENDIX I

Analysis of microtextures on quartz sand grains from lower Cook Inlet, Alaska

Monty A. Hampton, Arnold H. Bouma, Michael E. Torresan, and Ivan P. Colburn

Geology, v. 6, p. 105-110

1978

APPENDIX II

Bottom characteristics of lower Cook Inlet, Alaska

Arnold H. Bouma, Monty A. Hampton, Thomas P. Frost,
Michael E. Torresan, Robert C. Orlando, and John Whitney

U.S. Geological Survey
Open File Report 78-236
90 p.

1978

Pages 1-8 eliminated:
Pages 1-2: introduction; pages 3-8: bathymetry and distribution of bedforms (see App. V).

GRAIN SIZE PARAMETERS

Introduction

Grain size analyses were run in the laboratory using Rapid Sediment Analyzers. This technique is based on fall velocity through a high column of water. The data were next punch carded and fed to the computer under the heading sieve. The program provides several types of data such as cummulative percentages, statistical parameters and graphic presentations.

This section includes a discussion of the parameters provided, the graphic presentations, and a brief discussion about the findings and preliminary conclusions drawn from this aspect of the study.

Statistical Parameters

Quantitative evaluation and comparison of grain size distributions of sediment samples is possible through the use of statistical parameters. The two methods of determining the size distribution of a sand-size sample are sieving and settling tubes. Both systems give size data in millimeters and/or phi (ϕ) units, though the sieving method measures the physical size of particles, whereas the settling tube measures the settling velocities of the grains through water, which are then compared to the settling velocities of quartz spheres of known size. In other words, a small heavy mineral and a large light mineral may be hydraulic equivalents and fall into the same size range as measured by a settling tube, but the same two grains would be measured as being of quite different diameter in a sieve analysis.

Graphic Representation

The data obtained in a grain size analysis may be plotted in several ways. All methods use grain size as the abscissa and some measure of percentage frequency as the ordinate. It is usual to plot grain size in phi units, which relate logarithmically to millimeters 25: $-\log_2 d = \phi$, where d is grain diameter, and ϕ is size in ϕ -units.

The histogram is a bar graph, where the height of each bar represents the weight percent of grains in a particular size class. A frequency curve is a smooth curve through the midpoints of the bar tops. These types of plots are only pictorial representations, statistical parameters cannot be determined from them.

The cumulative curve is plotted by adding percentages in succeeding size grades and drawing a smooth curve through the points. On arithmetic ordinate paper the curve normally is S-shaped.

From the size analysis and its cumulative curve obtained through sieving or settling tube methods, statistical parameters can be calculated that quantitatively describe features of the sediment. The parameters and certain combinations of parameters can be compared and can give an indication of sedimentary environments of deposition.

Parameters

The parameters calculated in this study include:

1) "mode": the most frequently occurring grain size or sizes. It corresponds to the inflection points in the cumulative curve or the highest points on the frequency curve. The mode is useful in transport studies, especially when two or more sources are contributing sediment;

2) "median": half the particles by weight are larger than the median, and half are finer. It is easily found on the cumulative curve, it corresponds to the 50% mark;

3) "mean" (M_z): the average grain size. Several formulas can be used in calculating the mean. The most inclusive graphically derived is that given by Folk (1968):

$$M_z = (\phi 16 + \phi 50 + \phi 84)/3 \qquad (1)$$

where $\phi 16$, $\phi 50$, $\phi 84$ represent the size at 16, 50, and 84 percent of the sample by weight. Folk's formula is superior to that of Inman (1952) which is based on only two values. The Trask (1950) mean size is also included in our computor printout (App. I) although few people use it anymore.

4) "sorting": several methods exist for graphically determining the sorting, or uniformity, of sediments. In general, the best measures of sorting are those that encompass the greatest part of the size distribution. Folk (1968) introduced the "inclusive graphic standard deviation" (σ_1). It is considered to be the best graphically derived method of measuring the grain size variation in a sample. It is calculated using the formula:

$$(\sigma_1) = \frac{\phi 84 - \phi 16}{4} + \frac{\phi 95 - \phi 5}{6.6} \qquad (2)$$

where $\phi 84$, $\phi 16$, $\phi 95$, $\phi 5$ represent the phi values at the 84, 16, 95, and 5 percent markes on the cumulative curve. A verbal classification scale for sorting was present by Folk (1968): $\sigma_1 < 0.35$, very well sorted; $0.35-0.50\phi$, well sorted; $0.50-0.71\phi$, moderately well sorted; $0.71-1.0\phi$, moderately sorted; $1.0-2.0\phi$ poorly sorted; $2.0-4.0\phi$, very poorly sorted; $>4.0\phi$, extremely poorly sorted. Folk's method includes more of the curve than the measure introduced by Inman (1952) where sorting (σ_G) = $(\phi 84 - \phi 16)/2$. Trask's (1950) sorting coefficient (S_O) is used only with millimeter values and only includes the middle 50% of the curve.

5) "skewness": cumulative curves for sediment-size distributions may be the same in average size and sorting though they may be quite different in their degree of symmetry. Measures of skewness determine the degree to which a curve approaches symmetry. The most commonly used measure of skewness is Folk's "inclusive graphic skewness" (1968), determined by the formula:

$$Sk_1 = \frac{\phi 16 + \phi 84 - 2\phi 50}{2(\phi 84 - \phi 16)} + \frac{\phi 5 + \phi 95 - 2\phi 50}{2(\phi 95 - \phi 5)} \qquad (3)$$

This formula is preferred as it includes the skewness of the "tails" of the curve as well as the central portion. Other methods for determining skewness, notably those of Inman (1952) and Trask (1950) do not measure the tails of the curve and are of less value than Folk's (1968) method.

Symmetrical curves have a skewness equal to 0.00; those with a large proportion of fine material are positively skewed, those with a large proportion of coarse material are negatively skewed. A verbal classification for skewness suggested by Folk (1968) includes Sk_1 from -1.00 to -0.30: strongly fine skewed; +.30 to +0.10: fine skewed; +0.10 to -0.10: near symmetrical; -0.10 to -0.30: coarse skewed; and -0.30 to -1.00: strongly coarse skewed.

6) "Kurtosis": a measure of "peakedness" in a curve. A normal Gaussian distribution has a kurtosis of 1.00: it is a curve in which the sorting in the tails equals the sorting in the central portion. If a curve is better sorted in the central part of the curve than in the tails, it is said to be excessively peaked, or leptokurtic; if it is better sorted in the tails than in the central portion, it is flat-peaked or platykurtic. Folk's (1968) formula for kurtosis is given by

$$K_g = \frac{\phi 95 - \phi 5}{2.44(\phi 75 - \phi 25)} \qquad (4)$$

For normal curves $K_g = 1.00$, leptokurtic curves have $K_g > 1.00$, platykurtic curves have $K_g < 1.00$.

Method of Moments

All the above statistical parameters can be calculated using the method of moments. This method gives a somewhat truer picture of the sediment characteristics, but when calculated by hand, it is a tedious process. The computer program used in this study performs all the necessary calculations, greatly simplifying the determination. The first moment measure corresponds to the mean, the second to the standard deviation, the third to the skewness, and the fourth to the kurtosis.

Cook Inlet Samples

Surficial sediment samples from lower Cook Inlet were taken in June and July of 1976 aboard the R/V Sea Sounder. A modified van Veen grab sample, capable of taking an undisturbed surface sample of 40x60x30 cm was used to collect the unconsolidated sediments. The top two centimeters of each grab sample were used for grain size analyses.

Samples were taken from the bedform fields that occupy much of central lower Cook Inlet (Fig. 4). Water depths range from 40 to 100 m, averaging about 70 m. The area is one of very strong currents. Surface water velocities of 3 - 5 knots (150-250 cm/sec) are common during flood and ebb tides.

Grain size analyses of the samples show several gross trends. The mean grain size decreases more or less uniformly from north to south in the samples analyzed (Fig. 5). Concomitant with the decrease in grain size from north to south is an increase in the degree of sorting of the samples as indicated by the decrease in standard deviation (Figs. 6 and 7).

The apparent decrease in grain size from north to south in lower Cook Inlet may be due to one or several of the following: 1) it may simply be an artifact of sampling; not enough samples were taken to have a high confidence level in

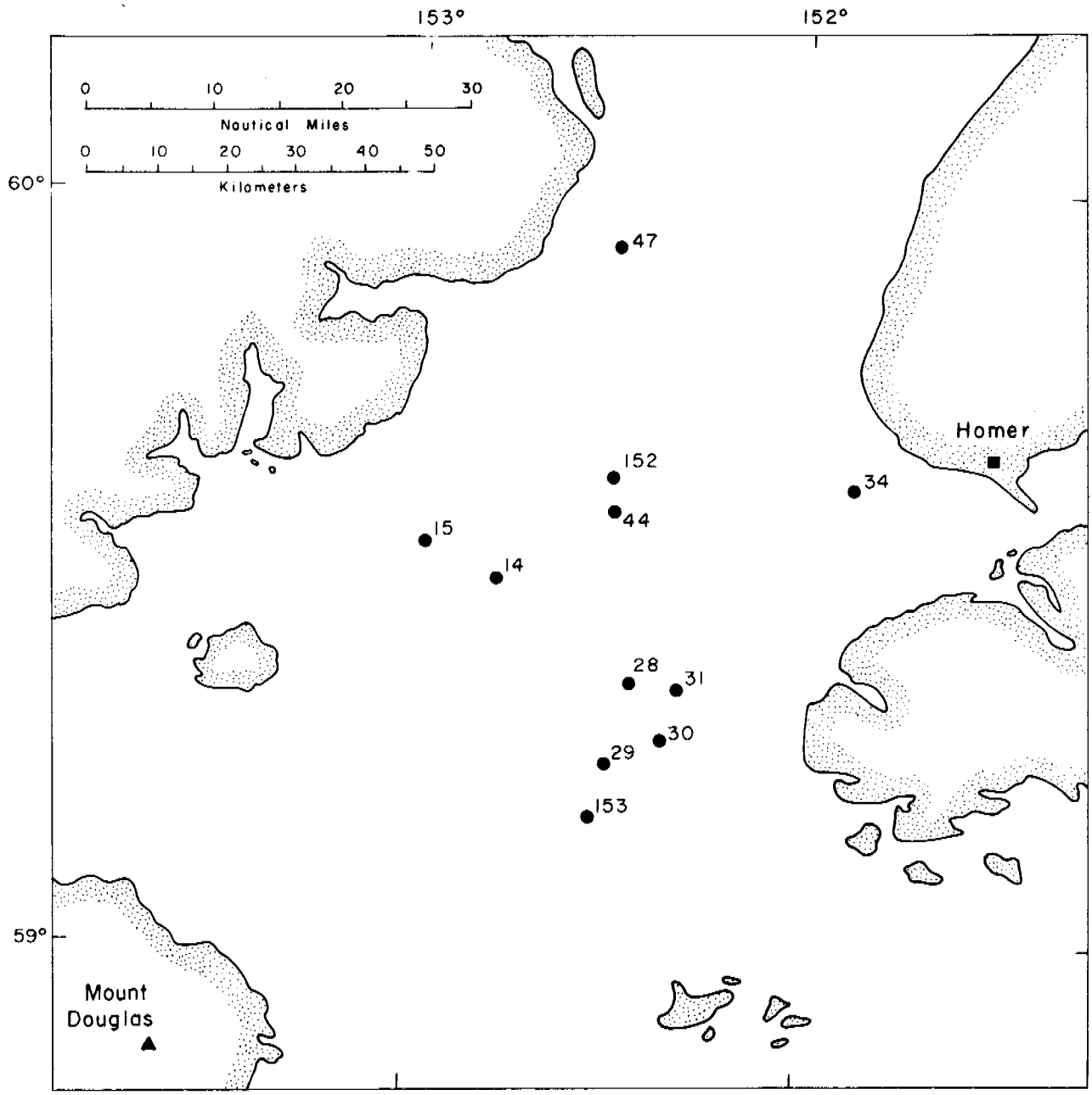

Figure 4. - Sample location map, lower Cook Inlet.

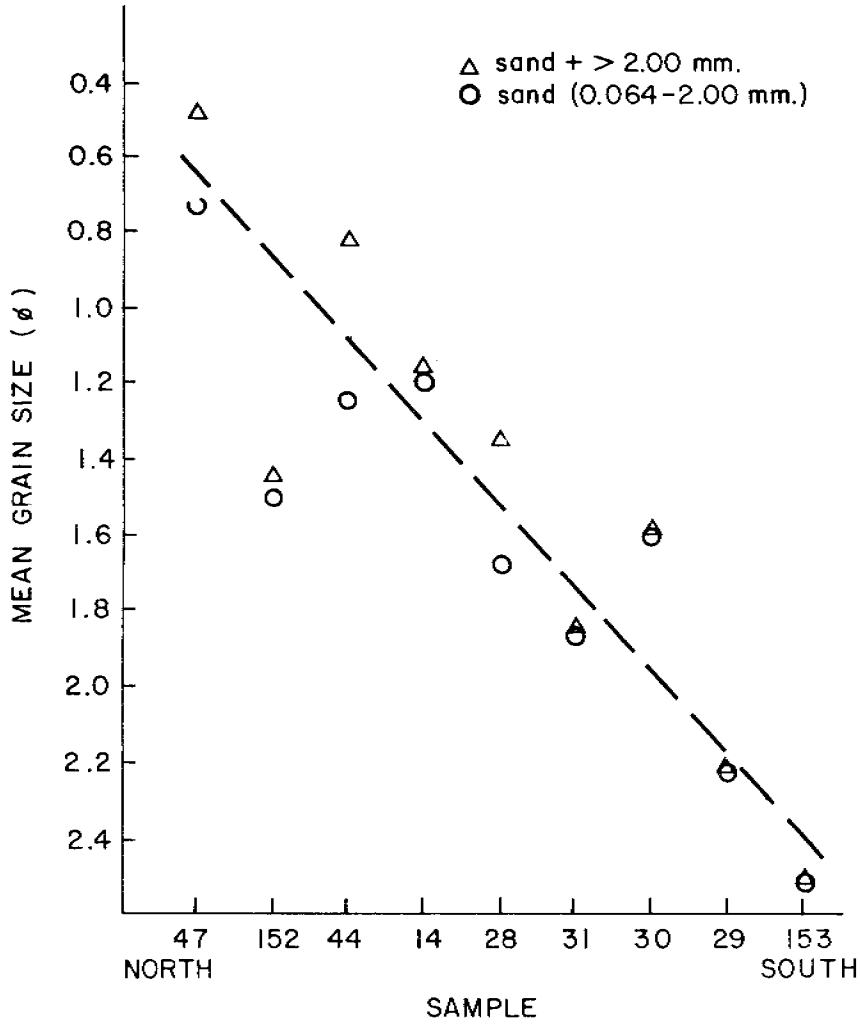

Figure 5.- Mean grain size along a north-south line, lower Cook Inlet.

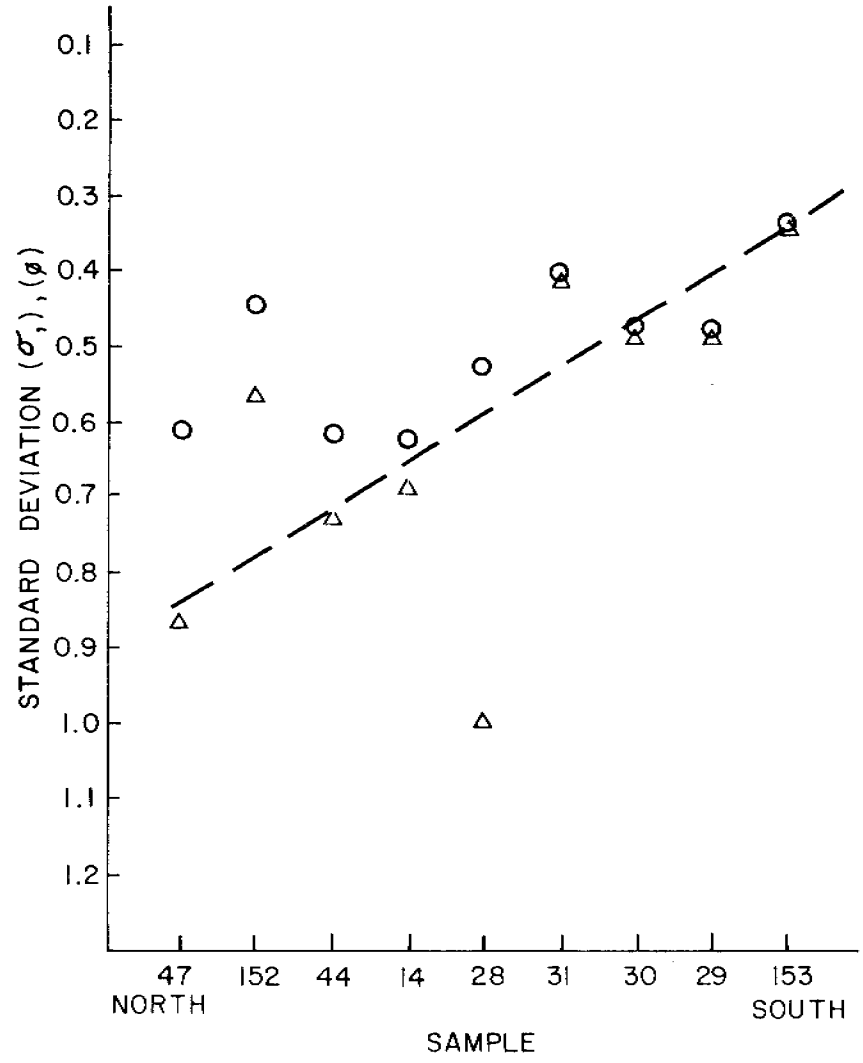

Figure 6.- Standard deviation along a north-south line, lower Cook Inlet

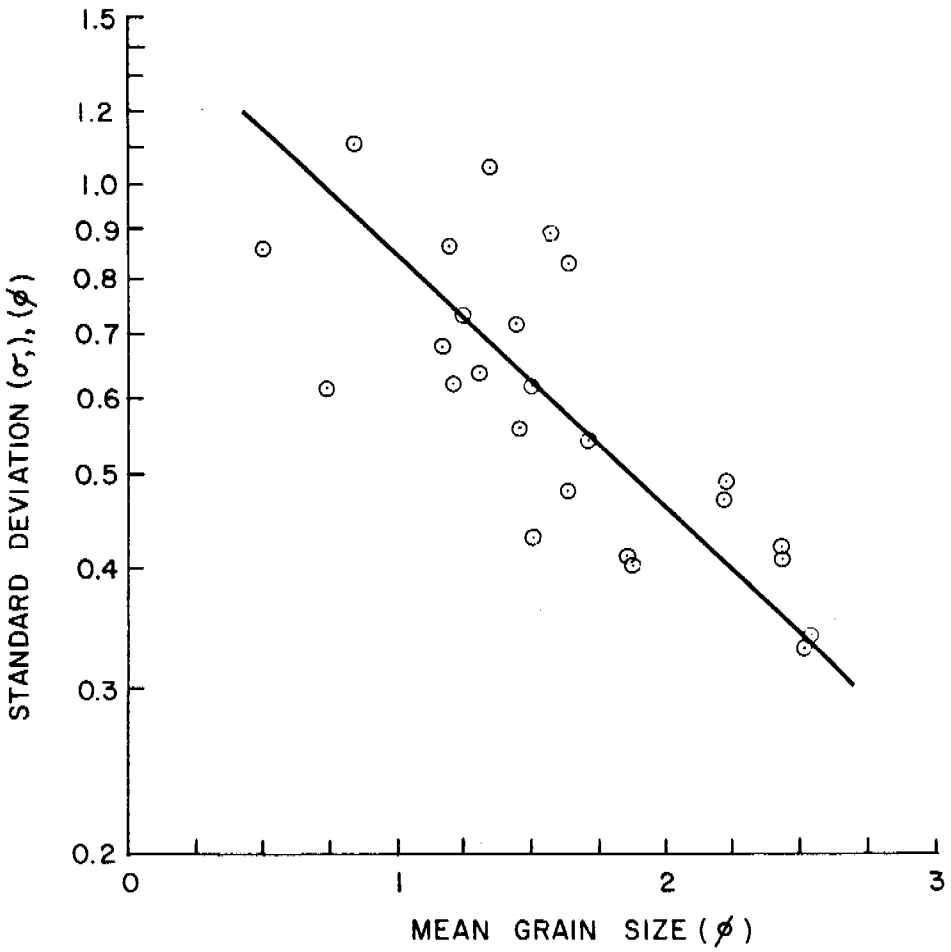

Figure 7.- Mean grain size vs. sorting, lower Cook Inlet.

the results, 2) it may reflect an original variation in mean grain size from north to south in lower Cook Inlet, 3) or it may be due to progressive sorting of the sediments by currents.

A systematic variation in grain size after the last glacial retreat from Cook Inlet is unlikely as glaciers are very poor sorting agents; glacial deposits are generally extremely poorly sorted mixtures of all size grades up to very large boulders. A more probably explanation is that the decrease in mean size and increase in sorting from north to south is due to progressive sorting by transport and winnowing.

Several lines of evidence support this interpretation. First, the majority of bedforms are consistently orientated with their steep faces toward the south indicating net transport in that direction (Bouma and Hampton, 1976; Bouma et al., 1977a). In addition, studies of quartz grain micro-surface textures indicate dominantly mechanical abrasion typical of aqueous transport in the bedform fields (Hampton and et al,, 1978). Quartz surface microtextures commonly associated with glacial action are also present in lower Cook Inlet, though, for the most part, these occur in an unmodified state rarely in the bedform fields (Hampton et al., 1978). Most original glacial microtextures present in the bedform fields have been overprinted with subaqueous transport features, indicating sufficient transport to subdue the original textures.

Inspection of the skewness and kurtosis reveals little information, primarily because so few samples are represented. The range in skewness is -0.5 to 0.4; most samples, however, are very close to symmetrical (0.0) in their size distribution (Fig. 8). Kurtosis shows a greater variation, from 0.28 to 1.96. There appears to be a slight tendency for the sediments to become negatively

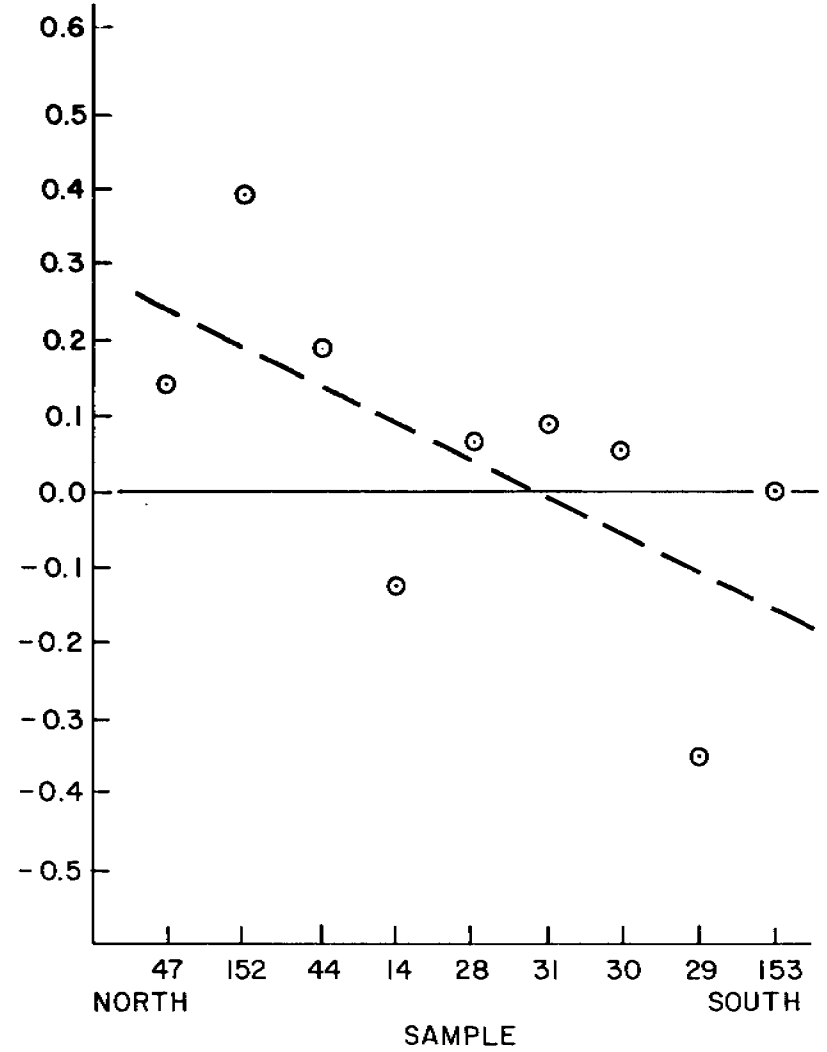

Figure 8.- Skewness along a north-south line, lower Cook Inlet.

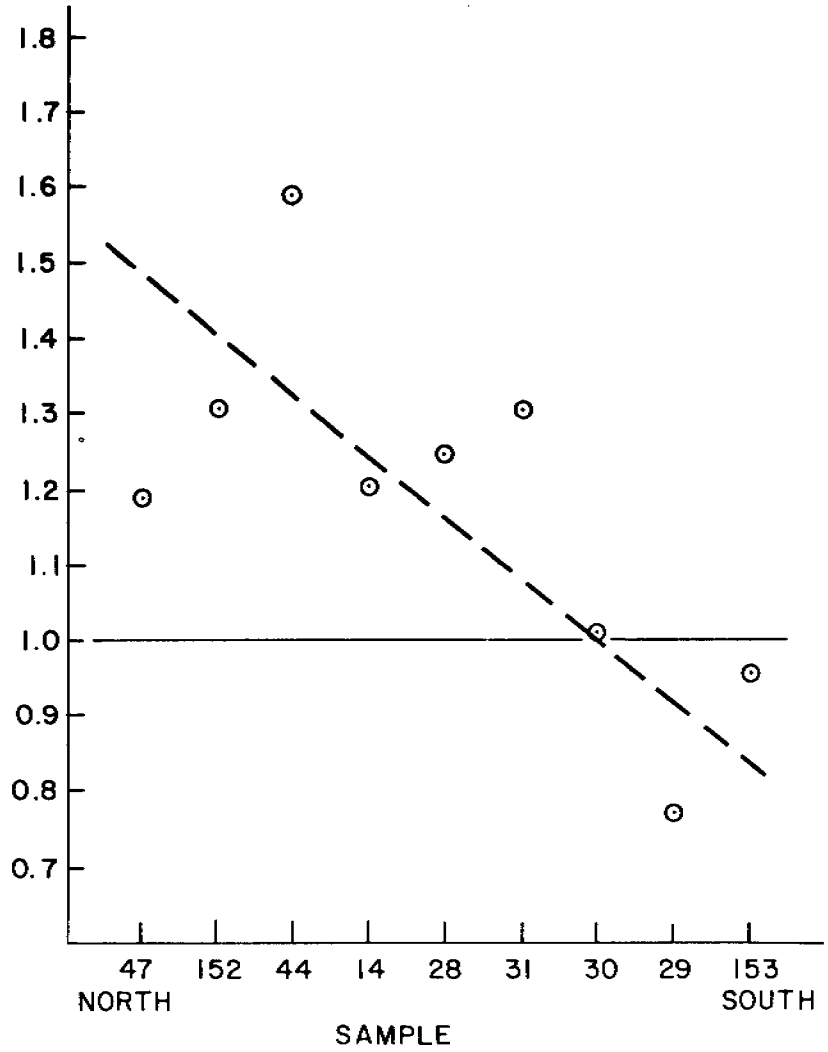

Figure 9.- Kurtosis along a north-south line, lower Cook Inlet.

skewed and platykurtic from north to south (Fig. 9). Grain size data are presented in Appendix I.

GENERALIZED ISOPACH MAP OF QUATERNARY SEDIMENTS

Sparker records from the 1976 cruise of the R/V SEA SOUNDER were used to make thickness measurements at 15 minute shot point positions of the uppermost sedimentary unit in lower Cook Inlet (Fig. 10). From these data, a generalized isopach map was constructed (Fig. 11).

Thicknesses were measured from the sea floor to an angular unconformity that shows distinctly on most of the records. Several thickness measurements were uncertain or indeterminable because of poor-quality records, shallow penetration, or the occurrence of the unconformity within the bubble pulse or a sea-bottom multiple. Where readings of "zero" thickness were recorded, the unconformity apparently rises to the sea floor and controls the sea floor geometry. Variations in the thickness of Quaternary sediments throughout lower Cook Inlet reflect a combination of variations in the elevations of the unconformity surface and of the sea floor.

In making the following maps, the assumption was made that the deformed rocks below the unconformity are of Tertiary age, judging from the on-land geology, and that the generally flat-lying sediments above the unconformity are primary and reworked glacially derived sediments deposited during Pleistocene-Holocene upper Tertiary age.

The thickness measurements were contoured only generally. Many thickness variations greater than one contour interval were ignored because they involve only one or two measurements. Consequently, many small basins and highs exist that do not show on the map. The areas south of Augustine Island and surrounding the Barren Islands are especially complex, and major portions of these areas were not contoured.

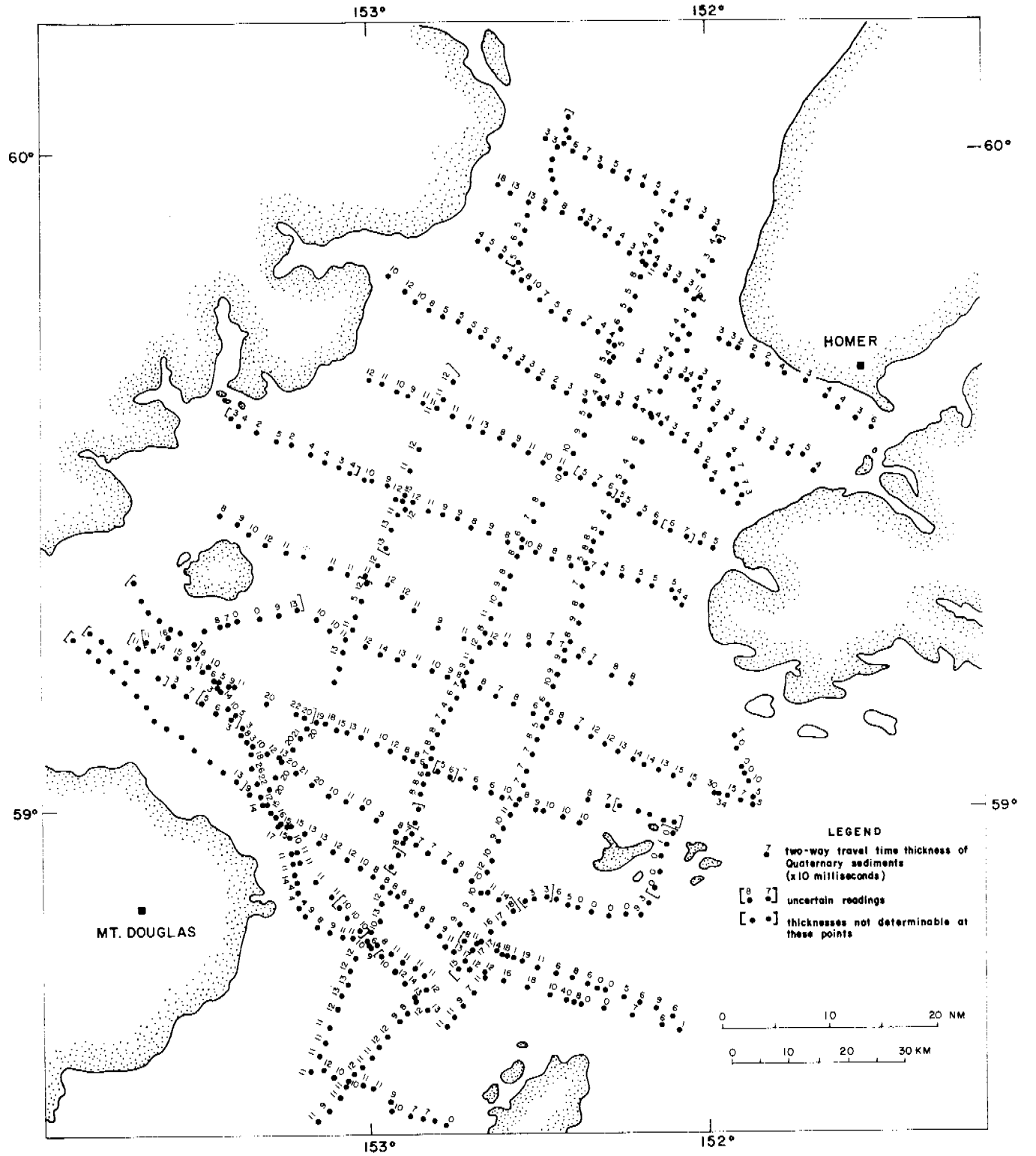

Figure 10. — THICKNESS MEASUREMENTS OF QUATERNARY SEDIMENTS LOWER COOK INLET

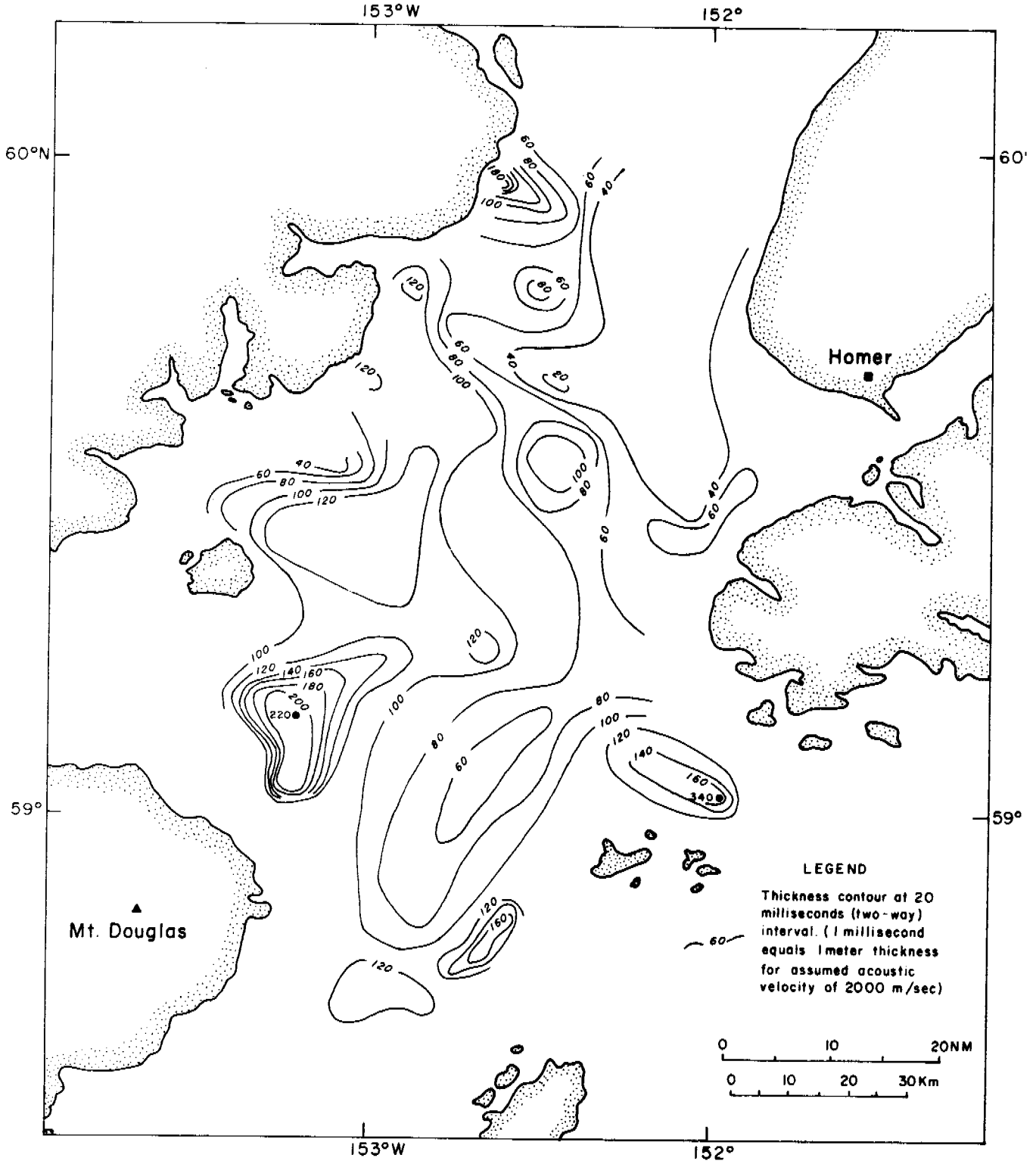

Figure 11.-GENERALIZED ISOPACH MAP OF QUATERNARY SEDIMENTS LOWER COOK INLET

REFERENCES

Bouma, A. H. and Hampton, M. A., 1976, Preliminary report on the surface and shallow subsurface geology of lower Cook Inlet and Kodiak Shelf, Alaska: U. S. Geological Survey Open-File Report 76-695, 36 p., 9 maps.

Bouma, A. H., Hampton, M. A. and Orlando, R. C., 1977b, Sand waves and other bedforms in lower Cook Inlet, Alaska. Marine Geotechnique, v.2, p.291-308.

Bouma, A. H., Hampton, M. A. Wennekens, M. P. and Dygas, Y. A., 1977a, Large dunes and other bedforms in lower Cook Inlet: Offshore Technology Conf. OTC 2737, p. 79-90.

Burbank, D. C., 1977, Circulation studies in Kachemak Bay and lower Cook Inlet. Rept. Alaska Dept. Fish and Game, Marine/Coastal Habitat Management, Anchorage, Alaska, 206 p.

Folk, R. L., 1968, Petrology of Sedimentary Rocks: Austin, Texas, Hemphills, 170 p.

Hampton, M. A. and Bouma, A. H., 1976, Seismic profiles of lower Cook Inlet and Kodiak Shelf, R/V SEA SOUNDER, June-July 1976: U. S. Geological Survey Open-File Report 76-848, 36 p., 9 rolls microfilm, 4 maps.

Hampton, M. A., Bouma, A. H., Torresan, M. C., and Colburn, I. P., 1978, Analysis of microtextures on quartz sand grains from lower Cook Inlet: Geology, v.6, p. 105-110.

Inman, Douglas L., 1952, Measures for Describing the Size Distribution of Sediments: Jour. Sed. Petrology, v. 22, 3, p. 125-145.

Trask, Parker D., 1950, Dynamics of Sedimentation, in Trask, Parker D., ed., Applied Sedimentation: New York, New York, John Wiley and Sons, p. 3-40.

APPENDIX I

Computor printout of sampling station data, grain size values, sediment parameters and graphic presentations of the surficial samples analyzed from lower Cook Inlet.

The computer printout shown in Appendix I gives all the pertinent data regarding the size alalyses of the sand samples from lower Cook Inlet. Each sample has five pages of printout; the top of each page gives the cruise identification, sample number and type (in all cases Soutar van Veen grabs) and sample length, which is not applicable in the case of grab samples. The first page gives the method of analysis, total sample weight, and particle size distribution in mm. and phi (ϕ) units, and the size class ratios. Because all samples were entirely composed of sand-size material, the ratios are in all cases non-existent. The second page gives the interpolated values used in calculating graphical statistics, which include Folk and Ward's (1968), Inman's (1952), and Trask's (1950) median, mean, sorting, skewness and kurtosis values. Moment measures and the class midpoints used in their calculation are also included on the second page. The third page gives the mode or modes, the fourth page presents a histogram of frequency versus size, and the fifth page gives a cumulative curve for the sample.

SEA276WG

CRUISE	STATION	SAMPLE TYPE,NUMBER	TOTAL LENGTH	SAMPLE CENTER	SAMPLE LENGTH	METHODS
S276WG	S-14	S 14	. M	. CM	. CM	1

#F:SV=20,ST= 0,H=0;WT:SV=30.3000,ST= 0.0000,H/P= 0.0000; PHI LIM:CS= 0.00,FN= 0.00

SAMPLE ANALYZED BY THE FOLLOWING METHOD(S):

SIZE RANGE	METHOD
2.0000- 0.0625MM	SIEVES

UNEDITED SAMPLE WEIGHTS IN GRAMS:

SIEVES	BSA	HYDROPHOTOMETER	PAN	INITIAL
30.3000				30.3000 (G)

PARTICLE SIZE DISTRIBUTION:

PHI	MM	PERCENT	CUM PERCENT
-0.7500	1.6818	0.660	0.660
-0.5000	1.4142	1.254	1.914
-0.2500	1.1892	1.320	3.234
0.0000	1.0000	1.485	4.719
0.2500	0.8409	2.013	6.733
0.5000	0.7071	3.036	9.769
0.7500	0.5946	8.680	18.449
1.0000	0.5000	13.366	31.815
1.2500	0.4204	19.571	51.386
1.5000	0.3536	19.670	71.056
1.7500	0.2973	14.587	85.644
2.0000	0.2500	8.812	94.455
2.2500	0.2102	3.135	97.591
2.5000	0.1768	0.891	98.482
2.7500	0.1486	0.528	99.010
3.0000	0.1250	0.363	99.373
3.2500	0.1051	0.198	99.571
3.5000	0.0884	0.165	99.736
3.7500	0.0743	0.132	99.868
4.0000	0.0625	0.132	100.000

SIZE CLASS RATIOS:

GRAVEL=	0.000PCT	GRAVEL/SAND=	0.000
SAND =	100.000PCT	SAND/SILT =	0.000
SILT =	0.000PCT	SILT/CLAY =	0.000
CLAY =	0.000PCT	SAND/CLAY =	0.000
MUD =	0.000PCT	SAND/MUD =	0.000
		GRAVEL/MUD =	0.000

SEA276WG

CRUISE	STATION	SAMPLE TYPE	SAMPLE NUMBER	TOTAL LENGTH	SAMPLE CENTER	SAMPLE LENGTH	METHODS
S276WG	S-14	S	14	. M	. CM	. CM	1

INTERPOLATED SIZES USED IN GRAPHICAL STATISTICS:

CUM_PERCENT	05.00	10.00	16.00	25.00	50.00	75.00	84.00	90.00	95.00	CUM_PERCENT
PHI	0.040	0.512	0.718	0.887	1.235	1.555	1.715	1.827	2.005	PHI
MM	0.9727	0.7015	0.6080	0.5408	0.4250	0.3404	0.3045	0.2818	0.2491	MM

GRAPHICAL STATISTICS:

FOLK_&_WARD_(PHI)		INMAN_(PHI)		IRASK_(MM)	
MEDIAN=	1.2346	MEDIAN=	1.2346	MEDIAN=	0.4250
MEAN =	1.2226	MEAN =	1.2166	MEAN =	0.4406
SORTING=	0.5472	SORTING=	0.4988	SORTING=	1.2605
SKEWNESS=	-0.1259	SKEW 16/84=	-0.0361	SKEWNESS=	1.0193
		SKEW 05/95=	-0.4251		
KURTOSIS=	1.2057	KURTOSIS=	0.9702	KURTOSIS=	0.2388

CLASS MID-POINTS(PHI) USED IN THE MOMENT CALCULATIONS:

-0.88	-0.63	-0.38	-0.13	0.13	0.38	0.63	0.88	1.13	1.38	1.63	1.88	2.13	2.38	2.63
2.88	3.13	3.38	3.63	3.88										

MOMENT MEASURES:

	PHI	MM
FIRST (ABOUT ORIGIN)=	1.1913	0.4379
SECOND (ABOUT MEAN) =	0.3817 VARIANCE	
SECOND (ABOUT MEAN) =	0.6178 STANDARD DEVIATION	
THIRD (ABOUT MEAN) =	-0.1876	
FOURTH (ABOUT MEAN) =	0.9987	

SEA276WG

CRUISE	STATION	SAMPLE TYPE/NUMBER	TOTAL LENGTH	SAMPLE CENTER	SAMPLE LENGTH	METHODS
S276WG	S-14	S 14	. M	. CM	. CM	1

MODAL ANALYSIS

1 MODE(S) DETECTED IN THIS SAMPLE.

PHI	MM	PERCENT	
-0.750	1.6818	0.6601	
-0.500	1.4142	1.2541	
-0.250	1.1892	1.3201	
0.000	1.0000	1.4851	
0.250	0.8409	2.0132	
0.500	0.7071	3.0363	
0.750	0.5946	8.6799	
1.000	0.5000	13.3663	
1.250	0.4204	19.5710	
1.500	0.3536	19.6700	** MODE **
1.750	0.2973	14.5875	
2.000	0.2500	8.8119	
2.250	0.2102	3.1353	
2.500	0.1768	0.8911	
2.750	0.1486	0.5281	
3.000	0.1250	0.3630	
3.250	0.1051	0.1980	
3.500	0.0884	0.1650	
3.750	0.0743	0.1320	
4.000	0.0625	0.1320	

SEA276WG

CRUISE	STATION	SAMPLE TYPE/NUMBER	TOTAL LENGTH	SAMPLE CENTER	SAMPLE LENGTH	METHODS
S276WG	S-14	S 14	. M	. CM	. CM	1

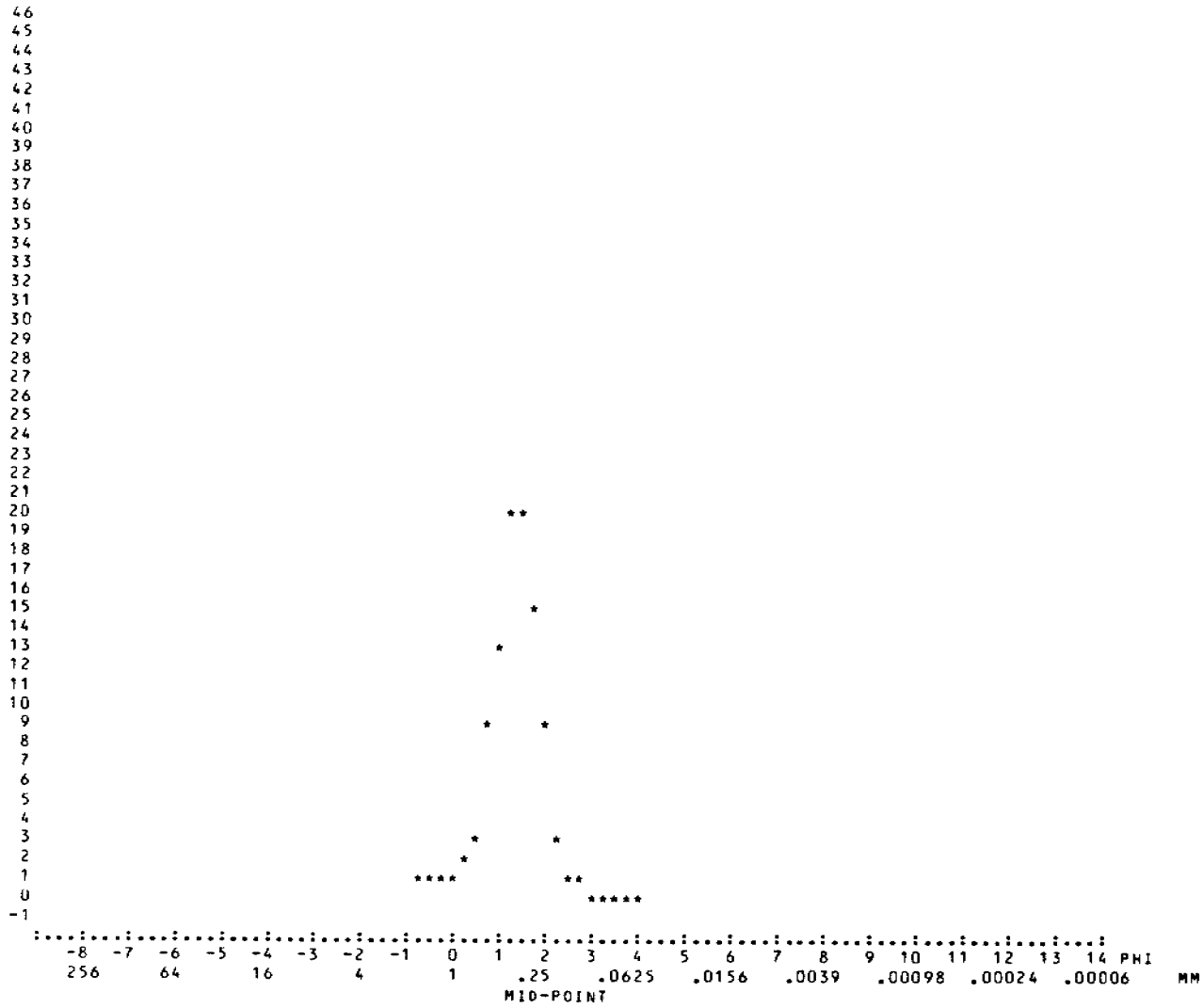

SEA276WG

CRUISE	STATION	SAMPLE TYPE/NUMBER	TOTAL LENGTH	SAMPLE CENTER	SAMPLE LENGTH	METHODS
S276WG	S-14	S 14	. M	. CM	. CM	1

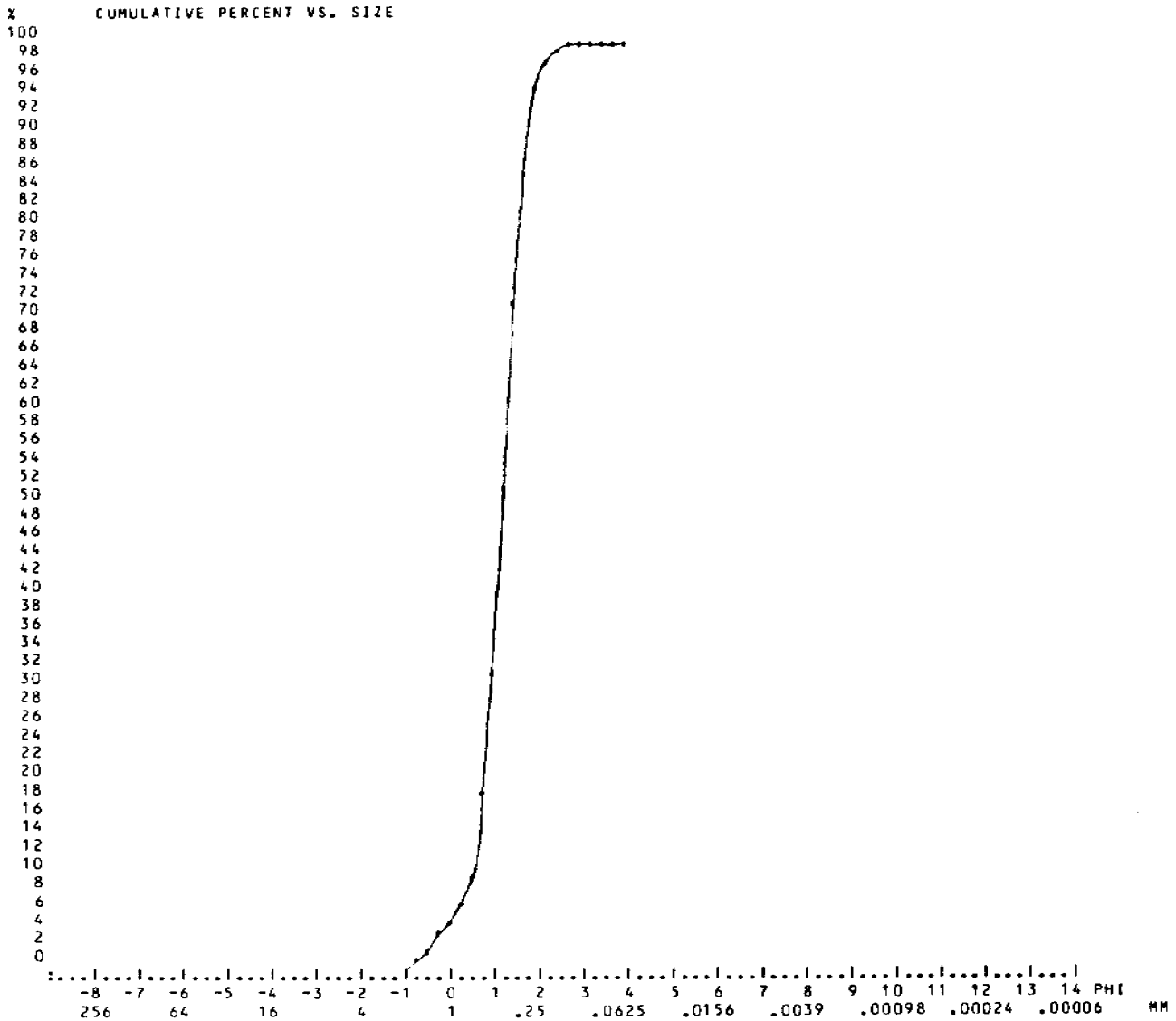

SEA276WG

CRUISE	STATION	SAMPLE TYPE,NUMBER	TOTAL LENGTH	SAMPLE CENTER	SAMPLE LENGTH	METHODS
S276WG	S-15	S15S1	. M	. CM	. CM	1

#F:SV=20,ST= 0,H=0;WT:SV=29.6200,ST= 0.0000,H/P= 0.0000; PHI LIM:CS= 0.00,FN= 0.00

SAMPLE ANALYZED BY THE FOLLOWING METHOD(S):

SIZE RANGE	METHOD
2.0000- 0.0625MM	SIEVES

UNEDITED SAMPLE WEIGHTS IN GRAMS:

SIEVES	BSA	HYDROPHOTOMETER	PAN	TOTAL
29.6200				29.6200 (G)

PARTICLE SIZE DISTRIBUTION:

PHI	MM	PERCENT	CUM PERCENT
-0.7500	1.6818	0.203	0.203
-0.5000	1.4142	0.709	0.912
-0.2500	1.1892	1.013	1.924
0.0000	1.0000	1.519	3.444
0.2500	0.8409	2.161	5.604
0.5000	0.7071	3.106	8.710
0.7500	0.5946	7.056	15.766
1.0000	0.5000	4.288	20.054
1.2500	0.4204	9.554	29.608
1.5000	0.3536	14.686	44.294
1.7500	0.2973	13.234	57.529
2.0000	0.2500	13.741	71.269
2.2500	0.2102	11.479	82.748
2.5000	0.1768	4.186	86.935
2.7500	0.1486	5.469	92.404
3.0000	0.1250	2.127	94.531
3.2500	0.1051	2.296	96.826
3.5000	0.0884	1.283	98.109
3.7500	0.0743	1.013	99.122
4.0000	0.0625	0.878	100.000

SIZE CLASS RATIOS:

GRAVEL=	0.000PCT	GRAVEL/SAND=	0.000
SAND =	100.000PCT	SAND/SILT =99999.999	
SILT =	0.000PCT	SILT/CLAY =	0.000
CLAY =	0.000PCT	SAND/CLAY =	0.000
MUD =	0.000PCT	SAND/MUD =99999.999	
		GRAVEL/MUD =	0.000

SEA276WG

CRUISE	STATION	SAMPLE TYPE,NUMBER	TOTAL LENGTH	SAMPLE CENTER	SAMPLE LENGTH	METHODS
S276WG	S-15	S15S1	. M	. CM	. CM	1

INTERPOLATED SIZES USED IN GRAPHICAL STATISTICS:

CUM_PERCENT	05.00	10.00	16.00	25.00	50.00	75.00	84.00	90.00	95.00	CUM_PERCENT
PHI	0.189	0.555	0.764	1.160	1.607	2.044	2.323	2.611	3.042	PHI
MM	0.8769	0.6808	0.5890	0.4475	0.3283	0.2425	0.1999	0.1637	0.1214	MM

GRAPHICAL STATISTICS:

FOLK_&_WARD_(PHI)		INMAN_(PHI)		TRASK_(MM)	
MEDIAN=	1.6069	MEDIAN=	1.6069	MEDIAN=	0.3283
MEAN =	1.5645	MEAN =	1.5434	MEAN =	0.3450
SORTING=	0.8220	SORTING=	0.7796	SORTING=	1.3585
SKEWNESS=	-0.0377	SKEW 16/84=	-0.0815	SKEWNESS=	1.0066
		SKEW 05/95=	0.0111		
KURTOSIS=	1.3223	KURTOSIS=	0.8292	KURTOSIS=	0.1982

CLASS MID-POINTS(PHI) USED IN THE MOMENT CALCULATIONS:

-0.88	-0.63	-0.38	-0.13	0.13	0.38	0.63	0.88	1.13	1.38	1.63	1.88	2.13	2.38	2.63
2.88	3.13	3.38	3.63	3.88										

MOMENT MEASURES:

	PHI		MM
FIRST (ABOUT ORIGIN)=	1.6000		0.3299
SECOND (ABOUT MEAN) =	0.6845	VARIANCE	
SECOND (ABOUT MEAN) =	0.8274	STANDARD DEVIATION	
THIRD (ABOUT MEAN) =	-0.0021		
FOURTH (ABOUT MEAN) =	0.1963		

SEA276WG

CRUISE	STATION	SAMPLE TYPE,NUMBER	TOTAL LENGTH . M	SAMPLE CENTER . CM	SAMPLE LENGTH . CM	METHODS
S276WG	S-15	S15S1				1

MODAL ANALYSIS

5 MODE(S) DETECTED IN THIS SAMPLE.

PHI	MM	PERCENT	
-0.750	1.6818	0.2026	
-0.500	1.4142	0.7090	
-0.250	1.1892	1.0128	
0.000	1.0000	1.5192	
0.250	0.8409	2.1607	
0.500	0.7071	3.1060	
0.750	0.5946	7.0560	** MODE **
1.000	0.5000	4.2876	
1.250	0.4204	9.5544	
1.500	0.3536	14.6860	** MODE **
1.750	0.2973	13.2343	
2.000	0.2500	13.7407	** MODE **
2.250	0.2102	11.4787	
2.500	0.1768	4.1864	
2.750	0.1486	5.4693	** MODE **
3.000	0.1250	2.1269	
3.250	0.1051	2.2957	** MODE **
3.500	0.0884	1.2829	
3.750	0.0743	1.0128	
4.000	0.0625	0.8778	

SEA276WG

CRUISE	STATION	SAMPLE TYPE,NUMBER	TOTAL LENGTH	SAMPLE CENTER	SAMPLE LENGTH	METHODS
S276WG	S-15	S15S1	. M	. CM	. CM	1

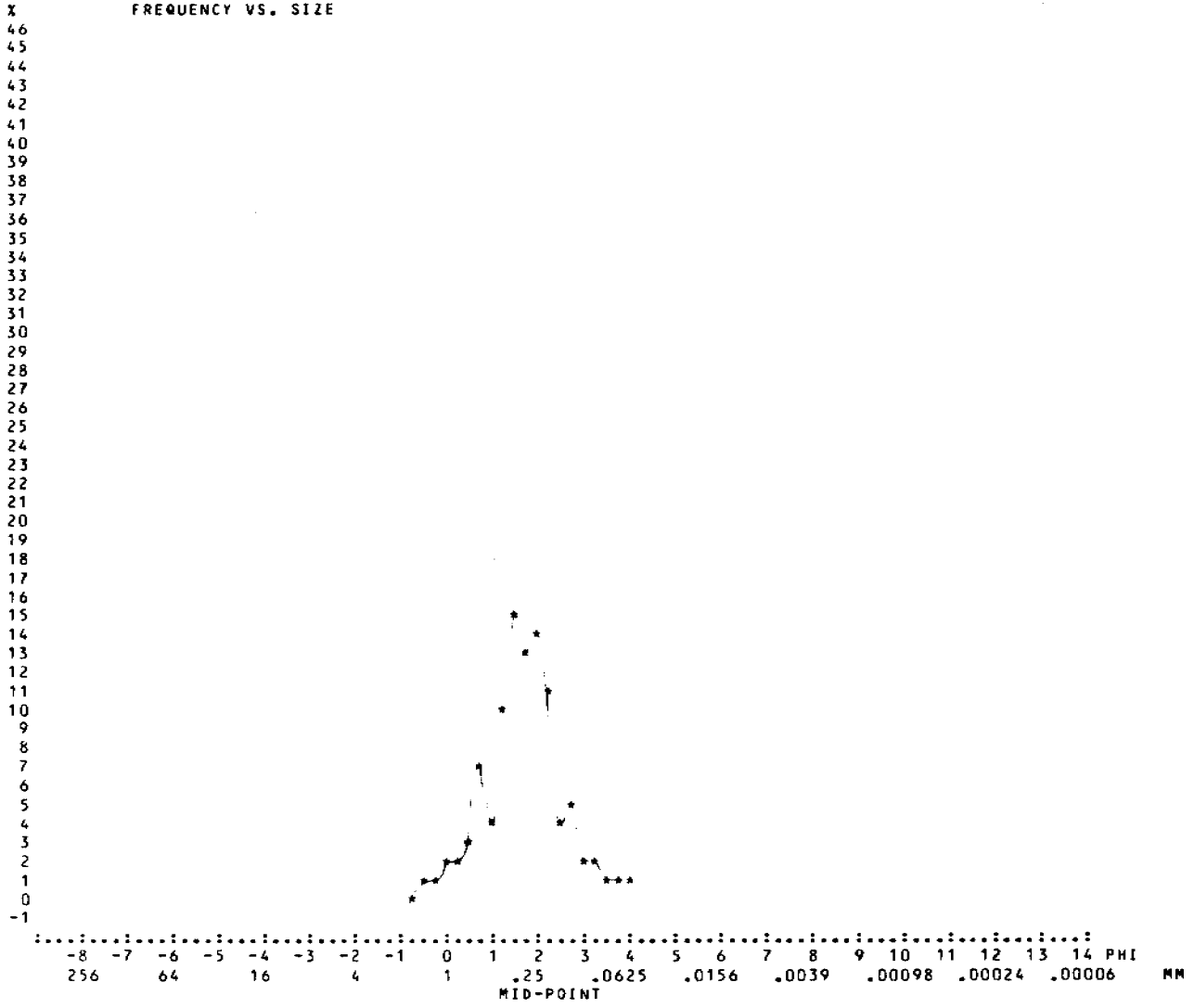

SEA276WG

CRUISE	STATION	SAMPLE TYPE,NUMBER	TOTAL LENGTH . M	SAMPLE CENTER . CM	SAMPLE LENGTH . CM	METHODS
S276WG	S-15	S15S1				1

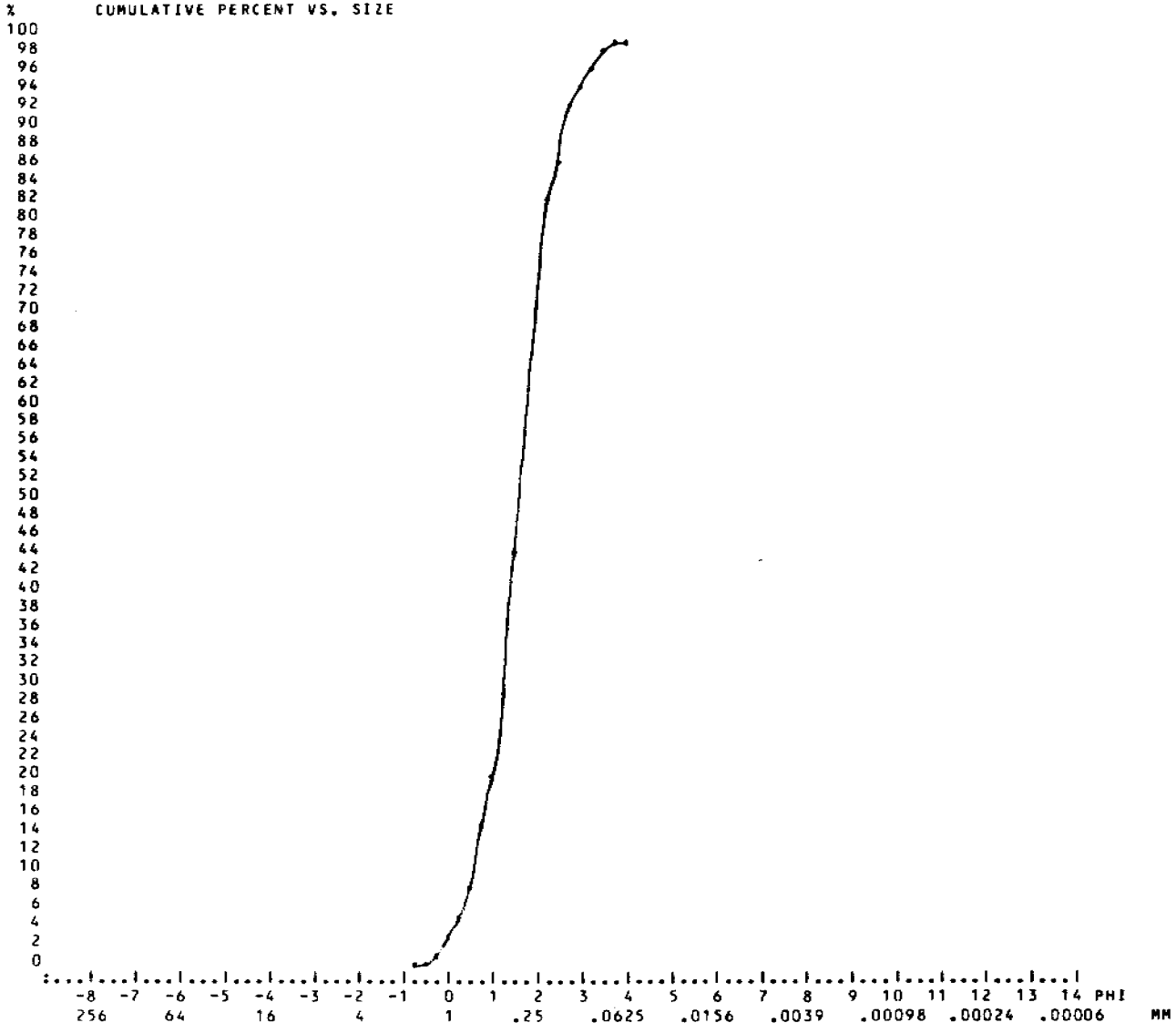

SEA276WG

CRUISE	STATION	SAMPLE TYPE,NUMBER	TOTAL LENGTH	SAMPLE CENTER	SAMPLE LENGTH	METHODS
S276WG	S-28	S28S1	. M	. CM	. CM	1

#F:SV=20,ST= 0,H=0;WT:SV=26.1000,ST= 0.0000,H/P= 0.0000; PHI LIM:CS= 0.00,FN= 0.00

SAMPLE ANALYZED BY THE FOLLOWING METHOD(S):

SIZE RANGE	METHOD
2.0000- 0.0625MM	SIEVES

UNEDITED SAMPLE WEIGHTS IN GRAMS:

SIEVES	BSA	HYDROPHOTOMETER	PAN	TOTAL
26.1000				26.1000 (G)

PARTICLE SIZE DISTRIBUTION:

PHI	MM	PERCENT	CUM PERCENT
-0.7500	1.6818	0.115	0.115
-0.5000	1.4142	0.268	0.383
-0.2500	1.1892	0.383	0.766
0.0000	1.0000	0.421	1.188
0.2500	0.8409	0.575	1.762
0.5000	0.7071	0.575	2.337
0.7500	0.5946	1.418	3.755
1.0000	0.5000	2.989	6.743
1.2500	0.4204	6.667	13.410
1.5000	0.3536	21.111	34.521
1.7500	0.2973	22.759	57.280
2.0000	0.2500	18.966	76.245
2.2500	0.2102	12.759	89.004
2.5000	0.1768	4.023	93.027
2.7500	0.1486	4.713	97.739
3.0000	0.1250	1.111	98.851
3.2500	0.1051	0.613	99.464
3.5000	0.0884	0.268	99.732
3.7500	0.0743	0.153	99.885
4.0000	0.0625	0.115	100.000

SIZE CLASS RATIOS:

GRAVEL	=	0.000PCT	GRAVEL/SAND	=	0.000
SAND	=	100.000PCT	SAND/SILT	=	99999.999
SILT	=	0.000PCT	SILT/CLAY	=	0.000
CLAY	=	0.000PCT	SAND/CLAY	=	0.000
MUD	=	0.000PCT	SAND/MUD	=	99999.999
			GRAVEL/MUD	=	0.000

SEA276WG

CRUISE	STATION	SAMPLE TYPE,NUMBER	TOTAL LENGTH	SAMPLE CENTER	SAMPLE LENGTH	METHODS
S276WG	S-28	S28S1	. M	. CM	. CM	1

INTERPOLATED SIZES USED IN GRAPHICAL STATISTICS:

CUM_PERCENT	05.00	10.00	16.00	25.00	50.00	75.00	84.00	90.00	95.00	CUM_PERCENT
PHI	0.882	1.154	1.303	1.439	1.668	1.981	2.099	2.310	2.528	PHI
MM	0.5425	0.4494	0.4052	0.3687	0.3147	0.2534	0.2334	0.2017	0.1734	MM

GRAPHICAL STATISTICS:

FOLK_&_WARD_(PHI)		INMAN_(PHI)		IRASK_(MM)	
MEDIAN=	1.6682	MEDIAN=	1.6682	MEDIAN=	0.3147
MEAN =	1.6901	MEAN =	1.7011	MEAN =	0.3110
SORTING=	0.4482	SORTING=	0.3978	SORTING=	1.2064
SKEWNESS=	0.0637	SKEW 16/84=	0.0827	SKEWNESS=	0.9436
		SKEW 05/95=	0.0924		
KURTOSIS=	1.2454	KURTOSIS=	1.0684	KURTOSIS=	0.2329

CLASS MID-POINTS(PHI) USED IN THE MOMENT CALCULATIONS:

-0.88	-0.63	-0.38	-0.13	0.13	0.38	0.63	0.88	1.13	1.38	1.63	1.88	2.13	2.38	2.63
2.88	3.13	3.38	3.63	3.88										

MOMENT MEASURES:

	PHI	MM
FIRST (ABOUT ORIGIN)=	1.6845	0.3111
SECOND (ABOUT MEAN) =	0.2930 VARIANCE	
SECOND (ABOUT MEAN) =	0.5413 STANDARD DEVIATION	
THIRD (ABOUT MEAN) =	-0.1833	
FOURTH (ABOUT MEAN) =	1.4095	

SEA276WG

CRUISE	STATION	SAMPLE TYPE,NUMBER	TOTAL LENGTH	SAMPLE CENTER	SAMPLE LENGTH	METHODS
S276WG	S-28	S28S1	. M	. CM	. CM	1

MODAL ANALYSIS
2 MODE(S) DETECTED IN THIS SAMPLE.

PHI	MM	PERCENT	
-0.750	1.6818	0.1149	
-0.500	1.4142	0.2682	
-0.250	1.1892	0.3831	
0.000	1.0000	0.4215	
0.250	0.8409	0.5747	
0.500	0.7071	0.5747	
0.750	0.5946	1.4176	
1.000	0.5000	2.9885	
1.250	0.4204	6.6667	
1.500	0.3536	21.1111	
1.750	0.2973	22.7586	** MODE **
2.000	0.2500	18.9655	
2.250	0.2102	12.7586	
2.500	0.1768	4.0230	
2.750	0.1486	4.7126	** MODE **
3.000	0.1250	1.1111	
3.250	0.1051	0.6130	
3.500	0.0884	0.2682	
3.750	0.0743	0.1533	
4.000	0.0625	0.1149	

SEA276WG

CRUISE	STATION	SAMPLE TYPE,NUMBER	TOTAL LENGTH . M	SAMPLE CENTER . CM	SAMPLE LENGTH . CM	METHODS
S276WG	S-28	S28S1				1

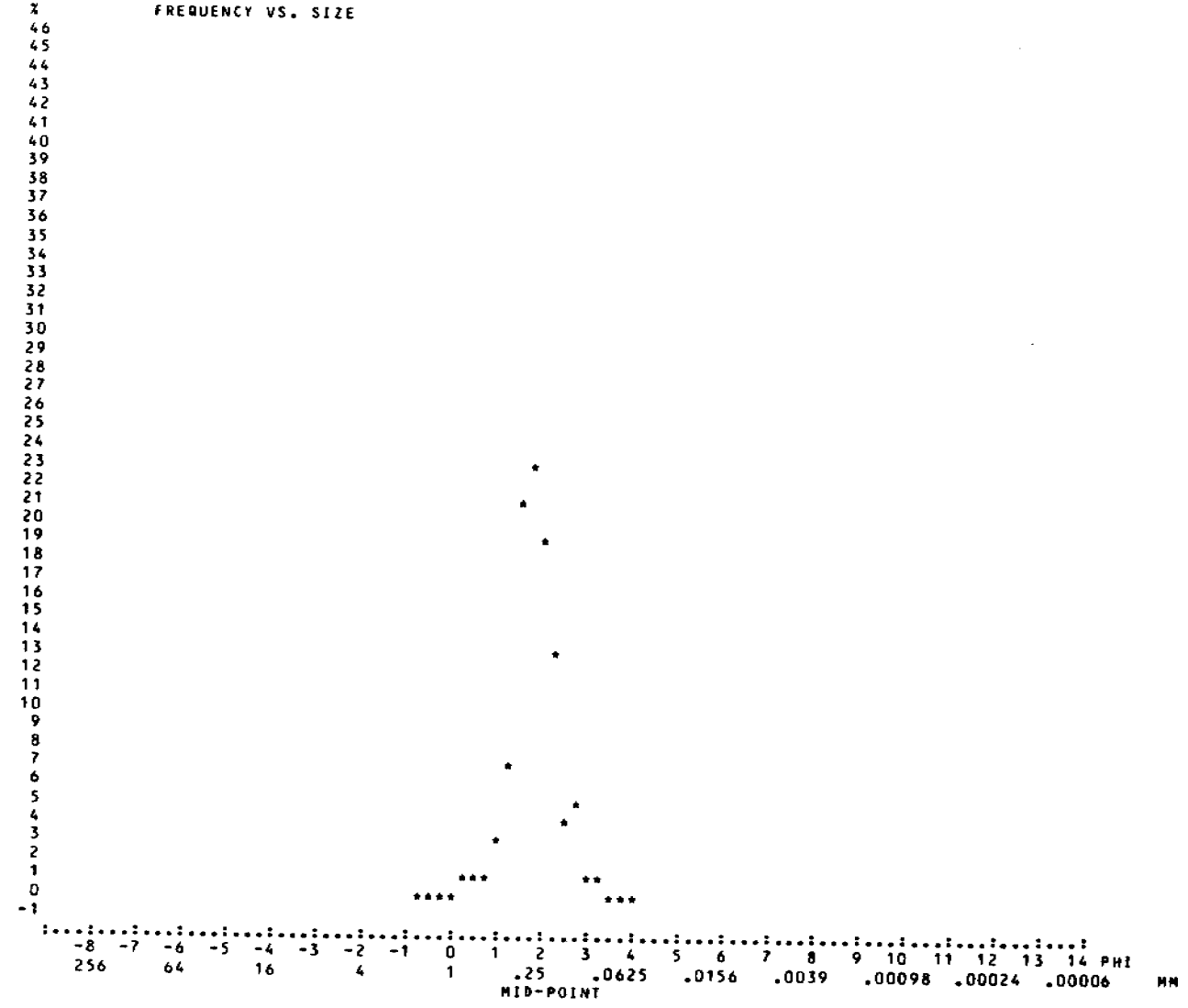

SEA276WG

CRUISE	STATION	SAMPLE TYPE,NUMBER	TOTAL LENGTH	SAMPLE CENTER	SAMPLE LENGTH	METHODS
S276WG	S-28	S28S1	. M	. CM	. CM	1

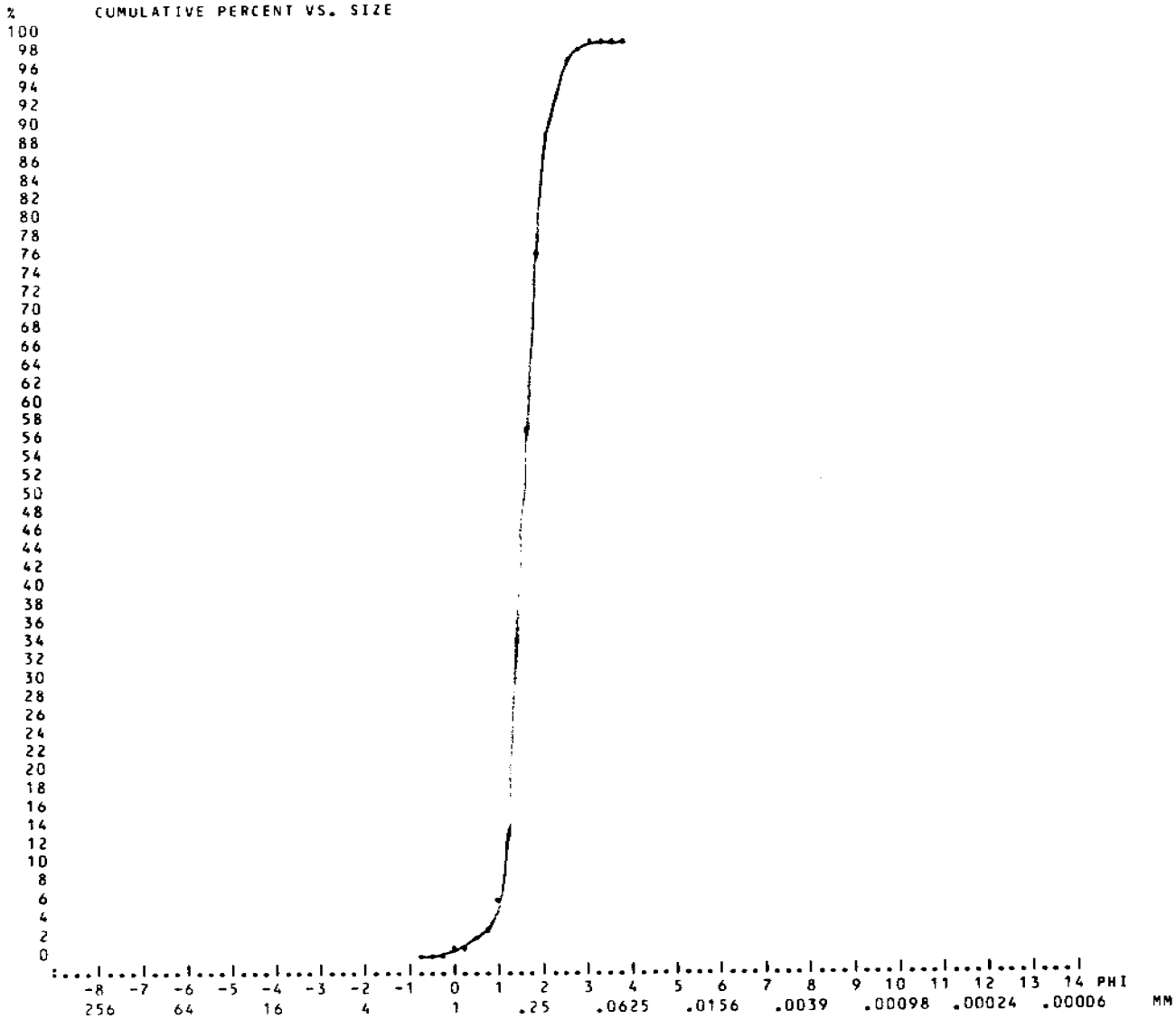

SEA276WG

CRUISE	STATION	SAMPLE TYPE,NUMBER	TOTAL LENGTH	SAMPLE CENTER	SAMPLE LENGTH	METHODS
S276WG	S-29	S29S1	. M	. CM	. CM	1

#F:SV=20,ST= 0,H=0;WT:SV=27.6300,ST= 0.0000,H/P= 0.0000; PHI LIM:CS= 0.00,FN= 0.00

SAMPLE ANALYZED BY THE FOLLOWING METHOD(S):

SIZE RANGE	METHOD
2.0000- 0.0625MM	SIEVES

UNEDITED SAMPLE WEIGHTS IN GRAMS:

SIEVES	BSA	HYDROPHOTOMETER	PAN	TOTAL
27.6800				27.6800 (G)

PARTICLE SIZE DISTRIBUTION:

PHI	MM	PERCENT	CUM PERCENT
-0.7500	1.6818	0.072	0.072
-0.5000	1.4142	0.072	0.145
-0.2500	1.1892	0.072	0.217
0.0000	1.0000	0.108	0.325
0.2500	0.8409	0.145	0.470
0.5000	0.7071	0.289	0.759
0.7500	0.5946	0.325	1.084
1.0000	0.5000	0.361	1.445
1.2500	0.4204	0.542	1.987
1.5000	0.3536	1.590	3.577
1.7500	0.2973	8.887	12.464
2.0000	0.2500	19.689	32.153
2.2500	0.2102	21.134	53.288
2.5000	0.1768	15.282	68.569
2.7500	0.1486	24.675	93.244
3.0000	0.1250	4.408	97.652
3.2500	0.1051	1.590	99.241
3.5000	0.0884	0.434	99.675
3.7500	0.0743	0.181	99.855
4.0000	0.0625	0.145	100.000

SIZE CLASS RATIOS:

GRAVEL=	0.000PCT	GRAVEL/SAND=	0.000
SAND =	100.000PCT	SAND/SILT	**********
SILT =	-0.000PCT	SILT/CLAY =	0.000
CLAY =	0.000PCT	SAND/CLAY =	0.000
MUD =	-0.000PCT	SAND/MUD	**********
		GRAVEL/MUD =	0.000

SEA276WG

CRUISE	STATION	SAMPLE TYPE,NUMBER	TOTAL LENGTH	SAMPLE CENTER	SAMPLE LENGTH	METHODS
S276WG	S-29	S29S1	. M	. CM	. CM	1

INTERPOLATED SIZES USED IN GRAPHICAL STATISTICS:

CUM_PERCENT	05.00	10.00	16.00	25.00	50.00	75.00	84.00	90.00	95.00	CUM_PERCENT
PHI	1.608	1.681	1.811	1.934	2.208	2.565	2.553	2.667	2.807	PHI
MM	0.3280	0.3119	0.2850	0.2616	0.2164	0.1690	0.1704	0.1575	0.1429	MM

GRAPHICAL STATISTICS:

FOLK_&_WARD_(PHI)		_INMAN_(PHI)___		_IRASK_(MM)___	
MEDIAN=	2.2081	MEDIAN=	2.2081	MEDIAN=	0.2164
MEAN =	2.1907	MEAN =	2.1821	MEAN =	0.2153
SORTING=	0.3671	SORTING=	0.3711	SORTING=	1.2444
SKEWNESS=	-0.0355	SKEW 16/84=	-0.0701	SKEWNESS=	0.9439
		SKEW 05/95=	-0.0013		
KURTOSIS=	0.7786	KURTOSIS=	0.6146	KURTOSIS=	0.3000

CLASS MID-POINTS(PHI) USED IN THE MOMENT CALCULATIONS:

-0.88	-0.63	-0.38	-0.13	0.13	0.38	0.63	0.88	1.13	1.38	1.63	1.88	2.13	2.38	2.63
2.88	3.13	3.38	3.63	3.88										

MOMENT MEASURES:

	__PHI___		___MM___
FIRST (ABOUT ORIGIN)=	2.2094		0.2162
SECOND (ABOUT MEAN) =	0.2185	VARIANCE	
SECOND (ABOUT MEAN) =	0.4674	STANDARD DEVIATION	
THIRD (ABOUT MEAN) =	-0.4674		
FOURTH (ABOUT MEAN) =	2.1667		

SEA276WG

CRUISE	STATION	SAMPLE TYPE,NUMBER	TOTAL LENGTH	SAMPLE CENTER	SAMPLE LENGTH	METHODS
S276WG	S-29	S29S1	. M	. CM	. CM	1

MODAL ANALYSIS
2 MODE(S) DETECTED IN THIS SAMPLE.

PHI	MM	PERCENT	
-0.750	1.6818	0.0723	
-0.500	1.4142	0.0723	
-0.250	1.1892	0.0723	
0.000	1.0000	0.1084	
0.250	0.8409	0.1445	
0.500	0.7071	0.2890	
0.750	0.5946	0.3251	
1.000	0.5000	0.3613	
1.250	0.4204	0.5419	
1.500	0.3536	1.5896	
1.750	0.2973	8.8873	
2.000	0.2500	19.6893	
2.250	0.2102	21.1344	** MODE **
2.500	0.1768	15.2818	
2.750	0.1486	24.6749	** MODE **
3.000	0.1250	4.4075	
3.250	0.1051	1.5896	
3.500	0.0884	0.4335	
3.750	0.0743	0.1806	
4.000	0.0625	0.1445	

SEA276WG

CRUISE	STATION	SAMPLE TYPE-NUMBER	TOTAL LENGTH	SAMPLE CENTER	SAMPLE LENGTH	METHODS
S276WG	S-29	S29S1	. M	. CM	. CM	1

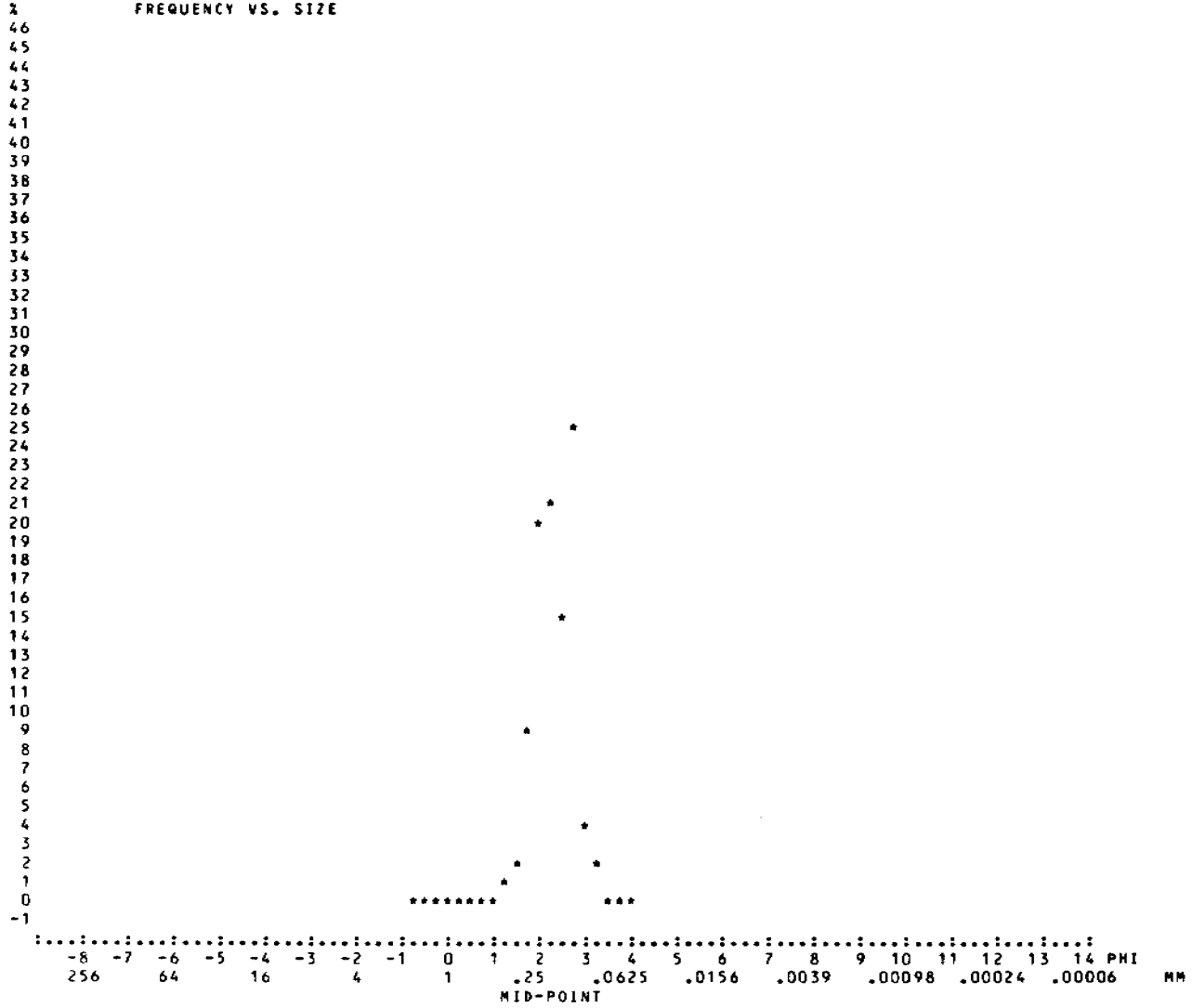

SEA276WG

CRUISE	STATION	SAMPLE TYPE,NUMBER	TOTAL LENGTH	SAMPLE CENTER	SAMPLE LENGTH	METHODS
S276WG	S-29	S29S1	. M	. CM	. CM	1

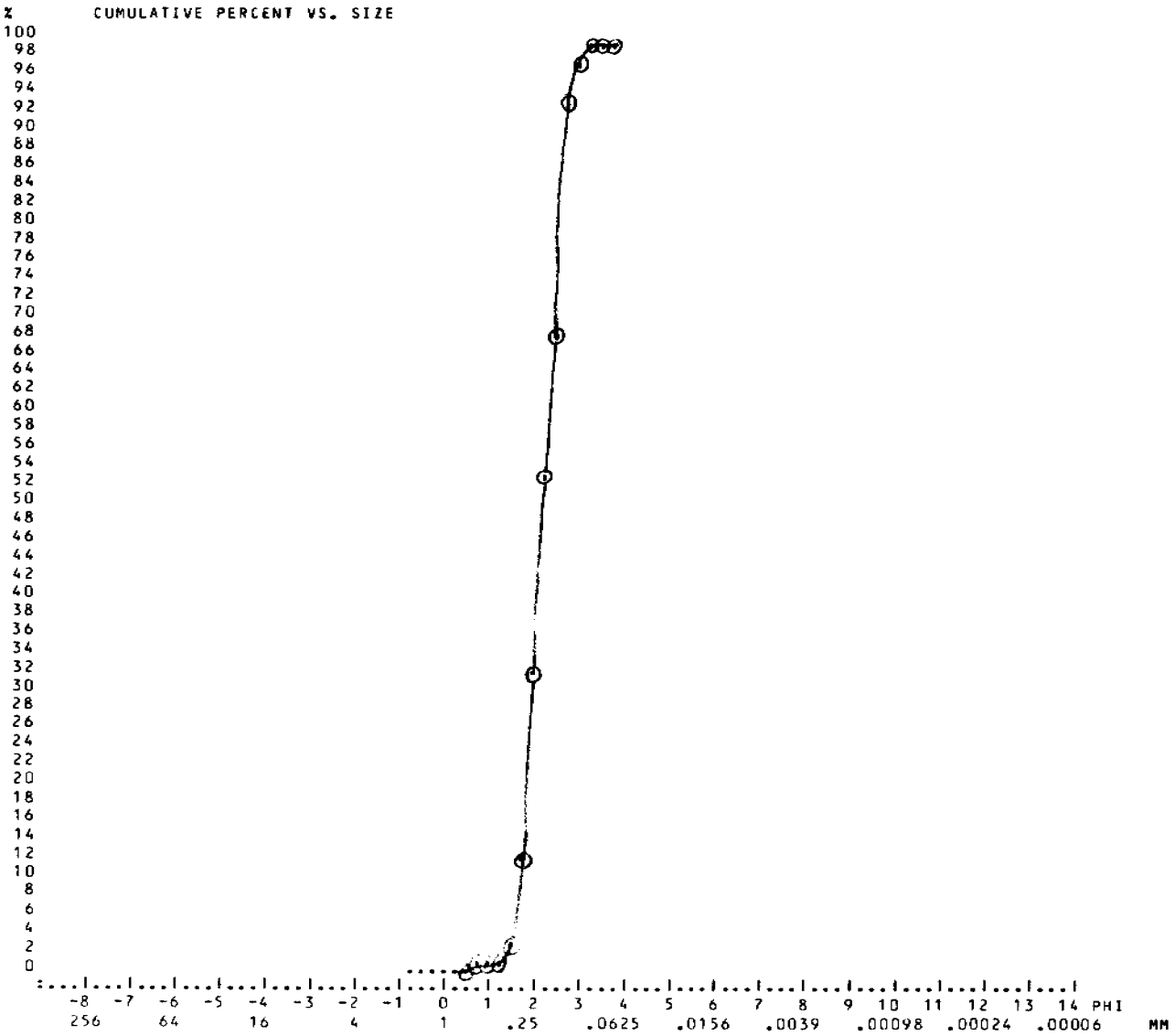

SEA276WG

CRUISE	STATION	SAMPLE TYPE,NUMBER	TOTAL LENGTH	SAMPLE CENTER	SAMPLE LENGTH	METHODS
S276WG	S-30	S30S1	. M	. CM	. CM	1

#F:SV=20,ST= 0,H=0;WT:SV=27.1600,ST= 0.0000,H/P= 0.0000; PHI LIM:CS= 0.00,FN= 0.00

SAMPLE ANALYZED BY THE FOLLOWING METHOD(S):

SIZE RANGE	METHOD
2.0000- 0.0625MM	SIEVES

UNEDITED SAMPLE WEIGHTS IN GRAMS:

SIEVES	BSA	HYDROPHOTOMETER	PAN	TOTAL
27.1550				27.1550 (G)

PARTICLE SIZE DISTRIBUTION:

PHI	MM	PERCENT	CUM PERCENT
-0.7500	1.6818	0.184	0.184
-0.5000	1.4142	0.147	0.331
-0.2500	1.1892	0.110	0.442
0.0000	1.0000	0.184	0.626
0.2500	0.8409	0.368	0.994
0.5000	0.7071	0.552	1.547
0.7500	0.5946	1.639	3.185
1.0000	0.5000	4.345	7.531
1.2500	0.4204	10.974	18.505
1.5000	0.3536	24.415	42.920
1.7500	0.2973	19.959	62.880
2.0000	0.2500	17.750	80.630
2.2500	0.2102	13.036	93.666
2.5000	0.1768	3.535	97.201
2.7500	0.1486	2.136	99.337
3.0000	0.1250	0.368	99.705
3.2500	0.1051	0.221	99.926
3.5000	0.0884	0.037	99.963
3.7500	0.0743	0.018	99.982
4.0000	0.0625	0.018	100.000

SIZE CLASS RATIOS:

GRAVEL=	0.000PCT	GRAVEL/SAND=	0.000
SAND =	100.000PCT	SAND/SILT =99999.999	
SILT =	0.000PCT	SILT/CLAY =	0.000
CLAY =	0.000PCT	SAND/CLAY =	0.000
MUD =	0.000PCT	SAND/MUD =99999.999	
		GRAVEL/MUD =	0.000

SEA276WG

CRUISE	STATION	SAMPLE TYPE,NUMBER	TOTAL LENGTH	SAMPLE CENTER	SAMPLE LENGTH	METHODS
S276WG	S-30	S30S1	. M	. CM	. CM	1

INTERPOLATED SIZES USED IN GRAPHICAL STATISTICS:

CUM_PERCENT	05.00	10.00	16.00	25.00	50.00	75.00	84.00	90.00	95.00	CUM_PERCENT
PHI	0.896	1.084	1.221	1.334	1.584	1.914	2.011	2.123	2.328	PHI
MM	0.5373	0.4718	0.4291	0.3966	0.3335	0.2654	0.2481	0.2295	0.1992	MM

GRAPHICAL STATISTICS:

FOLK_&_WARD_(PHI)		_INMAN_(PHI)___		_TRASK_(MM)___	
MEDIAN=	1.5844	MEDIAN=	1.5844	MEDIAN=	0.3335
MEAN =	1.6055	MEAN =	1.6160	MEAN =	0.3310
SORTING=	0.4146	SORTING=	0.3953	SORTING=	1.2224
SKEWNESS=	0.0591	SKEW 16/84=	0.0799	SKEWNESS=	0.9468
		SKEW 05/95=	0.0695		
KURTOSIS=	1.0125	KURTOSIS=	0.8111	KURTOSIS=	0.2708

CLASS MID-POINTS(PHI) USED IN THE MOMENT CALCULATIONS:

-0.88	-0.63	-0.38	-0.13	0.13	0.38	0.63	0.88	1.13	1.38	1.63	1.88	2.13	2.38	2.63
2.88	3.13	3.38	3.63	3.88										

MOMENT MEASURES:

	--PHI---		---MM---
FIRST (ABOUT ORIGIN)=	1.6011		0.3296
SECOND (ABOUT MEAN) =	0.2273	VARIANCE	
SECOND (ABOUT MEAN) =	0.4768	STANDARD DEVIATION	
THIRD (ABOUT MEAN) =	-0.2209		
FOURTH (ABOUT MEAN) =	1.2283		

SEA276WG

CRUISE	STATION	SAMPLE TYPE,NUMBER	TOTAL LENGTH	SAMPLE CENTER	SAMPLE LENGTH	METHODS
S276WG	S-30	S30S1	. M	. CM	. CM	1

MODAL ANALYSIS

1 MODE(S) DETECTED IN THIS SAMPLE.

PHI	MM	PERCENT	
-0.750	1.6818	0.1841	
-0.500	1.4142	0.1473	
-0.250	1.1892	0.1105	
0.000	1.0000	0.1841	
0.250	0.8409	0.3683	
0.500	0.7071	0.5524	
0.750	0.5946	1.6387	
1.000	0.5000	4.3454	
1.250	0.4204	10.9740	
1.500	0.3536	24.4154	** MODE **
1.750	0.2973	19.9595	
2.000	0.2500	17.7500	
2.250	0.2102	13.0363	
2.500	0.1768	3.5353	
2.750	0.1486	2.1359	
3.000	0.1250	0.3683	
3.250	0.1051	0.2210	
3.500	0.0884	0.0368	
3.750	0.0743	0.0184	
4.000	0.0625	0.0184	

SEA276WG

CRUISE	STATION	SAMPLE TYPE,NUMBER	TOTAL LENGTH	SAMPLE CENTER	SAMPLE LENGTH	METHODS
S276WG	S-30	S30S1	. M	. CM	. CM	1

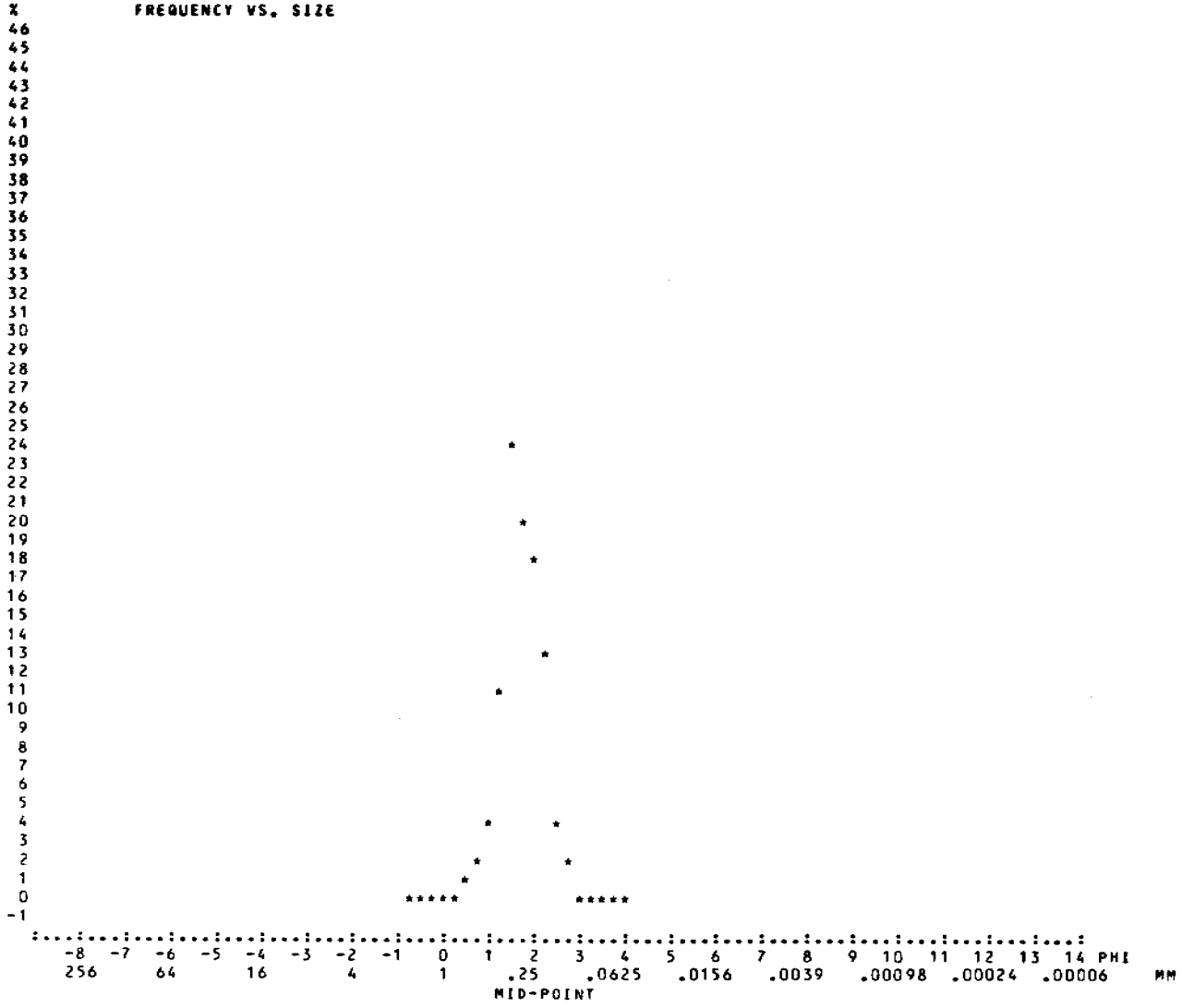

SEA276WG

CRUISE	STATION	SAMPLE TYPE,NUMBER	TOTAL LENGTH	SAMPLE CENTER	SAMPLE LENGTH	METHODS
S276WG	S-30	S30S1	. M	. CM	. CM	1

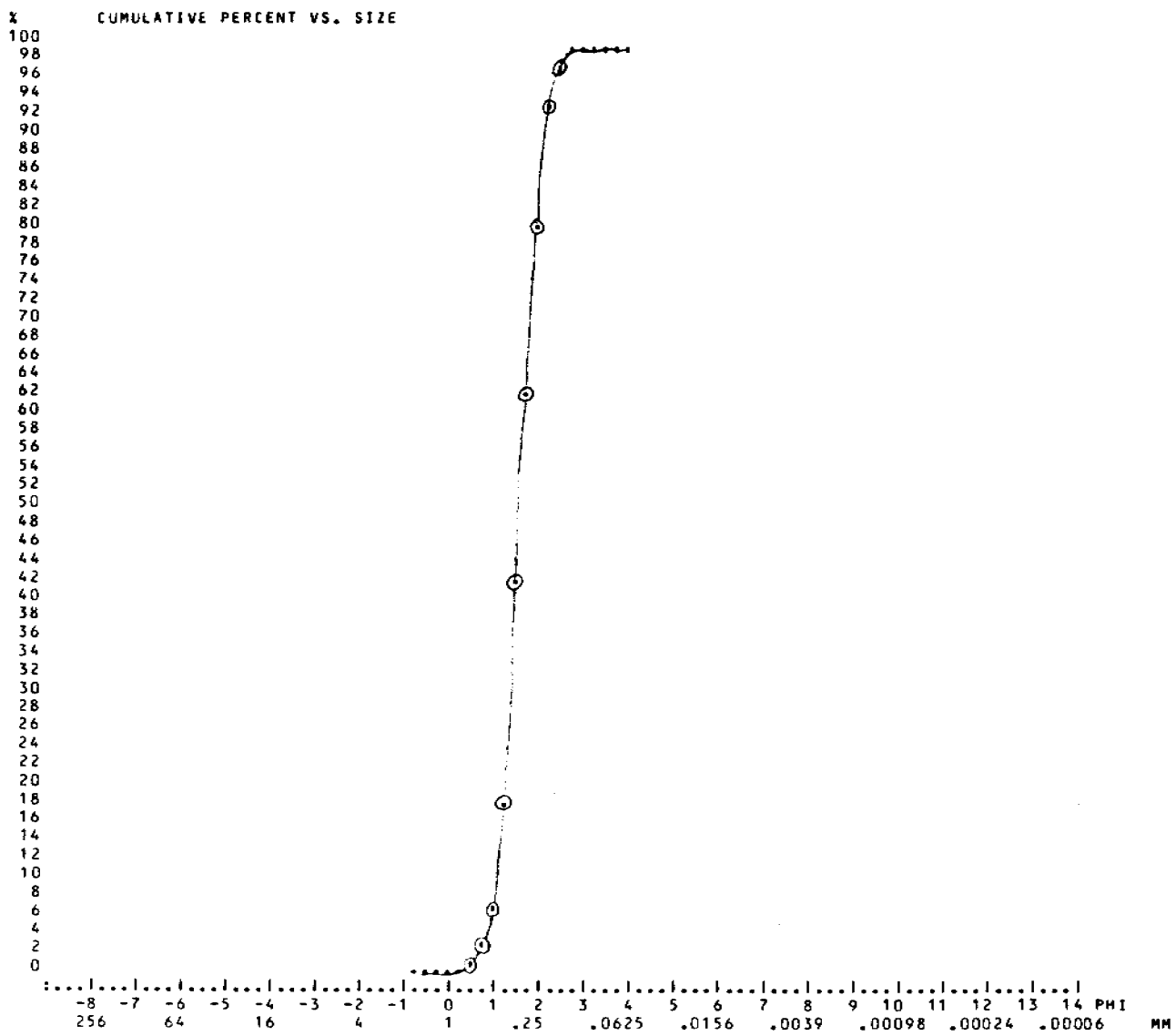

SEA276WG

CRUISE	STATION	SAMPLE TYPE,NUMBER	TOTAL LENGTH	SAMPLE CENTER	SAMPLE LENGTH	METHODS
S276WG	S-30	S30S2	. M	. CM	. CM	1

#F:SV=20,ST= 0,H=0;WT:SV=29.0800,ST= 0.0000,H/P= 0.0000; PHI LIM:CS= 0.00,FN= 0.00

SAMPLE ANALYZED BY THE FOLLOWING METHOD(S):

SIZE RANGE	METHOD
2.0000- 0.0625MM	SIEVES

UNEDITED SAMPLE WEIGHTS IN GRAMS:

SIEVES	BSA	HYDROPHOTOMETER	PAN	TOTAL
29.0800				29.0800 (G)

PARTICLE SIZE DISTRIBUTION:

PHI	MM	PERCENT	CUM PERCENT
-0.7500	1.6818	0.653	0.653
-0.5000	1.4142	1.238	1.891
-0.2500	1.1892	1.272	3.164
0.0000	1.0000	1.376	4.539
0.2500	0.8409	1.754	6.293
0.5000	0.7071	2.201	8.494
0.7500	0.5946	5.949	14.443
1.0000	0.5000	10.660	25.103
1.2500	0.4204	14.271	39.374
1.5000	0.3536	20.770	60.144
1.7500	0.2973	13.927	74.072
2.0000	0.2500	13.686	87.758
2.2500	0.2102	9.078	96.836
2.5000	0.1768	1.857	98.693
2.7500	0.1486	1.066	99.759
3.0000	0.1250	0.103	99.862
3.2500	0.1051	0.069	99.931
3.5000	0.0884	0.034	99.966
3.7500	0.0743	0.017	99.983
4.0000	0.0625	0.017	100.000

SIZE CLASS RATIOS:

GRAVEL	=	0.000PCT	GRAVEL/SAND	=	0.000
SAND	=	100.000PCT	SAND/SILT	=99999.999	
SILT	=	0.000PCT	SILT/CLAY	=	0.000
CLAY	=	0.000PCT	SAND/CLAY	=	0.000
MUD	=	0.000PCT	SAND/MUD	=99999.999	
			GRAVEL/MUD	=	0.000

SEA276WG

CRUISE	STATION	SAMPLE TYPE,NUMBER	TOTAL LENGTH	SAMPLE CENTER	SAMPLE LENGTH	METHODS
S276WG	S-30	S30S2	M	. CM	. CM	1

INTERPOLATED SIZES USED IN GRAPHICAL STATISTICS:

CUM_PERCENT	05.00	10.00	16.00	25.00	50.00	75.00	84.00	90.00	95.00	CUM_PERCENT
PHI	0.072	0.596	0.796	0.998	1.377	1.764	1.924	2.062	2.132	PHI
MM	0.9516	0.6614	0.5759	0.5006	0.3850	0.2943	0.2636	0.2395	0.2282	MM

GRAPHICAL STATISTICS:

FOLK_&_WARD_(PHI)		_INMAN_(PHI)___		_IRASK_(MM)___	
MEDIAN=	1.3771	MEDIAN=	1.3771	MEDIAN=	0.3850
MEAN =	1.3656	MEAN =	1.3598	MEAN =	0.3975
SORTING=	0.5940	SORTING=	0.5637	SORTING=	1.3041
SKEWNESS=	-0.1491	SKEW 16/84=	-0.0307	SKEWNESS=	0.9941
		SKEW 05/95=	-0.4888		
KURTOSIS=	1.1019	KURTOSIS=	0.8272	KURTOSIS=	0.2444

CLASS MID-POINTS(PHI) USED IN THE MOMENT CALCULATIONS:

-0.88	-0.63	-0.38	-0.13	0.13	0.38	0.63	0.88	1.13	1.38	1.63	1.88	2.13	2.38	2.63
2.88	3.13	3.38	3.63	3.88										

MOMENT MEASURES:

	--PHI---	---MM---
FIRST (ABOUT ORIGIN)=	1.3226	0.3998
SECOND (ABOUT MEAN) =	0.4052 VARIANCE	
SECOND (ABOUT MEAN) =	0.6365 STANDARD DEVIATION	
THIRD (ABOUT MEAN) =	-0.4064	
FOURTH (ABOUT MEAN) =	0.6487	

SEA276WG

CRUISE	STATION	SAMPLE TYPE,NUMBER	TOTAL LENGTH	SAMPLE CENTER	SAMPLE LENGTH	METHODS
S276WG	S-30	S30S2	. M	. CM	. CM	1

MODAL ANALYSIS
1 MODE(S) DETECTED IN THIS SAMPLE.

PHI	MM	PERCENT	
-0.750	1.6818	0.6534	
-0.500	1.4142	1.2380	
-0.250	1.1892	1.2724	
0.000	1.0000	1.3755	
0.250	0.8409	1.7538	
0.500	0.7071	2.2008	
0.750	0.5946	5.9491	
1.000	0.5000	10.6602	
1.250	0.4204	14.2710	
1.500	0.3536	20.7703	** MODE **
1.750	0.2973	13.9271	
2.000	0.2500	13.6864	
2.250	0.2102	9.0784	
2.500	0.1768	1.8569	
2.750	0.1486	1.0660	
3.000	0.1250	0.1032	
3.250	0.1051	0.0688	
3.500	0.0884	0.0344	
3.750	0.0743	0.0172	
4.000	0.0625	0.0172	

SEA276WG

CRUISE	STATION	SAMPLE TYPE,NUMBER	TOTAL LENGTH	SAMPLE CENTER	SAMPLE LENGTH	METHODS
S276WG	S-30	S30S2	. M	. CM	. CM	1

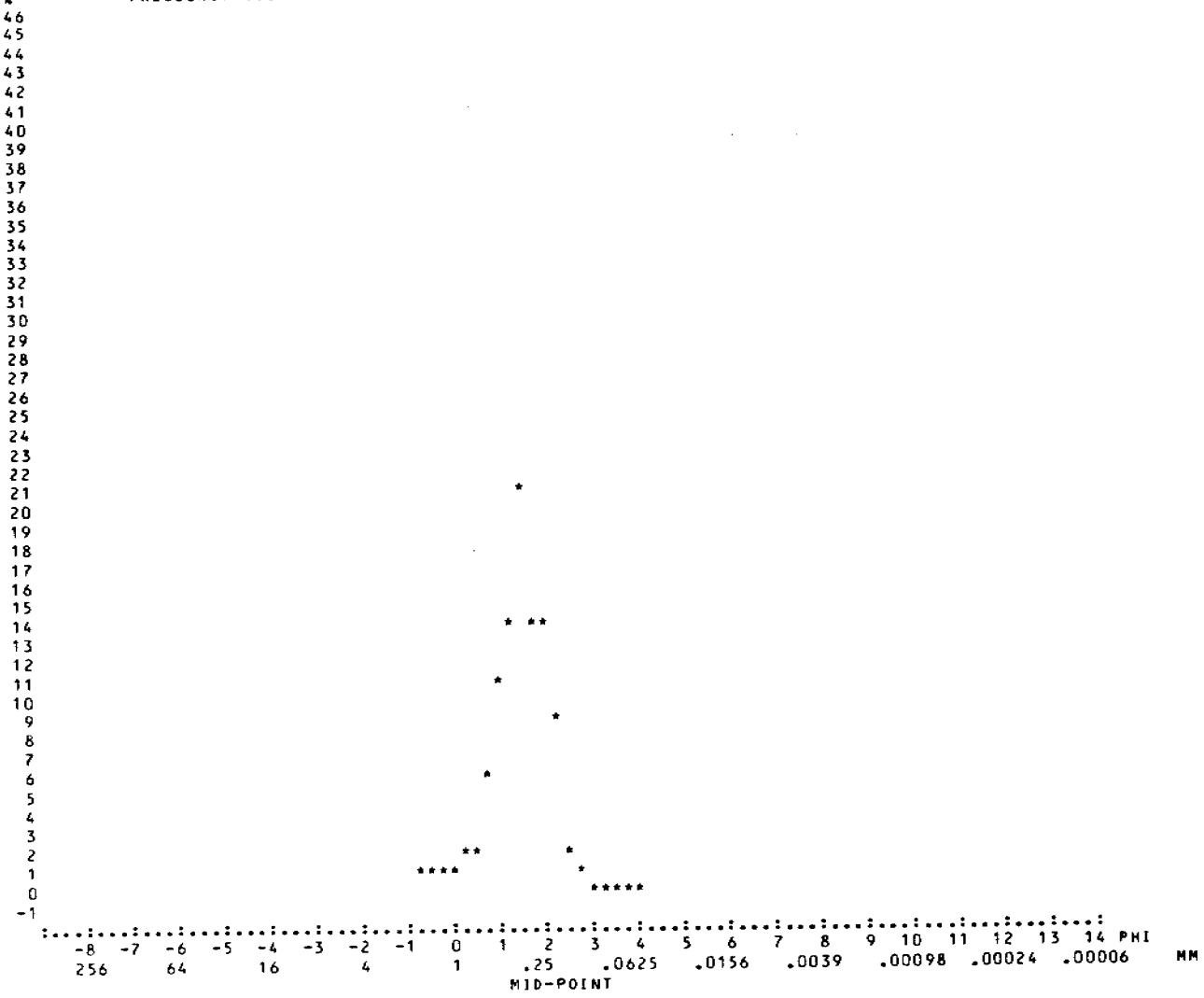

SEA276WG

CRUISE	STATION	SAMPLE TYPE/NUMBER	TOTAL LENGTH	SAMPLE CENTER	SAMPLE LENGTH	METHODS
S276WG	S-30	S30S2	. M	. CM	. CM	1

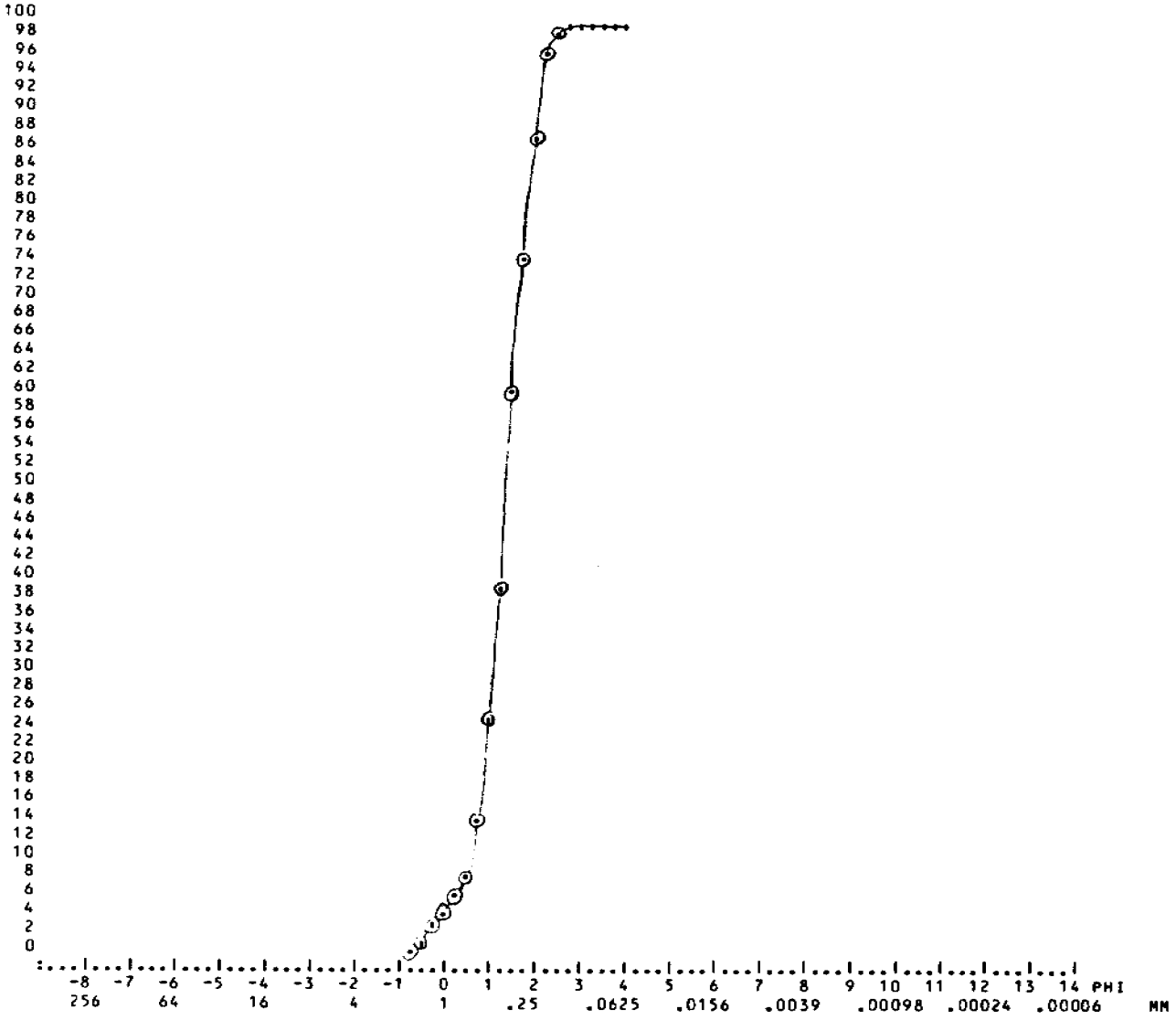

SEA276WG

CRUISE	STATION	SAMPLE TYPE,NUMBER	TOTAL LENGTH	SAMPLE CENTER	SAMPLE LENGTH	METHODS
S276WG	S-31	S31S1	. M	. CM	. CM	1

#F:SV=20,ST= 0,H=0;WT:SV=30.0000,ST= 0.0000,H/P= 0.0000; PHI LIM:CS= 0.00,FN= 0.00

SAMPLE ANALYZED BY THE FOLLOWING METHOD(S):

SIZE RANGE	METHOD
2.0000- 0.0625MM	SIEVES

UNEDITED SAMPLE WEIGHTS IN GRAMS:

SIEVES	RSA	HYDROPHOTOMETER	PAN	TOTAL
30.0000				30.0000 (G)

PARTICLE SIZE DISTRIBUTION:

PHI	MM	PERCENT	CUM PERCENT
-0.7500	1.6818	0.000	0.000
-0.5000	1.4142	0.000	0.000
-0.2500	1.1892	0.067	0.067
0.0000	1.0000	0.033	0.100
0.2500	0.8409	0.033	0.133
0.5000	0.7071	0.100	0.233
0.7500	0.5946	0.233	0.467
1.0000	0.5000	0.400	0.867
1.2500	0.4204	1.033	1.900
1.5000	0.3536	13.767	15.667
1.7500	0.2973	25.500	41.167
2.0000	0.2500	28.700	69.867
2.2500	0.2102	18.867	88.733
2.5000	0.1768	4.700	93.433
2.7500	0.1486	3.533	96.967
3.0000	0.1250	1.400	98.367
3.2500	0.1051	0.967	99.333
3.5000	0.0884	0.633	99.967
3.7500	0.0743	0.017	99.983
4.0000	0.0625	0.017	100.000

SIZE CLASS RATIOS:

GRAVEL=	0.000PCT	GRAVEL/SAND=	0.000
SAND =	100.000PCT	SAND/SILT	=99999.999
SILT =	0.000PCT	SILT/CLAY	= 0.000
CLAY =	0.000PCT	SAND/CLAY	= 0.000
MUD =	0.000PCT	SAND/MUD	=99999.999
		GRAVEL/MUD	= 0.000

SEA276WG

CRUISE	STATION	SAMPLE TYPE,NUMBER	TOTAL LENGTH . M	SAMPLE CENTER . CM	SAMPLE LENGTH . CM	METHODS
S276WG	S-31	S31S1				1

INTERPOLATED SIZES USED IN GRAPHICAL STATISTICS:

CUM_PERCENT	05.00	10.00	16.00	25.00	50.00	75.00	84.00	90.00	95.00	CUM_PERCENT
PHI	1.306	1.397	1.504	1.609	1.820	2.005	2.127	2.309	2.574	PHI
MM	0.4044	0.3797	0.3525	0.3278	0.2832	0.2491	0.2289	0.2018	0.1679	MM

GRAPHICAL STATISTICS:

FOLK_&_WARD_(PHI)		_INMAN_(PHI)___		_IRASK_(MM)___	
MEDIAN=	1.8203	MEDIAN=	1.8203	MEDIAN=	0.2832
MEAN =	1.8173	MEAN =	1.8158	MEAN =	0.2885
SORTING=	0.3478	SORTING=	0.3116	SORTING=	1.1470
SKEWNESS=	0.0872	SKEW 16/84=	-0.0145	SKEWNESS=	1.0187
		SKEW 05/95=	0.3844		
KURTOSIS=	1.3124	KURTOSIS=	1.0342	KURTOSIS=	0.2211

CLASS MID-POINTS(PHI) USED IN THE MOMENT CALCULATIONS:

-0.88	-0.63	-0.38	-0.13	0.13	0.38	0.63	0.88	1.13	1.38	1.63	1.88	2.13	2.38	2.63
2.88	3.13	3.38	3.63	3.88										

MOMENT MEASURES:

	--PHI---	---MM---
FIRST (ABOUT ORIGIN)=	1.8569	0.2761
SECOND (ABOUT MEAN) =	0.1594 VARIANCE	
SECOND (ABOUT MEAN) =	0.3993 STANDARD DEVIATION	
THIRD (ABOUT MEAN) =	0.3092	
FOURTH (ABOUT MEAN) =	1.3424	

SEA276WG

CRUISE	STATION	SAMPLE TYPE,NUMBER	TOTAL LENGTH	SAMPLE CENTER	SAMPLE LENGTH	METHODS
S276WG	S-31	S31S1	. M	. CM	. CM	1

MODAL ANALYSIS
2 MODE(S) DETECTED IN THIS SAMPLE.

PHI	MM	PERCENT	
-0.750	1.6818	0.0000	
-0.500	1.4142	0.0000	
-0.250	1.1892	0.0667	** MODE **
0.000	1.0000	0.0333	
0.250	0.8409	0.0333	
0.500	0.7071	0.1000	
0.750	0.5946	0.2333	
1.000	0.5000	0.4000	
1.250	0.4204	1.0333	
1.500	0.3536	13.7667	
1.750	0.2973	25.5000	
2.000	0.2500	28.7000	** MODE **
2.250	0.2102	18.8667	
2.500	0.1768	4.7000	
2.750	0.1486	3.5333	
3.000	0.1250	1.4000	
3.250	0.1051	0.9667	
3.500	0.0884	0.6333	
3.750	0.0743	0.0167	
4.000	0.0625	0.0167	

SEA276WG

CRUISE	STATION	SAMPLE TYPE,NUMBER	TOTAL LENGTH . M	SAMPLE CENTER . CM	SAMPLE LENGTH . CM	METHODS
S276WG	S-31	S31S1				1

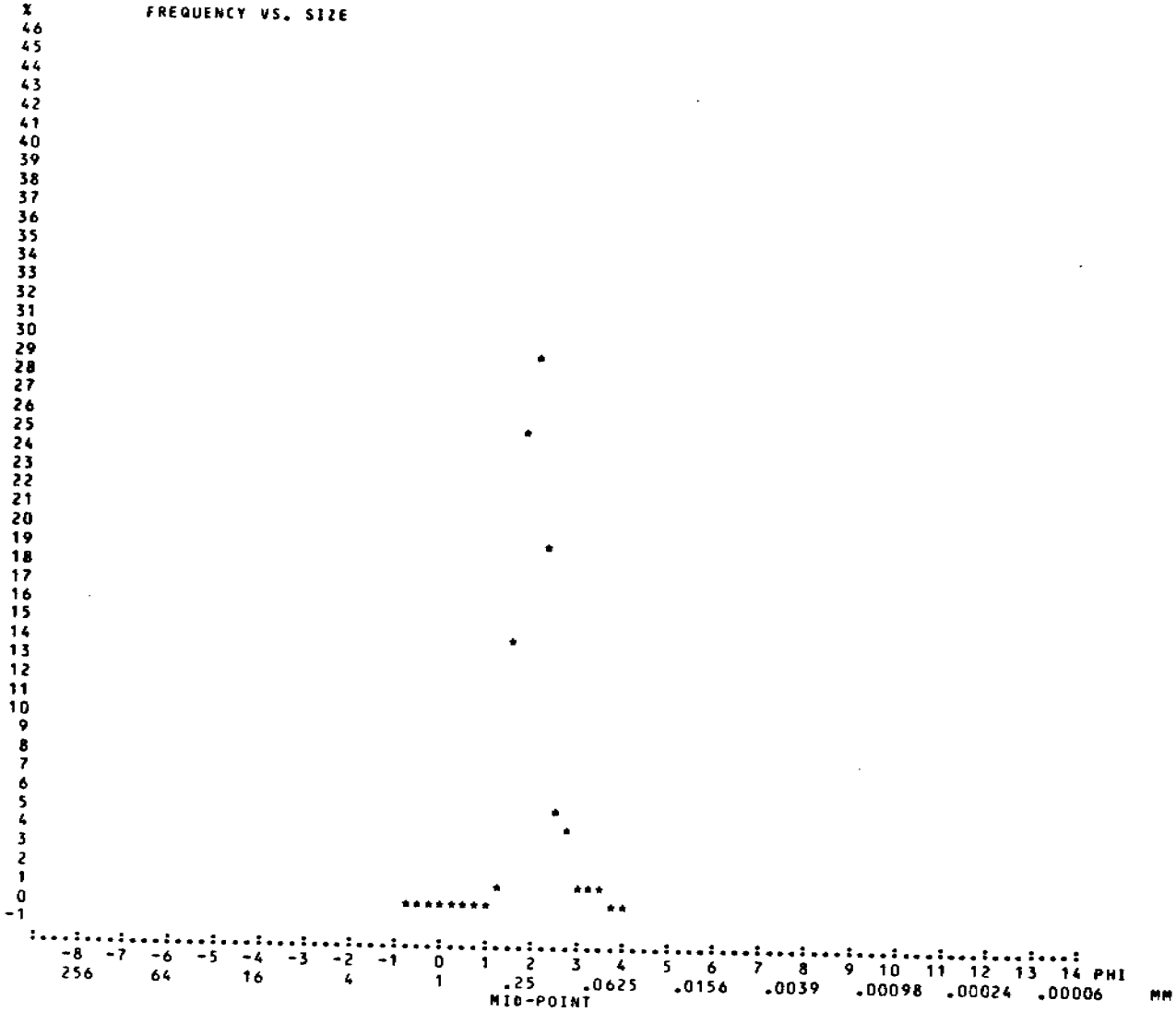

SEA276WG

CRUISE	STATION	SAMPLE TYPE,NUMBER	TOTAL LENGTH	SAMPLE CENTER	SAMPLE LENGTH	METHODS
S276WG	S-31	S31S1	. M	. CM	. CM	1

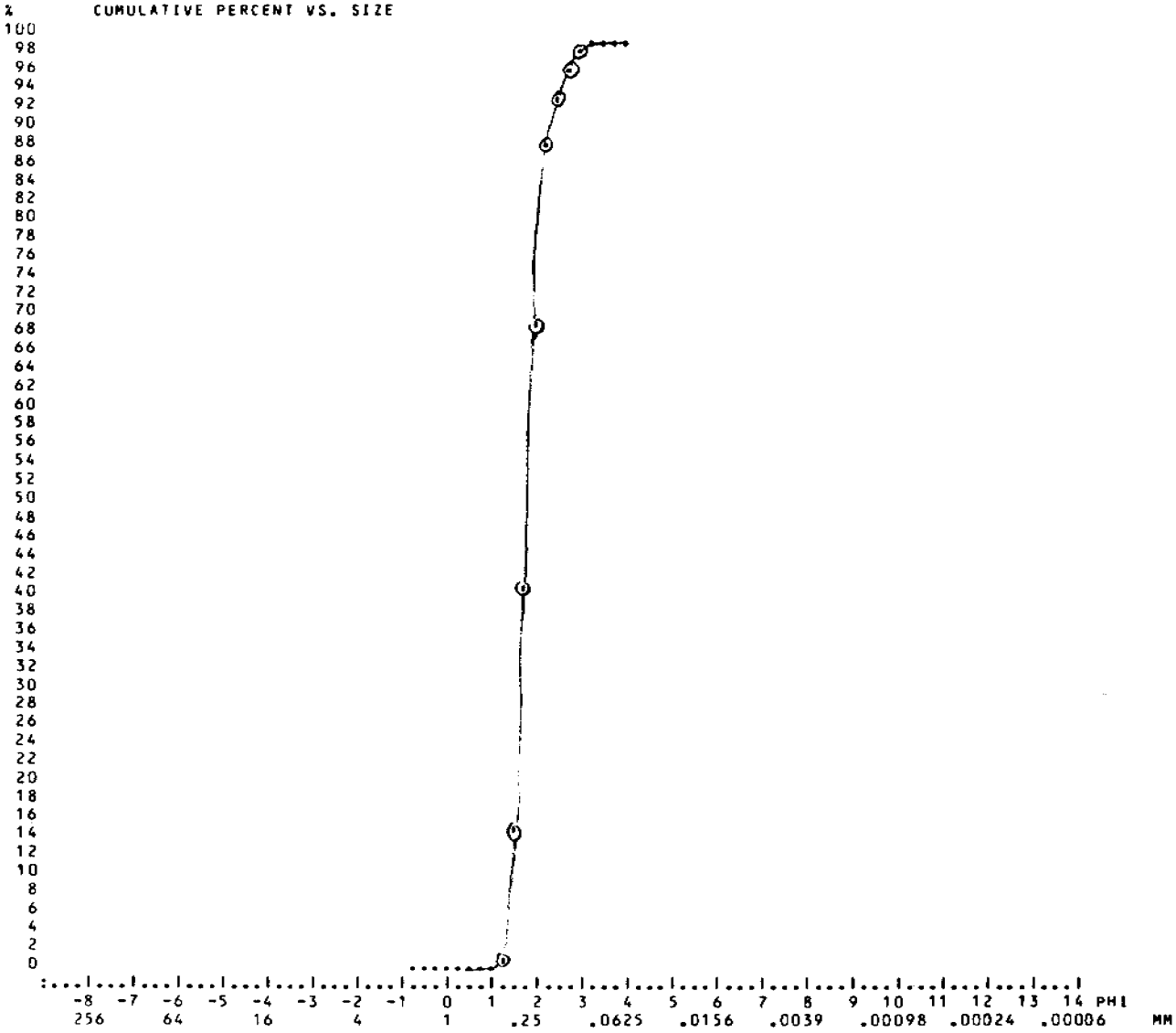

SEA276WG

CRUISE	STATION	SAMPLE TYPE,NUMBER	TOTAL LENGTH	SAMPLE CENTER	SAMPLE LENGTH	METHODS
S276WG	S-34	S34S1	. M	. CM	. CM	1

#F:SV=20,ST= 0,H=0;WT:SV=29.0500,ST= 0.0000,H/P= 0.0000; PHI LIM:CS= 0.00,FN= 0.00

SAMPLE ANALYZED BY THE FOLLOWING METHOD(S):

SIZE RANGE	METHOD
2.0000- 0.0625MM	SIEVES

UNEDITED SAMPLE WEIGHTS IN GRAMS:

SIEVES	BSA	HYDROPHOTOMETER	PAN	TOTAL
29.0500				29.0500 (G)

PARTICLE SIZE DISTRIBUTION:

PHI	MM	PERCENT	CUM PERCENT
-0.7500	1.6818	0.000	0.000
-0.5000	1.4142	0.000	0.000
-0.2500	1.1892	0.000	0.000
0.0000	1.0000	0.034	0.034
0.2500	0.8409	0.034	0.069
0.5000	0.7071	0.034	0.103
0.7500	0.5946	0.034	0.138
1.0000	0.5000	0.069	0.207
1.2500	0.4204	0.172	0.379
1.5000	0.3536	0.482	0.861
1.7500	0.2973	1.170	2.031
2.0000	0.2500	5.921	7.952
2.2500	0.2102	32.324	40.275
2.5000	0.1768	16.351	56.627
2.7500	0.1486	28.021	84.647
3.0000	0.1250	6.781	91.429
3.2500	0.1051	3.890	95.318
3.5000	0.0884	2.582	97.900
3.7500	0.0743	1.446	99.346
4.0000	0.0625	0.654	100.000

SIZE CLASS RATIOS:

GRAVEL =	0.000PCT	GRAVEL/SAND =	0.000
SAND =	100.000PCT	SAND/SILT =	99999.999
SILT =	0.000PCT	SILT/CLAY =	0.000
CLAY =	0.000PCT	SAND/CLAY =	0.000
MUD =	0.000PCT	SAND/MUD =	99999.999
		GRAVEL/MUD =	0.000

SEA276WG

CRUISE	STATION	SAMPLE TYPE,NUMBER	TOTAL LENGTH	SAMPLE CENTER	SAMPLE LENGTH	METHODS
S276WG	S-34	S34S1	. M	. CM	. CM	1

INTERPOLATED SIZES USED IN GRAPHICAL STATISTICS:

CUM_PERCENT	05.00	10.00	16.00	25.00	50.00	75.00	84.00	90.00	95.00	CUM_PERCENT
PHI	1.985	2.039	2.135	2.229	2.398	2.605	2.738	2.934	3.225	PHI
MM	0.2526	0.2433	0.2276	0.2133	0.1897	0.1643	0.1499	0.1308	0.1069	MM

GRAPHICAL STATISTICS:

FOLK & WARD (PHI)		INMAN (PHI)		IRASK (MM)	
MEDIAN=	2.3983	MEDIAN=	2.3983	MEDIAN=	0.1897
MEAN =	2.4240	MEAN =	2.4368	MEAN =	0.1888
SORTING=	0.3387	SORTING=	0.3016	SORTING=	1.1393
SKEWNESS=	0.2306	SKEW 16/84=	0.1276	SKEWNESS=	0.9740
		SKEW 05/95=	0.6860		
KURTOSIS=	1.3501	KURTOSIS=	1.0557	KURTOSIS=	0.2177

CLASS MID-POINTS(PHI) USED IN THE MOMENT CALCULATIONS:

-0.88	-0.63	-0.38	-0.13	0.13	0.38	0.63	0.88	1.13	1.38	1.63	1.88	2.13	2.38	2.63
2.88	3.13	3.38	3.63	3.88										

MOMENT MEASURES:

	PHI	MM
FIRST (ABOUT ORIGIN)=	2.4317	0.1853
SECOND (ABOUT MEAN) =	0.1732 VARIANCE	
SECOND (ABOUT MEAN) =	0.4162 STANDARD DEVIATION	
THIRD (ABOUT MEAN) =	0.2354	
FOURTH (ABOUT MEAN) =	1.0493	

SEA276WG

CRUISE	STATION	SAMPLE TYPE/NUMBER	TOTAL LENGTH	SAMPLE CENTER	SAMPLE LENGTH	METHODS
S276WG	S-34	S34S1	. M	. CM	. CM	1

MODAL ANALYSIS

2 MODE(S) DETECTED IN THIS SAMPLE.

PHI	MM	PERCENT	
-0.750	1.6818	0.0000	
-0.500	1.4142	0.0000	
-0.250	1.1892	0.0000	
0.000	1.0000	0.0344	
0.250	0.8409	0.0344	
0.500	0.7071	0.0344	
0.750	0.5946	0.0344	
1.000	0.5000	0.0688	
1.250	0.4204	0.1721	
1.500	0.3536	0.4819	
1.750	0.2973	1.1704	
2.000	0.2500	5.9208	
2.250	0.2102	32.3236	** MODE **
2.500	0.1768	16.3511	
2.750	0.1486	28.0207	** MODE **
3.000	0.1250	6.7814	
3.250	0.1051	3.8898	
3.500	0.0884	2.5818	
3.750	0.0743	1.4458	
4.000	0.0625	0.6540	

SEA276WG

CRUISE	STATION	SAMPLE TYPE/NUMBER	TOTAL LENGTH	SAMPLE CENTER	SAMPLE LENGTH	METHODS
S276WG	S-34	S34S1	. M	. CM	. CM	1

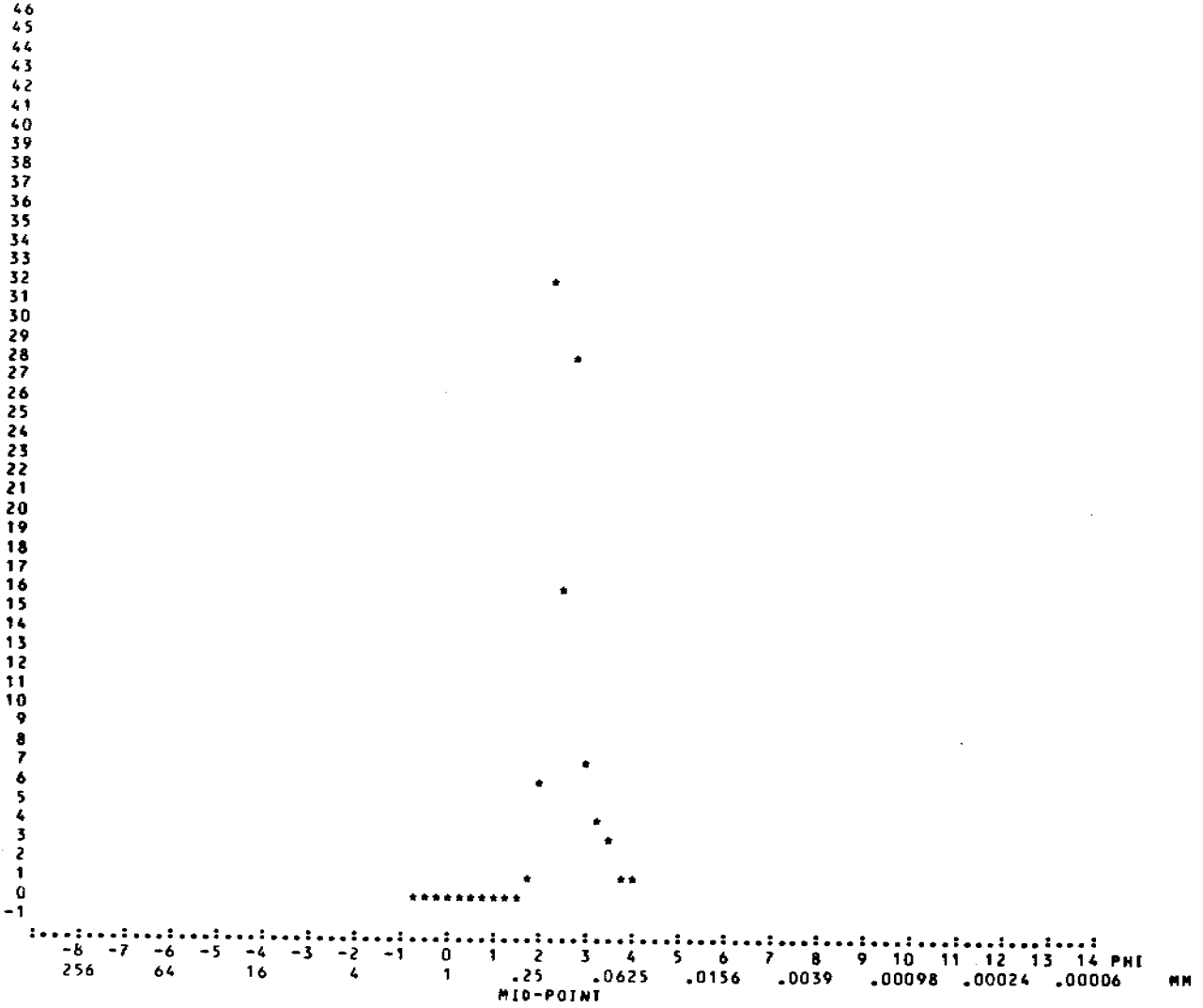

SEA276WG

CRUISE	STATION	SAMPLE TYPE,NUMBER	TOTAL LENGTH	SAMPLE CENTER	SAMPLE LENGTH	METHODS
S276WG	S-34	S34S1	. M	. CM	. CM	1

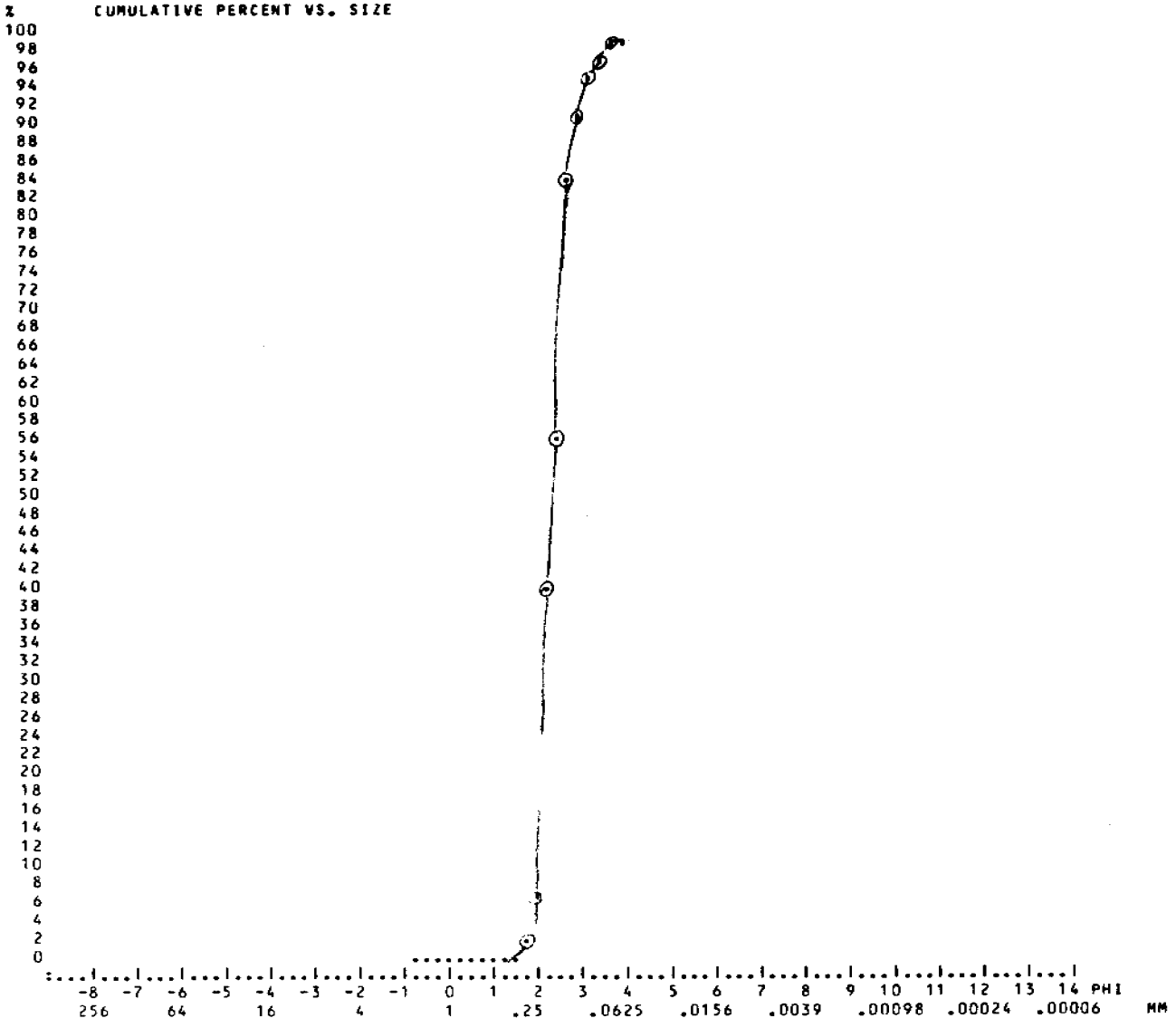

SEA276WG

CRUISE	STATION	SAMPLE TYPE,NUMBER	TOTAL LENGTH	SAMPLE CENTER	SAMPLE LENGTH	METHODS
S276WG	S-44	S 44	. M	. CM	. CM	1

#F:SV=20,ST= 0,H=0;WT:SV=29.0800,ST= 0.0000,H/P= 0.0000; PHI LIM:CS= 0.00,FN= 0.00

SAMPLE ANALYZED BY THE FOLLOWING METHOD(S):

SIZE RANGE	METHOD
2.0000- 0.0625MM	SIEVES

UNEDITED SAMPLE WEIGHTS IN GRAMS:

SIEVES	RSA	HYDROPHOTOMETER	PAN	TOTAL
29.0800				29.0800 (G)

PARTICLE SIZE DISTRIBUTION:

PHI	MM	PERCENT	CUM PERCENT
-0.7500	1.6818	0.344	0.344
-0.5000	1.4142	0.516	0.860
-0.2500	1.1892	0.653	1.513
0.0000	1.0000	0.928	2.442
0.2500	0.8409	1.651	4.092
0.5000	0.7071	1.685	5.777
0.7500	0.5946	2.992	8.769
1.0000	0.5000	3.542	12.311
1.2500	0.4204	10.488	22.799
1.5000	0.3536	30.502	53.301
1.7500	0.2973	17.297	70.598
2.0000	0.2500	12.895	83.494
2.2500	0.2102	8.047	91.541
2.5000	0.1768	2.682	94.223
2.7500	0.1486	3.542	97.765
3.0000	0.1250	0.963	98.728
3.2500	0.1051	0.585	99.312
3.5000	0.0884	0.275	99.587
3.7500	0.0743	0.206	99.794
4.0000	0.0625	0.206	100.000

SIZE CLASS RATIOS:

GRAVEL	=	0.000PCT	GRAVEL/SAND	=	0.000
SAND	=	100.000PCT	SAND/SILT	=	**********
SILT	=	-0.000PCT	SILT/CLAY	=	0.000
CLAY	=	0.000PCT	SAND/CLAY	=	0.000
MUD	=	-0.000PCT	SAND/MUD	=	**********
			GRAVEL/MUD	=	0.000

SEA276WG

CRUISE	STATION	SAMPLE TYPE/NUMBER	TOTAL LENGTH	SAMPLE CENTER	SAMPLE LENGTH	METHODS
S276WG	S-44	S 44	. M	. CM	. CM	1

INTERPOLATED SIZES USED IN GRAPHICAL STATISTICS:

CUM_PERCENT	05.00	10.00	16.00	25.00	50.00	75.00	84.00	90.00	95.00	CUM_PERCENT
PHI	0.390	0.844	1.135	1.276	1.484	1.822	2.004	2.170	2.514	PHI
MM	0.7632	0.5569	0.4555	0.4130	0.3574	0.2829	0.2494	0.2222	0.1751	MM

GRAPHICAL STATISTICS:

FOLK_&_WARD_(PHI)		_INMAN_(PHI)___		_IRASK_(MM)___	
MEDIAN=	1.4842	MEDIAN=	1.4842	MEDIAN=	0.3574
MEAN =	1.5408	MEAN =	1.5691	MEAN =	0.3479
SORTING=	0.5391	SORTING=	0.4346	SORTING=	1.2083
SKEWNESS=	0.0824	SKEW 16/84=	0.1953	SKEWNESS=	0.9143
		SKEW 05/95=	-0.0746		
KURTOSIS=	1.5941	KURTOSIS=	1.4436	KURTOSIS=	0.1944

CLASS MID-POINTS(PHI) USED IN THE MOMENT CALCULATIONS:

-0.88	-0.63	-0.38	-0.13	0.13	0.38	0.63	0.88	1.13	1.38	1.63	1.88	2.13	2.38	2.63
2.88	3.13	3.38	3.63	3.88										

MOMENT MEASURES:

	--PHI---		---MM---
FIRST (ABOUT ORIGIN)=	1.5069		0.3519
SECOND (ABOUT MEAN) =	0.3808	VARIANCE	
SECOND (ABOUT MEAN) =	0.6171	STANDARD DEVIATION	
THIRD (ABOUT MEAN) =	-0.1642		
FOURTH (ABOUT MEAN) =	1.1803		

SEA276WG

CRUISE	STATION	SAMPLE TYPE/NUMBER	TOTAL LENGTH	SAMPLE CENTER	SAMPLE LENGTH	METHODS
S276WG	S-44	S 44	. M	. CM	. CM	1

MODAL ANALYSIS

2 MODE(S) DETECTED IN THIS SAMPLE.

PHI	MM	PERCENT	
-0.750	1.6818	0.3439	
-0.500	1.4142	0.5158	
-0.250	1.1892	0.6534	
0.000	1.0000	0.9285	
0.250	0.8409	1.6506	
0.500	0.7071	1.6850	
0.750	0.5946	2.9917	
1.000	0.5000	3.5420	
1.250	0.4204	10.4883	
1.500	0.3536	30.5021	** MODE **
1.750	0.2973	17.2971	
2.000	0.2500	12.8955	
2.250	0.2102	8.0468	
2.500	0.1768	2.6823	
2.750	0.1486	3.5420	** MODE **
3.000	0.1250	0.9629	
3.250	0.1051	0.5846	
3.500	0.0884	0.2751	
3.750	0.0743	0.2063	
4.000	0.0625	0.2063	

SEA276WG

CRUISE	STATION	SAMPLE TYPE	SAMPLE NUMBER	TOTAL LENGTH	SAMPLE CENTER	SAMPLE LENGTH	METHODS
S276WG	S-44	S	44	. M	. CM	. CM	1

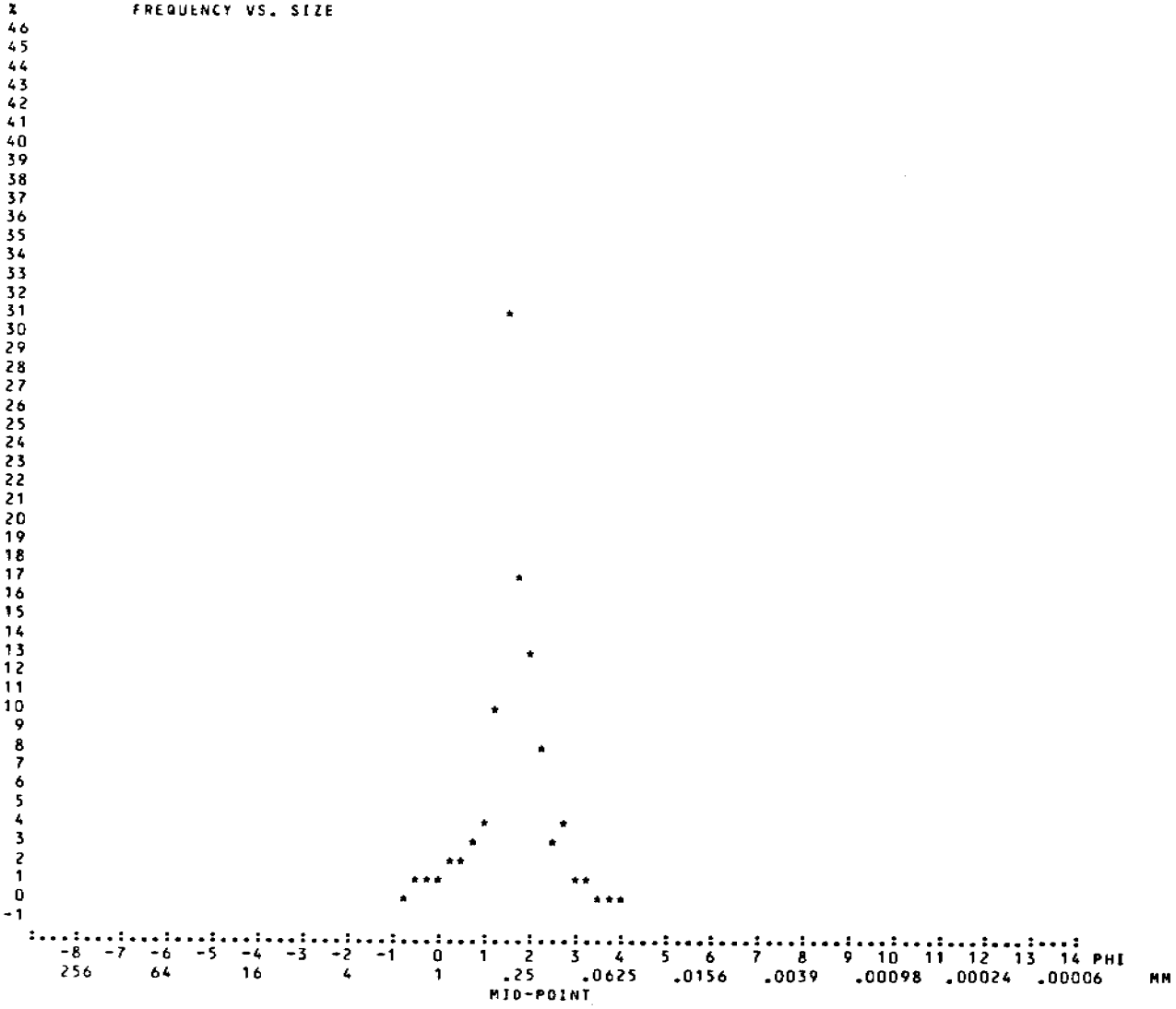

SEA276WG

CRUISE	STATION	SAMPLE TYPE/NUMBER	TOTAL LENGTH	SAMPLE CENTER	SAMPLE LENGTH	METHODS
S276WG	S-44	S 44	. M	. CM	. CM	1

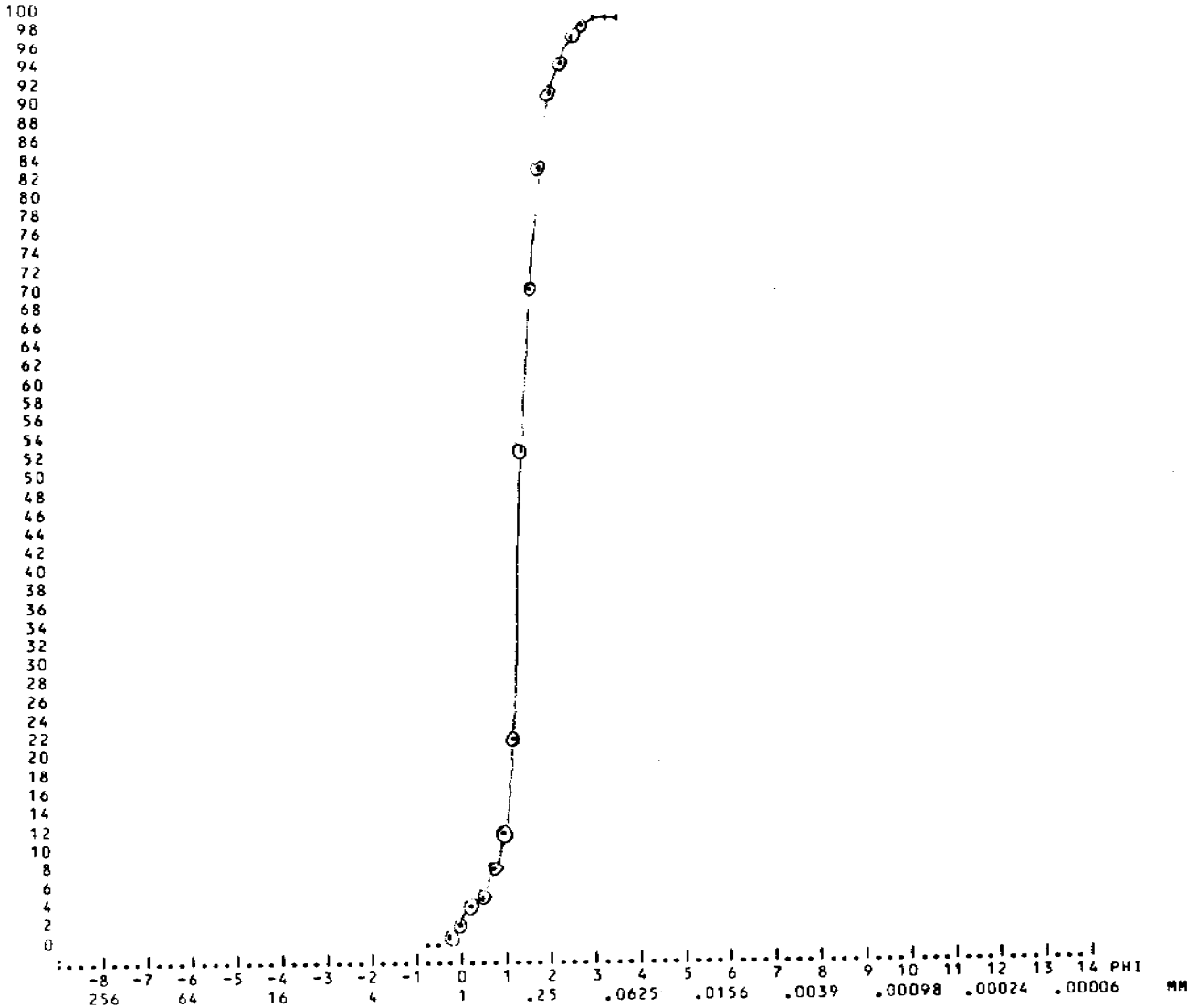

SEA276WG

CRUISE	STATION	SAMPLE TYPE,NUMBER	TOTAL LENGTH	SAMPLE CENTER	SAMPLE LENGTH	METHODS
S276WG	S-44S2	S44S2	. M	. CM	. CM	1

#F:SV=20,ST= 0,H=0;WT:SV=24.2800,ST= 0.0000,H/P= 0.0000; PHI LIM:CS= 0.00,FN= 0.00

SAMPLE ANALYZED BY THE FOLLOWING METHOD(S):

SIZE RANGE		METHOD
2.0000-	0.0625MM	SIEVES

UNEDITED SAMPLE WEIGHTS IN GRAMS:

SIEVES	BSA	HYDROPHOTOMETER	PAN	TOTAL
24.2700				24.2700 (G)

PARTICLE SIZE DISTRIBUTION:

PHI	MM	PERCENT	CUM PERCENT
-0.7500	1.6818	1.319	1.319
-0.5000	1.4142	2.678	3.997
-0.2500	1.1892	2.637	6.634
0.0000	1.0000	3.090	9.724
0.2500	0.8409	3.214	12.938
0.5000	0.7071	3.337	16.275
0.7500	0.5946	3.131	19.407
1.0000	0.5000	2.802	22.208
1.2500	0.4204	7.540	29.749
1.5000	0.3536	32.468	62.217
1.7500	0.2973	18.789	81.005
2.0000	0.2500	10.713	91.718
2.2500	0.2102	5.150	96.869
2.5000	0.1768	1.360	98.228
2.7500	0.1486	1.277	99.506
3.0000	0.1250	0.165	99.670
3.2500	0.1051	0.165	99.835
3.5000	0.0884	0.082	99.918
3.7500	0.0743	0.062	99.979
4.0000	0.0625	0.021	100.000

SIZE CLASS RATIOS:

GRAVEL=	0.000PCT	GRAVEL/SAND=	0.000
SAND =	100.000PCT	SAND/SILT =99999.999	
SILT =	0.000PCT	SILT/CLAY =	0.000
CLAY =	0.000PCT	SAND/CLAY =	0.000
MUD =	0.000PCT	SAND/MUD =99999.999	
		GRAVEL/MUD =	0.000

SEA276WG

CRUISE	STATION	SAMPLE TYPE,NUMBER	TOTAL LENGTH	SAMPLE CENTER	SAMPLE LENGTH	METHODS
S276WG	S-44S2	S44S2	. M	. CM	. CM	1

INTERPOLATED SIZES USED IN GRAPHICAL STATISTICS:

CUM_PERCENT	05.00	10.00	16.00	25.00	50.00	75.00	84.00	90.00	95.00	CUM_PERCENT
PHI	-0.403	0.022	0.479	1.133	1.471	1.653	1.798	1.945	2.091	PHI
MM	1.3224	0.9850	0.7174	0.4561	0.3607	0.3180	0.2877	0.2597	0.2348	MM

GRAPHICAL STATISTICS:

FOLK_&_WARD_(PHI)		_INMAN_(PHI)___		_IRASK_(MM)___	
MEDIAN=	1.4711	MEDIAN=	1.4711	MEDIAN=	0.3607
MEAN =	1.2493	MEAN =	1.1384	MEAN =	0.3870
SORTING=	0.7074	SORTING=	0.6592	SORTING=	1.1975
SKEWNESS=	-0.5039	SKEW 16/84=	-0.5047	SKEWNESS=	1.1147
		SKEW 05/95=	-0.9517		
KURTOSIS=	1.9650	KURTOSIS=	0.8916	KURTOSIS=	0.0952

CLASS MID-POINTS(PHI) USED IN THE MOMENT CALCULATIONS:

-0.88	-0.63	-0.38	-0.13	0.13	0.38	0.63	0.88	1.13	1.38	1.63	1.88	2.13	2.38	2.63
2.88	3.13	3.38	3.63	3.88										

MOMENT MEASURES:

	--PHI---	---MM---
FIRST (ABOUT ORIGIN)=	1.2470	0.4213
SECOND (ABOUT MEAN) =	0.5382 VARIANCE	
SECOND (ABOUT MEAN) =	0.7336 STANDARD DEVIATION	
THIRD (ABOUT MEAN) =	-0.5160	
FOURTH (ABOUT MEAN) =	0.5049	

SEA276WG

CRUISE	STATION	SAMPLE TYPE,NUMBER	TOTAL LENGTH	SAMPLE CENTER	SAMPLE LENGTH	METHODS
S276WG	S-44S2	S44S2	. M	. CM	. CM	1

MODAL ANALYSIS

3 MODE(S) DETECTED IN THIS SAMPLE.

--PHI--	---MM--	--PERCENT	
-0.750	1.6818	1.3185	
-0.500	1.4142	2.6782	** MODE **
-0.250	1.1892	2.6370	
0.000	1.0000	3.0902	
0.250	0.8409	3.2138	
0.500	0.7071	3.3375	** MODE **
0.750	0.5946	3.1314	
1.000	0.5000	2.8018	
1.250	0.4204	7.5402	
1.500	0.3536	32.4681	** MODE **
1.750	0.2973	18.7886	
2.000	0.2500	10.7128	
2.250	0.2102	5.1504	
2.500	0.1768	1.3597	
2.750	0.1486	1.2773	
3.000	0.1250	0.1648	
3.250	0.1051	0.1648	
3.500	0.0884	0.0824	
3.750	0.0743	0.0618	
4.000	0.0625	0.0206	

SEA276WG

CRUISE	STATION	SAMPLE TYPE,NUMBER	TOTAL LENGTH	SAMPLE CENTER	SAMPLE LENGTH	METHODS
S276WG	S-44S2	S44S2	. M	. CM	. CM	1

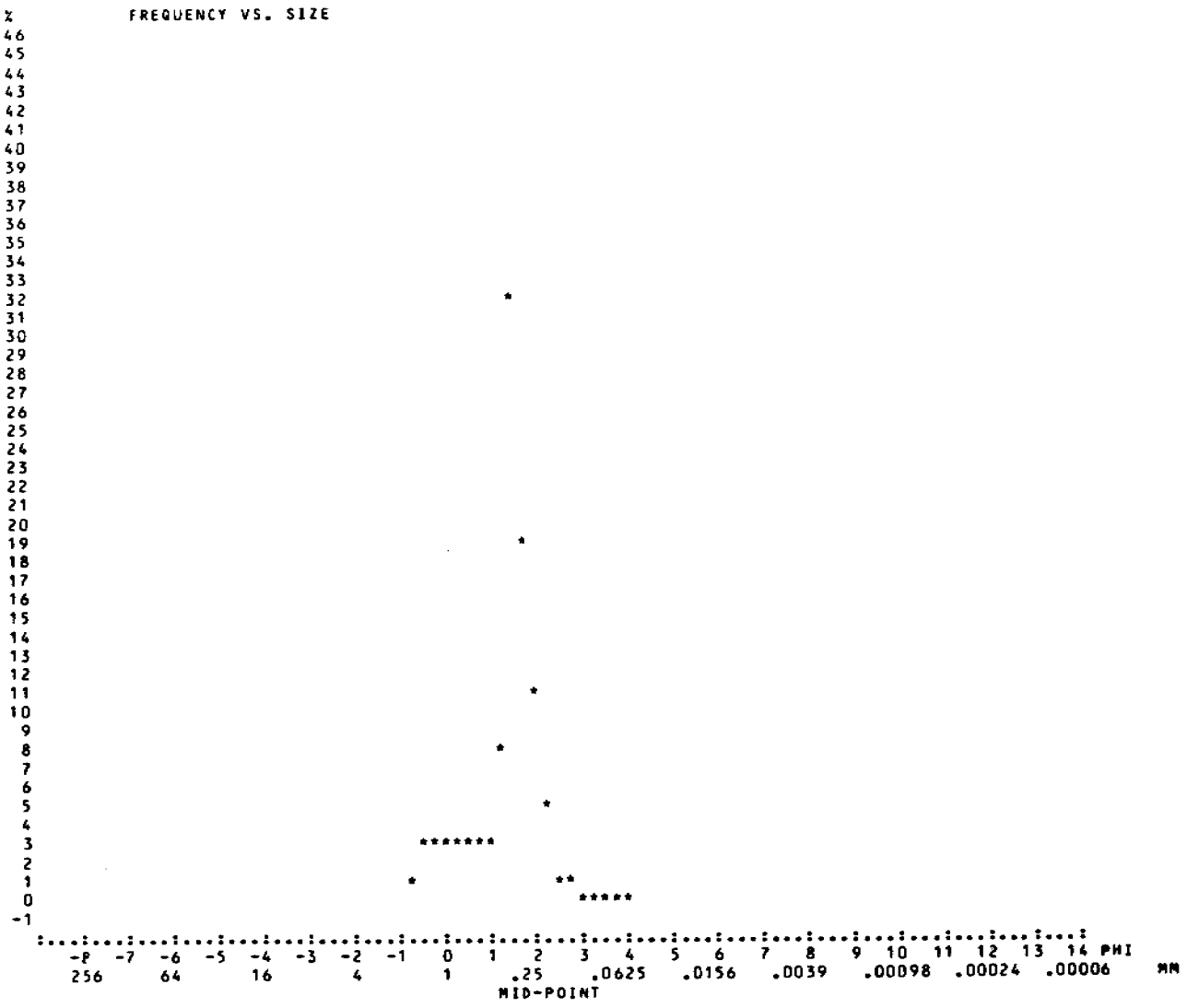

SEA276WG

CRUISE	STATION	SAMPLE TYPE/NUMBER	TOTAL LENGTH	SAMPLE CENTER	SAMPLE LENGTH	METHODS
S276WG	S-44S2	S44S2	. M	. CM	. CM	1

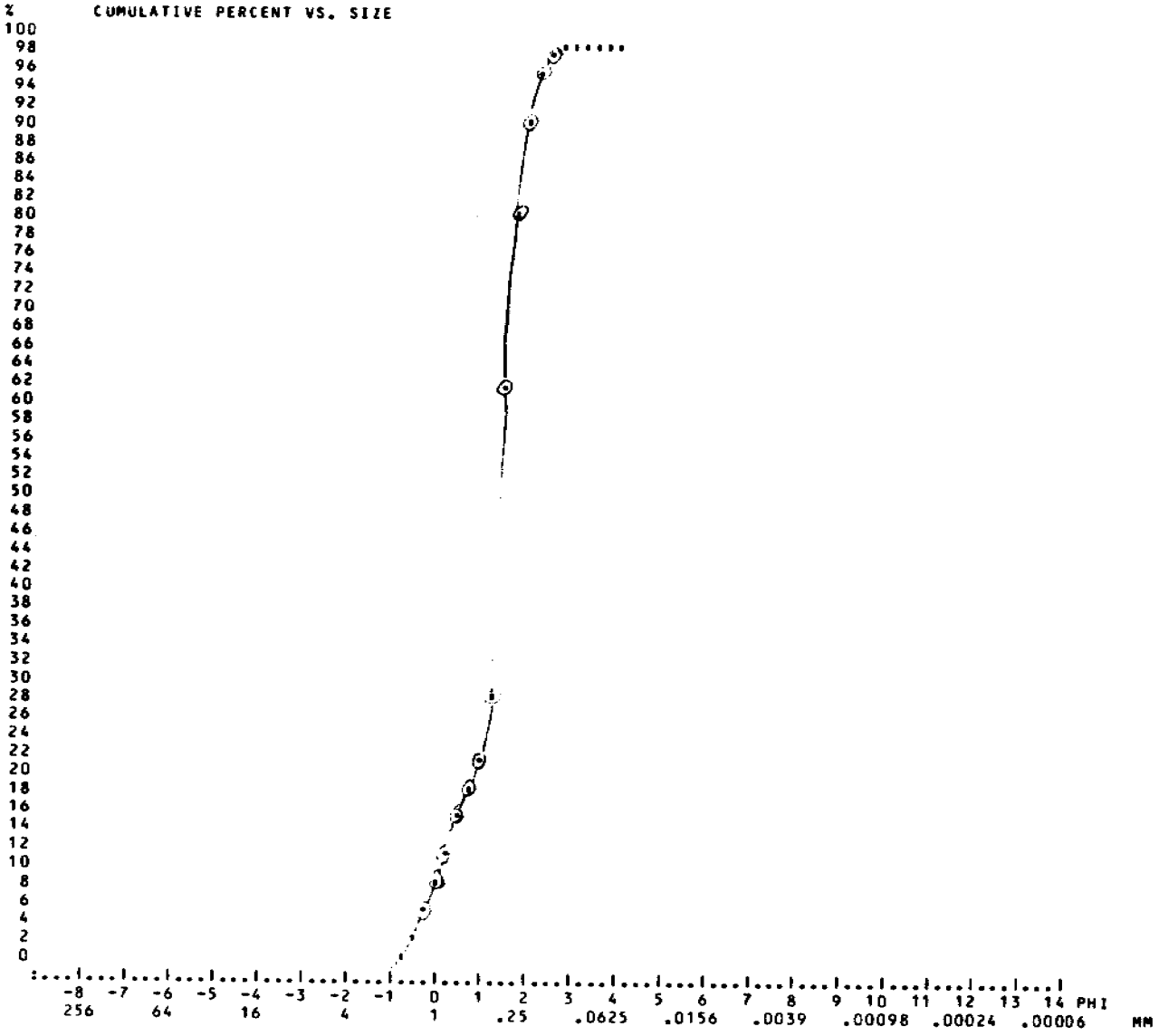

SIEVE...

CRITER	...	...	TEST LENGTH	SAMPLE CENTER	... LENGTH	METHODS
S27GWC	...	...	. %	. GM	. GM	1

AF:SV=... PHI LIM:CS= 0.00,FN= 0.00

SAMPLE ... FOR THE FOLLOWING METHOD(S):

...	METHOD
2.0000- ...	SIEVES

UNEDITED SAMPLE WEIGHTS IN GRAMS:

SIEVE	...	...	CAN	TOTAL
23.7800				23.7800 (G)

PARTICLE SIZE DISTRIBUTION:

PHI	...	PERCENT	CUM. PERCENT
-0.7500	1.0000	0.757	0.757
-0.5000	1.0000	0.000	0.757
-0.2500	1.0000	1.000	3.791
0.0000	1.0000	3.995	7.696
0.2500	0.8409	7.485	15.181
0.5000	0.7071	12.321	27.502
0.7500	0.5946	22.077	49.579
1.0000	0.5000	21.395	69.975
1.2500	0.4204	11.775	81.749
1.5000	0.3536	5.182	91.932
1.7500	0.2973	3.027	95.458
2.0000	0.2500	2.565	98.024
2.2500	0.2102	1.135	99.159
2.5000	0.1768	0.294	99.453
2.7500	0.1486	0.294	99.748
3.0000	0.1250	0.063	99.811
3.2500	0.1051	0.063	99.874
3.5000	0.0884	0.063	99.937
3.7500	0.0743	0.042	99.979
4.0000	0.0625	0.021	100.000

SIZE CLASS RATIOS:

GRAVEL	= 0.000 PCT	GRAVEL/SAND	= 0.000
SAND	= 100.000 PCT	SAND/SILT	=99999.999
SILT	= 0.000 PCT	SILT/CLAY	= 0.000
CLAY	= 0.000 PCT	SAND/CLAY	= 0.000
MUD	= 0.000 PCT	SAND/MUD	=99999.999
		GRAVEL/MUD	= 0.000

SEASAMPLE

CRUISE	STATION	LATITUDE	LONGITUDE	WATER DEPTH	SAMPLE CENTER	SAMPLE LENGTH	METHODS
S270A0	1-47	34°53'	[illegible]	. M	. CM	. CM	1

INTERPOLATED VALUES FROM CUMULATIVE GRAPHICAL STATISTICS:

CUM_PERCENT	5.00	10.00	16.00	25.00	50.00	75.00	84.00	90.00	95.00	CUM_PERCENT
PHI	-0.134	0.096	0.271	0.461	0.754	1.099	1.280	1.438	1.714	PHI
MM	1.094	0.9356	0.8269	0.7267	0.5930	0.4669	0.4117	0.3691	0.3048	MM

GRAPHICAL STATISTICS:

FOLK-WARD (PHI)		INMAN (PHI)		TRASK (MM)	
MEDIAN=	0.7559	MEDIAN=	0.7559	MEDIAN=	0.5930
MEAN =	0.7756	MEAN =	0.7756	MEAN =	0.5968
SORTING=	0.5047	SORTING=	0.5046	SORTING=	1.2476
SKEWNESS=	0.0404	SKEW 16/84=	0.1430	SKEWNESS=	0.9649
		SKEW 05/95=	0.0692		
KURTOSIS=	1.3681	KURTOSIS=	0.8352	KURTOSIS=	0.2293

CLASS MIDPOINTS (PHI) USED IN THE MOMENT CALCULATIONS:

-0.38	-0.63	-0.88	-1.13	1.13	0.38	0.63	0.88	1.13	1.38	1.63	1.88	2.13	2.38	2.63
2.88	3.13	3.38	3.63	3.88									

MOMENT MEASURES:

	PHI	MM
FIRST (ABOUT ORIGIN)=	0.7718	0.5857
SECOND (ABOUT MEAN) =	0.5215 VARIANCE	
SECOND (ABOUT MEAN) =	0.5670 STANDARD DEVIATION	
THIRD (ABOUT MEAN) =		0.6933
FOURTH (ABOUT MEAN) =		0.6731

SEA376WG

CRUISE	STATION	CORE NUMBER	TOTAL LENGTH	SAMPLE CENTER	SAMPLE LENGTH	METHODS
S276WG	S-47	34751	. M	. CM	. CM	1

MODAL ANALYSIS

1 MODE(S) ESTIMATED IN THIS SAMPLE.

--PHI--	----%---	--LOG(PHI)	
-0.750	1.6818	0.7509	
-0.500	1.4142	1.3036	
-0.250	1.1892	1.6400	
0.000	1.0000	3.7950	
0.250	0.8409	7.4053	
0.500	0.7071	12.3213	
0.750	0.5946	22.0774	** MODE **
1.000	0.5000	20.3953	
1.250	0.4204	11.7746	
1.500	0.3536	9.8823	
1.750	0.2973	3.8267	
2.000	0.2500	2.5452	
2.250	0.2102	1.1854	
2.500	0.1768	0.2944	
2.750	0.1486	0.2944	
3.000	0.1250	0.0631	
3.250	0.1051	0.0631	
3.500	0.0884	0.0631	
3.750	0.0743	0.0421	
4.000	0.0625	0.0210	

SEA276WG

CRUISE	STATION	SAMPLE TYPE,NUMBER	TOTAL LENGTH	SAMPLE CENTER	SAMPLE LENGTH	METHODS
S276WG	S-47	S47S1	. M	. CM	. CM	1

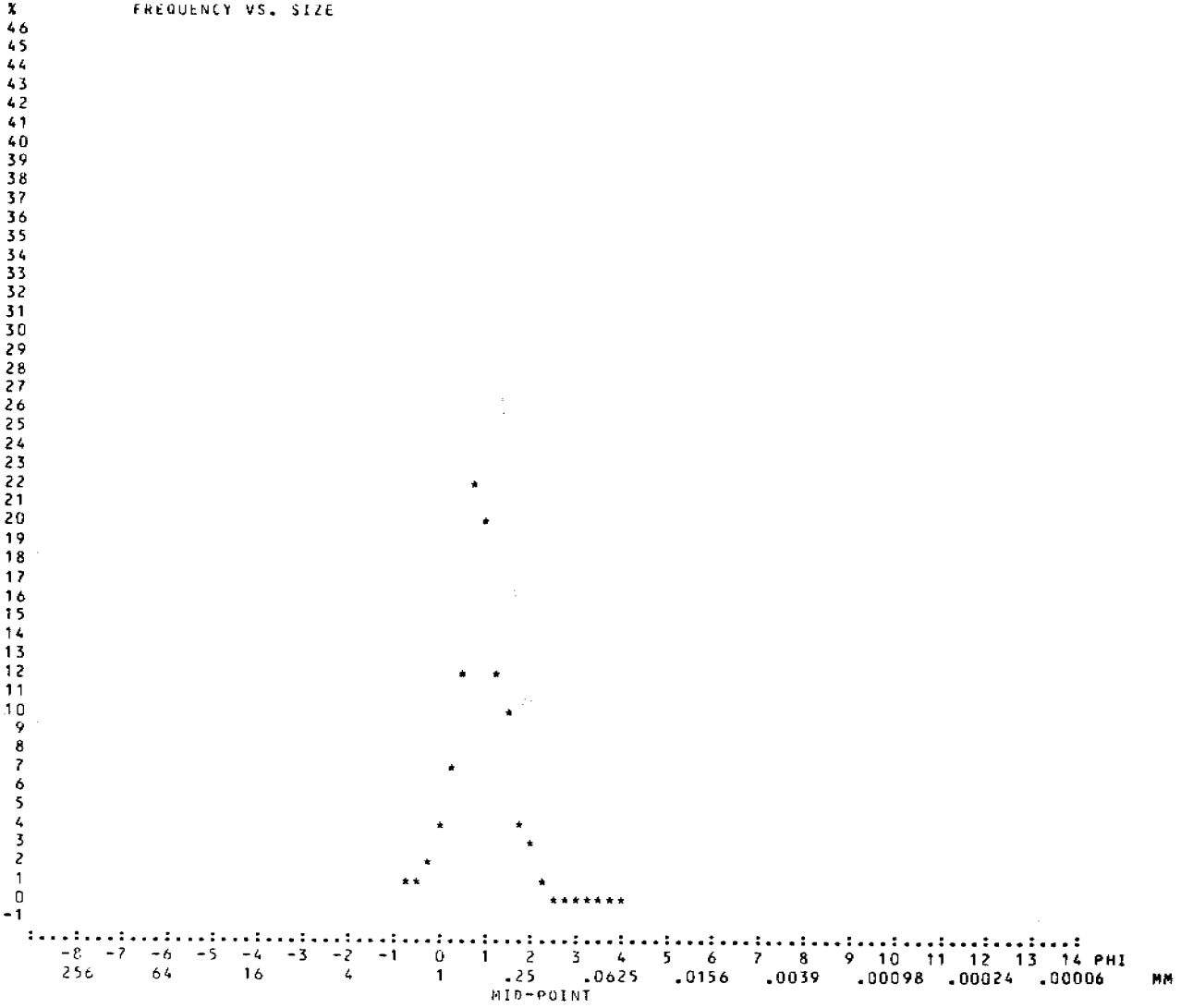

SEA37oWG

CRUISE	STATION	SAMPLE TYPE/NUMBER	TOTAL LENGTH	SAMPLE CENTER	SAMPLE LENGTH	METHODS
S276WG	S-47	S47S1	. M	. CM	. CM	1

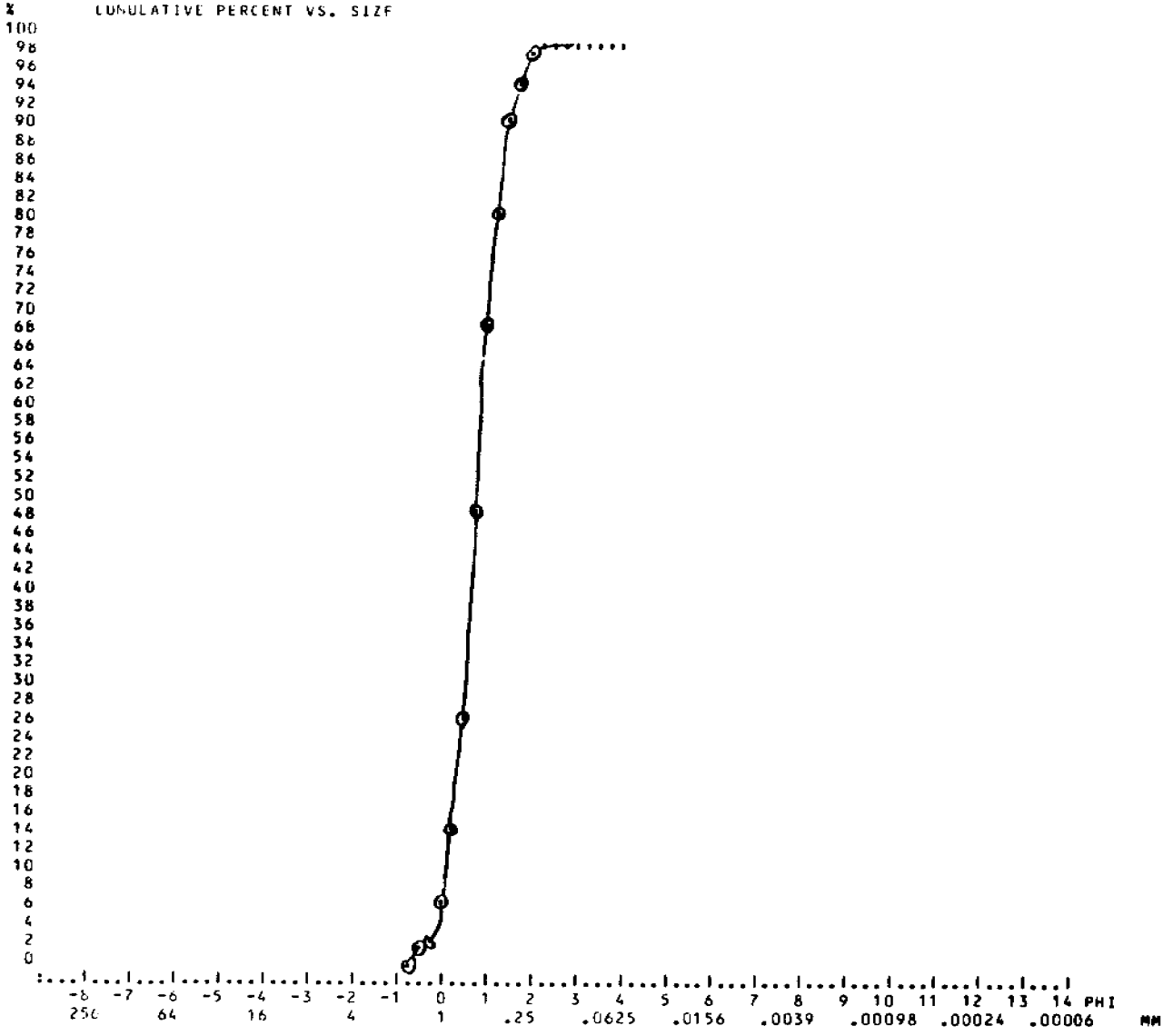

SEA276WG

CRUISE	STATION	SAMPLE TYPE,NUMBER	TOTAL LENGTH	SAMPLE CENTER	SAMPLE LENGTH	METHODS
S276WG	S-152	S152	. M	. CM	. CM	1

#F:SV=20,ST= 0,H=0;WT:SV=26.9200,ST= 0.0000,H/P= 0.0000; PHI LIM:CS= 0.00,FN= 0.00

SAMPLE ANALYZED BY THE FOLLOWING METHOD(S):

SIZE RANGE	METHOD
2.0000- 0.0625MM	SIEVES

UNEDITED SAMPLE WEIGHTS IN GRAMS:

SIEVES	RSA	HYDROPHOTOMETER	PAN	TOTAL
26.8700				26.8700 (G)

PARTICLE SIZE DISTRIBUTION:

PHI	MM	PERCENT	CUM PERCENT
-0.7500	1.6818	0.037	0.037
-0.5000	1.4142	0.037	0.074
-0.2500	1.1892	0.037	0.112
0.0000	1.0000	0.037	0.149
0.2500	0.8409	0.149	0.298
0.5000	0.7071	0.149	0.447
0.7500	0.5946	0.893	1.340
1.0000	0.5000	3.722	5.061
1.2500	0.4204	19.352	24.414
1.5000	0.3536	40.863	65.277
1.7500	0.2973	13.398	78.675
2.0000	0.2500	8.709	87.384
2.2500	0.2102	6.736	94.120
2.5000	0.1768	2.419	96.539
2.7500	0.1486	1.861	98.400
3.0000	0.1250	0.744	99.144
3.2500	0.1051	0.484	99.628
3.5000	0.0884	0.186	99.814
3.7500	0.0743	0.112	99.926
4.0000	0.0625	0.074	100.000

SIZE CLASS RATIOS:

GRAVEL =	0.000PCT	GRAVEL/SAND =	0.000
SAND =	100.000PCT	SAND/SILT =	**********
SILT =	-0.000PCT	SILT/CLAY =	0.000
CLAY =	0.000PCT	SAND/CLAY =	0.000
MUD =	-0.000PCT	SAND/MUD =	**********
		GRAVEL/MUD =	0.000

SEA276WG

CRUISE	STATION	SAMPLE TYPE/NUMBER	TOTAL LENGTH	SAMPLE CENTER	SAMPLE LENGTH	METHODS
S276WG	S-152	S152	. M	. CM	. CM	1

INTERPOLATED SIZES USED IN GRAPHICAL STATISTICS:

CUM_PERCENT	05.00	10.00	16.00	25.00	50.00	75.00	84.00	90.00	95.00	CUM_PERCENT
PHI	0.996	1.152	1.141	1.252	1.383	1.669	1.894	2.055	2.331	PHI
MM	0.5014	0.4502	0.4533	0.4198	0.3833	0.3144	0.2691	0.2406	0.1987	MM

GRAPHICAL STATISTICS:

FOLK & WARD (PHI)		INMAN (PHI)		IRASK (MM)	
MEDIAN=	1.3834	MEDIAN=	1.3834	MEDIAN=	0.3833
MEAN =	1.4729	MEAN =	1.5176	MEAN =	0.3671
SORTING=	0.3905	SORTING=	0.3763	SORTING=	1.1555
SKEWNESS=	0.3880	SKEW 16/84=	0.3565	SKEWNESS=	0.8984
		SKEW 05/95=	0.7443		
KURTOSIS=	1.3124	KURTOSIS=	0.7743	KURTOSIS=	0.2515

CLASS MID-POINTS(PHI) USED IN THE MOMENT CALCULATIONS:

-0.88	-0.63	-0.38	-0.13	0.13	0.38	0.63	0.88	1.13	1.38	1.63	1.88	2.13	2.38	2.63
2.88	3.13	3.38	3.63	3.88										

MOMENT MEASURES:

	PHI	MM
FIRST (ABOUT ORIGIN)=	1.4979	0.3541
SECOND (ABOUT MEAN) =	0.1911 VARIANCE	
SECOND (ABOUT MEAN) =	0.4371 STANDARD DEVIATION	
THIRD (ABOUT MEAN) =	0.5602	
FOURTH (ABOUT MEAN) =	1.7280	

SEA276WG

CRUISE	STATION	SAMPLE TYPE,NUMBER	TOTAL LENGTH	SAMPLE CENTER	SAMPLE LENGTH	METHODS
S276WG	S-152	S152	. M	. CM	. CM	1

MODAL ANALYSIS
1 MODE(S) DETECTED IN THIS SAMPLE.

PHI	MM	PERCENT	
-0.750	1.6818	0.0372	
-0.500	1.4142	0.0372	
-0.250	1.1892	0.0372	
0.000	1.0000	0.0372	
0.250	0.8409	0.1489	
0.500	0.7071	0.1489	
0.750	0.5946	0.8932	
1.000	0.5000	3.7216	
1.250	0.4204	19.3524	
1.500	0.3536	40.8634	** MODE **
1.750	0.2973	13.3978	
2.000	0.2500	8.7086	
2.250	0.2102	6.7361	
2.500	0.1768	2.4191	
2.750	0.1486	1.8608	
3.000	0.1250	0.7443	
3.250	0.1051	0.4838	
3.500	0.0884	0.1861	
3.750	0.0743	0.1116	
4.000	0.0625	0.0744	

SEA276WG

CRUISE	STATION	SAMPLE TYPE,NUMBER	TOTAL LENGTH	SAMPLE CENTER	SAMPLE LENGTH	METHODS
S276WG	S-152	S152	. M	. CM	. CM	1

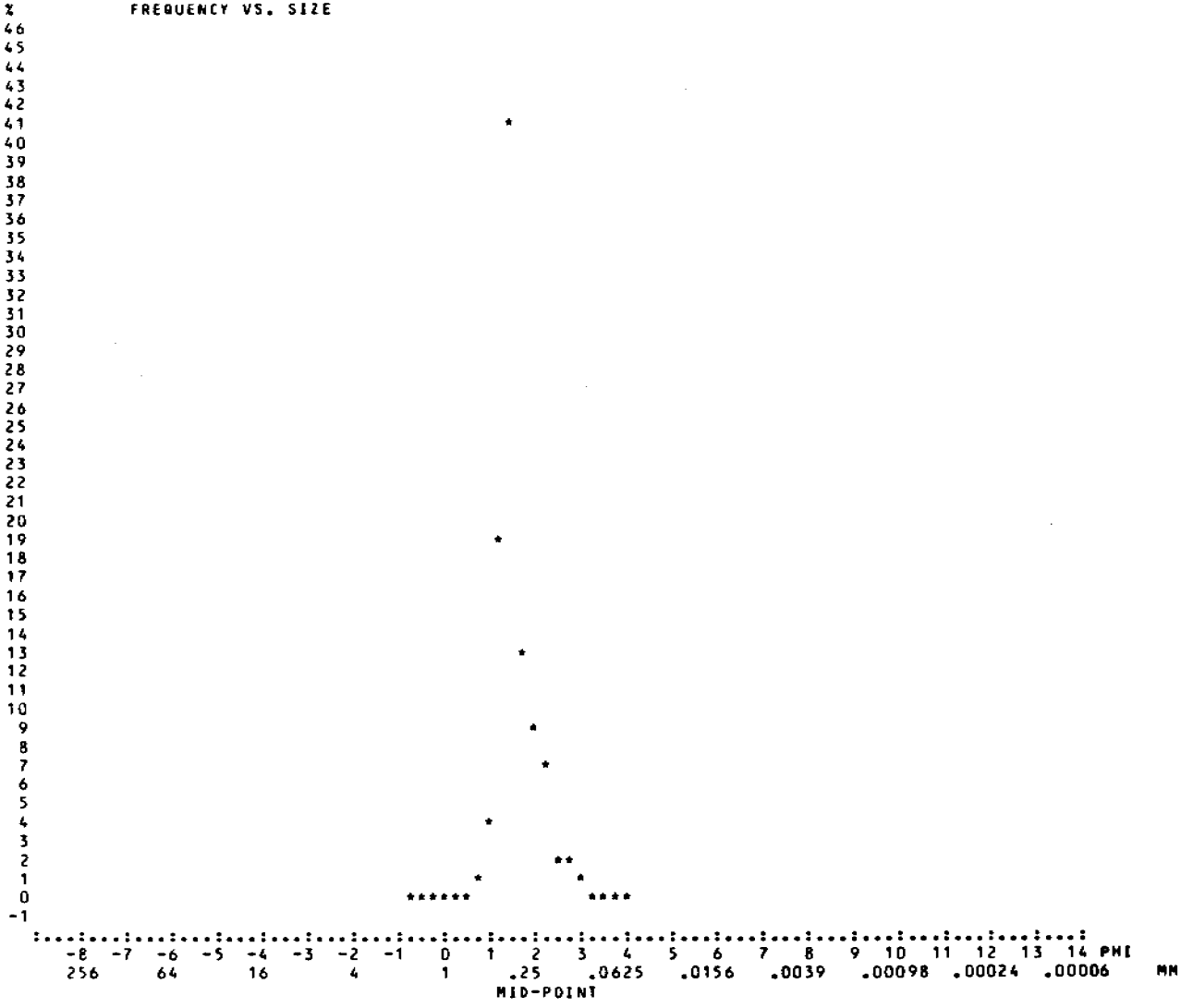

SEA276WG

CRUISE	STATION	SAMPLE TYPE,NUMBER	TOTAL LENGTH	SAMPLE CENTER	SAMPLE LENGTH	METHODS
S276WG	S-152	S152	. M	. CM	. CM	1

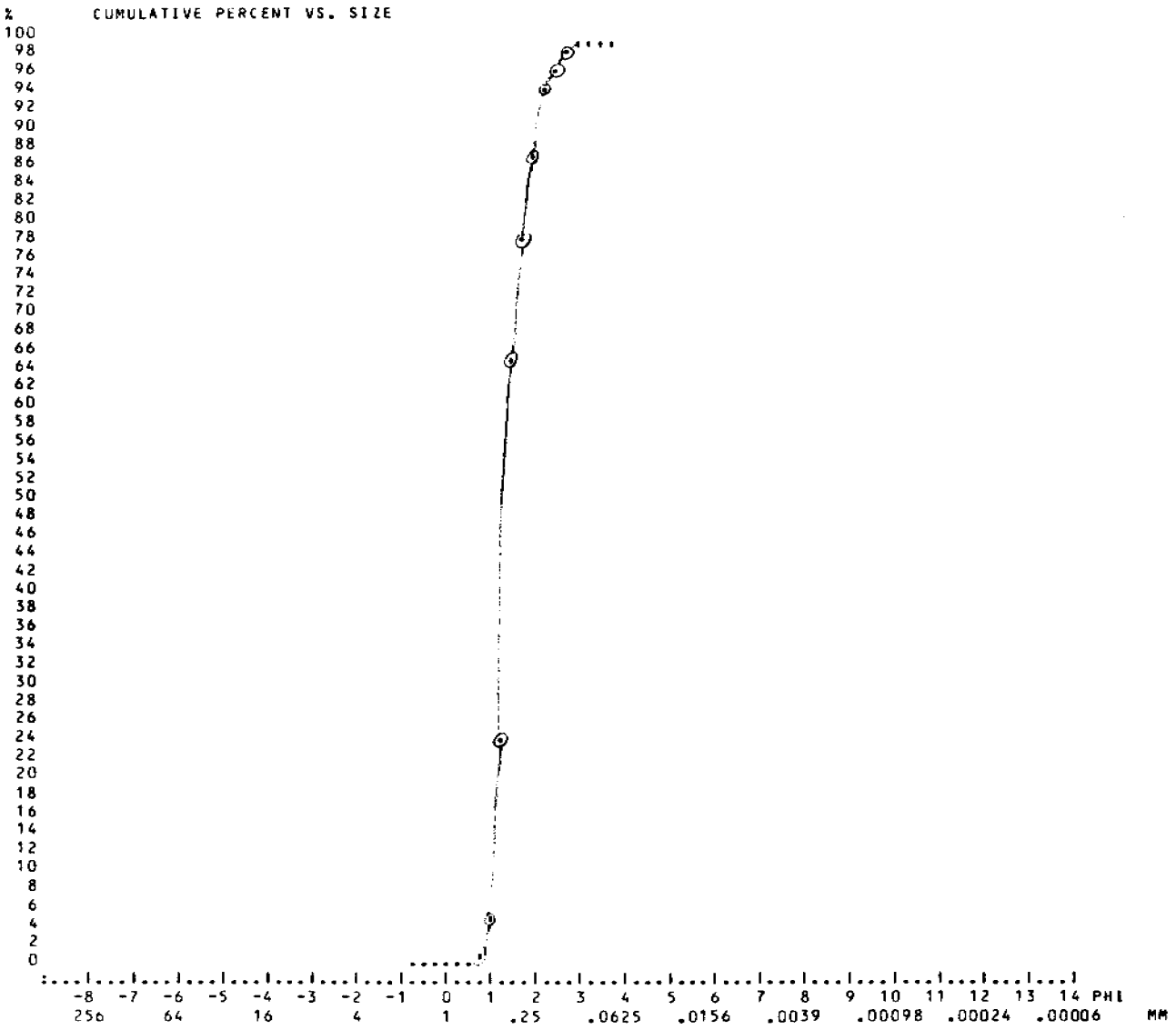

SEA276WG

CRUISE	STATION	SAMPLE TYPE,NUMBER	TOTAL LENGTH	SAMPLE CENTER	SAMPLE LENGTH	METHODS
S276WG	S-153	S153	. M	. CM	. CM	1

#F:SV=20,ST= 0,H=0;WT:SV=30.0500,ST= 0.0000,H/P= 0.0000; PHI LIM:CS= 0.00,FN= 0.00

SAMPLE ANALYZED BY THE FOLLOWING METHOD(S):

SIZE RANGE	METHOD
2.0000- 0.0625MM	SIEVES

UNEDITED SAMPLE WEIGHTS IN GRAMS:

SIEVES	BSA	HYDROPHOTOMETER	PAN	TOTAL
30.0600				30.0600 (G)

PARTICLE SIZE DISTRIBUTION:

PHI	MM	PERCENT	CUM PERCENT
-0.7500	1.6818	0.000	0.000
-0.5000	1.4142	0.033	0.033
-0.2500	1.1892	0.033	0.067
0.0000	1.0000	0.033	0.100
0.2500	0.8409	0.033	0.133
0.5000	0.7071	0.033	0.166
0.7500	0.5946	0.033	0.200
1.0000	0.5000	0.100	0.299
1.2500	0.4204	0.166	0.466
1.5000	0.3536	0.333	0.798
1.7500	0.2973	0.432	1.231
2.0000	0.2500	1.331	2.562
2.2500	0.2102	16.334	18.896
2.5000	0.1768	20.293	39.188
2.7500	0.1486	45.975	85.163
3.0000	0.1250	10.612	95.775
3.2500	0.1051	2.728	98.503
3.5000	0.0884	0.732	99.235
3.7500	0.0743	0.466	99.701
4.0000	0.0625	0.299	100.000

SIZE CLASS RATIOS:

GRAVEL =	0.000PCT	GRAVEL/SAND =	0.000
SAND =	100.000PCT	SAND/SILT =	**********
SILT =	-0.000PCT	SILT/CLAY =	0.000
CLAY =	0.000PCT	SAND/CLAY =	0.000
MUD =	-0.000PCT	SAND/MUD =	**********
		GRAVEL/MUD =	0.000

SEA276WG

CRUISE	STATION	SAMPLE TYPE,NUMBER	TOTAL LENGTH	SAMPLE CENTER	SAMPLE LENGTH	METHODS
S276WG	S-153	S153	. M	. CM	. CM	1

INTERPOLATED SIZES USED IN GRAPHICAL STATISTICS:

CUM_PERCENT	05.00	10.00	16.00	25.00	50.00	75.00	84.00	90.00	95.00	CUM_PERCENT
PHI	2.204	2.114	2.206	2.333	2.518	2.655	2.738	2.788	2.961	PHI
MM	0.2170	0.2310	0.2168	0.1984	0.1746	0.1587	0.1499	0.1448	0.1284	MM

GRAPHICAL STATISTICS:

FOLK_&_WARD_(PHI)		_INMAN_(PHI)___		_IRASK_(MM)___	
MEDIAN=	2.5177	MEDIAN=	2.5177	MEDIAN=	0.1746
MEAN =	2.4871	MEAN =	2.4719	MEAN =	0.1786
SORTING=	0.2478	SORTING=	0.2662	SORTING=	1.1181
SKEWNESS=	-0.0002	SKEW 16/84=	-0.1721	SKEWNESS=	1.0329
		SKEW 05/95=	0.2441		
KURTOSIS=	0.9629	KURTOSIS=	0.4217	KURTOSIS=	0.2302

CLASS MID-POINTS(PHI) USED IN THE MOMENT CALCULATIONS:

-0.88	-0.63	-0.38	-0.13	0.13	0.38	0.63	0.88	1.13	1.38	1.63	1.88	2.13	2.38	2.63
2.88	3.13	3.38	3.63	3.88										

MOMENT MEASURES:

	--PHI---	---MM---
FIRST (ABOUT ORIGIN)=	2.5187	0.1745
SECOND (ABOUT MEAN) =	0.1070 VARIANCE	
SECOND (ABOUT MEAN) =	0.3272 STANDARD DEVIATION	
THIRD (ABOUT MEAN) =	-0.5133	
FOURTH (ABOUT MEAN) =	5.0054	

SEA276WG

CRUISE	STATION	SAMPLE TYPE,NUMBER	TOTAL LENGTH	SAMPLE CENTER	SAMPLE LENGTH	METHODS
S276WG	S-153	S153	. M	. CM	. CM	1

MODAL ANALYSIS

1 MODE(S) DETECTED IN THIS SAMPLE.

PHI	MM	PERCENT	
-0.750	1.6818	0.0000	
-0.500	1.4142	0.0333	
-0.250	1.1892	0.0333	
0.000	1.0000	0.0333	
0.250	0.8409	0.0333	
0.500	0.7071	0.0333	
0.750	0.5946	0.0333	
1.000	0.5000	0.0998	
1.250	0.4204	0.1663	
1.500	0.3536	0.3327	
1.750	0.2973	0.4325	
2.000	0.2500	1.3307	
2.250	0.2102	16.3340	
2.500	0.1768	20.2927	
2.750	0.1486	45.9747	** MODE **
3.000	0.1250	10.6121	
3.250	0.1051	2.7279	
3.500	0.0884	0.7319	
3.750	0.0743	0.4657	
4.000	0.0625	0.2994	

SEA276WG

CRUISE	STATION	SAMPLE TYPE,NUMBER	TOTAL LENGTH	SAMPLE CENTER	SAMPLE LENGTH	METHODS
S276WG	S-153	S153	. M	. CM	. CM	1

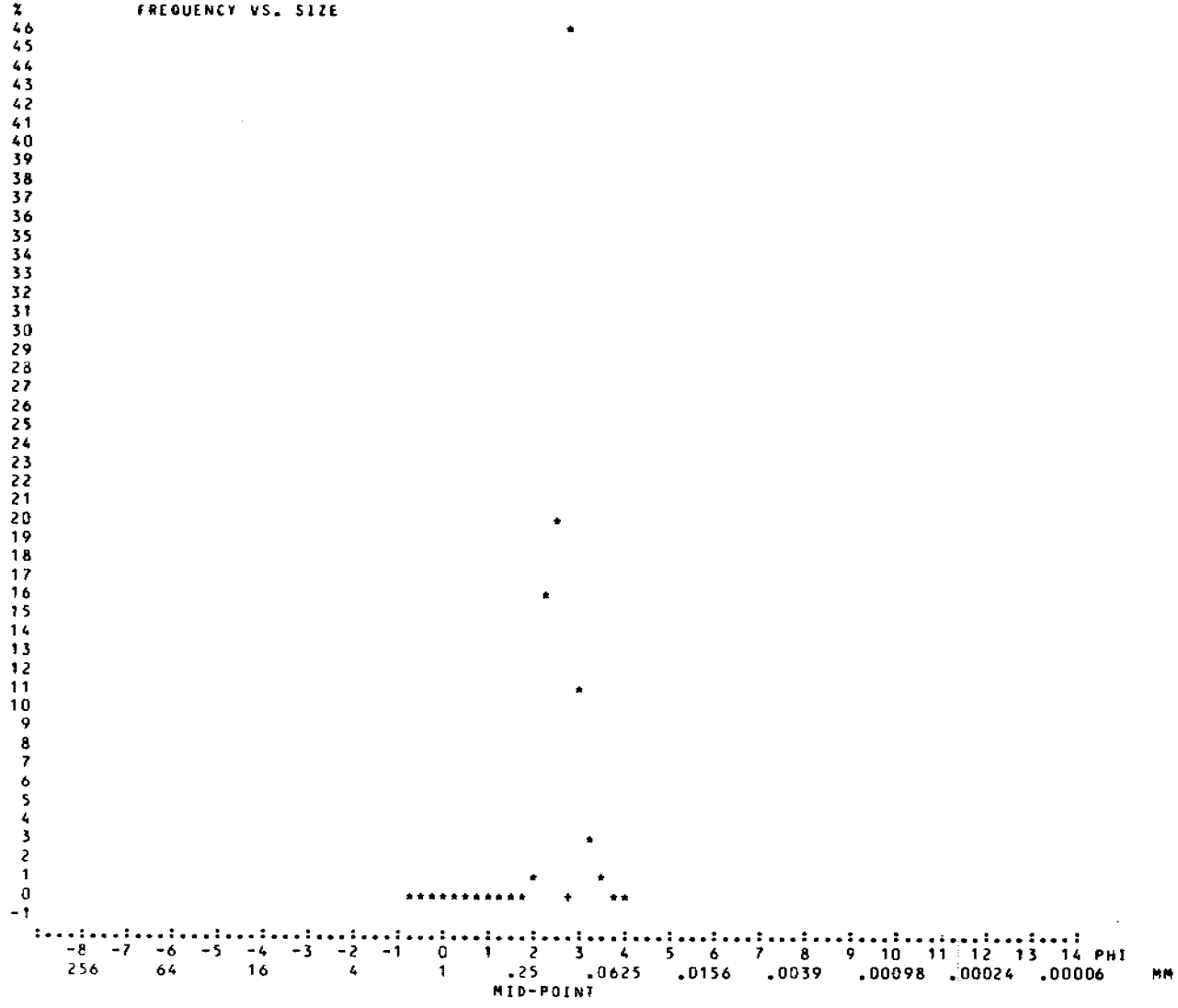

SEA276WG

CRUISE	STATION	SAMPLE TYPE/NUMBER	TOTAL LENGTH	SAMPLE CENTER	SAMPLE LENGTH	METHODS
S276WG	S-153	S153	. M	. CM	. CM	1

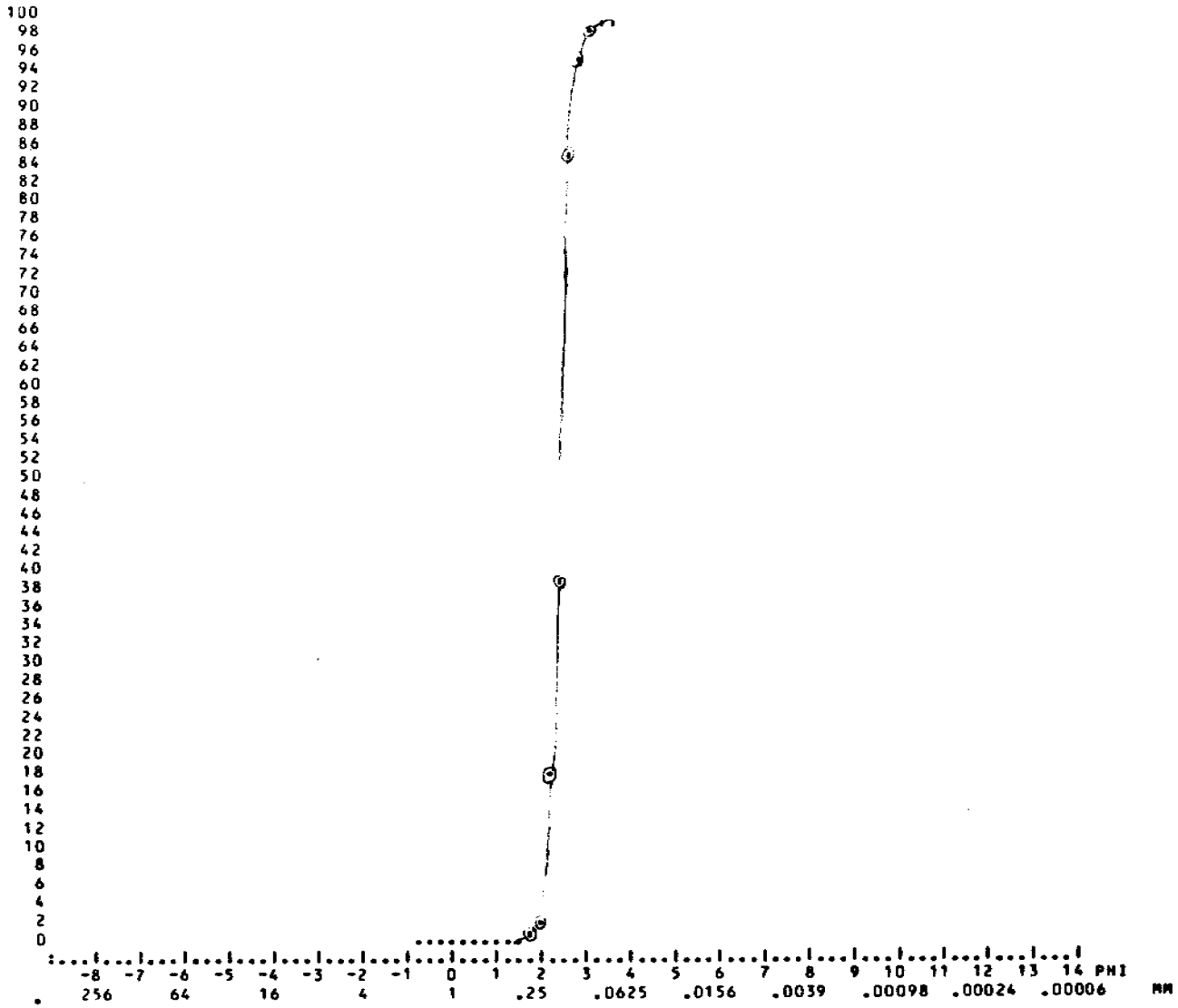

SEA276WG

CRUISE	STATION	SAMPLE TYPE,NUMBER	TOTAL LENGTH	SAMPLE CENTER	SAMPLE LENGTH	METHODS
S276WG	153-S1	S 153	. M	. CM	. CM	2

SUMMARY OF THE PREVIOUS 26 SAMPLES ** MEAN **
SAMPLES ARE LISTED IN ORDER OF INCREASING MEAN SIZE

SEQUENCE NO.			SAMPLE NAME			1ST MOMENT (PHI)
26	S276WG	S-153	S153	1	1	2.5187
13	S276WG	ES-153	S153	1	1	2.5175
21	S276WG	S-34	S34S1	1	1	2.4317
8	S276WG	ES-34	S34S1	1	1	2.4317
17	S276WG	S-29	S29S1	1	1	2.2094
4	S276WG	ES-29	S29S1	1	1	2.2022
20	S276WG	S-31	S31S1	1	1	1.8569
7	S276WG	ES-31	S31S1	1	1	1.8549
16	S276WG	S-28	S28S1	1	1	1.6845
18	S276WG	S-30	S30S1	1	1	1.6011
15	S276WG	S-15	S15S1	1	1	1.6000
5	S276WG	ES-30	S30S1	1	1	1.5951
2	S276WG	ES-15	S15S1	1	1	1.5530
22	S276WG	S-44	S 44	1	1	1.5069
25	S276WG	S-152	S152	1	1	1.4979
12	S276WG	ES-152	S152	1	1	1.4509
9	S276WG	ES-44	S 44	1	1	1.4502
3	S276WG	ES-28	S28S1	1	1	1.3540
19	S276WG	S-30	S30S2	1	1	1.3226
23	S276WG	S-44S2	S44S2	1	1	1.2470
14	S276WG	S-14	S 14	1	1	1.1913
6	S276WG	ES-30	S30S2	1	1	1.1629
1	S276WG	ES-14	S 14	1	1	1.1560
10	S276WG	ES44S2	S44S2	1	1	0.8258
24	S276WG	S-47	S47S1	1	1	0.7333
11	S276WG	ES-47	S47S1	1	1	0.4791

SEA276WG

CRUISE	STATION	SAMPLE TYPE,NUMBER	TOTAL LENGTH	SAMPLE CENTER	SAMPLE LENGTH	METHODS
S276WG	153-S1	S 153	. M	. CM	. CM	2

SUMMARY OF THE PREVIOUS 26 SAMPLES **STANDARD DEVIATION **
SAMPLES ARE LISTED IN ORDER OF DECREASING DEVIATION.

SEQUENCE NO.			SAMPLE NAME			2ND MOMENT (PHI)
10	S276WG	ES44S2	S44S2	1	1	1.1244
3	S276WG	ES-28	S28S1	1	1	1.0382
2	S276WG	ES-15	S15S1	1	1	0.8936
6	S276WG	ES-30	S30S2	1	1	0.8626
11	S276WG	ES-47	S47S1	1	1	0.8611
15	S276WG	S-15	S15S1	1	1	0.8274
23	S276WG	S-44S2	S44S2	1	1	0.7336
9	S276WG	ES-44	S 44	1	1	0.7201
1	S276WG	ES-14	S 14	1	1	0.6757
19	S276WG	S-30	S30S2	1	1	0.6365
14	S276WG	S-14	S 14	1	1	0.6178
22	S276WG	S-44	S 44	1	1	0.6171
24	S276WG	S-47	S47S1	1	1	0.6132
12	S276WG	ES-152	S152	1	1	0.5556
16	S276WG	S-28	S28S1	1	1	0.5413
5	S276WG	ES-30	S30S1	1	1	0.4931
4	S276WG	ES-29	S29S1	1	1	0.4920
18	S276WG	S-30	S30S1	1	1	0.4768
17	S276WG	S-29	S29S1	1	1	0.4674
25	S276WG	S-152	S152	1	1	0.4371
21	S276WG	S-34	S34S1	1	1	0.4162
8	S276WG	ES-34	S34S1	1	1	0.4162
7	S276WG	ES-31	S31S1	1	1	0.4065
20	S276WG	S-31	S31S1	1	1	0.3993
13	S276WG	ES-153	S153	1	1	0.3338
26	S276WG	S-153	S153	1	1	0.3272

NORMAL TERMINATION.
END OF INPUT DATA SET REACHED.

APPENDIX III

Dispersion of drill cuttings as a natural tracer to study depth of reworking of sediment in a field with small sand waves.

Arnold H. Bouma, Monty A. Hampton
Michael E. Torresan, and Robert C. Orlando

U.S. Geological Survey

March, 1978

DISPERSION OF DRILL CUTTINGS AS A NATURAL TRACER

Drill cuttings released from the semisubmersible OCEAN RANGER (Tract #489, Latitude 59°31' 06.3445"N, Longitude 152°38' 36.6037"W, waterdepth 218 ft) could be used as natural tracers to obtain insight into the horizontal and vertical dispersal patterns. The drilling rig was operating for a period of 100 days during the months June-September, 1977.

In total, seven stations were occupied with the BIG VALLEY, a 90-ft boat leased by Dames & Moore for specific studies. The samples were collected with our Soutar grab sampler and subsamples were cored with short plastic liner sections from the Soutar sampler.

The cores, collected from the sampler, were subsampled in 0.5 cm intervals and sieved over an 1-mm mesh screen to separate drill cuttings and shells from local seafloor material. Microscopic control proved this to be an acceptable procedure. Material smaller than 1 mm and larger than 63 microns was cleansed of soluble salts, organic and fine carbonate material, and an aliquot was then run in the Rapid Sediment Analyzer to obtain a grain size distribution curve. Material smaller than 63 microns proved insufficient to conduct effective size analysis. The material larger than 1 mm was dried, weighed and calculated as a percentage of the total sample. Additional sorting under the binocular microscope has to be done to effectively separate shell material from drill cuttings.

The drill cuttings consist of shale, sandstone, granite and gneiss. These petrographic elements are the same as found in the native seafloor material, which makes it impossible to separate cuttings from seafloor sediment when they are in the same size range because angularity disappears rapidly with distance of transport.

Preliminary examinations show that the size of the cuttings decreases rapidly away from the semisubmersible, which makes it difficult to utilize cores collected more than 250-300 m from the drilling operation.

Station #249 was located about 65 m northwest from the coordinate points of the semisubmersible. The overall percentage of drill cuttings in the 0.5 cm core intervals is extremely low which is an indication that active sediment transport takes place. The grain size distribution of the 1000-63 micron fraction is very uniform in a vertical sense (Fig. 1), which facilitates finding higher amounts of coarser material. Figure 1 shows significant peaks at a depth at 4.5-6.5 cm and one at 11.5-13.0 cm. Both depth zones may correspond to trough depths of ripples, making the coarser fraction a lag deposit that concentrates in troughs. Bioturbation was not observed, meaning that the vertical dispersal is due to mechnical action.

Station 251 was located 170 m west southwest and station 252 about 5½ nautical miles north of the drilling operation. The other samples collected have not been analyzed yet. Sample 251 shows high peaks at about 3, 4.5 and 12 cm, which corresponds to sample 249 (compare figures 1 and 2). The high peaks in sample 251 normally contain about 90% of shell material but preliminary microscopic examinations show that drill cuttings in these zones are higher too.

Station 252 results are more confusing and the core is not long enough to provide sufficient depth correlation. A few lithic fragments were observed but we are not sure if these are drill cuttings. The station was too far from the drilling operation to draw conclusive interpretations.

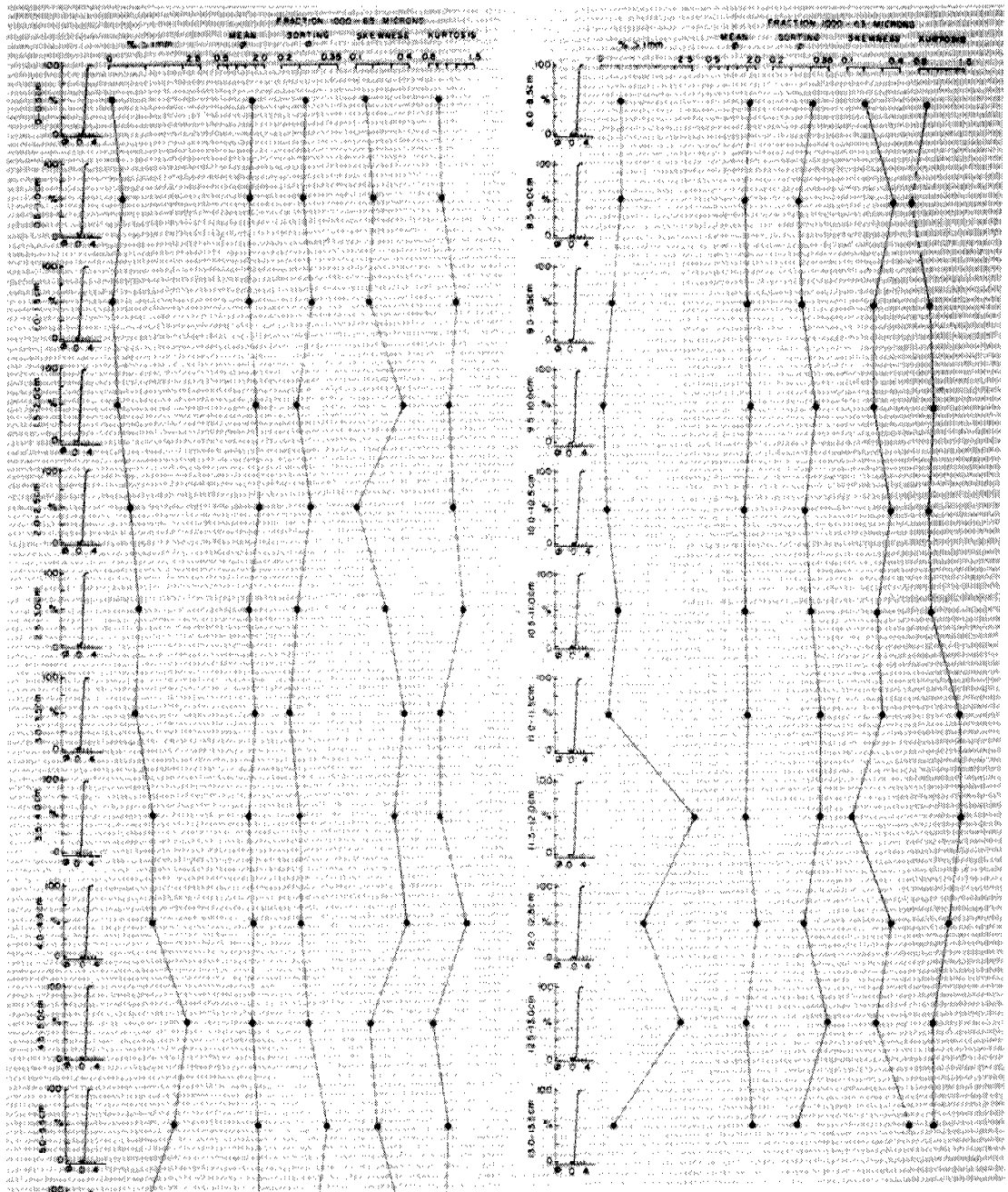

Figure 1. Vertical distribution of coarse fraction (greater than 1mm) and grain size parameters of the 1000-63 micron fraction. Core 249. (After Bouma and others, 1978b).

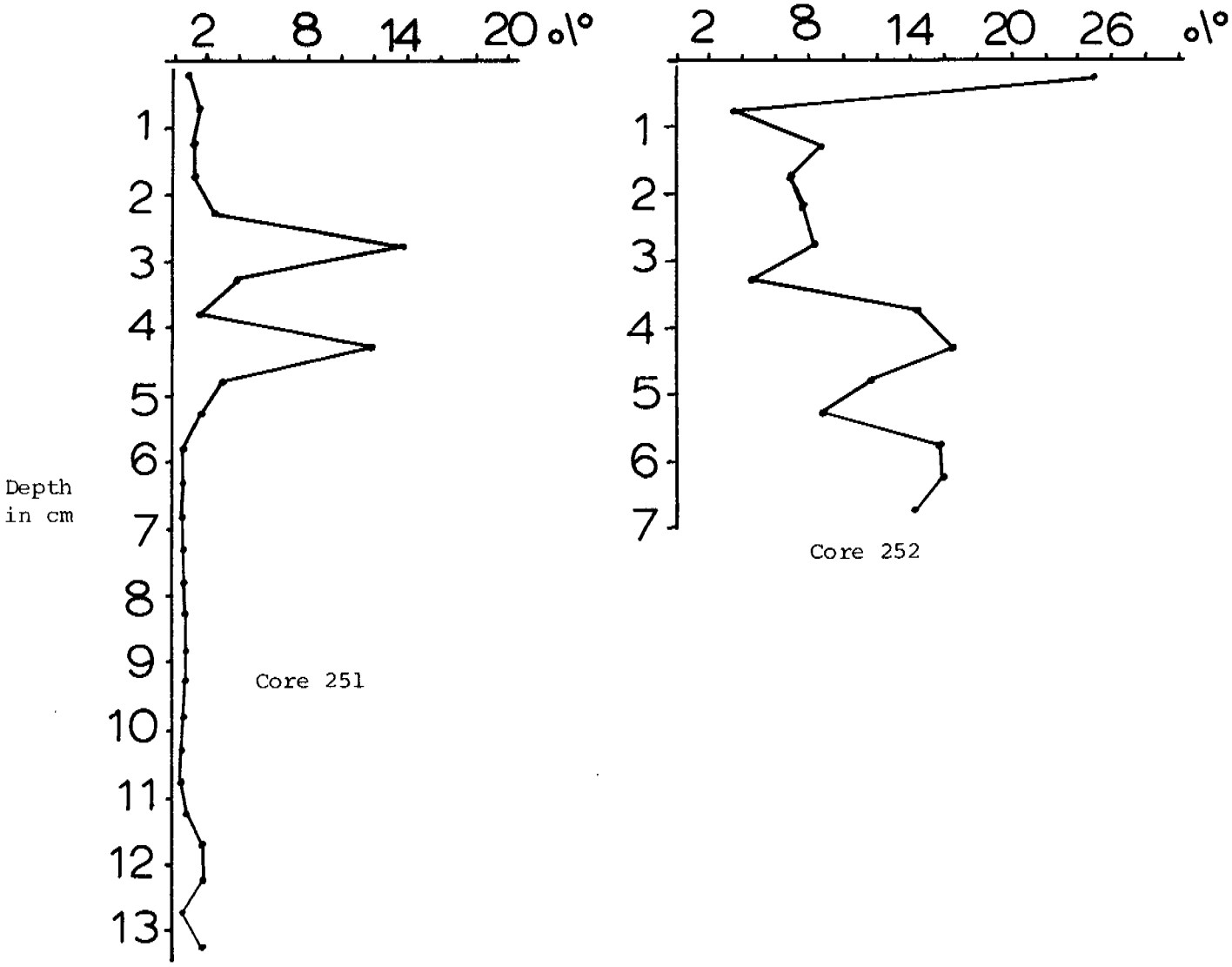

Figure 2. Percentage of coarse fraction (greater than 1 mm) in cores 251 and 252.

APPENDIX IV

Side-scan sonar observations of bedforms in the vicinity of Anchor Point, lower Cook Inlet Alaska.

Melvyn L. Rappeport
U.S. Geological Survey

March, 1978

A detailed study was initiated during the 1977 cruise to describe, quantify and spatially define the present seafloor morphology and sedimentological characteristics of a selected region within lower Cook Inlet, Alaska. This study was undertaken for the purpose of assessing the potential geological hazards to offshore structures and pipeline networks that might be associated with motion of non-cohesive sediments as migrating large marine bedforms.

The area of interest extends from 59°25'N to 59°45'N and from 151°55'W to 152°45'W. Two subregions within this larger area have received the bulk of our current efforts (Fig. 1). One region was centered on the site of the drilling platform D/V Ocean Ranger, (see App. III), whereas the second region encompasses the shallow broad shelf region just southwest of Anchor Point. Most of the following discussion is restricted to data obtained from these two areas.

Bathymetry - Water depths range from 30 to 90 m and slopes are gentle - averaging between 1-5 m/km. Of particular note is the bathymetric expression of two remnant terraces of probable glacial origin. One terrace is situated between the 30-40 meter isobaths and is best represented by a large tongue-like extension that partially bisects the eastern portion of the study region. The second terrace is found between the 50-60 m isobaths and is shown by the large flat portion just west of center of the study region. This latter terrace may be structural, or it may be constructional if it represents the confluence of a lateral moraine emanating from Kachemack Bay and one from the main axial trough of lower Cook Inlet. Bounding the terraces on the west is the main axial trough with depths in excess of 90 meters, and on the south-southeast by the smaller glacial trough extending outward from Kachemak Bay. Separating the two terraces is a small-tributary valley incised into the northern rim of the Kachemak channel (Fig. 2).

Tides and currents - Reports by Evans and others (1972), Meunch and others (1977), and Wagner and others (1969) have generally sketched out the main current circulation system operating within lower Cook Inlet. According to their interpretations, the circulation is dominated by the prevailing westerly flow in the Gulf of Alaska generated by sea surface slope contributions of the Alaskan current. Tidal flood currents move through Kennedy Entrance where they bifurcate. Most of this water is bathymetrically controlled and subsequently flows as a contour current along the base of the ramp that is found south of a line connecting Augustine Island with the Kenai Peninsula. Part of the tidal flow moves up-contour and drifts northward along the Kenai Coast and through the study area. Southwest of Kachemak Bay this flood water bifurcates once again with part moving into the bay and part moving along the coast. The ebb currents flow predominantly down the western half of lower Cook Inlet. Extensive cross flow phenomenon can be found in the central portion of the inlet and a region of shear instability is generated with confusing current patterns. The flow structure at greater (deeper) depths in the main axial trough region is as of yet unknown. It is tentatively inferred that the tidal flow structure is as follows: bottom flood currents are channeled up the Kachemak channel with part moving into the bay while the rest moves up the isobaths through the tributary valley to join with the outflow from the bay and surface currents - all moving northward along the coast in the region of Bluff Point. On the western half, the flood waters are weaker as far as surface currents indicate, because

the prominent bathymetric high extending to the southeast from the central zone of the ramp apparently channelizes bottom flow up the tributary valley and not toward the northwest. On the otherhand, ebb bottom currents tend to remain channelized in the main axial trough, as bathymetric highs on either side of the main channel south of the Forelands act to restrict the ebb flow to the main channel.

Mean diurnal tidal ranges vary from an average of 4.2 meters at the mouth of the inlet to 5.4 meters at Seldovia. The higest tidal range near the Kenai Peninsula is 7.9 meters and the lowest is 1.8 meters with an average of 5.5 m. (Alaska OCS, 1976).

Surface tidal current volocities have been reported by Wagner and others (1969) and Burrell & Hood (1967) as moderate, attaining a mean of 3.8 knots (196 cm/s) with a maximum of over 6.5 knots (335 cm/s) at monthly tidal extremes. Currents as strong as 8 knots (412 cm/s) have been reported by Visser (1969).

Underwater television observations along the surface of large sand waves within lower Cook Inlet (Bouma and other, 1977) at a site adjacent to the western boundary of the overall study area, indicated sand moving over the bottom velocities, ranging from 2 to 30 cm/s. The variability of these visually inferred velocities appears to be highly dependent on relative position on the sand wave.

Winds and waves - Waves in excess of 6 m (19.7 feet) have been reported for lower Cook Inlet by fisherman during periods of severe weather, and during a Chinook wind, westerly winds are intensified as they are funneled through mountain passes west of Kamishak Bay, resulting in wind velocities exceeding 100 knots (51.5 m/s). Most storm weather, however, is generated in the Gulf of Alaska and then moves into the inlet through Shelikof Strait.

Percentage frequency information on wave heights is minimal; however, as reported in the final environmental statement for the proposed outer continental shelf oil and gas lease sale in lower Cook Inlet, the frequency of wave heights in excess of 3.5 meters (11.5 feet) for January is 5-7 percent while for July less than 5 percent. In either case, it can be seen that large wave activity is not uncommon for this region.

For sediment transport estimates under wave effects, the typical winter storm condition in lower Cook Inlet, in particular within our study region, would comprise the following: water depth - 50 meters; wind fetch 200 nm; wind speed 35 knots and duration 12 hours. Using this simplified model information and empirical charts for wave parameters versus these conditions (Ippen, 1966) it is possible to determine the overall wave parameters. Significant wave height was determined to be 4.7 m (15.5 feet) and the wave period to be approximately 10 seconds. Because the significant wave height is statistical measure, some 16-17 percent of the wave heights will be in excess of this number. Therefore the reported storm wave heights and those calculated from the model are in reasonable correspondence. For the Chinook winds, it is more difficult to model, because the winds flow cross the inlet rather than up inlet and fetch

lengths and average water depths are quite variable, yet wave heights in excess of 3.5 meters would be more likely to occur. A deep water wavelength corresponding to the 3.5 meter wave height and corresponding period would be roughly 160 meters with a shallow water wavelength of 230 meters. Water depths to wavelength ratios for the study area are therefore within the range of intermediate water depth limits for waves (Ippen 1966, p. 94) and thus would have an influence on the bottom. Stokes second order theory for intermediate water depths yields estimated orbital velocities in the 90-100 cm/s range. This value is well above the critical transport velocity for sand, and therefore considerable storm-induced bottom sediment transport can be expected.

Observed bedforms near Anchor Point - The subregion off Anchor Point has been surveyed intensively during the field work of past summer. A total of 175 km of side-scan sonar traverses were run, a number of underwater television and bottom camera stations were made, and more than 275 km of 3.5 kHz, 12 kHz and uniboom information obtained. Trackline to trackline spacing varied from 0.25 to 1.0 km. From this sonar data a preliminary bedform map was constructed (Fig. 3). The sonographs show a rich variability of bedform types including constructional forms as well as erosional forms. A nearly complete morphological hierarchy was observed ranging from small, medium and large sand waves through small and medium dunes to sand patches. Interspersed regions of hard bottom with thin sand ribbons and hard bottom composed of pebbly or shelly lag deposits were observed as well as areas of acoustically smooth bottom and acoustically rough terrain-primarily comprising boulder and gravel fields.

The bedform morphologies in the far western section of the Anchor Point subregion show a marked north to south linearity whereas the central zone is noted by its intertongued pattern of bedform fields, and the eastern section demonstrates a return to a linear pattern. Analyses of the corresponding bathymetry suggests that these patterns are somehow controlled or at least partially controlled by local isobath variations. The central intertongued zone is located on the 30-40 meter terrace whereas the far western section is located on the slope that leads from the upper terrace down to the 50-60 m terrace. The apparent parallelism of the bedform fields with the local isobaths in the far western section suggests that high velocity flood and/or ebb currents dominate the morphologies, whereas on the shallower central and eastern regions tidal current effects are weaker and the corresponding bedform distributions are more irregularly arranged. The influence of circulation in Kachemak Bay and the scarcity of sand must also affect the types and extent of bedform fields on the shallower portions of the study area. Also, the shallower central and eastern sections may show the effects of large winter storm waves as discussed perviously. A region of partly eroded sand waves in the southern part of the mapped region, together with the irregularity of distributions and the high percentage of gravel, could be the direct result of storm-generated flows. In particular, sonographs taken along the eastern side of the study area show a bottom that appears to be currently undergoing reconstruction of a thin sand sheet into sand ribbons over a previously storm-degraded pattern.

The initial appraisal of the side-scan sonar shows a possible bedform progression from west to east up the local isobaths that is analagous to the tidal transport succession proposed by Belderson and others (1970) for the North Sea. Those authors showed a progression down the tidal velocity gradient from 1) bedrock and gravel to 2) sand ribbons to 3) sand waves to 4) smooth sand and then 5) sand patches. We observed an upslope progression from a boundary area with sand patches and narrow sand ribbons to a "hard" bottom to a field with small to medium sand waves and finally succeeded by a zone with small dunes on the edge of the flat area. Representative sonographs of this progression can be found in Bouma and others (1978b). It is proposed that the observed progression represents the corresponding 1) -3) part of Belderson's model where the velocities decrease the upslope direction.

REFERENCES

Alaska OCS Office, "Lower Cook Inlet, final environmental impact statement", Alaska Outer Continental Shelf Office, Bureau of Land Management, Anchorage, Alaska (1976), 3 volumes.

Belderson, R.H., Kenyon, N.H. and Stride, A.H., "Holocene sediments on the continental shelf west of the British Isles", Inst. Geol. Sci. Rept. (1970), No. 70, 159-170.

Bouma , A.H., Hampton, M.A., Rappeport, M.L., Whitney, J.W., Teleki, P.G., Orlando, R.C., and Torresan, M.E. (1978b), "Movement of sand waves in lower Cook Inlet, Alaska, Preprints Offshore Technology Conference, OTC Paper 3311, in press.

Burrell, D.C. and Hood, D.W., (1967), "clay-inorganic and organic-inorganic association in equatic environments, Part II, Feb. '66 - June '66, Prog. Rept. R67-3 to AEC., Inst. Marine Sci., Univ. Alaks, Fairbanks, 275 p.

Evans, C.D., Buck, E.H., Buffler, R.T., Fisk, S.G., Forbes, R.B., and Parker, W.B., "The Cook Inlet environment - a background study of available knowledge", Univ. of Alaska Resource and Science Center, Alaska Sea Grant Program, Anchorage (1972), 132 p.

Ippen, A.T., Ed. (1966) "Estuary and Coastline Hydrodynamics", McGraw-Hill, 744 p.

Meunch, R.D., Charell, R.L. and Mofjeld, H.D., "Summer circulation in lower Cook Inlet, Alaska", Trans. Amer. Geoph. Union, (1977), v. 58, 1173 (abstr.)

Visser, R.C., "Platform design & construction in lower Cook Inlet, Alaska", J. Petrol. Techn., (1969), 411-420.

Wagner, D., Murphy, R.S. and Behlke, C., "A program for the collection, storage, and analysis of baseline environmental data for Cook Inlet, Alaska", Rept. No. IWR-7, Inst. Water Res., Univ. of Alaska, Fairbanks (1969), 248 p.

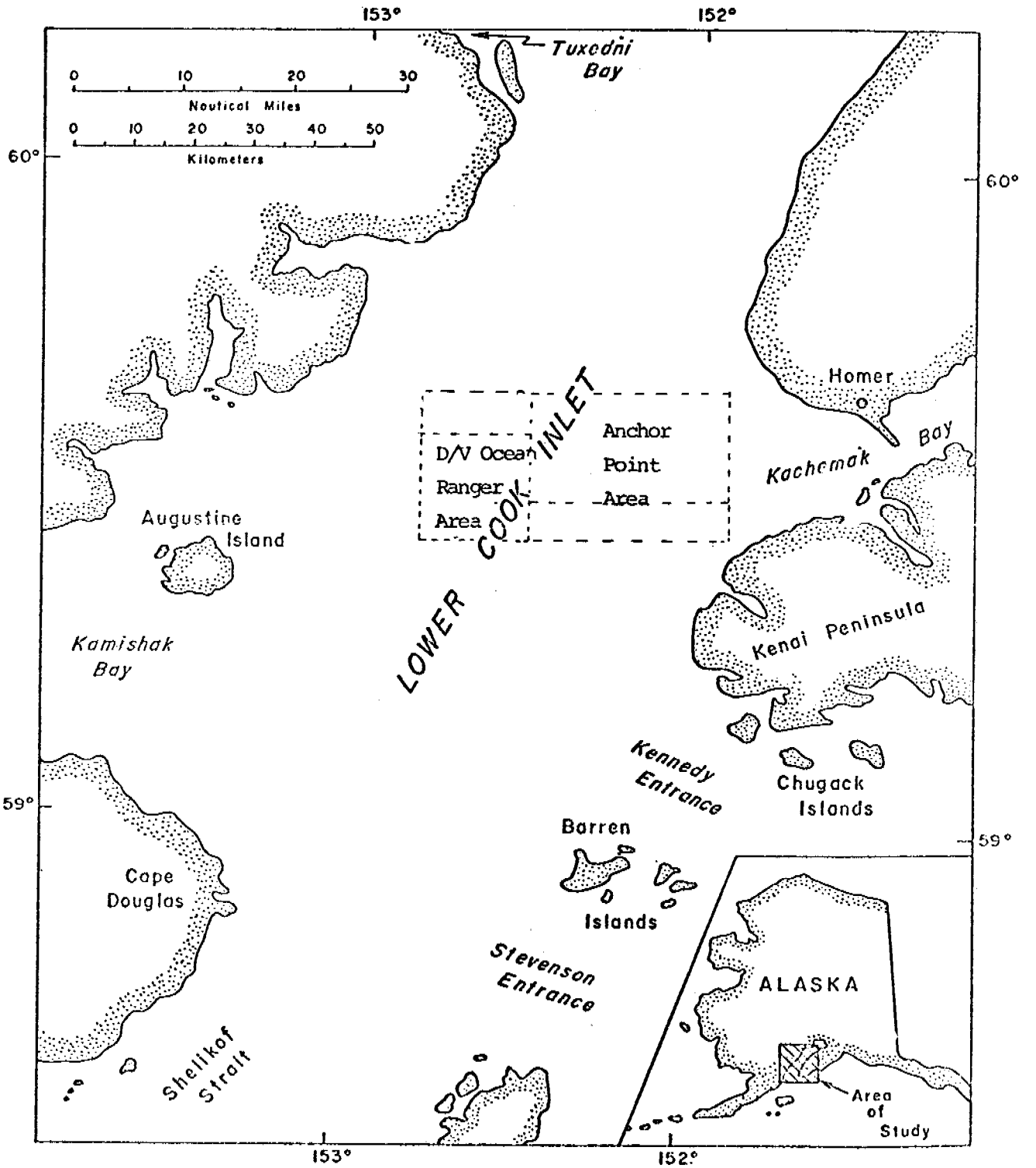

figure 1. Lower Cook Inlet index map.

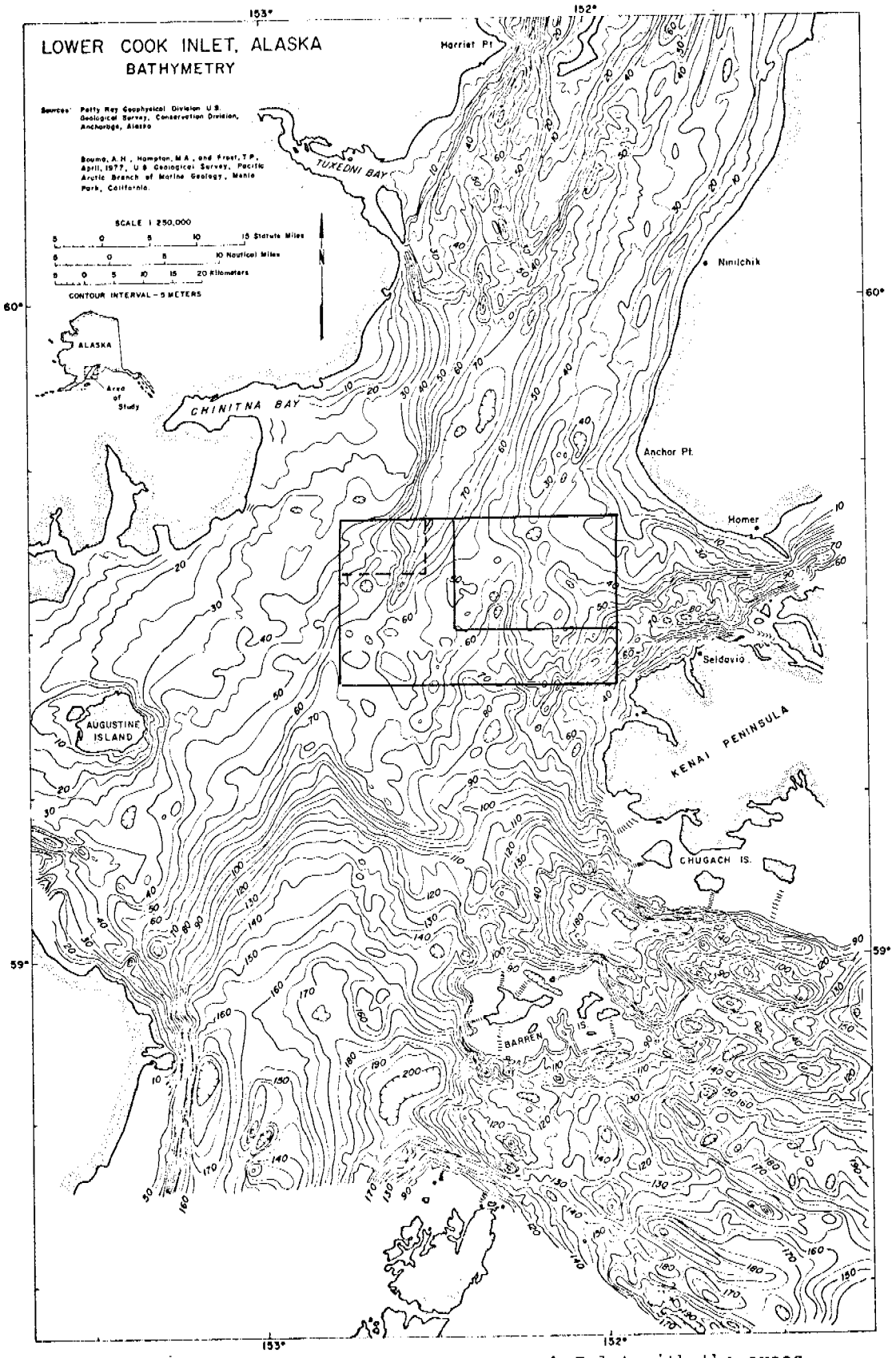

Figure 2. Bathymetry of lower Cook Inlet with the areas of detailed studies indicated.

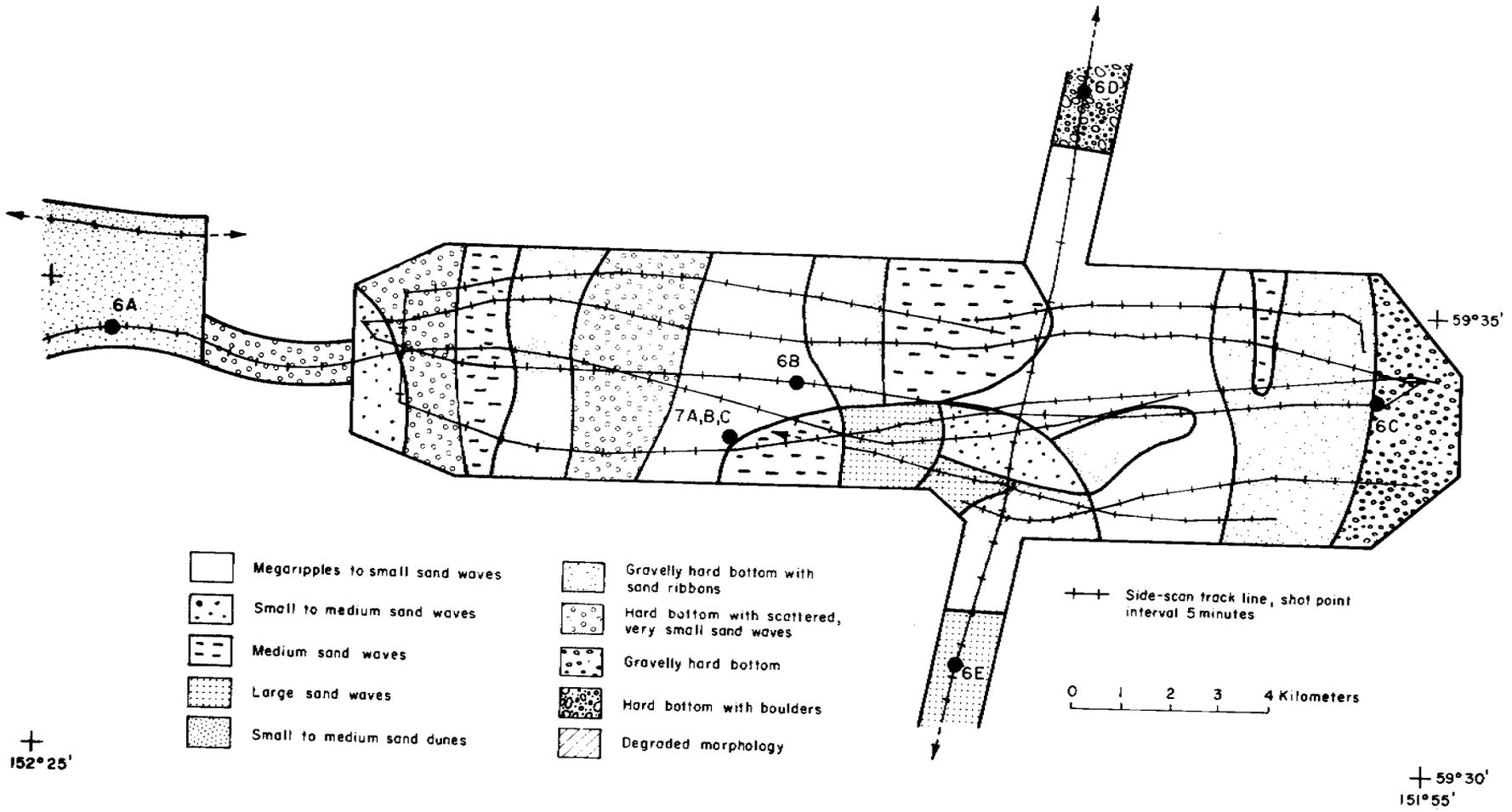

Figure 3. Study area off Anchor Point with tracklines and bedform fields. Large dots with numbers refer to bottom photographs presented in Bouma and others, 1978b.

APPENDIX V

Bathymetry of lower Cook Inlet

Arnold H. Bouma and Monty A. Hampton

1978

BATHYMETRY OF LOWER COOK INLET

The bathymetry of lower Cook Inlet is best defined as being complex in nature, preventing an easy description. The area can be divided into three smaller ones (Fig. 1), each composed of a number of typical physiographic characteristics.

Northern lower Cook Inlet

This area starts at Kalgin Island, is bounded on the east and west by land, and at the south by a ramp at the latitude of approximately 59°15'. Along the eastern side - Kenai Lowlands - a platform or terrace is present that gradually slopes toward the west. In the south this platform only occupies the northern part of Kachemak Bay where it is bounded at the south by a relatively deep channel. Along the western side - Chigmit Mountains - a similar platform occurs that slopes toward the east. Its southern boundary also consists of a channel-type depression running along Mt. Douglas. This western platform becomes very narrow off Redoubt Volcano and is cut by a channel extending from Tuxedni Bay. A volcanic island - Augustine Island - forms part of this platform.

The central part of lower Cook Inlet between the latitude of Ninilchik (about 60°N) and Seldovia (about 59°30') forms a central depression bounded by the 60 m isobath. At its northern side it bifurcates into two channels, divided by a platform adjacent to Kalgin Island. Near the latitude of Seldovia the 60 m isobaths come close together, the central depression shoals, and south of this constriction a triangular body exists in the shape of a delta that terminates at the ramp. The largest bedforms found in northern Cook Inlet are more or less restricted to the axial part of the central depression and to the deltaic - shaped area south of the 60 m isobath constriction (Fig. 2).

Southern lower Cook Inlet

This part of lower Cook Inlet is bounded primarily by escarpments forming a basin in its center. Due to lack of detailed bathymetric information from Shelikof Strait we don't know how this deeper part extends to the south.

On its northern side this area is bounded by a "boomerang-shaped" slope or ramp that starts at a depth of about 70 m and terminates at about 12-130 m with slopes ranging from 0.3 to 0.6°. On its western side it is bounded by a steep slope along Mt. Douglas and on its eastern side by a platform around the Barren Islands, a submerged platform between Shuyak Island and the Barren Islands, and a type of ridge extending north from the Barren Islands to the ramp.

The central part deepens gradually toward the south and it contains two deeper areas, one at the base of the slope off Cape Douglas and one adjacent to the platform between Shuyak Island and the Barren Islands. The latter one is in excess of 200 m deep. In between these local deeps a slightly irregular bathymetry can be observed with local highs and a local deep.

Sediments in this southern part of lower Cook Inlet, at least in its central area north of the latitude of the Barren Islands, are muddy sands, in contrast to the ramp itself and the area farther north, where sand is found.

The top of the eastern part of the ramp is devoid of large bedforms. From this area down, the smooth bottom changes to medium-sized bedforms, going over into large ones, which in turn become smaller and die out at the base of the ramp.

Eastern lower Cook Inlet

The eastern part of lower Cook Inlet includes the bathymetrically complex areas known as Stevenson Entrance in the south and Kennedy Entrance in the north. The Barren Islands and a submerged ridge extending in ESE direction form the dividing zone.

Stevenson Entrance contains two depressions, elongate and parallel to the ridge extending from the Barren Islands. Both shoal to the west to a depth of about 120 m and less, which constitutes the platform between Shuyak Island and the Barren Islands.

Kennedy Entrance is more complex in its bottom morphology. This northern passage from the Pacific Ocean to Cook Inlet starts off as a deep (east side of Figure 1), then divides into two shallower channels with a short ridge in between, and then comes together again between the Barren Islands and Ilizabeth Island (western one of the Chugach Islands) to form a deep basin. From there it shoals and bends via NNW to a northern direction forming an identation in the 60 m isobaths at the latitude of Seldovia.

This bathymetric shape of Kennedy Entrance provides a passage for the incoming Pacific Ocean water directing the flood along the eastern side of lower Cook Inlet, separating the bottom water bathymetrically from the central depression. The ridge between the Barren Islands and the ramp likely also has an effect on the path of the incoming deeper water, although the higher ramp certainly will steer part of this water along its face toward the west. Near the northern termination of Kennedy Entrance one finds the entrance of the channel into the Kachemak Bay. This channel has a similarity to the central depression in that it also contains several deeper basins and has a constricted mouth formed by the 60 m isobaths.

The bathymetry of lower Cook Inlet has a strong effect on the direction of tidal bottom flows as can be observed by the bottom characteristics, such as the direction of bedform fields (see Appendix IV). Because of the complexity of the bathymetry, bottom circulation can also be expected to be complex.

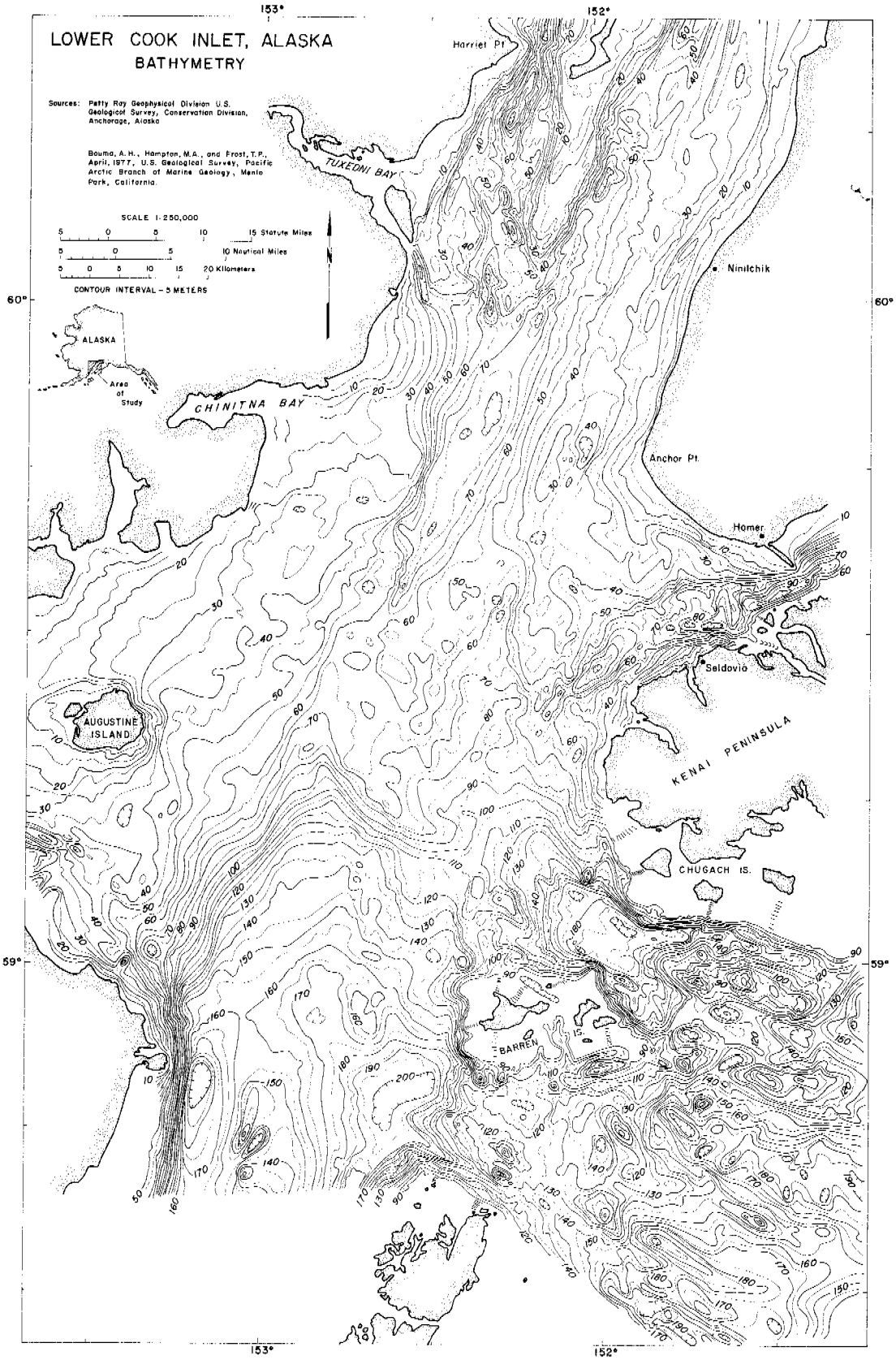
LOWER COOK INLET, ALASKA
BATHYMETRY
Sources: Petty Ray Geophysical Division U.S. Geological Survey, Conservation Division, Anchorage, Alaska
Bouma, A.H., Hampton, M.A., and Frost, T.P., April, 1977, U.S. Geological Survey, Pacific Arctic Branch of Marine Geology, Menlo Park, California.
SCALE 1-250,000
15 Statute Miles
10 Nautical Miles
20 Kilometers
CONTOUR INTERVAL - 5 METERS
ALASKA
Area of Study
153°
152°
60°
59°
Harriet Pt.
TUXEDNI BAY
CHINITNA BAY
Ninilchik
Anchor Pt.
Homer
Seldovia
KENAI PENINSULA
AUGUSTINE ISLAND
CHUGACH IS.
BARREN

Figure 1.

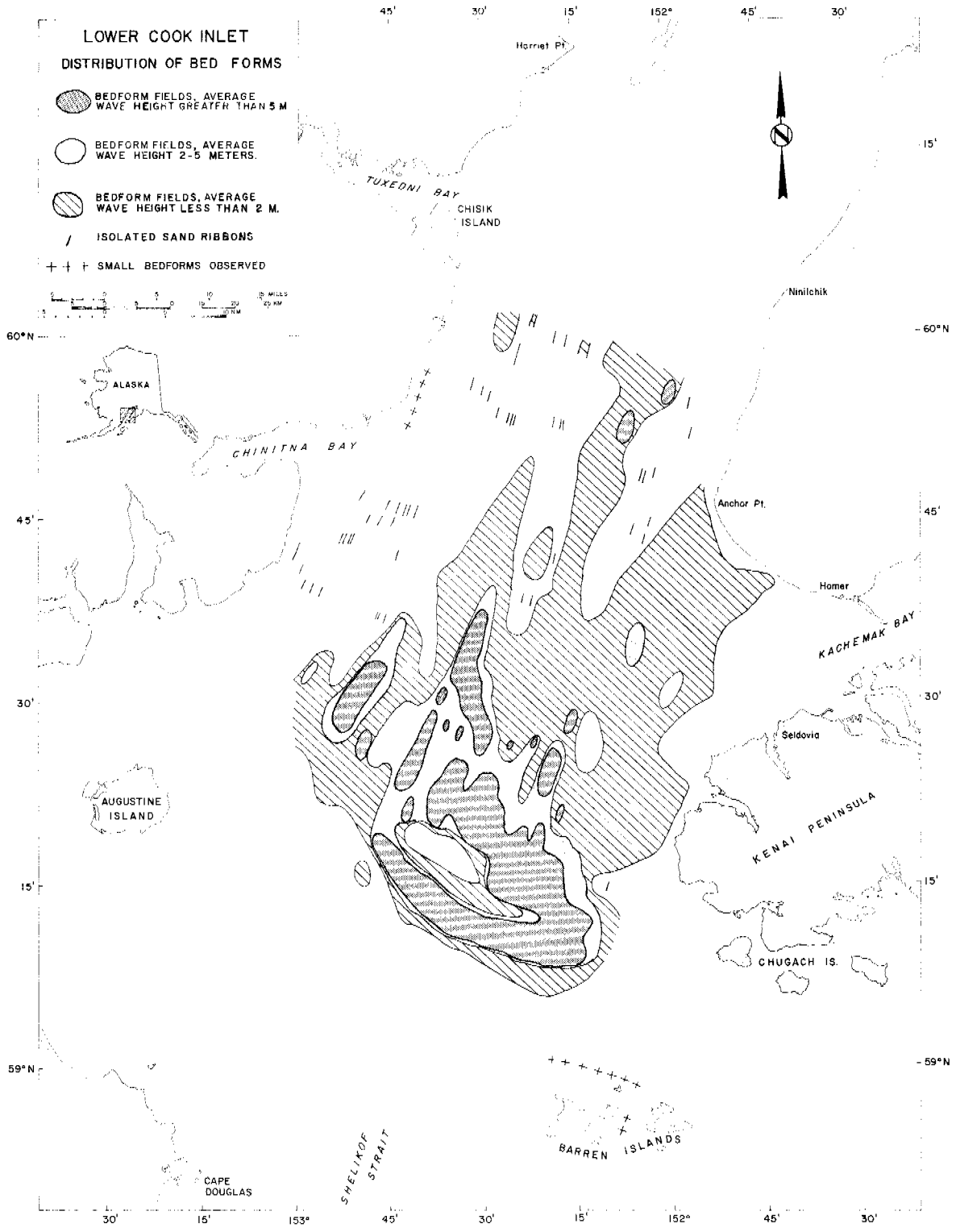
LOWER COOK INLET
DISTRIBUTION OF BED FORMS
BEDFORM FIELDS, AVERAGE WAVE HEIGHT GREATER THAN 5 M
BEDFORM FIELDS, AVERAGE WAVE HEIGHT 2-5 METERS.
BEDFORM FIELDS, AVERAGE WAVE HEIGHT LESS THAN 2 M.
ISOLATED SAND RIBBONS
SMALL BEDFORMS OBSERVED
45'
30'
15'
152°
Harriet Pt.
TUXEDNI BAY
CHISIK ISLAND
Ninilchik
60°N
ALASKA
CHINITNA BAY
Anchor Pt.
Homer
KACHEMAK BAY
Seldovia
AUGUSTINE ISLAND
KENAI PENINSULA
CHUGACH IS.
59°N
SHELIKOF STRAIT
BARREN ISLANDS
CAPE DOUGLAS
153°

Figure 2.

APPENDIX VI

Slope instability near the shelf break, western Gulf of Alaska

Monty A. Hampton and Arnold H. Bouma

Marine Geotechnology
v. 2, p. 309-331

1977

APPENDIX VII

Hydrocarbon gases in sediments from the western Gulf of Alaska

Keith A. Kvenvolden and George D. Redden
U.S. Geological Survey

March 1978

Hydrocarbon Gases in Sediments from the Western Gulf of Alaska

Keith A. Kvenvolden and George D. Redden

During the 1977 field season (S7-77), eleven surface and near-surface sediment samples were collected from seven sites in the Western Gulf of Alaska and were analyzed for hydrocarbon gases methane: (C_1), ethane (C_2), ethane ($C_{2:1}$), propane (C_3), propene (C_3), isobutane (i-C_4), and n-butane (n-C_4). The seven stations were located on specific geologic features. The objective of the work was to determine how the concentration and composition of hydrocarbon gases in the sediments vary with respect to these features.

Samples for gas analyses were recovered by gravity and piston coring, and one grab sample was taken. From the 8-cm (I.D.) core liner were removed one or two 10-cm long segments. Sediment core from each segment was extruded into a pre-weighed, 1-qt. can that had been previously prepared with two septa-covered holes near the top. The can was filled with distilled water that had been purged with helium to remove any dissolved hydrocarbon gases. From the can 100-ml of water was removed. A double friction top was sealed in place and the 100-ml headspace was purged with helium through the septa. The can was inverted and frozen. Later, the contents of the can were thawed. The cans were shaken for ten minutes to extract gases into the headspace. From the can about 5-ml of gas mixture was removed in a gas-tight syringe. Exactly one ml of this mixture was injected into a modified Carle 311 Analytical Gas Chromatograph equipped with both flame ionization and thermal conductivity detectors. The instrument was calibrated by means of a standard mixture of hydrocarbon gases prepared by Matheson Gas Company. Calculations of concentrations of gases were determined from chromatograms by measuring heights of

peaks representing the gases. Partition coefficients were used to correct for differences in gas solubilities. Concentrations are reported as nL/L of wet sediment.

Stations 224, 225, and 226 were associated with a slump mass of Middle Albatross Bank on the continental slope southeast of Kodiak Island. Station 224 was located in the slump mass itself. In the core taken here, both C_1 and C_2 increase significantly with depth. Station 225 was at the headwall scarp at the top of the slump mass. The surface sample, and particularly the sample from 140-150 cm depth, both have anomalously high concentrations of C_1, C_2 and C_3. The deep sample may be saturated with C_1. Both samples smelled of H_2S. Samples from Station 226 came from original, undisturbed continental slope sediments. This station was positioned both above the headwall and the slump. Concentrations of hydrocarbon gases from one sample (101-111 cm) were low.

One sample from gas analysis was obtained from Chiniak Trough (Station 231). C_1 concentration in this sample was moderately high. The sample, composed mainly of volcanic ash, came from a silled trough with quiet sedimentation.

Stations 239 and 240 were associated with a slump mass of Stevenson Trough. Station 239 was in the headwall above the slump and Station 240 was in the slump. Concentrations of C_1 in samples from both of these stations were low, and, in contrast to the slump off Middle Albatross Bank, C_1 concentrations do not increase significantly with depth.

At the last Station (241), also off Stevenson Trough, a single surface sample of "typical" continental slope sediment was analyzed. C_1 concentration is low and the ratio $C_1/(C_2 + C_3)$ is also low. Low $C_1/(C_2 + C_3)$ ratios are commonly observed in surface samples from Arctic marine sediments.

These few samples show that hydrocarbon gases are present in sediments from the Western Gulf of Alaska in variable concentrations. In one slump mass off of Middle Albatross Bank, C_1 increased dramatically with depth, but in the other slump mass off of Stevenson Trough, no significant gradient exists over the interval sampled. The most significant concentrations of hydrocarbon gases were found at Station 225. This gas is undoubtedly of biological origin. These sediments may be gas-charged and therefore may be unstable. Gases at the other stations are also probably of biological origin. There is no evidence in the samples studied here for seepage of petroleum-derived hydrocarbon gases.

Table 1 - Hydrocarbon Gases - Western Gulf of Alaska (S7-77)

Sta/Smpl	Interval (cm)	Water Depth (m)	Concentrations (nL/L set sediment) C_1	C_2	$C_{2:1}$	C_3	$C_{3:1}$	i-C_4	n-C_4	$\frac{C_1}{C_2 + C_3}$
224 - G1	0-10	992	2890	50	25	18	6	-	-	43
"	120-130	"	77700	1400	19	20	-	-	-	55
225 - P1	0-10	601	22800	460	82	122	32	10	26	39
	140-150	"	28,700,000	15000	-	203	-	-	-	1880
226 - P1	101-111	360	5650	37	19	5	-	-	-	133
231 - G1	71-81	170	48400	62	19	66	6	-	-	378
239 - G1	150-160	965	6060	75	25	25	-	7	7	60
	290-300	"	8530	112	50	91	25	13	13	42
240 - G1	70-80	1415	4040	37	19	10	-	-	-	85
	210-220	"	5600	50	19	20	6	-	-	80
241 - S1	0-10	603	4920	156	57	91	25	27	27	20

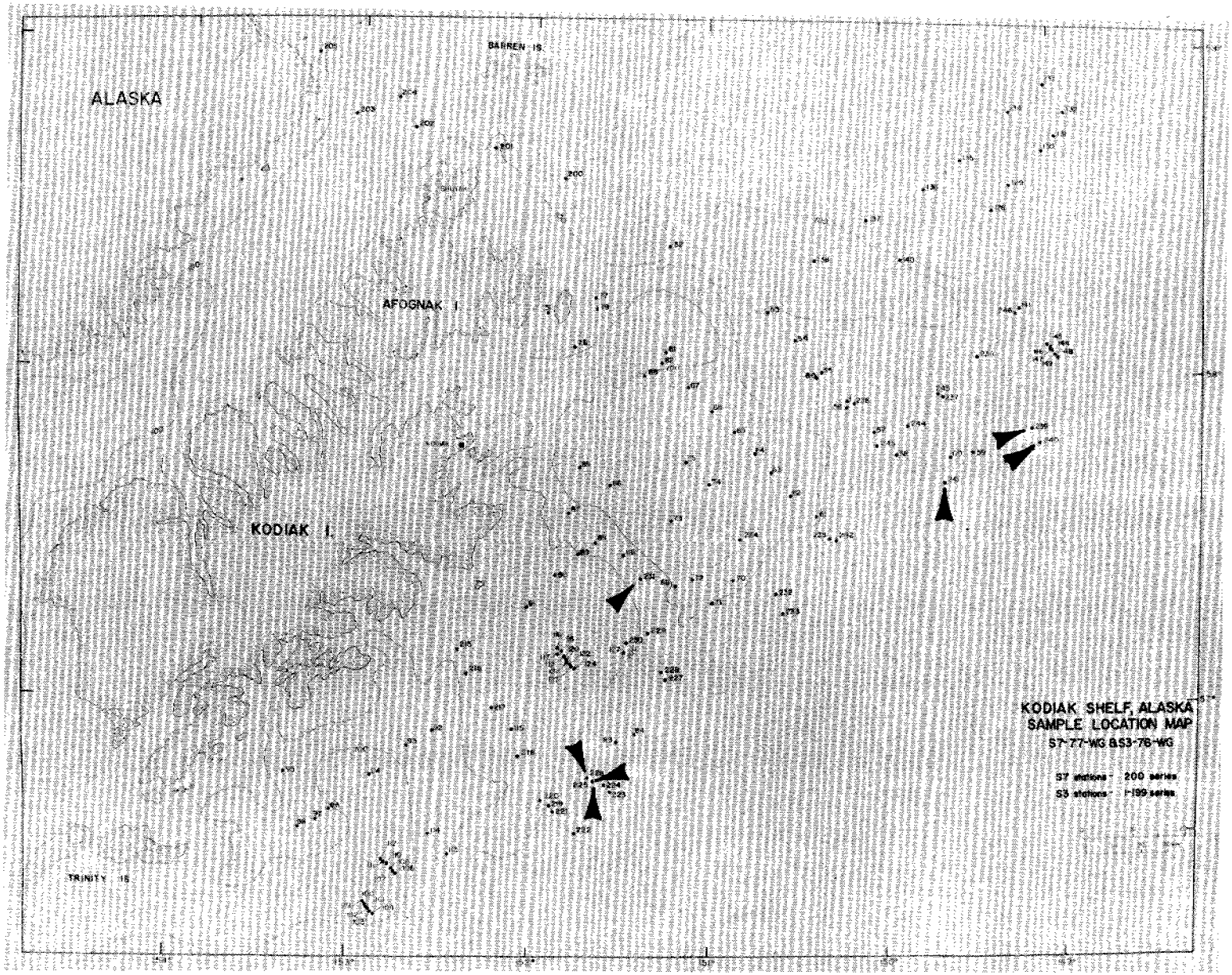
ALASKA
BARREN IS.
AFOGNAK I.
KODIAK I.
TRINITY IS.
KODIAK SHELF, ALASKA
SAMPLE LOCATION MAP
S7-77-WG BS3-76-WG
S7 stations - 200 series
S3 stations - 199 series

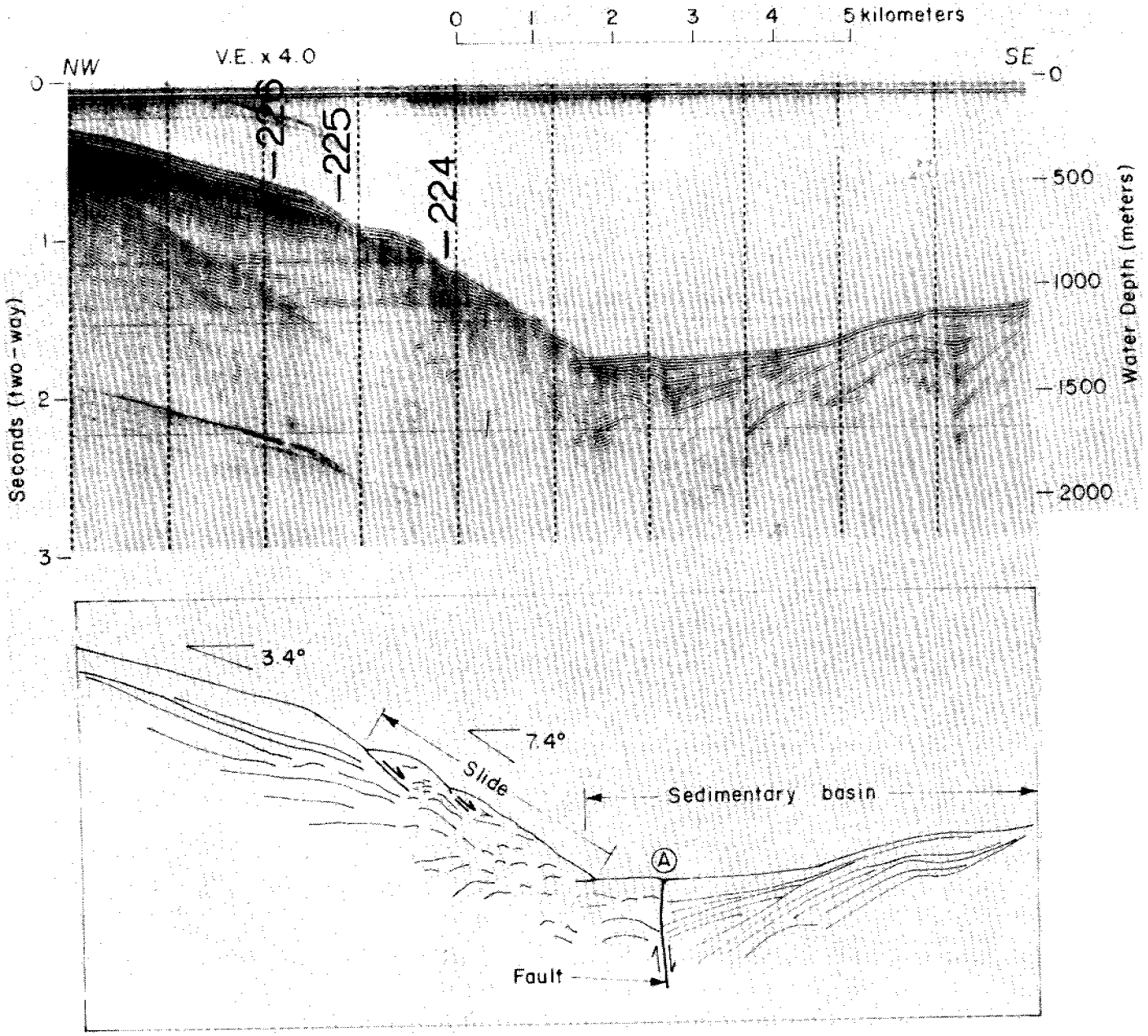
0 1 2 3 4 5 kilometers
NW
V.E. x 4.0
SE
-226
-225
-224
0
1
2
3
Seconds (two-way)
-0
-500
-1000
-1500
-2000
Water Depth (meters)
3.4°
7.4°
Slide
Sedimentary basin
A
Fault

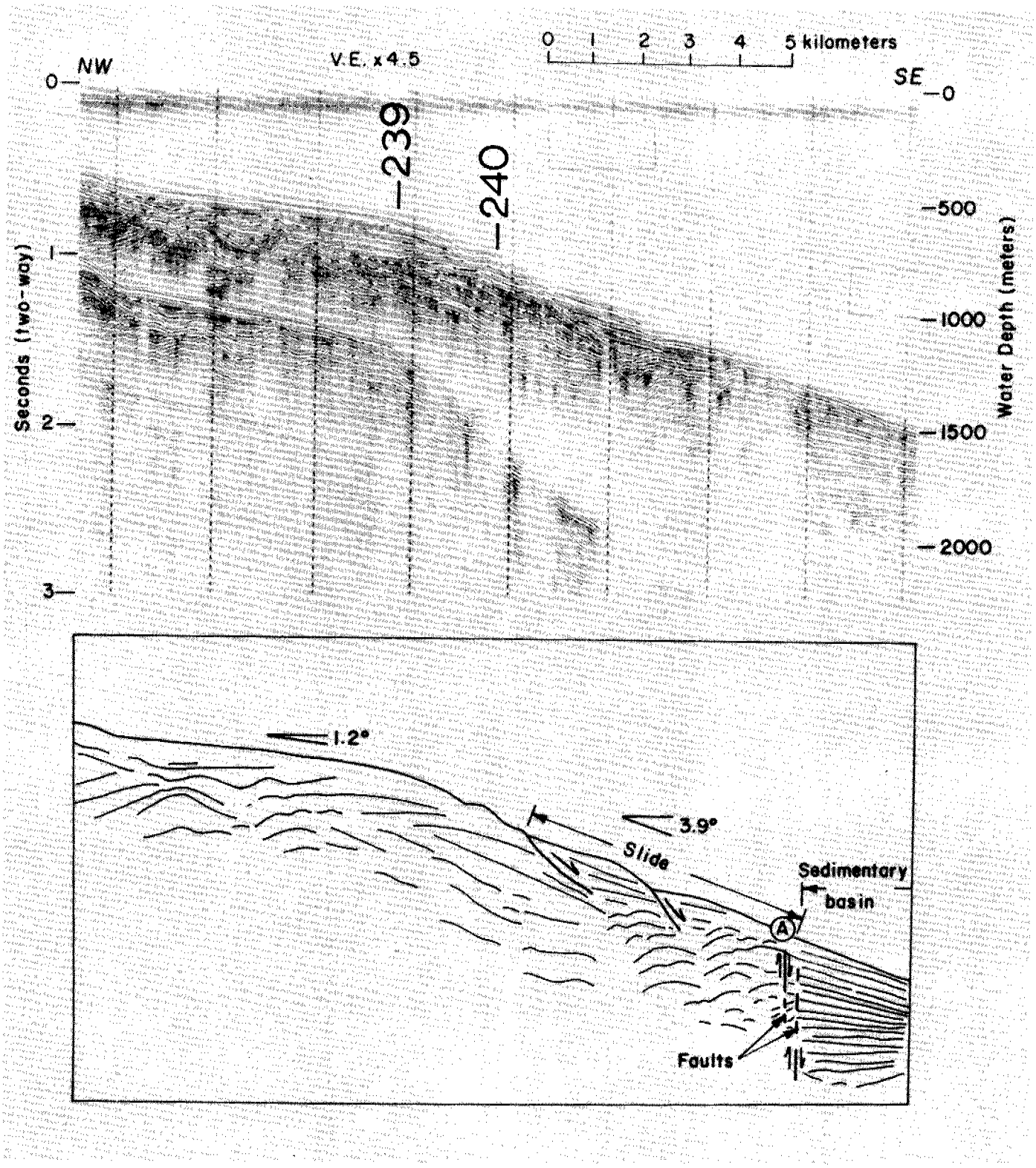
0 1 2 3 4 5 kilometers
NW
V.E. x 4.5
SE
0
239
240
500
1000
1500
2000
Seconds (two-way)
Water Depth (meters)
1
2
3
1.2°
3.9°
Slide
Sedimentary basin
A
Faults

APPENDIX VIII

Bryozoa from Cook Inlet and Kodiak Shelf, Alaska

Richard Rezak and Arthur J. Leuterman
Texas A & M University
Department of Oceanography
College Station, Texas

February 1978

APPENDIX

Bryozoa from Cook Inlet and Kodiak Shelf Alaska

by

Richard Rezak and Arthur J. Leuterman
Texas A & M University
Department of Oceanography

Ten samples, taken by the R/V SEA SOUNDER during the period June 18 - July 30, 1976, were sent to the senior author for analysis of possible coralline algae. The samples were collected with a Soutar modification of the Van Veen sampler and a chain dredge. Water depths at these stations vary from 35 m to more than 200 m (Fig. 1 and 2).

Shipboard descriptions of the material sampled refer to an abundant fauna of molluscs, small sea-fans, brittle stars, etc. (Bouma and Hampton, 1976). Laboratory examination reveals an abundance of Bryozoa. A breakdown beyond families may provide environmental characteristics and depth zonations which can not be done with the data given in Table I. However, no coralline algae are present in any of the samples examined.

The absence of algae in these samples is an enigma. Adey and MacIntyre (1973) indicate that coralline algae will grow within the Arctic Circle to depths greater than 40 m. Water turbidity is the controlling factor in depth distribution within this range. No nephelometry measurements were made on that cruise which prevents an in depth discussion on the viability of coralline algae near the station locations. The waters of Lower Cook Inlet seem to be low in suspended clay material but high in small animals and plants which may prevent sufficient light penetration (A. H. Bouma, personal communication). The senior author has samples of articulated coralline algae sand that had washed up on the beach on the east side of Kodiak Island. Also articulated coralline algae are abundant in Pirate Cove, Sitka Sound, Alaska (Charles M.

Hoskins, personal communication). An explanation for the absence of coralline algae in samples from stations 4 and 9 must await further investigations. The remaining stations are probably too deep for coralline algae at this latitude.

Bibliography

Adey, W. H. and MacIntyre, I. G., 1973, Crustose coralline algae: a re-evaluation in the geological sciences. Geol. Soc. America Bull., v. 84, p. 883-904.

Bouma, A. H. and Hampton, M. A., 1976, Preliminary report on the surface and shallow subsurface geology of lower Cook Inlet and Kodiak shelf, Alaska. U.S. Geol. Survey Open-file Rept. 76-695, 36 p., 9 plates.

TABLE I

Bryozoa of Cook Inlet and the Kodiak Shelf

Cook Inlet

	No. of Specimens
Station 4, depth 40 m, Encrusting Cheilostomes	3
Station 9, depth 35 m	
Order: Cheilostomata	
Suborder: Anasca	
Division: Cellularina	
Family: Scrupocellaridae	57
Scrupocellaria sp.	6
Family: Electrinidae	
Electra sp.	1
Family: Cribrilinidae	2
Family: Membraniporidae	
Membranipora sp.	2
Suborder: Ascophora	
Family: Celleporidae	
Family: Myriozoidae	1
Myriozoum tenue	1
M. sp.	29
Unidentified encrusting Cheilostomes	7
Order: Cyclostomata	
Tubulipora sp.	7
Entalophora sp.	5
Crisia sp.	10
Family: Lichenoporidae	2
Station 9D, depth 35 m	
Order: Cheilostomata	
Suborder: Anasca	
Family: Menbraniporidae	8
Suborder: Ascophora	
Unidentified encrusting Cheilostomes	3
Myriozoum sp.	4
Order: Cyclostomata	
Family: Tubuliporidae	1
Family: Entalophoridae	
Entalophora sp.	1

Station 19, depth 200 m	
Order: Ctenostomata	
Family: Pedicellinidae	2
Order: Cheilostomata	
Suborder: Anasca	
Family: Scrupocellaridae	21
Scrupocellaria sp.	8
Family: Membraniporidae	3
Family: Cribrilinidae	
(?) *Membraniporella* sp.	1
Suborder: Ascophora	
Family: Microporellidae	
Microporella spp.	35
Microporella (?) n.sp.	1
M. vibraculifera	1
Fenestrulina malusi var. *umbonata*	3
Family: Myriozoidae	
Myriozoum sp.	2
Order: Cyclostomata	
(?) *Oncousoecia* sp.	1
Station 44, depth 62 m	
Order: Cheilostomata	
Suborder: Anasca	
Family: Membraniporidae	1
Suborder: Ascophora	
Hippothoa sp.	1
(?) *Smittina* sp.	1
Family: Celleporidae	3
Order: Cyclostomata	
Tubulipora sp.	3
Entalophora sp.	2

Kodiak Shelf

Station 51, depth 60 m	
Order: Cheilostomata	
Suborder: Anasca	
Division: Cellularina	
Family: Scrupocellaridae	6
(?) *Tricellaria* sp.	2
Suborder: Ascophora	
Hippothoa divaricata	1
(?) *Porella* sp.	1
Schizoporella sp.*	1
Myriozoum spp.	29
M. subgracile	15
M. cf. *tenue*	3
Order: Cyclostomata	
Entalophora sp.	1

* encrusting on *Myriozoum* sp.

Station 61, depth 112 m	
Order: Cheilostomata	
Suborder: Ascophora	
Microporella sp.	1
Branching Cheilostome	1
Order: Cyclostomata	
Entalophora sp.	1
cf. *Lichenopora* sp.	1
Station 62, depth 102 m	
Order: Cheilostomata	
Suborder: Ascophora	
Microporella sp.	1
Order: Cyclostomata	
Tubulipora sp.	2
Family: Lichenoporidae	1
Lichenopora sp.	4
Station 66, depth 77 m	
Order: Cheilostomata	
Suborder: Anasca	
Family: Scrupocellaridae	2
Family: Membraniporidae	3
Family: Cribrilinidae	1
Suborder: Ascophora	
Hippothoa sp.	2
cf. *Lacerna* sp.	1
Myriozoum sp.	2
Order: Cyclostomata	
Family: Lichenoporidae	1
Station 138, depth 60 m	
Order: Cheilostomata	
Suborder: Anasca	
Family: Scrupocellaridae	2
Family: Microporidae	
Microporina borealis	126
Suborder: Ascophora	
Smittina sp.	1
Microporella so.	6
Myriozoum spp.	41
Family: Celleporidae	4
Order: Cyclostomata	
Family: Tubuliporidae	2

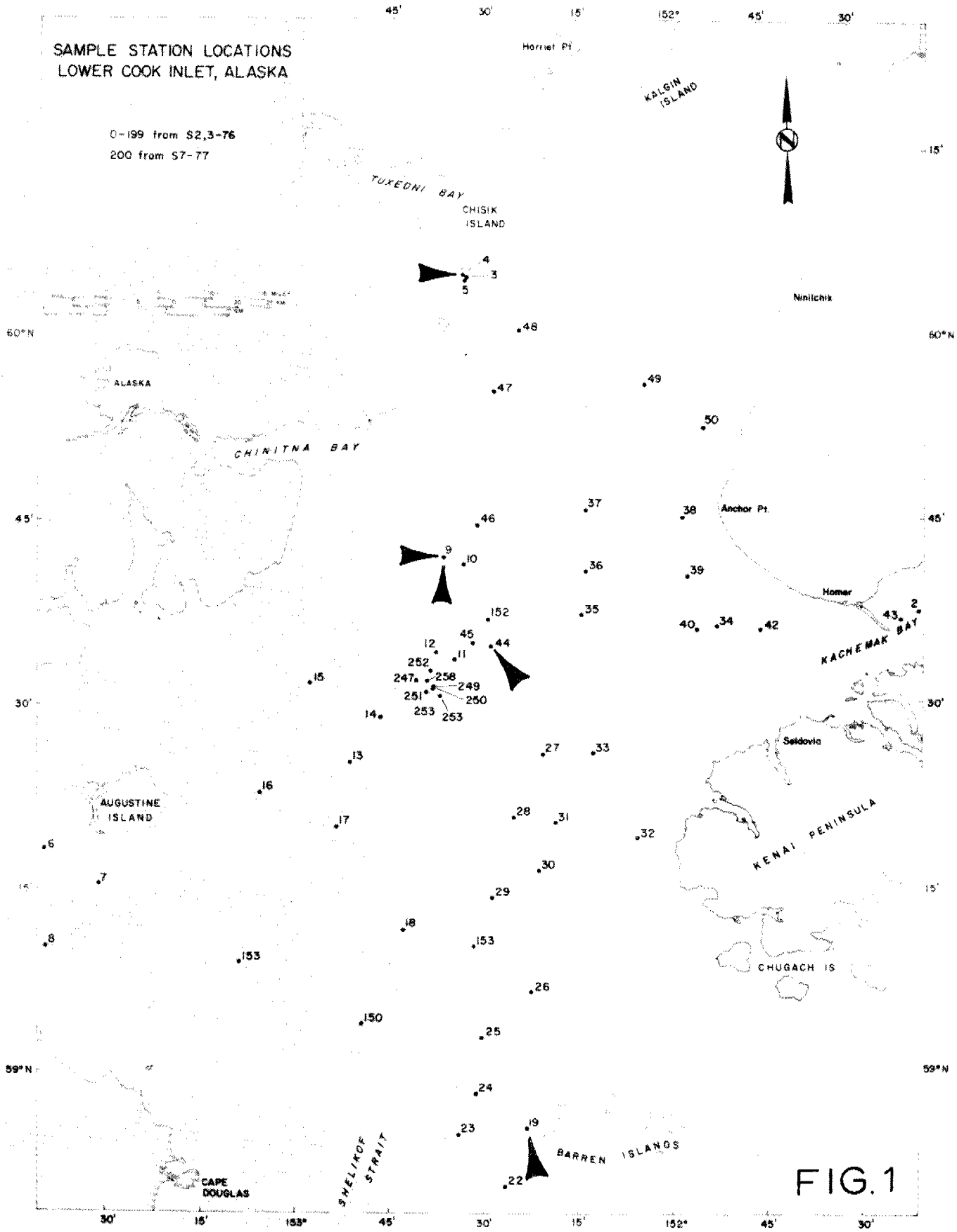
SAMPLE STATION LOCATIONS
LOWER COOK INLET, ALASKA
0-199 from S2,3-76
200 from S7-77
45'
30'
15'
152°
45'
30'
Harriet Pt
KALGIN ISLAND
TUXEDNI BAY
CHISIK ISLAND
Nanilchik
60°N
ALASKA
CHINITNA BAY
Anchor Pt.
Homer
KACHEMAK BAY
Seldovia
KENAI PENINSULA
AUGUSTINE ISLAND
CHUGACH IS
BARREN ISLANDS
SHELIKOF STRAIT
CAPE DOUGLAS
59°N
153°

FIG. 1

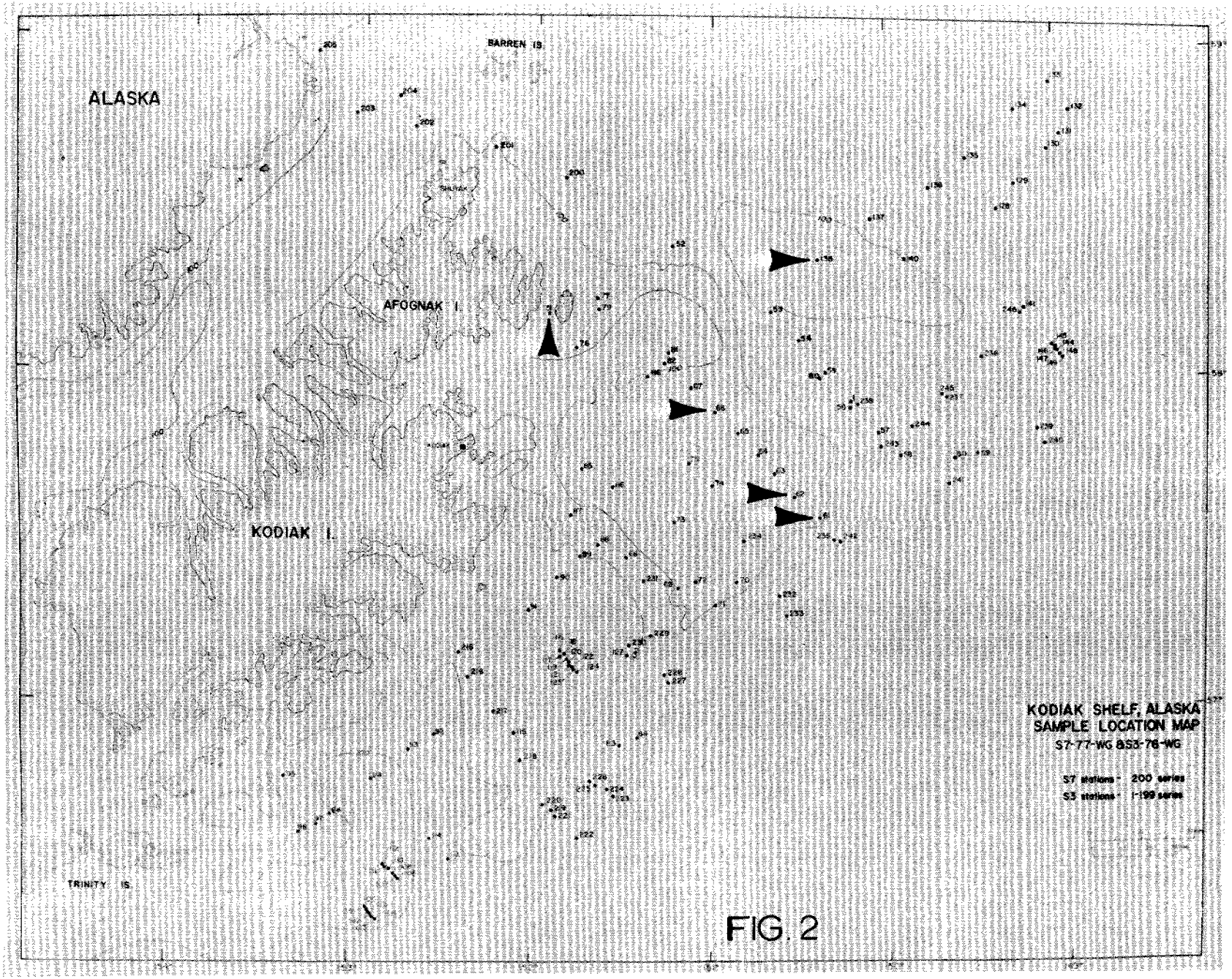
ALASKA
BARREN IS.
AFOGNAK I.
KODIAK I.
TRINITY IS.
KODIAK SHELF, ALASKA
SAMPLE LOCATION MAP
S7-77-WG & S3-76-WG
S7 stations - 200 series
S3 stations - 1-199 series

FIG. 2

FAULTING, SEDIMENT INSTABILITY, EROSION, AND DEPOSITION HAZARDS OF THE NORTON BASIN SEAFLOOR

ANNUAL REPORT OF THE PRINCIPAL INVESTIGATOR FOR THE YEAR ENDING MARCH, 1978

HANS NELSON

Research Unit #429

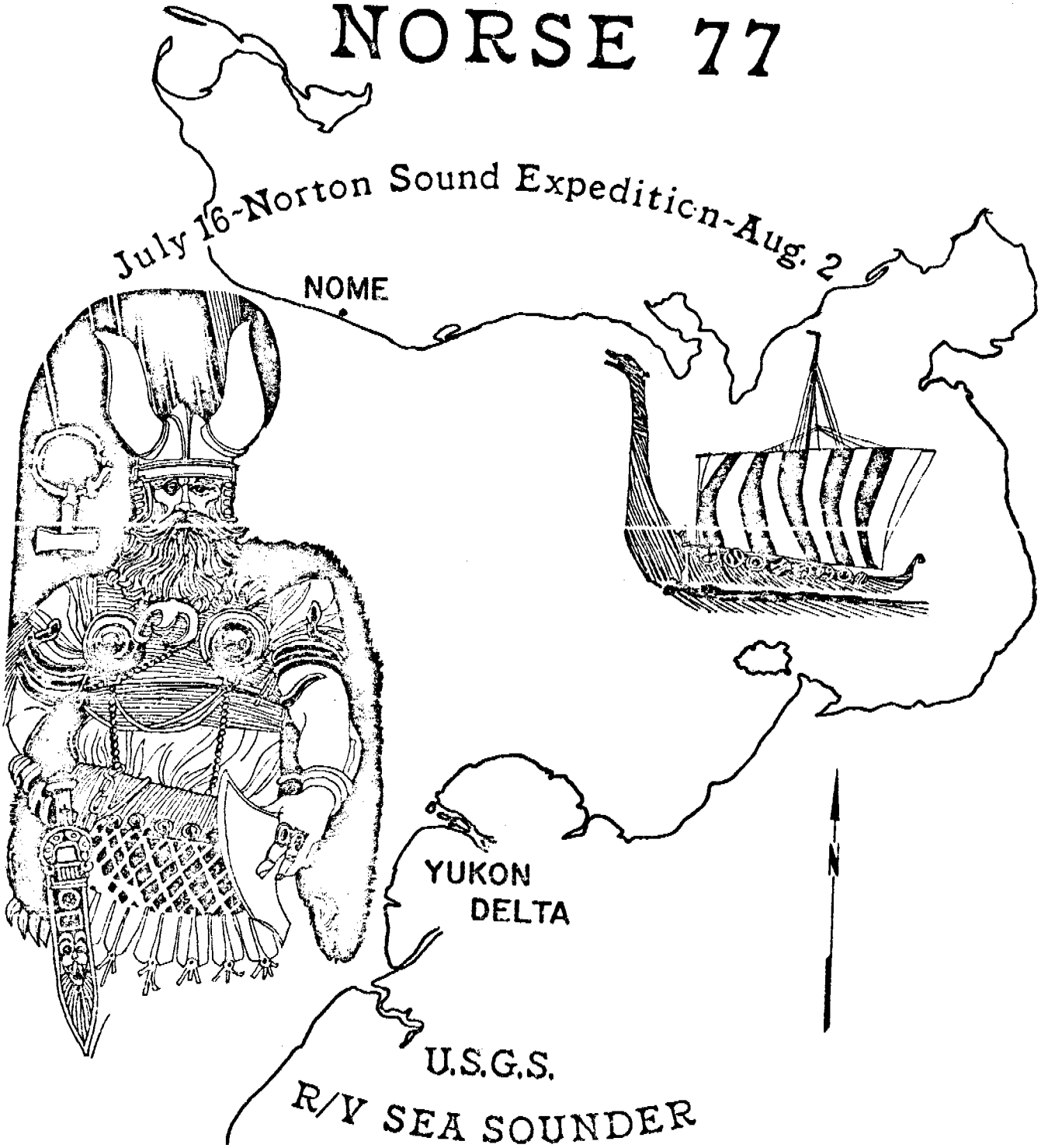

TABLE OF CONTENTS

Faulting, Sediment Instability, Erosion, and Deposition Hazards of the Norton Basin Sea Floor - Annual Report 1978

Hans Nelson and Devin R.Thor

I. SUMMARY

Environmental evaluation of geologic phenomena in northern Bering Sea indicates faulting, ice gouging, bottom currents, storm surges, and gas-charged sediment pose potential problems to development of offshore resources (Nelson, 1977; Nelson and Thor, 1977) (Fig. A1). Surface and near-surface faults are prominent along the entire northern margin of Norton Basin but Holocene fault activity is difficult to determine because strong current scour may be preserving or exhuming old scarps. Active migration of gas and seismicity along some of the traces suggests that recent movement occurs on certain fault segments in northern Norton Basin. Surface and near-surface faults are rare in west central Norton Basin and become more common along the southwest margin, particularly in straits areas northeast and north of St. Lawrence Island. Definition of the major Kaltag fault system and possible recent activity in southeastern Norton Basin await inshore research of the R.V. KARLUK. The reconnaisance mapping of surface scarps and near-surface faults will be terminated with this report except for inshore areas of R.V. KARLUK research. Determination of recent activity depends mainly on completion of seismicity studies.

Potentially unstable near-surface sediment results from apparent thermogenic gas charging in a local area 40 km south of Nome and from a wide region of biogenic gas charging in north central Norton Sound. Geophysical, geotechnical, and geochemical evidence indicate that hydrocarbon gases of subsurface, thermogenic origin apparently migrate into the near-surface sediment along fault zones 30-40 km south of Nome. Subbottom reflector terminations on continuous seismic reflection profiles outline a large zone of anomalous acoustic responses about 9 km in diameter and at 100 m depth that may be caused by a subsurface accumulation of gas. Gas migration from the subsurface accumulation to the surface sediment is indicated by smaller zones of reflector terminations observed in high-resolution profiles and more rapid penetration of the vibracorer in sediment at sites of surface acoustic anomalies. Sediment from a vibracore taken at such a site showed unusually high concentrations of hydrocarbon gases heavier than methane and also significant quantities of gasoline-range hydrocarbons. The gas composition and presence in near-surface sediment above a thick underlying section with acoustic anomalies suggest both a potential petroleum source at depth and a possible hazard for any future drilling activity in this area. Any artificial structures penetrating the apparent large gas accumulation at 100 m or associated faults with gas-charged sediment may provide direct avenues for uncontrolled gas migration to the sea floor. Such structures also may encounter reduced bearing capacity in this gas-charged substrate.

Small (3 to 8 m in diameter), shallow (<.5 m deep), circular-shaped craters observed on sonographs over a large area of north central Norton Sound

may be formed by present-day gas venting. The craters are associated with near-surface peat layers, gas-rich sediment, and acoustic anomalies observed in high-resolution seismic reflection profiles. Near-surface peat layers from 1-2 m below the sea floor have been vibracored throughout northern Bering Sea. These peaty muds are non-marine, pre-Holocene deposits with abnormal amounts of organic C (>5%) and biogenic methane gas generated from the buried organic debris. This gas-charged near-surface sediment causes sporadic acoustic anomalies due to the attenuation of sound waves in low density peaty muds and gas-charged sediment. Both acoustic anomalies and gas craters occur only where freshwater mud is now covered by a relatively thin (1-2 m) layer of Holocene mud. Where Holocene mud is thicker near the Yukon delta or grades into sand in Chirikov Basin, no craters are found.

In non-storm conditions, the near-surface gas may be trapped by thin modern muds. Apparently the gas escapes and forms craters during periodic storms that cause rapid changes in pore water pressures because of sea level set up, seiches, storm waves, and unloading due to sediment resuspension and erosion of covering muds. Gas venting and sediment depressions often formed during peak storm periods, have been associated with pipeline breaks in the oil producing regions of the North Sea and the Gulf of Mexico. The near-surface gas-charged sediment and peaty mud also may exhibit reduced bearing strength for gravity-type offshore platforms.

Ice scouring of bottom sediment is found everywhere throughout northeastern Bering Sea where water depths are less than 20 m, but also has been noted in water depths up to 30 m. Ice gouge furrows cut into bottom sediment a maximum of 1 m and occur most often and ubiquitously as solitary gouges. Pressure ridge raking is most common around the shoals of the Yukon prodelta because of the presence of a well-developed ice shear zone. Most of Norton Sound is affected by some degree of ice gouging as are the margins and sand ridge shoal areas of Chirikov Basin.

Much of the gouging in the Sound is probably caused by pressure ridges formed along shear zones as Norton Sound pack ice moves past the stationary shorefast ice. The combination of pronounced Yukon prodelta shoals and ice convergence offshore from the delta area account for the high density of gouging in this area. Because ice gouging is a pervasive scouring agent, any bottom facilities such as cables or pipelines should be buried below the depth of potential gouge penetrations. The base of any gravity structures on the sea floor and supporting substrate also should be protected from ice keels.

In certain areas of the intense ice gouging, large scour depressions are associated with the gouge furrows and silty muds. This series of large (25 to 150 m in diameter), irregularly shaped, shallow (up to 1 m deep) depressions in Yukon-derived, silty, sandy mud occurs along the southwestern margin of the Yukon prodelta area and on the flanks of an extensive, shallow trough in north-central Norton Sound. The depressions usually are associated with increased bottom steepness and regions of higher bottom current speeds. Some of the northern depressions are found near sea-floor scarps of unknown origin; those west of the prodelta front are definitely associated with ice-gouge furrows. Apparently, in regions where current speed is increased because of constriction of water flow along flanks of troughs, shoals, or prodelta fronts, any further disruption of current flow by slump scarps or

ice-gouge furrows initiates scour of the Yukon River derived sediment to form large, shallow depressions.

Presence of current scour depressions outlines regions where any artificial structure disrupting current flow may cause extensive erosion of Yukon mud and potentially hazardous undercutting of the structure. Even buried structures may be subject to scour because naturally occurring ice gouges may be greatly broadened and deepened by strong currents to expose the buried structure. Full assessment of this geologic hazard requires long-term current monitoring in specific scour regions to predict current intensity and periodicity, especially during major storms when combined storm tide and wave currents may be several times greater than normal currents.

In sandy substrates, especially in strait areas, strong bottom currents result in migrating fields of mobile bedforms. Sand waves, 1 to 2 m high with wavelengths of 10 to 20 or 150 to 200 m, and ripples 4 cm high with 20 cm wavelength, occupy the crests and some flanks of a series of large, linear sand ridges lying west of the Port Clarence area (Field and others, 1977; Nelson and others, 1977; Cacchione and others, 1977). Ice gouges are found in varying states of preservation on several ridges. This indicates active sand wave modification and recent movement. Survey tracklines of 1976 were replicated in 1977 and local changes in bedform type and trend further substantiate recent bedform activity. Movement of small-scale sand waves and bedload transport occur during calm weather, but maximum change of large-scale sand waves may take place when northerly current flow is enhanced by sea level set-up from major southwesterly storms. Strong north winds from the arctic, however, reduce the strength of the continuous northerly currents and thereby reduce the amount of bedload transport and activity of mobile bedforms near Bering Strait. Port Clarence is the only natural harbor north of the Bristol Bay area and its use as a future port is quite possible if resource development takes place in the northeastern Bering Sea. The long-term dynamics of the largest mobile bedform areas surrounding the entrance to Port Clarence must be defined so that realistic recommendations can be made for depth of burial or "safe" corridors for pipelines and sea-floor structures.

In conclusion, present knowledge suggests that the offshore region surrounding the Yukon Delta and eastern Bering Strait areas have the combination of the most severe geologic hazards (Fig. A1). Faulting and current scour are most intense near Bering Strait, but similar less severe conditions exist near Anadyr and Shpanberg Strait. Ice gouge, bottom-current scour and storm surge activity are all intense over a wide area around the shallow prodelta area. Apparent gas cratering occurs throughout north central Norton Sound. Dynamics of mobile bedforms, scour depressions, storm surge deposits, and gas craters must be ascertained before extent of these hazards can be fully assessed. Our confirmation of a thermogenic hydrocarbon seep 40 km south of Nome is likely to cause a quantum jump in interest and development in Norton Basin. This points to the urgent need for a continued strong program of environmental research in this outer continental shelf area.

SUMMARY BIBLIOGRAPHY - YEAR ENDING MARCH, 1978

Cacchione, D.A., Drake, D.E., Nelson, C.H., 1977, Sediment transport in Norton Sound, Alaska, (abs.):Transaction of AGU, EOS, v. 58, no. 6 p. 408.

Clukey, E.C., Nelson, Hans, and Newby, J.E., 1978, Geotechnical properties of northern Bering Sea sediment: U.S. Geological Survey Open File Rept. No. 48p.

Field, M.E., Nelson, Hans, Cacchione, D.A., and Drake, D.E., 1977, Dynamics of bedforms of an epicontinental shelf: northern Bering Sea (abs.): Transactions Am. Geophys. Union, EOS, v. 58, no. 12, p. 1162.

Nelson, Hans, Field, M.E. , Cacchione, D.A., and Drake, D.E., 1978, Activity of mobile bedforms on northeastern Bering shelf, in Environmental Assessment of the Alaskan Continental Shelf, Ann. Rept. of Principal Investigators for the year ending March, 1978, v. _____, Env. Res. Lab., Boulder, Colo., NOAA, U.S. Dept. of Commerce, (in press).

Holmes, M.C., Cline, J.D., and Johnson, J.L., 1978, Geological setting of Norton Basin gas seep: Proc. 10th Ann. Offshore Tech. Conf., v. , OTC paper #3052 (in press).

Howard, J.D., and Nelson, Hans, 1977, Physical and biological sedimentary structures of Norton Sound, Alaska (abs.): Geol. Soc. America, abstracts with programs, v. 9, no. 7, p. 1028.

Johnson, J.L., and Holmes, M.L., 1977, Prelimnary report on surface and subsurface faulting in Norton Sound and Northeastern Chirikov Basin, Alaska, in: Environmental Assessment of the Alaskan Continental Shelf, Ann. Rept. of Principal Investigators for the year ending March, 1977, v. XVIII, Env. Res. Lab., Boulder, Colo., NOAA, U.S. Dept. of Commerce, p. 14-41.

Johnson, J.L. and Holmes, M.L., 1978, Final report on surface and subsurface faulting in Norton Sound and Northeastern Chirikov Basin, Alaska, in: Environmental Assessment of the Alaskan Continental Shelf, Ann. Rept. of Principal Investigators for the year ending March, 1978, vol.____ (in press).

Kvenvolden, K.E., Rapp, J.B., and Nelson, Hans, 1978, Low molecular weight hydrocarbons in sediments from Norton Sound: Am. Assoc. Petroleum Geologists Bull., (abs.) (in press).

Larsen, M.C., Nelson, Hans, Thor, D.R., 1978, Potential hazard of scour depressions in Yukon silt, in: Environmental Assessment of the Alaskan Continental Shelf, Ann. Rept. of Principal Investigators for the year ending March, 1978 v. _____, Env. Res. Lab., Boulder, Colo., NOAA, U.S. Dept. of Commerce, (in press).

Larsen, B.R., Nelson, Hans, Patry, J.J. and Heropoulos, Christopher, 1978, Trace metal content of bottom sediment in northern Bering Sea, Final

Report, in: Environmental Assessment of the Alaskan Continental Shelf, Ann. Rept. of Principal Investigators for the year ending March, 1978, v. _____, Env. Res. Lab., Boulder, Colo., NOAA, U.S. Dept. of Commerce, (in press).

Nelson, Hans, 1977, Faulting, sediment instability and deposition hazards of the Norton Basin sea floor, in: Environmental Assessment of the Alaskan Continental Shelf, Qtrly Rept. of Principal Investigators, Oct.-Dec., 1976, v. 4, Env. Res. Lab., Boulder, Colo., NOAA, U.S. Dept. of Commerce, p. 14-41.

Nelson, Hans, 1977, Ice gouging and other environmental geologic problems of northern Bering Sea, in: Blean, K.M. (ed.), United States Geological Survey in Alaska: Accomplishments during 1976: U.S. Geol. Survey Cir., 751-B, p. B98.

Nelson, Hans, 1977, Large-scale bedforms and potential scour areas in northern Bering Sea: in: Environmental Alaskan Assessment of the Continental Shelf, Ann. Rept. of Principal Investigators for the year ending March, 1977, v. XVIII, Env. Res. Lab., Boulder, Colo., NOAA, U.S. Dept. of Commerce, p. 120-129.

Nelson, Hans, 1977, Potential sea-floor instability from gas-rich sediments and sediment depression craters, in: Environmental Assessment of the Alaskan Continental Shelf, Ann. Rept. of Principal Investigators for the year ending March, 1977, v. XVIII, Env. Res. Lab., Boulder, Colo., NOAA, U.S. Dept. of Commerce, p. 79-92.

Nelson, Hans, 1977, Storm surge effects, in: Environmental Assessment of the Alaskan Continental Shelf, Ann. Rept. of Principal Investigators for the year ending March, 1977, V. XVIII, Env. Res. Lab., Boulder, Colo., NOAA, U.S. Dept. of Commerce, p. 111-119.

Nelson, Hans, 1977, Summary of faulting, sediment instability, and erosion and deposition hazards of Norton Basin sea floor, in: Environmental Assessment of the Alaskan Continental Shelf, Ann. Rept. of Principal Investigators for the year ending March, 1977, v. XVIII, Env. Res. Lab., Boulder, Colo., NOAA, U.S. Dept of Commerce, p. 1-13.

Nelson, Hans, 1977, Trace metal content of bottom sediment in northern Bering Sea, in: Environmental Assessment of the Alaskan Continental Shelf, Qtrly. Rept. of Principal Investigators, Oct.-Dec., 1976, v. 3, Env. Res. Lab., Boulder, Colo., NOAA, U.S. Dept. of Commerce, p. 305.

Nelson, Hans, 1977, Trace metal content of bottom sediment in northern Bering Sea, in: Environmental Assessment of the Alaskan Continental Shelf, Ann. Rept. of Principal Investigators for the year ending March, 1977, v. XVIII, Env. Res. Lab., Boulder, Colo., NOAA, U.S. Dept. of Commerce, p. 300-320.

Nelson, Hans, and Creager, J.S., 1977, Displacement of Yukon-derived sediment from Bering Sea to Chukchi sea during the Holocene: Geology, v. 5, p. 141-146.

Nelson, Hans, Holmes, M.L., Thor, D.R., and Johnson, J.L., 1978, Continuous Seismic reflection data, Sea 5-76-BS cruise, northern Bering Sea: U.S. Geological Survey Open File Rept. (in press).

Nelson, Hans, Larsen, B.R., Jenne, E.A., and Sorg, D.H., 1977, Mercury dispersal from lode sources in the Kuskokwim River drainage, Alaska: Science, v. 198, p. 820-824.

Nelson, Hans, and Thor, D.R., 1977, Environmental geologic hazards in Norton Basin, Bering Sea (abs.): Geol. Soc. America, abstracts with programs, v. 9, no. 7, p. 1111.

Nelson, Hans and Thor, D.R., 1977, Faulting, sediment instability, erosion and deposition hazards of Norton Basin Sea Floor, in: Environmental Assessment of the Alaskan Continental Shelf, Qtrly. Rept. of Principal Investigators, April-June, 1977, v. I, Env. Res. Lab., Boulder, Colo., NOAA, U.S. Dept. of Commerce, p. 120-129.

Nelson, Hans, Cacchione, D.S., Field, M.A., Drake, D.E., and Nilsen, T.H., 1977, Complex ridge and trough topography on a shallow current-dominated shelf, northwest Alaska: Am. Assoc. of Petroleum Geologists, Bull., v. 61, p. 817.

Nelson, Hans and Thor, D.R., 1978, Summary of faulting, sediment instability, erosion and deposition hazards of the NOrton Basin sea floor: Environmental Assessment of the Alaskan Continental Shelf, Ann. Rept. of Principal Investigators, for year ending March, 1978, v.____, Env. Res. Lab., Boulder, Colo., NOAA, U.S. Dept. of Commerce, (in press).

Nelson, Hans, Kvenvolden, K.E., and Clukey, E.C., 1978, Thermogenic gas in sediment of Norton Sound, Alaska, Proc. of OTC., 1978, 12 p. (in press).

Nelson, Hans and Kvenvolden, K.E. and Clukey, E.C., 1978, Potential hazards of thermogenic gas in near-surface sediment of Norton Sound, Alaska, in: Assessment of the Alaskan Continental Shelf, Ann. Rept. of Principal Investigators for the year ending March, 1978, v.____, Env. Res. Lab., Boulder, Colo., NOAA, U.S. Dept of Commerce, (in press).

Nelson, Hans, Rowland, R.W., Stoker, S., and Larsen, B.R., Interplay of Physical and biological sedimentary structures of the Bering Sea epicontinental shelf: Jour. Sed. Petrology, (in review), 70 p.

Nelson, Hans, Thor, D.R., and Sandstrom, M.W., 1978, Modern biogenic gas craters (sea floor "pockmarks") on the Bering shelf, Alaska In: Environmental Assessment of the Alaskan Continental Shelf, Ann. Rept. of Principal Investigators for the year ending March, 1978, v. XV__, Env. Res. Lab., Boulder, Colo., NOAA, U.S. Dept. of Commerce, (in press).

Newby, John, Clukey, E.C., and Nelson, Hans, 1977, Preliminary report - physical properties and geotechnical characteristics of northern Bering Sea sediments, in: Environmental Assessment of the Alaskan Continental shelf, Ann. Rept. of Principal Investigators for the year ending March, 1977, v. XVIII, Env. Res. Lab., Boulder, Colo., NOAA, U.S. Dept. of Commerce, p.42-78.

Patry, J.J., Larsen, B.R., Nelson, Hans and Heropoulos, Christopher, 1977, Trace metal content of bottom sediment, northern Bering Sea, in: Environmental Assessment of the Alaskan Continental Shelf, Qtrly. Rept. of Principal Investigators, April-June, 1977, v. I, Env. Res. Lab., Boulder, Colo., NOAA, U.S. Dept. of Commerce, P. 846-856.

Thor, D.R., Nelson, Hans, and Evans, J.E., 1977, Preliminary assessment of ice gouging in Norton Sound, Alaska, in: Environmental Assessment of the Alaskan Continental Shelf, Qtrly. Rept. of Principal Investigators for the year ending March, 1977, v. XVIII, Environmental Research Lab., Boulder, Colo., NOAA, U.S. Dept. of Commerce, p. 93-110.

Thor, D.R. and Nelson, Hans, 1978, Continuous seismic reflection data. Sea 5-77-BS cruise, northern Bering Sea: U.S. Geological Survey Open File Rept. (in press).

Thor, D.R. and Nelson, Hans, and Williams, R.O., 1978, Environmental geologic studies in northern Bering Sea, in: Blean, K.M. (ed.), United States Geological Survey in Alaska, Accomplishments during 1977, 4 p. (in press).

Thor, D.R. and Nelson, Hans, 1978, Faulting, sediment instability, erosion and deposition hazards of Norton Basin Sea Floor, in: Environmental Assessment of the Alaskan Continental Shelf, Qtrly. Rept. of Principal Investigators, Aug.-October, 1977, Env. Res. Lab., Boulder, Colo., NOAA, U.S. Dept. of Commerce, , p. 628-649.

Thor, D.R., and Nelson, Hans, 1978, Faulting, sediment instability, erosion and deposition hazards of Norton Basin Sea Floor, in: Environmental Assessment of the Alaskan Continental Shelf, Qtrly. Rept. of Principal Investigators, Nov., 1977,-Jan., 1978, v. ____, Env. Res. Lab., Boulder, Colo., NOAA, U.S. Dept. of Commerce, (in press).

Thor, D.R., Nelson, Hans and Williams, R.O., 1978, Ice gouging in Norton Sound, Alaska, in: Environmental Assessment of the Alaskan Continental Shelf, Ann. Rept. of Principal Investigators for the year ending March, 1978, v. ____, Env. Res. Lab., Boulder, Colo., NOAA, U.S. Dept. of Commerce, (in press).

II. INTRODUCTION

A. General Nature and Scope of Study

This research addresses geological hazards that may result from surface and near-surface faulting, sediment instability, and erosion and deposition processes in the Norton Basin region (Fig. A2). Geological baseline parameters and process information also are generated that provide valuable ancillary information for other interdisciplinary studies. For example, data on sediment texture is presented that is crucial to understanding sediment dynamics questions encountered in RU 430 or benthic organism distribution. Opportunities to collect baseline information on trace metals, and light and heavy hydrocarbon fractions in surface and subsurface hydrocarbons also have been provided. These data are important inputs for RU 413 and for NOAA studies of light hydrocarbon gas seeps.

B. Specific Objectives

To meet our objective of defining recently active faults we are reviewing all old sparker and airgun records to trace fault origins. These are then compared with new reconnaissance data on surface and near-surface faulting observed in high-resolution records. Our goal for sediment stability problems is to characterize soils engineering index properties of the sediment and compare this with other near-surface sediment parameters of gas content, seismic acoustic anomalies, mass movement evidence, and storm sand and peat stratigraphy to determine areas where sediment failure is possible. By studying bedforms on side-scan sonar records, thickness of Holocene sediment on high-resolution seismic records, and stratigraphy of storm sand layers, we hope to determine regions where currents and waves cause excessive disruption of the sea bed. Detailed analysis of the side-scan sonar records also permits assessment of regions of intense ice gouging.

C. Relevance to problems of petroleum development

In this extremely shallow epicontinental shelf area similar to the North Sea (Fig. A3), the stability and maintenance of drilling rigs, production platforms, pipelines, and shoreline based facilities in the Norton Basin area are all threatened by potential hazards of active faulting, thermogenic gas charged sediments, thixotropic sediment, ice gouging, and sediment scour caused by current and wave erosion. Potential problems of biogenic gas venting and sediment collapse during storm wave interaction with the bottom must be understood prior to construction and installation of sea-floor structures for petroleum development.

III and IV. CURRENT STATE OF KNOWLEDGE IN THE STUDY AREA

A significant number of sediment studies and some deep-penetration seismic profiling had been accomplished in the Norton Basin region prior to the advent of OCS studies in the summer of 1976[1]. Reconnaissance studies with high-resoluton geophysical systems and sampling for cruise S5-76-BS concentrated on the eastern portion of Norton Basin and Norton Sound. The cruise being addressed in this report, S5-77-BS, concentrated on reconnaissance studies in Chirikov Basin and topical studies at several selected sites in Norton Basin (Fig. A4). The S5-77-BS cruise consisted of three weeks field work during July, 1977, and covered 2900 km of geophysical tracklines and collected 3.5 kHz, 12 kHz, 200 kHz, Uniboom, minisparker, side-scan sonar, and 160 kJ single-channel sparker seismic data (Fig. A5). Forty-eight stations were occupied where 29 box cores, 10 vibracores, and 11 Soutar van Veen grab samples were collected (Fig. A5).

V. SOURCES, METHODS, AND RATIONALE OF DATA COLLECTION

The nature of previous work in this large geographical area dictated the rationale for the study methods. Lack of any nominated areas also influenced decisions. The consequence is a concentration on broad reconnaissance of good, high-resolution geophysics and side-scan sonar data and of new sampling methods of vibracoring at scattered locations over the whole region. Last year's work has uncovered a much greater extent of sand wave fields near St. Lawrence Island and south of Nome, new regions of scour depression in Norton Sound, new areas of thermogenic and biogenic gas-charged sediment. As a result, in the 1978 summer field season, reconnaissance work will be completed and some time will be spent further studying topical areas which evolved from reconnaissance work (Fig. A4). These topical studies include the sand wave fields west of Port Clarence, and northwest and northeast of St. Lawrence Island, the thermogenic gas seep south of Nome, the biogenic gas craters in central and eastern Norton Sound, and the scour depression areas northwest and northeast of the Yukon delta.

Specific methods for each facet of the study are outlined in detail in the results secton. The research results are subdivided into six topics, each of which comprises a separate sub-report with different authors.

[1]See summary bibliography in Nelson et al., 1974; Oceanography of the Bering Sea, Occasional Publication No. 2, edited by Hood, D.W. and Kelly, E.J., Institute of Marine Science, Univ. of Alaska, Fairbanks, AK, p. 485-516. (note insert paper b) #(PG)

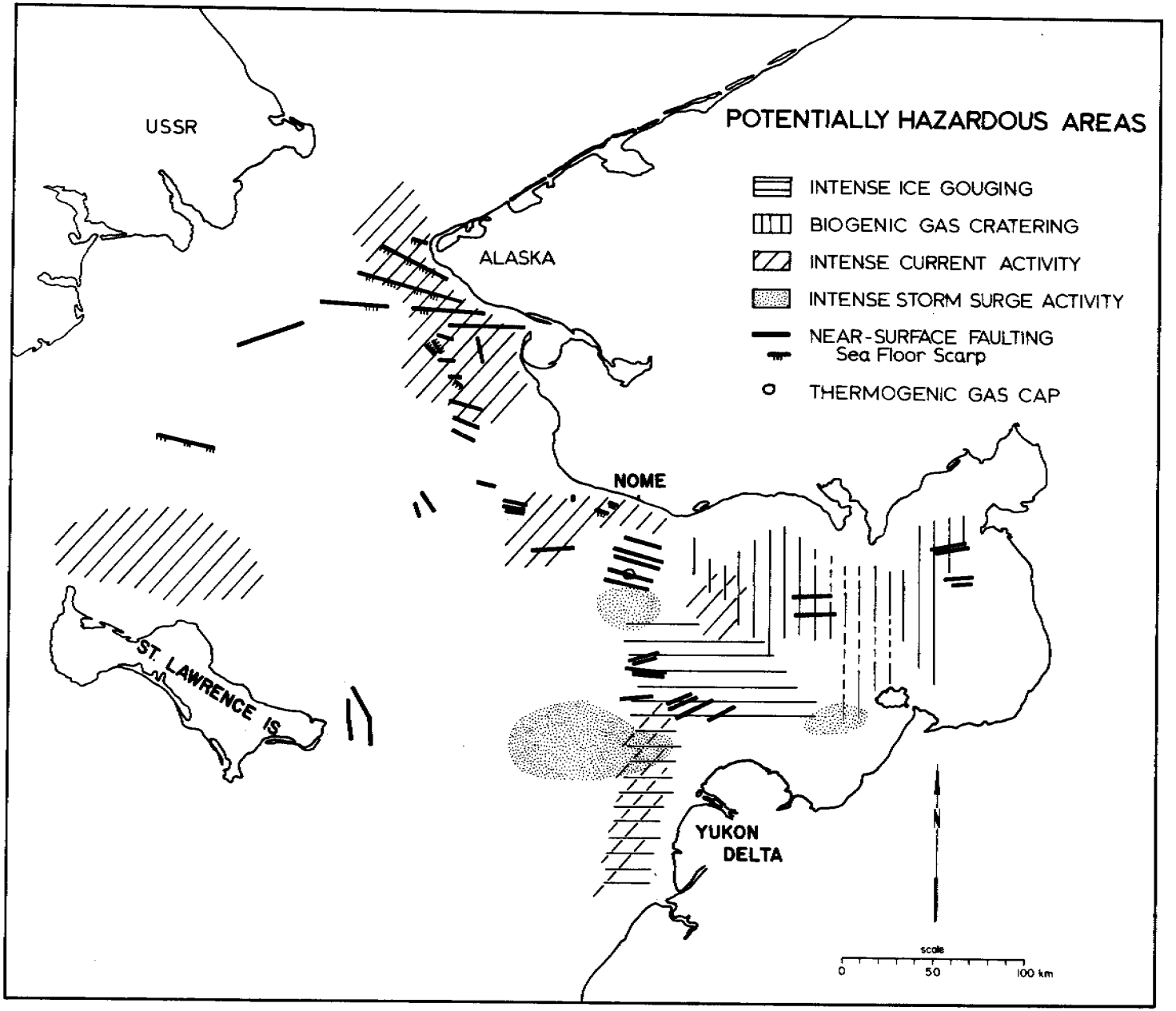

Figure A1. Summary of potentially hazardous regions in northeastern Bering Sea.

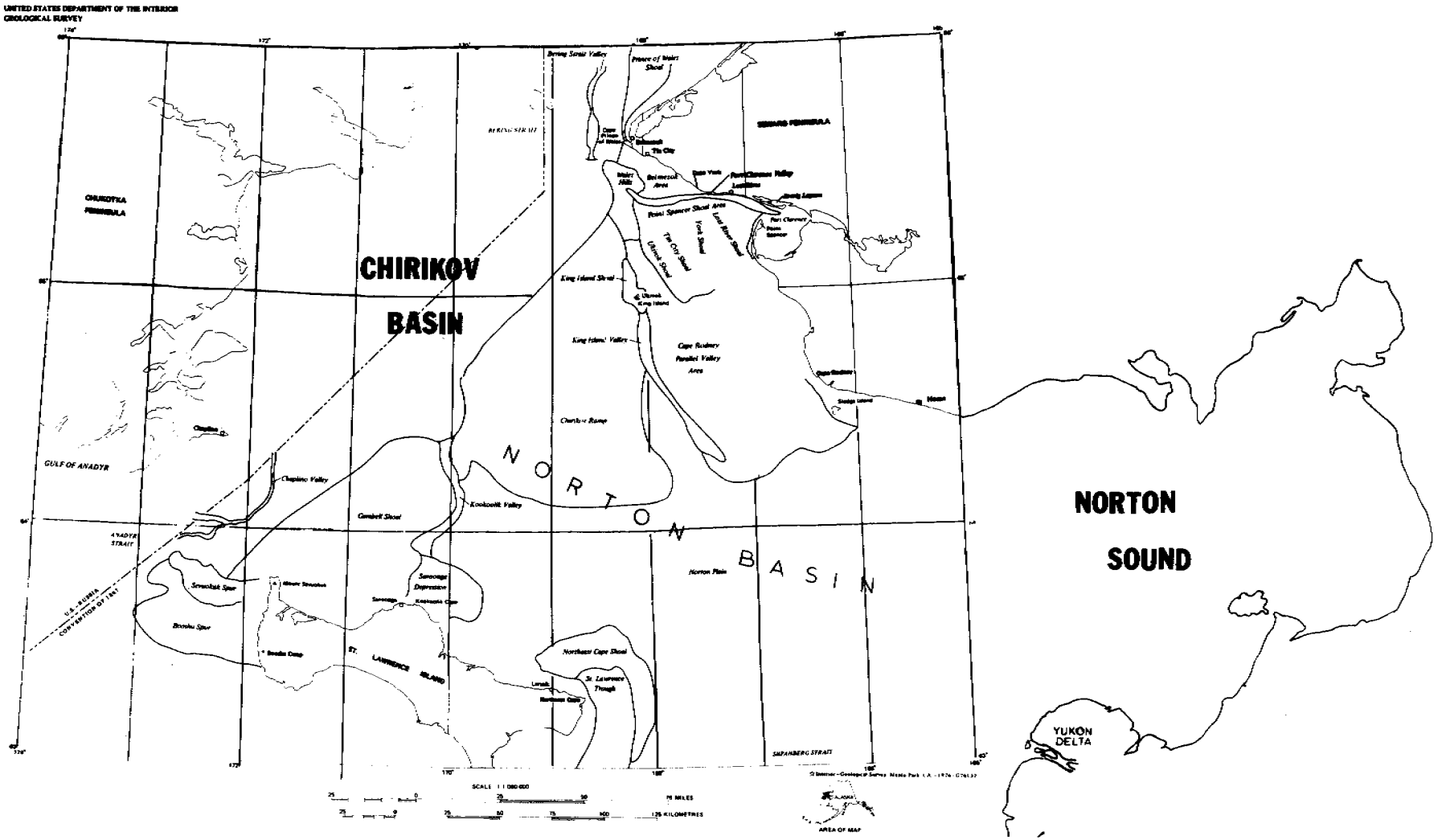

Figure A2. Physiographic subdivisions of the Chirikov Basin and Norton Sound.

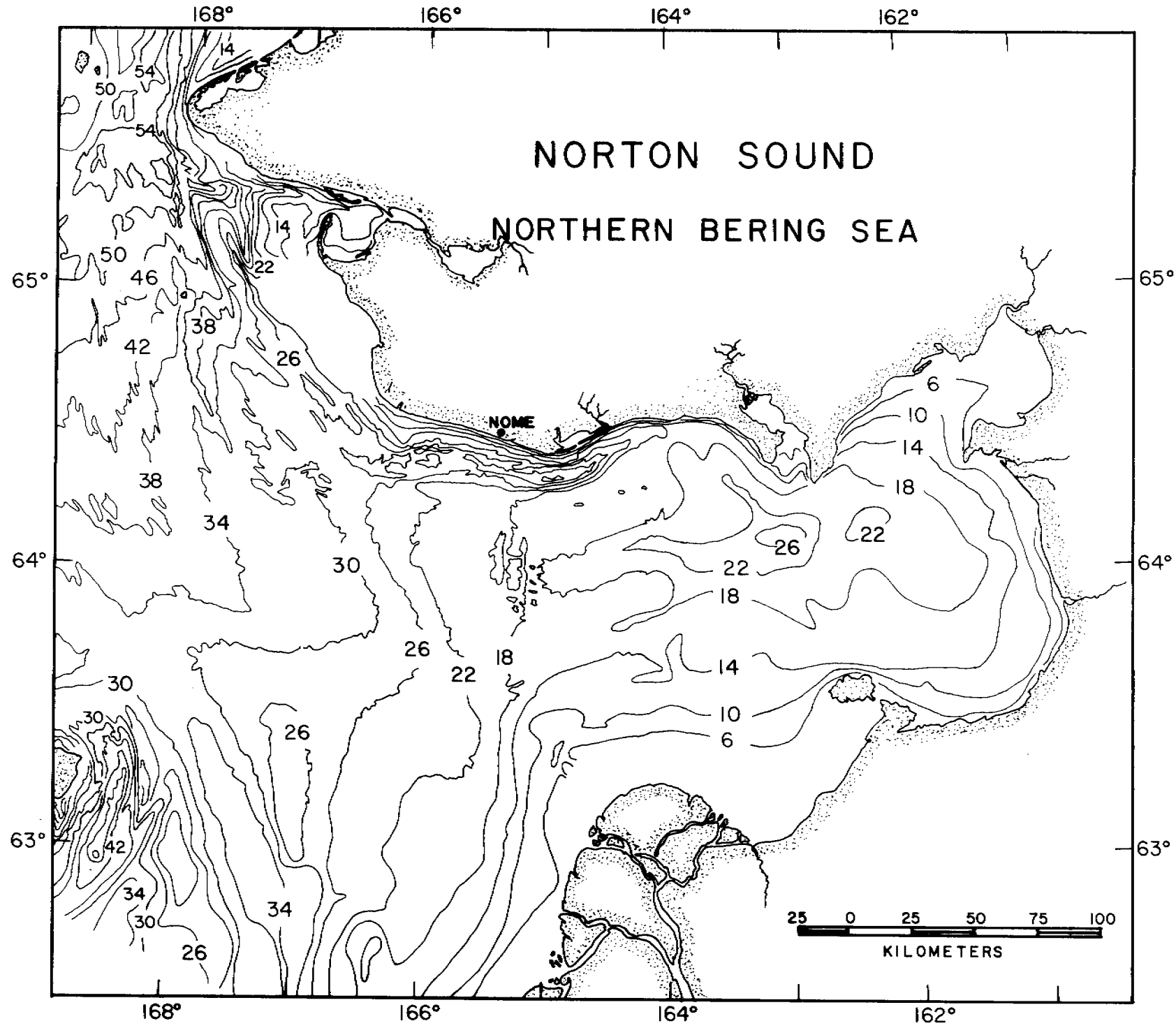

Figure A3. Bathymetry of northeastern Bering Sea.

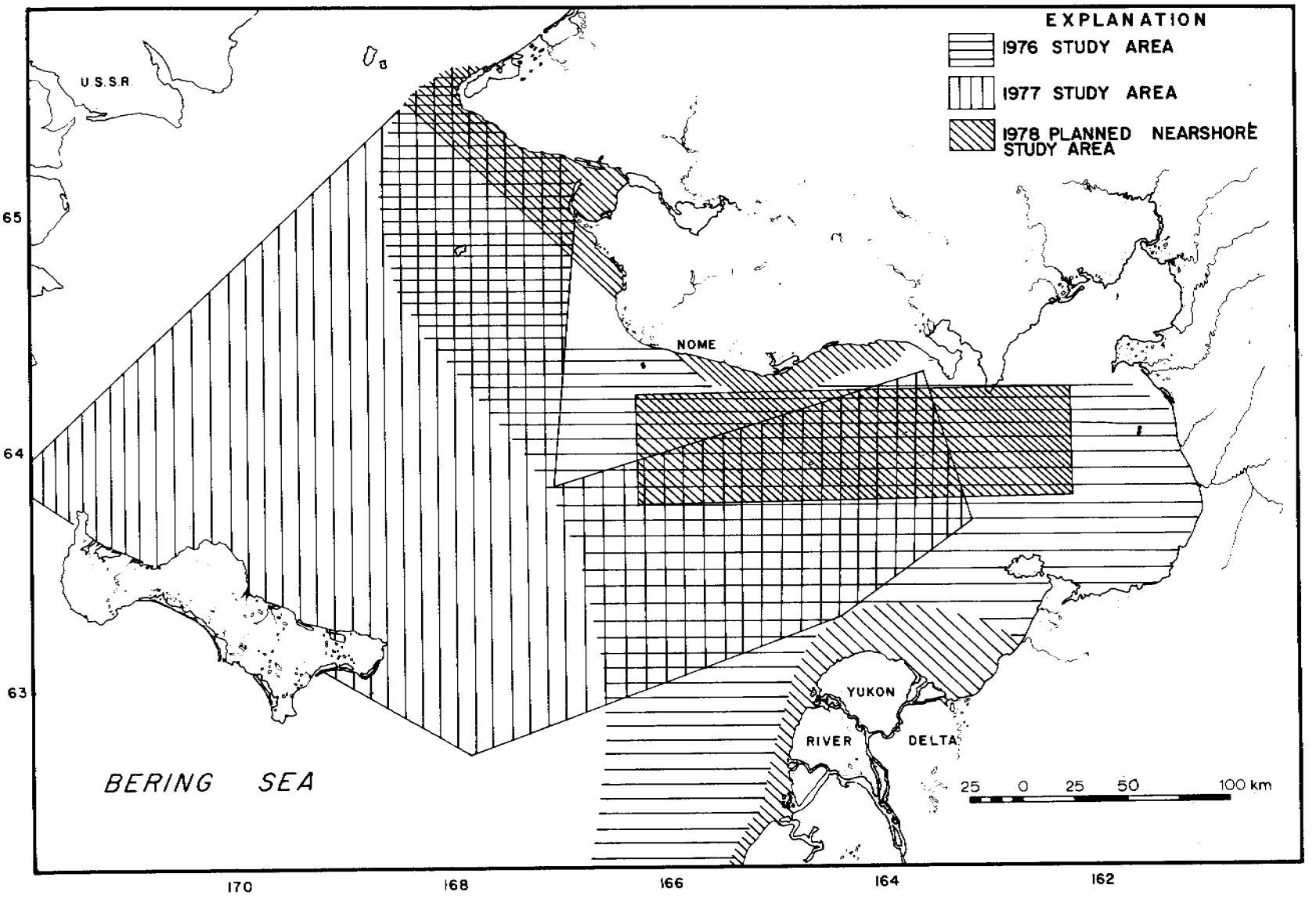

Figure A4. Areas covered by 1976 and 1977 studies, and areas of planned studies in 1978.

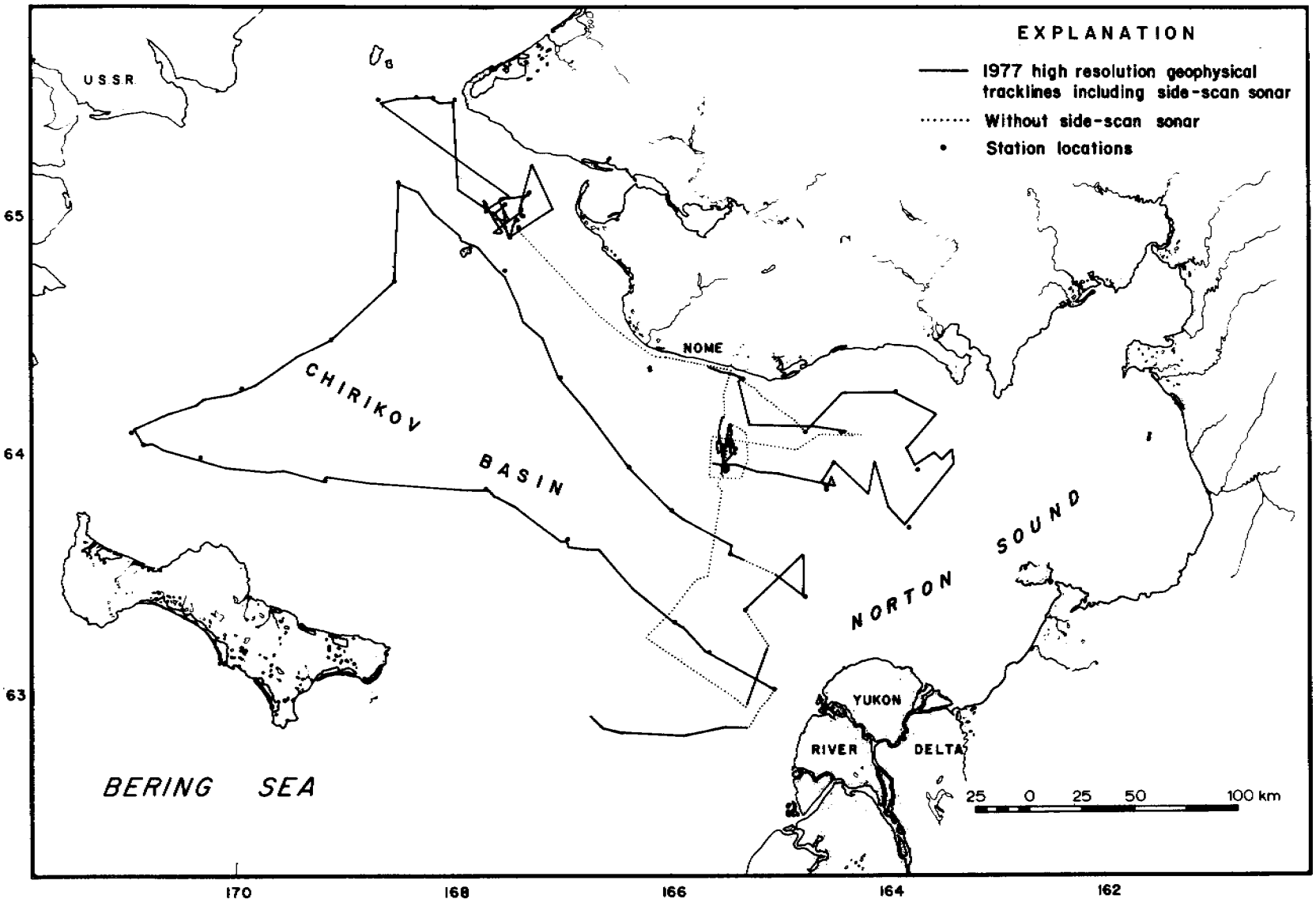

Figure A5. High-resolution seismic proflie tracklines (160 kJ sparker, Uniboom, 3.5 kHz), side scan sonar tracklines, and sampling stations from Sea-5-1977 cruise.

VI. RESULTS

B. REPORT ON SURFACE AND SUBSURFACE FAULTING IN NORTON SOUND AND CHIRIKOV BASIN, ALASKA

By

Janice L. Johnson and Mark L. Holmes

SUMMARY

Seismic reflection data were obtained in July 1977 by the U. S. Geological Survey aboard R/V SEA SOUNDER along 2800 km of track in Norton Sound and northeastern Chirikov basin. These data and records from several previous surveys were analyzed in order to determine the location, extent, and possible age and activity potential of offshore faulting. Acoustic reflection records were obtained using sparkers (160 and 0.8 kilojoule), Uniboom (1200 joule), and 3.5 kHz subbottom profiler. Sidescan sonar measurements were made along some of the tracklines whenever the large sparker was not deployed.

Maps showing the distribution of surface, near-surface, and deeper subbottom faults show that faulting occurs most commonly within 50 km of the margins of Norton basin, the deep sedimentary trough which underlies Norton Sound and Chirikov basin. A smaller number of faults were detected in the central regions of the basin.

Surface fault scarps were seen in several places in northern Chirikov basin. These sea-floor offsets ranged in height from 5 to 15 m along several west-trending faults which may be associated with some of the major transcurrent faults in Alaska. The existence of these scarps

indicates possible disturbance of sedimentary deposits over the fault, although the scarps may have been maintained by non-deposition. Evidence from both onshore and offshore field studies indicate that movement along these faults may have occurred between 12,000-120,000 years ago.

Many northwest-trending faults were mapped around the margins and in the central regions of Norton basin; they appear to show increasing displacement with depth and a thickening of the strata as they dip basinward away from the fault. These characteristics indicate a more or less continual movement along the faults as Norton basin was subsiding. The lack of recorded earthquakes in Norton basin during historical time implies that either activity along the offshore faults has ceased, or that movement is taking place at a slow but steady rate, preventing a buildup of strain and consequent earthquake-producing ruptures.

The west-trending faults in northern Chirikov basin appear to offset, and therefore postdate, the northwest trending faults which parallel the Norton basin axis. These two intersecting trends may have resulted from a change in the direction of regional compression during late Tertiary or early Quaternary time.

Considerable sea-floor relief hampered identification of surface scarps associated with offshore faults near St. Lawrence Island; and horizontal (transcurrent) motions along these faults may have taken place during Quaternary time in conjunction with movements on the Kaltag Fault which displaced Pleistocene deposits in western Alaska.

CONTENTS

INTRODUCTION

Geological and geophysical studies were carried out by U. S. Geological Survey personnel aboard R/V SEA SOUNDER in Norton Sound and Chirikov basin during July 1977 (Fig. B1). Acoustic survey systems used included 160 and 0.8 kilojoule sparkers, a 1200 joule (four transducer) Uniboom, a 3.5 kHz bathymetric/subbottom profiling system, and sidescan sonar. This section of the annual report deals primarily with an interpretation of the extent and hazard potential of the surface and subsurface faults shown on the sparker and Uniboom records. Discussions of the 3.5 kHz and sidescan sonar data will be found in other sections.

The geophysical data obtained on this recent USGS cruise has been supplemented in places by seismic reflection information which was collected on previous expeditions by the USGS, NOAA, and the University of Washington (Fig. B1). In 1967 a joint USGS/University of Washington cruise obtained 4200 km of 150 joule sparker data (Grim and McManus, 1970), and 3200 km of 120 kilojoule sparker records (Scholl and Hopkins, 1969). High-resolution seismic reflection surveys were conducted in 1967 in the nearshore region south of Nome between Sledge Island and Cape Nome (Tagg and Greene, 1973). Walton et al. (1969) shot 3840 km of single channel 40 in^3 air gun records during a joint USGS/NOAA (then ESSA) survey in 1969, and that same year an additional 800 km of 150 joule sparker records were collected in Chirikov basin on a joint USGS/University of Washington cruise. Johnson and Holmes (1977) reported on preliminary results of a study of recent faulting in the northern Bering Sea, based primarily on examination of approximately 3000 km of seismic reflection data collected aboard R/V SEA SOUNDER in September and October 1976. Holmes

et al. (1978) obtained an additional 675 km of single channel air gun reflection data and 13 refraction profiles in Norton Sound during a survey conducted by the USGS aboard R/V LEE in October 1977.

All seismic records, sidescan records, and navigational data from the 1976 and 1977 R/V SEA SOUNDER cruises are on microfilm. Copies can be obtained from the National Geophysical and Solar-Terrestrial Data Center, EDS/NOAA, Boulder, Colorado 80302, or from the Alaska Technical Data Unit, USGS, 345 Middlefield Road, Menlo Park, California 94025.

METHODS

This section discusses the instrumentation and procedures used in collecting navigation and acoustic survey data on the R/V SEA SOUNDER cruise in July 1977.

Navigation

Navigational information was obtained by two independent systems. A Magnavox satellite navigator with integrated Teledyne Loran C received inputs from the ship's speed log and gyro. This system computed dead reckoning positions every two seconds and the data were stored on magnetic tape and a teleprinter. Performance of the system was degraded somewhat by proximity to the Loran C master station at Port Clarence and the high elevation of many of the satellites during transit.

A Motorola mini-Ranger system was used to obtain fixes every seven and one-half minutes which were recorded on paper tape in digital form. This system measures the range to two or more shore-based transponders which were maintained by survey personnel on land. On a few occasions the included angle between the transponders was too small to permit obtaining reliable fix information.

Fixes were plotted at least every fifteen minutes on the navigational charts with appropriate notations made at the time of major course and speed changes. Radar and line-of-sight bearings were sometimes used to augment the other navigational information, and navigational accuracy probably averaged ± 150 m.

Acoustic Survey Techniques

Figure B1 shows the tracklines for the 1977 R/V SEA SOUNDER cruise, as well as those of previous expeditions on which seismic reflection data were collected. The figure also notes which acoustic systems were used during the various cruises. The bathymetry-subbottom profiler and sidescan sonar systems used aboard R/V SEA SOUNDER will be briefly discussed, although interpretation of these data will be, as previously mentioned, found in other sections of the report.

Seismic profiling operations aboard R/V SEA SOUNDER were carried out at speeds ranging from 4-6 knots. It was found that speeds greater or less than this range resulted in generation of "ship noise" by the propulsion machinery which produced a significant amount of interference on the records.

Sparker. A Teledyne SSP (Seismic Section Profiler) was used to obtain 325 km of single channel seismic reflection records in Norton Sound and northeastern Chirikov basin. Power output was normally 160 kilojoules, but was reduced to 120 kilojoules at times because of equipment casualties. The signals were received by a Teledyne 100-element Hydrostreamer and processed through a Teledyne seismic amplifier before being printed off a modified Raytheon PFR (Precision Fathometer Recorder). Frequency pass band was normally set at 20-98 Hz, and sweep and fire rate was 4 seconds. The records were annotated at 30 minute intervals with date, time (GMT), line number, water depth, and appropriate instrument settings. Changes in course, speed, or instrumentation were noted when they occurred.

Maximum penetration achieved by the sparker was approximately 2.1 km. The quality of the records was affected adversely by the shallow water and the generally flat nature of the bottom and subbottom reflectors. The shallow depth caused the water bottom multiple to appear at small distances below the initial sea-floor reflection, thus partially obscuring signals from deeper reflectors. The flat subbottom layering produced intra-formational or "peg-leg" multiples which also obscured or interfered with the primary reflections. In only a few places was an acoustic basement detected; more commonly the reflection amplitudes slowly decreased as the signal was attenuated in the sedimentary section.

Uniboom. Approximately 2800 km of high-resolution records were obtained using a hull-mounted EG & G Uniboom system consisting of four transducer plates. Total power level for this array was 1200 joules. An EG & G model 265 hydrophone streamer (10-element) was used as a receiver. Records were printed on an EPC 4100 recorder after passing through a Krohn-Hite filter. Sweep and fire rate was normally 1/4 second, although a 1/2 second sweep was used on occasion. The filter pass band was typically set from 400-4000 Hz. Time marks were made at 5 minute intervals and record annotations similar to those for the sparker were made at 15 minute intervals.

The quality of the Uniboom records was most affected by sea state, surficial bottom sediment type, and machinery generated ship noise. The hydrophone streamer was towed alongside the ship and only 20-30 cm below the surface. Consistently choppy seas were responsible for a significant amount of noise on the record which sometimes totally obscured subbottom

reflectors. Maximum penetration achieved was approximately 100 m, but was typically less than 75 m. Whenever coarse-grained and hard sediments were encountered penetration was severely reduced, and in some instances, such as near the Yukon Delta, the records are very poor.

Bathymetry/Subbottom Profiler. These data were collected along 2800 km of track using a Raytheon 3.5 kHz CESP II system. A hull-mounted transducer array consisting of 12 TR-109A units was used to send and receive the signals. Pulse generation and correlation functions were done by a CESP II (Correlator Echo Sounder Processor) and a PTR-105B (Precision Transmitter Receiver) was used as a tone burst amplifier during pulse transmission. Sweep and fire rates were normally 1/2 second. Time marks were made every 5 minutes and the records were annotated and depth measurements taken at 15-minute intervals.

Clarity of the records and amount of penetration varied considerably over the survey area. This system seemed less sensitive to ship-generated noise than the Uniboom, but the 3.5 kHz records were more adversely affected by hard bottom sediment. The long (50 msec) pulse generated during transmission also created an internal "ringing" in the transducer array which masked not only the weak subbottom reflections but sometimes the bottom echo as well in shallow water. Penetration ranged from 0-20 m.

Sidescan Sonar. An EG & G sidescan sonar system was used to record 1000 km of good to high quality data. Scales (sweeps) of 50 m and 100 m were used, and the "fish" altitude above the sea-floor was maintained at approximately 10 percent of the scale being used. The sidescan system was used in shallow water areas of known or suspected sand waves and ice-gouge features, and at such times the sparker system was shut down and its associated arc cables and hydrostreamer were brought aboard to prevent their fouling the sidescan cable.

GEOLOGIC SETTING

Tectonic Framework

The structural features and evolution of the Bering Sea continental shelf have been discussed by Scholl and Hopkins, 1969; Scholl et al., 1968; Pratt et al., 1972; Churkin, 1972; Lathram, 1973; Nelson et al., 1974; and Marlow et al., 1976. Figure B2 shows the major Cenozoic structures of western Alaska and eastern Siberia.

The general tectonic framework is characterized by large scale oroclinal bending forming two distinct flexures in central Alaska and eastern Siberia concave toward the Pacific Ocean. The Bering and Chukchi continental shelves are part of the broad intervening structural arc which is concave toward the Arctic Ocean.

This large scale oroclinal folding appears to have been completed before Oligocene time (Nelson et al., 1974), but continued activity along the major Alaskan transcurrent faults has displaced upper Tertiary and Quaternary sediment in several places on land and beneath the shelf areas (Patton and Hoare, 1968; Scholl et al., 1970; Grim and McManus, 1970). Total horizontal (right-lateral) movement along some of these large transcurrent faults has been approximately 130 km since the beginning of the Tertiary (Grantz, 1966; Patton and Hoare, 1968).

Regional Geology

Norton Basin. The geology of Norton basin has been discussed by Moore, 1964; Scholl and Hopkins, 1969; Grim and McManus, 1970; Tagg and Greene, 1973; Nelson et al., 1974; and Holmes et al., 1978. A submarine seepage of natural gas 40 km south of Nome has been described by Cline and Holmes (1977). Seismic reflection data suggest that the basin area is about 130,000 km^2; maximum basin depth has recently been estimated to be approximately 5.5 km (Anon., 1976). The basin probably contains as much as 180,000 km^3 of sediment.

The basin fill consists of three major stratified units (Homes et al., 1978), which are in turn covered by a thin mantle of Quaternary sediment (Grim and McManus, 1970; Tagg and Greene, 1973; Nelson and Creager, 1977). The lowermost unit in the basin, with a velocity of 4.9 km/sec (Holmes et al., 1978), may consist of Cretaceous nonmarine sandstones similar to those mapped onshore in the Koyukuk geosyncline (Patton and Hoare, 1968; Cobb, 1974). A velocity discontinuity at the top of this unit indicates that this interface may be an erosional unconformity.

Two other units of the basin fill can also be distinguished on the basis of compressional velocities (Holmes et al., 1978). A strong reflector on the reflection records corresponds to an apparent unconformity separating those units; the unconformity lies at a depth of about 1.2 km near the basin axis and approaches to within a few tens of meters of the sea floor near the basin margins. The compressional velocities above this unconformity are low, ranging from 1.6 to 2.1 km/sec; this section is probably composed of recent marine and glaciomarine sediment and loosely cemented sandstones and shales. The higher velocities (2.3-3.7 km/sec) below the

unconformity are more characteristic of compact or indurated sandstones and shales (Grant and West, 1965; Gardner et al., 1974). The unconformity was probably formed during the late Miocene marine transgression which inundated the northern Bering Sea continental shelf (Nelson et al., 1974). Strata of the unit below the unconformity form a broad synclinorium whose principal axis trends generally northwest; the beds of the upper unit are more nearly flat-lying.

Although younger Quaternary deposits everywhere cover the older Cenozoic and Mesozoic basin fill, some onshore outcrops and drill-hole data give clues as to the nature of the two upper units. Nonmarine coal-bearing strata of late Oligocene age are exposed on northwestern St. Lawrence Island (Patton and Csejtey, 1970), and several offshore holes drilled by the U.S. Bureau of Mines near Nome encountered marine sands and clayey silts of early Pliocene age at a subbottom depth of approximately 18 m (Scholl and Hopkins, 1969; Nelson et al., 1974). Late Miocene or early Pliocene marine limestone was recovered from a dredge haul 30 km south of St. Lawrence Island, just outside the basin.

These facts and the regional stratigraphic patterns indicate that the basin fill probably consists of late Cretaceous and lower to middle Tertiary sedimentary rock in the lower two units and upper Tertiary and Plio-Pleistocene sedimentary rocks and sediment in the upper unit. All direct evidence suggests that the lower units are nonmarine, but the size of the basin is such that unseen transitions to marine facies could occur within this sequence.

Acoustic Basement. The high compressional velocity contrast across the acoustic basement is indicative of a marked lithologic change at this interface (Holmes et al., 1978). Velocities of 5.5 to 6.5 km/sec are characteristic of igneous and metamorphic rocks (Grant and West, 1965), indicating that Norton basin is probably floored by a basement surface formed on strata which are analogous to the diverse older rocks which occur on land around the basin margins. Sedimentary, metamorphic, and igneous rocks of Precambrian through Mesozoic age are exposed on the Chukotka Peninsula (Nalivkin, 1960); and Seward Peninsula is formed primarily of Paleozoic sedimentary and metamorphic units with some Mesozoic and Cenozoic intrusive and extrusive rocks. Mesozoic sedimentary rocks (some slightly metamorphosed) and Cenozoic volcanics have been mapped onshore in the Yukon-Koyukuk basin east and southeast of Norton Sound (Miller et al., 1959; Patton and Hoare, 1968). At the southern margin of Norton basin, St. Lawrence Island is constructed mainly of Paleozoic, Mesozoic, and Cenozoic intrusive and extrusive rocks with some Cenozoic sedimentary deposits (Miller et al., 1959; Scholl and Hopkins, 1969; Patton and Csejtey, 1970). The acoustic basement probably represents an erosional surface which has been steepened by tectonic subsidence during development of Norton basin.

RESULTS AND DISCUSSION

Observed Faults and Structures

Locations of faults observed on seismic reflection profiles from Norton Sound and Chirikov basin are shown in Fig. B3. The majority of faults, especially those extending close to the sea floor, occur within 50 km of the basin margins. Most faults in Chirikov basin and western

Norton Sound trend northwest in alignment with the major axis of Norton basin. Synclinal and anticlinal axes mapped by Greene and Perry (unpub.), and shown in Johnson and Holmes (1977, Fig. B3), reflect this same trend. In eastern Norton Sound, the structural grain is nearly east-west.

Seismic records from the basin margins generally show sediments of the upper two units of basin fill, the Main Layered Sequence of Scholl and Hopkins (1969), resting with onlap unconformity against the eroded surface of the acoustic basement. The single channel seismic reflection systems were unable to resolve acoustic basement in the deeper basin areas where sediment thickness exceeded 2 km. Numerous faults offset the acoustic basement, often displacing overlying sediments. Many normal and antithetic faults displace the basin fill and extend to within 100 meters of the sediment surface. A few of these have topographic expression as fault scarps.

Faulting appears to be most complex, and the fault density is highest, in the area west of Port Clarence (Fig. B3). Several west-trending faults appear to intersect, and can be seen to offset, the dominant pattern of northwest-trending faults. These west-trending faults must therefore be younger than the others, and may be indicative of a change in the direction of regional compression during Quaternary time.

One of the major faults comprising this major east-west trend is the Bering Strait Fault (BSF) of Hopkins (unpub.). It forms the northern boundary of the Bering Strait Depression (BSD) named by Greene and Perry

(unpub.) and appears to extend for over 90 km west from Port Clarence (Fig. B3). A south-facing scarp 5 meters high marks the fault near the Bering Strait Depression. The scarp decreases in height eastward; no trace of the fault has been found beneath Port Clarence. This fault appears to have been active as recently as 12,000 years ago (Hopkins, unpub.).

The Port Clarence Rift (PCR) (Hopkins, unpub.) is a narrow fault-bounded depression extending eastward from the Bering Strait Depression; the fault along the northern margin of the depression is probably equivalent to the Cape York Fault of Greene and Perry (unpub.). This northern fault has a scarp 9 meters high near the Bering Strait Depression, which decreases to the east. No trace of this fault has been observed beneath Port Clarence, but displacement of bedrock beneath Grantley Harbor has been suggested as evidence for extension of the Port Clarence Rift further to the east. The Rocks beneath Grantley Harbor have experienced 16 km of left-lateral movement (Hopkins, unpub.). Several other west-trending faults with scarps up to 15 m high have been observed in the area west of Port Clarence (Fig. B3).

The rough seafloor topography north of St. Lawrence Island made identification of fault scarps difficult, but a few have been tentatively mapped (Fig. B3). A large west-trending fault has been inferred by Hopkins (unpub.) to parallel the northern coast of St. Lawrence Island and bend northward before reaching the western end of the island (Fig. B3). Existence of the St. Lawrence Fault Zone (SLF) is based on swarms of volcanic vents which trend N80^{o}W through the axis of the Kookooligit

Mountains, and on the extension of these volcanic rocks into offshore regions. Hopkins has suggested that movement along this fault has been left-lateral. Possibly it is related to movement along the Kaltag Fault (KF), a large transcurrent fault in western Alaska that has been known to displace Pleistocene sediments onshore.

Many deep-seated and near-surface normal faults occur in the central part of Norton basin, although no surface expressions of these have been identified. An increase in displacement with depth, and apparent thickening of beds on the downthrown side of these faults, indicates that they are probably growth faults along which movement has taken place more or less continuously during the major episodes of basin subsidence.

Several subbottom faults occur along the southern and eastern margins of Norton Sound (Fig. B3). Short line segments indicate faults have been observed on one crossing, and therefore, their exact orientation is unknown. However, several faults appear to parallel the trend of the Kaltag Fault; others may represent splays of the Kaltag Fault. No surface scarps were associated with the near-surface faults along the eastern margin of Norton Sound.

Fault Activity and Hazard Potential

Surface fault scarps in northern Chirikov basin are associated with the Bering Strait Fault, the Port Clarence Rift, and other nearby faults (Fig. B3). The Bering Strait Fault and Port Clarence Rift may represent extensions or splays of the large transcurrent faults which have been mapped in western Alaska and Seward Peninsula (Fig. B2). The scarps may have been caused by recent vertical movement on these faults, and therefore would indicate a definite hazard to man-made structures placed over

or near these fault zones. There is also the possibility, that the faults have been inactive for some time, and the scarps have been maintained by nondeposition or lack of erosion. Currents west of Port Clarence flow almost normal to the trend of these scarps, and carry almost one third of the Yukon River sediment load into the Chukchi Sea (Nelson and Creager, 1977). The persistence of the surface expression of the faults in spite of apparently vigorous erosional agents would argue for the fault scarps to be recently formed features.

The Bering Strait Fault must have formed between 12,000 and 120,000 years ago; evidence exists that a lake was formed during the Wisconsin glaciation when development of the fault scarp dammed a northward-flowing river west of present day Port Clarence. Marine terraces on Seward Peninsula may have been uplifted during the Illinoian glaciation as a result of movement along the fault 130,000 years ago. Although no specific age can be given to movements along these faults in northern Chirikov basin, the area should definitely be considered as potentially hazardous to placement of structures on the bottom in the vicinity of the fault scarps.

Only a few surface scarps have been noted in association with faults along the northern side of the St. Lawrence Island or in southern and eastern Norton Sound; the rough sea-floor topography in this area makes identification of fault scarps difficult. Movement may have occurred along these faults during Tertiary and Quaternary time in conjunction with known displacement in western Alaska along the large transcurrent Kaltag Fault. Further study is necessary to determine if this represents a hazard to resource development.

Earthquake records show an almost complete lack of epicenters beneath Norton basin. This lack of seismicity can be interpreted to indicate either inactivity or, conversely, that strain release is being accomplished by small but frequent adjustments along the faults. The growth nature of most of the northwest trending faults which parallel the Norton basin axis support the latter interpretation, although the rate of basin subsidence may have decreased since the end of Pleistocene time when rising sea-level opened Bering Strait and resulted in a significant change in deposition patterns in the northern Bering Sea.

CONCLUSIONS

Based on the foregoing discussion, the following conclusions may be made regarding the faulting observed in Norton Sound and Chirikov basin:

1. Faults are most numerous in a belt approximately 50 km wide around the margins of Norton basin. Near surface faults are more numerous in central Norton basin than previously reported, but are still less prevalent than around the periphery of the basin. Most of the faults trend generally northwest, with the basinward sides down-dropped; antithetic faults are also common, resulting in series of narrow horsts and grabens along the basin margins. These faults and the many associated anticlinal and synclinal folds involving the basin fill and acoustic basement are the result of tectonic activity which occurred during subsidence and filling of the 5.5-km deep Norton basin. Initial subsidence of the basin probably began during late Cretaceous time, and has continued to the present with two apparent major interruptions during early and late Tertiary time.

2. Surface scarps up to 15 m high are associated with some of the long west-trending faults in northern Chirikov basin. These scarps can indicate either recent activity or persistence due to lack of erosion or burial by sedimentation since the last movement. Scarps occur on the Bering Strait Fault and on the northern side of the Port Clarence Rift, and movement along these faults possibly occurred as recently as 12,000 years ago in conjunction with uplift of marine terraces on Seward Peninsula.

3. The west-trending faults in northern Chirikov basin intersect and appear to offset the northwest-trending faults and structures south of Bering Strait. This relationship implies that the west-trending features postdate the main Norton basin structures; the different trends could also be indicative of a shift in regional compressive axes.

4. None of the faults can definitely be classed as historically active, however the area of northern Chirikov basin west of Port Clarence should be considered potentially hazardous to any bottom mounted structures. The fault scarps in this region are still well defined in spite of the swift currents and bottom sediment transport which occur normal to the trend of the fault zones. Basin subsidence is probably still taking place, and the lack of recorded earthquakes beneath Norton basin may indicate that strain release is being accomplished by small but frequent movement along some of these faults.

5. West-trending subbottom faults without surface fault scarps occur along the southern margin of Norton basin. These may represent splays or displacements related to the Kaltag Fault, one of the major transcurrent faults in western Alaska. Movement along onshore portions of the Kaltag Fault have displaced Pleistocene deposits, but data regarding age of movements along the offshore portion are inconclusive.

REFERENCES

Anonymous, 1976, Prospective basins included in Alaska OCS sale plans: The Oil and Gas Journal, v. 74, p. 126-130.

Churkin, M., Jr., 1972, Western boundary of the North American continental plate in Asia: Geol. Soc. America Bull., v. 83, p. 1027-1036.

Cline, J. D., and M. L. Holmes, 1977, Submarine seepage of natural gas in Norton Sound, Alaska: Science, v. 198, p. 1149-1153.

Cobb, E. H., 1974, Synopsis of the mineral resources of Alaska: U.S. Geological Survey Bull. 1307, 53 p.

Gardner, G.H.F., L. W. Gardner, and A. R. Gregory, 1974, Formation velocity and density--the diagnostic basis for stratigraphic traps: Geophysics, v. 39, p. 770-780.

Grant, F. S., and G. F. West, 1965. Interpretation theory in applied geophysics: McGraw-Hill, New York, p. 8.

Grantz, A., 1966, Strike-slip faults in Alaska: U.S. Geol. Survey Open-File Report, 82 p.

Grim, M. S., and D. A. McManus, 1970, A shallow seismic-profiling survey of the northern Bering Sea: Marine Geology, v. 8, p. 293-320.

Holmes, M. L., J. D. Cline, and J. L. Johnson, 1978, Geological setting of the Norton basin gas seep: Proceedings, 1978 Offshore Technology Conference (in press).

Johnson, J. L., and M. L. Holmes, 1977, Preliminary report on surface and subsurface faulting in Norton Sound and northeastern Chirikov basin, in Environmental Assessment of the Alaskan Continental Shelf, v. XVIII, Hazards and Data Management, Annual Reports of Principal Investigators: U.S. Dept. of the Interior, Bureau of Land Management, p. 14-41.

Lathram, E. H., 1973, Tectonic framework of northern and central Alaska, in Pitcher, M. G., ed., Arctic Geology: Tulsa, Okla., American Assoc. Petroleum Geologists Mem. 19, p. 351-360.

Marlow, M. S., D. W. Scholl, A. K. Cooper, and E. C. Buffington, 1976, Structure and evolution of Bering Sea shelf south of St. Lawrence Island: American Assoc. of Petroleum Geologists Bull., v. 60, p. 161-183.

Miller, D. J., T. G. Payne, and G. Gryc, 1959, Geology of possible petroleum provinces in Alaska: U.S. Geol. Survey Bull. 1094, 131 p.

Moore, D. G., 1964, Acoustic reconnaissance of continental shelves: Eastern Bering and Chukchi Seas, in Miller, R. L., ed., Papers in Marine Geology, Shepard commemorative volume: New York, MacMillan Co., p. 319-362.

Nalivkin, D. V., 1960, The geology of the U.S.S.R.: New York, Pergamon Press, 170 p.

Nelson, C. H., D. M. Hopkins, and D. W. Scholl, 1974, Tectonic setting and Cenozoic sedimentary history of the Bering Sea, in Herman, Y., ed., Marine Geology and Oceanography of the Arctic Seas: New York, Springer-Verlag, p. 119-140.

Nelson, C. H., and J. S. Creager, 1977, Displacement of Yukon-derived sediment from Bering Sea to Chukchi Sea during Holocene time: Geology, v. 5, p. 141-146.

Patton, W. W., Jr., and J. M. Hoare, 1968, The Kaltag fault, west-central Alaska: U.S. Geol. Survey Prof. Paper 600-D, p. D147-D153.

Patton, W. W., Jr., and B. Csejtey, Jr., 1970, Preliminary geologic investigations of western St. Lawrence Island, Alaska: U.S. Geol. Survey Prof. Paper 684, 15 p.

Pratt, R. M., M. S. Rutstein, F. W. Walton, and J. A. Buschur, 1972, Extension of Alaskan structural trends beneath Bristol Bay, Bering shelf, Alaska: Jour. Geophys. Research, v. 77, p. 4994-4999.

Scholl, D. W., E. C. Buffington, and D. M. Hopkins, 1968, Geologic history of the continental margin of North America in Bering Sea: Marine Geology, v. 6, p. 297-330.

Scholl, D. W., and D. M. Hopkins, 1969, Newly discovered Cenozoic basins, Bering Sea shelf, Alaska: Amer. Assoc. Petroleum Geologists Bull., v. 53, p. 2067-2078.

Scholl, D. W., M. S. Marlow, J. S. Creager, M. L. Holmes, S. C. Wolf, and A. K. Cooper, 1970, A search for the seaward extension of the Kaltag fault beneath the Bering Sea: Geol. Soc. America, Abs. with Program, Cordilleran Sect., v. 2, p. 141-142.

Tagg, A. R., and H. G. Greene, 1973, High-resolution seismic survey of an offshore area near Nome, Alaska: U.S. Geol. Survey Prof. Paper 759-A, 23 p.

Walton, F. W., R. B. Perry, and H. G. Greene, 1969, Seismic reflection profiles, northern Bering Sea: ESSA Operational Data Report C+GS DR-B

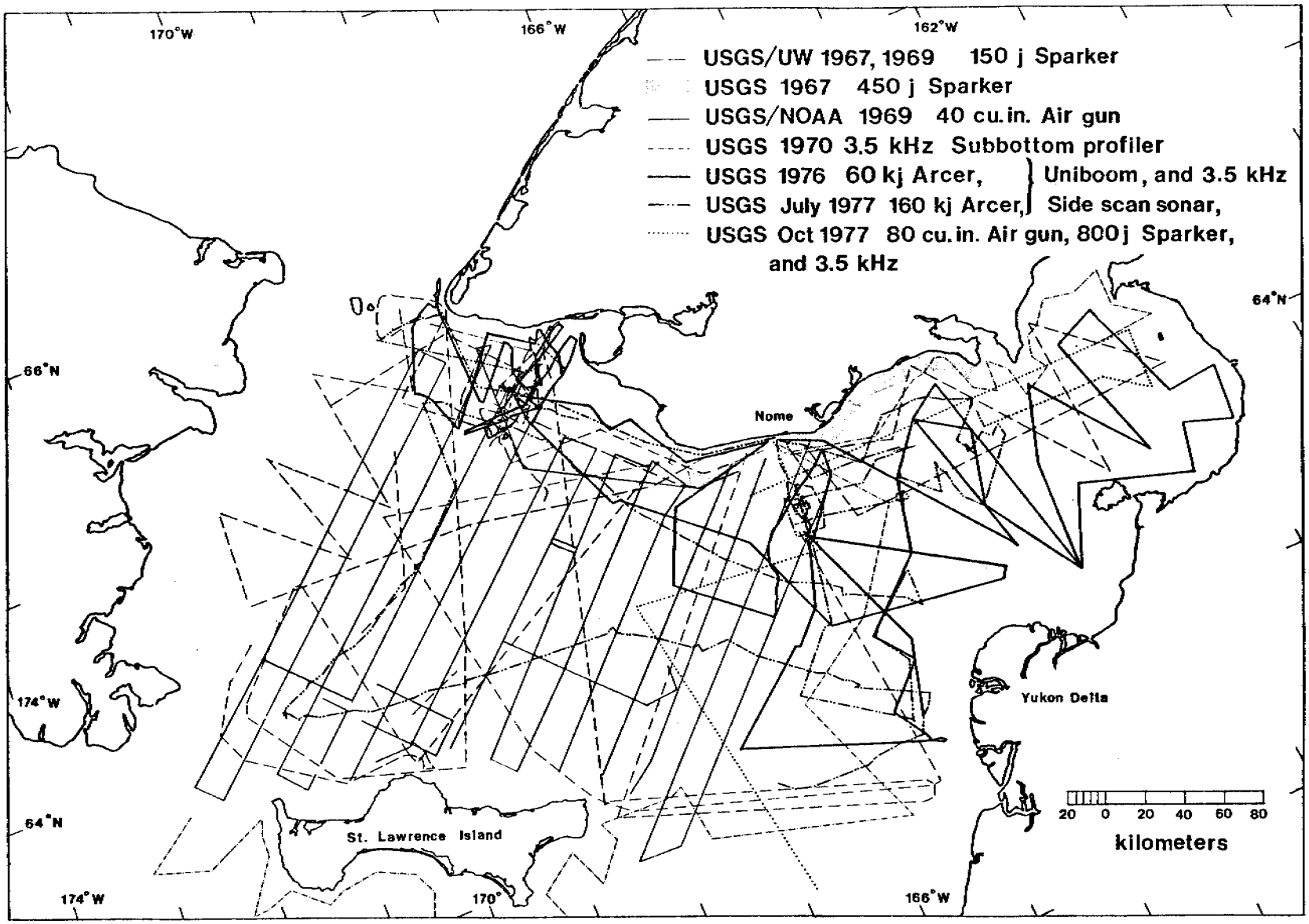

Figure B1. Coverage of geophysical studies conducted in northeastern Bering Sea.

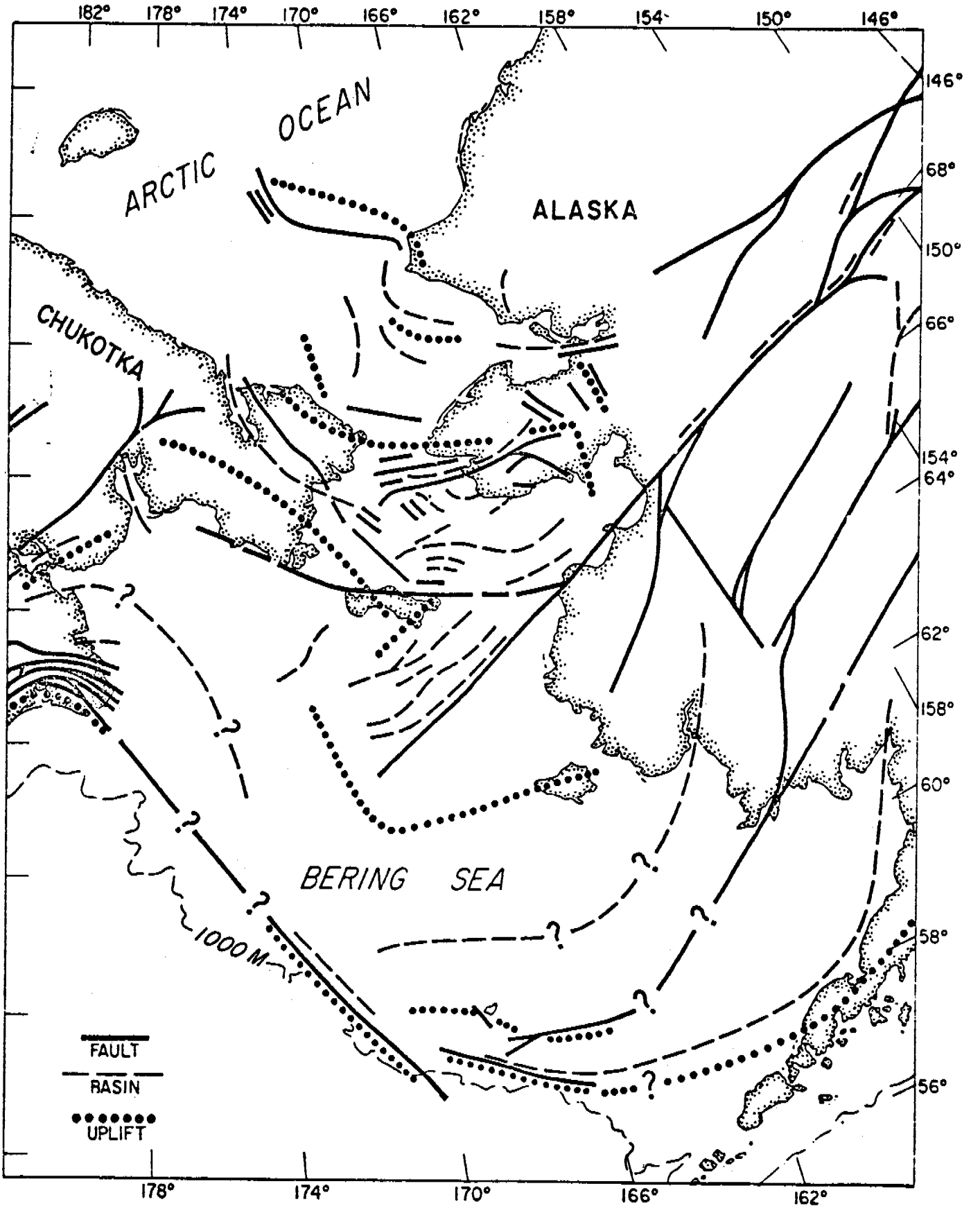

Figure B2. Regional tectonic map of northern Bering Sea area.

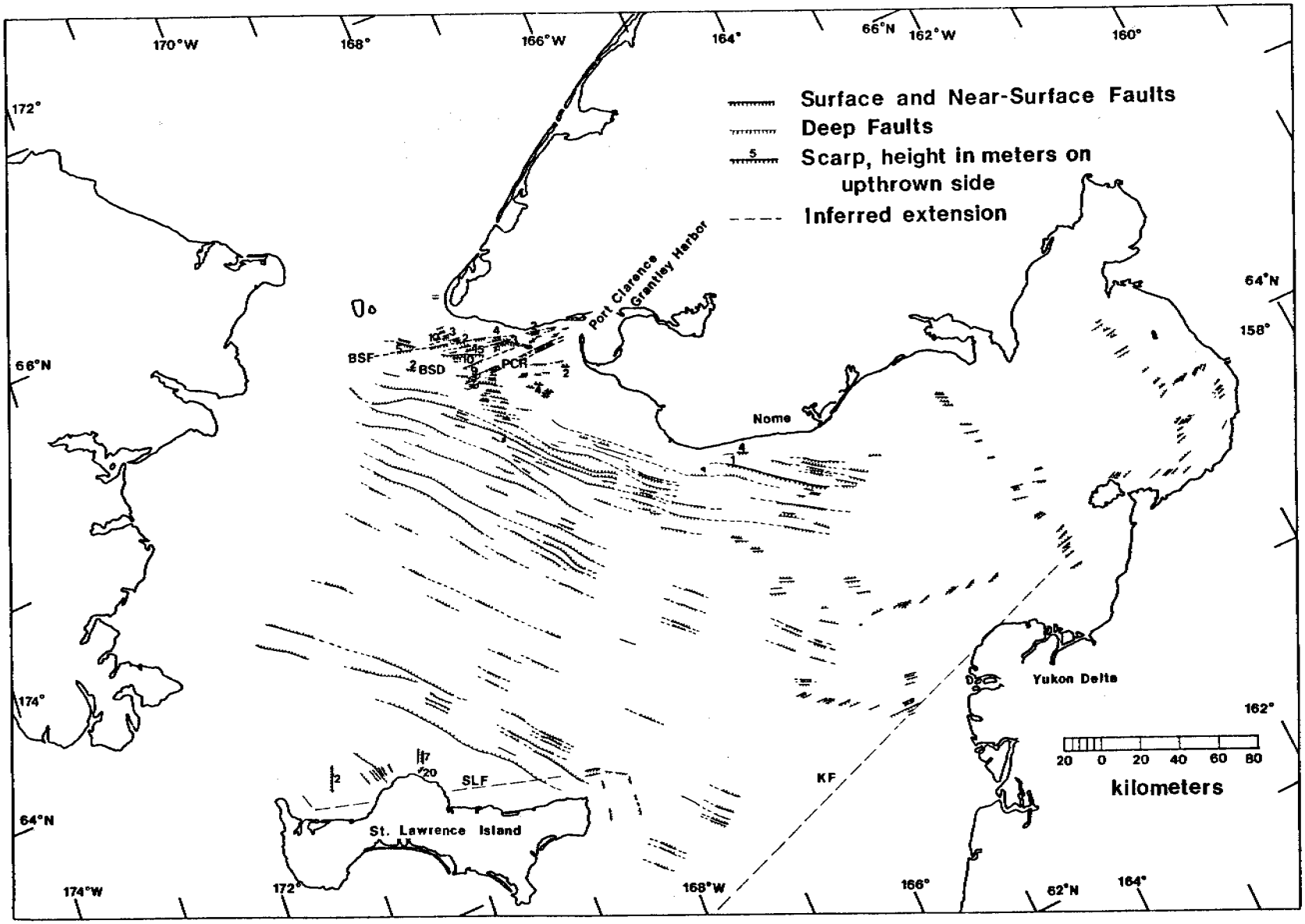

Figure B3. Faults in Chirikov Basin and Norton Sound.

VI. RESULTS

C. Identification of Thermogenic Gas-charged Sediment in Norton Basin and Potential Hazards

Hans Nelson, Keith A.Kvenvolden and Edward C. Clukey

Introduction

In the summer of 1976, Cline and Holmes (1977) discovered unusual concentrations of hydrocarbon gases, particularly gases heavier than methane, in the water column of Norton Sound (fig. C-1). The epicenter of the gas plume is coincident with a near-surface zone of northwest-trending faults about 40 km south of Nome, Alaska. The distribution of these gases, coupled with an assessment of the geochemistry, geology, and geophysics of the area, indicated the nearby presence of a seep of thermogenically derived gases from a possible petroleum reservoir (Cline and Holmes, 1977; Holmes and Cline, 1977).

In the field season of 1977, we investigated the gas content of the bottom sediment beneath the hydrocarbon-rich plume. We wanted to know where and how the possible seepage would manifest itself in the surface and near-surface sediments and whether such a seepage into sediment presented a geologic hazard. We anticipated that a combination of detailed deep-penetration and high-resolution geophysical techniques together with geotechnical properties and the organic geochemical characteristics of the sediment could precisely define the source of the water column anomaly and the location of a potential petroleum resource. This paper describes application of these techniques to outline (a) the presence of an apparent large (9 km diameter) subsurface gas accumulation, (b) several locations where leakage into near-surface sediment presumably is occurring, and (c) one location where apparent gas craters and thermogenic hydrocarbons are detected in the sediment.

A potential source of the major hydrocarbon accumulation from which the near-surface manifestations are derived is provided by an underlying Tertiary basin, Norton basin. This basin contains up to 5.5 km of marine and continental sediment (fig. C-1) (Holmes et al., in press). A thin layer of mixed Pleistocene marine, glacial, and lacustrine deposits overlies the Tertiary deposits (Nelson and Hopkins, 1972; Nelson and Creager, 1977). Holocene silty sand 1-3 m thick covers Pleistocene deposits at the seep site where the depth of water is about 20 m. Detailed characteristics of the oceanographic and geologic setting are given in Holmes et al., (in press).

Methods

A detailed grid of high-resolution reflection profiling and side-scan sonographs, and a limited amount of deep-penetration seismic profiling, was obtained in the region of the gas plume epicenter (fig. C-1). The geophysical instruments consisted of an EG&E side-scan sonar with a 100-m sweep, an 800-joule EG&G Uniboom utilizing 4 hull-mounted transducers, a 3.5-kHz Raytheon subbottom profiling system with 12 hull-mounted transducers, a 12-kHz echo sounder, an extra recorder displaying the Uniboom signal filtered at 1500

to 5,500-Hz to detect bubbles in the water column, and a 160-kJ arcer system. This array of profiling systems was used to map patterns of acoustic anomalies and also to detect any associated sea-floor gas craters of water column bubble streams caused by leaking gas.

Because no point sources of leaking gas (bubbles) were observed in side-scan sonar, bubble detector or other high-resolution profiling records, a general reconnaissance grid of vibracorer holes was drilled along the trace of a near-surface fault close to the epicenter of the water column anomaly (fig. C-1); some cores were positioned in specific locations of acoustic anomalies and others outside them for background data (figs. C-1 and 2). Kiel vibracores with a maximum penetraton of 2-m were taken at stations 14 through 17. The vibracorer failed at station 18, thus terminating the coring program. Van Veen surface samples were taken at stations 15, 17, and 18; a box core was obtained at station 16. Station 14 was located to the north of the expected seep location, and thus served as a control. Stations 15, 16, and 18 were located above a fault that was thought to be a possible conduit for the gas seep. Station 17 was positioned south of the locus of the seep as mapped in 1976, but was located within a newly outlined fault and acoustic anomaly zone. At all vibracoring sites except station 18, approximately 30 minutes of underwater television scanning of the sea floor was videotaped, and 20 bottom photos were taken with a 70-mm film camera.

At selected sites throughout Norton Sound, a sea-floor penetrometer was deployed to map relative penetraton and determine regions of anomalously deep penetration. The penetrometer measured the relative stiffness of the upper meter of sediment by dropping a probe of known weight (5.3 kg) a known distance 6-7 cm) above the sea floor to provide a standardized measurement of penetraton at each site.

At all five coring sites, the rate of penetraton of the vibracorer was recorded. Thus, the rate of penetration in sediment associated with acoustic anomalies could be compared with those normal sediments without anomalies, and effects from the possible presence of gas could be judged.

To test for unusual amounts of gas in cores, measurements for shear strength and subsamples of known volume were taken in vertical sequence down the cores immediately upon retrieval. Water contents, percent pore water saturation, and bulk densities of the samples were calculated from the measured appropriate weight-volume relations. The percent pore water saturation was evaluated by subtracting the volume of the solid particles in each sample from the total volume of the sample, to determine the volume of pore space, and then dividng the measured volume of water by that difference. If the measured volume of water was not equal to the available pore space (i.e., saturation <100 percent), then part of the pore space may have been occupied by hydrocarbon gas. Some pore water may have been lost by drainage after core retrieval and by evaporation before sampling. Effects due to drainage appear to be noticeable near the base of most cores, where there were commonly marked decreases in percent pore water saturation (fig. C-3b).

Although physical disturbance of sedimentary structures and stratigraphy in vibracores is minimal, loss of gas, like loss of pore water, may be significant. Unlike pore water, gas may be lost at the sea floor because of the vibracoring process. Once the core reaches the sea surface, any drainage

of pore water also will cause loss of gas. The mid-section in the vertical sequence will be the most reliable for gas content, although even these samples will not be quantitative and can only provide a qualitative estimate of the gases. Because of the greater loss of pore water and exposure of the open ends of the core barrel to ambient conditions, the top and bottom samples of a core will be the least reliable for geotechnical and geochemical samples.

The rectangular cores recovered with the Kiel vibracorer were split so that the central part could be sampled in 5-9-cm-long segments at several intervals down the core for gas analyses. Loss of hydrocarbon through this sampling procedure is likely, and the recovered samples probably do not contain quantities of *in situ* gas. The volume of the sample segments from the core was measured for use in determining gas concentrations. Van Veen and box cores, which have the greatest exposure to ambient conditions of any samples, were subsampled with a stainless steel tube that recovered a 10-cm-long core of 0.42 L volume. Sediment splits from all sampling devices were analyzed for hydrocarbon gases by the following procedure:

A sediment sample was placed in a 1-qt. paint can which was immediately filled with helium-purged water. From the can, 100 mL of water was withdrawn, the can was sealed, and the resulting 100 mL headspace was purged with helium through septa previously attached to the can. The can was shaken for ten minutes on a paint-can shaker to release interstitial gas into the 100 mL headspace. exactly 1 mL of this gas mixture was analyzed on a Carle Model 311 analytical gas chromatograph equipped with both flame ionization and thermal conductivity detectors to obtain complete separation of common hydrocarbon gases containing as many as four carbon atoms. Hydrocarbons with five and more carbon atoms (C_5+) were analyzed as a single backflush peak. Gas concentrations were calculated from the chromatograms by measuring the heights of peaks representing the various gases present in the mixture. Partition coefficients were used to correct for the differences in solubilities of the gases. Concentrations of methane are reported in μL/L wet sediment; the other gases are reported in nL/L wet sediment (Table C-1).

Results

The high-resolution records show that near-surface acoustic anomalies are common throughout this general region and can be of two general types. Profiling records in figures C-2b and C-2c over station 17 exhibit an acoustic response consisting of sharp termination of subbottom seismic reflectors and weak multiple reflectors on the record, indicating nearly complete absorption of the seismic signal. Profiling records near stations 15 (fig. C-2d) and 16 and numerous other locations in Norton Basin (Holmes and Cline, 1977; Nelson, unpub. data) show acoustic anomalies of the second type, where the subbottom record is acousticaly turbid, but strong surface multiple reflectors occur in the lower part of the record beneath the upper anomaly zone. This second type of acoustic anomaly appears to be generated by highly reflective surface sources in contrast to the first type of anomaly. In the seismic profile shown in figure C-2d it also is apparent that subbottom reflectors outline the edges of buried channels, and that the acoustic anomaly occurs directly beneath the channel floor. In this region of glaciated terrain (Nelson and Hopkins, 1972), it is quite likely that such buried channel floors contain gravel layers producing "reflective" type anomalies rather than "absorptive" types.

The moderate-penetration geophysical records from the 160-kJ arcer system exhibited a widespread subsurface "absorptive" type acoustic anomaly in the vicinity of station 17 (figs. C-1 and C-2a). Our records and also those of Holmes et al. (in press) show a reflector termination anomaly about 100 m below the sea floor; this acoustically turbid zone is about 9 km wide. Near station 17 is a narrow zone where an upward continuation of this anomalous acoustic reponse extends close to the sea floor (Fig. C-2a).

The 3.5-kHz and Uniboom high-resolution seismic profile records show "absorptive" acoustic anomalies at station 17 (figs. C-2b and C-2c) which appear to be a near-surface continuation of the same "absorptive" type anomaly seen in the moderate-penetration arcer records. The greater resolution in these records shows that, in some areally restricted zones, the surface of the large, deeper acoustically anomalous zone rises suddenly to within a meter of the sea floor (Figs. C-1 and C-11a,b, and c). Vibracore samples penetratng only 2 m into the sea floor can therefore provide significant information about the cause of the smaller near-surface anomalies as well as their possible relations to the much deeper and wider anomaly patterns observed in the moderate-penetration arcer profiles.

The sequence of high-resolution and moderate-penetration geophysical records also disclosed previously undetected faults (B and C in figs. C-1 and C-2e) south of fault A, which was known from previous work (Nelsn, unpub. data; Walton et al, 1969). Correlation between seismic records from adjacent tracklines revealed near-surface "absorptive" acoustic anomalies associated with the projected fault traces in the vicinity of stations 17 and 18 (fig. C-1). The high-resolution records crossing the projected trace of the newly defined fault C show an "absorptive" type of anomaly covering a 1 x2 km area around station 17 (fig. C-1). Station 18, on the westward projection of a well-defined near-surfae fault to the east (A, figs. C-1 and C-2e), is located over a surficial acoustic anomaly similar in size and type to that at station 17. Unfortunately, we have no moderate-penetraton records to define the possible occurence of a deeper and larger associated subsurface acoustic anomaly near station 18, or between stations 17 and 18 where a series of smaller "absorptive" type anomalies occur close to the sea floor (Fig. C-1).

Geotechnical properties also are anomalous at stations 17 and 18 (fig. C-3). At these locaions, the rate of penetraton of the vibracorer (fig. C-3a) was much greater than that encountered at statons 14, 15, and 16 even though all five sites are covered by the same type of Yukon mud. The penetrometer readings at stations 17 and 18 were three times greater than that of surrounding areas. Penetrometer readings elsewhere in Norton Sound are low except in the east-central region where near-surface peat layers and high quantities of biogenic gas are found (Nelson, 1977), and in the southeastern area where the sediment has a high clay content.

Water saturation percent below the 20-cm-thick surface mixed layer(Nittrouer, et al., in press), where bioturbation and other physical and chemical processes may have affected gas contents, also appeared to be consistently lower in sediment at station 17 compared to sediment at stations 14, 15, and 16 (fig. C-3b). Coring artifacts (evaporation and drainage at the ends of the barrel) also may have masked true relations of water saturation percent except in the middle parts of the cores.

At stations 14, 15, and 16, the concentrations of hydrocarbon gases from sediment showed no distinctive trends, nor were the concentrations anomalous in any way (Table c-1); $C_1/(C_2 + C_3)$ was always greater than 50. At station 17, however, the $C_1/(C_2 + C_3)$ ratio showed a minimum value of 6[1], and the sediment contained anomalous gas concentrations and compositions compared to sediment at other stations. For example, the maximum amounts of n-butane, and isobutane, were 1.3, 76, 4, 6, and 52 times greater, respectively, than in samples from the other three stations.

Representative gas chromatograms from sediment at approximately the same depth at stations 17 and 14 emphasize the marked difference in concentration and composition of gases at the two sites (fig. C-4). Of particular interest at station 17 is the C_5+ peak; this peak represents gasoline-range hydrocarbons that are present in anomalous amounts at all depths below the mixed layer at staton 17. The C_5+ peak was not measured because of the lack of a suitable standard.

Although the compositions and the concentratons of gases in sediments at station 17 are anomalous, the amounts measured are well below saturation. For example, we estimate that the solubility of methane in the interstitial water of these samples at a water depth of 20 m is about 50 mL/L of wet sediment. The maximum concentration of methane measured was only about 0.1 mL/L.

Discusson

The geophysical and geotechnical observations, coupled with data on composition of hydrocarbon gases in the bottom sediments (especially the low $C_1/(C_2 + C_3)$ ratios and the presence of gasoline-range hydrocarbons), suggest that thermogenic gas has leaked into near-surface sediment of Norton Sound. The occurrence of hydrocarbon gases of anomalous composition at statoion 17 coincides with the presence of acoustically turbid zones on seismic-reflection records. A principal cause for such acoustically turbid zones ("absorptive" acoustic anomalies) may be the presence of gas bubbles in the sediment (Schubel and Scheimer, 1973). The higher penetration rates of the vibracore and the greater penetration of the bottom penetrometer are a result of lower shearing resistance of the sediment that may be due in part to included gas. Lower shearing resistance is related to the development of excess pore pressures (i.e., pressures greater than hydrostatic) that may be a consequence of gas in bubble phase within interstitial pore spaces (Sangrey, 1978). The lower pore water saturation percentages in sediment at station 17 are believed to indicate that gas bubbles may occupy part of the pore space within the sediment (Fig. C-3).

In addition to acoustic anomalies and geotechnical measurements, television observations of numerous sea-floor pits, 10-40 cm diameter at station 17, also suggest the presence of gas that may have vented from

[1]This ratio has been used as a measure to determine the possible sources of hydrocarbon gases (Bernard, et al., 1976).Ratios less than 50 suggest that hydrocarbon gases may be from thermogenic sources, i.e. may be from thermogenic sources, i.e., they result from the same kind of thermal processes which generate petroleum. On the other hand, ratios greater than 50 suggest that gases from biogenic, microbial processes are present.

sediment into the water (fig. C-5). The lack of pits at all stations except 17, and the size, irregular shapes, and lack of ridges or sediment mounding around the pits negate a biological origin and suggest an origin as gas vents. Some pits contain vertical holes descending to unknown depths and resemble underwater fumaroles observed in the bottom of Crater Lake, Oregon (Nelson, unpub. data). No core samples, videotape recordings of underwater television scans, or bottom photographs were taken at station 18, where geophysical and geotechnical data also suggest that gas in bubble phase may be present in surficial sediment.

The geophysical, geotechnical, and geological evidence suggests that the sediment at station 17 is gas-charged. However the measured concentrations of hydrocarbon gases, although anomalously high, are well below saturation and the formation of free gas bubbles in sediment pore space. In part this contradiction may be explained by loss of gas and pore water during coring and sample processing. Another contributin factor may be inhomogeneity or gas distribution in the sediment as shown by the sporadic occurrence of gas pits on the sea floor and variable gas concentrations down the core.

In the sediment at station 17, the hydrocarbon gases are distributed irregularly, suggesting they are being selectively oxidized, metabolized, or fractionated by some process. Of the gases measured, only propane and n-butane increase continuously with depth (Table C-1). Contents of ethane and isobutane are erratic both in concentraton and distribution. The highest concentrations of thse gases as well as methane are found in the middle interval of the core, where the lowest water saturation values occur. Contents of ethane and propane remain nearly constant with depth and are comparable to concentrations found in most sediments from other station locations. These unsaturated gases are probably biologically derived and are not significant components of the actual seep gas.

The variable gas cncentrations with depth in the sediment may relate to the sampling procedure itself. It was very difficult to recover samples efficiently from the vibracore in a manner that assured minimum loss of gases. The sediment is silty sand that could not be recovered as discrete blocks of material. Even if there has been selective loss of gases in some samples from core 17, this loss has not overshadowed the primary observation that the gases remaining were clearly anomalous in composition relative to the gases in sediments at the other station locations. Cline and Holmes (1977)showed that the gases in the hydrocarbon-rich plume in the water had a minimum $C_1/(C_2 + C_3)$ ratio of about 40 and they used a dynamic model to predict a C_2/C_3 ratio of 1.7 for the initial gas phase in the sediment. On the basis of these calculations and other consideratons, they suggested that the hydrocarbon deposit from which the gas is leaking contains liquid petroleum as well as natural gas. Our data show a minimum $C_1(C_2 + C_3)$ rato of 6 and a minimum C_2/C_3 of about 3. Also, gasoline-range hydrocarbons are present as indicated by the C_5+ peak (Fig. C-4). Therefore, our data point in the same directon as those of Cline and Holmes (1977). Apparently, much of the hydrocarbon gas in sediments at station 17 is of thermogenic origin, and it is likely that the gas source is associated with a liquid petroleum occurrence in Norton Basin.

The general appearance of the large (9 km diameter, subsurface (-100 m) acoustic anomaly associated with the Norton Sound gas seep is similar to features observed on seismic records taken over large subsurface gas caps of

petroleum reservoirs in developed offshore oil fields (Holmes et al.,1978). In Norton Sound, the seep at station 17 over this acoustic anomaly is located beneath the southern apex of a large gas plume observed in the water column (Fig. C-1) (Cline and Holmes, 1977). The highest hydrocarbon concentrations measured in the plume were at a station 5.5 km north of station 17; concentrations decreased northward and westward from this station, as would be expected in a region with north-northwest water currents. (Coachman, et al., 1976). This relation and the highly pitted sea floor (fig. C-5) surrounding station 17 suggest that gas leaking into the water column around this site is a major source of the gas plume observed in the water. The presence of other local, surficial acoustic anomalies and abnormal geotechnical properties indicates that several other possible seep sources for the water plume exist between stations 17 and 18.

Our work indicates that high-resolution profiling, together with geotechnical and geochemical techniques can aid petroleum prospecting. High-resolution seismic profiles may be used in conjunction with deep-penetraton seismic records to trace acoustic anomalies from deep, large subsurface sources to surface locations. Regions with near-surface"absorptive" type acoustic anomalies merit additional testing but those with "reflective" type anomalies for example stations 15 and 16 along the eastern half of fault A (fig. C-2d), do not because they are unrelated to anomalous gas concentrations. Scans over absorptive" anomaly sites with bubble detectors, side-scan sonar, underwater television, and bottom camera can help detect specific gas vents. Geotechnical probes may be deployed to locate areas of anomalous soil engineering properties indicating potential gas-charged sediment. Shallow cores for gas samples should be taken only in areas exhibiting a combination of (a) "absorptive" acoustic anomalies on deep-penetration and high-resoluton seismic records, and (b) charcteristics of gas-charged sediment such as sea-floor pitting, low shearing resistance and low water-saturation values.

Cores for gas and geotechnical sampling need to reach depths greater than one-half meter to obtan a representative subsurface sample and to note sequential changes in gas types and concentratons with depth. For example, normal (background) gas concentrations and pore water saturation values were measured in surface samples at station 17, although they were clearly anomalous deeper in the sediment (Table C-1). Apparently, the surface mixed layer, up to one-half meter in depth (Nittrouer et al., in press) and actively reworked by biological, chemical, and physical processes, yields samples unsuitable for reliable identification of gases and geotechnical properties of surficial sediment.

Gases from submarine seeps have been sampled previously (Bernard et al., 1976; Clifton et al., 1971; Reed and Kaplan, 1977), by capturing and analyzing gas bubbles emanating from the sea floor. We know of only one published report, by Carlisle, Bayliss, and Van Delinder (1975), in which marine bottom sediments contained evidence for a seep of thermogenic gas. We used their general approach and with modified methods have apparently confirmed that potential seeps of thermogenic gas can be identified by analyses of hydrocarbons dissolved in the pore waters of marine sediment.

Application of our combined geophysical, geotechnical, and geochemical techniques suggests that the sea floor at staton 18 in northern Norton Sound

exhibits the desirable criteria for further testing by coring. Seismic records show an area of acoustically turbid sediment at staton 18 equal in size to that at station 17 (fig. C-1). Sediment with a high degree of penetrability also occurs there (fig. C-3a). Unfortunately, television and bottom camera data are absent, and lack of core recovery prevented gas analysis of subsurface samples at station 18 in 1977. However a high priority will be put on collection of bottom surface imagery and of deeper sediment samples for analysis during the next field season. Smaller acoustic anomaly zones representing potential targets also exist in the area between stations 7 and 18 (fig. C-1).

If indeed gas is seeping into the sediment at station 17 from a possible large subsurface accumulation at relatively shallow depths (-100 m) (Holmes and Cline, 1977), a potential hazard to petroleum development may exist in the broad 9-km-diameter area over the gas accumulation (fig. C-1). Observed patterns of near-surface acoustic anomalies indicate that the subsurface gas may be seeping out of several sea-floor locations associated with near-surface faults; these steeply dipping faults may act as pathways for upward migration of gas from the subsurface accumulation (figs. C-1 and C-2E). Because there appears to be a thick subsurface sequence of gas-charged sediment (Holmes et al., 1977), penetration or even near penetration of this large accumulation by artificial structures may provide direct avenues for uncontrolled gas migration to the sea floor.

The presence of gas also may cause a reduction in the strength and bearing capacity of the near-surface sediment and present potential hazards for offshore gravity structures and pipeline installations. Soil engineering anomalies have already been measured at stations 17 and 18 where gas seeps are suspected.

Conclusions

1. One source of a large hydrocarbon-gas plume previously observed in the water column of Norton Sound has been identified in sediment at station 17 (fig. 1). The gas apparently migrates to the sea-floor surface along faults dipping steeply toward a large subsurface gas accumulation. Significant geophysical and geotechnical anomalies at station 18 suggest additional potential seep sites over a fault trace 12 km northwest of station 17. All evidence points to a possible new petroleum resource area 45 km south of Nome.

2. Our combination of several geophysical systems, geotechnical probes, and shipboard gas chromatography provides an effective means for resource exploration. Geophysical methods permit mapping of anomalous acoustic responses that might be caused by gas-charged sediment. These targets can then be tested for (a) "absorptive" acoustic anomalies suggesting near-surface gas, (b) low shear resistance of the sediment possibly indicating gas charging, (c) composition of dissolved hydrocarbons to discriminate between biogenic and thermogenic gas sources. Near-surface core sampling must, however, penetrate beneath the surface mixed layer of sediment to obtain representative gas and geotechnical samples.

3. A potential hazard to development of this possible petroleum resource in Norton Basin is presented by the observed shallow, subsurface (about -100 m) occurrence of a possible large gas accumulation (9 km diameter). Any

artificial structures penetrating the gas accumulation or associated faults may provide direct avenues for uncontrolled gas migration to the sea floor. Near-surface gas-charged sediments associated with the large, subsurface accumulaton, may seriously reduce the bearing capacity for offshore structures and pipelines.

Acknowledgments

We thank the scientific staff and crew of the R/V Sea Sounder for assistance in collection and processing of samples at sea, and particularly we thank J.B. Rapp for help in gas chromatographic analyses. Numerous beneficial discussions on acoustic anomalies in seismic profiles were held with M.L. Holmes, M.S. Marlow, and D.R. Thor. Devin Thor also assisted with figure compilation and drafting along with R.O. Williams, M.C. Larsen, J.J. Patry, and S.A. Bailey. Beneficial review comments were provided by M.L. Holmes and G.E. Claypool.

REFERENCES

Bernard, B.B., Brooks, J.M., and Sackett, E.M., 1976, Natural gas seepage in the Gulf of Mexico: Earth and Planetary Sci. Letters, v. 31, p. 48-54.

Carlisle, C.I., Bayliss, G.S., and Van Delinder, D.G., 1975, Distribution of light hydrocarbon in sea-floor sediments: Correlations between geochemistry, seismic structure, and possible reservoired oil and gas, in Proc. of the 1975 Annual Offshore Technology Conference, OTC paper no. 3, p. 65-70.

Cline, J.D., Distribution of light hydrocarbons, C_1-C_4, in Norton Sound and Chukchi Sea, in Environ. Assessment of the Alaskan Continental Shelf, Qtrly. Repts., Oct.-Dec.,1976, Environ. Rsch. Lab., NOAA, U.S. Dept. Commerce, Boulder, Colorado, 46 p.

Cline, J.D., and Holmes, M.L., 1978, Submarine seepage of natural gas in Norton Sound, Alaska, in Proc. of 10th Annual Offshore Technology Conference, OTC paper no. 3052 (in press).

Cline, J.D., and Holmes, M.L., 1977, Submarine seepages of natural gas in Norton Sound, Alaska: Science, v. 198, p. 1149-1153.

Clifton, H.E., Greene, H.G., Moore, G.W., and Phillips, R.L., 1971, Methane seep off Malibu Point following the San Fernando earthquake, in The San Fernando, California earthquake of February 9, 1971: U.S. Geol. Survey Prof. Paper 733, p.112-116.

Coachman, L.K., Aagaard, K., and Tripp, R.B., 1976, Bering Strait: The regional physical-oceanography: Univ. Washington Press, Seattle, Wa., 186 p.

Holmes, M.L. and Cline, J.D., 1977, Acoustic anomalies and seeping gas in Norton Basin: Geol. Soc. America Abs. with Programs, v. 9, no. 7, p. 1022.

Holmes, M.L., Cline, J.D., and Johnson, J.L., 1978, Geologic setting of the Norton Basin gas seep, in Proc. of 10th Annual Offshore Technology Conference, OTC paper no. 3051 (in press).

Nelson, C.H., and Hopkins, D.M., 1972, Sedimentary processes and distributon of particulate gold in northern Bering Sea: U.S. Geol. Survey Prof. Paper no. 689, 27 p.

Nelson, C.H., Hopkins, D.M., and Scholl, D.W., 1976,Cenozoic sedimentary and tectonic history of the Bering Sea, in Hood, D.W., and Kelley, E.J., (eds.), Oceanography of the Bering Sea: Univ. of Alaska, Inst. of Marine Sci., Occasional Pub., no. 2, p. 485-516.

Nelson, C.H., and Creager, J.S., 1977, Displacement of Yukon derived sediment from Bering Sea to Chukchi Sea during the Holocene, Geology, v. 5, p.

141-146.

Nelson, C.H., 1978, Potential sea-floor instability from gas-rich sediments and sediment depression craters, in Environ. Assessment of the Alaskan Continental Shelf, Ann. Rept. of Principal Investigators for Year Ending March, 1977: Environ. Rsch. Lab., NOAA, U.S. Dept. Commerce, Boulder, Colorado, v. 18, p. 79-92.

Nittrouer, C.A., Sternberg, R.W., Carpenter, R., and Bennett, J.T., 1978, The use of Pb-210 geochronology as a sedimentological tool: Application to the Washington continental shelf: Marine Geology, (in press).

Reed, W.E., and Kaplan, I.R., 1977, The chemistry of marine petroleum seeps: Jour. Geochem. Explor., v. 7, p. 255-293.

Sangrey, D.A., 1977, Marine geotechnology-state of the art, Marine Geotech., v. 2, no. 1 p. 45-80.

Schubel, J.R., and Scheimer, E.W., 1973, The cause of the acoustically impenetrable, or turbid, character of Chesapeake Bay sediments: Marine Geophys. Researches, v. 2, p. 61-71.

Table C-1. Content of Low Molecular Weight Hydrocarbons in Core Sediment Samples

Interval Sampled (cm) V= vibracore VV= Van Veen B= box core		μL/L	nL/L						
		C_1	C_2	$C_{2:1}$	C_3	$C_{3:1}$	n-C_4	iC_4	$\frac{C_1}{C_2 + C_3}$
Station 14									
7-12	V	10.7	51	34	27	10	11	11	138
40-45	V	13.8	56	46	31	15	tr	tr	158
80-85	V	8.2	90	52	43	31	tr	tr	62
95-100	V	5.7	73	54	41	24	tr	tr	51
Station 15									
0-10	VV	9.9	53	166	70	72	26	9	81
10-15	V	50.3	33	34	22	19	10	10	928
70-75	V	28.8	38	28	18	9	-	-	514
115-120	V	31.7	70	50	43	24	21	10	279
135-139	V	35.5	114	53	164	22	38	19	128
Station 16									
0-10	B	8.6	21	31	26	15	-	-	183
10-15	V	5.1	38	34	22	9	-	-	86
50-55	V	7.8	27	28	18	9	-	-	175
90-95	V	9.3	27	39	18	9	-	-	205
130-135	V	12.0	60	67	40	24	10	-	121
152-157	V	14.6	60	62	54	24	-	-	128
Station 17									
0-10	VV	3.9	55	48	34	22	8	-	44
10-18	V	101	857	27	21	8	12	8	115
60-69	V	99	8626	24	24	7	tr	946	11
100-109	V	113	6600	-	64	14	28	982	17
145-159	V	6.7	770	44	313	14	187	286	6
160-164	V	18	2005	45	620	22	231	433	7
Station 18									
0-10	VV	0.74	26	43	17	11	-	16	17

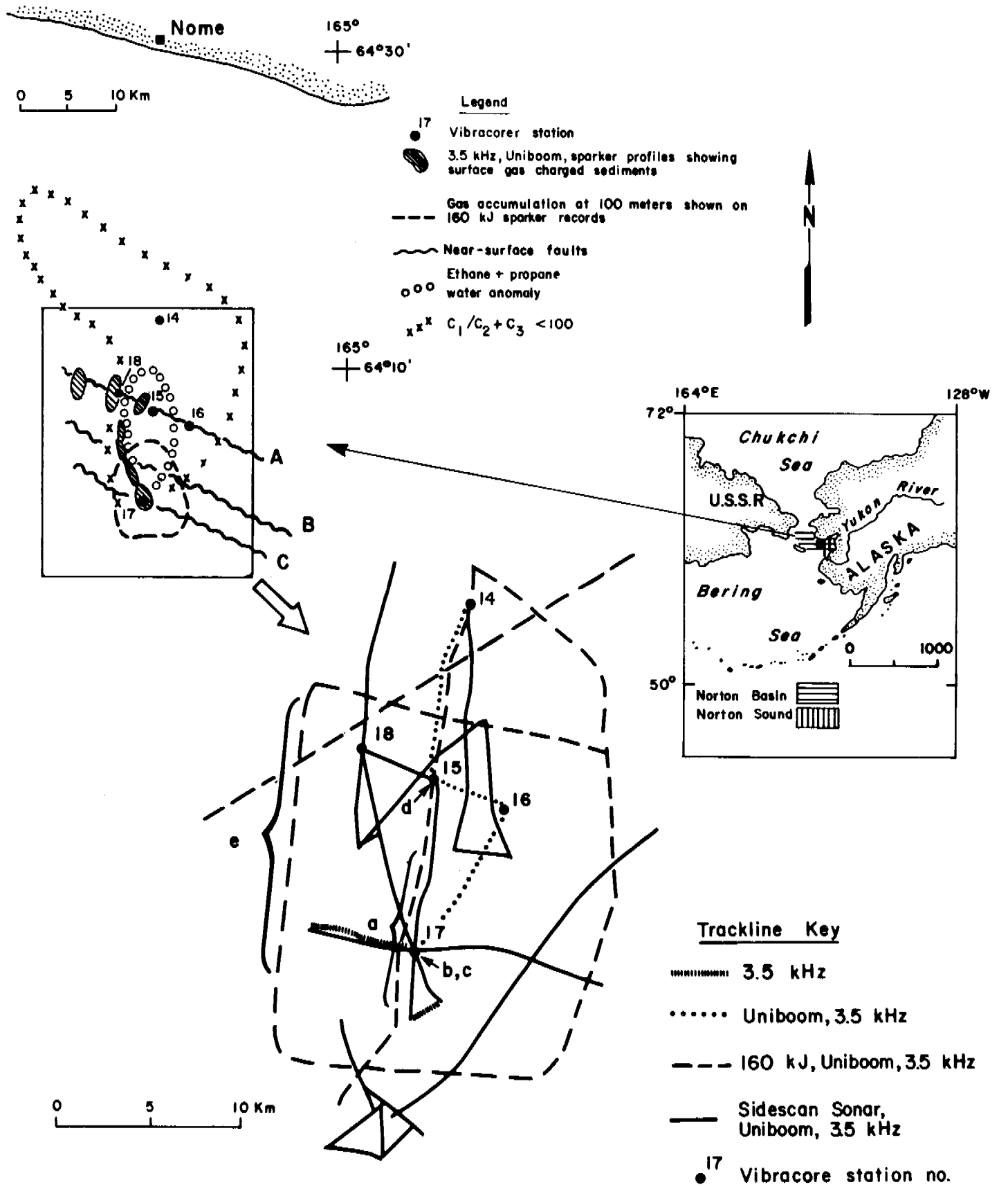

Figure 1 Location of region of thermogenic gas-rich sediment and water in Norton Sound showing geophysical tracklines and vibracore station locations. Outline of possible gas accumulation is after Holmes et al., (in press) and data on gas content in water is after Cline (1977). Capital letters key near-surface fault traces discussed in this paper.

Figure C-2 Acoustic anomalies observed in continuous seismic profiles from the gas seep region. The station number above the records indicates vibracore station locations shown in Figure 1. The locations of seismic record examples are also keyed on the trackline map in Figure 1.

(a) Small near-surface acoustic anomaly connecting to a large subsurface acoustic anomaly (possible gas cap at 100 m) shown on our 120 kJ arcer record closest to vibracore station 17.

(b) Uniboom profile acoustic anomaly at vibracorer station 17.

(c) 3.5 kHz profile acoustic anomaly at vibracore station 17.

(d) Uniboom acoustic anomalies over buried channels near fault A and vibracore station 15.

(e) Arcer profile across faults A, B, and C. Acoustic anomalies obscure apparent location of fault A projected from other adjacent records.

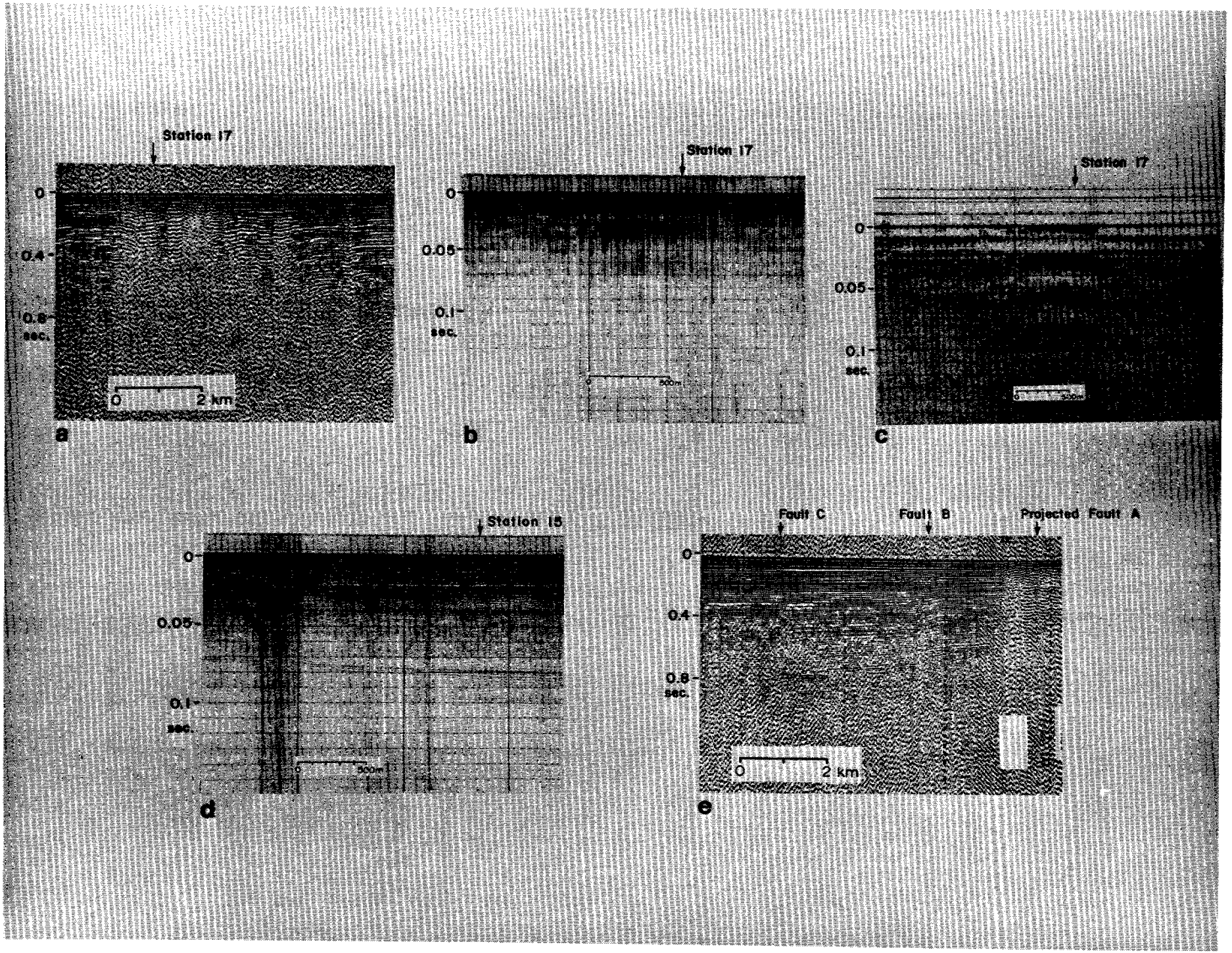
Station 17
0
0.4
0.8
sec.
0
2 km
a
Station 17
0
0.05
0.1
sec.
500m
b
Station 17
0
0.05
0.1
sec.
500m
c
Station 15
0
0.05
0.1
sec.
500m
d
Fault C
Fault B
Projected Fault A
0
0.4
0.8
sec.
0
2 km
e

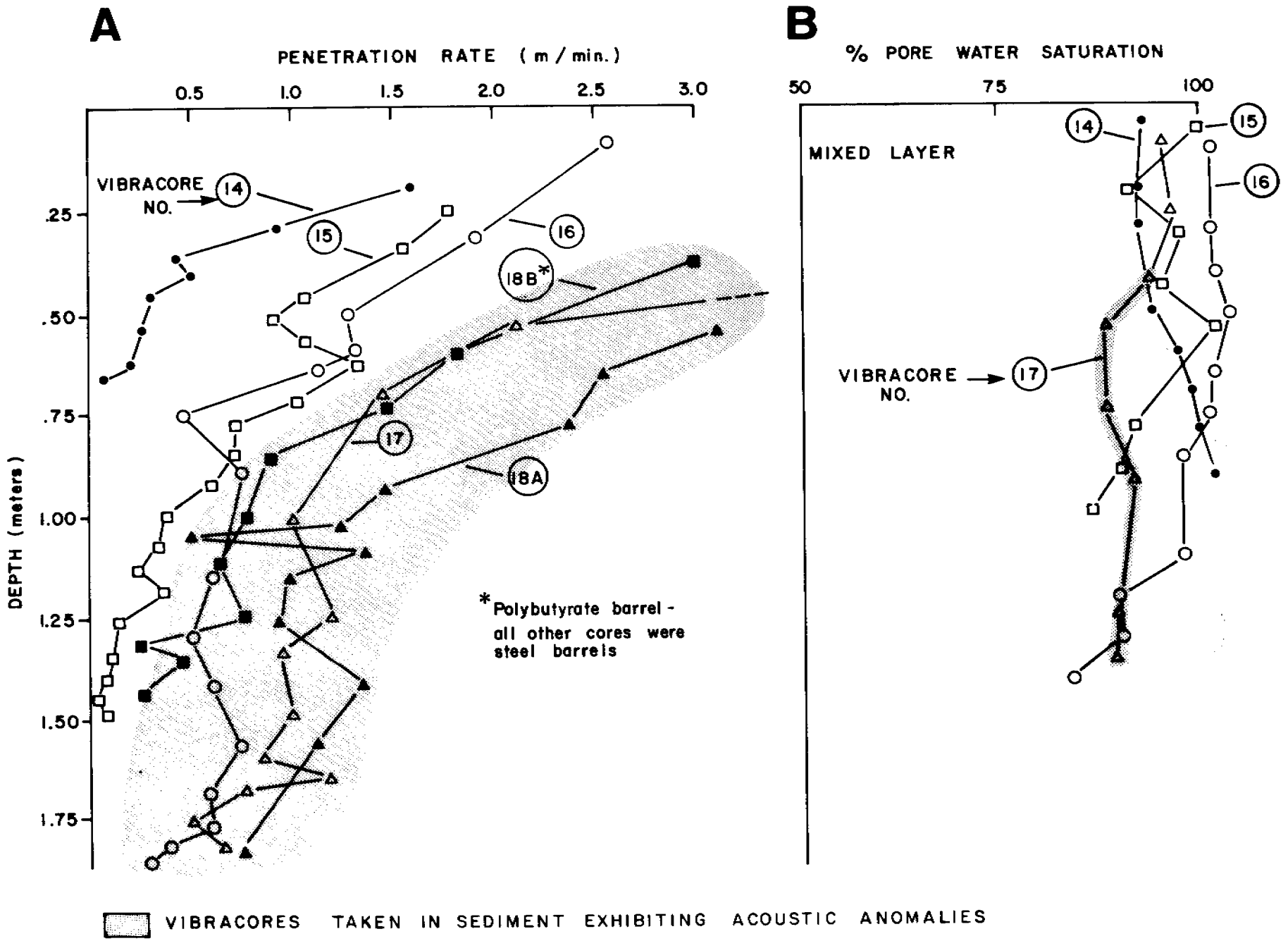

Figure C-3 Vibracore penetration rates and percent pore water saturation at sites in the thermogenic gas-rich area of Norton Basin (see Figure 1 for vibracore station locations). Profiles in Part B were constructed by using three-point moving averages of original values.

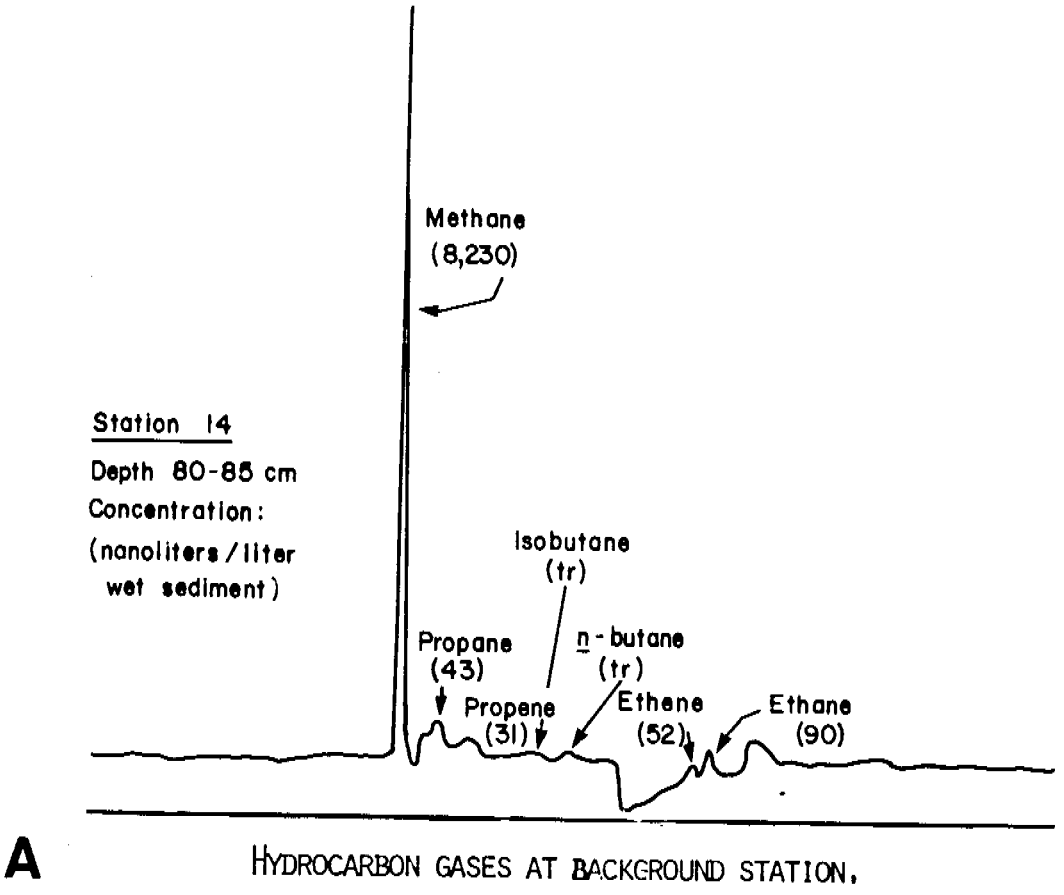

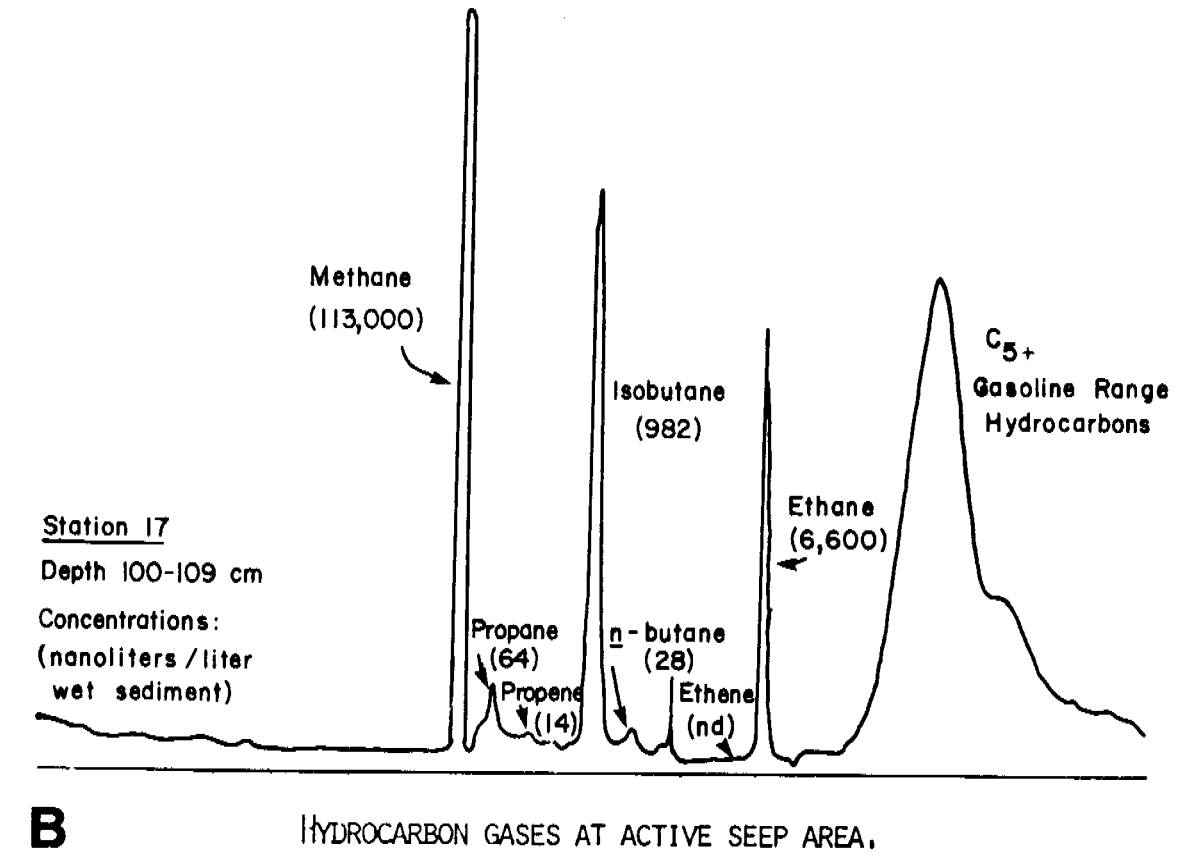

Figure C-4 Representative hydrocarbon gas chromatograms (A) at background site of vibracore station 14 and (B) at thermogenic gas-rich site of station 17 (see Figure 1 for location of vibracore stations).

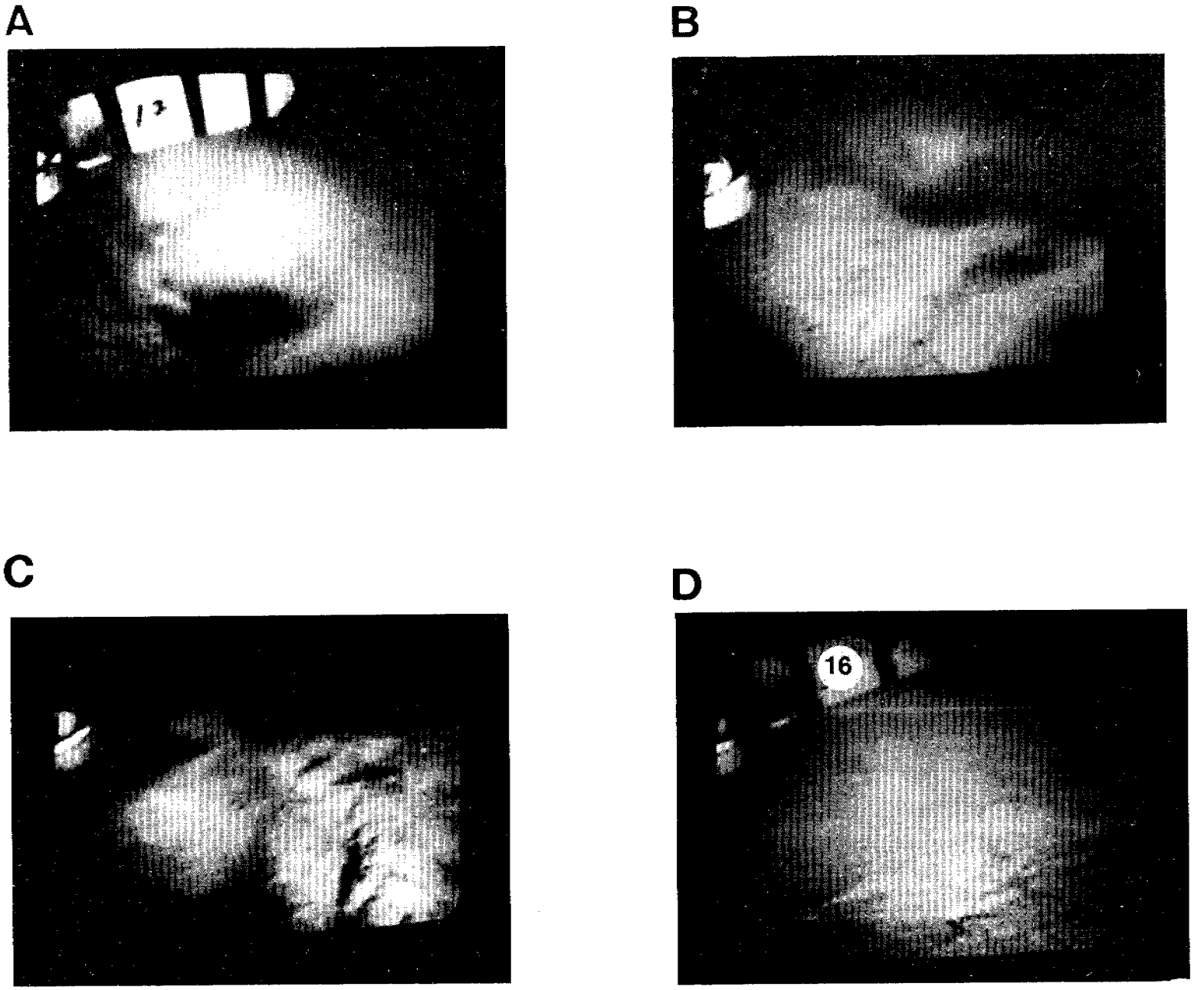

Figure C-5 Photos A to C show sea floor pits observed in underwater television along a 1-km traverse across the region of acoustic anomalies surrounding station 17. Photo D shows normal non-pitted sea floor observed at station 16. Black stripes on the compass vane are 2 cm wide.

VI. RESULTS

D. Modern Biogenic Gas-generated Craters (Sea Floor "Pockmarks") on the Bering Shelf, Alaska

Hans Nelson, Devin R. Thor, and Mark W. Sandstrom

Introduction

We have observed widespread occurrence of small (3-8 m diameter) circular pits or craters in north-central Norton Sound of the Bering Sea epicontinental shelf; a few similar craters are also present near Port Clarence. These features resemble so called "pockmarks" observed on numerous other broad shelf areas (King and MacLean, 1970; Anonymous, 1977; Platt, 1977). The origin of these sea floor depressions has been ascribed to a wide variety of processes from relict depressions of melting permafrost, to relicts of meteorite showers, to gas and fluid escape structures (Anonymous, 1977).

We hypothesize that the craters in Bering sea floor are caused by modern generation and venting of biogenic gas. The purpose of this paper is to describe this new occurrence of craters or pockmarks, show the application of interdisciplinary geological, geophysical, geochemical, and geotechnical techniques to verify our hypothesis, and point out the potential hazard to that these features may present to future petroleum development. In the petroleum producing regions of the North Sea and Gulf of Mexico, problems have been associated with sediment depression craters apparently caused by gas venting at the sea floor (Garrison, 1974; Per Stokke, oral communication, 1977).

Methods

Data for this study were gathered during 1976 and 1977 summer field seasons aboard the R/V SEA SOUNDER. Seismic data pertinent to this paper include 2,800 km of Uniboom trackline and 2,200 km of side-scan sonar trackline (Fig. D-1). The Uniboom system utilized four hull mounted E. G. and G. transducer plates with a total power output of 1,200 joules. The 105 Hz, E. G. and G. side-scan sonar system recorded at 50 m and 100 m sweeps (scales). The altitude of the transducer fish was maintained at approximately 10 percent of the scale being used.

Surface sediment samples were obtained with a 60-cm stainless steel boxcore or a frame-supported Soutar Van Veen grab sampler that was chemically free of hydrocarbon contamination. Subsurface samples were obtained with a Kiel vibracorer from stations in northern Norton Basin. Sediment subsamples were collected as soon as possible after the sampling device was brought on deck; the sediment was placed into 600 ml tin cans, and the cans were filled with distilled water to maintain a constant headspace of approximately 50 ml and then flushed with helium prior to sealing the can.

Low molecular weight hydrocarbons (LMWHC) were determined by static headspace analysis of the canned samples using gas chromatography. The cans

were shaken, punctured, and 1 ml samples of the gas headspace were injected into the gas chromatograph. A Carle #311 Analytical Gas Chromatograph, equipped with a flame ionization detector, utilized a series of columns that allowed complete separation of C_1 through C_4 alkanes and alkenes. Standardization was conducted by injecting 1 ml samples of a gas standard into the gas chromatograph.

Gas remaining in the can after shipboard gas analysis was collected in 20 ml vacutainers and stored for mass spectrometric analysis. Methane in the gas samples was purified from carbon dioxide and other hydrocarbons by passing it through a trap held at -180°C and collecting it on activated charcoal held at -180°C. The methane was quantitatively converted to carbon dioxide for mass spectrometric analysis by combustion in an oxygen atmosphere at 900°C using the method of Kaplan and others (1970).

Geologic Setting

Norton Sound is an elongate, east-west trending marine reentrant in northwestern Alaska (Fig. D-1). It is bounded on the north by the Seward Peninsula and on the southwest by the Yukon Delta. The sea floor of the sound is flat, lacking topographic irregularities except for a broad, shallow trough in the northern part. Most of the sound is between 10 to 20 m deep (Fig. A-3).

Sea-level lowering of late Pleistocene time caused the Norton Sound area to be subaerially exposed (Nelson and Hopkins, 1972). During this time, fluvial processes and tundra vegetation characterized the area (Hopkins, 1967) and peaty, organic rich mud was deposited over much of the region (Fig. D-2). This freshwater sediment generally contains 5-10 times more organic carbon than does overlying marine sediment which consists of 0.5 to 1.0% organic carbon (Nelson, 1977). The C_{14} ages of the upper surface of non-marine sediment ranges from 10,120 - 16,400 years B. P. and confirms its pre-transgressive history and continental origin on an emergent landmass (Steven Robinson, written communication, 1978; USGS Radiocarbon dates W-2686, 155, 157, 159, 357 and 352).

Post-glacial sea-level rise flooded most of Norton Sound and initiated marine sedimentation from 12,000 B.P. to 9,000 B.P. (Nelson and Creager, 1977). During Holocene time 0-10 meters of fine-grained sandy, silt derived from the Yukon River prograded over Norton Sound (McManus and others, 1977; Nelson and Creager, 1977). The Holocene marine sediment typically is less than two meters thick in the region of the sea floor craters (see cores 121, 125, 131 in Fig. D-2; Nelson and Creager, 1977).

Crater Morphology and Distribution

Small, circular-shaped pits are observed on the sea floor over a large area of central and eastern Norton Sound (Fig. D-3). These craters range from one to ten meters in diameter, average two meters in diameter, and are probably less than half a meter deep since their relief is not evident on the horizon line of sonographs or 200 kHz fathograms (Fig. D-4). Neither rims or mounds around the craters have been observed on sonographs; their

absence is characteristic in other pockmark occurrences (King and MacLean, 1970; Per Stokke, written communication, 1978). Cross-section shape of the craters cannot be determined because less than 0.5 m scale of detail is easily masked by wave motion and is beyond the resolution capabilities of our present shipboard recording equipment. However, most craters probably are relatively shallow and flat floored; if they were conical, geometry would dictate depths greater than .5 m and such shapes would probably be evident on records. The fairly smooth, convex-up "saucer" shape of craters probably results because (1) the silty substrate tends to seek minimum relief equilibrium after crater formation by sides flowing toward the center, and (2) the constant oscillatory pounding of wave motion on the bottom causes shear failure in soft sediments (Henkel, 1970), thus causing crater sides to collapse toward the center of the crater.

Although we lack side scan data in the central area of the crater field, crater distribution seems to radiate outward to less dense areas from two areas of greatest concentration in east-central Norton Sound (Fig. D-3). Change from high density to low density is fairly gradational. Areas of maximum concentration reach a high of 134 craters/km of trackline or over 5,000 craters/km^2, although such high densities are rare; typical concentrations range from 200 to 1000 per km^2.

Geophysical Characteristics of Crater Areas

High-resolution seismic profiles in Norton Sound generally are characterized by parallel, horizontal reflectors with common acoustic anomalies except in the area north of the modern Yukon delta (Figs. D-1 and D-4). Acoustic anomalies generally represent acoustically impenetrable near-surface zones in the sediment and occur as (1) total termination of subsurface reflectors with weak or absent multiples (Fig. D-4), or (2) hyperbolic forms just below the surface, replacing normal reflectors, but with strong multiples. Anomalies range from sporadic, few-meter-long features on the seismic profile to several kilometers-long continuous features. Both types of acoustic anomalies are distributed throughout the Norton Sound area and in many cases are associated with specific locations of the small, circular craters or pockmarks.

There are two possible explanations that appear to be mainly responsible for acoustic anomalies in Norton Sound, sharp contrasts in sediment type and presence of gas-charged, peaty Pleistocene mud. Gravels in buried channels may act as a multifaceted, dense reflector surface and thus create a hyperbolic anomaly (see d in Fig. C-2). Peat and or gas-charged sediment may act as an "acoustic sponge" absorbing all reflective energy because of the large density difference between gas-rich peat and sediment (Kepkay and Barrett, 1977; Schubel and Schiemer, 1973; Keen and Piper, 1976). The extensive reflector termination anomalies and occurrence of peat with high gas content in east-central Norton Sound suggests that gas charged sediment is a major cause of acoustic anomalies in sediment of the crater field area.

Organic Geochemistry of Sediment in Crater Areas

Low molecular weight hydrocarbons (C_1 - C_4) (LMWHC) are present in the sediment of Norton Sound (Table D-1). These hydrocarbons may be derived from microbial degradation of organic material (biogenic gas) or from thermocatalytic processes (thermogenic gas). Biogenic gas is usually characterized by $C_1/C_2 + C_3$ ratios >50, $C_1/\Sigma C_1\text{-}C_4$ ratios >0.99, and $\delta^{13}C$ values lighter than -60‰ (Bernard and others, 1976; Stahl, 1974). Thermogenic gas usually has $C_1/C_2 + C_3$ ratios less than 50, $C_1/\Sigma C_1\text{-}C_4$ ratios less than 0.95, and $\delta^{13}C$ values heavier than -50‰ (Bernard and others, 1976).

Gas chromatographic analysis of the LMWHC in Norton Sound sediment indicates that the gas is predominantly methane (>99%) with small amounts of ethane, ethylene, propane, propylene and iso- and n-butane (Table D-1). The $C_1/C_2 + C_3$ and $C_1/\Sigma C_1\text{-}C_4$ ratios (>1000 and >0.99, respectively) and $\delta^{13}C$ values (-69 to -75‰) for the gases in these sediments indicate that the LMWHC are derived from biogenic processes. High concentration of organic carbon in the peaty mud (1-5%) suggests suitable organic material is present for microbial anaerobic decomposition and methane production to occur.

The chemical composition and $\delta^{13}C$ values of the LMWHC (Table D-1) measured in these sediments rule out the possibility that high methane concentration in the sediment is related to a possible thermogenic gas seep in western Norton Sound reported by Cline and Holmes (1977) and Nelson, Kvenvolden and Clukey (this volume).

Cline (1976) detected relatively high C_2 and C_3 concentrations in the water column, yet no methane anomalies were detected here or elsewhere in bottom waters of central Norton Sound.

Methane content in surface sediment, like bottom water, exhibits no anomalies (Fig. D-5); however, subsurface values increase several orders of magnitude in Pleistocene peaty mud in the areas with craters (see 121, 125, 131 in Figs. D-2 and D-3). Samples at the base of the vibracores in the crater area, have methane content measured was very close to saturation or bubble phase as calculated utilizing the method of Yamamoto et al. (1976)[1]. Both Holocene marine and Pleistocene freshwater sediment contain much lower methane content in non-crater areas (see cores 137 and 15 in Figs. D-2 and 3).

The variation in organic carbon content also correlates with methane content and may predict presence of high methane concentration in crater areas where methane measurements are not available. For example, very high organic carbon content is found in Pleistocene peaty mud in an area with craters near Port Clarence. In contrast, organic carbon content appears to be significantly lower in Pleistocene freshwater mud in areas where no craters are found, yet the basic stratigraphy is similar to other crater areas (see 15 in Fig. D-2; Nelson, unpublished data).

---

[1] $\frac{41 \pm 5 \text{ ml } CH_4 \text{ (STP)}^a}{1 \text{ seawater}} \times \frac{1 \text{ mM}}{22.4 \text{ ml}} = \frac{1.8 \pm 0.2 \text{ mM}}{1 \text{ seawater}}$

Assuming 30-36‰ salinity and 0-8°C temperature variation. Effect of pressure at these shallow depths (<25 m) appears to be insignificant (MacDonald and Wong, 1975).

Relationship of Craters to Sea Floor Geology, Geophysics and Geochemistry

The craters in northern Bering Sea are very recent features because they are present within modern ice gouge grooves and relict, buried craters have not been observed in seismic profiles (Fig. D-4). Bering shelf craters are found only in areas with a thin (1-3 m), cover of Holocene fine-grained mud, generally Yukon silt (McManus et al., 1977); where mud becomes sandier, average crater size seems to increase. Where mud is thicker craters are lacking and acoustic anomalies are not present. No craters have been found in Chirikov Basin where transgressive gravel and fine sand covers the sea floor. However, mud-covered swales between sand ridges off Port Clarence do contain craters (Fig. D-2).

Craters are usually present in areas where acoustic anomalies occur at very shallow depths; although there does not seem to be a definite one to one correlation between anomaly and crater occurrence. Other large (50-150 m diameter) irregular shaped, flat-bottomed depressions are found in Yukon mud of Norton Sound, but these are never associated with acoustic anomalies (see Larsen et al., this volume); instead, they appear to be related to regions of strong current energy, ice-scoured bottom, and sea floor scarps. The crater areas and associated numerous large reflector-termination anomalies appear to be correlated with gas-charged sediment and/or near-surface peat. The areas of sea floor craters occur where the near-surface peat is most organic rich (greater than 5% organic C) and, consequently, contains the highest quantity of methane. The methane content apparently is saturated or in bubble phase at many places in the peaty mud causing absorbitive acoustic anomalies (Schubel and Schiemer, 1973). The lack of anomalies under some crater areas may be due to the lack of gas in subsurface sediment because of recent outgassing.

Lack of measurement of saturated methane content probably best is explained by loss of gas and pore water during coring and sample processing. Samples in which methane content close to saturation were measured had been vibrated out of the sea floor and then split. This exposed them to atmospheric conditions prior to analysis and considerable gas could have escaped. The high methane content remaining at the time of analysis suggests that the in situ sediment was saturated with methane and could cause the observed acoustic anomalies. Because measurements of both organic carbon and methane vary stratigraphically down section and from place to place, it is likely that in situ variance of organic carbon and bacterial methane production may in part explain sporadic occurrence of acoustic anomalies (Reeburg and Heggie, 1977).

Crater Genesis

All evidence indicates that high methane concentration results from microbial decomposition (Claypool and Kaplan, 1974; Reeburg and Heggie, 1977) of organic detritus in the subsurface Pleistocene peaty mud. Methane concentration sometimes reaches the saturation point and causes gas charging of this sediment (Martens and Berner, 1977; Martens, 1976). The observed subsurface stratigraphic relationships, and measured geotechnical properties of peaty mud, all point to gas venting as the origin of small surface craters

in Norton Sound. Increased organic content in sediment normally increases water content and compressibility while decreasing shear strength and density (Whelan and others, 1976). This effect can be demonstrated in peaty mud of Norton Sound because normal increase in shear strength and water content does not occur in peat zones (Clukey et al., 1978). These characteristics, together with the high compressibility of peaty mud, increase the chance of gas venting.

Two basic mechanisms for gas venting can be proposed. The first postulates that continuous piping or local degassing may maintain craters as continually active gas vents on the sea floor. The second and favored hypothesis, proposes that gas is intermittently vented, particularly under severe storm conditions. In the first case, generally continuous bubbling should be apparent and this has never been observed on any seismic and "bubble detector" profiles. Also, with more or less continuous degassing, the entire sediment section should generally be underconsolidated, and it is not (Clukey et al., 1978). Instead, sediment typically is overconsolidated as might be expected from intermittent rapid sediment degassing, collapse, and densification. Continual degassing should allow the continuous reworking of sediment to form a crater with a deep conical cross-section and a surface shape elongated parallel to the strong eastward and westward diurnal and storm tide seiching in this area (see Cacchione and Drake, this volume); however, round surface and flat-bottomed cross-section shapes are postulated. Continual venting over the large area of Norton Sound should enrich surface sediment and near bottom water in methane, yet neither of these are apparent (see surface samples in Fig. D-5; Cline, 1976).

In contrast, the extremely low content of gas in overlying Holocene marine sediment compared to that at depth (Fig. D-5) suggests that gas diffusion to the surface is poor, even through a few tens of centimeters of sediment. This indicates that gas generated in peaty muds will build up with time and be entrapped relatively close to the surface, particularly throughout northern Norton Sound where pre-transgressive peaty muds are only thinly buried. When this gas enriched, compressible sediment comes under increased stress from rapidly fluctuating storm wave pressures, gas venting, sediment collapse, and surface crater formation seem quite tenable.

The presence of craters themselves and high quantities of methane trapped beneath marine mud suggest that gas venting is periodic rather than by slow diffusion to the surface. Such periodic gas venting on this extremely shallow shelf is most likely associated with the storm surge events of this region. Significant sea surface set-up is common in Norton Sound (Fatheur, 1975) and the immense movement of water into the region should affect bottom sediment pressures. Also, the associated storm waves can cause rapid fluctuation in wave loading and sedimentation regime on the sea floor. In addition to rapid pressure changes, extensive sediment unloading may occur because of sediment resuspension by storm waves (Nelson and Creager, 1977).

The lack of acoustic anomalies and craters in the Yukon prodelta area suggests that gas saturation in subsurface sediment is maintained at a delicate equilibrium state. Greater sediment loading of the thick Holocene delta wedge over the Pleistocene sediment in the prodelta area may prevent subsurface gas

content from reaching bubble phase, whereas storm wave loading over thin Holocene sediment may trigger gas ebullation from Pleistocene sediment.

Geologic Significance

Characteristics of craters or pockmarks in northern Bering Sea correlate with basic observations of these features on other shelves (King and MacLean, 1970; Anonymous, 1977; Platt, 1977; Josenhaus et al., in press). The Bering Sea craters are found in the surface sediment with the finest grain size in the region, this confirms that a sealing surface unit with fine-grained texture is required to cause crater formation. The craters on the Bering shelf have the greatest density and smallest size known to date. Since Holocene sediment of the Bering shelf is the thinnest and coarsest of any crater area observed to date, observations there correlate with other findings that the thicker and coarser-grained the surface unit is, the larger and fewer are the craters (Josenhaus and others, in press). On both the Scotian and North Sea shelves crater formation is not thought to be active because crater patterns and lineation appear to relate to deeper structure and numerous relict, buried pockmarks are found. In contrast, the Bering shelf setting provides an example of an active system with no apparent correlation to subsurface structure, only to lithology and present day biogenic methane formation.

Widespread deposition of organic-rich paralic sediment during the Pleistocene history of regression, emergence, and transgression over epicontinental shelf areas suggests that this dynamic process of gas cratering should be a world-wide phenomenon, particularly where thin deposits of Holocene mud may form a seal over gas-generating paralic sediment. Ancient analogs, perhaps indicated by vertical escape structures and filled craters, should be searched for in the extensive stratigraphic record of past epicontinental sea deposits.

Conclusions

Numerous craters (up to 5000 per km^2) cover the sea floor of Norton Sound where there is a high potential for petroleum resource development. The craters are small (2 to 5 m in diameter), shallow (less than 1 m deep), circular pits observed on sonographs over 20,000 km^2 of northern Norton Sound, and locally west of Port Clarence. They are associated with acoustic anomalies seen on high-resolution seismic profiles, near-surface peat layers, and gas-rich sediment observed in vibracores.

Widespread occurrence of shallow subsurface, but thick (>1.5 m) sapropelic mud layers have been found in box cores and vibracores throughout the northern Bering Sea. These peaty muds are nonmarine pre-Holocene deposits that are now covered by a relatively thin layer (1 to 3 m) of Holocene marine mud in the area of crater development. Abnormal amounts of methane gas are found in the buried organic-rich mud (5 to 7% organic carbon). This gas is predominantly methane (C_1/C_2+C_3 = 256 to 7669) and has carbon isotope (δC^{13}) values of -69 to -75 parts per thousand, both indicating the gas is derived from biologic as opposed to thermogenic processes. Decomposition of organic debris in the mud causes gas charging of the near-surface sediment. The peaty and gaseous zones attenuate sound waves and cause numerous acoustic anomalies on high-resolution seismic profile records from the cratered area.

The process of crater formation presently is active, because craters disrupt modern ice gouges. Apparently under non-storm conditions, the gas may be trapped in the peaty mud in a quasisaturated state by the cover of Holocene mud. Periodically, possibly during storms, the gas escapes through the thin Holocene sediment veneer and forms craters. Gas escape may be facilitated by changing pore water pressures during storm surges when a) sea-level sets up and seiches, b) storm waves cause rapid fluctuation in hydrostatic pressures, and, c) unloading results from erosion of overlying mud. Where the insulating cover of Holocene mud is more than several meters thick, around the Yukon Delta, acoustic anomalies and craters are absent.

Present Hazards and Future Studies

John Platt (1977), E, G&G, International, Singapore states that the crucial aspects to ascertain for hazards assessment in a pockmark area are whether craters are presently active and are associated with shallow gas pockets. The crater fields of Bering shelf appear to be guilty on both counts. As a result, spanning craters and shallow gas pockets may be hazardous to siting of offshore facilities and abundance of such features over large areas in Norton Sound makes avoidance of siting over them nearly impossible.

Confirmation of present day crater activity and shallow gas processes in the sediment of Norton Basin must be made to assess potential hazards to man-made structures or facilities. The most complete analysis of gas generation processes can be accomplished by deep stratigraphic sampling of Pleistocene peaty mud. Study of present activity of craters can best be undertaken by diving observations and long-term *in situ* probes to measure gas content and wave loading. To assess modern activity, divers can observe presence of bubbles, amount of bioturbation within craters, consolidation state and gas content of sediment in craters, and conical or flat-bottomed nature of craters.

Acknowledgments

We would like to thank Keith Kvenvolden and John Rapp for providing geochemical analyses and helpful discussion of chemical analytical results. We greatly appreciate the help of Steven Robinson for C_{14} dating of freshwater peat samples. We also thank Per Stokke for sharing his thoughts and some unpublished data on cratering in other parts of the world, and Mark Holmes for his help in interpreting seismic records. Dwight Sangrey and Edward Clukey provided beneficial discussion on geotechnical characteristics of gas-charged sediment. We again commend the officers, crew and scientific staff for excellent cooperation and assistance in collection of data at sea.

REFERENCES CITED

Anonymous, 1977, Pockmarks puzzle the geologists: Offshore Engineer, June Issue, p. 51.

Bernard, B. B., Brooks, J. M., and Sackett, W. M., 1976, Natural Gas Seepage of the Gulf of Mexico: Earth and Planetary Science Letter, v. 31, p. 48-54.

Claypool, G. E. and Kaplan, I. R., 1974, The origin and distribution of methane in marine sediments, in Kaplan, I. R., (ed.), Natural gases in marine sediments: New York, Plenum Press, p. 99-140.

Cline, Joel, 1976, Distribution of light hydrocarbons, C_1 - C_4, in Norton Sound and Chukchi Sea, in Environmental Assessment of the Alaskan Continental Shelf, Principal Investigators Reports, 1-31 December 1976, Environmental Research Laboratories, National Oceanographic and Atmospheric Agency, U.S. Dept. of Commerce, Boulder, Co., p. 215-261.

Cline, J. D. and Holmes, M. L., 1977, Submarine seepage of natural gas in Norton Sound, Alaska: Science, v. 198, p. 1149-1153.

Clukey, E. C., Nelson, Hans, and Newby, J. E., 1978, Geotechnical properties of northern Bering Sea sediments: U.S. Geological Survey Open File Report No. , 48 p. (in press).

Craig, H., 1953, Isotopic standards for carbon and oxygen correction factors for mass spectrometric analysis of carbon dioxide: Geochim. Cosmochim. Acta 12, p. 133-149.

Fathauer, T. F., 1975, The Great Bering Sea Storms of 9-12 November 1974: Weatherwise Magazine, Am. Meterological Society, v. 28, p. 76-83.

Garrison, L. E., 1974, The instability of surface sediments on parts of the Mississippi Delta front: Open File Report May, 1974, U.S. Geological Survey, Corpus Christi, Texas.

Henkel, D. J., 1970, The role of waves in causing submarine landslides: Geotechnique, v. 20, p. 75-80.

Josenhaus, H. W., King, L. H., and Fader, G. B., in press, A side scan sonar mosaic of pockmarks on the Soctian shelf: Canadian Jour. Earth Science.

Kaplan, I. R., Smith, J. W., and Ruth, E., 1970, Carbon and sulfur concentration and isotopic composition in Apollo 11 lunar samples: Geochim. Cosmochim. Acta, Supplement I, v. 1317, p.

Keen, M. J. and Piper, D. J. W., 1976, Kelp, methane, and an impenetrable reflector in a temperate bay: Canadian Jour. Earth Sci., v. 13, p. 312-318.

Kepkay, P. E. and Barrett, D. L., , The acoustic signature of gassy muds in two coastal inlets of Atlantic Canada: Unpub. MS., Dalhousie Univ., Halifax N.S.

King, L. H. and MacLean, Brian, 1970, Pockmarks on the Scotian shelf: Geol. Soc. Am. Bull., v. 81, p. 3141-3148.

Martens, C. S., 1976, Control of methane sediment-water bubble transport by macroinfaunal irrigation in Cape Lookout Bight, North Carolina: Science, v. 192, p. 998-999.

Martens, C. S. and Berner, R. A., 1977, Interstitial water chemistry of anoxic Long Island Sound sediments. 1. Dissolved gases: Limnol. Oceanogr., v. 22, p. 10-25.

MacDonald, R. W. and Wong, C. S., 1975, Factors influencing the degree of saturation of gases in seawater: in Adams, W. A., (ed.), Chem. and Phys. of Aqueous Gas Solutions: Electrochemical Soc. Inc., New Jersey, p. 214-232.

McManus, D. A., Venkataratham, Kolla, Hopkins, D. M., and Nelson, Hans, 1977, Distribution of bottom sediments on the continental shelf, northern Bering Sea: U.S. Geological Survey, Prof. Paper 759-C, p. C1-C31.

Nelson, C. H. and Hopkins, D. M., 1972, Sedimentary processes and distribution of particulate gold in the northern Bering Sea: U.S. Geological Survey Prof. Paper 689, 27 p.

Nelson, C. H. and Creager, J. S., 1977, Displacement of Yukon-derived sediment from Bering Sea to Chukchi Sea during Holocene time: Geology, v. 5, p. 141-146.

Platt, John, 1977, Significance of pockmarks for engineers: Offshore Engineer, August Issue, Letters and Book Section.

Reeburgh, W. and Heggie, D. T., 1977, Microbial methane comsumption reactions and their effect on methane distribution in freshwater and marine environments: Limnol. Oceanography, v. 22, p. 1-9.

Schubel, J. R. and Schiemer, E. W., 1973, The cause of the acoustically impenetrable, or turbid, character of Chesapeake Bay sediments: Marine Geophys. Researches, v. 2, p. 61-71.

Stahl, W., 1974, Carbon isotope fractionations in natural gases: Nature, v. 251, p. 134-135.

Whelan, T., Coleman, J. M., Roberts, H. H., and Sahayda, J. V., 1976, The occurrence of methane in sediments and its affect on soil stability, in Selected Papers from the Mississippi Delta Project: U.S. Geological Survey, Corpus Christi, Texas, p. 1-24.

Yamamoto, S., Alcauskas, J. B., and Crozier, T. E., 1976, Solubility of methane in distilled water and seawater: Jour. Chem. Eng. Data 21, p. 78-80.

Table D-1. Biogenic gas content and carbon isotope ratios of vibracore samples taken in the gas crater area of north-central Norton Sound.

Sample	Depth (cm)	concentration (μ M/gm dry sediment)			$\delta^{13} C_{PDB}$ (a)
		CH_4	$CH_4/C_2H_6+C_3H_8$	$CH_4/\Sigma\ CH_4 - C_4H_{10}$	
121 VIBR	10-20	0.67	49	0.974	n.d. (b)
	60-70	5.91	256	0.995	n.d. (b)
	170-180	201.97	6536	0.999	-72.16
125 VIBR	72-80	38.07	3626	0.999	n.d. (b)
	148-150	149.91	n.d.	n.d.	-68.94
131 VIBR	70-75	4.19	873	0.998	n.d. (b)
	160-165	173.31	7669	0.999	-75.01

(a) measured relative to PDB standard (Craig, 1953)

(b) n.d. = not determined. Insufficient gas available for isotopic measurement.

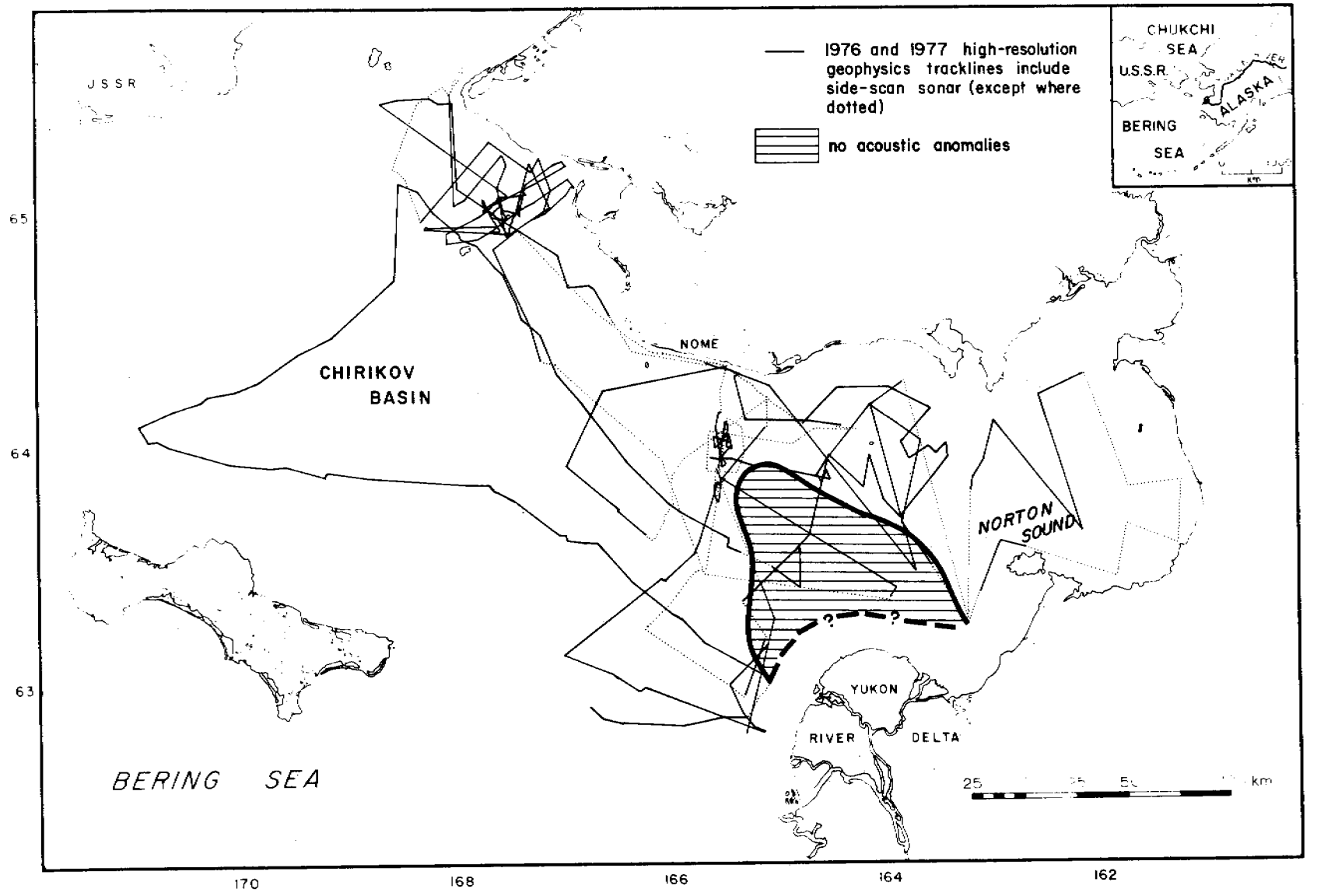

Figure D-1. Index map showing 1976 and 1977 high-resolution seismic profile tracklines and the area which lacks acoustic anomalies.

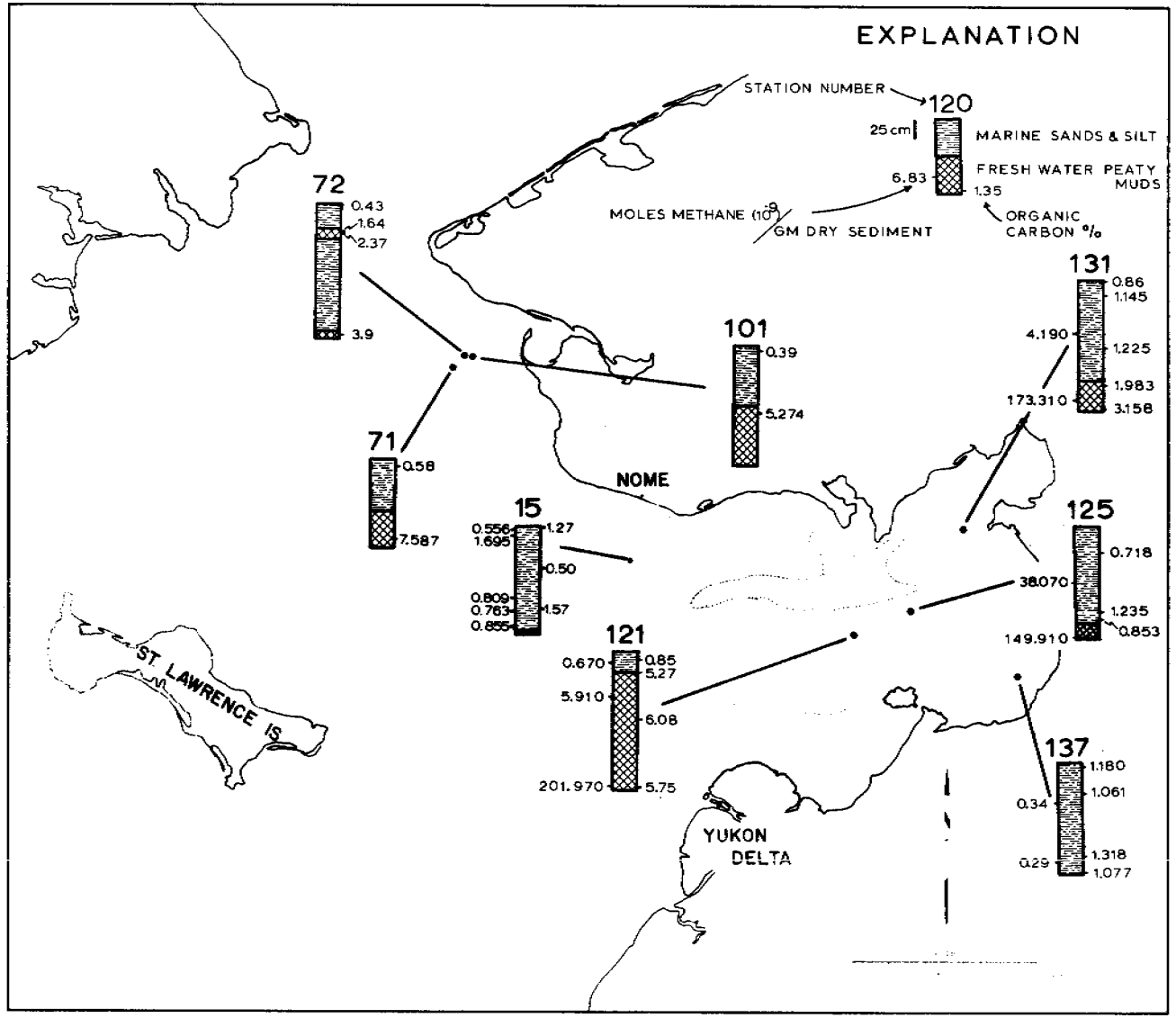

Figure D-2. Presently known locations of freshwater peaty muds in northeastern Bering Sea and comparison of organic carbon content and methane content with normal marine sediment overlying these pre-transgressive deposits.

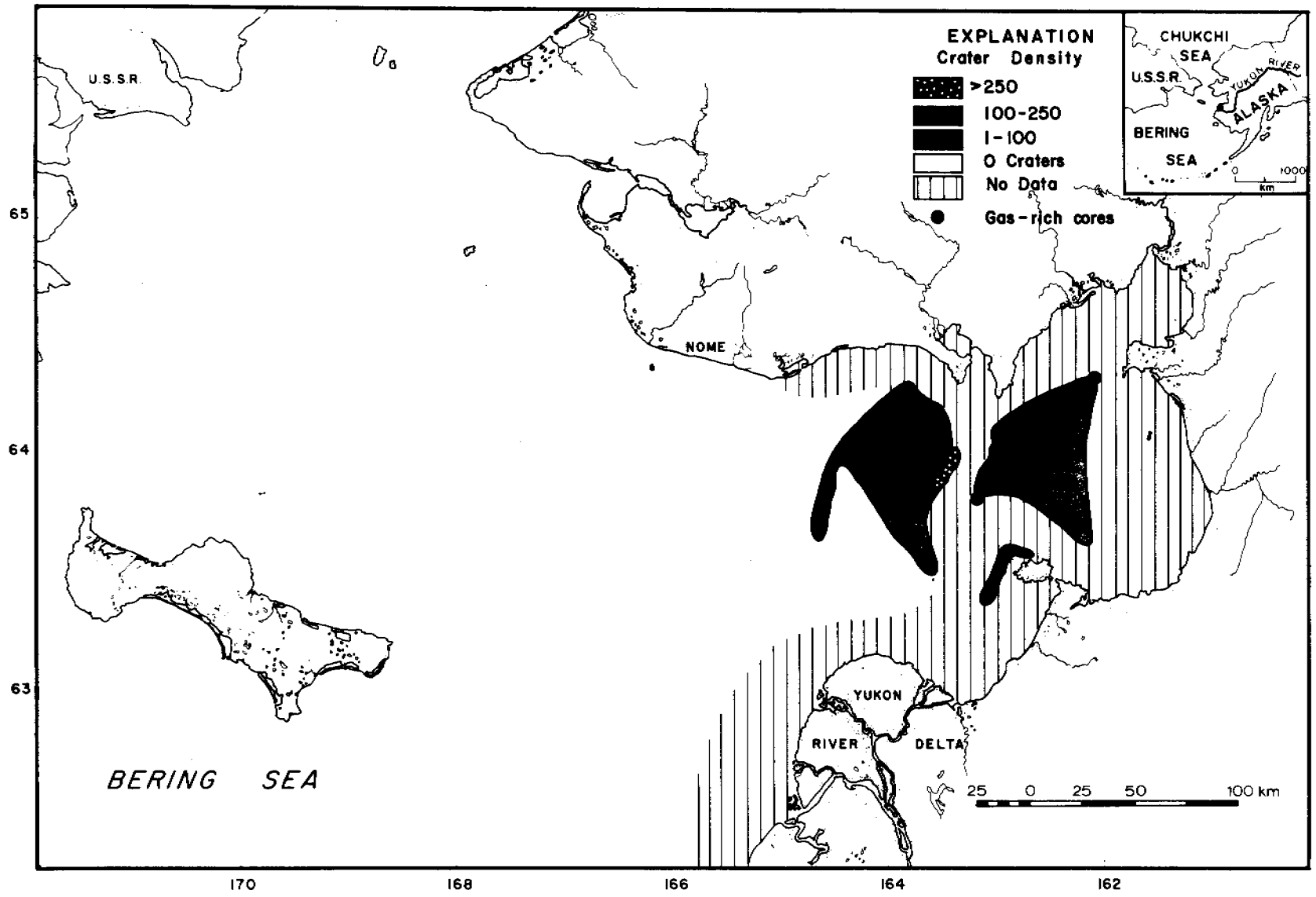

Figure D-3. Distribution and density of craters on the sea floor of Norton Sound. Dots show locations of Fig. 2 cores 121, 125, and 131 that contain gas-rich sediment.

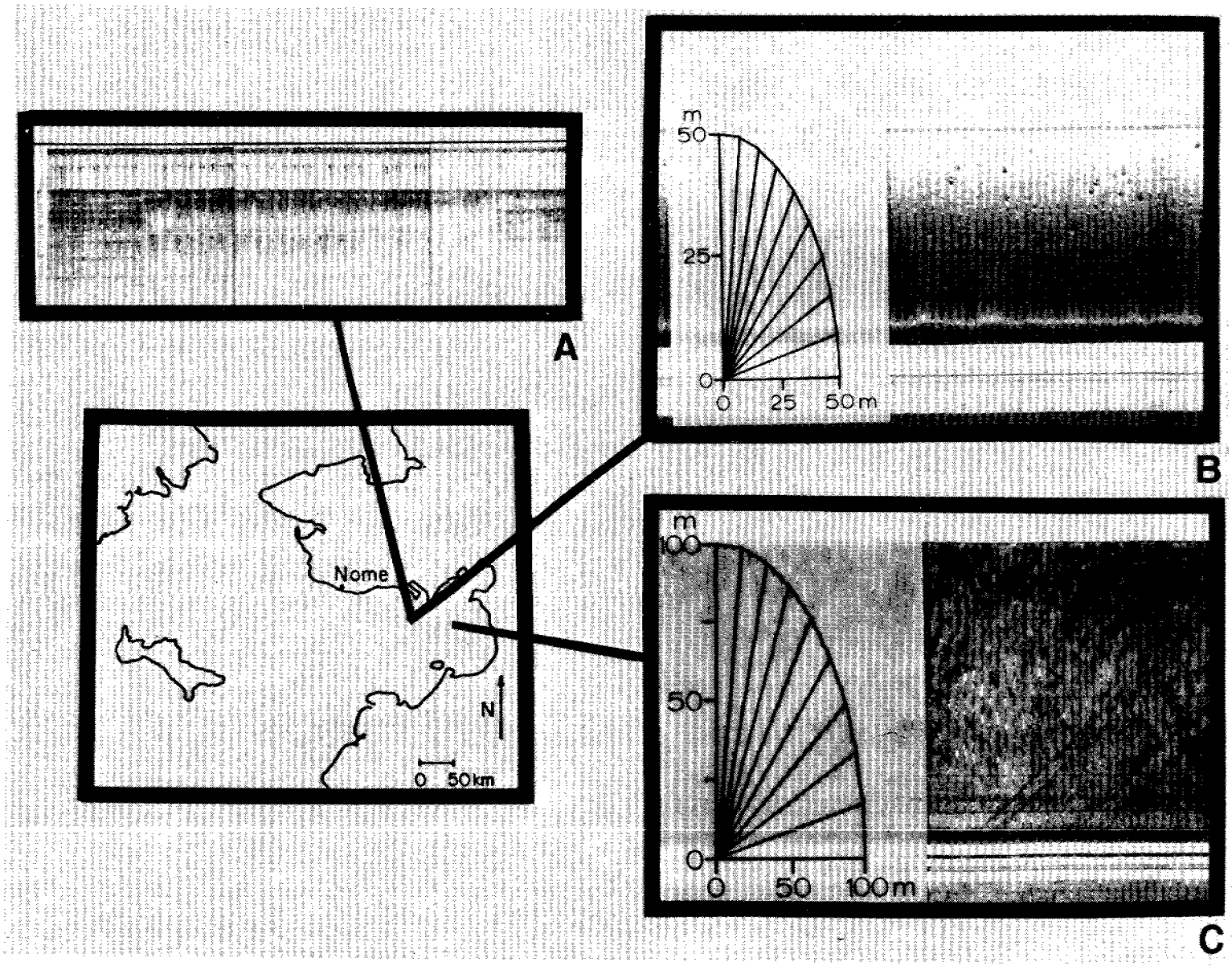

Figure D-4. A - characteristic acoustic anomaly on Uniboom profile.
B - characteristic craters on sonograph associated with acoustic anomalies, as shown in "A".
C - craters formed within an ice gouge.

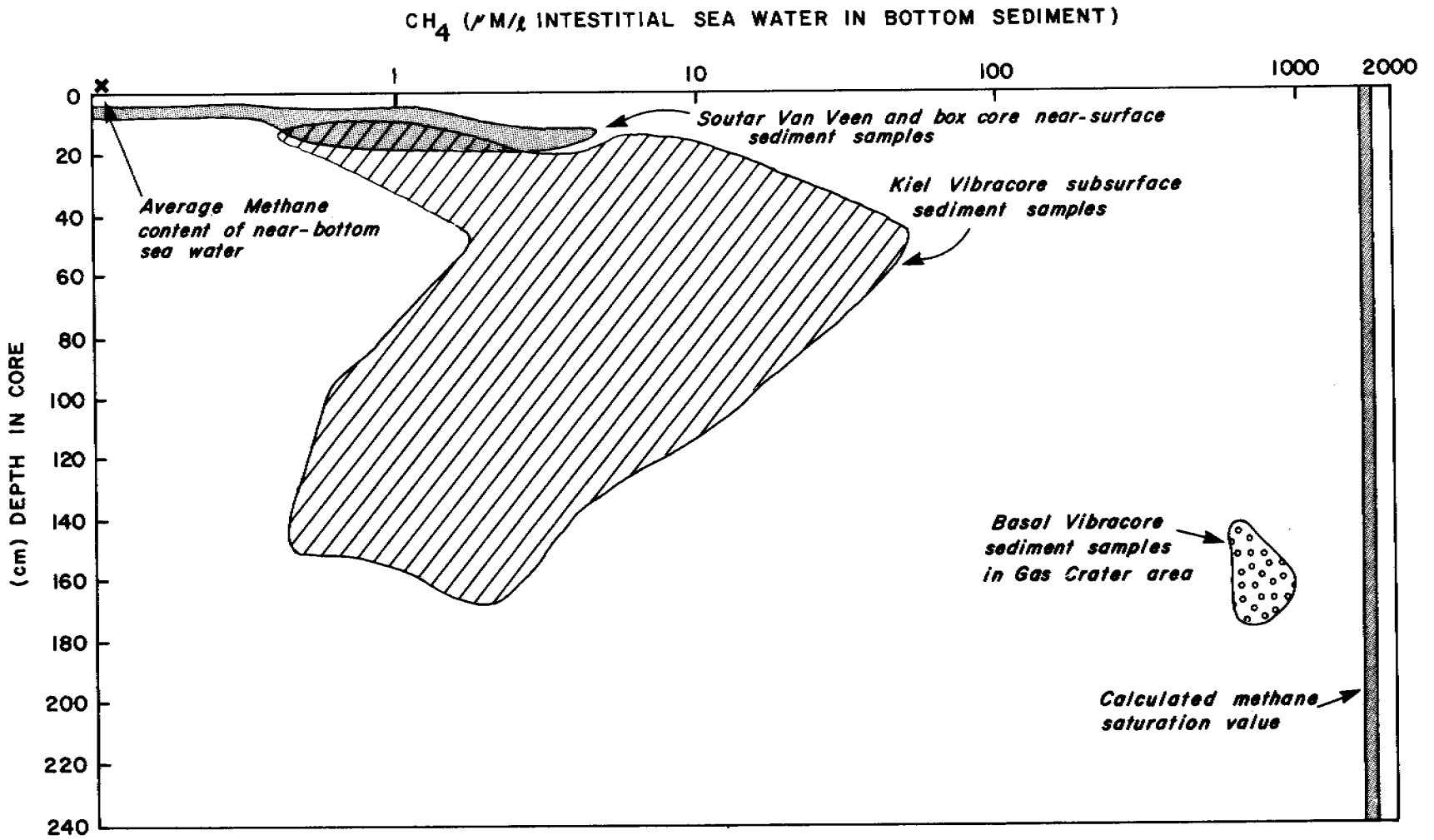

Figure D-5. Characteristic CH_4 content of sediment samples in Norton Basin. Average methane content in near-bottom water from Cline, 1976; calculation of saturation after Yamamoto et al., 1976 and shown in footnote 1 on p.

VI. RESULTS

E. Potential Hazards of Ice Gouging over the Norton Basin Sea Floor

Devin R. Thor, Hans Nelson, Ronald O. Williams

Introduction

The study of ice-related hazards is part of the geo-environmental evaluation of Norton Basin, Alaska, by the U.S. Geological Survey (Fig. E-1).

Extensive previous research has been accomplished on the affects of ice on shelf sediment in arctic regions such as the Beaufort Sea (Reed and Sater, 1974), but not in subarctic regions such as the Bering Sea. It is apparent from our studies that a variety of gouging features occurs throughout the northeastern Bering Sea, even though ice conditions are not as severe as in arctic regions. This study assesses the distribution, density, and intensity of ice gouging in the northeastern Bering Sea. Water depths in northeastern Bering Sea range from 30 - 50 m in Chirikov Basin to 10 - 25 m in Norton Sound (Fig. A-3). Important geomorphologic features in the study area include the series of ridges and swales that parallel the shoreline off Port Clarence, and the extensive shoals (less than 10 m water depth to 30 km from shore) of the Yukon prodelta (Fig. A-3).

Methods

Data were gathered during September, 1976 and July, 1977, aboard R/V SEA SOUNDER, operated by the U.S. Geological Survey. Approximately 3,400 km of side-scan sonar trackline was obtained (Fig. E-1). Normally, Uniboom, 12 kHz, 3.5 kHz, and 200 kHz units were run simultaneously with the side-scan for additional bottom and subbottom information. Ship speed during side-scan sonar operation ranged from 4 to 6 knots, but most of the time averaged 5 knots. Navigation is discussed in the B section of this report.

An E.G. and G. side-scan sonar system, consisting of a dual-channel graphic recorder and a towed transducer fish, was used to evaluate ice gouging. Side-scan sonar, an alternate method to conventional vertical echo sounding, employs an acoustic beam whose axis is slightly below horizontal. This acoustic beam (105 kHz) can resolve small topographic irregularities and small objects on the sea floor down to about 10 cm of relief; reflected echoes are graphically recorded in a form that approaches a plan view map. Discussions on theoretical and practical aspects of side-scan operation and interpretation can be found in Belderson and others (1972) and Flemming (1976). Normally the side-scan was operated at 100 m sweep (the range on either side of the ship for which data is recorded), although many times the 50 m sweep was used to help resolve details of the gouging. In addition, a 200 kHz high-resolution fathometer was operated to measure the depth of ice gouges. Vertical relief of gouges is generally masked by sea swell and ship motion that is recorded as 0.25 to 1 m relief on the fathometer record and the horizon line of the sonographs.

Gouge data were collected fom the sonographs by counting the number, measuring the trend, and noting the time occurrence of all gouges seen on the records. Distortion of features on the sea floor occurs parallel to the line of travel due to ship's speed. A distortion ellipse protractor, which corrects for the apparent angle produced by ship's speed, was used to measure gouge angle with respect to ship's track to obtain absolute compass trend of gouges. This information was then normalized to 10 km intervals by: 1) graphing the measured trends at 10 degree increments on a rose diagram and noting ,the average dominant and subordinate trend or trends, and 2) noting the number of gouges per 10 km interval. Each average trend per given interval was then plotted on the base map to define areas of similar trend and density of gouging.

Ice Conditions and Movement

The northern Bering Sea and southern Chukchi Sea are overlain by annual ice during the months of November through June (Muench and Ahlnas, 1976; Shapiro and Burns, 1975). Depending on the severity of the winter, multi-year ice may also form in southern Chukchi Sea. Pack ice (any free-floating ice regardless of origin) thickness has been reported up to 12 m in the Bering Sea and up to 20 m in the southern Chukchi Sea when it is stacked up in pressure ridges (Anderson, 1959). General ice formation in open sea pans in Norton Sound is 0.3 to 2 m thick (William Dupre', David Drake, pers. comm.). Shorefast ice (ice which is anchored to the land) extends seaward to about the 10 m isobath and is best developed in Norton Sound (Ralph Hunter, written comm., 1976; Dupre', 1977, Stringer and others, 1977) (Fig. E-2).

Analysis of ERTS photography (William Dupre', pers. comm.; Stringer and others, 1977; Muench and Ahlnas, 1976; Shpiro and Burns, 1975) has contributed to a preliminary understanding of ice dynamics in the Bering Sea. Pack ice in the northern Bering Sea originates from in situ northeastern Bering Sea and advected Chukchi Sea ice. Although Chukchi Sea ice usually moves in a northward direction, there are short-lived episodes of rapid deformation and subsequent southerly movement of pack ice through the Bering Strait and into the northern Bering Sea (Shapiro and Burns, 1975). These events are controlled by atmospheric and oceanographic processes.

Ice movement in the northeastern Bering Sea is controlled by the interplay of: 1) prevailing winter northeasterly geostrophic wind (Muench and Ahlnas, 1976), 2) erratic onshore wind (N.O.A.A., 1974), 3) north-flowing water current on the eastern side of the Bering Sea (Coachman and others, 1976), and 4) a counter clockwise gyre in Norton Sound (Nelson and Creager, 1977) (Fig. E-3). Late winter and early spring winds tend to push ice generally southward, whereas waning late spring winds allow pack ice to be increasingly influenced by the north-directed water current (Fig. E-3). In Norton Sound the dominant direction of ice movement is southwestward out of the sound under the influence of the northeasterly winds (Fig. E-2). Periodic changes in wind and water current tend to move ice in and out of the sound, thereby making it possible for even advected Chukchi Sea ice to work its way into Norton Sound. The dominant southwesterly movement of ice out of the sound tends to create a zone of divergence, and consequetly an area of new ice generation, in the northeastern part of the sound and a zone of convergence in the southwestern or Yukon prodelta area of the sound (William Dupre', pers. comm., Stringer and others, 1977) (Fig. E-2).

The junction between the shorefast ice of the Yukon prodelta area and the seasonal pack ice is a shear zone where moving pack ice shears past stationary fast ice (Dupre', 1977, Stringer and others, 1977). Characteristics of shear zones in areas of convergence are colliding, pancaking, and deformation of the edges of the fast ice and pack ice, resulting in the formation of pressure ridges and extremely thick stacks of ice. The best developed pressure ridges in the northeastern Bering Sea occur around the Yukon prodelta where Bering Sea pack ice on the western prodelta and Norton Sound pack ice on the northern prodelta form good shear zones.

Types of Ice Gouging

Two basic types of ice gouge have been recognized on the sea floor of the northeastern Bering Sea: 1) solitary gouging and 2) pressure ridge raking.

A solitary gouge (Figs. E-4A-E) is a groove produced by a single keel of ice plowing through the surficial sediment (Reimnitz and others, 1973; Reimnitz and Barnes, 1974) (Fig. E-5A and B). Solitary gouges are the dominant type of scour mark on the sea floor of the Bering. They are ubiquitous throughout Norton Sound, although the highest density of solitary gouges occurs around the prodelta of the Yukon (Fig. E-6).

Solitary gouge widths range from 5-10 m to 50-60 m, although gouges 15-25 m are most common. Gouge patterns range from straight to sinuous, to sharp-angled turns (Fig. E-4). Depths of gouges, as measured on the horizon line of the sonographs (Fig. E-4E) and on the 200 kHz fathometer (Fig. E-5B), can be up to 1 m. Most gouges area 0.25-0.5 m or less, because they are too shallow to show relief on the horizon line of the sonograph. Without seeing the gouge as it is being cut, it is impossible to know if these depths represent the actual limit of incision or if the gouge was deeper and subsequently caved in.

Pressure ridge raking (Figs. E-4F-G) is produced by a wide base of ice pressure ridge keels plowing or "raking" the bottom sediment, creating numerous parallel furrows (Reimnitz and others, 1973; Reimnitz and Barnes, 2974). Raking is sparse in comparison with solitary gouges, and is mainly found in the prodelta area of the Yukon where locally it is denser than solitary gouging. Zones of raking observed on sonographs are 50-100 m to several kilometers wide. The deepest incisions by raking are about 1 m, but as with solitary gouges, raking usually is less than 0.25-0.5 m deep.

In most cases the feature called a solitary gouge in this paper does not imply that a "solitary" piece of ice is responsible for the gouge. A solitary piece of ice does not have the momentum to gouge sediment (Reimnitz and Barnes, 1974; Sackinger and Rogers, 1974). It takes the momentum of moving pack ice to plow ice keels through sediment. Therefore, whether it is a single-pronged keel or a multi-pronged pressure ridge keel, it is the driving force of the pack ice that causes gouging.

Trend and Distribution of Gouges

Analysis of gouge trend and density enabled recognition of five areas of similar trending gouges (areas I-V) and one area (VI) practically devoid of gouges (Fig. E-6). Directional trends represented by the rose diagrams in Figure E-6 show the number of gouges in a given area and the trend of the gouging. Absolute movement direction of the ice could not be determined. Criteria to make such determinations, such as gouge terminal moraines, was not evident on the sonographs.

There are two major points that can be made concerning ice gouging in the Bering Sea. Gouging is related to: (1) water depth and geomorphology, and (2) location of the shear zone and oceanographic conditions. Seventy-eight percent of all gouging occurs in water 10-20 m deep (Fig. E-7). The largest area of shallow water in northeastern Bering Sea is Norton Sound, and it is in the area of the Yukon prodelta that eighty-five percent of all gouging occurs (Fig. E-6). Gouging found in water 20-30 m deep is concentrated on the ridge crests of the ridge and swale topography west of Port Clarence, on a sand/gravel ridge just northwest of St. Lawrence Island, and on the western flanks of the Yukon prodelta. A definite correlation can be made with the trend of ice gouging, geomorphology and orientation of ice shear zones. In areas I and II (Fig. E-6), the major trend direction is "parallel to isobaths". There is more data scatter in areas III through IV, but a general paralleling of isobaths and the coastline is evident. Pack ice moving southwestward out of Norton Sound forms an east-west trending shear zone probably because of interplay of winds moving ice westward and currents moving ice eastward. Bering Sea pack ice moving either north with currents or south with winds forms a north-south trending shear zone on the west side of the Yukon prodelta area. The pressure ridges formed along these shear zones and thick Bering Sea or advected Chukchi Sea ice caught in the shear zone can account for the type and trend of gouging observed on the sonographs. The lack of gouging in Chirikov Basin is because of greater water depths and the lack of shear-zone pressure- ridge complexes. Pressure ridges which develop in the relatively deeper water off Port Clarence only infrequently feel bottom.

Ice Gouging as a Geologic Process

Although no direct measurements were made in the field to determine the age and longevity of gouges, there are several lines of evidence to suggest that the gouges are modern phenomena that recur annually and are relatively ephemeral. Several ice gouges have been found in sand wave fields on crests of ridges west of Port Clarence (see Field and others, this volume) and in ripple fields in the nearshore area of Nome. These gouges cross through ripple and sand wave fields which are in dynamic equilibrium with present wave or current motion and both old gouges highly modiefied by ripples and fresh gouges are found (Fig. E-4A and B); therefore the gouges must be modern.

Storm waves can resuspend and transport surficial sediment (Nelson and Creager, 1977), as can tidal currents and dynamic currents (Cacchione and Drake, this volume) in Norton Sound. Thus gouges will tend to be either eroded or buried, because they are not in equilibrium with the dynamic physical oceanographic processes in the Bering Sea. Biological reworking of

surficial sediment is an active and ongoing process in Norton Sound (Nelson and others, in prep.) and this also would tend to cause the destruction of gouges.

It has been noted that gouges in the Beaufort Sea in water depths of less than 20 m can be smoothed over in one season (Reimnitz and Barnes, 1974). The wave and current regimes are considerably more active in the Bering Sea and Norton Sound. Smoothing over of gouge form could be caused by: 1) the saturated, silty substrate tending to seek a minimum relief equilibrium after gouge formation caused by the sides flowing or slumping toward the center, and 2) the constant oscillatory pounding of wave motion on the bottom would cause shear failure in the soft sediment (Henkel, 1970), thus causing gouge sides to collapse toward the center of the gouge. The "dish-shape" profile of most gouges (Figs. E-4E and G) indicate this is a viable process. Therefore, the relatively rapid destruction of gouges by the above mentioned processes reinforces the idea that gouges are ephemeral features constantly reforming each winter.

Ice gouging as an erosive agent

The sharpness of gouge morphology is higly dependent on the substrate being gouged. The form of the gouge in figure E-5A and also some examples in figure E-4 indicate a fairly competent substrate capable of maintaining a pronounced rim. Sampling has shown the bottom of Norton Sound to be silty Yukon mud that will hold a shape better than coarser-grained sediment. Gouge form in sandy substrate, such as that found on the shoals off of Port Clarence, is smoother looking because sand lacks the cohesion to hold steep walls (Fig. 4-A).

Mixing of bottom sediment and deformation of the substrate are important processes in densely gouged areas, such as those found around the Yukon prodelta. A zone of deformed sediment in box core #48 (11-18 cm interval, Fig. E-5C) is most probably due to an ice gouge event that has since been buried by sedimentation. The deformed zone probably represents disruption on the periphery of the actual gouge incision (Fig. E-5B).

Prominent, large depressions on the western prodelta of the Yukon also seem to be indirectly related to ice gouging. These depressions are broad (50-150 m wide) and fairly shallow (0.6-0.8 m deep) (Larsen and others, this volume). The fine-grained nature of Yukon sediment makes it relatively cohesive, therefore any plowing action by ice not only gouges the sediment, but may also dislodge cohesive blocks of the sediment. Once started, a depression apparently can continue to grow by erosion by locally strong currents (Larsen and others, this volume).

Ice as a depositional agent

The extensive shoals of the Yukon prodelta coincide with the seaward extent of shorefast ice, stamukhi (grounded pressure ridges) and dense ice gouging (Figs. E-2 and E-5). Reimnitz and Barnes (1974) have noted this relationship in the Colville Delta area in the Beaufort Sea and have hypothesized that pressure ridges and stamukhi may act as sediment traps or

dams, channelize winter currents, or bulldoze sediment to form shoals. A cycle is formed in the sense that shoal areas determine the extent of shorefast ice and the location of a shear zone and pressure ridges, which in turn cause the shoals to develop. Dupre' (1977 and this volume) has postulated that the geomorphology of the Yukon Delta and prodelta is highly controlled by the ice.

Conclusions

1). Northeastern Bering Sea is affected by ice gouging even though it is in a subarctic region. Gouges occur in water depths of 30 m or less, but they occur most commonly in depths of 20 m or less.

2). Gouging occurs as solitary gouges, formed by single-keeled pieces of ice, and as pressure ridge raking, formed by multi-keeled pressure ridges plowing into the sediment. Maximum incision depth is about 1 m.

3). Gouging forms in shear zones where pressure ridges are well developed and where single pieces of thick ice, caught in pack ice movement, touch bottom. Pressure ridges form where moving pack ice collides, deforms, and pancakes with the stationary edge of shorefast ice. Single pieces of thick ice may originate in northeastern Bering Sea or may be advected southern Chukchi Sea ice.

4). The dominantly southwesterly movement of Norton Sound ice produces a zone of convergence around the Yukon prodelta and divergence in the eastern part of the sound. Convergence produces a well developed shear zone and pressure ridging, therefore the prodelta has the highest density of gouging in northeastern Bering Sea (Fig. E-8).

5). The area around Nome is one of divergence or only minimal shearing, therefore gouge density is low (Fig. E-8).

6). The shear zone west of Port Clarence occurs in water too deep for most ice to touch bottom, ice which does touch bottom forms solitary gouges on the crests of the sand ridges.

7). The main part of northeastern Bering Sea, Chirikov Basin, does not have any ice gouging.

8). Ice gouging is an important mixer of surficial sediment in intensely gouged areas.

9). Ice gouging may disrupt bottom smoothness in such a way that in areas of Yukon sediment in high current zones, current scour produces broad, shallow depressions.

Suggestions for Futher Study

1). There is a lack of data in water shallower than 10 m because the draft of the R/V SEA SOUNDER restricts piloting to water deeper than 10 m. The R/V KARLUK (1.3 m draft) will be used during the summer, 1978 field season

to fill in the information gap in water less than 10 m.

2). Recurrence of ice gouging will be tested off of Nome and Port Clarence since both places are probable logistics centers for any future resource development. Precisely located tracklines (± 50 m using miniranger navigation) have been run and will be repeated during field work in the summer of 1978 to check gouging recurrence.

3.) Ice gouge studies conducted by the authors will be integrated with ice movement studies being conducted by other N.O.A.A. OCSEAP projects (Stringer, RU #257; Dupre', RU #208) and with ice research from the Alaska Oil and Gas Associations.

Acknowledgements

We thank William Dupre' (University of Houston) for data concerning pack ice movement and shorefast ice limits, Ralph Hunter (U.S.G.S., Menlo Park) for data on shorefast ice limits, and David Drake (U.S.G.S., Menlo Park) for data on ice thickness. Valuable discussions on ice processes and sonograph interpretation were held with Peter Barnes, Erk Reimnitz, and Larry Toimil (U.S.G.S., Menlo Park). The officers, crew, and technical staff of the R/V SEA SOUNDER made data collection a successful and enjoyable endeavor.

References Cited

Anderson, W.R., 1959, First under the North Pole: New York, World Pub. Co., 137 p.

Belderson, R.H., Kenyon, N.H., Stride, A.H., and Stubbs, A.R., 1972, Sonographs of the sea floor: New York, American Elsevier Pub. Co., 185 p.

Coachman, L.K., Aagaard, K., and Tripp, R.B., 1976, Bering Strait: The regional physical oceanography: Seattle Washington Univ. Press, 186 p.

Dupre', W.R., 1977, Yukon Delta coastal processes study: Environmental assessment of the Alaskan continental shelf, Ann. Rept. of the Principal Investigators for the year ending March, 1977, Environmental Research Lab., National Oceanographic and Atmospheric Adm., Dept. of Commerce, v. XIV, p. 508-553.

Flemming, B.W., 1976, Side-scan sonar: A practical guide, in Side Scan Sonar, A comprehensive presentation: E.G. and G. environmental Equipment Division, Waltham, Mass., p. A-1 - A-45.

Fleming, R.H., and Heggarty, D., 1966, Oceanography of the southeastern Chukchi Sea, in Willimovsky, M.H., and Wolfe, J.M., eds., Environment of Cape Thompson region, Alaska: Washington, D.C., U.S. Atomic Comm., p. 697-754.

Goodman, J.R., Lincoln, J.H., Thompson, T.G., and Zeusler, F.A., 1941, Physical and chemical investigations: Bering Sea, Bering Strait, Chukchi Sea during the summers of 1937 and 1938: Washington Univ. Pubs. in Oceanography, v. 3, no. 4, p. 105-169 and app. p. 1-117.

Henkel, D.J., 1970, The role of waves in causing submarine landslides: Geotechnique, v. 20, p. 75-80.

Husby, D.M., 1969, Report of oceanographic cruise U.S.C.G.C. NORTHWIND, northern Bering Sea-Bering Strait-Chukchi Sea, July 1969: U.S. Coast Guard Oceanog. Rept., no. 24, 75 p.

_____1971, Oceanographic investigations in the northern Bering Sea and Bering Strait, June-July 1969: U.S. Coast Guard Oceanog. Rept., no. 49, 50 p.

McManus, D.A., and Smyth, C.S., 1970, Turbid bottom water on the continental shelf of northern Bering Sea: Jour. Sed. Petrology, v. 40, p. 869-877.

Muench, R.D. and Ahlnas, K., 1976, Ice movement and distribution in the Bering Sea from March to June 1974: Jour. Geophys. Research, v. 81, no. 24, p. 4467-4476.

Nationnal Oceanic and Atmospheric Administration, 1974, Local climatological data - Annual Summary with comparative data for Nome, Unalakeet, Shismaref and Wales, Alaska.

Nelson, Hans and Creager, J., 1977, Displacement of Yukon-derived sediment from Bering Sea to Chukchi Sea during Holocene time: Geology, v. 5, p. 141-146.

Nelson, C.H., and Hopkins, D.M., 1972, Sedimentary processes and distribution of particulate gold in the northern Bering Sea: U.S. Geol. Survey Prof. Paper 689, 27 p.

Pratt, R., and Walton, F., 1974, bathymetric map of the Bering shelf: Boulder, Colo., Geol. Soc. America, scale 1:1,440,000.

Reed, J.C. and Sater, J.E., eds., 1974, The coast and shelf of the Beaufort Sea: Arlington, Virginia, Arctic Inst. North Am., 750 p.

Reimnitz, Erk, and Barnes, P.W., 1974, Sea ice as a geologic agent on the Beaufort Sea shelf of Alaska, in Reed, J.C. and Sater, J.E., eds., The coast and shelf of the Beaufort Sea: Arlington, Virginia, Arctic Inst. North Am., p. 301-351.

Reimnitz, Erk, Barnes, P.W., and Alpha, T.R., 1973, Bottom features and processes related to drifting ice: U.S. Geol. Survey, Miscellaneous field studies, map MF-532.

Sackinger, W.M. and Roger, J.C., 1974, Dynamics of break-up in shorefast ice, in Reed, J.C. and Sater, J.E., eds., The coast and shelf of the Beaufort Sea: Arlington, Virginia, Arctic Inst. North Am., p. 367-376.

Shapiro, L.H., and Burns, J.J., 1975, Satellite observations of sea ice movement in the Bering strait region: Climate of the Arctic, Rept., Univ. of Alaska, Fairbanks, p. 379-386.

Stringer, W.J., Barrett, S.A., Balvin, Nita, and Thomson, Diane, 1977, Morphology of Beaufort, Chukchi, and Bering Seas near-shore ice conditions by means of satellite and aerial remote sensing: Environmental Assessment of the Alaskan Continental Shelf, Ann. Rept. of Principal Investigators for the year ending March, 1977, Environmental Research Lab., National Oceanographic and Atmospheric Admin., Dept. of Commerce, v. XV, p. 42-150.

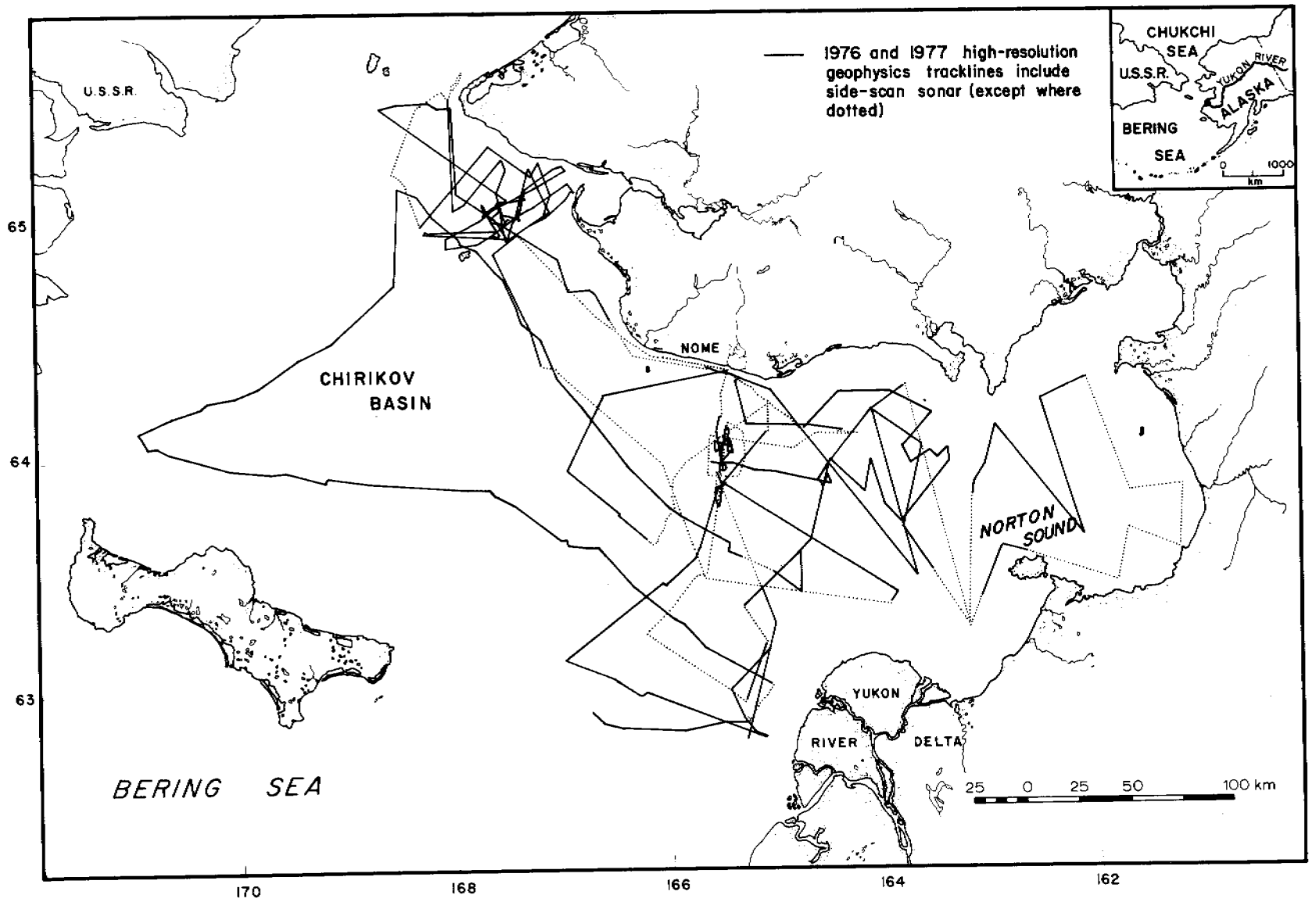

Figure E1. Index map and chart of high-resolution geophysical and side-scan sonar tracklines covered by the R/V SEA SOUNDER in northeastern Bering Sea during S5-76-BS and S5-77-BS cruises.

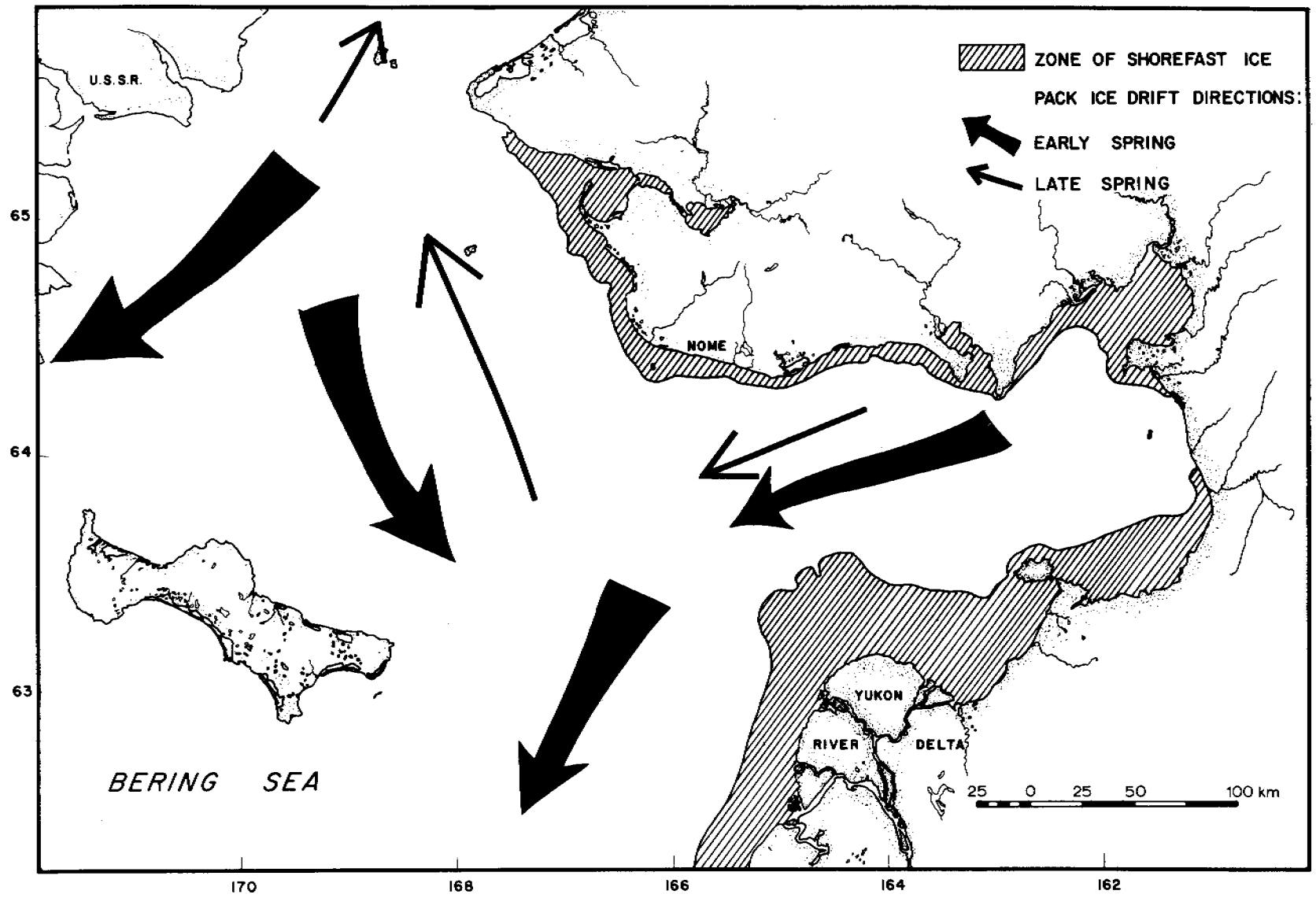

Figure E2. Drift directions of pack ice in northern Bering Sea, adapted from Meunch and Ahlnas (1976). Zone of shorefast ice is based on evaluation of LANDSAT imagery (Dupre', 1977; Ralph Hunter, pers. comm.).

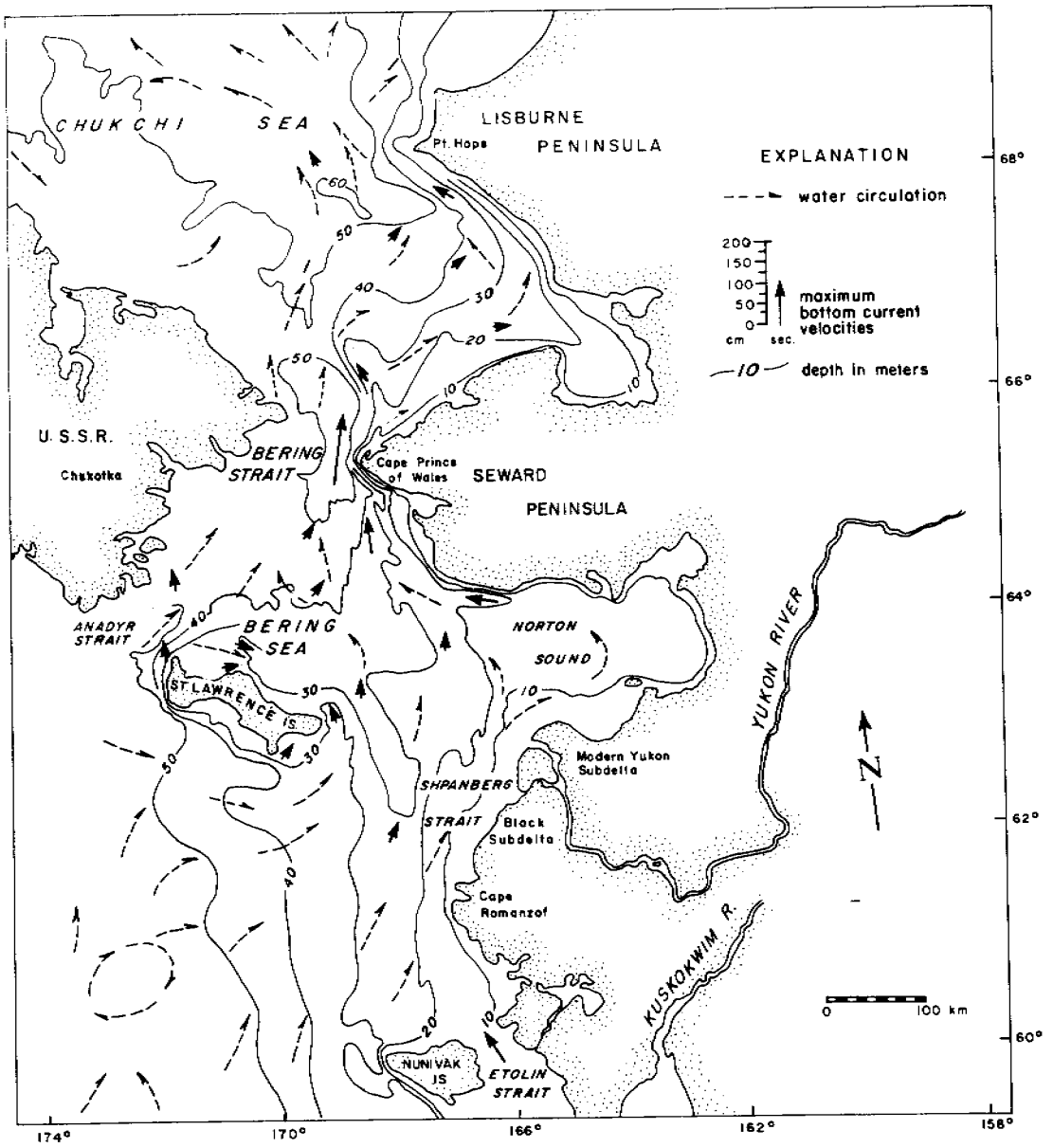

Fig. E-3 Northeastern Bering Sea and southern Chukchi Sea, showing water circulation, distribution of Alaskan Coastal Water, measured bottom-current velocities, and bathymetry. Compilation sources include Goodman and others (1942), Fleming and Heggarty (1966), Husby (1969, 1971), McManus and Smyth (1970), Nelson and Hopkins (1972), Pratt and Walton (1974), and Coachman and others (1976).

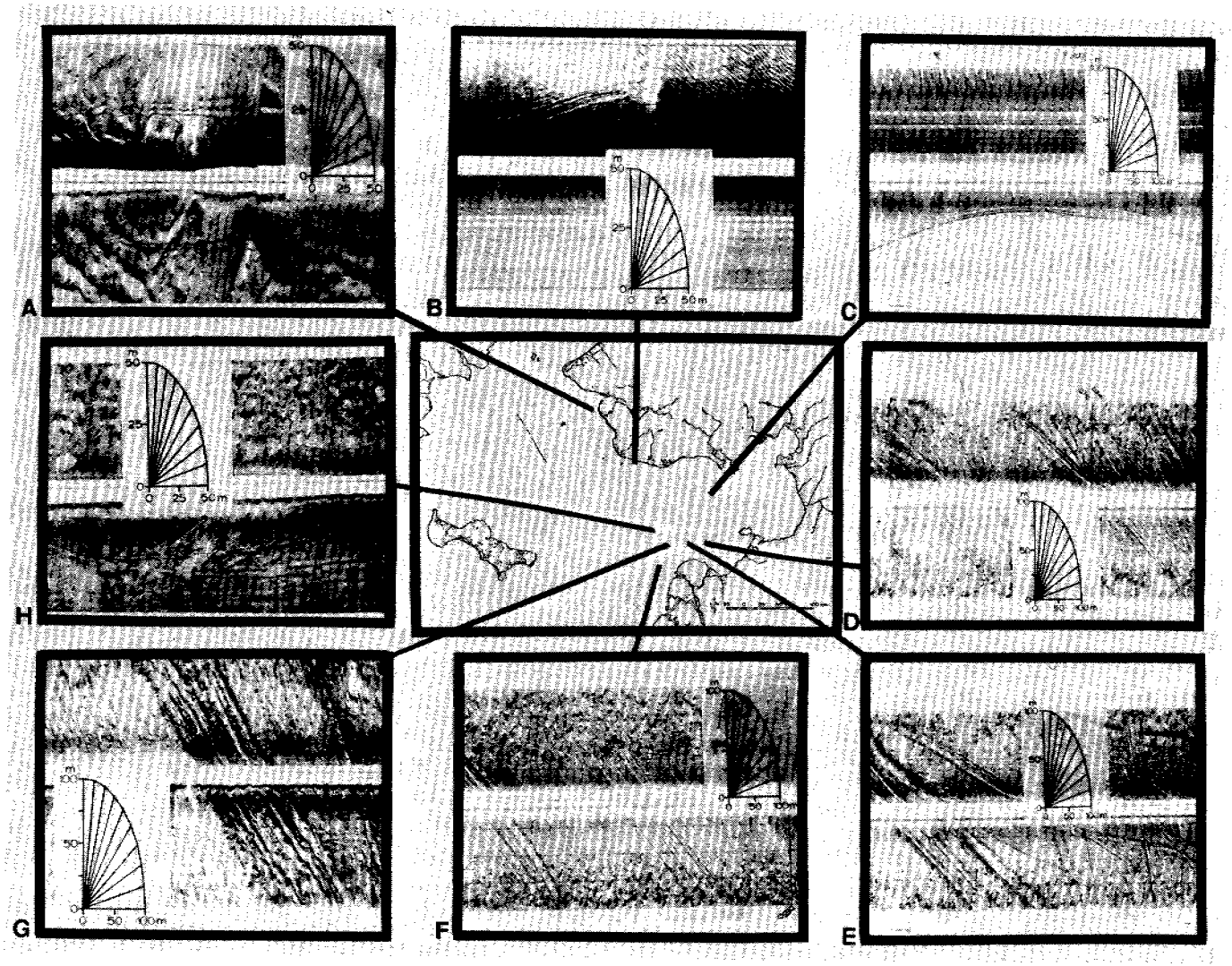

Figure E4. Ice gouges observed on sonographs taken over the sea floor of the northeastern Bering Sea. A and B - solitary gouges in ripple field. C, D, E - examples of solitary gouges, example E shows depth of incision on the sonograph horizen line. F and G - examples of pressure ridge raking, example G shows depth of incision on the sonograph horizen line. H - example of depressions associated with ice gouging.

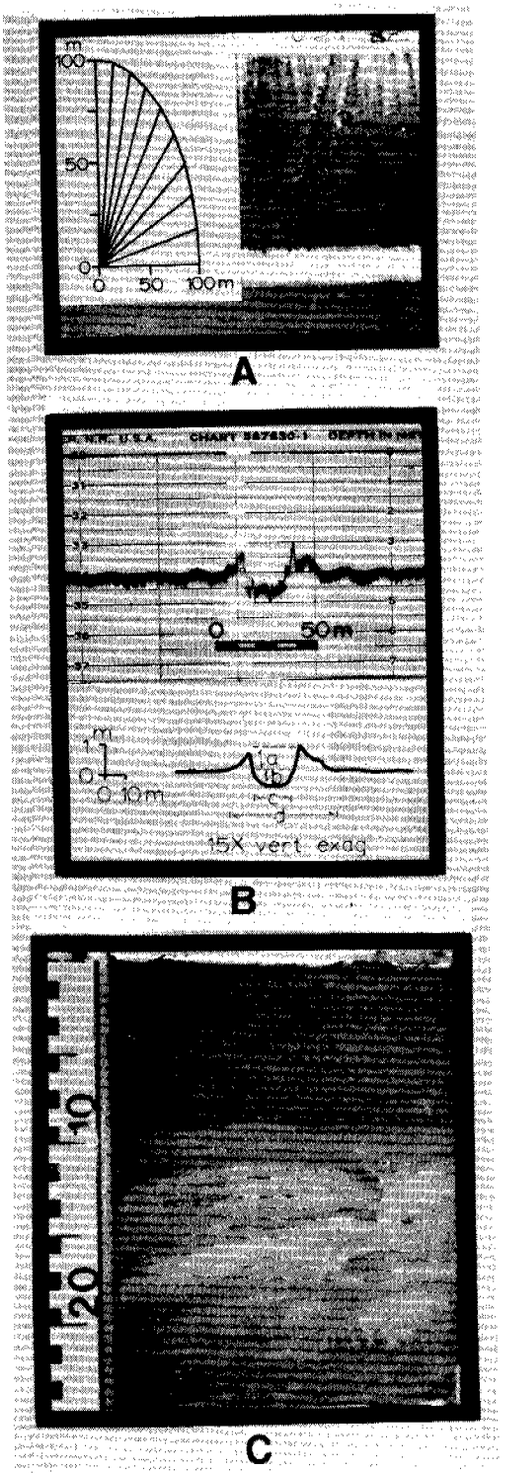

Figure E5. A - solitary gouge on a sonograph. B - 200 kHz profile and diagrammatic representation of gouge in A. Features of gouge include: a) incision depth as measured from gouge bottom to a horizontal line projected across sediment surface. b) height of sediment mounded on the gouge edge, c) width of incision, d) width of disruption zone caused by the gouging process. C - box core slab showing subsurface (11-18 cm interval) dissruption probably due to a past gouge event.

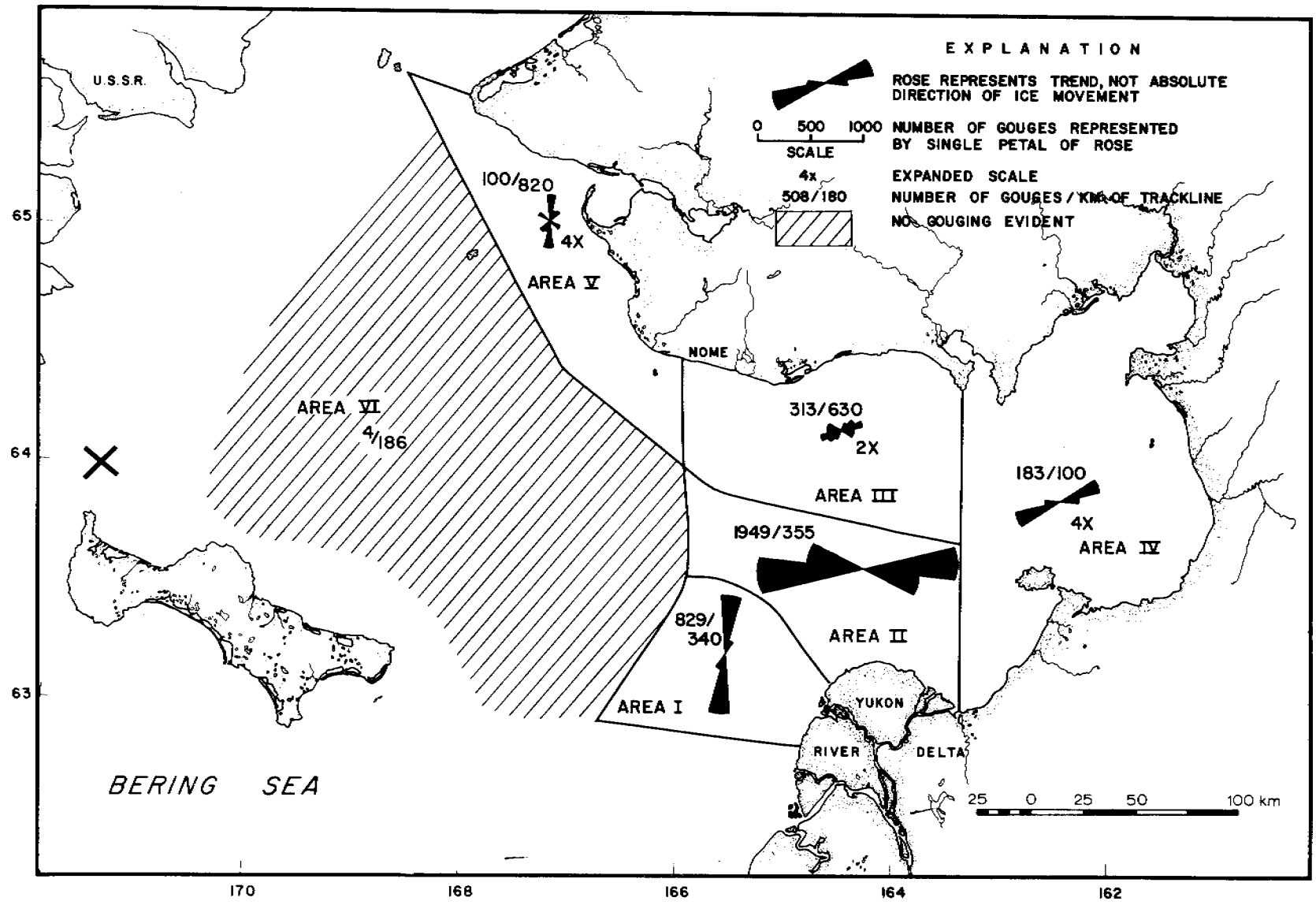

Figure E6. Ice gouging in northeastern Bering Sea. Rose diagrams represent trend and number of gouges; data are trends and not indicators of absolute motion. Division into areas I - VI is based on zones of similar trending gouges.

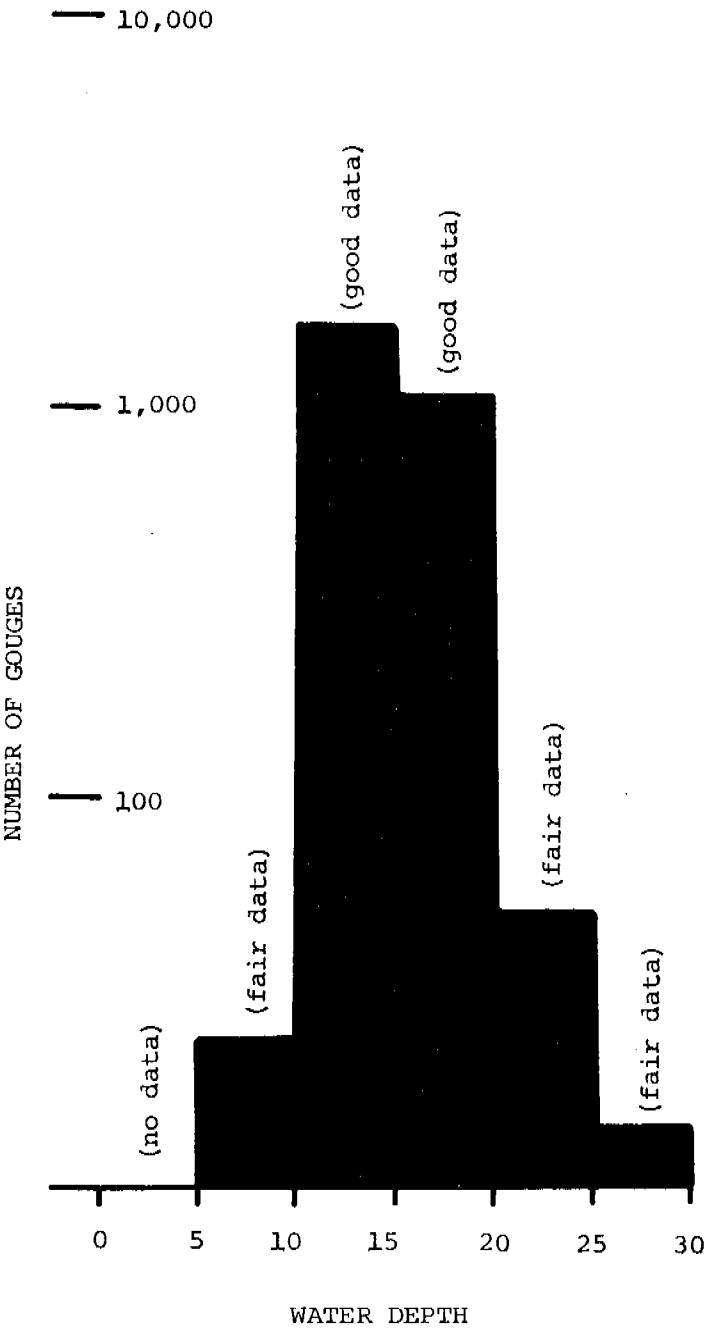

Figure E7. Histogram of gouge frequency versus water depth.

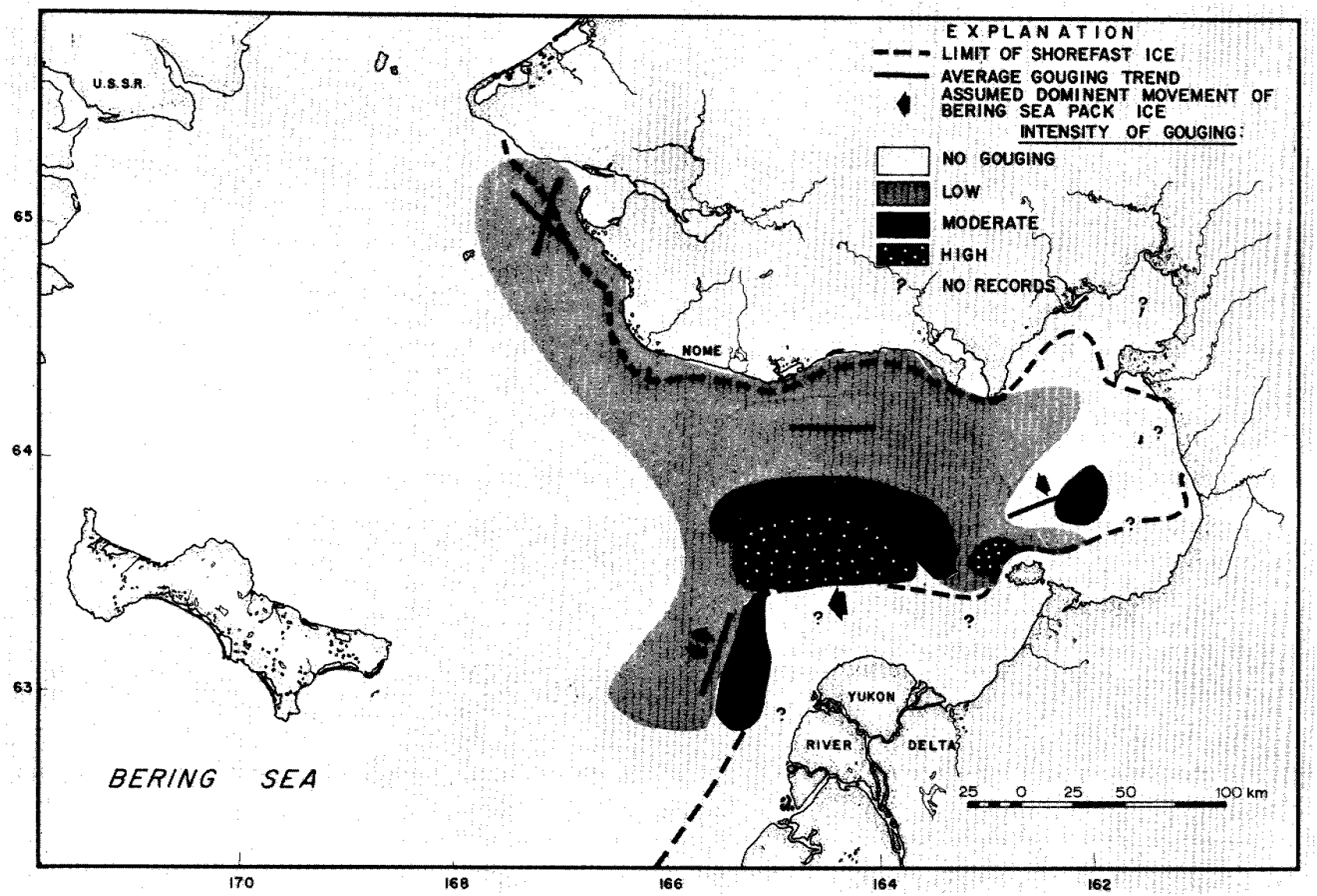

Figure E8. Summary of ice gouging in northeastern Bering Sea. The high density of gouging around the Yukon Delta is due to a well developed shear zone around the prodelta where shorefast ice interacts with southwestward moving Norton Sound pack ice, and north or south moving Bering Sea pack ice. Lower density of gouging in the rest of Chirikov Basin is due to greater water depths where only the deepest keels can touch bottom.

VI. RESULTS

F. Scour Depressions and Zones in Norton Sound

Matthew C. Larsen, Hans Nelson and Devin R. Thor

Introduction

Local occurrences of broad (50-150 m), shallow (less than one meter deep) depressions have been noted on sonographs taken in Norton Sound. These features exhibit a much greater diameter, more irregular shape, and flatter bottom than the small, conical gas craters described in section D. Unlike modern craters caused by gas venting at the sea floor (Garrison, 1974), these depressions may be caused by presently active sediment scour and therefore may present hazards to development of petroleum facilities (Demars et al., 1977; Herbich, 1977; Palmer, 1969; Posey, 1971). Such geologic hazards are of concern because Norton Basin shows promise of future resource development (Nelson, Kvenvolden and Clukey, this volume).

A program of intensive substrate reconnaissance employing side scan sonar, bottom photography, underwater television, sediment grain size analysis, and examination of current dynamics has been initiated to ascertain if the large depressions represent areas of intense scour. This paper describes depressions and correlates them with current regime, topography, and sediment type, to predict potentially hazardous scour areas for any future resource development.

Methods

A total of 3400 km of trackline of E. G. & G. side scan sonar was collected at 5 knots and primarily at 100 m sweep, during the 1976 and 1977 field seasons aboard the R/V SEA SOUNDER (Fig. E-1). Scour occurrence, extent, and morphology were examined on sonographs and located on a base map. A more detailed account of side scan operations is found in part E of this report.

During the 1977 field season 35 sediment samples were obtained in previously unsampled areas of Norton Basin. These samples augment an extensive previous sampling grid of over 500 sample locations. Sample preparation included washing to remove salts and oxidation of the organic fraction using Hydrogen Peroxide. Grain size was determined through standard textural analysis techniques using rapid settling tubes for the 2 mm to 0.063 mm size fraction, and the T.S.S. Hydrophotometer for the 0.044 mm to 0.004 mm range. Coarse fractions, greater than 2 mm, were dry sieved and weighed. The resulting data were compiled and statistically analysed by computer. Statistical measures include particle size distribution, size class ratio, cumulative percents, mean size, median size, sorting, skewness, kurtosis and moment measures.

Bottom current data were compiled and adapted from numerous previous studies of current velocity and direction conducted in Norton Basin (Coachman, Aagaard, and Trip, 1976; Fleming and Heggarty, 1966; Goodman et al., 1942; Husby, 1969, 1971; McManus et al., 1974; McManus and Smyth, 1970; Nelson and Creager, 1977). Bottom current readings were taken by lowering a current meter

to approximately one meter off the bottom. Thus, most of the compiled measurements are temporally unrelated, which results in fairly consistent current velocities, but conflicting current direction data. A map showing mean current regimes greater than 20 cm per second was compiled for Norton Sound (Fig. F-1); these data are not presented for Chirikov Basin where no apparent scour features are present.

At each of 30 stations in Norton Basin approximately 30 minutes of underwater television scanning was videotaped and 20 bottom photographs were taken with a 70mm format black and white still camera. Large scale features such as scour depressions were not noted on videotape or photographs due to the limited field of view of the system. However, the technique of scanning the substrate with underwater television proved to be effective in examining small-scale bottom features such as animal burrows, sediment characteristics, and ripple bedforms. The most significant problem encountered with photographic and TV scanning was sediment turbidity in the water column. Because of strong bottom-currents and the Yukon River suspended sediment load, bottom turbidity was a particular problem in the south-central area of Norton Sound in areas surrounding the Yukon Delta.

Morphology of Depressions

Zones of scour occur in two principle areas of Norton Sound, the most extensive being the west and north portions of the Yukon prodelta where ice gouging is frequently associated with the scoured area. The second zone is located 50 km southeast of Nome on the western flank of a broad shallow trough where water depth is greater than 20 m (Fig. F-1 and A-3). Isolated scour is also found on the eastern end of the trough and 10 km west of Stuart Island (Fig. F-1).

The shape of scour features varies from individual, more or less elliptical depressions, 10 to 30 m in diameter, to large zones of scour with irregular margins, 80 to 150 m wide (Fig. F-2). All observed depressions appeared to have very sharp edges with a broad flat bottom between the steep walls.

Sonographs over scour zones southeast of Nome were of sufficient quality that relief could be measured on the horizon line of the sonograph (Fig. F-3). Scour in this location was 60 to 80 cm deep. Side scan reflectors at this measurable location are on the same order of magnitude as all other observed scour features which indicates that 60 to 80 cm may be a standard depth for scour in Norton Sound.

Current Regimes and Bottom Character

Regional current direction in the northeastern Bering Sea is to the north at a mean velocity of 20 to 25 cm per second (Coachman et al., 1976). This flow slows down and swings in a counter-clockwise gyre into western Norton Sound. Tidal movement of water in Norton Sound is east-west and the highest non-storm velocities of 30 cm/sec. have been measured during spring tidal cycles (Cacchione and Drake, this volume) in 80 days of continuous measurement taken within one meter of the bottom by the GEOPROBE instrument (Cacchione and Drake,

in press) (see Fig. F-1 for location). The maximum current speed observed was 70 cm/sec. during an autumn storm of 2 to 3 days duration (Cacchione, this volume). Storm wave components contribute part of maximum current speeds observed.

Normal current velocities under non-storm conditions are low in eastern Norton Sound, and range between 5 to 10 cm/sec.; current speeds increase toward the center of the Sound and are maximum at the western end. Bottom-current velocities in scour areas on the Yukon prodelta and in the trough area southeast of Nome (Fig. A-3) range from 10 to 35 cm/sec. during non-storm conditions. The mean bottom-current velocity in both scour areas is about 20 cm/sec. (Fig. F-1).

Bottom photography shows ripple bedforms in both scour areas (Fig. F-4). Photos on either side of the scour area show a flat, fine-grained substrate with no visible bedforms. Water column turbidity off the Yukon delta prevented adequate visibility for good photographs at most stations. However, rippled sediment was photographed in the area of large scour zones northwest of the delta. Ripples in scour areas on the prodelta and south of Nome are asymmetric with a 10 to 15 cm wavelength and a height of 3 to 5 cm.

Grain size of bottom sediment in Norton Sound ranges from 0.16 mm to 0.007 mm (2.6 phi to 7.5 phi) (very fine sand to fine silt). The mean size over the general area is approximately 0.063 mm (4 phi) (sand-silt boundary) (Fig. F-5). Sediment lithology varies in the two main areas of current scour. Yukon prodelta sediment is typically fine sand and silt with a small percentage of clay (McManus et al., 1977). Small wood fragments and other organics account for a small percentage of river sediment. Sediment grain size values range from 25 to 50 percent sand, 40 to 70 percent silt, and 5 percent clay. Mean grain size is 0.044 mm (4.5 phi). Sediment in the trough southeast of Nome is typified by coarser grain sediment. Size values range from 65 to 78 percent sand, 20 to 30 percent silt, and 8 percent clay. Mean grain-size is slightly coarser than prodelta sediment and is 0.058 mm (4.1 phi). Sediment in Chirikov Basin is coarser than that found in Norton Sound, and ranges from a mean diameter of 4 mm to 0.125 mm (-2 to 3 phi) (gravel to fine sand).

Genesis of Depressions

All areas with sediment depressions share common elements of topographic setting and are associated with small scale morphologic disruption of the sea floor. Depressions on the western edge of the Yukon prodelta are situated on a gradual slope of less than 0.5° (Fig. A-3). A slope of this magnitude generally is insufficient for gravity slumping, however it can focus wave energy and constrict strong water currents moving from the Bering Sea into the increasingly more shallow Yukon prodelta. Depressions in northern Norton Sound also are located on a slope at the edge of a shallow east-west trending trough (Fig. A-3) and in this setting scarps are apparent (Fig. F-2). Ebbing tidal currents may be concentrated on the western face of the trough, due to east-west motion of tidal water masses. On both of these topographic slopes small scale ripple forms are found that indicate presence of stronger current regimes compared to other areas of Norton Sound where ripples are absent (Fig. F-4).

Depressions in Norton Sound all occur in areas covered by Holocene Yukon silt (McManus et al., 1977), but the grain size 0.044 mm to 0.063 mm

(4.0 to 4.5 phi) is coarser than other regions of Norton Sound (Fig. F-5). This again shows that areas with depressions are associated with the regions of strongest current regime, as current measurements verify (Fig. F-1).

Evidence at the GEOPROBE site, situated just west of the northern set of depressions in similar silt-sized sediment (Fig. F-1), shows that critical shear velocities are only occasionally exceeded under the normal current regime of the region (Cacchione and Drake, this volume). However, during storm conditions, the shear velocities are doubled and large amounts of suspended sediment are detected by the GEOPROBE transmissometer and nephelometer. Since the GEOPROBE site is considered quite representative of the general Norton Sound environment, we infer that storm conditions provide an adequate mechanism for intense scour of Yukon silt. Our independent evidence of coarser grain size and ripple fields indicates that scour in Norton Sound should be most intense in the areas where the depressions occur (Figs. F-4 and F-5).

The presence of seafloor scarps and ice gouges, often expanded into large depressions, suggests that similar to areas of bedforms in fine sand (Southard, 1977; Southard and Dingler, 1971) disruption of otherwise flat bottom by gouging or scarps provide a mechanism for initiation of silt scour. Once the irregularities in the substrate and the current regimes of storm conditions are present, flow separation over the disruption should occur and the downstream eddy would strip out sediment to a certain depth and distance downstream until the wake died out (Southard, oral communication, 1978). Thus, large scale, flat-floored scour depressions would be formed and could consequently be maintained by the normal current regime (Southard, Ibid). Small scale ripples are the only bedforms that have been observed to form in the grain size ranges that are present in Norton Sound (Southard, 1977; Harms et al., 1975). Consequently, the large scour depressions we observe may be another characteristic response to strong current and wave regimes, when currents are focused on silt covered slopes with topographic disruptions. In Chirikov Basin, where generally stronger current regimes and coarser grain size exist, the sea floor response is fields of large-scale, active bedforms (see Fig. G-1 and section G, this volume).

Potential Geologic Hazards in Scour Areas

A newly recognized geologic hazard in this subarctic region is presented by the synergistic effect of strong storm currents and ice gouging that triggers formation of large scour depressions in Yukon silt. Scour is a recognized problem along routes of subsea pipelines because it can expose and leave lengths of pipeline unsupported (Demars et al., 1977). Extensive undermining of pipelines poses serious risks of stress and structural damage.

Gravity structures are used in shallow water areas of well consolidated undersea sediments like Norton Basin. They are stable by virtue of their large mass and broad base (approximately 100 m in diameter), that gives them a low center of gravity (Gerwick, 1976). Problems in gravity structure stability arise from differential settling of sediment at the base, which can be initiated by compaction of poorly consolidated substrate material, or loss of substrate support by current scour (Palmer, 1976; Wilson and Able, 1973).

Another extremely critical problem to recognize is that any type of natural or artificial flow disruption of storm derived currents over Yukon sediment will set off intense scour. Thus, in the scour areas outlined to date (Fig. F-1) any artificial structures on the sea floor will trigger a large region of scour around the disrupting structure, similar too, but probably of larger magnitude than that recognized near pier pilings (Palmer, 1970).

Conclusions and Suggested Future Research

Sediment scour in Yukon silts and very fine grained sand is common in two areas of Norton Sound. It is associated with high current velocity, small scale ripple fields, and topographic disruptions, especially ice gouging. Consequently, potential petroleum development in these areas of Norton Sound faces many scour hazards. Pipelines can be damaged during annually occuring storms by scour that can leave them unsupported for lengths of up to 150 m. Loss of substrate support by current scour may also be a serious problem affecting stability of gravity structures.

Suggested future work and analysis in Norton Sound is necessary to examine the process of current scour. Better photographic documentation, precisely located sediment sampling, *in situ* substrate engineering property tests, and diver observation of scour zones is planned as part of the 1978 field program off the R/V KARLUK. To fully assess scour processes, long term monitoring of bottom currents, suspended sediment movement, and sea floor response by *in situ* measurement systems is required in areas of scour depressions.

REFERENCES

Cacchione, D. A. and Drake, D. E., in press, A new instrument system to investigate sediment dynamics on continental shelves: Marine Geology.

Coachman, L. K., Aagaard, Knut, and Tripp, R. B., 1976, Bering Strait: The regional physical oceanography: Univ. of Washington Press.

Demars, K. R., Nacci, V. A., and Wang, W. D., 1977, Pipeline failure: a need for improved analyses and site surveys: Offshore Technol. Conf. Prepr. V., pp. 63-70.

Fleming, R. H., and Heggarty, D., 1966, Oceanography of the southeastern Chukchi Sea, in: Wilimovsky, N. J. and Wolf, J. M., eds., Environment of Cape Thompson Region, Alaska: U.S. Atomic Comm., p. 697-754.

Garrison, Louis E., 1974, The instability of surface sediments on parts of the Mississippi Delta front: Open file report May, 1974, U.S. Geological Survey, Corpus Christi, Texas.

Gerwick, B. C., Jr., 1976, Condeep - in 400 ft. of water, concrete caisson requires no piles: Civil Engineering, ASCE-April, v. 46, no. 4, p. 54-56.

Goodman, J. R., Lincoln, J. H., Thompson, T. G., and Zeusler, F. A., 1942, Physical and chemical investigations: Bering Sea, Bering Strait, Chukchi Sea during the summers of 1937 and 1938: Univ. of Wash. Pub. in Oceanography, v. 3, no. 4, p. 105-169, and Appendix, p. 1-117.

Harms, J. C., Southard, J. B., Spearing, D. R., and Walker, R. G., 1975, Depositional environments as interpreted from primary sedimentary structures and stratification sequences: Soc. Econ. Paleontologists and Mineralogists Short Course No. 2, Dallas, 161 p.

Herbich, J. B., 1977, Wave induced scour around offshore pipelines: Offshore Technol. Conf. Paper, v. , p. 79-84.

Husby, D. M., 1969, Report of oceanographic cruise U.S.C.G.C. NORTHWIND, northern Bering Sea - Bering Strait - Chukchi Sea, July 1969: U.S. Coast Guard Oceanographic Report, no. 24, 75 p.

Husby, D. M., 1971, Oceanographic investigations in the northern Bering Sea and Bering Strait, June-July 1969: U.S. Coast Guard Oceanographic Report, no. 40, 50 p.

McManus, D. A., Venkataratham, K., Hopkins, D. M., and Nelson, C. H., 1974, Yukon River sediment on the northernmost Bering Sea shelf: Jour. Sed. Pet., v. 44, no. 4, p. 1052-1060.

McManus, D. A. and Smyth, C. S., 1970, Turbid bottom water on the continental shelf of northern Bering Sea: Jour. Sed. Pet., v. 40, p. 869-877.

Moore, D. G., 1964, Acoustic-reflection reconnaissance of continental shelves: Eastern Bering and Chukchi Seas, in: Miller, R. L., ed., Papers in marine geology (Shepard volume): New York, Macmillan Co., p. 319-362.

Nelson, C. H. and Hopkins, D. M., 1972, Sedimentary processes and distribution of particulate gold in the northern Bering Sea: U.S. Geol. Survey Prof. Paper 689, 27 p.

Nelson, C. H. and Creager, J. S., 1977, Displacement of Yukon-derived sediment from Bering Sea to Chukchi Sea during Holocene time: Geology, v. 5, p. 141-146.

Palmer, H. D., 1969, Wave-induced scour on the seafloor, in Civil engineering in the oceans, II, American Society of Civil Engineers, New York, p. 703-716.

Palmer, H. D., 1970, Wave-induced scour around natural and artificial objects: Doctoral Dissertation, Dept. Geol. Sciences, Univ. of Southern California, 172 p.

Palmer, H. D., 1976, Sedimentation and ocean engineering structures, in: Stanley, D. J. and Swift, D. J. P., eds., Marine sediment transport and environmental management: New York, John Wiley and Sons, Inc., p. 519-534.

Posey, C. J., 1971, Protection of offshore structures against underscour: Journal of the Hydraulics Div., Proc. Am. Soc. Civil Eng., v. 97, no. HY7, p. 1011-1016.

Southard, J. B. and Dingler, J. R., 1971, Flume study of ripple propagation behind mounds on flat sand beds: Sedimentology, v. 16, p. 251-263.

Southard, J. B., 1977, Erosion and transport of fine cohesive marine sediments (abs.): EOS, Trans. Amer. Geophys. Union, v. 58, no. 12, p. 1161.

Sundborg, A., 1956, The river Klaralven; a study of fluvial processes: Geograf. Ann., v. 38, p. 125-316.

Wilson, N. D. and Abel, W., 1973, Seafloor scour protection for a semi-submersible drilling rig on the Nova Scotian shelf: Offshore Technol. Conf. Prepr., v. 2, p. 631-646.

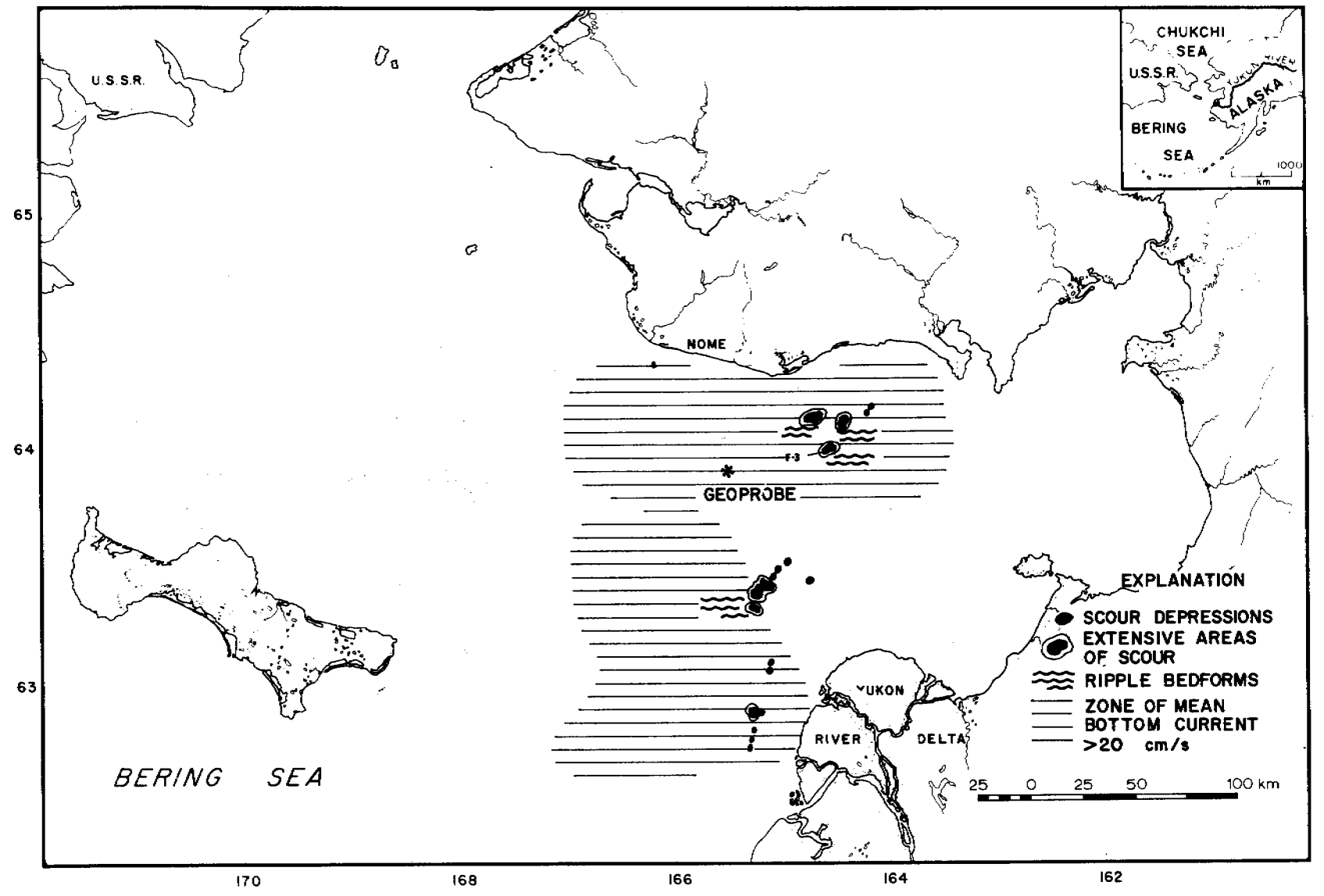

Figure F-1. Location of scour depressions, extensive scour and ripple zones, and strongest bottom currents in Norton Sound.

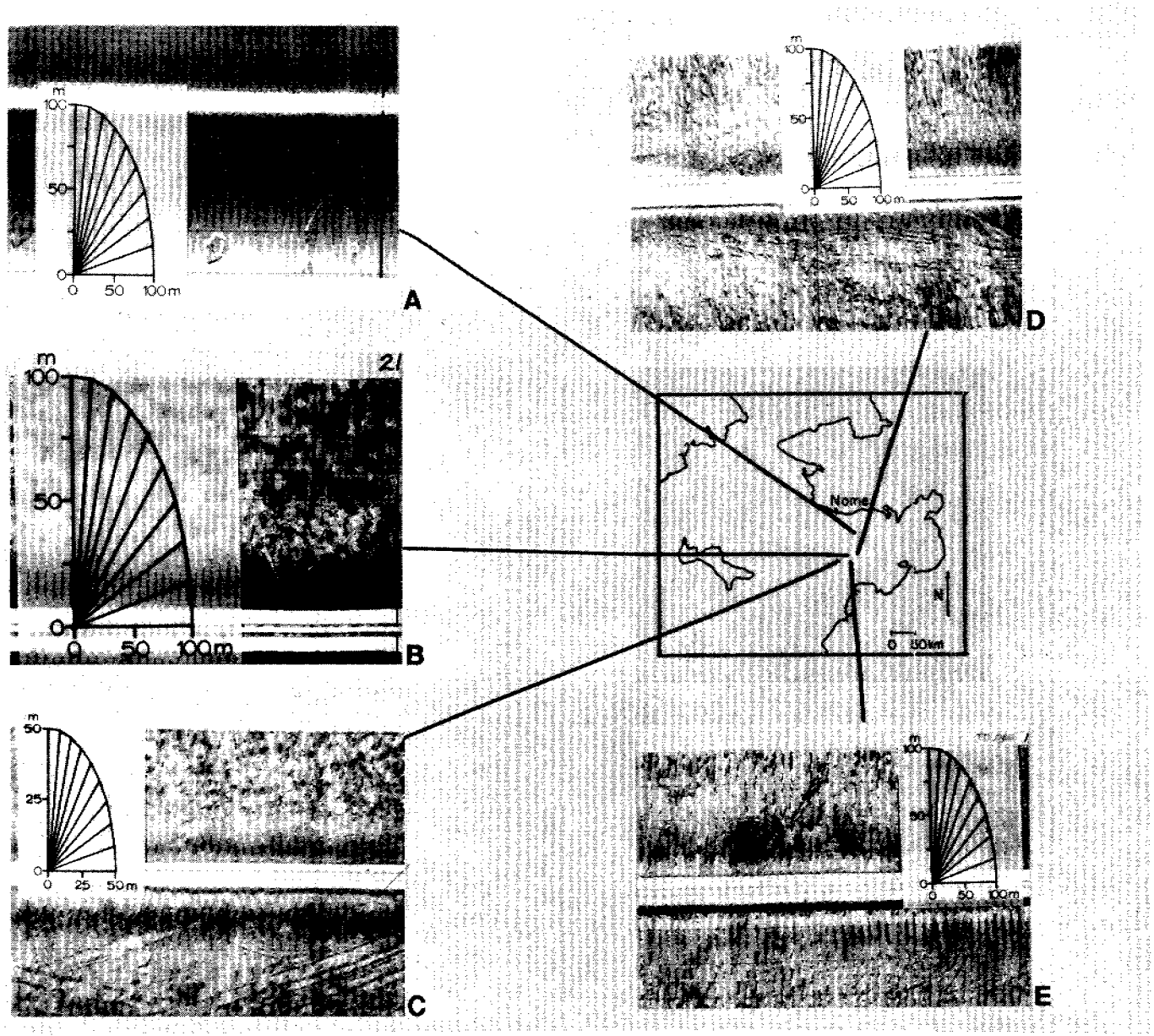

Figure F-2. Side scan sonograph examples of scour features. A and B are examples of individual depressions. C, D and E show large zones of scour associated with ice gouge.

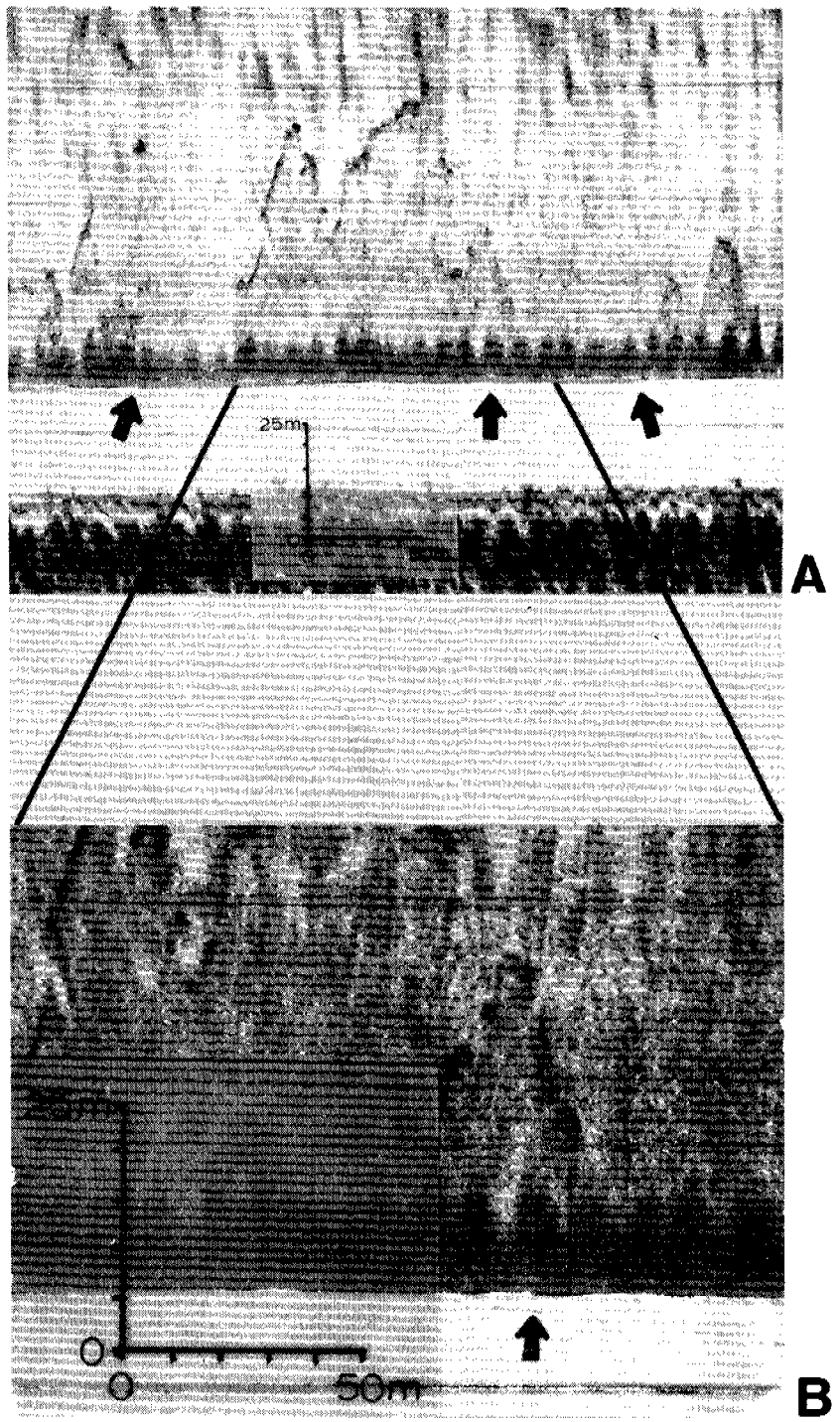

Figure F-3. Example of large scour zone (location keyed on Fig. F-1). Photo B is an expanded version of A. Arrows point to scarps defining scour margins which are crossed by sonograph horizon line.

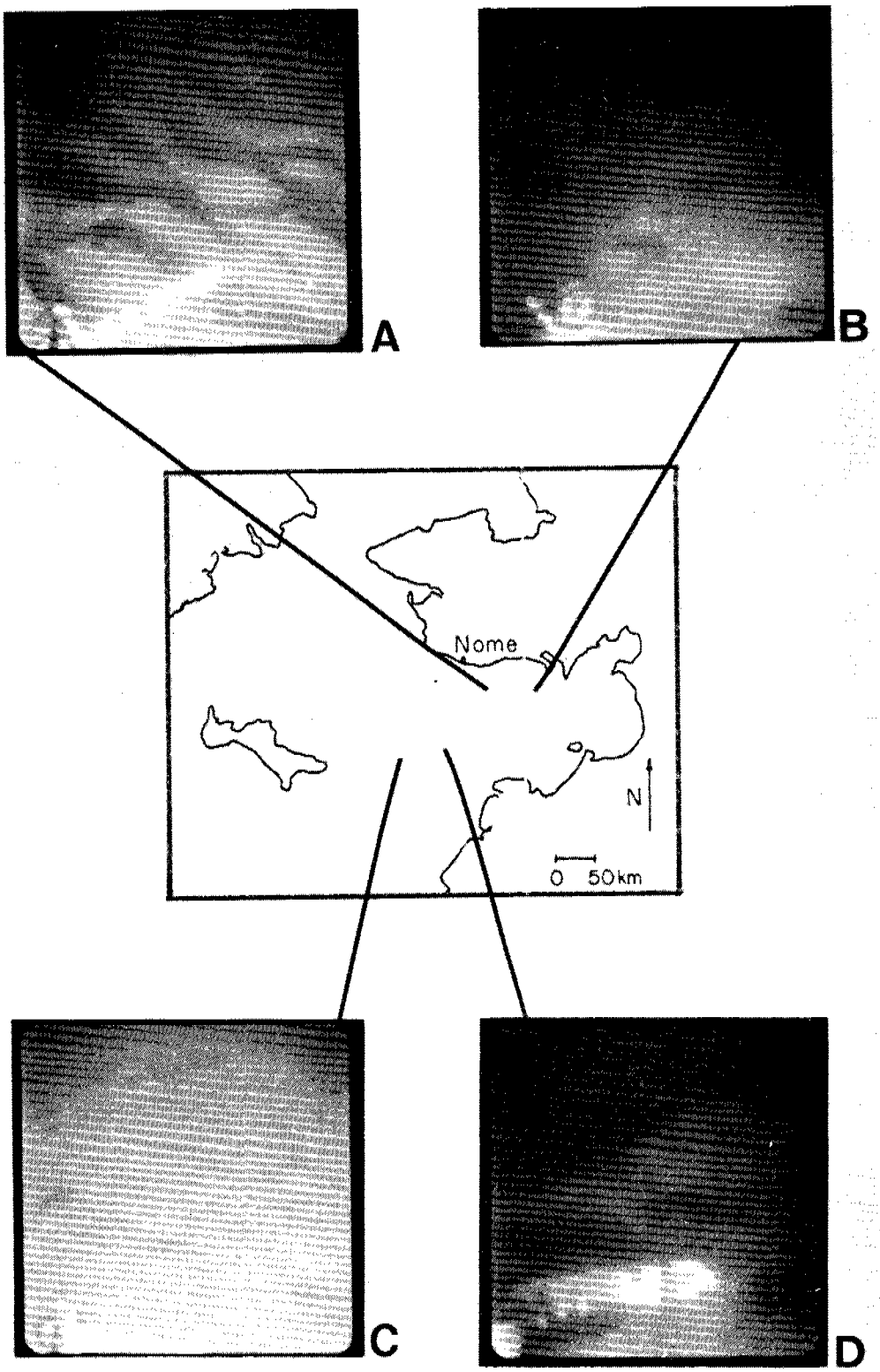

Figure F-4. 70 mm bottom photographs showing ripple zones in scour areas. Scale: black strip on compass vane is 2 cm wide.

Photos A and D: scour area ripples with 10 to 15 cm wavelength.
Photos B and C: normal bottom without ripples or scour.

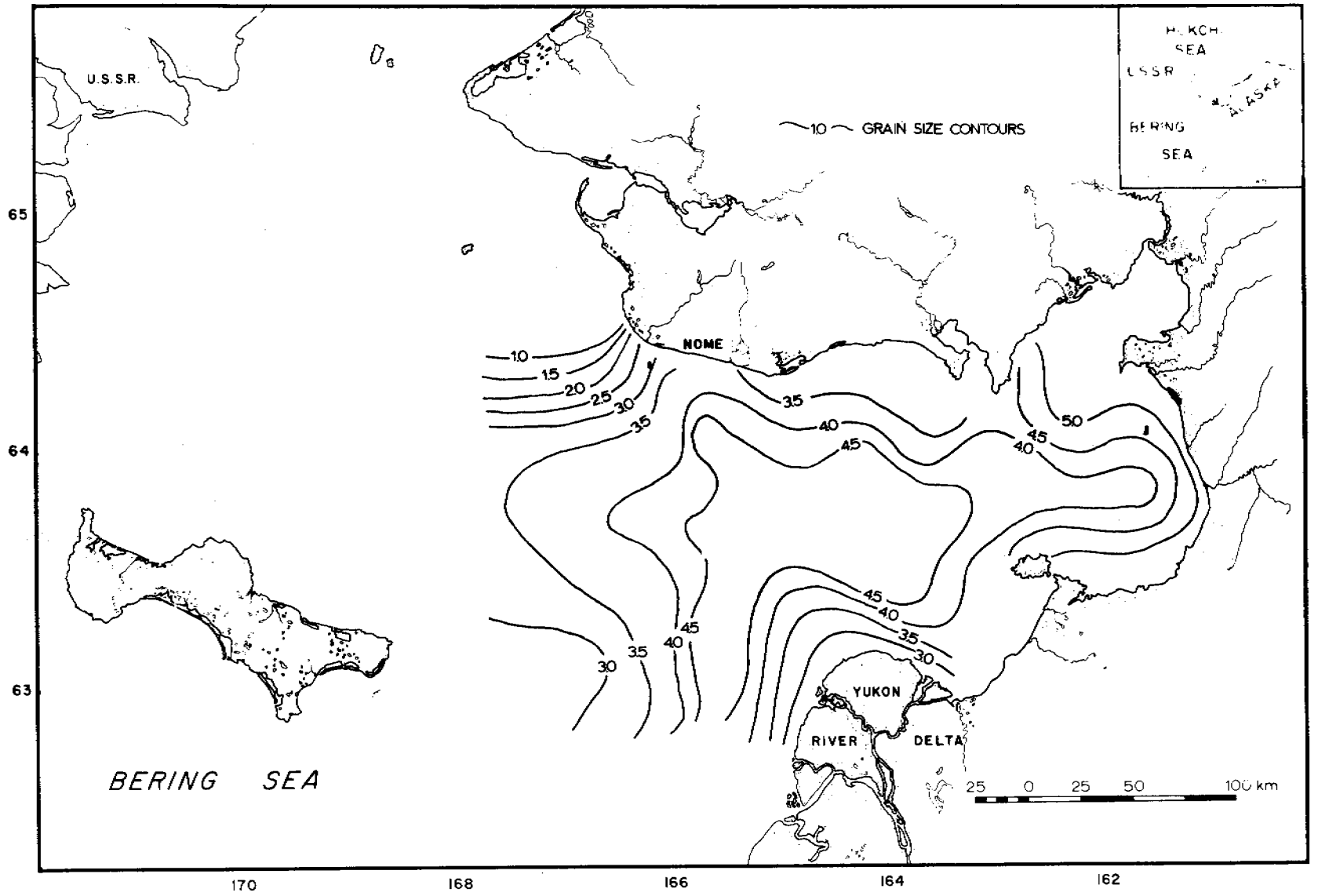

Figure F-5. Contour map of sediment grain size distribution in mean phi in Norton Sound. Values represent first moment calculation at each station.

VI. RESULTS

G. Areas of Active, Large Scale Sand Wave and Ripple Fields with Scour Potential on the Norton Basin Sea Floor

Hans Nelson, Michael E. Field, David A. Cacchione, and
David E. Drake

Introduction

Strong dynamic currents are present throughout much of the northern Bering Sea, particularly where westward land projections interject into the northward flow, such as in the eastern Bering Strait area (fig. G-1) (Fleming and Heggarty, 1966). In such regions large bedforms develop and migrate to form an unstable sea floor that can be a potential hazard to platform foundations and pipelines. Such potentially hazardous areas must be identified, their history assessed, and magnitude of future problems predicted. This paper outlines regions of mobile bedforms (fig. G-1) and presently known aspects of their dynamic activity.

Identification and Distribution of Bedform and Scour Features

Large bedforms and scour features can be recognized and mapped with side-scan sonar profles and basic internal structure sometimes can be determined by high-resoltuion profiles (fig. G-2; see Methods in sections B-D for a description of techniques). Detailed surficial observations can be made with underwater television and bottom photos, and subsurface stratigraphic history may be determined by analyses of vibracores and box cores (figs. G-3 and 4).

In general, only small scale bedforms and large scale scour features (fig. F-1) are found in Norton Sound (fig. G-1). Chirikov Basin on the other hand is characterized by coarser grain size than Norton Sound (fig. F-5) (Nelson and Hopkins, 1972; McManus et al., 1974 and 1977), and numerous fields of mobile bedforms. In the vicinity of Sledge Island, most of the sea floor has been stripped bare of sediment (Nelson and Hopkins, 1972), suggesting intense current scour. Just east and west of the scoured region and extending across the nearshore area of the Nome coastal plain, extensive sand wave and ripple fields are found (fig. G-1).

From Pt. Spencer spit west to King Island a series of sand ridges and swales exist (fig. G-2). The crest of each shoal is covered with sand waves of varying types and sizes (fig. G-5). To the north of the ridge and swale area toward Bering Strait, extensive sand ribbon fields are found with occasional sand dune areas (fig. G-1); however, the area is not completely surveyed. The sand ribbon fields indicate a sediment-starved region and possibly one prone to current scour as the current speeds intensify toward Bering Strait (fig. E-3). Further north within Bering Strait itself, gravel and shell pavements are noted (Nelson and Hopkins, 1972) in addition to sporadic occurrences of extremely large sand waves (Grim and McManus, 1970).

Off the eastern and western ends of St. Lawrence Island, major sand ridge and swale topography is known (Hopkins et al., 1976), and ripple fields are common to the northwest off St. Lawrence Island (fig. G-1).

Character and Origin of Mobile Bedform Features

In the ridge and swale area between King Island and the mainland, swale areas appear to undergo erosion periodically. Generally, a thin veneer of fine, modern mud at the surface overlies Pleistocene peaty mud (fig. G-6). Fine mud, signifying sluggish currents, typically deposit rapidly in depressions (fig. G-7). The lack of thick deposits, and very old radiocarbon dates close to the surface, however, suggest that muds periodically are swept away so that there has been no net mud accumulation for thousands of years. In fact, a radiocarbon date on peat 20 cm below the surface of the swale between Tin City and York Shoal was >30,000 BP, indicating that significant quantities of younger sediment had been stripped away, possibly by currents (fig. G-6).

In contrast to swales, sand ridges are definitely constructive as is shown in the sparker seismic profiles (figs. G-8 and 9). The morphology of inner shoals mirrors the shape of the modern Pt. Spencer spit and these shoals may be ancient analogues (fig. G-3). Indeed, depths of shoal crests coincide with proposed still-stand depths of ancient submerged strandlines noted elsewhere in northern Bering Sea (Nelson and Hopkins, 1972). Sand ridges behind large obstructions to the northward current flow, such as King Island and Cape Prince of Wales (see area north of 88 in fig. G-3), may be lee side accumulations of sediment unrelated to past paralic environments.

Although formation of the basic ridge structures (15-30 km long, see cross-hatched areas in fig. G-3), may relate to past transgressive history, these structures also have a modern history of modification by development of sand waves and ripple fields. Sand waves are 1 to 2 m high and have crest spacings of either 10 to 20 m or 150 to 200 m (figs. G-9 and G-10E) Superimposed on the sand waves are smaller scale current asymmetric (figs. G-10B and C) and wave oscillation (fig. 10A) ripples with heights approximately 4 to 10 cm and wavelengths approximately 20 to 100+ cm. Except for the oscillation ripples, bedforms of all sizes are asymmetric to the north, and their asymmetry coincides with the prevailing northward flowing dynamic currents (fig. E-3) (Coachman et al., 1976).

Growth and movement of the sand wave fields on crests is definitely intermittent, just like the apparent erosional history of the swales. Ice gouges observed to cut sand wave fields on inner shoals in the summer of 1976 proved that no change in the sand wave fields had occurred at a minimum since the previous winter, or possibly for many years before, depending on how recently the gouge occurred. At the time we studied the area in the fall of 1976, only low speed oscillatory bottom currents up to 15 cm/sec (fig. G-11) were measured. Underwater television observation showed only the development of oscillation ripples (Fig. G-10A) and only decayed, inactive sand wave bedforms were seen on sonographs (figs. G-10D and E). Thus, sand wave movement was active neither then nor apparently for some time before. However, a piece of wood found at 30 cm depth in a sand wave had an age of 1155 BP (Teledyne Isotopes #I-9773). This date proved that sand wave scour had been active to this depth since sea level has reached its present height, and that sand waves are not relict features from some past time of lower sea level.

Data collected in the field season of 1977 indicates that significant activity has occurred since the 1976 survey. In some areas with replicate side-scan lines, large scale sand waves have reformed from decayed fields and developed subsets of smaller scale sand waves offset at an angle (fig. G-10E); however, sand waves on some other ridges remained unmodified from 1976 to 1977 (fig. G-10D). Underwater television videotapes show that small scale ripple fields were undergoing active modification at the time of observation in 1977. Instead of oscillation ripples observed during the storm conditions in 1976, there were actively migrating asymmetric straight-crested ripples in the troughs (fig. G-10C) and linguoid ripples on the upcurrent face of sand waves (fig. G-10B). Northward flowing bottom current speeds measured with the shipboard profiling current meter ranged from 20-40 cm/sec, and near bottom average current speed was 24 cm/sec (fig. G-12).

Observations of a series of ice gouges also confirms that there has been recent, active migration of sand waves near Port Clarence (fig. G- 13). Ice gouges range from fresh to highly modified by sand wave migration (fig. G-12 F); thus, extensive movement of some sand wave fields has occurred recently. Lack of modification of gouges (fig. G13) and continued presence of decayed bedforms in some locations indicate that current activity in the Port Clarence area varies both in time and space. Only long term current measurements from from several locations will solve the complexity of current regimes and allow predictability of mobile bedform activity.

Conclusions and Needs for Further Study

Surveys in September 1976 during a period of subsiding storm waves from the north showed only oscillatory movement of sand on ripple crests. A maximum speed of the north-flowing coastal current of about 15 cm/sec was measured near the bottom and no net bedload movement was observed. Fresh-looking ice gouges cutting inshore ripples indicated that bedload movement had been negligible in this zone since ice break-up in the spring. The second survey, in July 1977, was made during very calm weather, yet significant bedload movement was observed on ridge crests at water depths of 10 to 30 m. Northward flowing bottom currents measured up to 40 cm/sec. Linguoid ripples were observed moving on the stoss slope of sand waves and straight-crested ripples in the troughs. Ice gouges on deeper ridge crests in varying states of preservation indicated active bedload transport.

Sand wave movement and bedload transport apparently occur during calm weather and maximum change apparently occurs when major southwesterly storms generate sea level set-up in the eastern Bering Sea that enhances northerly currents. Strong north winds from the Arctic, however, reduce the strength of the continuous northerly currents and thereby reduce the amount of bedload transport.

Studies to date indicate that the most extreme scour potential exists in regions of sand ribbons and gravel plus shell pavement within straits areas (fig. G-1). The Port Clarence sand wave area has the most rapidly changing relief and the scour in sand wave troughs may reach depths of up to 2 m (Fig. G-9). Data from replicate lies in 1976 and 1977 show that such scour may occur in some areas of the Port Clarence sand wave field each year (fig. G-10).

Future studies require reoccupation of key sites within the sand wave field to determine stability. Long measurements for several months must be made of current velocity and suspended sediment, especially during times of storm stress. Detailed side-scan profiling is required at locations of suspected current scour and stratigraphic history must be investigated with deep vibracoring to determine depth of active scour, and periodicity and extent of bedform movement.

Acknowledgements

Devin Thor, Mathew Larsen, Terry Hallinan, William Richmond, Jeff Patry and James Evans compiled data and prepared figures. We thank the officers, crew, and shipboard scientific staff for their concerted effort in the detailed study of sand wave areas.

References Cited

Coachman, L.K., Aagaard, Knut, and Tripp, R.B., 1976, Bering Strait: The regional physical oceanography; Univ. of Washington Press, 186 p.

Fleming, R.H., and Heggarty, D., 1966, Oceanography of the southeastern Chukchi Sea, in Wilimovsky, N.J., Wolfe, J.M., (eds.), Environemnt of Cape Thompson Region, Alaska: U.S. Atomic Energy Commission, p. 697-754.

Grim, M.S., and McManus, D.A., 1970, A shallow seismic profiling survey of the northern Bering Sea: Marine Geology, v. 8, p. 293-320.

Hopkins, D.M., Nelson, Hans, Perry, R.B., and Alpha, Tau Rho, in press, Physiographic subdividsions of the Chirikov Basin, northern Bering Sea; U.S. Geol. Survey Prof. Paper 759-B, (published in cooperation with) National Ocean Survey, National Oceanographic and Atmospheric Administration.

McManus, D.A., Venktaratham, K., Hopkins, D.M., and Nelson, C.H., 1974, Yukon River sediment on the northernmost Bering Sea shelf: Jour. Sed. Pet., v. 44, no. 4, p. 1052-1060.

McManus, D.A., Venkataratham, Kolla, Hopkins, D.M., and Nelson, Hans, 1977, Distribution of bottom sediments on the continental shelf, northern Bering Sea: U.S. Geol. Survey, Prof. Paper 759-C, p. C1-C31.

Nelson, C.H., and Hopkins, D.M., 1972, Sedimentary processes and distribution of particulate gold in the northern Bering Sea: U. S. Geol. Survey Prof. Paper 689, 27 p.

Nelson, C. H., and Creager, J.S., 1977, Displacement of Yukon-derived sediment from Bering Sea to Chukchi Sea during Holocene time: Geology, v. 5, pp. 141-146.

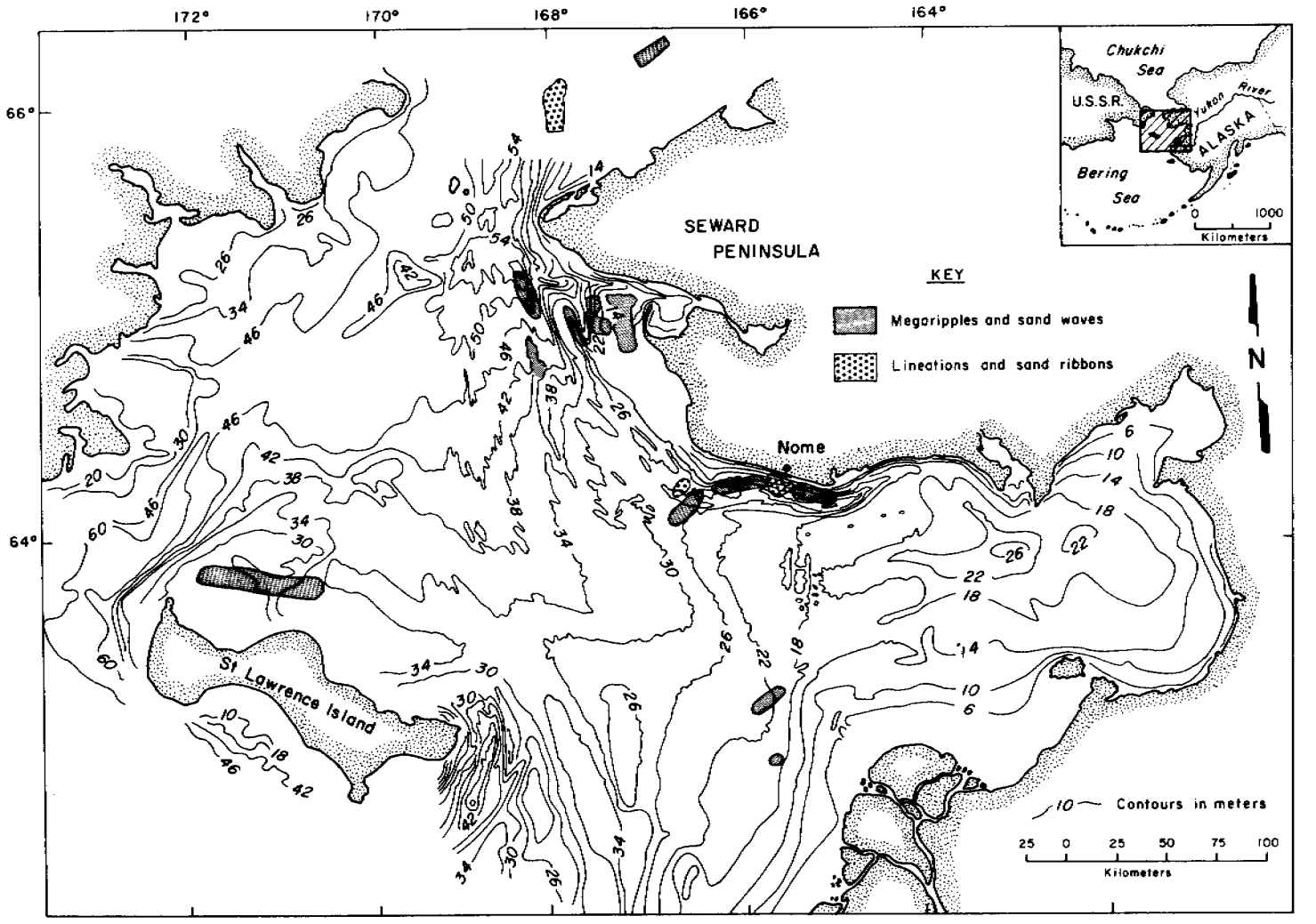

Figure G-1. Index map of Northern Bering Sea showing major areas of mobile bedforms.

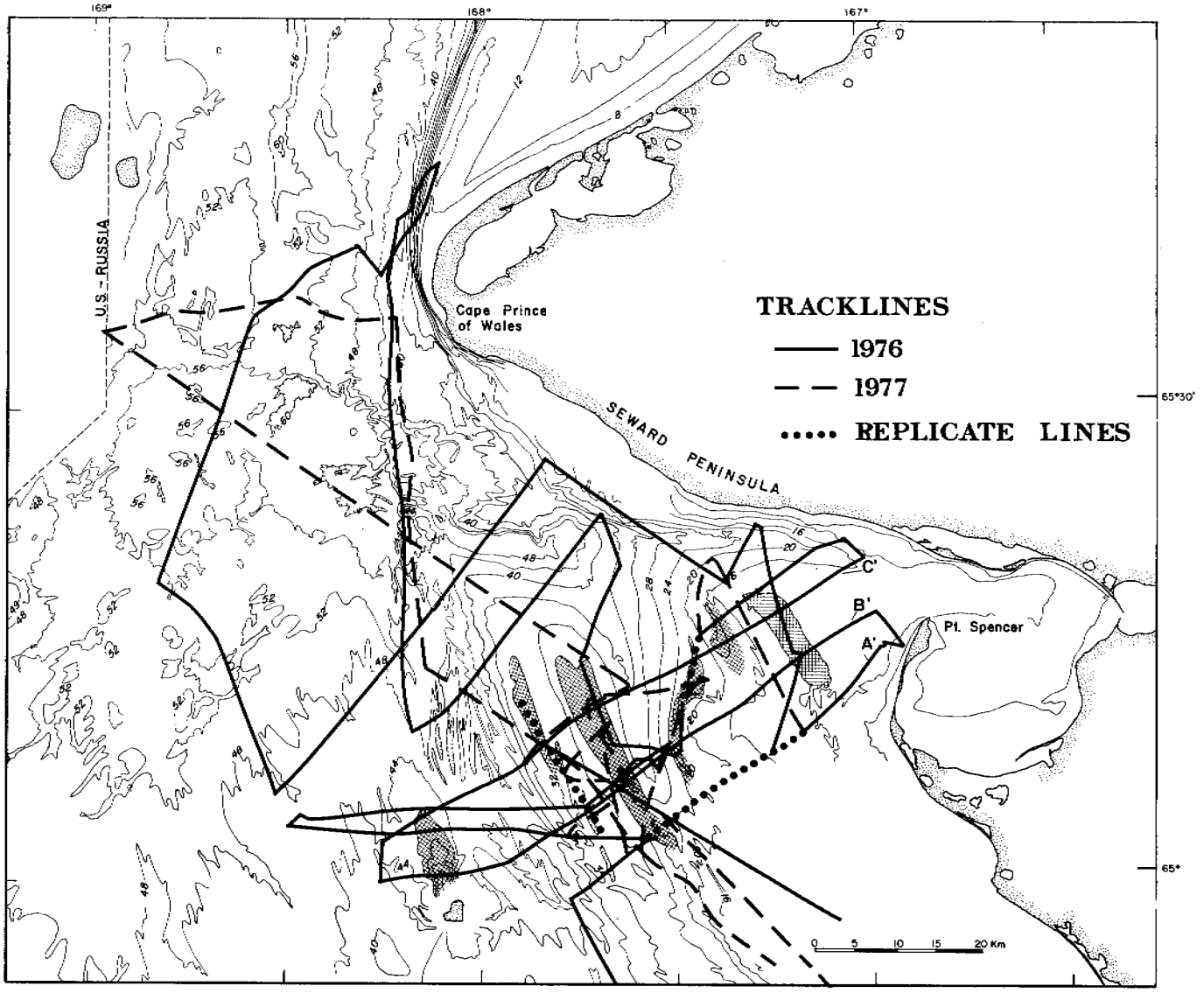

Figure G-2. Detailed high-resolution seismic profile and side scan tracklines collected in 1976 and 1977 in northeastern Chirikov Basin. Miniranger precision navigation was used to replicate tracklines. Bathymetric contours are in meters; hatchered areas outline major sand ridges that exhibit sand-wave fields.

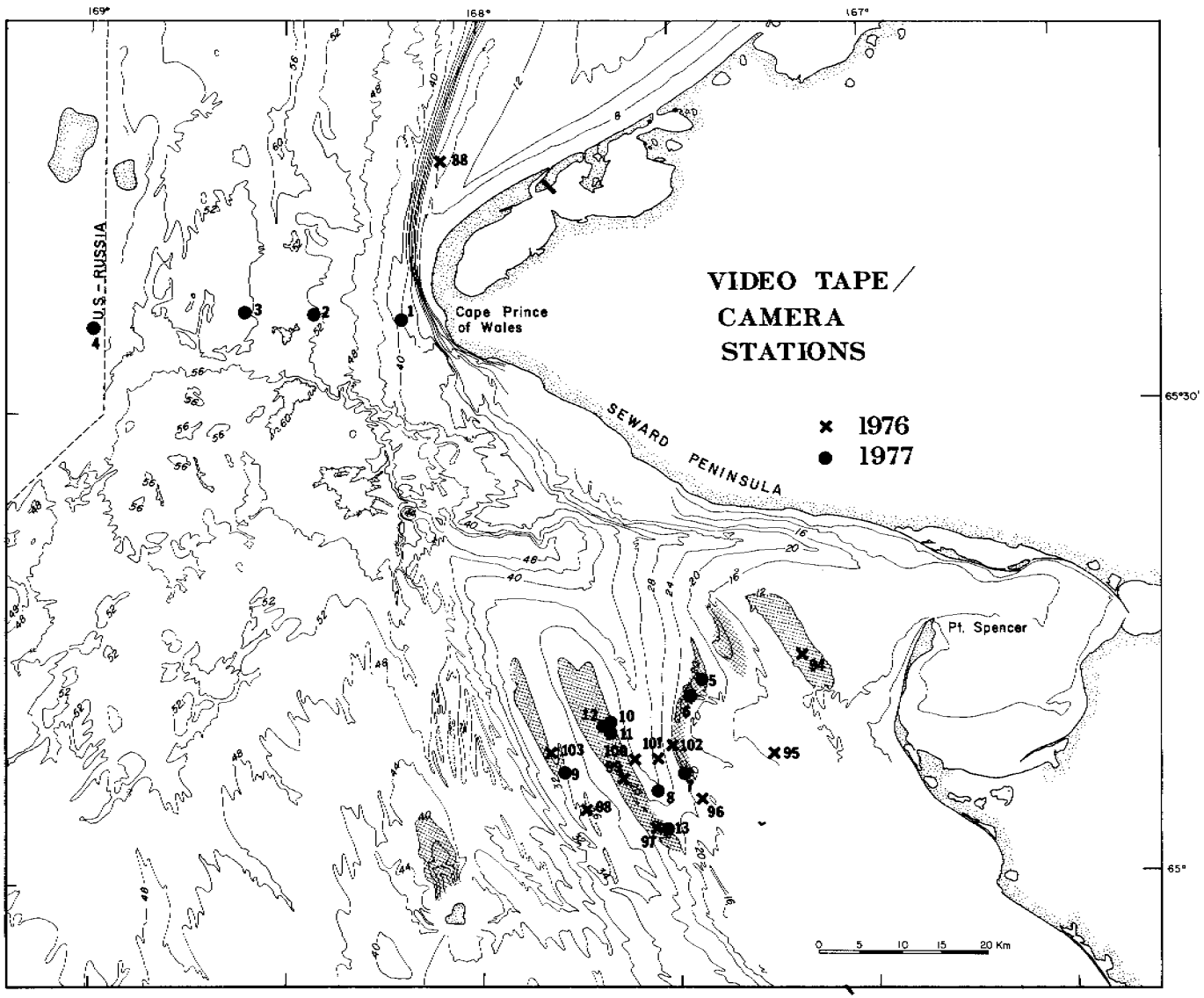

Figure G-3. Detailed transects of underwater television and bottom camera stations taken in northeastern Chirikov Basin. Bathymetric contours are in meters; hatchered areas outline major sand ridges that exhibit sand-wave fields.

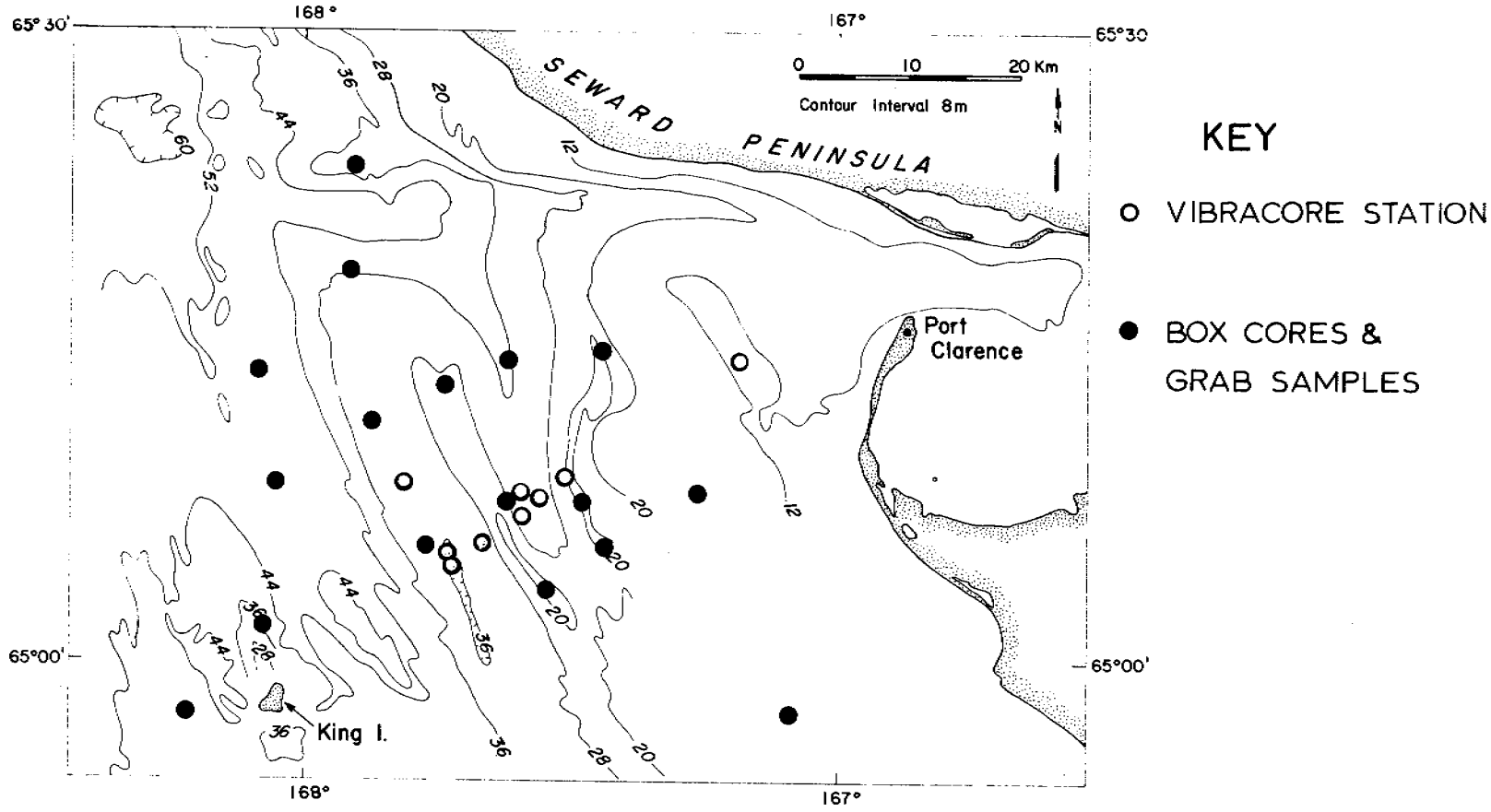

Figure G-4. Location of detailed sampling stations in area of sand ridges west of Port Clarence, Alaska.

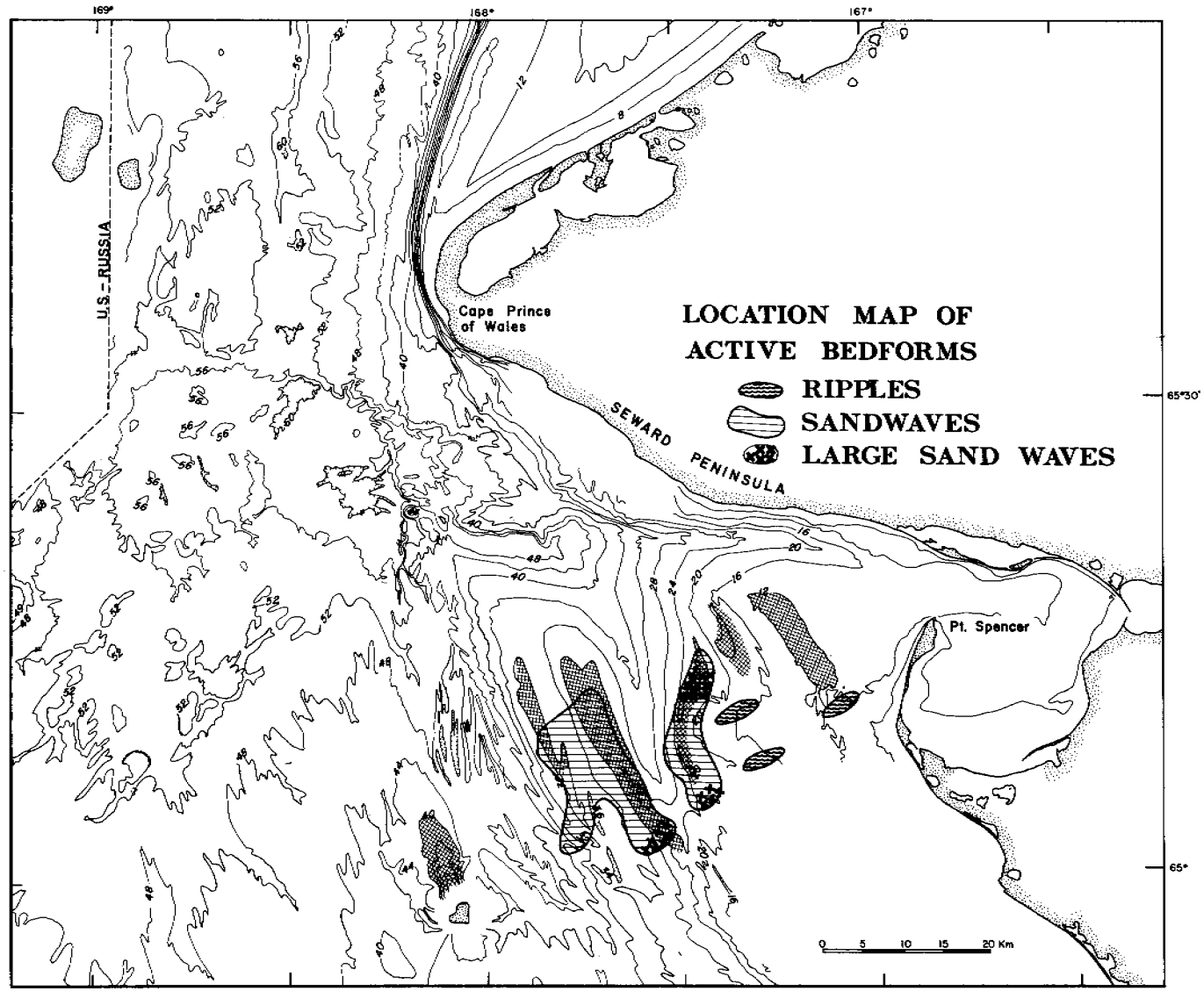

Figure G-5. Location of active bedforms in northeastern Chirikov Basin. Bathymetric contours are in meters; hatchered areas outline major sand ridges that exhibit sand-wave fields.

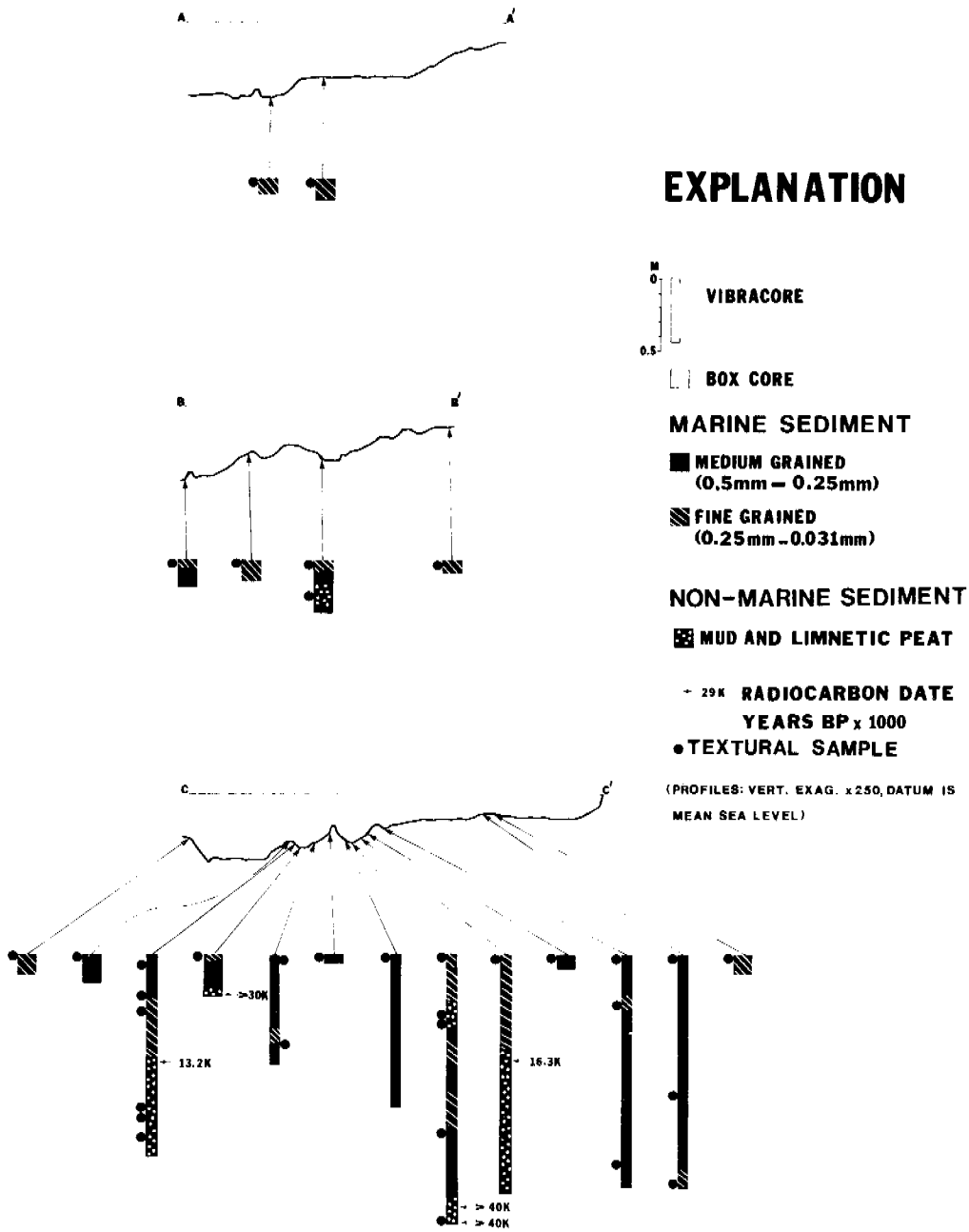

Figure G-6. Stratigraphy of near-surface sediment observed in box and vibracores from sampling transects across sand ridges near Port Clarence. Location of transects is shown in figure G-2.

SEDIMENT DISTRIBUTION

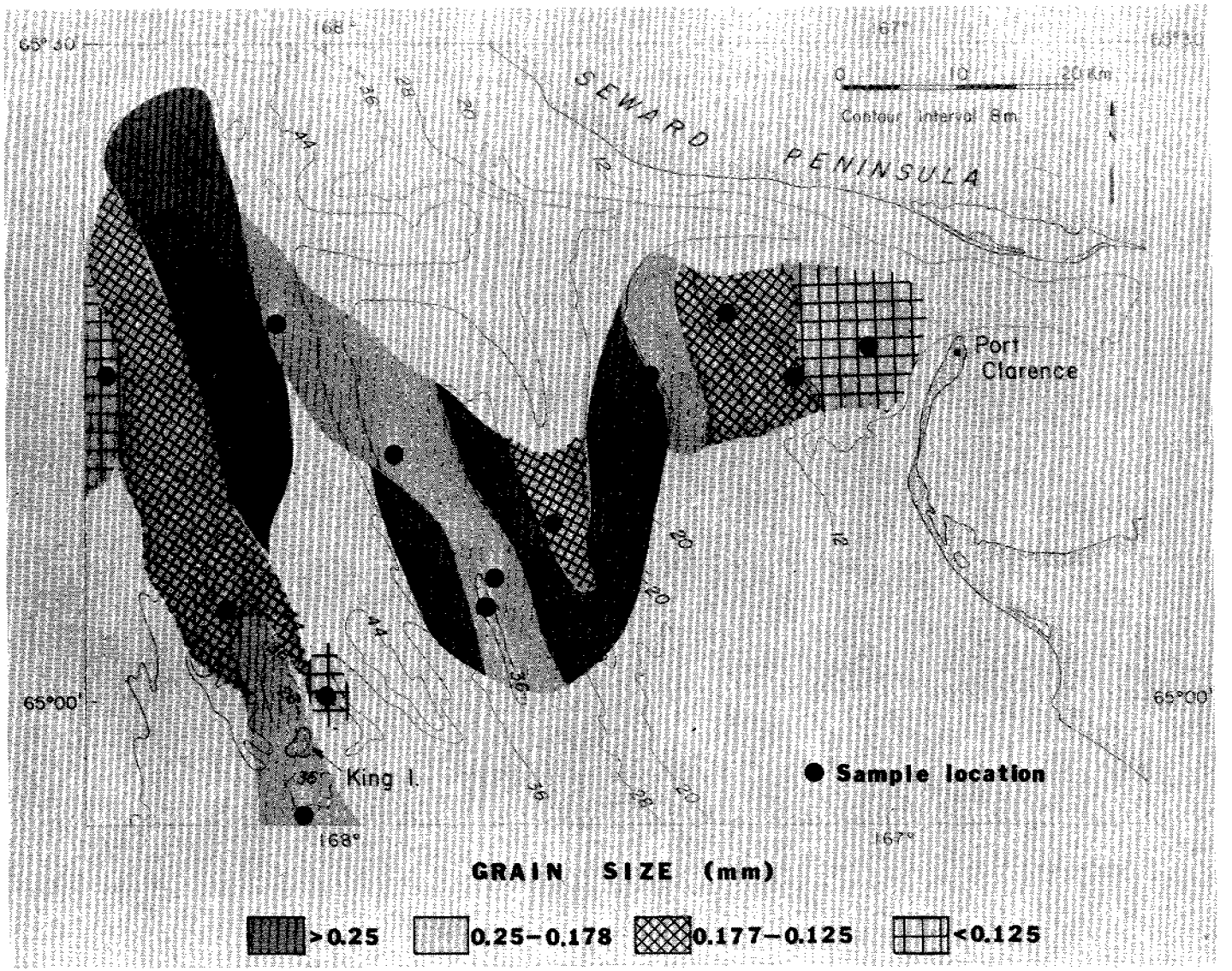

Figure G-7. Grain-size distribution in sand ridge area west of Port Clarence.

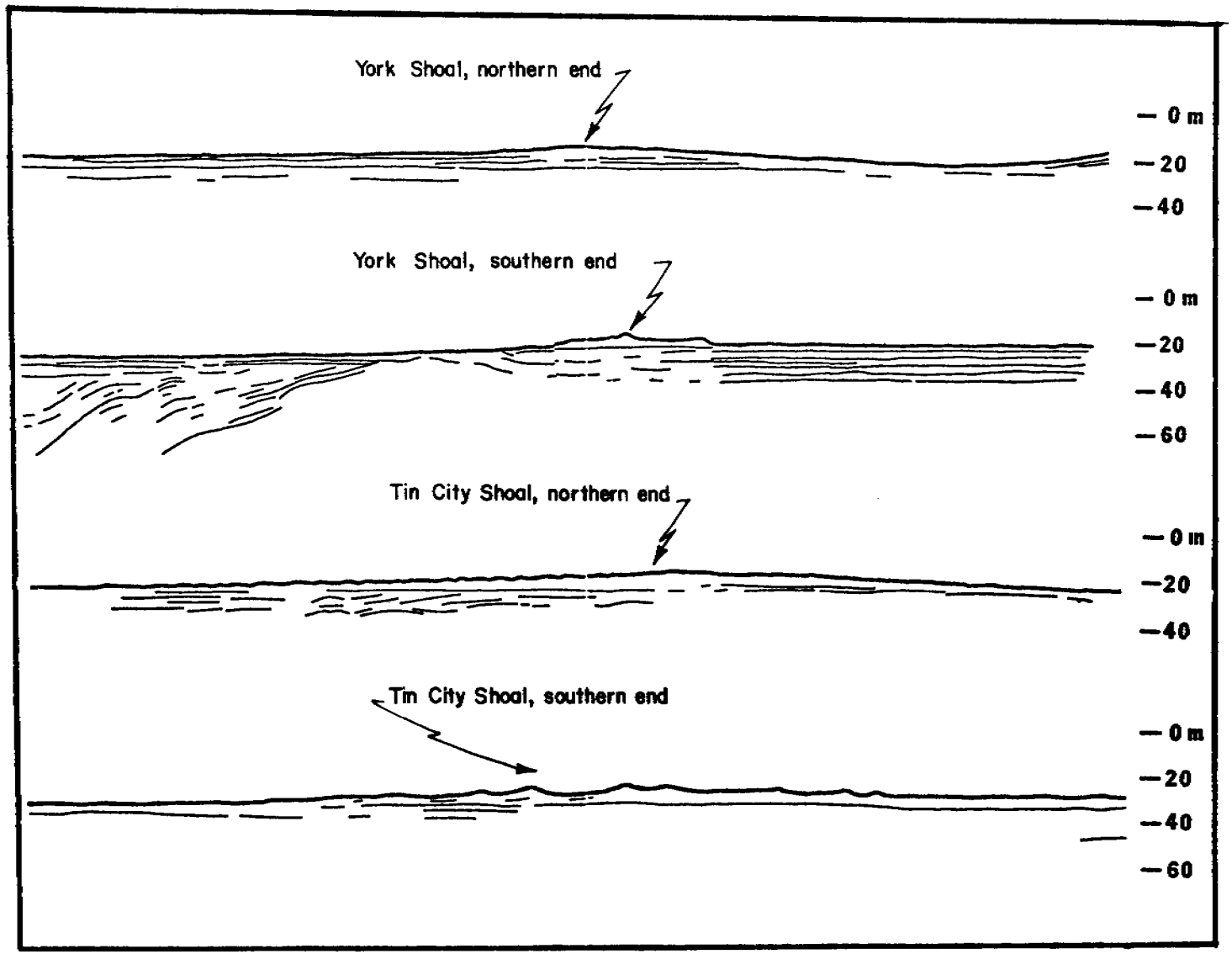

Figure G-8. Line drawings of high-resolution seismic profiles across major sand ridges shown in figure G-2. Note that the "sand ridges" are constructional features overlying parallel or folded, older sediment. Names of ridges are given in figure A-2.

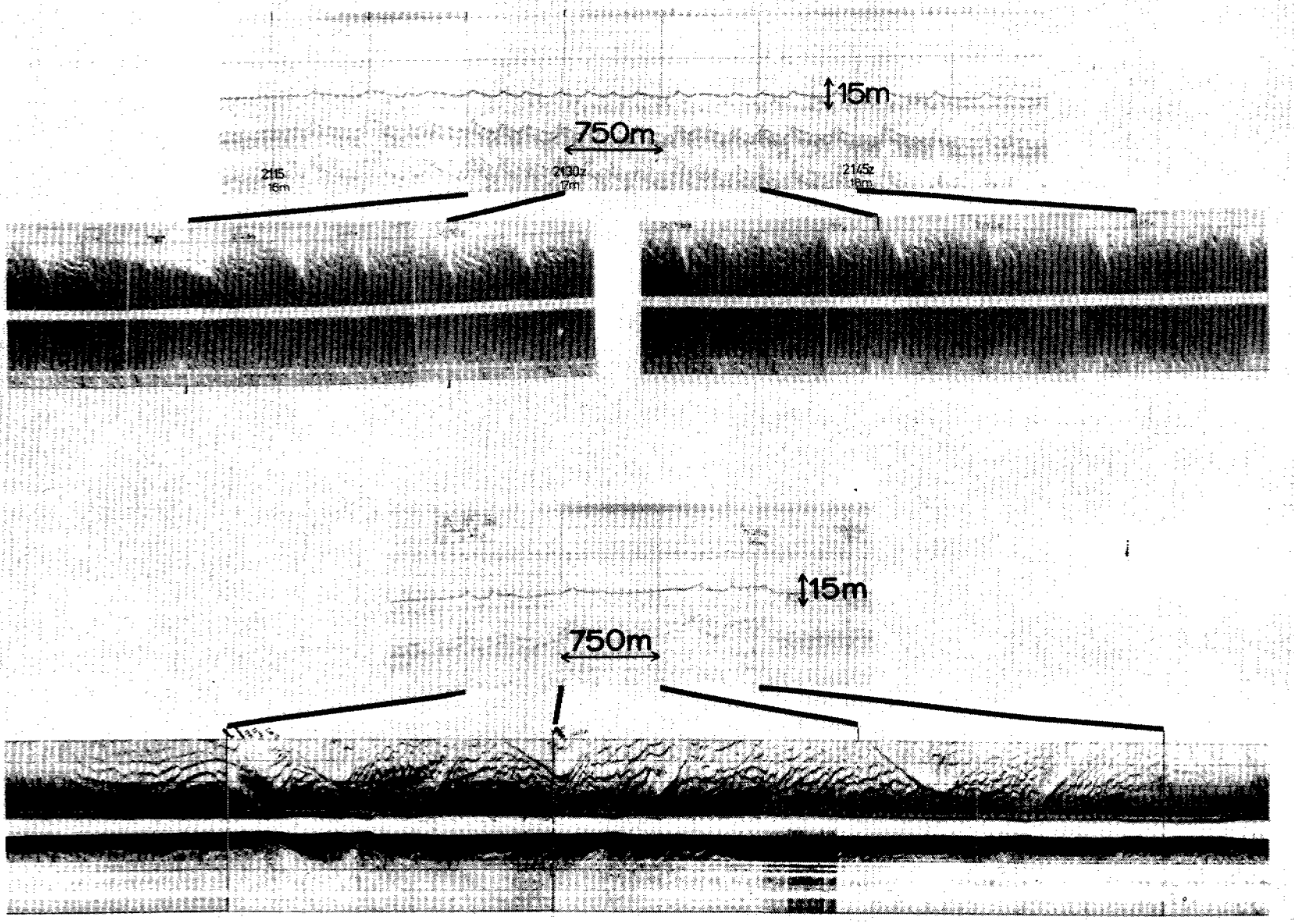

Figure G-9. 3.5 kHz seismic profiles with associated sonographs taken over sand ridges covered by large and small-scale, active sand waves. Records are from the York Shoal area shown in Figure A-2.

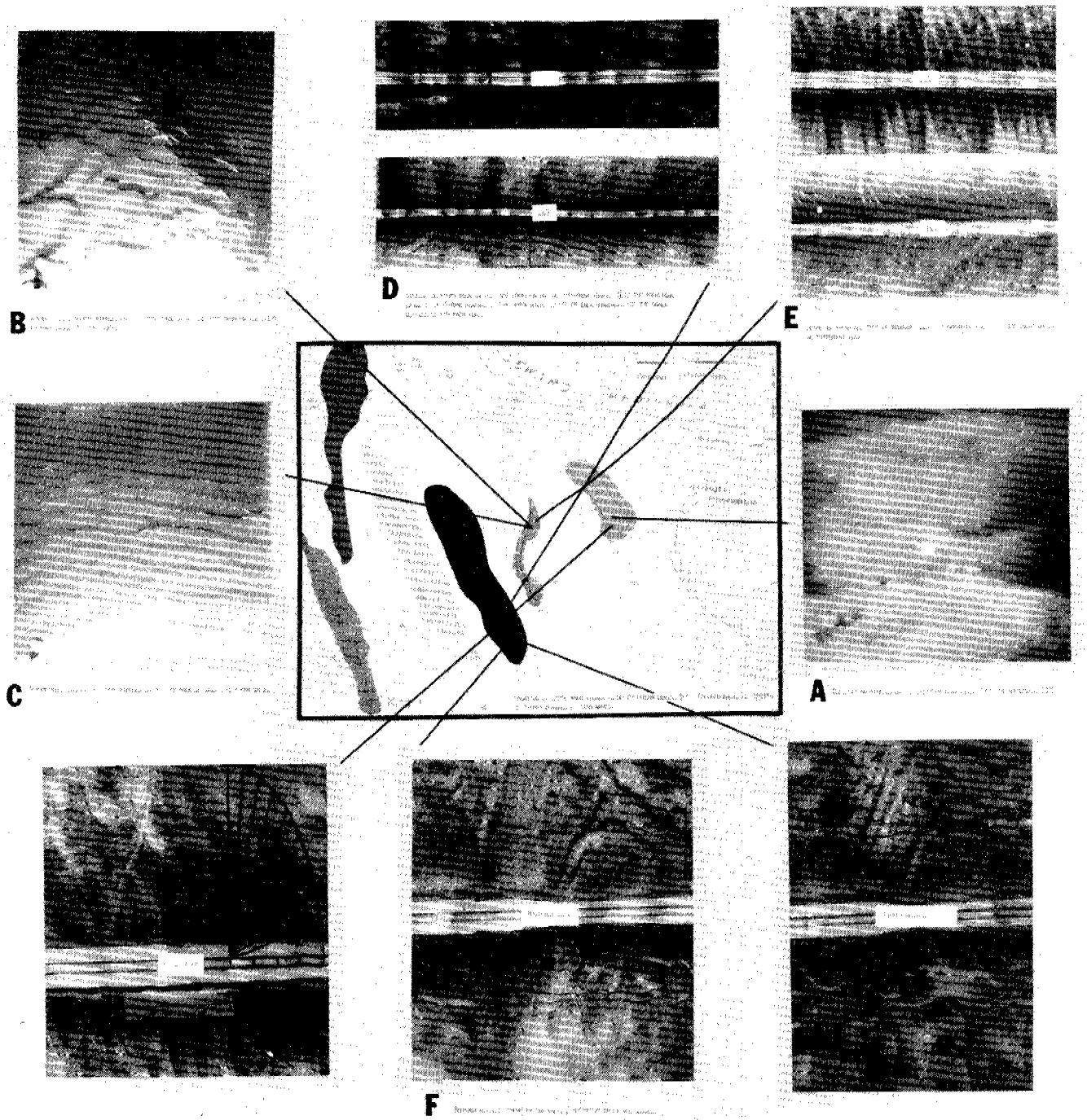

Figure G-10. Bedforms and ice gouges observed on sand ridges west of Port Clarence. A- videotape photo of oscillation ripples taken on the crest of Lost River Shoal in September, 1976(ripple height approximately 4 cm and wave length about 20 cm; water depth 12 m). B- Bottom camera photo of asymmetric linguoid ripples on the stoss face of a sand wave on York Shoal taken in July, 1977 (ripple height approximately 2-3 cm and wave length about 10 cm; water depth 20m). C- Bottom camera photo taken at same location as B showing asymmetric straight-crested ripples of the same scale, but located in a trough between sand waves of .5m wave height, approximately. D- Sonographs of unchanged sand waves on the crest of Tin City Shoal. E. Sonographs of sand waves on York Shoal that changed from decayed bedforms in 1976 to two active sets of bedforms in 1977(large-scale waves 2m high and 150-200 m wave length; small-scale waves .5 m high and 10-20m wave length). F-Series of sonographs showing different stages of ice gouge modification by actively migrating sand wave fields.

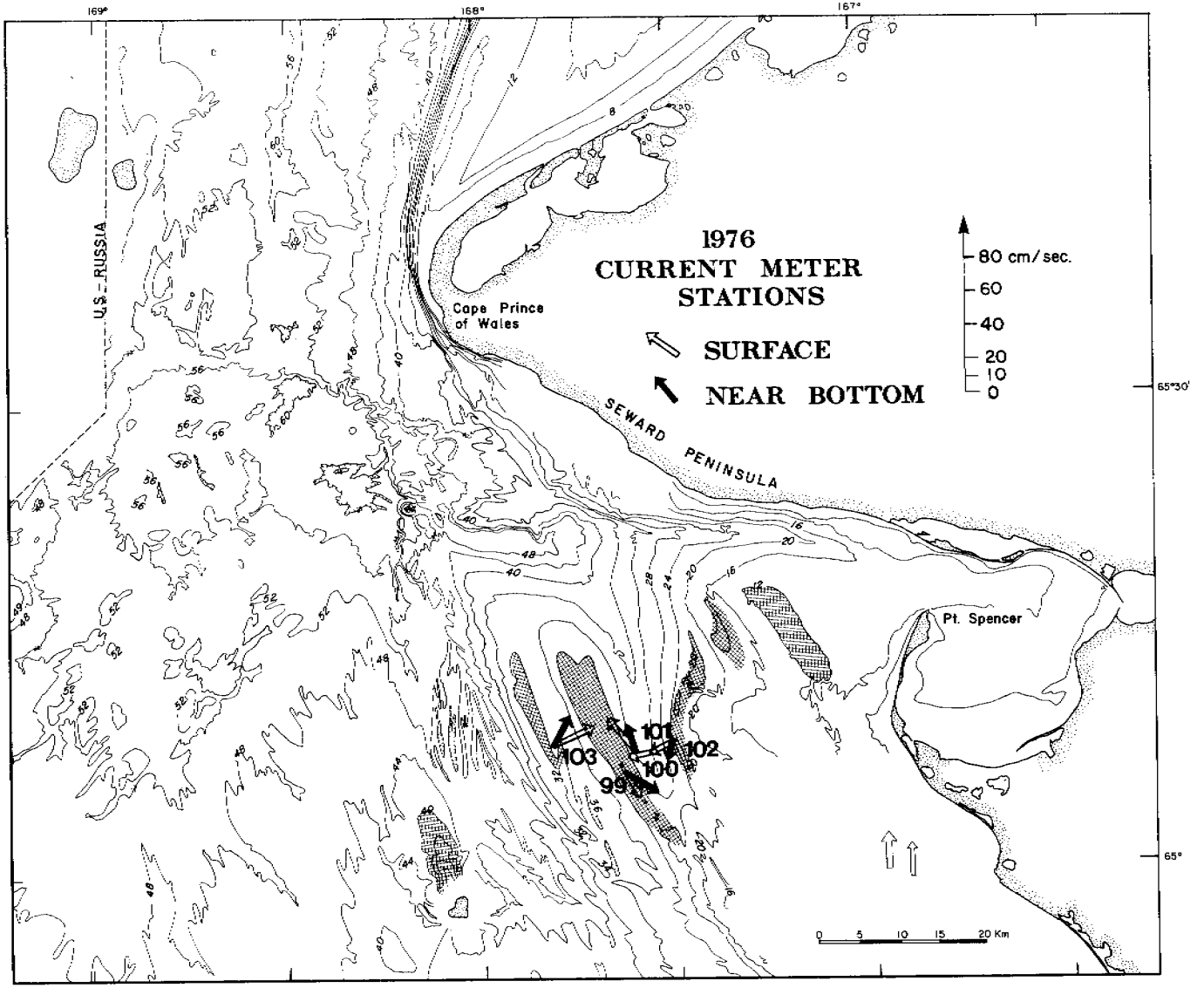

Figure G-11. Summary of profiling current meter data collected at stations in the sand wave fields west of Port Clarence in September, 1976. Hatchured area depicts region of major sand ridges with sand wave fields; contour interval is 4 meters.

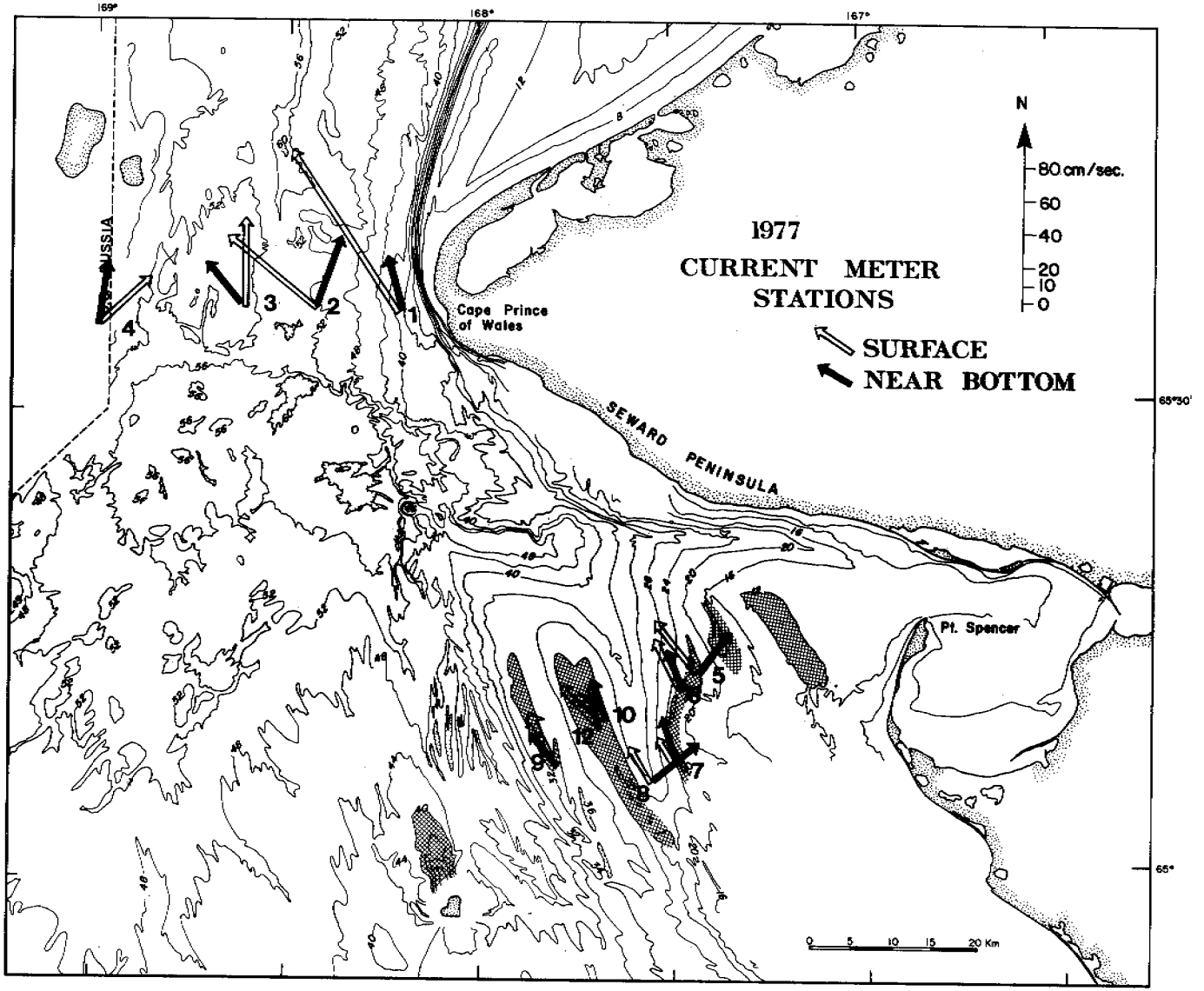

Figure G-12. Summary of profiling current meter data collected at stations in the sand wave fields west of Port Clarence and in Bering Strait during July, 1977. Hatchured area depicts region of major sand ridges with sand wave fields; contour interval is 4 meters.

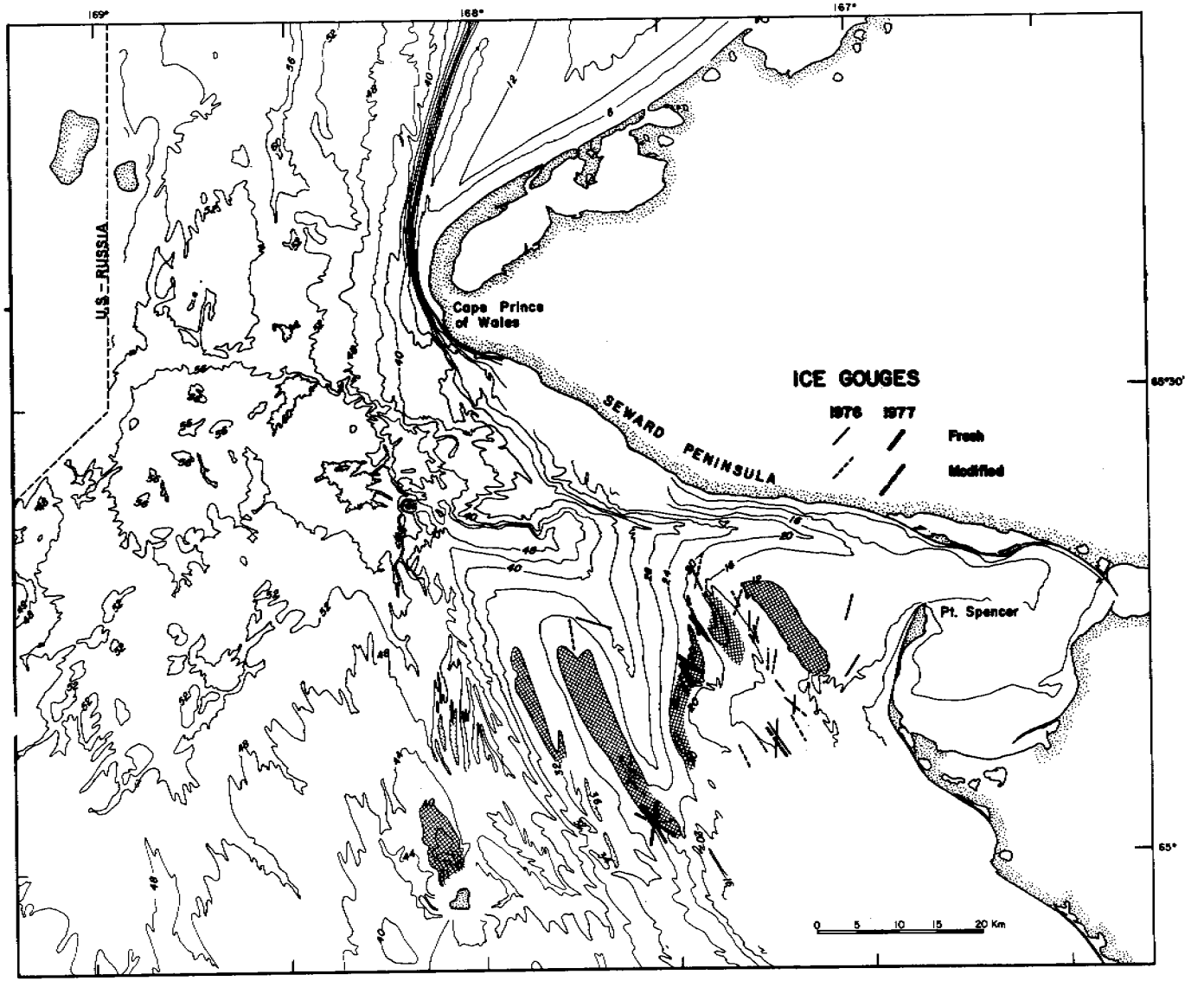

Figure G-13. Modification of ice gouges by actively migrating sand waves that is observed in sonographs taken in the area west of Point Spencer, Alaska. Hatchured areas depict sand ridge crests with sand waves ; contour interval is 4 meters.

FIRST ANNUAL REPORT

Research Unit RU-430
Reporting Period 3/31/77-4/1/78
Number of pages:

Sediment Transport in Norton Sound - Northern Bering Sea, Alaska

Principal Investigators: David A. Cacchione
David E. Drake

U.S. Geological Survey
Menlo Park, California

1 April 1978

Table of Contents

I. SUMMARY

A multi-faceted investigation of sediment dynamics in Norton Sound and other sections of the Northern Bering Sea was conducted to define the principal pathways and mechanisms of bottom and suspended materials transport during the past two years. During 1977 the principal investigators (D. Cacchione and D. Drake) on this research unit organized and conducted two research cruises in Norton Sound to deploy and recover two in situ GEOPROBE (Geological Processes Bottom Environmental) tripods and to obtain water samples, light transmission and current profiles, sediment samples and geophysical records. Additionally, a winter-time program involving helicopter operations to collect suspended matter samples beneath the ice cover in western Norton Sound was carried out by D. Drake in February, 1978. The results of this work, including data analysis and laboratory findings, are directly relevant to the evaluation of potential pollutant dispersal and occurrences of excessive, possibly hazardous, erosional events caused by storms.

Distributions of suspended matter in July 1977 were essentially the same as those found in September-October 1976. The pattern is dominated by a broad tongue of turbid water trending northwest across the mouth of Norton Sound from the Yukon Delta. Mixed Yukon and Alaskà coastal current water carrying large amounts of suspended silt extends through the entire water column along this transport pathway.

Mud deposits in the eastern part of the area are supplied by weak or intermittent currents which transport Yukon detritus eastward along the southern coast of the Sound. The presence of a remnant body of winter water in the inner Sound probably is important in the accumulation of a blanket of mud in this area. Pollutants entering this eastern "cul-de-sac" may be retained for relatively long periods owing to the limited water exchange with the outer part of Norton Sound.

It can now be demonstrated that storms play a major part in the transport of sediment in Norton Sound. Preliminary calculations show that suspended sediment transport during one 1977 storm exceeded transport during the 2 months of fairweather preceeding the storm. Thus, sediments (and potentially pollutants) which have been temporarily deposited on the sea floor can be suddenly remobilized during a short storm.

We have recently completed the field work for our winter sampling project in Norton Sound. Preliminary results show that ice transport of sediment may be highly significant in the Norton Sound area. This mechanism for sediment and pollutant transport should receive further study. Samples of the water column contained substantial amounts of suspended matter. In fact, concentrations appear only slightly lower than in the summertime. It is clear that suspended sediment transport is important beneath the winter ice cover and is not dependent upon wave action and wind-driven currents.

Owing to electronic failures in one of the GEOPROBE systems, only the tripod located about 50 km south of Nome provided useable data for the entire 80 day period of operation. Time-series data on currents, pressure, temperature, and suspended sediment concentrations were obtained near the sea floor at this site.

The GEOPROBE data verify the extreme importance of storm generated waves and currents in both resuspending and transporting away the modern sediment. The shipboard data provide a snapshot of the patterns and pathways of this transport. The daily tidal cycle ("mixed") and the fortnightly tide both are important in establishing the local suspended and bottom sediment conditions in western and probably all of Norton Sound. High currents during peak spring tides generate enough bottom shear to initiate motion of the bottom sediment. The high silt content and organic materials retard this movement, producing a condition of equilibrium between the tidal stresses and the character (bed configuration and sediment texture) of the sea floor. Storm events disrupt this equilibrium by causing excessive shear stresses that erode and transport the bed materials. During non-storm, i.e. tidal or normal periods, material from the high level Yukon source can be deposited when turbulent bottom stresses are considerably lower.

The above discussion and that presented in subsequent sections emphasize the dynamic nature of material movements in this region. Storm currents, tides, and waves generate highly variable, often energetic, bottom stresses and water transport whose temporal and spatial distributions must be understood in order to predict the fate of pollutants introduced there. This work has attempted to unravel these complicated processes in the hope of alerting planners for future resource development and aiding the engineering design of this development.

II. INTRODUCTION

A. General nature and scope

This research unit is designed to investigate the transport of sediments and other materials in the Northern Bering Sea, with special attention on Norton Sound. This work is part of a larger program of continental margin sediment dynamics in which the principal investigators have been involved since July, 1975. The overall program is directed at increasing our understanding of the pathways, rates, and mechanics of sediment movement in a variety of geological settings. A major topic of this research is the complicated interrelationships of sediment movement and hydrodynamics stresses that occur in the marine environment. Temporal contrasts like those caused by seasonal cycles and quiescent versus storm conditions are of particular interest.

The Northern Bering Sea is characterized by several unique and extreme environmental conditions: (1) sea ice covers the sea surface over 50 percent of the year, (2) late summer to early fall storms that travel along the polar front often bring severe local weather to the area, and (3) the Yukon River effluent, second largest of North American rivers, enters the system at the southwestern side of Norton Sound (Fig. 1).

Based on several years of cruise data collected under OCSEAP support, Nelson (1977, 1978) has developed a comprehensive picture of the geological and geophysical setting for this region. His work has provided the in-depth background that is a necessary prerequisite for the more topically focused research in this project. For example, Nelson and Creager (1977) and others have shown that the enormous flux of sediment introduced at the mouth of Norton Sound annually by the Yukon River has not yielded sediment accumulations commensurate with the rate of supply. The causes and modes of transport for this apparent exit of most Yukon River materials from the immediate region of Norton Sound are topics included in this investigation.

The scope of research in this project also includes topics such as (1) patterns and rates of transport of sediments, nutrients, and pollutants as suspended load in the Northern Bering Sea, (2) patterns and rates of transport in the sedimentary bedforms located west of the Seward Peninsula; (3) wintertime suspended sediment concentrations in western Norton Sound.

B. Specific objectives

The principal objective of this work is to develop an understanding of the relationships between suspended and bottom sediment transport in Norton Sound and the hydrodynamic regime that causes this transport. Specific objectives of the past year included:

(1) deployment of two GEOPROBE (Geological Processes Bottom Environmental) tripods in Norton Sound for about 3 months;

(2) continued development of computer soft-ware techniques for handling the Geoprobe data sets, including time-series analysis of the pressure, current meter, temperature and light transmission/scattering data;

(3) production of site-specific temporal histories (plots and statistics) of sediment transport parameters (shear velocity, roughness coefficients, flux vectors) and hydrodynamic values (maximum currents, tidal and storm currents, etc.);

(4) completion of maps showing the spatial distributions of suspended sediments for the period of the cruise (July, 1977);

(5) measurement and display of suspended sediment concentrations beneath the ice cover in western Norton Sound.

C. Relevance to problems of petroleum development

This research is extremely pertinent to two major impact areas of petroleum development in the marine environment: (1) transport of materials including pollutants; and (2) hazardous sea floor conditions produced by erosion caused by currents and waves.

The data and analyses produced in this work will enable future engineers, scientists, and other personnel to make better estimates of transport pathways for oil that is spilled in Norton Sound and the northwestern Bering Sea. The transport patterns of suspended fine materials (like Yukon river silts and clays) are indicators of the paths oil will take in the average or mean sense (long times > 1 month); the transport vectors produced at specific sites will better define the temporal variability of the oil transport.

This information is immediately useful to chemists and biologists who are assessing the impact that oil and trace metals might have on the local Norton Sound and Bering Sea environment. Oil that is absorbed by the fine suspended organic and inorganic material and that is mixed into the bottom sediments will be transported by the regional mean currents. The higher frequency currents such as tidal flow and surface wave-induced currents add local complications to the transport effects. For example, a tidal current average of about 10 cm/sec during the ebb stage in Norton Sound (typical for the data) will produce transport over about 4.5 km during the 12 hour half-cycle. Biota over this distance would be affected by the local transport of pollutants and nutrients.

The ability to predict accurately the movements of pollutants in the sea is strongly dependent on our knowledge of local transport processes. Specific geographic regions, like Norton Sound, will have unique aspects to the mechanisms which control the paths and amounts of material that is moved. This study attempts to identify and elaborate upon the most important transport-producing mechanisms in this region, and to relate these mechanisms to entrainment and movement of near-bottom materials. The eventual understanding which this study has as its goal will hopefully permit an accurate description of bottom transport of sediments, pollutants, nutrients, and other particulate matter in Norton Sound.

As recent events have all too often proven, when a large oil spill occurs at sea near our coasts, public and private attention is immediately focused on its environmental and economic impact. Those in charge of clean-up operations, managers of offshore land programs, political leaders, and concerned citizens

want to know where the spilled oil will go, how quickly will it move, and how large an area will be affected. Two specific aspects of this research project relate directly to this problem of oil spills at sea: first, excessive erosion can cause collapse of seafloor pipelines; second, the transport of oil near and along the sea floor will be controlled by those processes that also control the transport of sediments.

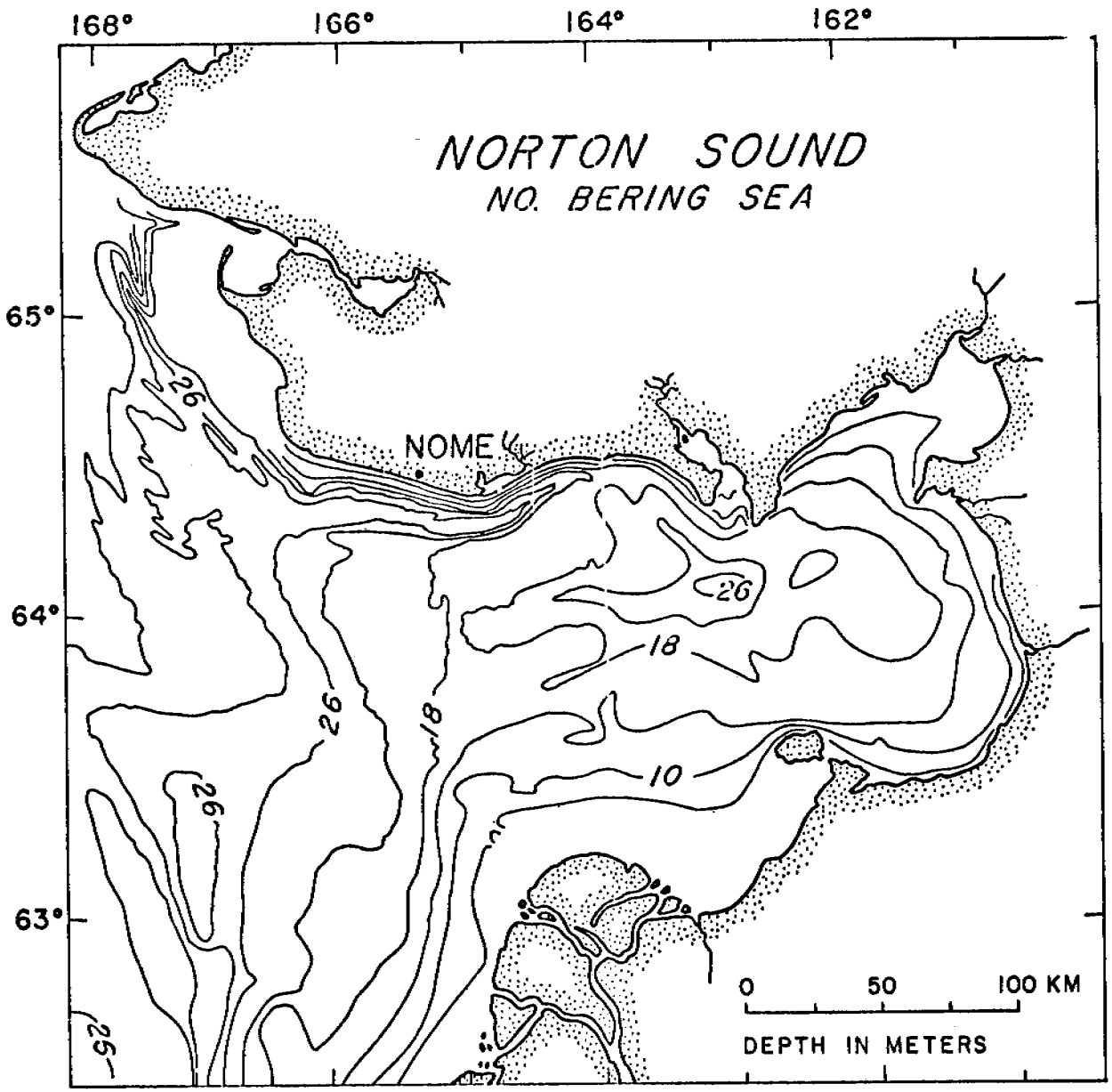

Figure 1. Bathymetric chart of Norton Sound, Alaska.

III. CURRENT STATE OF KNOWLEDGE

The suspended and bottom sediments found in Norton Sound are nearly all derived from the Yukon River, which discharges about 70 to 100 million tons of material per year into the southwestern corner of this area (Fig. 1). Despite this enormous sediment source, Nelson and Creager (1977) and McManus et al. (1974) show that in recent times (<5000 years B.P.) modern Yukon fine sands and silts have been accumulating on the Yukon subdelta in southern Norton Sound at a surprisingly low rate. This thin accumulation of sediments has been attributed to the erosive action of storms that occur in the early fall prior to the formation of ice cover (Nelson and Creager, 1977). The fine-grained fraction of Yukon-derived materials is presumably transported through the Northern Bering Sea by the Alaskan Coastal Current and deposited in the southern Chukchi Sea (Nelson and Creager, 1977; McManus et al., 1974).

Modern Yukon very fine sands and silts do not form a continuous blanket in Norton Sound. Despite the proximity of this large sediment supply, the modern muds tend to deposit along the southern border of the Sound leaving substantial areas in the north-central portion with little or no recent cover. The distribution of Yukon mud is consistent with sediment transport and water circulation patterns revealed by our studies and those of Coachman, Muench and Charnell (RU 541). The explanation for the slow rates of accumulation in the northern half of the Sound was not known prior to our work in 1977. We now believe this situation is the result of strong tidal and storm currents along with an advective transport pattern that diverts the bulk of the Yukon silt to other areas.

Investigations of the large-scale current patterns in the northern Bering and Chukchi Seas have been summarized by Coachman et al. (1976). When viewed in a regional sense, the mean circulation is relatively simple. Bering Sea shelf water flows toward the Arctic Ocean and the magnitude of this transport is modulated primarily by atmospheric pressure changes. Owing to topography, the current speeds increase toward the north; the effect of flow constriction is particularly apparent, north of 64°30'N latitude. Bottom sediments in the approaches to Bering Strait are predominantly sands which have been molded into a progression of bedform types that are characteristic of progressively stronger bottom currents. There is no chance for permanent deposition of fine-grained sediments in this area (north of 64°30') and suspended material moves rapidly through Bering Strait and into the Chukchi Sea.

Whereas the regional flow field is reasonably well known, the physical oceanography of Norton Sound has only recently been examined. As is typical of most investigations of "unknown" areas the initial gains in knowledge tend to come easily but the detail needed to achieve a quantitative understanding comes only after several years of intensive research.

Studies in 1976 by Muench, Charnell and Coachman (1977) and Cacchione and Drake (1977) were the first adequate investigations of the physical oceanography of Norton Sound. Among many results the following should be noted:

1. Muench et al (1977) suggested that the circulation in the outer portion of Norton Sound is characterized by a cyclonic gyre.

2. Exchange of water between the outer Sound and the eastern "cul-de-sac" is limited. In fact, the bottom water in the cul-de-sac late in the summer of 1976 was probably remnant from the previous winter (Muench et al., 1977).

3. GEOPROBE data for September-October 1976 showed that tidal currents were surprisingly strong 60 km south of Nome in 18 m of water. Sediment transport calculations suggested that the tidal currents plus the mean should produce bed shear stresses close to those needed to initiate motion (Cacchione and Drake, 1977).

4. The regional sampling by Cacchione and Drake revealed a pronounced tongue of turbid water originating near the Yukon Delta and extending across the mouth of Norton Sound toward the Nome coast.

With these results in mind, we were anxious to revisit the area during the early summer of 1977 to deploy two GEOPROBES and 3 PMEL/NOAA current meter moorings and obtain a second set of suspended sediment measurements. The results of this work are discussed in this report. In addition, our previous work, and the work of other researchers, has been confined to the ice-free season. This produces an obvious bias and, therefore, we proposed to sample the area in the winter of 1978. This proposal was funded and the winter work has been carried out in conjunction with K. Aagaard (Univ. of Washington). A preliminary discussion of this project is included in Section X of this report.

Increased transport of sediments on continental shelves during storm periods has been discussed by Smith and Hopkins (1972, p. 143), Drake et al., (1972) and Butman (1976). In a body of water like Norton Sound, whose depth is everywhere less than 30 meters (average depth about 18 meters), bottom stresses generated by wind-driven waves and currents can be expected to dominate the patterns of sediment movement. The added questions of whether sediment transport during the relatively longer periods of calm summer weather or beneath the winter ice cover are important must also be addressed. We will discuss the impact of storms in the present report and recent work should provide information on the winter regime.

IV. STUDY AREA

Norton Sound is a shallow arm of the Northern Bering Sea, located on the western margin of Alaska, south of the Seward Peninsula (Fig. 1). It is approximately rectangular in shape, 250 km long in an E-W direction, and 130 km long in a N-S direction. Water depth is everywhere less than 30 meters; average depth is 18 meters. Nome, Alaska, population 2400, is situated along the northwest coast.

Although we have concentrated our work within Norton Sound we have also collected data in Bering Strait and in the "sand wave" fields west of Cape Clarence. In addition, C. H. Nelson (USGS) collected water samples for suspended sediment analysis in previously unsampled areas north of Saint Lawrence Island. These data will be incorporated in future reports.

V. DATA COLLECTION

A. Overview

As in our previous work, there were two distinct, complementary facets to the data collection effort during the past year, each important to the various objectives. An intensive shipboard sampling program of hydrographic and geological stations was carried out in Norton Sound during a 6-day scientific cruise on R/V SEA SOUNDER (7 July - 12 July 1977). The station locations shown in Figure 2 were designed to give adequate coverage of the entire area of interest as well as to provide data at locations of special interest (eg. off the Yukon River). A summary of hydrographic, geological and geophysical data collected during this cruise is presented in Appendix A.

Secondly, two GEOPROBE tripods were deployed in Norton Sound at locations shown in Figure 1. Tripods 1 and 2 were emplaced on July 8 and July 10, respectively, from R/V SEA SOUNDER and recovered on the R/V S.P. LEE on October 10 and 12, respectively. The latter cruise was conducted principally to make the recovery of the tripods; no additional data relevant to this project was collected on that cruise.

Two additional, unique aspects to our work were accomplished this past year. First, a field team led by D. Drake together with a research team from University of Washington (Seattle) used helicopter support to collect suspended sediment data from beneath the ice cover in western Norton Sound during the period February 18 - March 5, 1978. These data are discussed in a subsequent section.

The shipboard data were normally collected in a planned sequence. Typically, at each station a current meter profile (speed and direction), light transmission profile, C-T-D profile, water bottle samples for suspended sediments and salinity, and surface temperature were obtained. At each GEOPROBE site and current meter mooring location (see below) we additionally obtained bottom TV/70 mm photographs, bottom sediment samples, closely-spaced side-scan sonar and other geophysical transects, and in-situ penetrometer measurements. Between stations we typically conducted geophysical surveys including 3.5 kHz, 12 kHz and uniboom profiling.

Also, two investigators from NOAA, PMEL, Seattle (R. Muench, principal investigator and J. Hazlitt) participated in the cruise on R/V SEA SOUNDER during 7-12 July 1977. Three PMEL shallow water current meter moorings were launched from R/V SEA SOUNDER at sites of mutual interest in Norton Sound (Fig. 1). The PMEL personnel also aided in obtaining the conductivity-temperature-depth (C-T-D) measurements using a C-T-D system that was installed temporarily on R/V SEA SOUNDER under OCSEAP guidance. The cooperative efforts of PMEL researchers (R. Charnell and R. Muench) have been particularly helpful in the execution of our field work and during the analysis of oceanographic data.

B. Shipboard Data

Thirty-four anchor stations were occupied in July 1977 aboard the R/V SEA SOUNDER (Fig. 2). At each location we made a standard set of observations

which included:

1. a C-T-D cast using a Plessey 9040 sensor which was loaned to us by NOAA/PMEL.

2. a profile of current speed and direction using a Hydro Products Savonius rotor and vane sensor. Observations were made at 2 m increments to 1 m above the sea floor.

3. a light transmission and temperature profile using a Martek 100 cm beam transmissometer.

4. surface and subsurface water samples were collected using Hydro Products PVC water samplers ("Van Dorn bottles").

The CTD data were recorded on magnetic tape and subsequently processed by R. Muench at PMEL. Data from the profiling current meter and the transmissometer were recorded manually.

Water samples were collected in order to determine the concentrations of suspended particulate matter. Samples were immediately transferred to rinsed polyethylene bottles and filtered (within 2 hours) through preweighed 0.4 um Nuclepore polycarbonate filters. In general, one liter samples were processed except in those cases when the filter clogged early. The sample filters and a series of control filters were reweighed in our shore laboratory after drying for 2 hours at 50°C. Studies of the membrane filtration technique for determination of suspended sediment concentrations have shown the following degrees of precision:

1. Nuclepore filters (47 mm diameter) can be weighed to $\pm$ 6 µg without resorting to special handling. This is always <2% of the concentrations in one liter of water in Norton Sound.

2. Multiple samples from a single Van Dorn bottle generally agree to within 20% of the mean value. Typically the reproducibility improves with an increase in the suspended load.

In view of the errors inherent in the filtration technique, we believe that the significance of concentration differences of 0.5 mg/l and less can be questioned.

In addition to our observations at anchor, we collected temperature and salinity data for the surface water while underway using a Plessy thermosalinograph. Also a series of about 40 surface water samples were recovered between stations in order to provide a more detailed description of the suspended matter distribution.

C. GEOPROBE Data

Two GEOPROBE tripods were launched during the July cruise (see above and Fig. 2). They were recovered in October 1977 from the R/V S.P. LEE. Unfortunately, the digital data obtained at site G2 (at the easternmost site)

were unusable because of an electronics failure in the recording system. The cause of the failure has been identified and corrected, but the data on the tape recorded during the experiment could not be saved.

On the brighter side the data from G1 has been processed and, as discussed in section VI below, produced 80 days of continuous, reliable measurements. Less than 0.1% of the records contained errors. Each of the error records has been corrected by a polynomial interpolation scheme.

An illustration of the GEOPROBE tripod launch at site G1 is shown in Fig. 3. The tripod dimensions are 3.3 meters between centers of each footpad and 3.5 meters high. The entire system weighs about 500 kg in air. The details of the instrument system are given in Appendix B and were also discussed in last year's annual report for this project.

During this year's field program 80 consecutive days of hourly averages (1920 averages) of bottom current speed and direction as sensed with a Savonius rotor and vane mounted about 1.5 m above the sea floor were obtained. An equal number of hourly averages of bottom pressure were obtained with a very sensitive quartz-crystal oscillator type of sensor. Thermistors mounted at 5 cm and 200 cm above the sea floor were used to obtain discrete hourly values of bottom water temperatures. Similarly, a nephelometer/transmissometer mounted at 200 cm above the sea floor gave hourly values of light scattering/transmission over the 80 day period.

Four small diameter (4 cm) electromagnetic current sensors arranged in a vertical array at 20 cm, 50 cm, 70 cm, and 100 cm above the sea floor were used to obtain hourly "bursts" of horizontal bottom current velocities at each level. From these data, vertical profiles of horizontal velocity (i.e. velocity shear) could be derived for each "burst." Each "burst" sample, taken once per hour, consisted of sixty successive measurements of velocity at each probe; the measurements were taken at a rate of once per second. Thus each "burst" was one minute in duration. Additionally, bottom pressure was also "burst" sampled. Each "burst" record consists of 8 components of current speed (two at each probe) and one pressure reading. About 1900 "bursts" were obtained.

The bottom photographs obtained with the GEOPROBE tripods, although considerably improved from last year, are only marginally usable because of the high degree of backscatter ("washout"). In addition, a malfunction in the programmer section of the electronics packages for both tripods caused the camera system to sequence through the entire 100 foot film roll in less than one day. The system was set to obtain one picture every 4 hours throughout the duration of the experiment.

Figure 2. Station locations for R/V SEA SOUNDER cruise during 7-12 July, 1977. GEOPROBE sites (G1 is the westernmost and G2 the easternmost) and NOAA mooring locations are also shown.

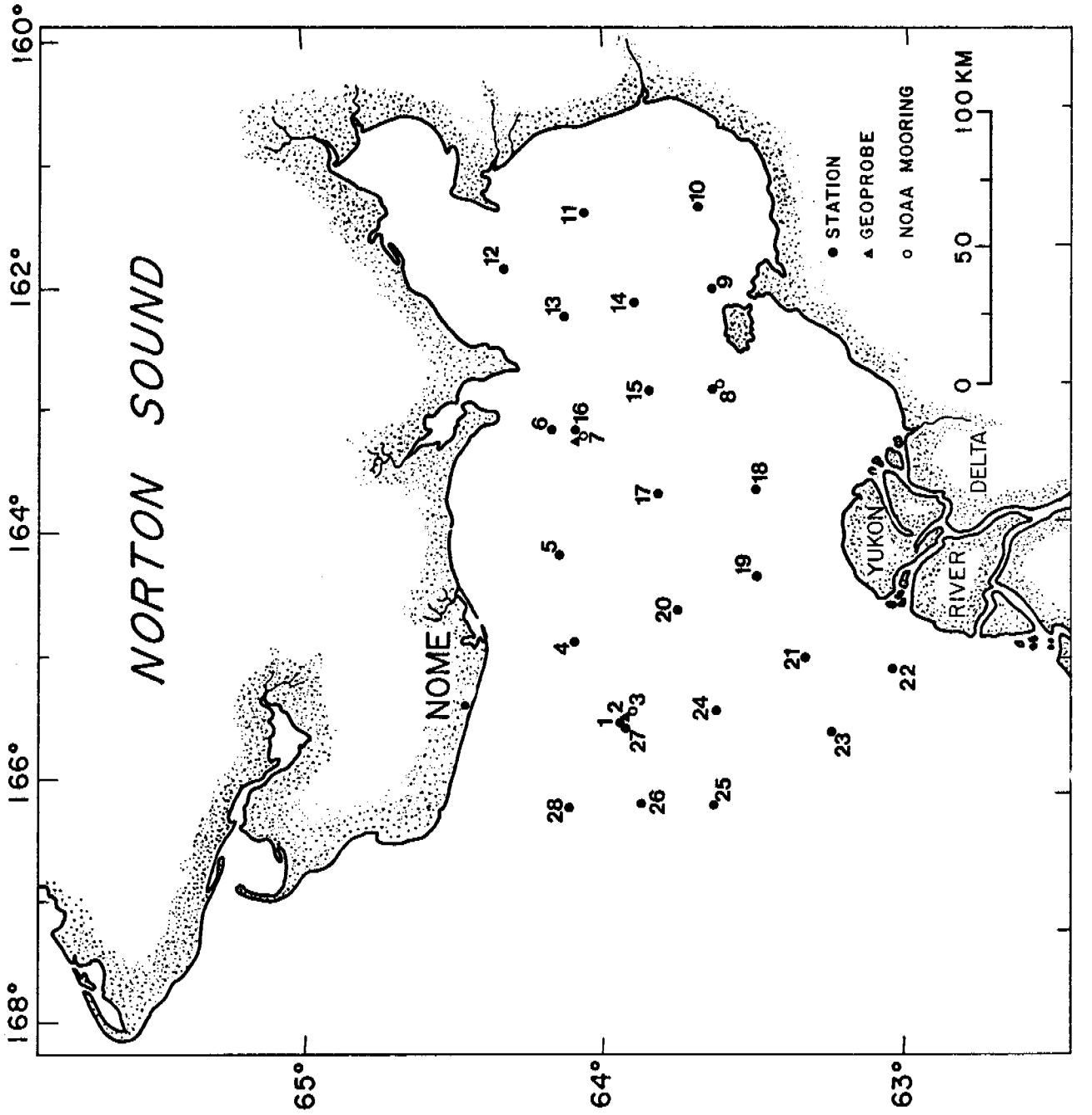

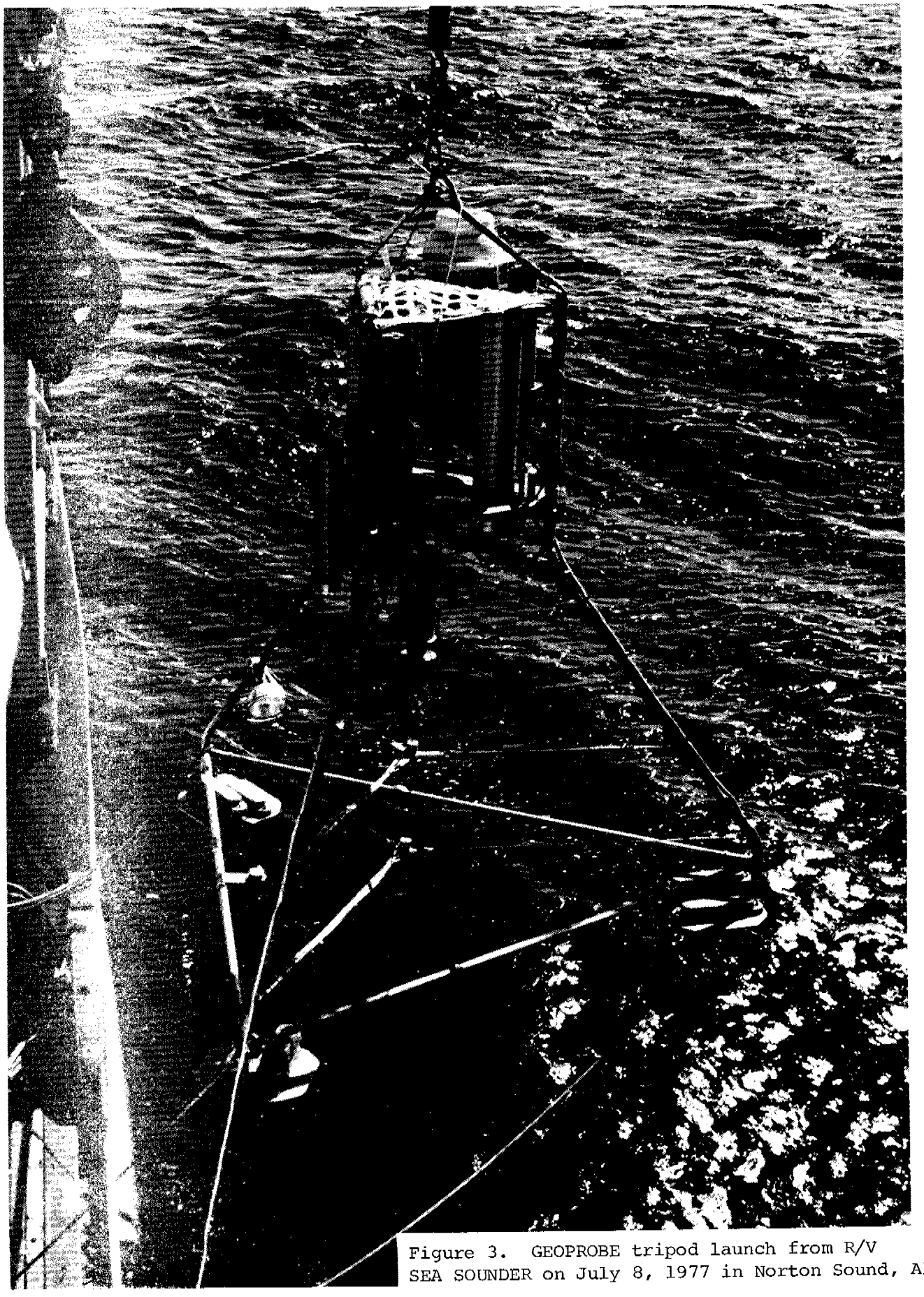

Figure 3. GEOPROBE tripod launch from R/V SEA SOUNDER on July 8, 1977 in Norton Sound, Alaska

VI. RESULTS

A. Suspended matter distribution

1. Surface water

Concentrations of total suspended matter (TSM) at the surface ranged from 0.2 mg/l at the mouth of Norton Sound to 65.8 mg/l 20 km west of the Yukon Delta (Fig. 4). Microscope inspection of the suspended matter shows that all samples except those at the mouth of the Sound are dominated by inorganic fine silt and clay. Point counts of the low concentration samples demonstrate that 30-60% of the material is plankton.

The distribution of TSM in the surface water is simple and the influence of Yukon River effluent is obvious. Concentrations are highest near the major western distributaries of the Yukon and decrease rapidly westward into the northward-flowing Alaskan coastal current. Although there is clear evidence that Yukon sediment is carried into the eastern portion of Norton Sound, it is apparent that the tongue of turbid water extending across the mouth of the Sound toward the Nome coast is a more important transport pathway.

Our observations in the vicinity of the delta are restricted by the shoalness of the delta front sediment body. In order to examine the sediment transport system within 20 km of the delta we have studied LANDSAT images from the period 1973-1977. These data reveal a consistent pattern of southerly suspended matter transport along the western shore of the delta and westward transport along the northern shore.

2. Subsurface distributions

Concentrations of TSM near the sea floor (1 m above bottom) ranged from about 1 mg/l at the mouth of the Sound and off Port Clarence to 26.6 mg/l at our station closest to the delta (Fig. 5). In general, the near bottom TSM values were from 2 to 3 times higher than surface water concentrations. Exceptions to this occurred near the Yukon delta where surface concentrations substantially exceeded those present near the bottom (see Fig. 4).

The distribution of TSM near the sea floor is similar to the pattern present in the surface water. Of particular interest is the strong gradient in TSM west of the delta and the tongue of sediment-charged water extending to the northwest from the delta.

Combustion analysis and microscope study of the near bottom TSM show that inorganic silt and clay comprise >85% of the particulate matter. Textural analysis of the near bottom suspended matter has been accomplished using a Model TAII Coulter Counter. The sediment was prepared for size analysis by ultrasonification of portions of the sample filters for periods of 20 minutes. This method reduces all of the material to discrete particles and is thus comparable to the standard method for textural analysis of fine-grained bottom sediments. After size analysis of the ultrasonified material, selected samples were reanalyzed after stirring gently for periods of 2-6 hours. This second analysis showed that the size distribution of the suspended matter rapidly

changed. The change noted in all cases involved an increase in 12-20 μm particles at the expense of 2-6 μm particles. Evidently, aggregation of several particles occurs rapidly even in very dilute suspensions of Norton Sound sediment. The upper size limit of such aggregates would depend on the concentration of particles and the turbulence (shearing) of the suspension.

The results of the Coulter Counter work are presently being analysed in detail. At this point the following preliminary conclusions seem justified:

1. a neglible amount of sand-sized material is in suspension at 1 m above the sea floor except in the Bering Strait.

2. The suspended matter in Norton Sound is typically very poorly sorted (in the dispersed, ultrasonified state) and exhibits a weak mode at 2-8 μm.

3. Silt (4-62 μm) comprises 70-95% of the suspended matter near the bottom.

4. Suspensions in Bering Strait are substantially coarser-grained than elsewhere in the northeastern Bering Sea. Sand was present in amounts of 10-25% at levels of up to 10 m above the sea floor during July 1977. Particles up to 200 μm in diameter were in suspension at 1 m over the bottom.

3. Light transmission and density cross-sections

Two east-west cross-sections showing the subsurface distribution of water density (as sigma-t) and light beam transmission values are presented in Figures 6 and 7. The northwestward-trending plume of turbid water from the Yukon is clearly shown and it is evident that high concentrations of TSM extend from the surface to the bottom in this area. In the central and eastern portions of the Sound the water column becomes strongly two-layered with warm, low salinity surface water overlying cold (0 to 2°C) and saline (32-34%) bottom water. Studies in 1976 by Muench et al. (1977) and also during our survey in July 1977 strongly suggest that the bottom water in the eastern part of Norton Sound is remnant from the winter season of ice formation and production of cold, saline water (Muench et al., in prep.). It is noteworthy that this remnant water contains substantial amounts of suspended particulate matter (Figs. 5 and 7). Moreover, the bottom sediments in this area are principally fine silt and clay from the Yukon River and rates of deposition are relatively high (Nelson and Creager, 1977).

4. Current measurements

In July 1977, 49 current meter profiles were obtained during our cruise and the following cruise of C. H. Nelson. All of these data were collected while the SEA SOUNDER stood at anchor in order to minimize errors due to motion of the ship. In addition current speed and direction data were recorded for 40 days at two sites near GEOPROBES I and II by Bob Muench of PMEL.

The direction and speed data from our shipboard profiling meter showed significant changes in both parameters from station to station and in cases where stations were re-occupied. Our 1976 GEOPROBE data had demonstrated the importance of tidal currents in Norton Sound and, therefore, we suspected that the observed variability was caused by the semi-diurnal tide. This conclusion has been confirmed by the moored current measurements obtained in 1977.

Because of the strong tidal currents, it is clear that current direction data from the shipboard profiler are of limited value. However, the speed data can be used to estimate the spatial distribution of flow field "energy" in Norton Sound and along the Seward coast (Fig. 8) provided a sufficiently large number of measurements is available. It should be noted that the near-bottom current speed observations (Fig. 8) represent the combined effects of all forcing mechanisms operating at a given, short period of time; the assumption is that the data were collected randomly with respect to the tides and that variations in other forcing mechanisms over the total collection period were not significant.

Despite these limitations the current speed data reveal a logical pattern of "energy" variations. The northeastern Bering Sea shelf can be subdivided into 4 parts based on the energy of the near-bottom currents and presumably their ability to transport sediments. In 3 of the 4 areas the average speeds are essentially equal to or greater than the current speeds that are generally required to initiate motion of non-cohesive sand and coarse-silt sediments. Speeds in the fourth area, east of Cape Darby and Stuart Island, decrease to an average of about 7 cm/s. This current magnitude, if representative of the area, is not capable of transporting all but the finest silt and clay particles.

It is worth noting that the moored current measurements (site G1) at 1 m above the sea floor 60 km south of Nome are in good agreement with the average speeds obtained by the shipboard observations in the outer and central portion of Norton Sound.

B. GEOPROBE site surveys

An intensive geological and geophysical survey of the launch site is normally conducted prior to the launch of a GEOPROBE tripod. This survey usually includes geophysical profiling using 3.5 kHz, 12 kHz, uniboom and side-scan sonar systems on R/V SEA SOUNDER. Once a suitable location has been identified, with no extreme bathymetric irregularities, underwater television displays and 70 mm bottom camera photographs are taken along with samples of the bottom sediments. Immediately following the tripod launch, a routine sampling station is taken that includes C-T-D, transmissometer, and current profiles, and water bottles.

The group of illustrations shown in Figure 9 and Figure 10 show the results of these GEOPROBE site surveys for the July, 1977 cruise in Norton Sound. The 3.5 kHz and uniboom seismic records shown in Figure 9 demonstrate the generally flat-lying subsurface reflectors. The thin, acoustically transparent layer of surface sediments seen in the 3.5 kHz profile is typical of western

Norton Sound. This layer probably represents the most recent deposits of the very fine sand to muddy silts shown in surface samples. The dramatic feature in the side-scan record (Fig. 9) is an ice gouge that is located about 3 km north-northwest of site G1. The dominant gouge is about 5-8 m wide and has an arcuate trend. Its fresh appearance suggests it was formed recently, probably during the previous winter. A narrower, linear trace of a less intense ice gouge intersects the larger feature near the middle of the record. The mottled texture in the side-scan record is mostly instrument induced "noise"; however, the fine-grained, irregular patchiness near the center probably represents the small-scale bottom irregularities that are present. The bottom photograph in Figure 9 shows a typical bed irregularity, a short-crested incipient sediment ripple. These low ripples and the animal mounds have vertical relief of a few (2-3) centimeters.

Figure 10 contains a series of results from the site survey at G2. The acoustically transparent layer shown by the 3.5 kHz record from site G1 is not as well-defined in the similar record shown in this figure. The 3.5 kHz record for site G2 does show many disrupted acoustic reflectors near the surface which Nelson (1977, 1978) has attributed to gas effects. The subsurface disturbances are also apparent in the uniboom records (Fig. 10).

The side-scan sonar records near site G2 (Fig. 10) did not show evidence for ice gouging; however, the bottom echoes showed many circular or near-circular holes or "pits" with diametral scales of about 1 m or less. A possible explanation for these depressions as collapse structures caused by local sub-surface gas accumulation and release has been given by Nelson (1977, 1978). Another alternative explanation is that the holes are caused by burrowing animals.

The local surface relief at site G2 was similar to that at site G1, about 2-3 cm, caused by animal mounds and patches of sediment ripples. Shelly debris and clams are evident in the bottom photographs (Fig. 10) and box cores (Fig. 10). The sediment surface to a depth of 3-4 cm is again characterized by a soft, ooze-like layer whose greenish-brown color contrasts with the dark green underlying material (Fig. 10).

The topmost several centimeters (about 3-4 cm in Fig. 9) at the GEOPROBE site contain nearly equal amounts by weight of sand and silt/clay sizes. Table 1 is a size-frequency distribution for the surface sample at site G1. The mean size is 3.3Ø (0.7 mm). The material is moderate to poorly sorted. The surface layer at site G1 contains a considerable amount of organic material. The soft, loosely packed upper few centimeters of the samples typically have a greenish brown color. Bioturbation was evident in each of the box core samples; the dominant burrowing organisms were several varieties of worms and molluscs. (Nelson, 1977 and 1978, presents more information on the organism - sediment interaction).

Again like at site G1 there is evidence for a rich organic content in the surface material at site G2 due to excrement, mucoid materials, and organisms. The sediment size classes for this area are shown in Table 2. Mean grain size is 3.0Ø(1.3 mm) with moderate sorting.

The bottom water densities at each site after deployment were σ_t =24.4 at site G1 and σ_t = 27.5 at site G2. Bottom suspended sediment concentrations (at 1 m above the bottom) were 4.4 mg/l and 2.7 mg/l for sites G1 and G2, respectively. At both sites the dominant size class was silt in the suspended materials about 1 m above the bottom.

C. GEOPROBE sensor data

The GEOPROBE system recovered at site G1 (Fig. 2) provided 80 consecutive days of time-series digital data on currents, pressure, temperature, and light scattering/transmission near the sea floor (July 8 - September 25, 1977). No digital data were obtained at site G2 (see section V for explanation). The complete data set of hourly averages are presented in this section to demonstrate the wealth of information which one GEOPROBE can provide and to point out the critical significance of long-term measurements in trying to understand a dynamic and complex geological and oceanographic region like Norton Sound.

1. Current data

a. **Hourly averages**

Currents are measured at 5 positions on each GEOPROBE tripod as shown in Figure 11. As discussed in section V (see above) the rotor/vane values represent average currents for each 1 hour interval; each e-m current sensor produces "burst" measurements taken one per second for 60 seconds during each 1 hour interval. The hourly averages for each current sensor over the entire 80 day period are shown in Appendix C. Also shown for each sensor are the statistics and histograms of speed and direction for the entire record.

Several significant results are obvious in the current data and are pointed out here. Refer to Appendix C for the figures.

(1)The speed and direction records are dominated by a tidal periodicity for the first 57 days (to about September 5). The tidal current has a mixed periodicity with a dominant diurnal component prevalent in the more intense E-W motion. A distinct spring-neap fortnightly cycle is evident, with relatively low currents with confused direction occuring during the neap stage. For example, CM 4 has weak, neap tidal current-speeds during the period around July 10 and again 2 weeks later on July 24, August 8, etc. The strongest tidal currents occur during peak springs: achieving speeds of about 25 cm/sec at CM 1 to about 35 cm/sec at CM 4. The E-W tidal currents are very energetic; these records compare favorably with the current meter record taken by PMEL near site G1 (not shown).

(2) The current records show events that are longer in duration than the daily tidal cycle. For example, on July 24-25, September 4-7, and especially during September 13-16 and subsequently the current speed records show prolonged periods (>1 day) of increased, non-tidal flows. As will be discussed below, these events are correlated with increased wind speeds and wind direction shifts.

(3) The dominant low frequency non-tidal flow (daily-averaged) is generally northward, with a added eastward component at CM 1 and CM 4 (Appendix C - "stick" diagrams). The small magnitudes of the daily averages, denoted by the short "sticks" in the daily vector records are statistically insignificant. However, the large northward daily component during September is significant and occurs during strong southerly winds. The progressive vector plots essentially estimate the daily drift over the 80 day record at each sensor, and show the north-northeastward motion (about 2.5 km/day or 3 cm/sec at CM 4).

(4) The storm-intensified bottom flow during September 13-15 has hourly average values (i.e. burst averaged) of nearly 25 cm/sec at 20 cm above the bed (CM 1) and greater than 40 cm/sec at 100 cm above the bed (CM 4).

(5) Strong non-tidal flows subsequent to the September 13-15 storm event are quite evident. The N-S component has a marked northward component of about 10 cm/sec at CM 4 throughout the period September 17 to September 26 except for a sharp southward reversal on September 21-22 and the diurnal overtones. The other sensors show a similar northward polarization during the post-storm period.

Graphs of the power spectra for each time-series record of burst-averaged currents are also given in Appendix C. The kinetic energy spectrum for each sensor shows that the diurnal and semi-diurnal components dominate the motion field; however, a lower frequency peak (not significant at 95% confidence interval) is present at a period of about 140 (58 days). The spectral plots for E-W and N-S components generally show largest power at the diurnal period.

b. Burst data

The e-m current sensors were sampled each second over a single 60 second burst to obtain measurements of the surface wave-induced currents. The data are too numerous to present as time series plots for the entire 1,900 burst sequences. The total number of burst data points for each e-m current sensor is about 1.2×10^5.

Examples of the burst data are shown for selected burst sequences on July 13 (Figs. 12-14), July 25 (Figs. 15-17), and September 14 (Figs. 18-20). The lower graph on each figure is the "burst" pressure data, also sampled once per second.

The most significant finding is that the large surface waves and swell (1-2 m) during September 13-14 occurred during strong southwesterly winds (~20 knots) that persisted for over 24 hours. Additionally, this was a period of high spring tides. The combined wind-driven, wave-induced, and tidal currents produced near-bottom currents of 60-70 cm/sec at the times of measurements.

The maximum periods of the wave motion derived from the pressure data was 5 sec., 7 sec., and 11 sec. (Figs. 14, 17, 20). The relatively long periods during the strong winds in September 13-14 are particularly significant because of the shallow water depth of 20 m at site G1. These waves probably were swell that had propagated into the area from the SW.

c. Other data

Figure 21 contains GEOPROBE sensor data for the first 30 days (July 8 - August 7) of the 1977 experiment. The uppermost graph shows hourly averages of current speed obtained with the rotor/vane sensors. Semi-diurnal tidal motion and two fortnightly tidal cycles are quite obvious in this record. Spring tidal current speeds have daily maxima of 25-32 cm/sec; neap tidal current maxima are 10-15 cm/sec.

The plots of light transmission (TRANS) and light scattering (NEPHEL) in Figure 21 are presented as relative units of measurement taken once each hour (basic interval). The relatively persistent, low levels of scattering, about 0.24 relative, corresponds to about 3-5 mg/l as derived from calibration data (not shown here). These levels are representative of the "normal" conditions in the region of measurement as determined by independent shipboard sampling (about 4.4 mg/l).

Light transmission is more sensitive to turbidity fluctuations than scattering at relatively low levels of suspended concentrations. Therefore, the diurnal fluctuations in light transmission, not apparent in the scattering record (July 8 - July 21), correspond to real changes in the turbidity levels (about 1-2 mg/l peak-to-peak). These tidal fluctuations in turbidity are correlated with similar diurnal oscillations in the temperature data. A more detailed examination of these results shows several significant features:

(a) The oscillations are distinctly diurnal, not semi-diurnal.

(b) Periods of low temperatures ("cold") are correlated with values of low turbidity ("clear").

(c) During times of neap tide (July 8, July 23, August 6) both turbidity and temperature are relatively steady.

The above features suggest that tidal advection, specifically the E-W diurnal motion evident in the current speed (E-W) values (Appendix C) transports water into and out of Norton Sound, sweeping past site G1. This mechanism is a more plausible explanation for the observed values than vertical advection or mixing caused by the internal tide because of the correlation of "cold" with "clear" water. Since the bottom water is colder and more turbid than the surface layer, a vertical mixing or advection process would presumably cause a correlation of "cold" with "turbid" values. The horizontal tidal advection implies then that with a rms diurnal tidal speed of about 10 cm/sec, reversing lateral E-W transport of about 4.5 km will occur every 12 hours.

Even more noteworthy in Figure 21 is the unusual "event" that occurs on July 25, characterized by a sudden increase in scattering, decrease in transmission (i.e. sharp increase in turbidity), and a significant speed increase due to a non-tidal current. The peak NEPHEL value of 2.0 relative corresponds to about 50 mg/l in sediment concentrations, an order of magnitude increase over the "normal" levels.

Figure 22 shows the weather data recorded at the National Weather Service station at Nome (about 30 miles to the north) during the period of this unusual event. Hourly values of wind speed, wind direction and air pressure are plotted in this figure. The wind data show a regular diurnal cycle, with wind speeds generally lower during the late evening-early morning hours. During July 24 wind speeds increase to 9-10 m/sec (about 20 knots) and become persistent, above 12 knots, over the next several days. Wind direction also becomes steadier from the SE during this period. Air pressure drops off, suggesting the passage of a low pressure center through the region. The higher surface waves caused by the

increased wind stress produced maximum oscillatory bottom currents as high as cm/sec (Fig. 17). The increased, sustained wind stress, occurring at the end of a neap stage in the tidal regime, apparently also caused an increase in magnitude and duration of the mean bottom current speed. The combined effect of higher wave-induced and wind-driven currents produced a bottom stress competent enough to cause the relatively large increase in concentrations of suspended materials (~ 50 mg/l). The sudden onset and equally sudden decrease in the concentration values are probably a result of initial resuspension of fine-materials that had settled out locally during the immediately preceding time of neap tide, and to increased upward turbulent mixing of the higher near-bottom suspended load by vigorous wave activity.

The effects on sediment movement at site G1 caused by a storm passage are even more vividly depicted in Figures 23 and 24. Figure 23 shows that during the last 20 days of the experimental period, the concentrations of suspended materials were high enough to obscure totally the light transmission path (except for a 2 day period on September 12-14). The current speed data in Figure 23 are from the hourly rotor/vane values; it was judged from the data and from the high degree of algal fouling of the rotor upon recovery that at some period after September 16 the rotor values are unreliable. The current speed data in Figure 24 are taken from CM4 and are judged to be reliable for the entire period. Note that the two current sensors (rotor and CM4) produce very similar results until about September 16.

The atmospheric data (wind speed, direction and surface pressure) show the storm passage and the subsequent "unsettled" weather quite clearly. The bottom pressure shows an "inverted barometer" effect as the atmospheric low passed through. The surface pressure analysis and storm track for September 14 is shown in Figure 25. Wind speeds of 10 m/sec (~20 knots) are exceeded during September 14 - 16; wind directions are generally south-southwesterly. The unusually large sediment concentration values greater than 100 mg/l on September 14 are followed by several periods of very high concentration levels. These high concentrations are correlated with relatively high values of mean bottom currents generally flowing northward. The strong winds and long durations also produce very high surface waves. Waves that have apparently propagated in from the SW along the storm track direction as swell are evident in Figures 18-20. The waves are as high as 2 m and have periods as long as 11 seconds, suggestive of a "deep" water origin in the southern Bering Sea.

Table 1: Grain size distribution by weight for surface sediment sample at GEOPROBE site G1.

GRAIN SIZE (Ø)	CUMULATIVE WEIGHT %	WEIGHT %
-1.00	0.25	0.25
-0.75	0.25	0
-0.50	0.25	0
-0.25	0.25	0
0.00	0.25	0
0.25	0.50	0.25
0.50	0.50	0
0.75	0.75	0.25
1.00	0.75	0
1.25	1.0	0.25
1.50	1.0	0
1.75	1.0	0
2.00	1.0	0
2.25	1.25	0.25
2.50	1.50	0.25
2.75	2.0	0.50
3.00	3.5	1.50
3.25	15.0	11.50
3.50	4.200	27.00
3.75	76.0	34.00
4.00	92.0	16.00
4.00+	100.0	8.00

Totals: 51.3% sand
48.7% silt/clay

Table 2: Grain size distribution by weight for surface sediment sample at GEOPROBE site G2.

GRAIN SIZE (Ø)	CUMULATIVE WEIGHT %	WEIGHT %
-1.00	-	0
-0.75	-	0
-0.50	-	0
-0.25	-	0
0.00	-	0
0.25	-	0
0.50	-	0
0.75	-	0
1.00	1.5	1.50
1.25	3.5	2.00
1.50	7.5	4.00
1.75	14.0	6.50
2.00	25.0	11.00
2.25	36.5	11.50
2.50	44.0	7.50
2.75	53.0	9.00
3.00	64.0	11.00
3.25	86.0	22.00
3.50	95.0	11.00
3.75	98.0	3.00
4.00	100.0	2.00
4.00+	100.0	0

Totals: 68.2% sand
37.8% silt/clay

Figure 4. Total suspended matter in the surface water, July 1977.

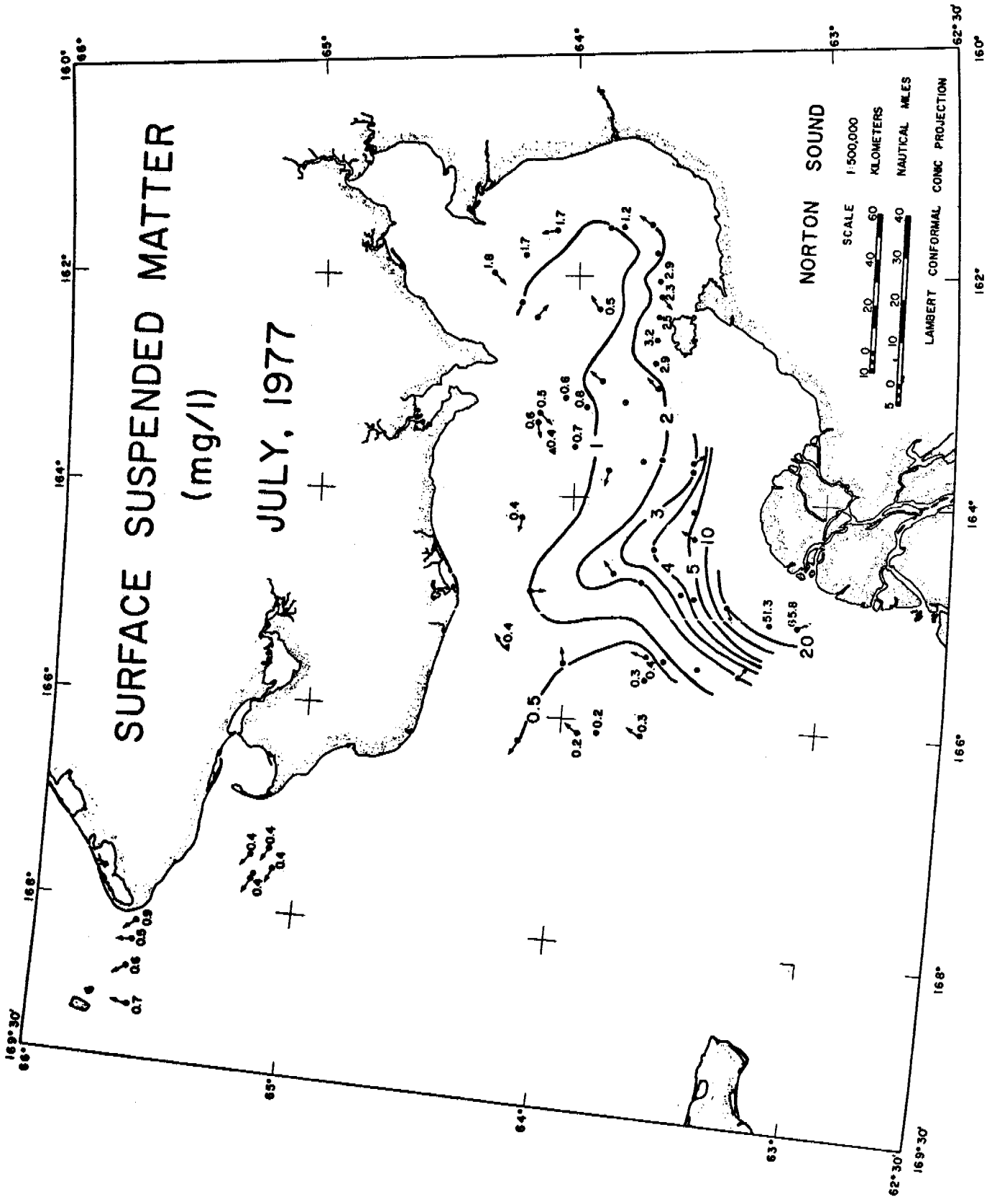

Figure 5. Total suspended matter in the near bottom waters, July 1977.

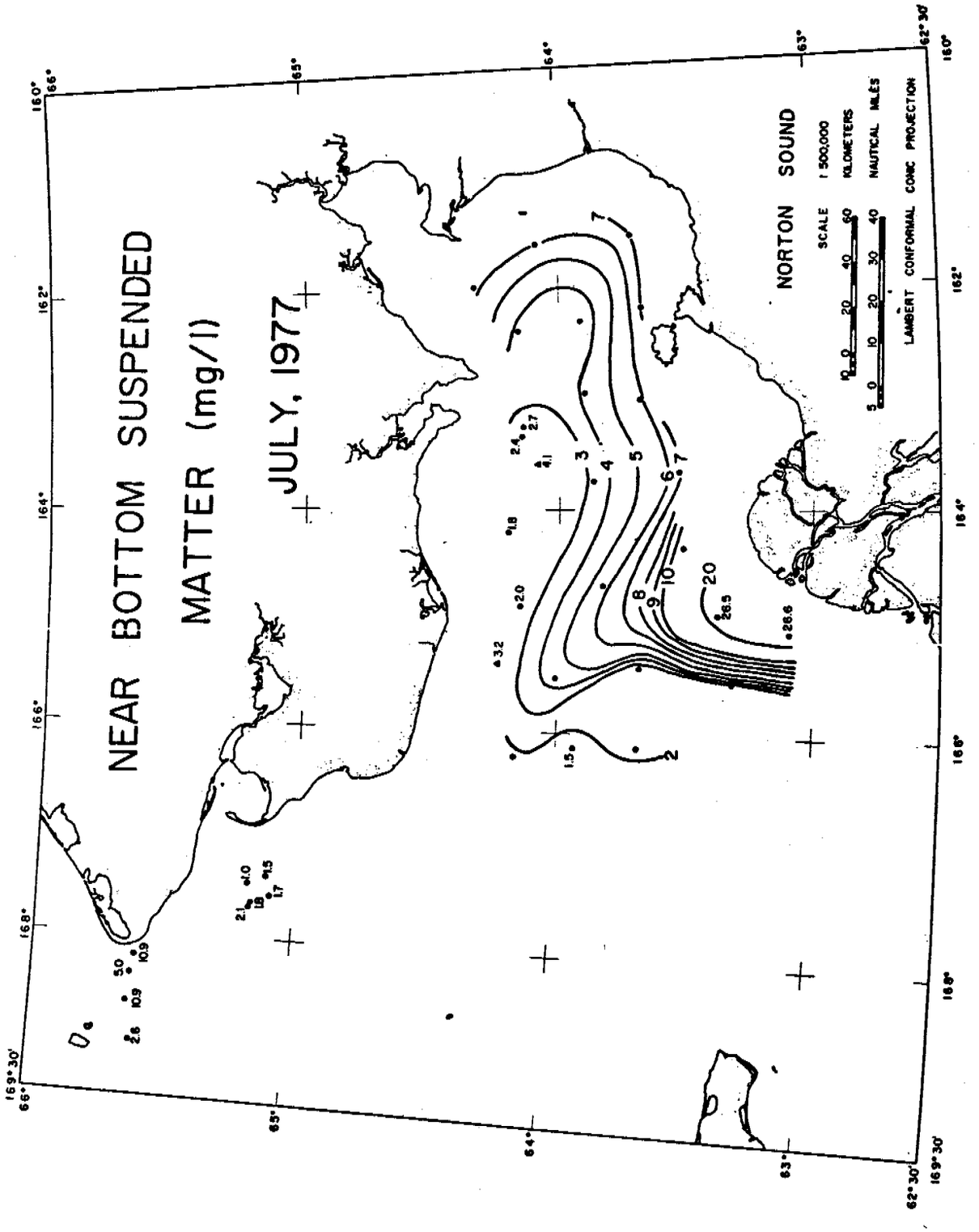

Figure 6. Light transmission (100 cm) and sigma-t distributions along an E-W section in Norton Sound, July 1977. Refer to figure 2 for station locations. Note that low values of light transmission indicate higher concentrations of suspended matter (compare to figs. 4 and 5).

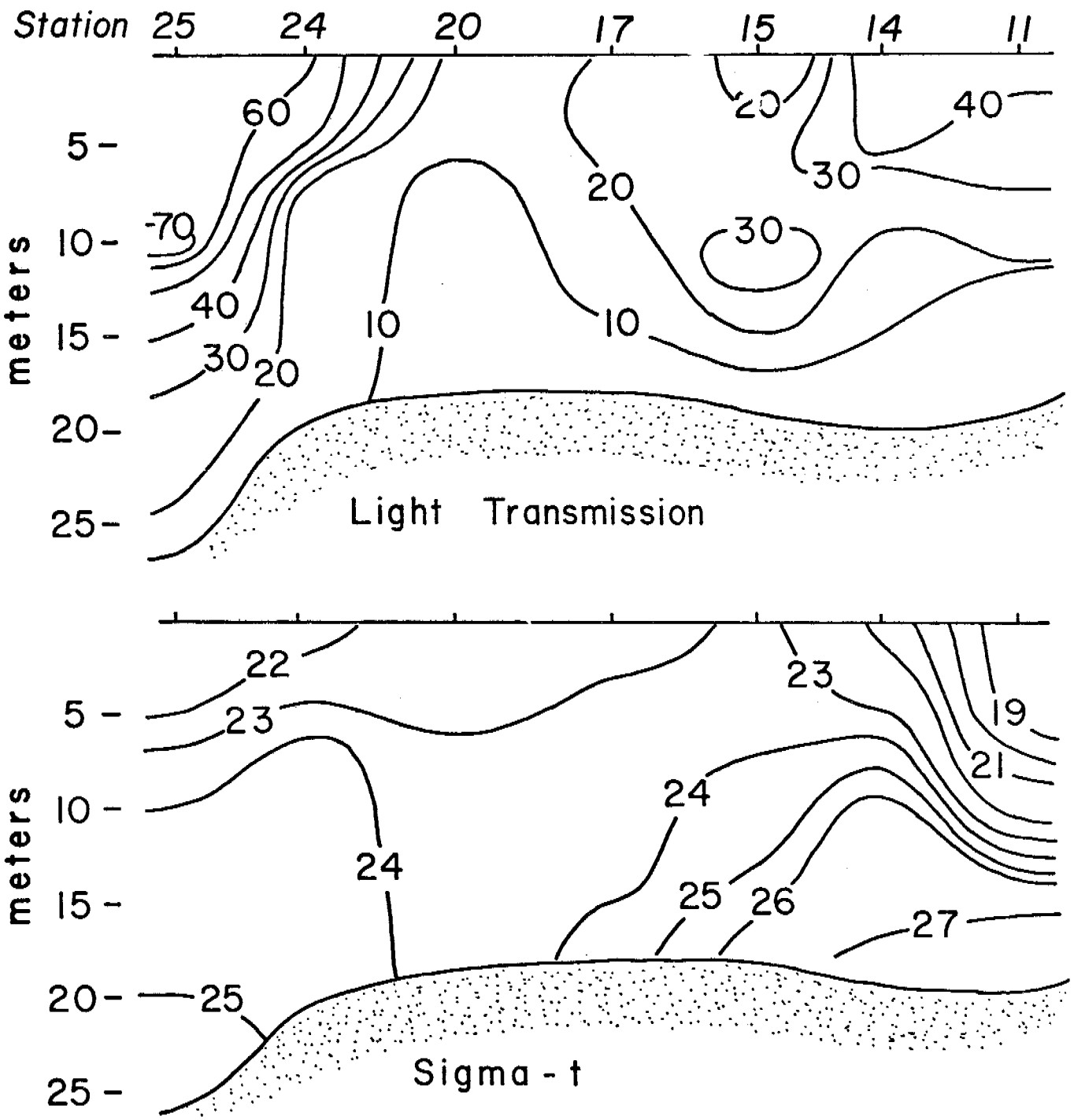

Figure 7. Light transmission (100 cm) and sigma-t distributions along an E-W section in Norton Sound, July 1977. Refer to figure 2 for station locations. Note the presence of anomalously dense bottom water in the eastern portion of the area.

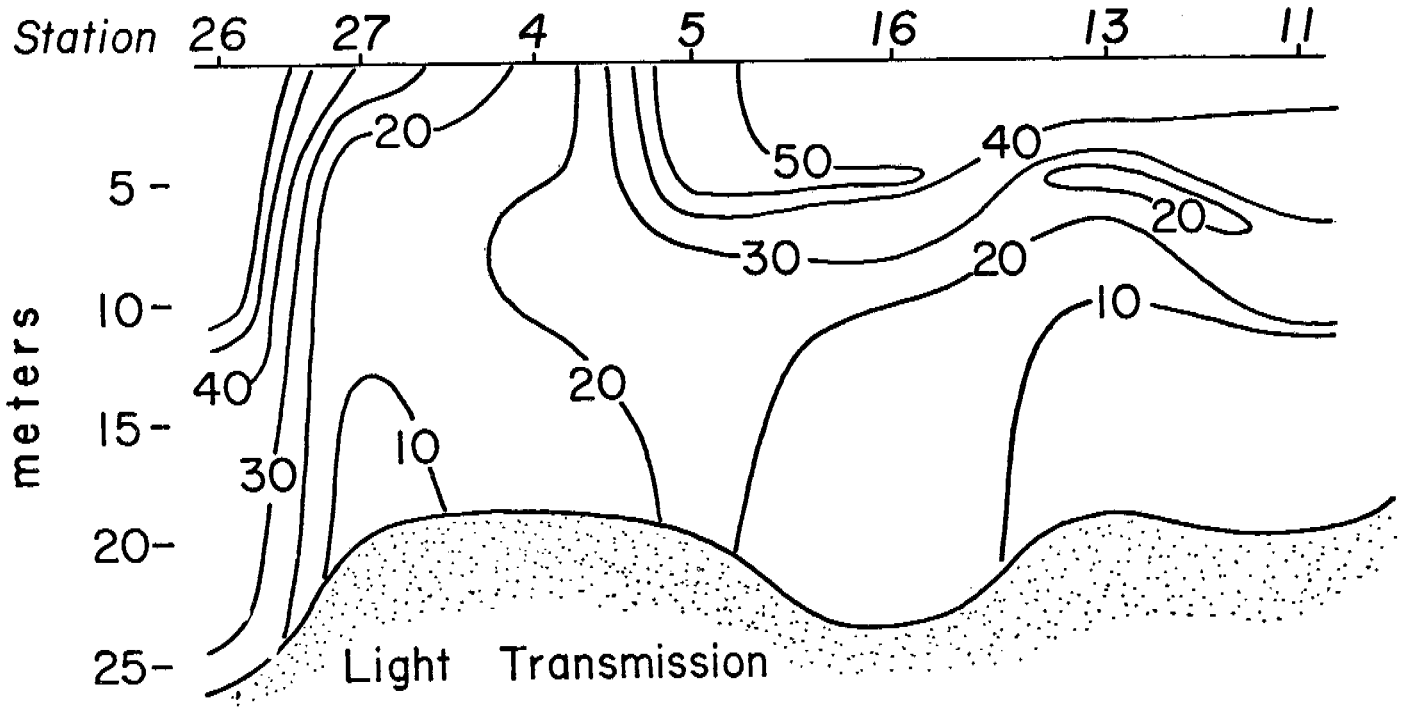

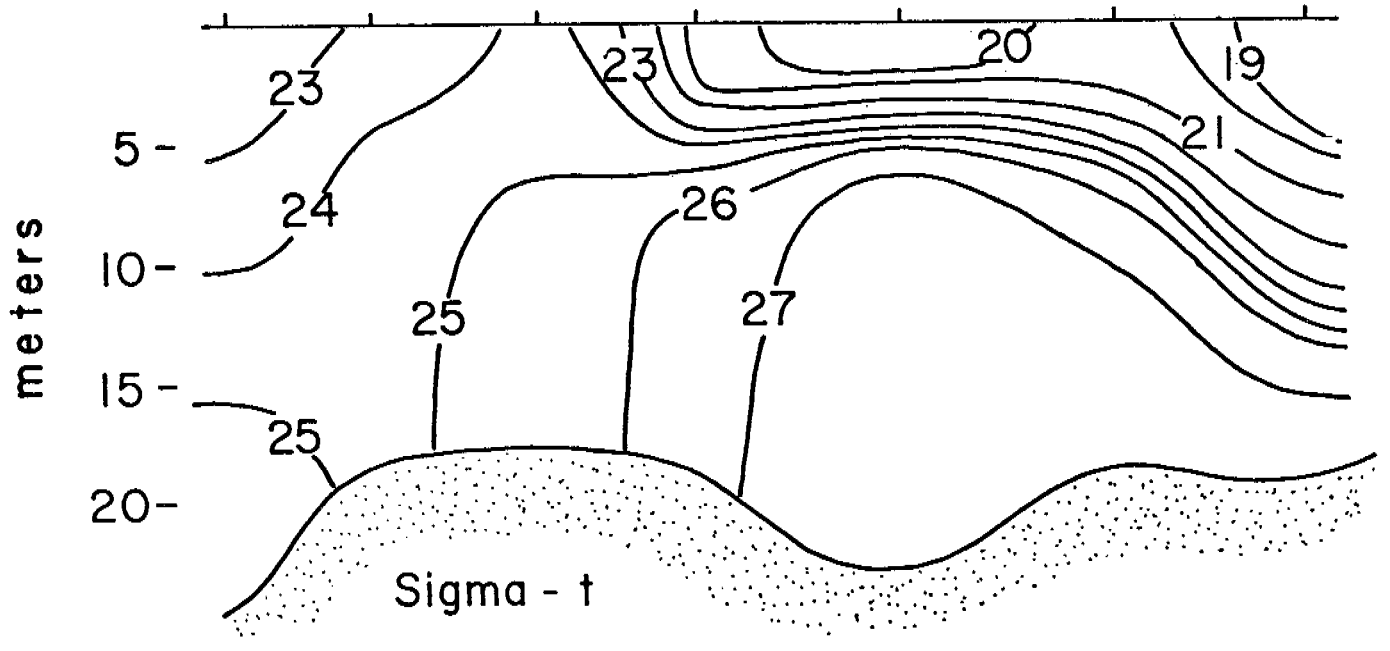

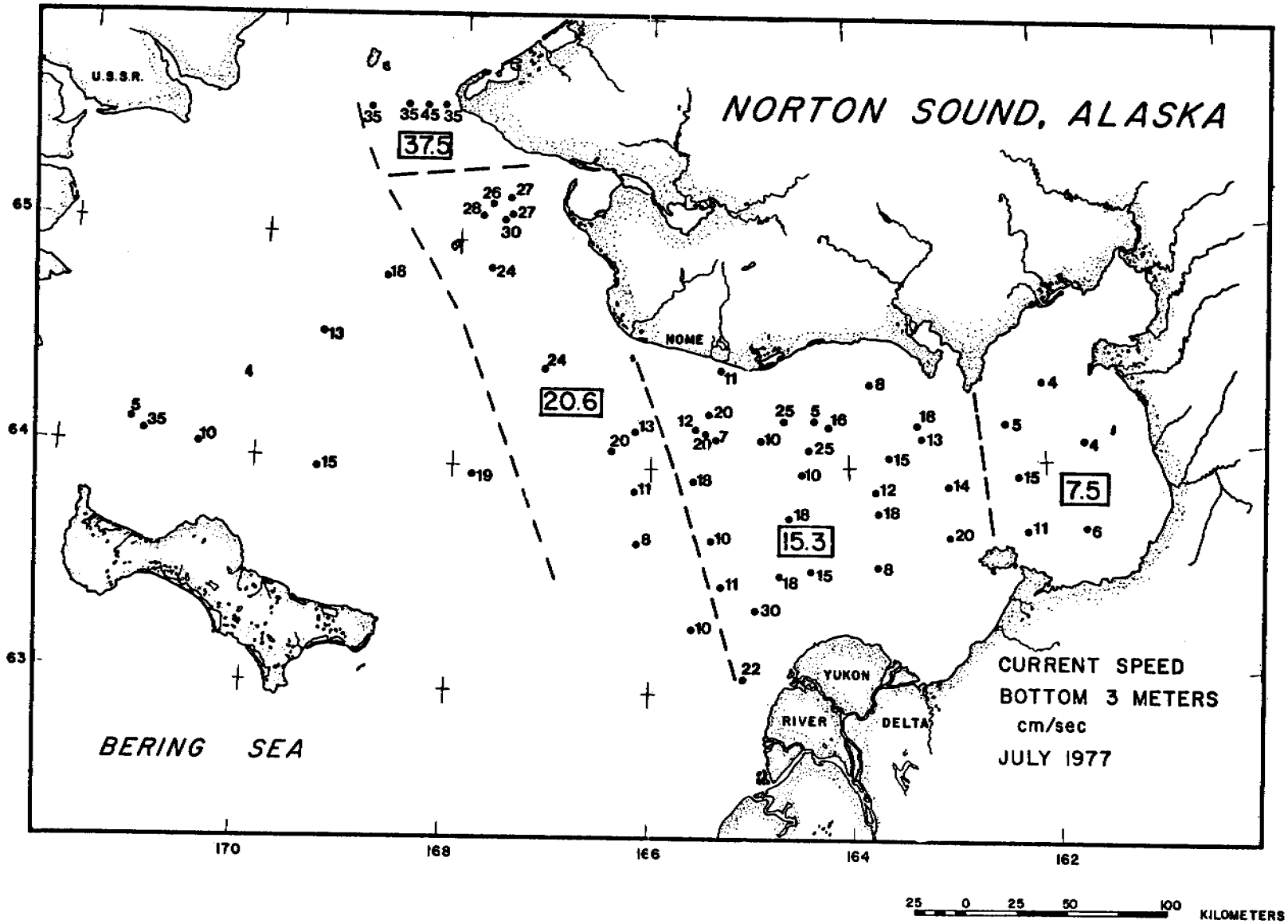

Figure 8. Current speeds measured in the near bottom water (1 to 3 m above the sea floor) of the northern Bering Sea during July 1977. The values within the boxes are the averages for each area. C. H. Nelson kindly provided data that were collected following our cruise.

Figure 9. Site survey data from GEOPROBE site G1 (64°00.0'N, 165°,29.5'W).

- a. geophysical records
- b. box core slab; numbers are in centimeters
- c. bottom photograph taken from an underwater television display at site G1. The horizontal scale of the photograph is about 50 cm.

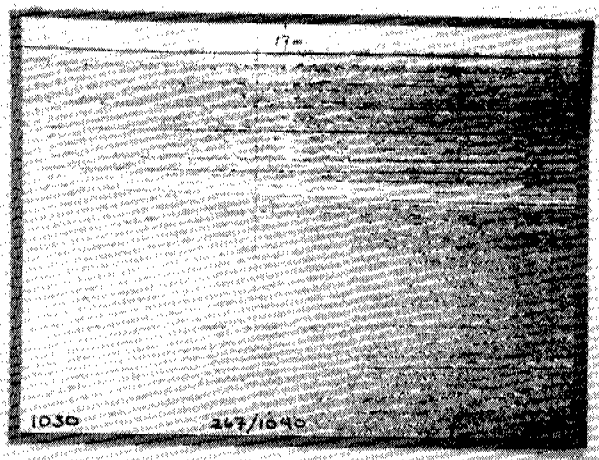

3.5 kHz

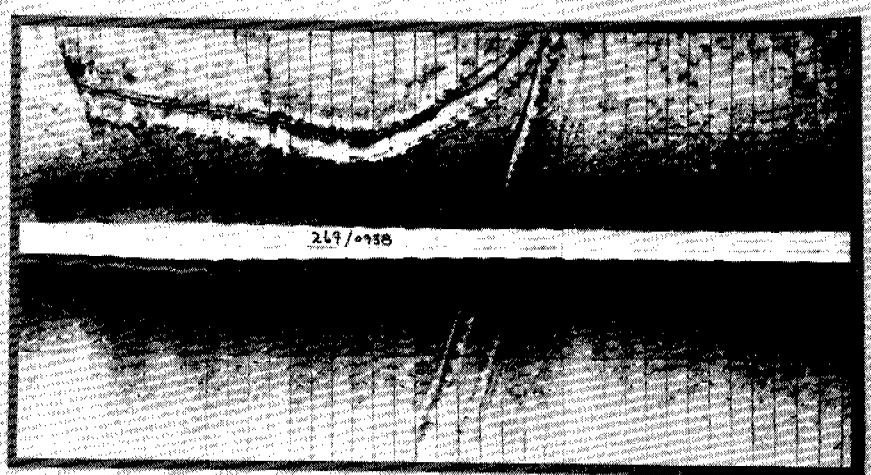

SIDESCAN SONAR

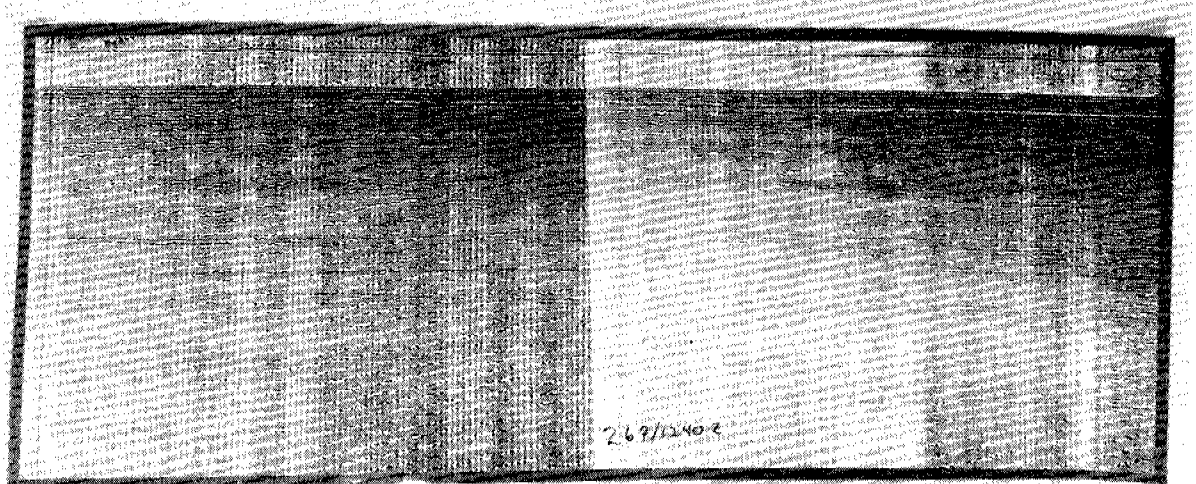

UNIBOOM

9 a

9 b

9 c

Figure 10. Site survey data from GEOPROBE site G2 (64°09.0'N, 163°21.3'W).

- a. geophysical records
- b. box core slab; numbers are in centimeters
- c. bottom photograph taken from an underwater television display of the seafloor at site G2. The horizontal scale of the photograph is about 50 cm.

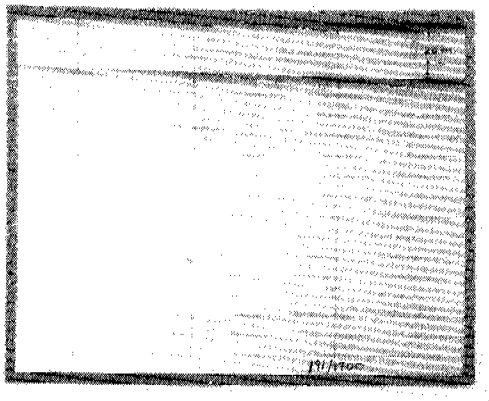

12 kHz

SIDESCAN SONAR

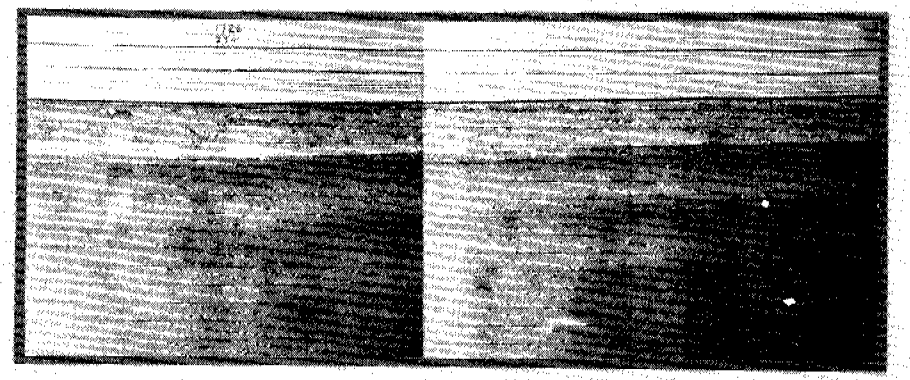

3.5 kHz

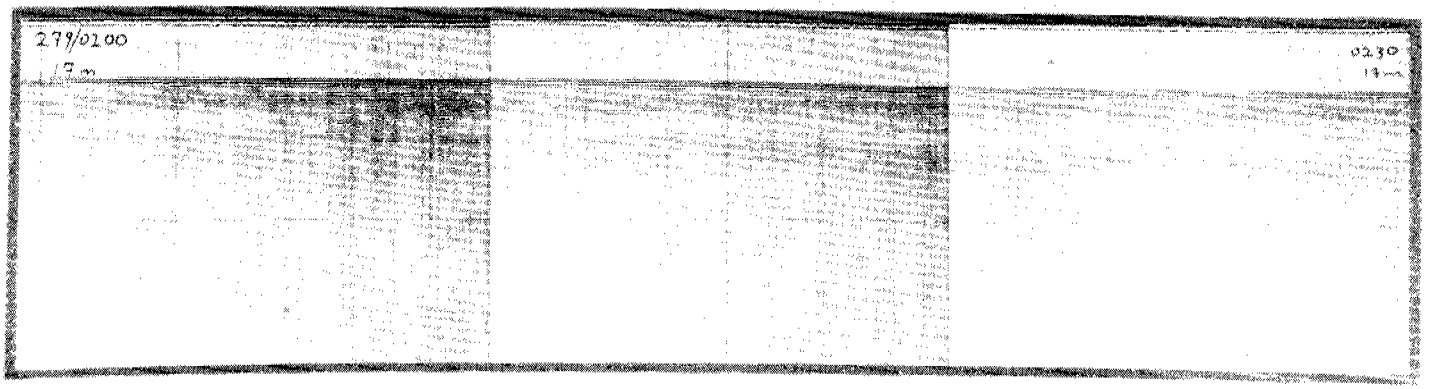

UNIBOOM

10 a

10 b

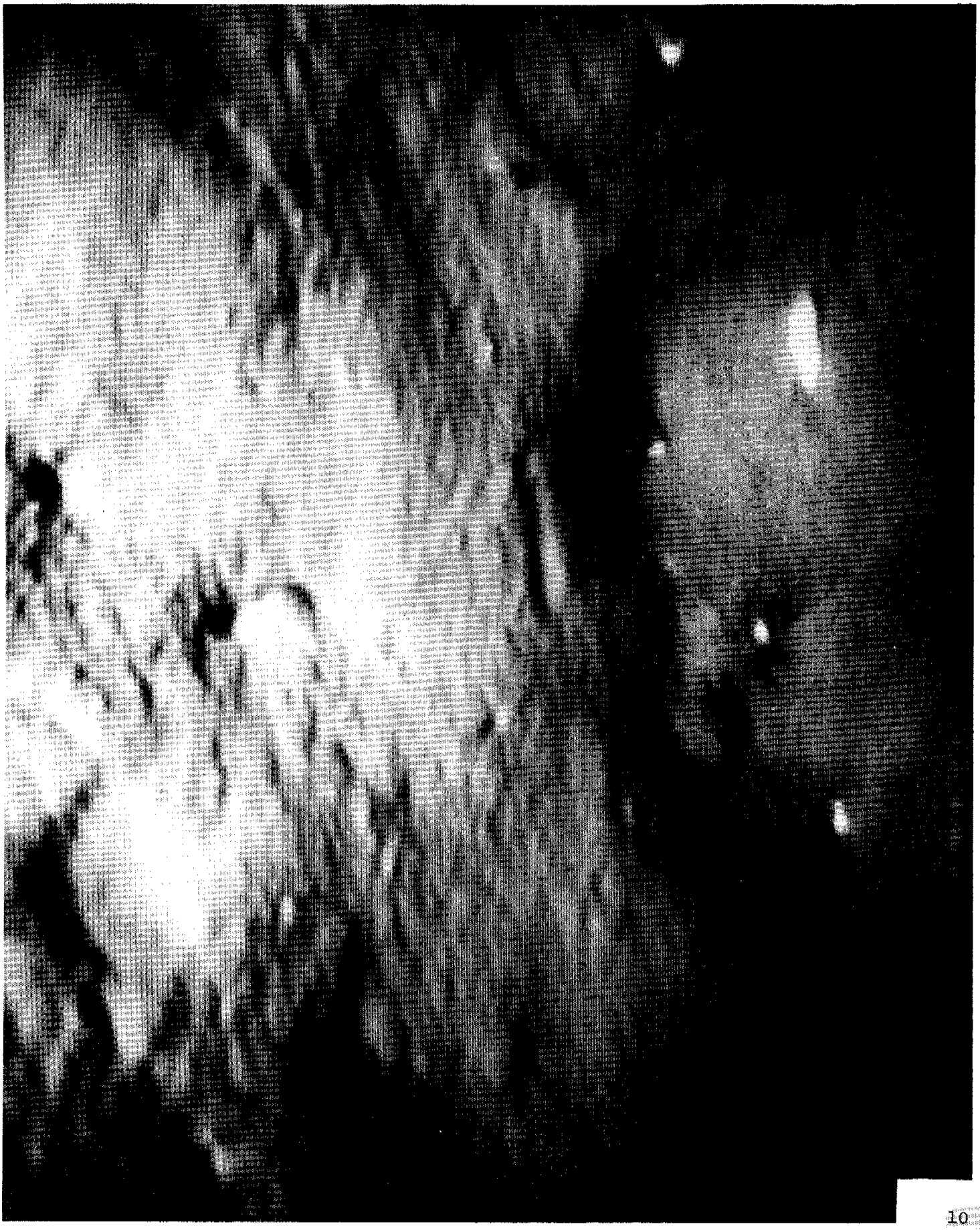
10 c

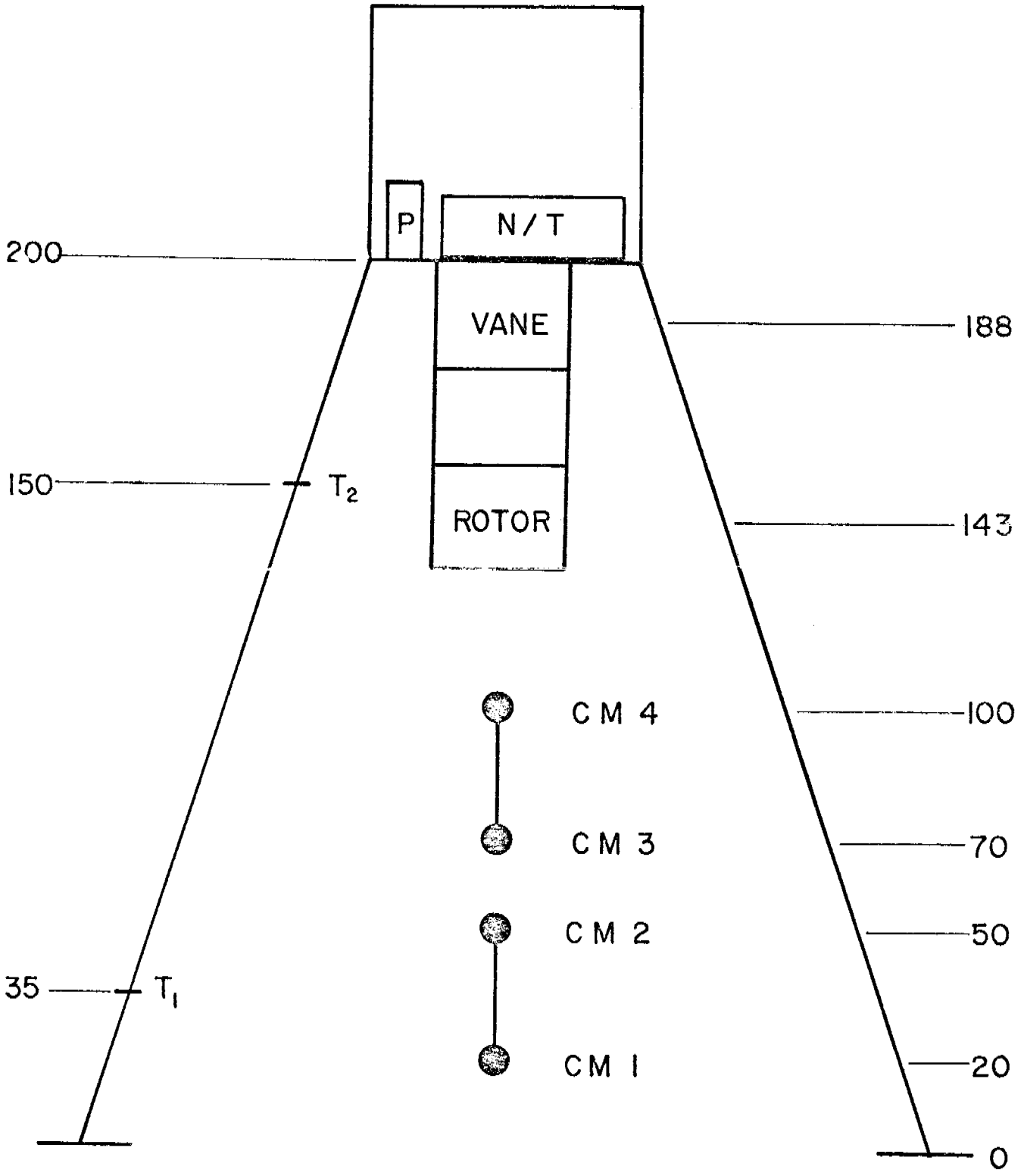

Fig. 11 Schematic of GEOPROBE tripod. All distances are given in centimeters from the base of the foot pads.

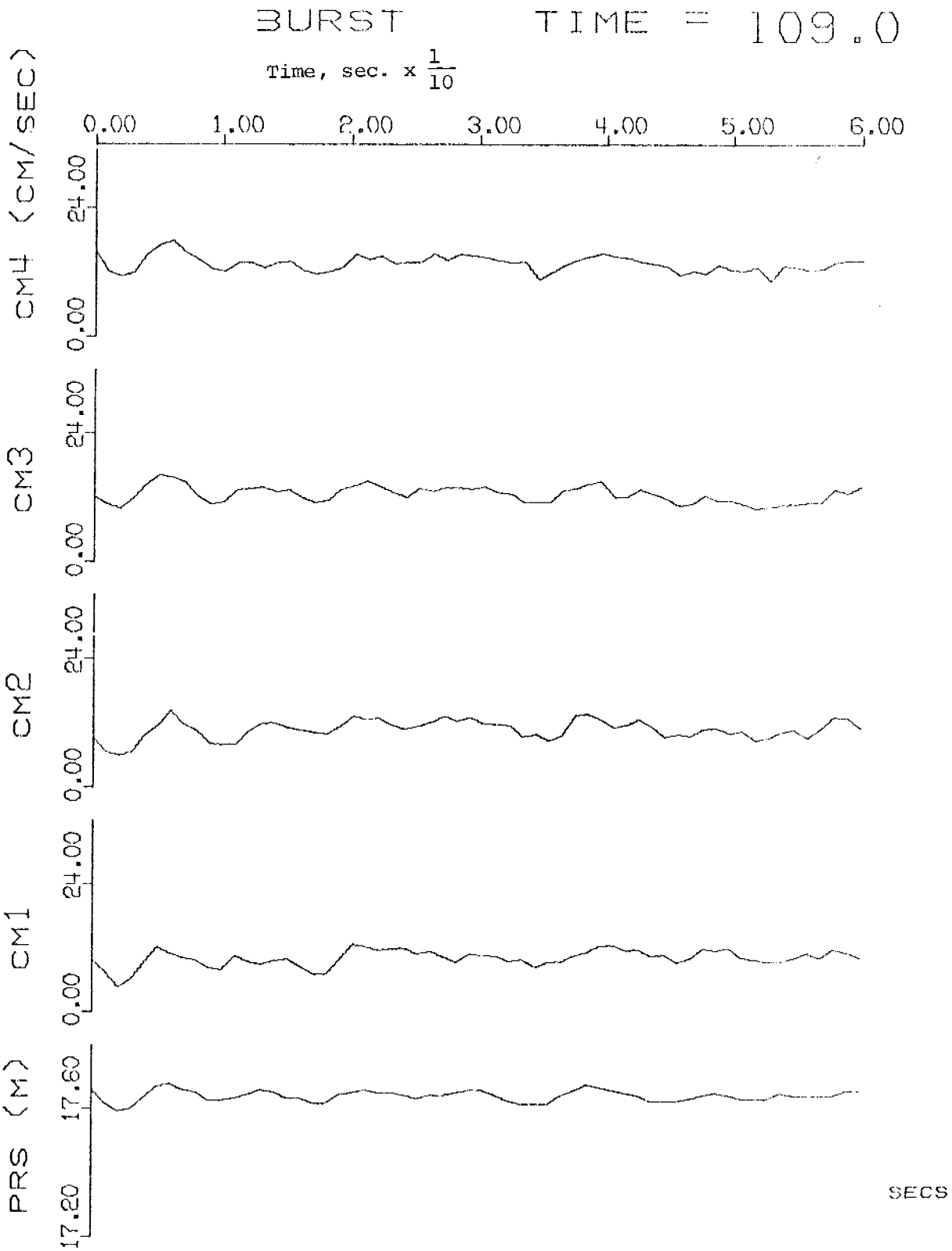

Fig. 12 "Burst"electromagnetic current sensor (CM) and pressure sensor (PRS) data taken at 0800 local time, July 13, 1977. There are 60 data points for each plot; lines have been drawn point-to-point by computer.

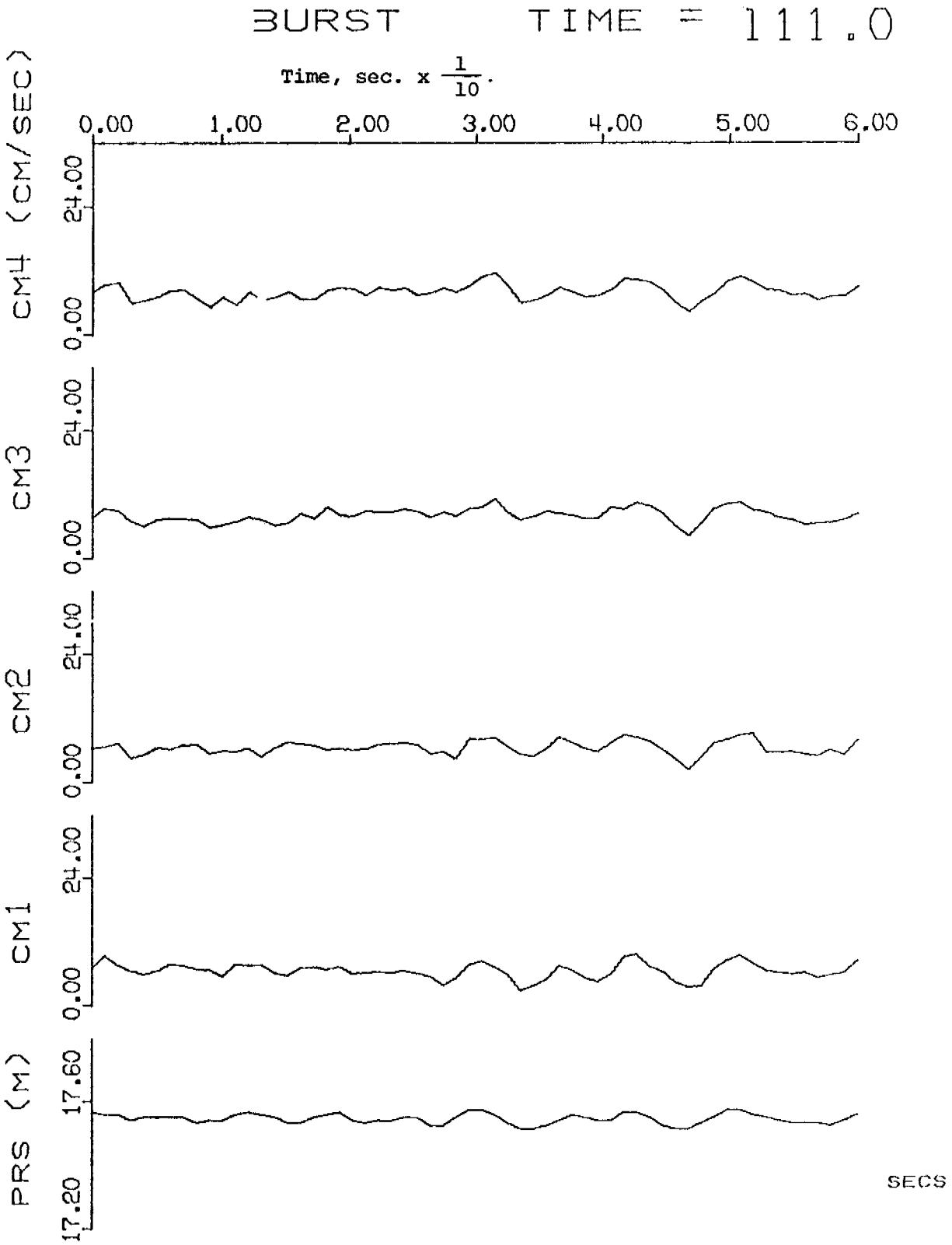

Fig. 13 "Burst current and pressure data similar to Fig. 12 except taken two hours later at 1000 local time, July 13, 1977.

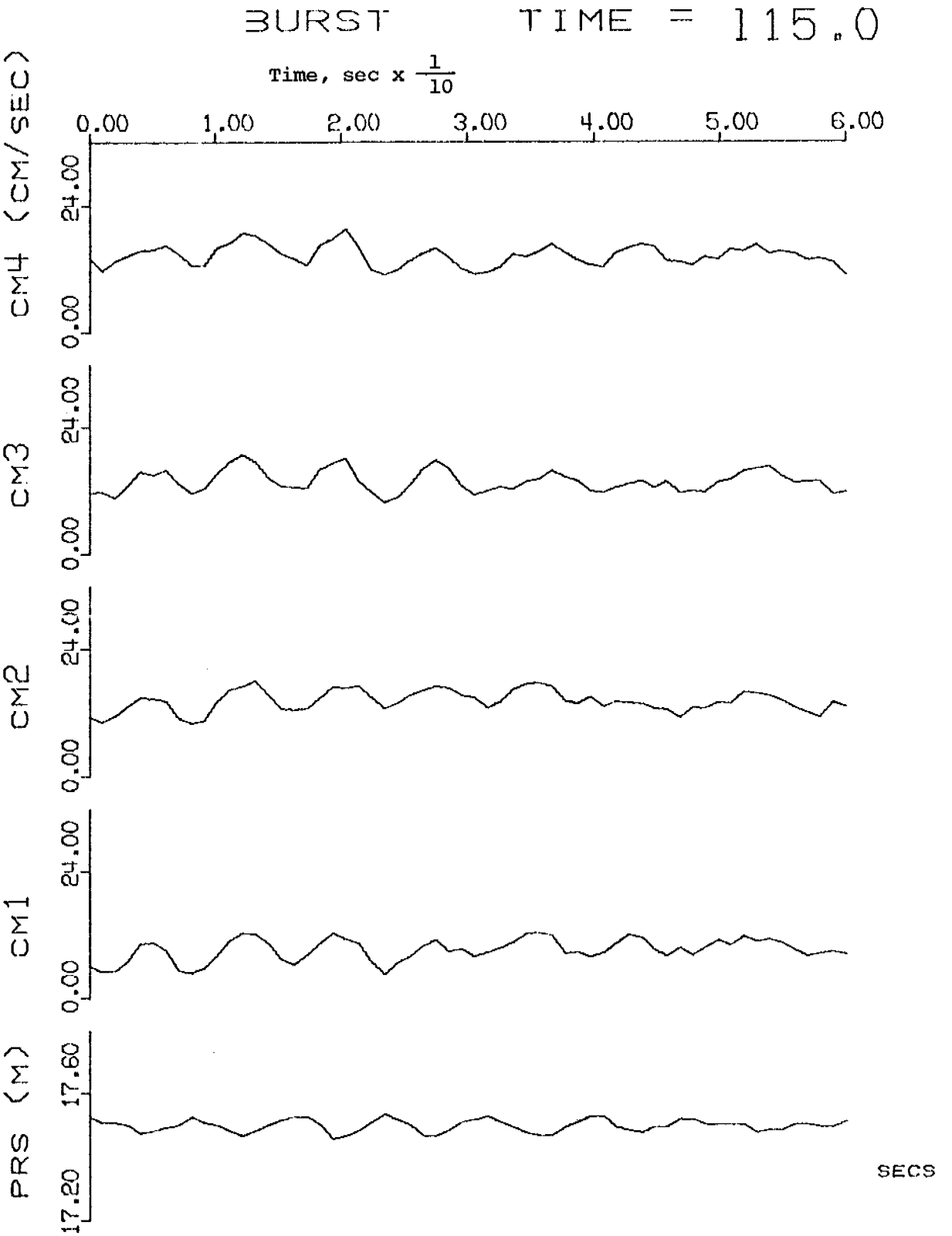

Fig. 14 "Burst" current and pressure data similar to Fig. 12 except taken four hours later at 1200 local time, July 13, 1977.

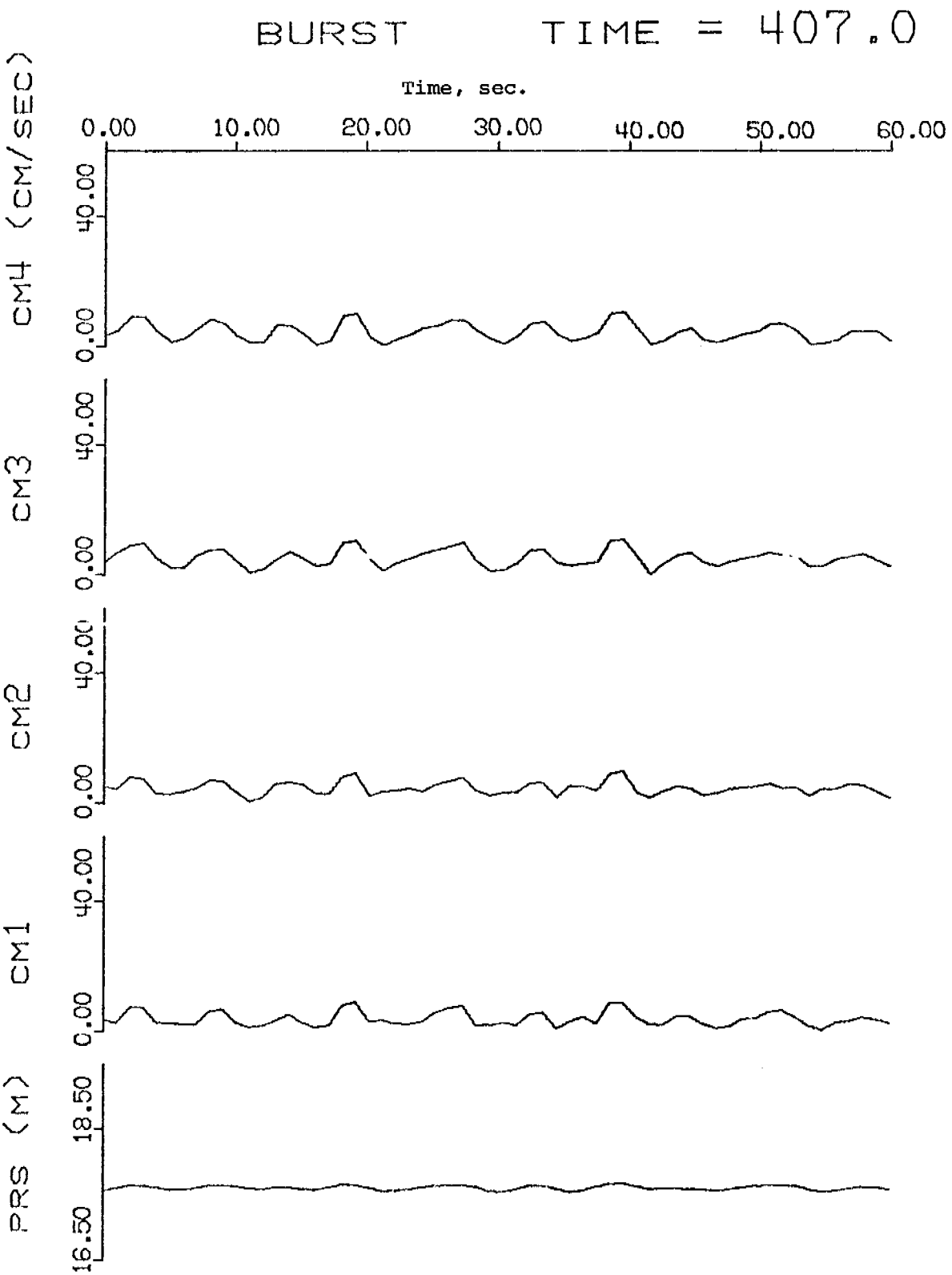

Fig. 15 "Burst" electromagnetic current sensor (CM) pressure sensor (PRS) data taken at 0100 local time, July 25, 1977. There are 60 data points for each plot; lines have been drawn point-to-point by computer.

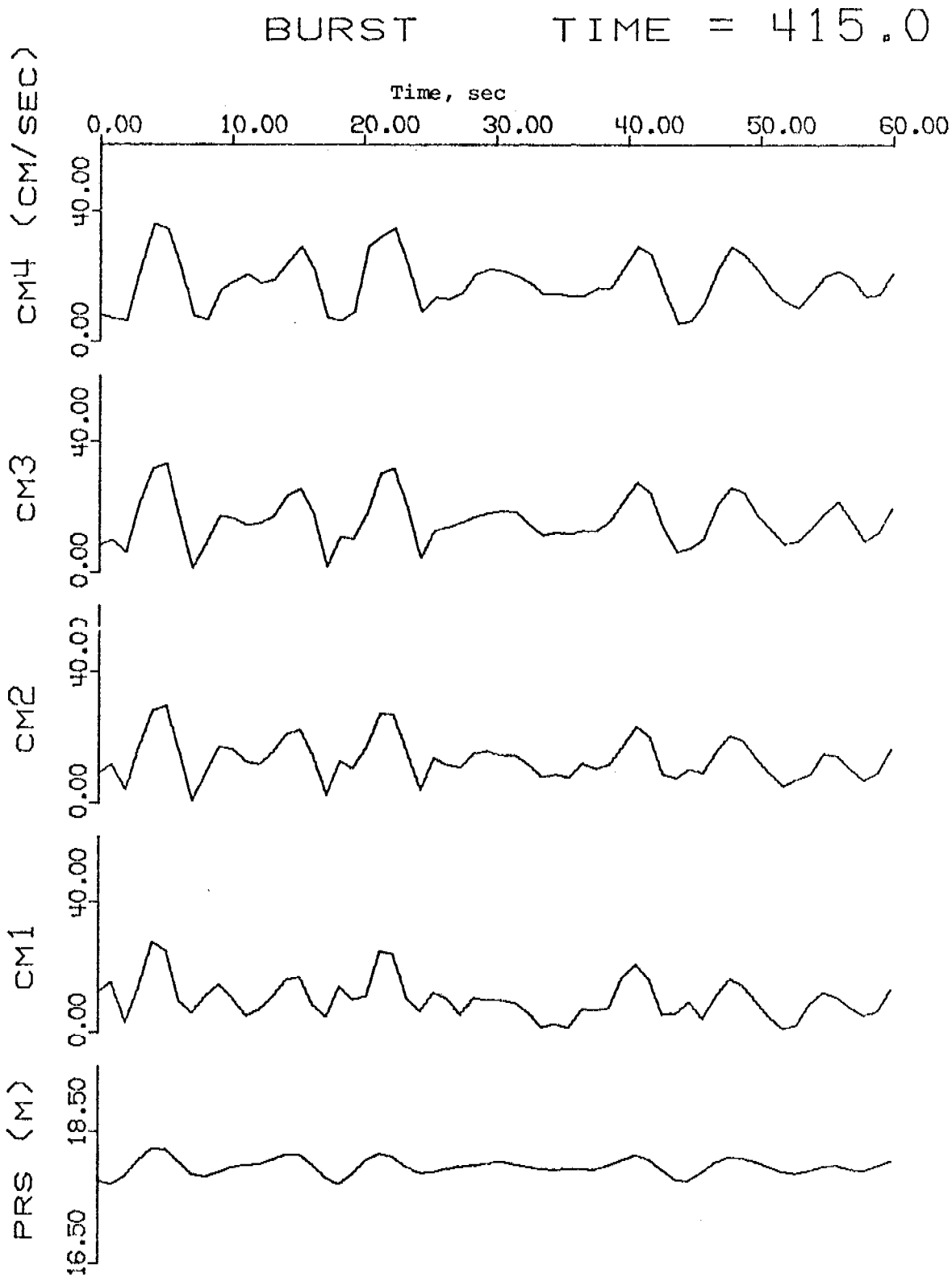

Fig. 16 "Burst" current (CM) and pressure (PRS) data similar to Fig. 15 except taken 8 hours later at 0900 local time, July 25, 1977.

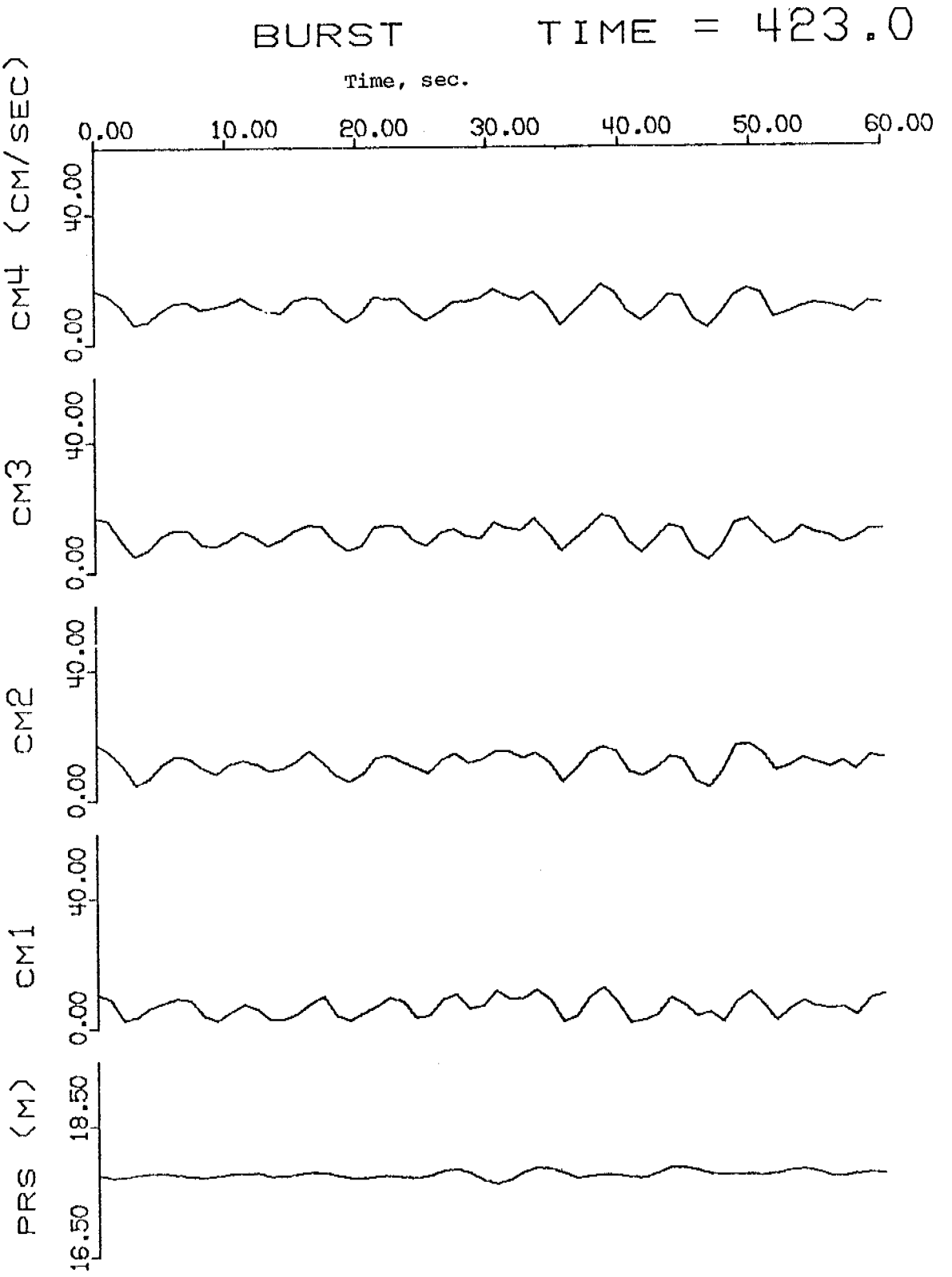

Fig. 17. "Burst" current (CM) and pressure (PRS) data similar to Fig. 15 except taken 16 hours later at 1700 local time, July 25, 1977.

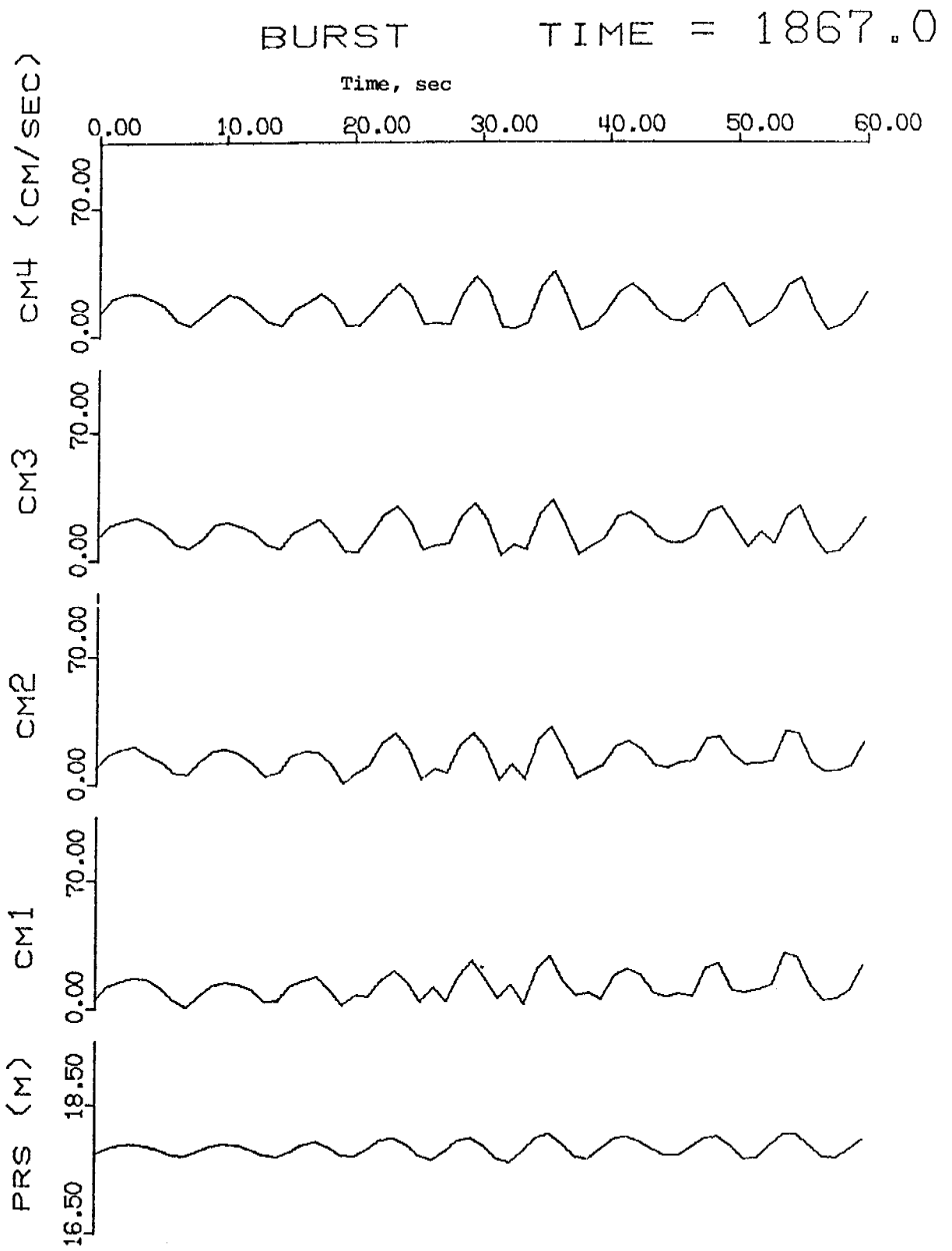

Fig. 18 "Burst" electromagnetic current sensor (CM) and pressure sensor (PRS) data taken at 0000, local time, September 14, 1977.

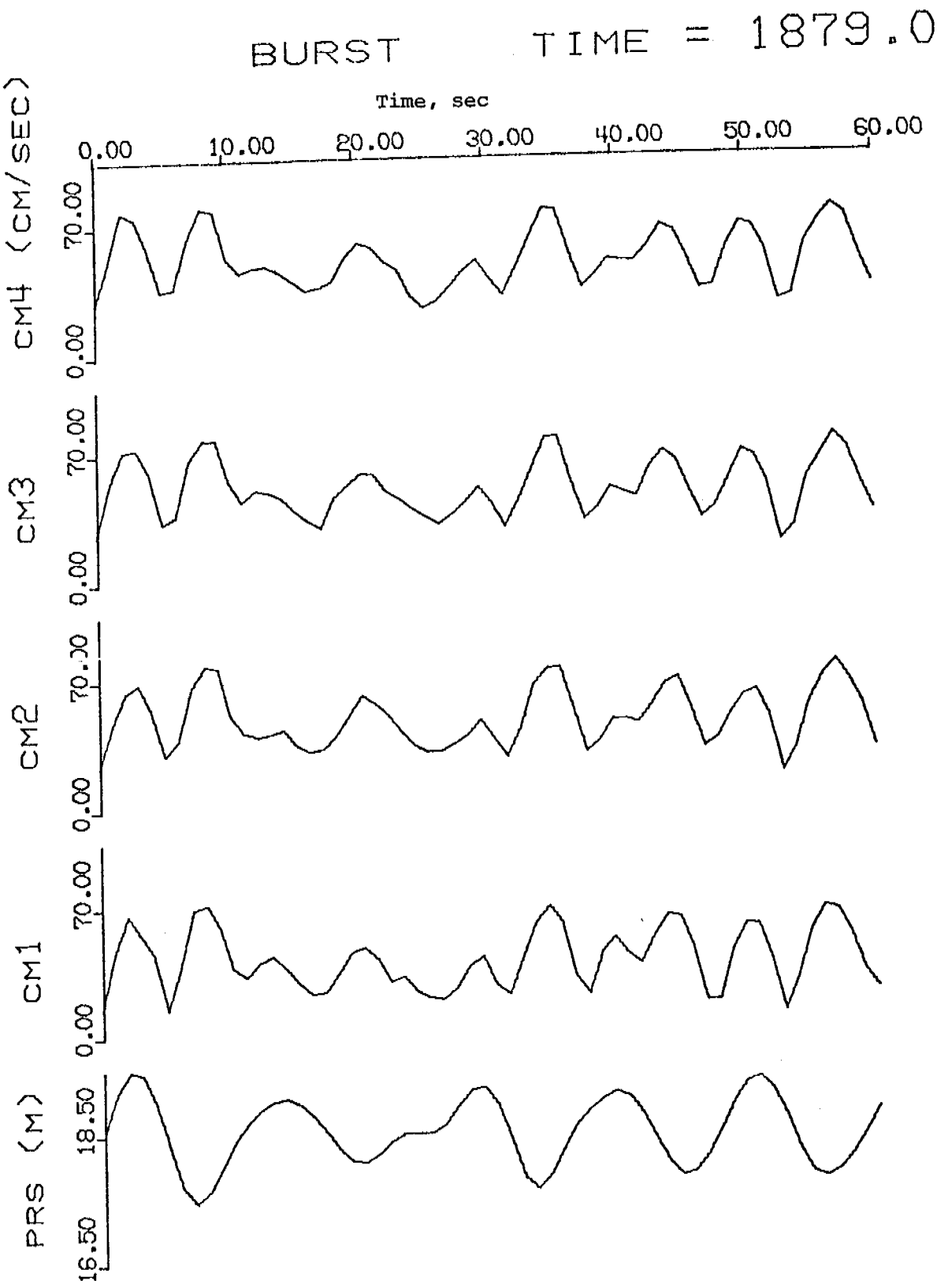

Fig. 19 "Burst" current (CM) and pressure (PRS) data similar to Fig. 18 except taken 12 hours later at 1200, local time, September 14, 1977.

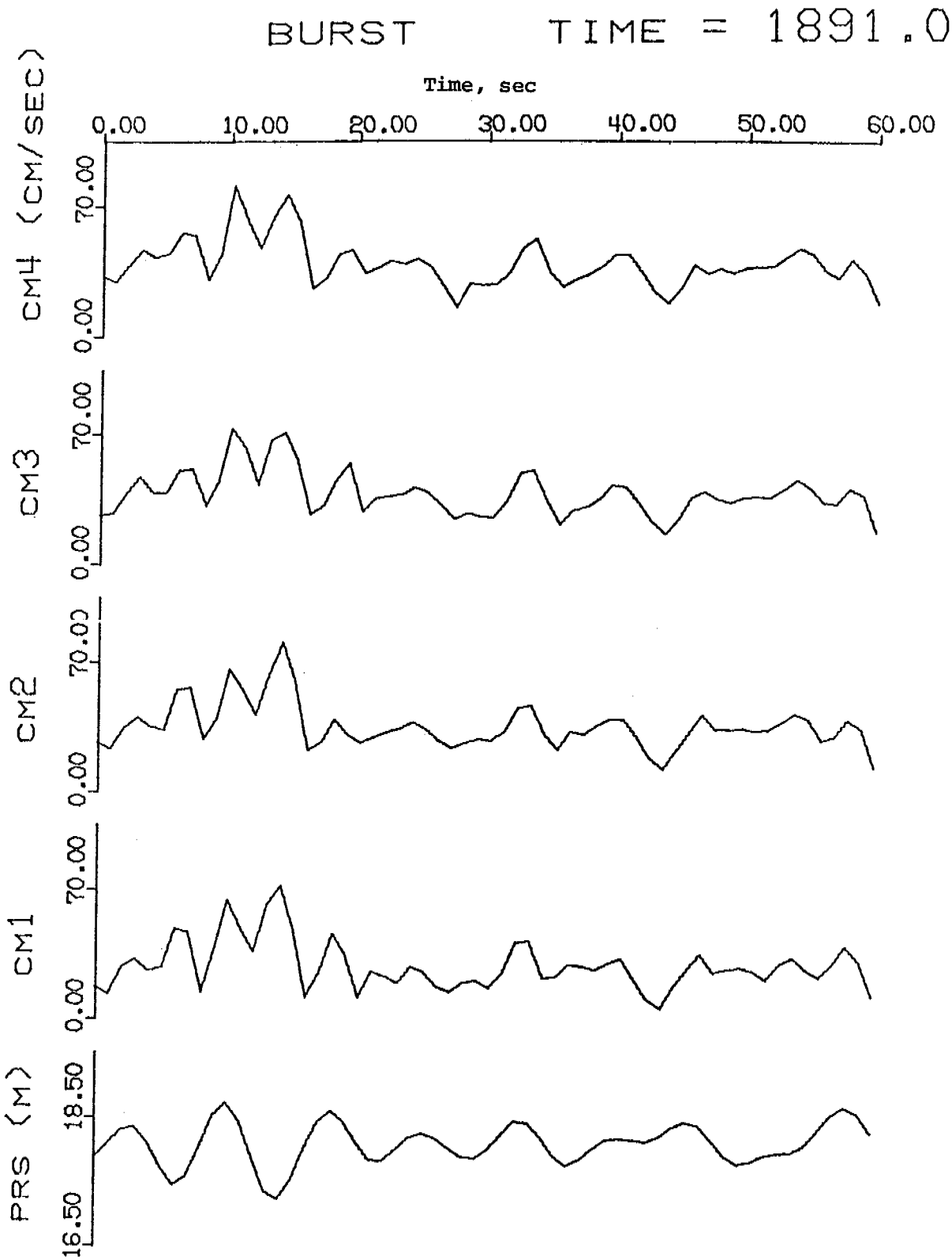

Fig. 20 "Burst" current (CM) and pressure (PRS) data similar to Fig. 18 except taken 24 hours later at 0000 local time, September 15, 1977.

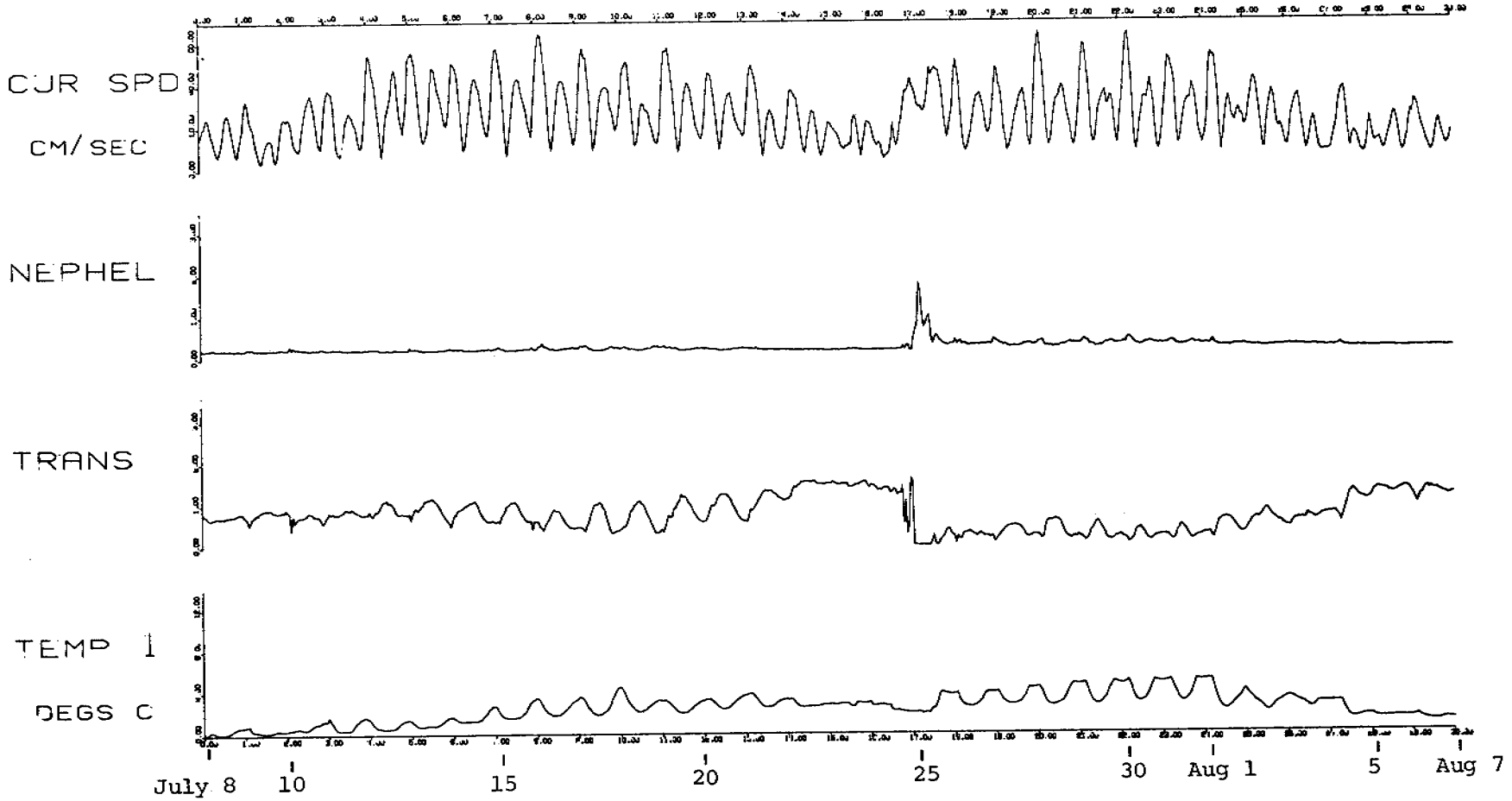

Fig. 21 Hourly GEOPROBE data taken over the 30 day period, 0000, July 8 - 0000, Aug. 7, 1977. Current speed (CUR SPD) at top are hourly averages obtained with the Savonius rotor. Light scattering (NEPHEL) and light transmission (TRANS) are in relative units; value for these and for temperature (TEMP 1) were taken once each hour. Horizontal axis is in days.

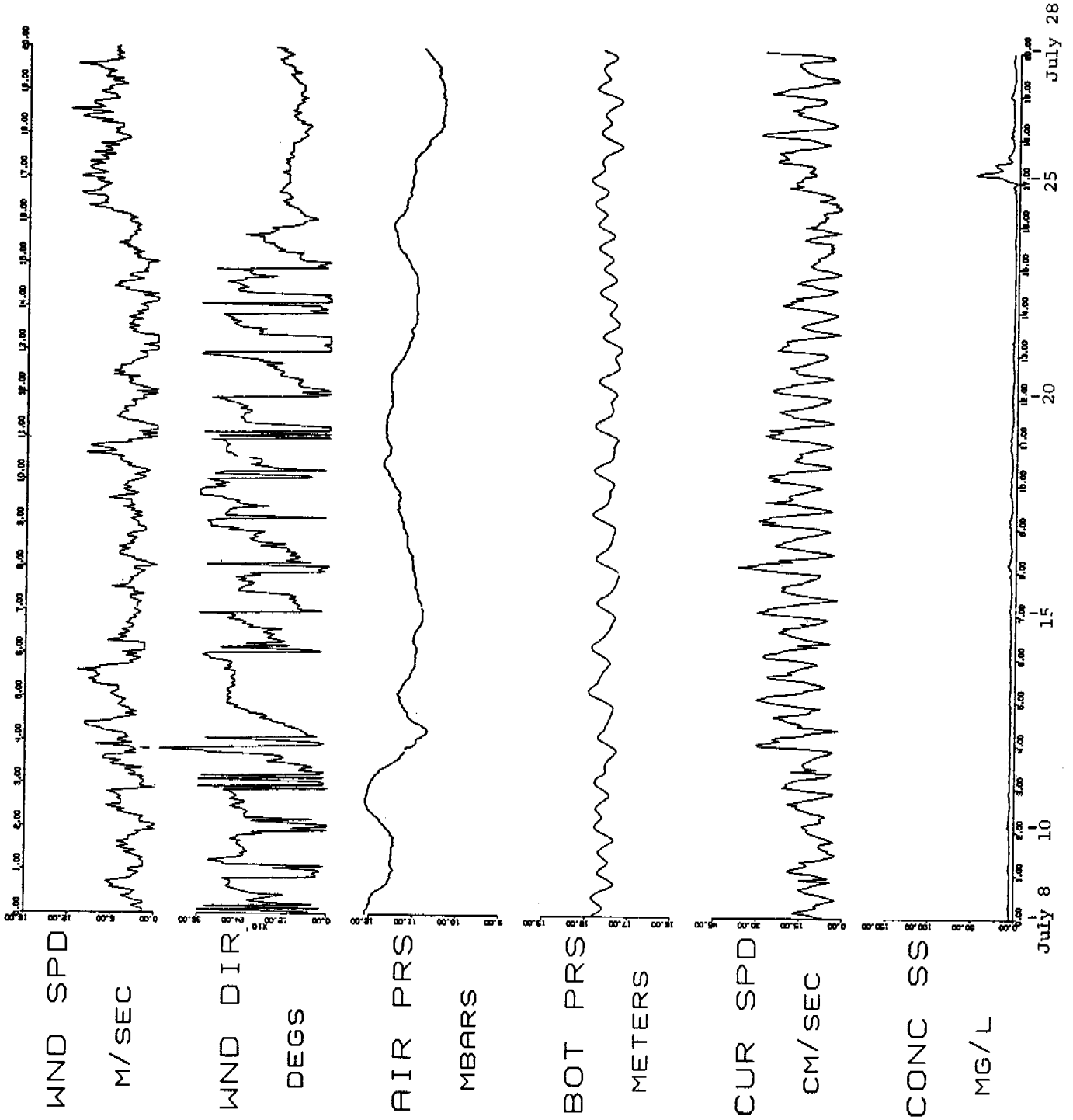

Figure 22. Meterological and GEOPROBE data taken over the 20 day period 0000, July 8 - 0000, July 28, 1977. Wind speed (WND SPD), wind direction (WND DIR), and surface air pressure (AIR PRS) were recorded hourly by the National Weather Service at Nome, Alaska. Bottom pressure (BOT PRS) and current speed (CUR SPD) were taken with GEOPROBE sensors. Concentration of suspended sediments (CONC SS) was derived from the light scattering (nephelometer) values using calibration data.

Fig. 23 Hourly GEOPROBE data taken over the 20 day period, 0000, Sept. 7 - 0000, Sept. 27, 1977. Current speed (CUR SPD) at top are hourly averages obtained with the Savonius rotor. Light scattering (NEPHEL) and light transmission (TRANS) are in relative units; value for these and for temperature (TEMP 1) were taken once each hour. Horizontal axis is in days.

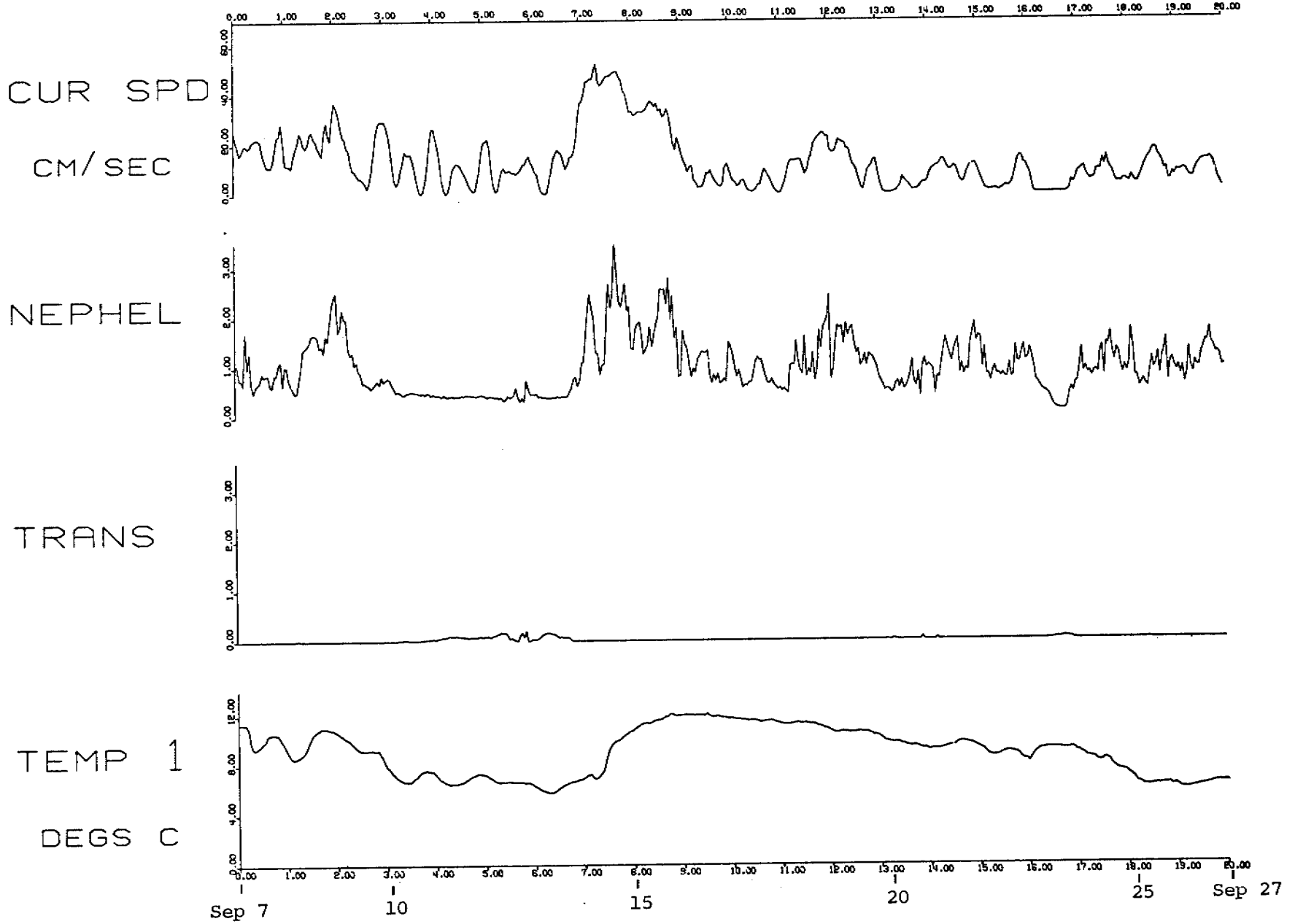

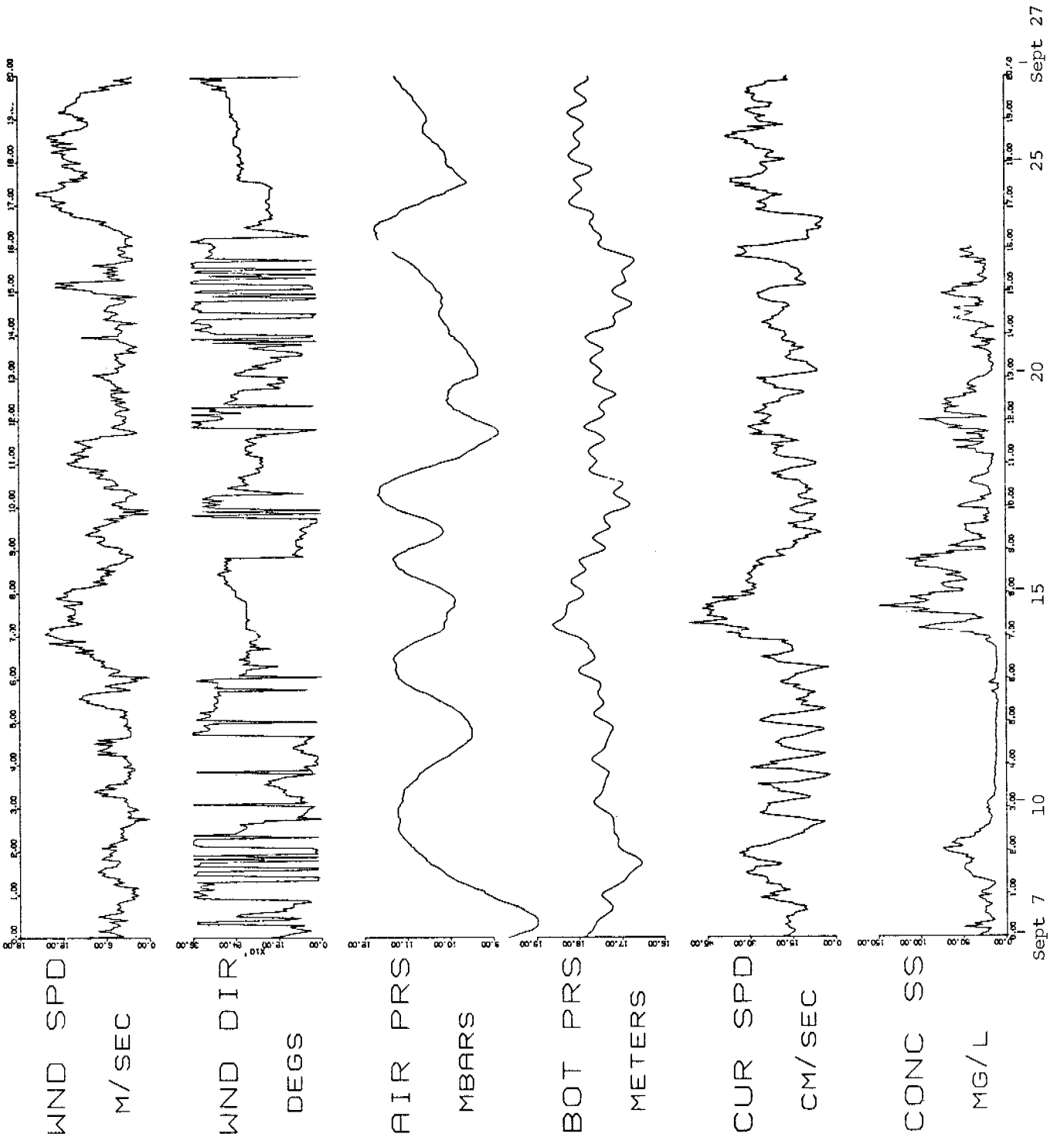

Figure 24. Meterological and GEOPROBE data taken over the 20 day period 0000, September 7 - 0000, September 27, 1977. Wind speed (WND SPD), wind direction (WND DIR), and surface air pressure (AIR PRS) were recorded hourly by the National Weather Service at Nome Alaska. Bottom pressure (BOT PRS) and current speed (CUR SPD) were taken with GEOPROBE sensors. Concentration of suspended sediments (CONC SS) was derived from the light scattering (nephelometer) values using calibration data. Concentration data for the last 4 days are available but not plotted owing to a computer malfunction.

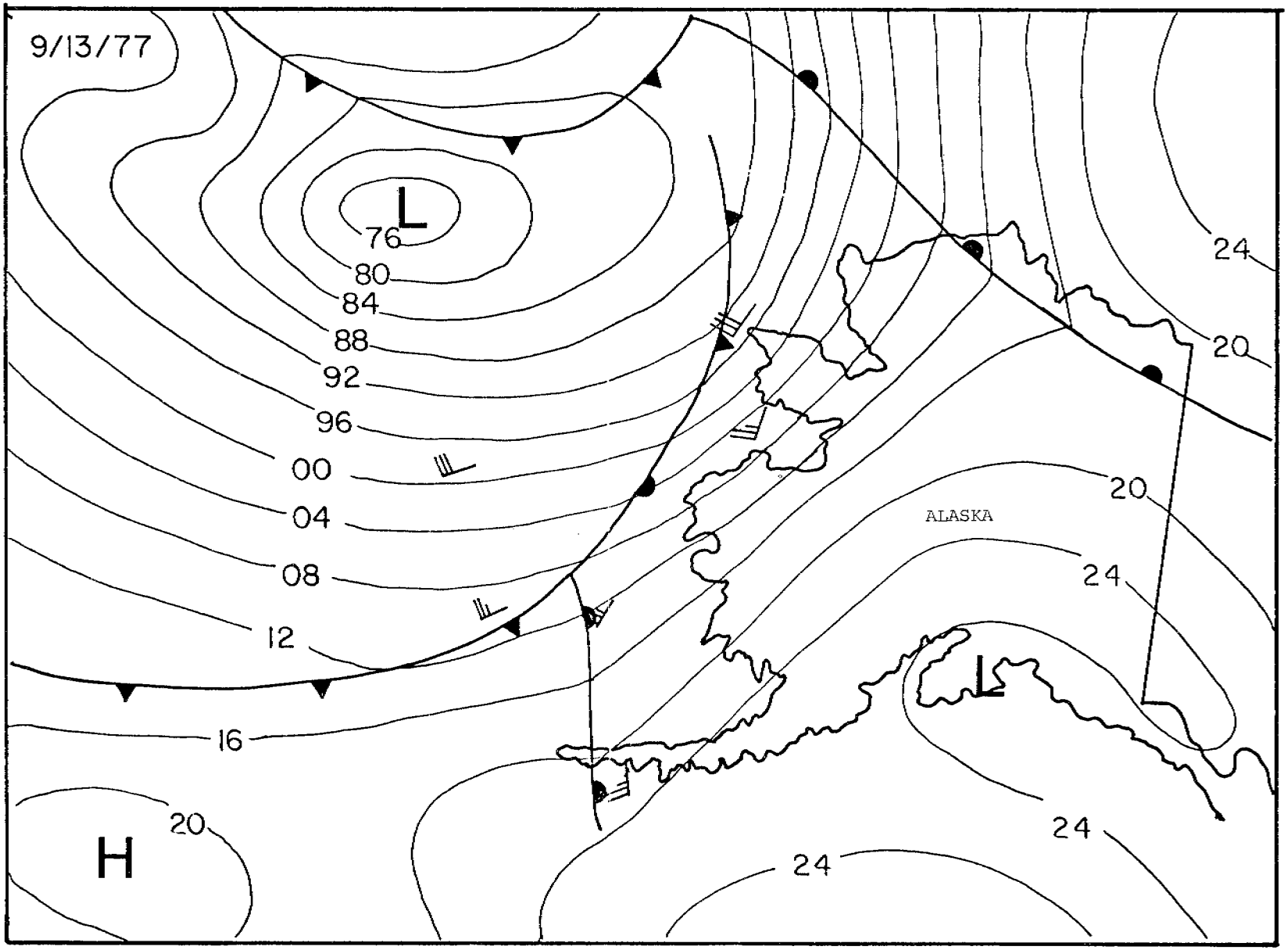

Figure 25. Surface pressure analysis for September 14, 1977 copied from a weather facsimile chart at the National Weather Service office in Nome, Alaska.

VII. DISCUSSION

A. Transport pathways of suspended matter

Three transport pathways are important in the dispersal of terrigenous silt and clay delivered by the Yukon River:

1. initial transport (during the summer months at least) is characterized by westerly and southerly flow within 20 km of the Yukon Delta. Turbid water commonly extends south to Cape Romanzof and on 29 June 1977, a NOAA satellite image suggests transport as far south as Hazen Bay. This transport pattern, evident on satellite images, is rather surprising because one would expect that the density distribution would generate currents to the north and east around the delta front (owing to Coriolis effect). We suspect that the observed current is the result of entrainment of nearshore water by the Alaskan coastal current as it flows northward past Cape Romanzof. W. Dupre (RU 208) has found that embayments to the south of the major Yukon River distributaries contain large amounts of modern Yukon silt. This finding provides independent evidence to support the importance of southward nearshore flow.

2. The suspended matter that is moved southward along the west shore of the delta either accumulates in "low energy" lagoons and bays or returns within the Alaskan Coastal Current. Our studies, the studies of Muench et al. (1977), and a large body of data collected over the years by L. Coachman and his associates (Univ. of Washington) demonstrate a nearly "unidirectional" flow of shelf water northward between the mainland and St. Lawrence Island. This flow is driven by the difference in sea level between the Bering Sea and the Arctic Ocean and the need to replace water lost from the Arctic Ocean to the Atlantic Ocean.

   As this current, the Alaska Coastal Current, flows past Norton Sound it tends to mix with the turbid Yukon water in the vicinity of the delta. This mixed water then extends across the mouth of the Sound toward the Nome coast (Figs. 6 and 7). There is no question that the currents immediately N and NW of the delta are complex. Nevertheless, the distributions of both surface and near bottom suspended matter demonstrate the existence of this important northward transport pathway. Muench et al. (1977) have postulated a mean circulation system that is dominated by a cyclonic gyre centered in the outer portion of the Sound north of the delta. In order to obtain agreement between our results and this circulation pattern, it is necessary to postulate a split in the northward flow near the Yukon delta with part of the water moving directly across the Sound and another part moving into the Sound to feed the cyclonic gyre.

   Obviously, more long-term current measurements are needed to fully describe the flow field in Norton Sound.

3. Bottom sediments in the inner part of Norton Sound are clearly derived from the modern Yukon River (Nelson and Creager, 1977). In fact, accumulation rates of mud in this area (east of Cape Darby - Stuart Island) are among the highest on the northern Bering Sea shelf. Suspended matter distributions in 1977 and also in 1976 (Cacchione and Drake, 1977) suggest transport of Yukon silt and clay eastward past Stuart Island. However, the available data do not support a strong interchange of water between the inner and outer parts of Norton Sound (Muench et al., 1977; Drake et al., 1977). Satellite images tend to show a steep gradient decrease in TSM at the surface near Stuart Island such that the bulk of the suspended matter is confined to Pastol Bay (west of Stuart Island).

   The effects of wind stress on the circulation in the Sound are not well understood but it seems likely that periods of strong westerlies (which are common in the summer) would drive surface water eastward along the southern coast and into the inner Sound. West and southwest winds exceeding 15 knots occur on about 3-4 days during each of the summer months (based on weather records at Nome); winds come from the southwest quadrant approximately 40% of the time. It is possible that flow into the inner Sound occurs whenever the wind stress is sufficient to overcome the effects of other forcing mechanisms.

   It is safe to say that the transport of suspended matter eastward from the delta is not as important as other transport pathways. However, the sediment that is carried into the inner part of Norton Sound tends to remain there. We believe that key factors in this sediment retention are the low energy of bottom currents in this area and the limited exchange of bottom water with the outer Sound (as shown by the presence of remnant, winter bottom water well into the ice-free season). Of these two factors we suspect that the latter is the more significant because TSM concentrations in the remnant water are relatively high indicating that this water, although isolated, is not motionless. Current data collected by R. Muench within the postulated remnant water body southwest of Cape Darby (Fig. 2) show tidal currents of up to 30-40 cm/s but essentially no net motion. It seems likely that a similar but less vigorous current regime also would characterize the bottom water within the inner Sound.

B. Comparison of 1976 and 1977 Results

Suspended sediment distributions on many continental shelves exhibit a large degree of spatial and temporal variability. It is probable that much of the variability is caused by wind-driven transport combined with variable rates of fine sediment resuspension by wave action.

The data for Norton Sound in late summer of 1976 and early summer of 1977 reveal strikingly similar suspended sediment patterns (see Cacchione and Drake, annual OCSEAP report April, 1977). In both cases the distributions at the surface and near the bottom are dominated by a tongue of turbid water

that originates along the western side of the Yukon Delta and extends across the mouth of Norton Sound toward Bering Strait. Temperature and salinity values show that this water is a mixture of Alaska Coastal Current water and Yukon River water.

These results along with the GEOPROBE measurements indicate that current patterns and speeds in the outer portion of the Sound are caused principally by the tides and the regional transport of Bering Sea shelf water toward the Chukchi Sea. In particular, it appears that the regional flow establishes, to a large degree, the mean circulation pattern in the Sound whereas the relatively strong tidal currents (primarily constrained to flow E-W) serve to maintain particles in suspension and also resuspend materials at times of spring tides. Tidal excursions are approximately 4 to 5 km with only a small net motion. Consequently, they act as a diffusing element. The "clarity" of the observed suspended matter distributions (ie. the sharpness of boundaries between clear and turbid waters) suggests the importance and consistency of the regional advective flow regime.

The situation is different in the inner portion of Norton Sound (east of Cape Darby and Stuart Island). Here the suspended matter distribution tends toward greater uniformity, particularly in September 1976. This suggests that tidal and wind-driven currents are more significant compared to advection. As discussed above, the inner portion of Norton Sound is strongly two-layered and the lower layer is water formed during the winter months. Substantial advective motion must be restricted to the low density surface layer and vertical mixing clearly must be minimal across the pycnocline (Muench et al., 1977).

The eastern part of Norton Sound is, in effect, an excellent sediment trap. We suspect that the only reason it is not collecting Yukon River mud more rapidly is that the circulation system near the delta diverts the bulk of the sediment to other areas.

VII. DISCUSSION

C. Temporal variability

The GEOPROBE tripod data provide a valuable time history of near-bottom measurements of fluid and sediment parameters at site G1 (Fig. 2) for the 80 day deployment period. A complete listing and plot of all data was not included because of the large volume of numbers that are generated by one GEOPROBE station tape. Only the most pertinent information is given in section VI.

One of the most significant results is the contrast in the local dynamic conditions that occurs during "normal" and stormy periods. The "normal" near-bottom flow field at G1 is characterized by the data shown in Figures 21 and 22 for the period July 8 - July 24. During this time tidal forcing dominates the hourly mean values of pressure, bottom current, temperature and turbidity. Small perturbations in the tidally-dominated "normal" regime occur, principally due to short periods of increased wind-driven currents and waves.

The tidal bottom currents are most intense during spring tides, commonly achieving values of greater than 30 cm/sec at 1 m above the sea floor. During neap, the daily maximum currents at 1 m are much reduced, typically less than 15 cm/sec during the smallest tides. As Figure 22 shows, the bottom pressure has a definite change in pattern during the fortnightly cycle. The spring tides are strongly mixed with two unequal highs during each daily cycle; the neaps are more nearly a diurnal type.

Figures 23 and 24 point out the extreme importance of storm conditions in affecting the sediment transport pattern in this area. The relatively high, sustained values of hourly-averaged bottom current speed and the persistent northward directions are indicative of active, large transport of materials. These wind-generated events appear to overwhelm the rythmic pattern that is the "normal" condition.

In terms of evaluating the fluid motion at the sea floor for its effect in the transport of sediments, two of the most critical parameters are shear velocity, u_*, and bed roughness, z_o, where

$$u_* = \tau o/\rho \; ; \qquad (1)$$

τo is the bottom shear stress
ρ is fluid density

and z_o is the roughness length in the Karman-Prandtl turbulent boundary layer equation

$$u/u_* = \frac{1}{k} \ln \left(\frac{z + z_o}{z_o} \right), \qquad (2)$$

u is the velocity at a distance z above the bed; k ~0.4 is von Karman's constant.

To compute u_* and z_o from equation (2) u can be measured at several levels (z) above the bed. If more than two levels are used then the validity of equation (2) can also be estimated. Since the 4 GEOPROBE e-m current sensors are operated within the bottom tidal boundary layer, these measurements afford a unique data set to derive u_* and z_o values. Figure 26 shows examples of the hourly current speed profiles obtained during neap, spring, and storm conditions. The maximum values

of u_* and the maximum speed at 1 m are highest during the storm; spring tide values are significantly greater than during neap.

The threshold value of u_* to initiate movement of non-cohesive sediment can be estimated from the modified Shields Diagram (Madsen and Grant, 1976), even when the flow is unsteady. The critical, or threshold, value of u_* for the mean particle size of 0.07 mm at site G1 is 1.3 cm/sec. This value, together with u_* values in Figure 26 suggest that incipient sediment motion in the vicinity of site G1, occurs during storms and spring tides. The added effects of organic materials (cohesive) and finer-grained sediments (<62μ) are not well understood; Jumars (1977) and Southard (1977) have discussed these problems with regard to sediment transport and pointed out the poor state of knowledge in this area. Possibly the binding caused by mucoid surface materials explains the patchiness of the sediment ripples throughout the central western Norton Sound area. Also, the high silt content would tend to inhibit ripple formation and transport in these bedforms.

Another important part of the overall transport pattern in this region is demonstrated by Figure 27. Daily average values of u_* and z_o were computed by first taking averages of u at each level over consecutive 24 hour periods. These new daily-averaged values of u, called <u>, were then used in equation (2) to derive daily averaged values of u_* and z_o, which are shown in Figure 27. Throughout the 80 day period, all vertical profiles of <u> fit a logrithmic curve to within 2%. The maximum standard error of estimate of any single value of <u> that derives from using the logrithmic profile is 0.03 cm/sec (an incredible result!).

Figure 27 clearly shows the effect of the fortnightly tidal cycle on shear velocity. The dashed line is the estimated critical value of u_* of 1.3 cm/sec. During times of peak spring tides, u_* exceeds or equals the critical value. Storm periods during September generate the highest shears. The relatively small change in z_o, even during the storm period is interesting and somewhat surprising.

The above discussion did not directly assess the effects of surface waves. Obviously, during times of high winds, the larger waves would be expected to contribute a substantial increase to the instantaneous bed shear stress. In Section VI examples of the wave-induced currents were shown (Fig. 12-20). The added stress from these waves will produce local resuspension when the combined wave-induced and lower frequency components cause u_* to exceed the critical value. In a water depth of about 20 m, waves of 0.5 m in height with periods of 6 sec, typical of this area over normal conditions, produce maximum wave-induced bottom currents of about 7-8 cm/sec. The bottom stresses contributed by these normal wave conditions, when combined with spring tidal currents certainly would produce initial motion and resuspension of bottom sediment.

As a final part in this discussion, it appears that there exists a relatively thin bottom layer of high concentrations of suspended sediment whose total concentration and thickness waxes and wanes with the tidal cycles. This dense cloud of suspended materials apparently thickens to above 2 m during peak spring tides and during storms, and thins to about 1 m or less during neaps. Bottom photographs from the GEOPROBE system show evidence for this turbid bottom layer at site G1. This layer should produce lower values of eddy viscosity due to the turbulence-damping effects of high suspended loads, probably altering the values of u_* (Smith and McLean, 1977). These effects will have significant implications for regional numerical models of the circulation.

Figure 26. Current speed, u, in cm/sec measured at 4 levels with the electromagnetic current sensors plotted against the natural logarithm of distance above the sea floor (ln z) at different times during the 80 day period, 8 July - 27 September 1977 in Norton Sound, Alaska. Maximum values of shear velocity, u_*, are shown.

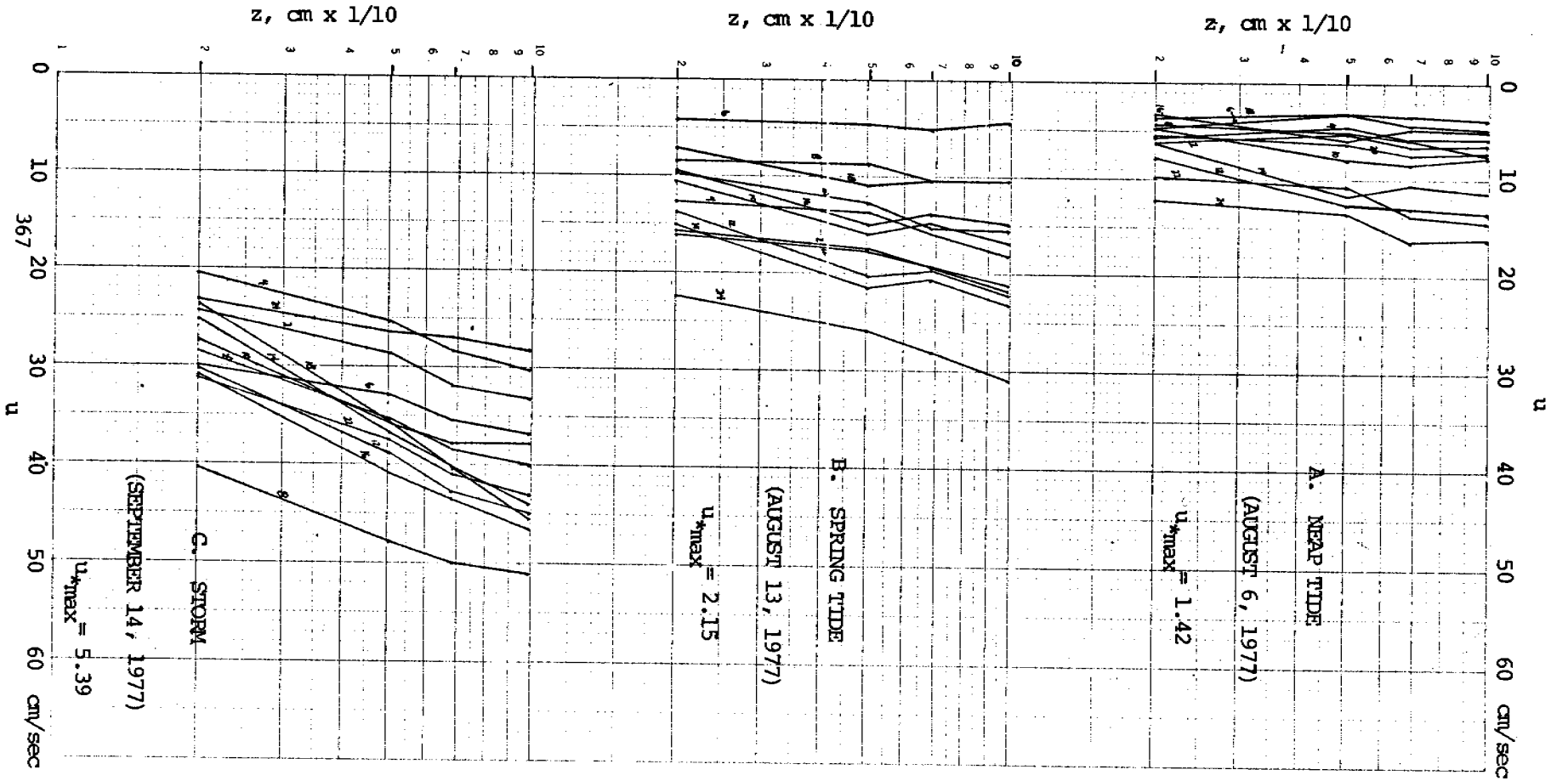

Figure 27. Daily values (averages) of shear velocity (u_*), bed roughness (z_o), and sediment flux (Flux) derived from GEOPROBE data taken at site G1 during the 80 day period, 8 July - 27 September, 1977. Sediment flux is computed from

$$\text{Flux} = \vec{u}\,(100)\cdot C$$

where $\vec{u}$ is the daily averaged velocity in cm/sec at 100 cm above the bed and C is daily averaged concentration in mg/l at about that level. The "stick" points in the direction of flux and the length of the "stick" gives the amount of flux.

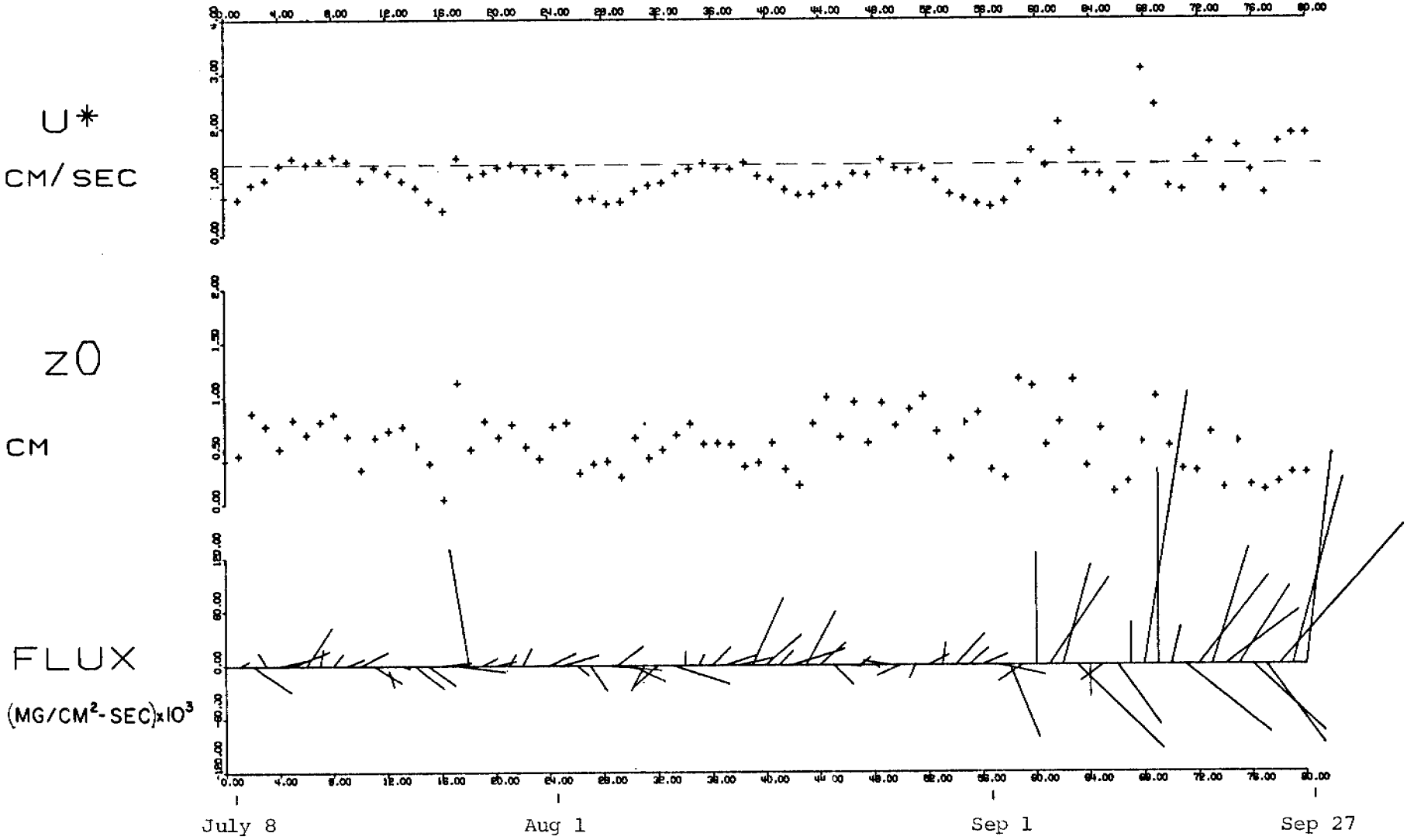

VIII. CONCLUSIONS

A. Suspended sediment transport

1. Satellite images and photographs show that the major distributary of the Yukon River discharges sediment near the southern boundary of the modern delta complex. Of the two other distributaries, the one which enters Pastol Bay in Norton Sound appears to transport the least amount of water and sediment (W. Dupre, personal communication, 1977). In effect, the initial discharge of Yukon River sediment is not directed into Norton Sound but occurs some 60-70 km to the south along a section of the coast that is relatively unprotected. This fact combined with the relative lack of highly cohesive clay particles in the Yukon material probably accounts for the absence of major mud deposits near the southern Yukon distributary.

2. Nearshore currents (within ~20 km of the shore) tend to flow toward the west and south around the front of the Yukon Delta based on studies of LANDSAT data. The mechanism that causes this flow is not known but it is evident that fine particles are transported as far south as Cape Romanzof and, at times, as far as Hooper and Hazen Bays. It should be noted that littoral sediment transport along the delta shore is probably directed toward the north in response to long period waves from the southwest. Consequently, the form of the delta reflects the transport and deposition of littoral sand and coarse silt.

3. Seaward of the southward nearshore flow, the current reverses to northerly within the Alaskan Coastal Current. Satellite images clearly reveal broad, elongated plumes of suspended matter trending northward from the vicinity of Cape Romanzof. A substantial amount of fine-grained Yukon Sediment from the two major distributaries on the western side of the delta makes a journey of some 150 km south only to return to the mouth of Norton Sound via the Alaska Coastal Current.

4. This mixture of Yukon and Alaska Coastal Current water in turn mixes with turbid water to the northwest of the delta and then continues across the mouth of Norton Sound. The result is pronounced surface and near bottom plumes of suspended silt and clay. The location of this transport pathway coincides exactly with the distribution of modern Yukon prodelta deposits (McManus et al., 1977).

5. During deployment of GEOPROBE I, located in the path of the suspended sediment plume, concentrations of TSM near the bottom were 4.4 to 4.6 mg/l. The GEOPROBE nephelometer data show that concentrations remained at approximately the same level during the entire summer except during storms. This evidence suggests that the plume is a consistent feature of the sediment transport system (see Figs. 3 and 4).

6. Storm-generated currents and waves produce tremendous increases in the amount of suspended sediment within 2 m of the sea floor and in the magnitude of the sediment flux. Combined wave and wind-driven currents exceeded 70 cm/sec at 1 m above the bottom during a storm in September 1977. Concentrations during this period were at least 20 times higher than concentrations prior to the storm

and net water transport northward increased by a factor of about 10. Thus, the amount of sediment moved in suspension during one day of the storm exceeded the transport that had occurred during the preceeding 3 months of fairweather. A thorough analysis of this storm and several lesser events in 1977 is in progress. At this point it is safe to conclude that storms play a major role in the transport and deposition of sediment in the northern Bering Sea.

7. Bottom waters in the eastern portion of Norton Sound and in the shallow trough in the north-central part of the area appear to be remnant from the winter season. The preservation of this anomalously dense water well into the summer demonstrates that there is a limited exchange of subsurface water between the outer and inner portions of the Sound. Suspended matter which settles into this water body would be trapped and most likely deposited during slack tide periods. The remnant winter water was present only in the eastern cul-de-sac (east of Cape Darby and Stuart Island) in September-October 1976. This portion of Norton Sound is floored by a relatively thick accumulation of fine silt and clay derived from the Yukon River.

B. Temporal sediment dynamics (GEOPROBE data)

The GEOPROBE system deployed about 50 km south of Nome produced 80 consecutive days of time-series data on bottom currents, pressure, temperature, light transmission and light scattering. Analyses of these data show the following features:

1. During periods of increased surface wind stress, especially during the storm of September 13-14, 1977, bottom currents as high as 70 cm/sec generated instantaneous shear velocities (u_*) in excess of 6 cm/sec (equivalent to a shear stress of about 40 dynes/cm^2. Storm-driven currents, waves, tides and mean flow all contributed to this large bottom stress. These shear velocities exceed the critical values of 1.3 cm/sec by amounts that are extremely significant. Bedload transport rates for non-cohesive sediments are generally proportional to the third-power of the shear velocity.

2. Daily and fortnightly tidal stresses both regulate the "average" character of the sea floor. Spring tides commonly cause bottom stresses that reach or exceed the estimated critical values. During neap, these stresses are significantly lower. This result, together with photographs of the bottom bottom at site G1, suggests that a tidally maintained bottom layer of suspended materials thickens and thins with the spring and neap cycle.

3. Large surface waves, generated in the deeper water of southern Bering Sea refract into the western Norton Sound area, generating abnormally large bottom stresses. Waves with heights of 1.5-2m and periods of 9-11 seconds were measured during the September stormy period. Wave-induced bottom currents as high as 40 cm/sec were recorded.

IX. NEEDS FOR FURTHER STUDY

Sediment transport studies must include a sufficient number of long-term measurements of both current and sediment parameters. The observational periods should be long enough to properly evaluate infrequent events and sampling rates should be adequate to study high frequency mechanisms such as surface waves. Furthermore, most shelf processes tend to vary seasonally and, therefore, a full year of data is needed. In short, future studies of sediment transport in the Norton Sound area should emphasize current meter and light scattering measurements at perhaps 8 to 10 mooring sites.

A second problem is the present lack of data on the sediment discharge of the Yukon River. Most researchers use Lisitzin's estimate of 100×10^6 tons but this may be in error by 30-40 million tons. This uncertainty makes sediment budget calculations impossible.

Finally, additional studies of the remnant water in Norton Sound should be undertaken. These should focus on the dynamics of this water body and the possibility that storms may flush the layer out or at least cause significant mixing.

X. 4th QUARTER OPERATIONS

During February 18 to March 5, Dave Drake, Chuck Totman and Pat Wiberg were in Nome, Alaska to carry out winter season sampling of the Norton Sound area in cooperation with Knut Aagaard of the University of Washington. Although the field program began slowly owing to equipment problems and bad flying weather, the final 10 days in the area produced excellent results.

A total of 95 water and ice samples were recovered from 38 stations in the outer part of Norton Sound and along the southwestern coast of Seward Peninsula (table 3). These samples were filtered through preweighed Nuclepore filters at the end of each day. Twelve light transmission profiles were obtained before it was decided to curtail that part of the program in order to lighten the load in the helicopter and achieve a better equipment/fuel ratio. It was felt that the amount of lost information was not critical because the light transmission profiles showed that the water column was well mixed with no significant stratification of suspended matter.

The membrane filters have been reweighed in Menlo Park and we have begun to analyze the particulate matter. Preliminary results, based on field observations and initial sample analysis, are as follows:

1. the prevailing winds and the storm winds at Nome are from the north and east and, rarely, from the southeast during the winter. The result is a nearly continuous drift of ice from the inner Sound to the west and southwest. Consequently, thick ice is essentially lacking east of Cape Darby and we could not sample that area.

2. ice slabs containing "zones" or layers that were discolored by sediments were common at all locations in outer Norton Sound but especially north of the Yukon Delta. Samples of this turbid ice show sediment concentrations of up to 1 gram/liter whereas the "clean" ice contained a few milligrams/liter of particulate matter. The appearance of the sediment-rich ice did not suggest adfreezing of bottom sediment but rather incorporation of suspended matter within forming ice layers (at the base of the floating ice "pancakes"). If this is correct, the addition of these layers to the ice must have occurred in shallow water close to a major source of sediment. The fact that "dirty ice" was present throughout the outer Sound and off Port Clarence shows that the ice motion is significant.

3. Suspended sediment concentrations in the water column ranged from about 1 mg/liter to over 8 mg/liter. The highest concentrations were present at stations closest to the Yukon Delta. A preliminary comparison of these values with data collected in July 1977 shows only a small decrease in the winter. Analyses are underway to determine the composition of the suspended matter. However, at this point, it appears that sediment transport is substantial in Norton Sound with or without an ice cover.

4. the suspended matter concentrations in the winter and the evidence of significant ice movement by wind and currents suggest that the

tidal and mean currents are capable of resuspending bottom sediments (since there is virtually no sediment coming from the Yukon River after November) and causing significant transport.

5. observations in the field indicated that the area north and northwest of the Yukon delta is a convergence zone where the ice is highly fractured and pressure ridging seemed more intense.

   Presumably some of this ice grounds on the sea floor around the delta each year under the nearly constant forcing of the prevailing north and northeasterly winds. Nelson and Thor (RU 429) have found that ice gouges are common along the front of the Yukon Delta.

During the 4th quarter we have continued our analysis of GEOPROBE data from 1976 and 1977. We have emphasized the 80 day record obtained in 1977 and most of the results of this work are presented in this report.

The journal MARINE GEOLOGY has accepted our paper discussion the GEOPROBE system; a preprint of this article is appended. In addition, we expect to submit two papers for publication within the next few months. One will present an in-depth analysis of our GEOPROBE boundary layer measurements with special attention to the 1977 storm. The second will discuss regional patterns of water motion and sediment transport with particular emphasis on suspended matter transport and the fate of Yukon River detritus. Additional journal articles will be prepared as our data and laboratory analyses continue.

Table 3.

NORTON 1978

Winter Project

Station	Lat.	Long.	Depth	Sample Depths	Conc. (mg/l)
1	64°25.7	165.18.6	22 m	3 m	1.35
				15 m	1.60
2	64°22.0	165°16.2	31 m	3 m	2.54
				25 m	1.87
3	64°17.2	165°14.5	22.5 m	5 m	3.44
4	64°10.9	165°12.1	17.5 m	15 m	4.34
5	64°4.0	165°9.9	17.5 m	3 m	3.69
6	63°55.2	165°6.5	17.5 m	3 m	3.65
7	63°45.2	165°3.2	17.5 m	3 m	5.79
				Ice Chunk	1791.0
8	63°40.9	164°57.0	17.6 m	3 m	5.90
				14 m	6.14
9	64°18.2	164°3.0	16.5 m	3 m	1.52
				8 m	1.50
10	64°12.7	163°53.3	18.5 m	3 m	2.01
11	63°57.2	166°57.7		4 m	1.88
12	63°57.9	166°36.6	33 m	5 m	2.29
				SFC Slush	347.64
				Ice Sample	7.7
13	64°00.8	166°11.4		3 m	1.71
				11 m	1.66
14	65°2.0	165°42.5	21 m	3 m	2.19
				19 m	2.06
15	64°1.9	165°26.9	19.65 m	2.5 m	2.14
				9.5 m	2.30
				18.5 m	2.41
16	64°04.2	165°10.0	18.8 m	3 m	2.18
				8.75 m	2.66
				17.75 m	2.89
17	64°4.9	165°52.1	19 m	3 m	3.29
				9 m	2.99
				18 m	3.30
18	64°5.9	164°33.5	20.8 m	3 m	3.24
				19.8 m	3.15
				Ice Sample	9.77
19	64°7.1	164°7.6	22.2 m	3 m	2.65
				21.2 m	3.99

Table 3. (cont'd)

NORTON 1978

Winter Project

Station	Lat.	Long.	Depth	Sample Depths	Conc. (mg/l)
20	64°36.1	166°32.0	20.5 m	2.5 m	1.89
				10 m	2.04
				19 m	2.18
21	64°32.8	166°49.1	27.5	2.5 m	2.15
				26.5 m	1.94
22	64°29.3	167°9.5	28-30 m	27-28 m	1.99
				SFC Slush	27.1
23	64°25.1	167°26.9	30 m	3 m	1.35
				29 m	1.43
				Ice Chunk	965.5
24	63°27'	166°51.5'	27 m	3 m	1.35
				26 m	1.39
				Ice	6.0
25	63°31.4'	167°12.7'	27 m	3 m	1.52
				26 m	1.85
				Ice	159.9
26	63°31.7'	167°35'	29.5 m	3 m	2.01
				28.5 m	2.07
				Ice	94.9
27	64°54.1'	168°11.7'	40.3 m	3 m	1.50
				39.3 m	1.68
				Ice	120.6
28	64°59.2'	167°53.8'	43 m	3 m	1.44
				42 m	2.22
				Ice	3.80
29	65°1.9'	167°36.5'	46 m	3 m	1.24
				45 m	1.32
				Ice	9.35
30	65°5.3'	167°19.7'	21 m	3 m	1.17
				20 m	1.27
				Ice	2.31
31	64°1.0'	164°12.0'	21 m	3 m	2.35
				20 m	2.76
				Ice	5.62
32	63°53.2'	164°10.9'	17.5 m	3 m	3.48
				16.5 m	3.93
33	63°48.8'	164°25.3'	18 m	2.5 m	4.44
				16.5 m	5.91

Table 3. (cont'd)

NORTON 1978

Winter Project

Station	Lat.	Long.	Depth	Sample Depths	Conc. (mg/l)
34	63°37.7'	164°22.2'	13.3 m	3 m	8.37
				12.3	8.44
35	63°34.8'	164°5.7'	13 m	3 m	8.00
				12 m	7.98
				Ice	9.90
36	63°38.8'	163°46.4'	15 m	3 m	4.24
				14 m	5.30
				Ice	9.30
37	63°40.3'	163°34.8'	15 m	3 m	2.59
				14 m	3.03
				Ice	9.66
38	64°28.1'	166°1.5'	21 m	3 m	2.06
				20 m	1.78
39	64°22.4'	166°13.9'	(CTD only)		

REFERENCES

Butman, B., 1976, Sediment transport on east coast continental shelves: Proc. of NSF/IDOE workshop, Vail, Colorado.

Cacchione, D. A. and Drake, D. E., 1977, Sediment transport in Norton Sound, northern Bering Sea, Alaska: Annual Report to NOAA/OCSEAP, Juneau, Alaska, 19 p.

Coachman, L. K., Aagaard, K., and Tripp, R. B., 1976, Bering Strait, the regional physical oceanography: Seattle, Univ. of Washington Press, 186 p.

Drake, D. E., Kolpack, R. L., and Fischer, P. J., 1972, Sediment transport on the Ventura-Oxnard Shelf, California; in Swift, D. J. P., Duane, D. B., and Pilkey, O. H., eds., Shelf sediment transport; process and pattern: Stroudsburg, Pa., Dowden, Hutchinson and Ross, Inc., p. 307-331.

Drake, D. E., Cacchione, D. A., and Muench, R., 1977, Movement of suspended and bottom sediment in Norton Sound, Alaska, (abs.): Geol. Soc. Amer. Abstracts with Programs, 9(7), p. 956.

Gust, G. and Walger, E., 1976, The influence of suspended cohesive sediments on boundary-layer structure and erosive activity of turbulent seawater flow: Marine Geology, 22, p. 189-206.

Jumars, P., 1977, Sediment flux and animal foraging patterns, (abs.): Trans. Amer. Geophys. Union, 58(12), p. 1161.

Madsen, O. S. and Grant, W. D., 1976, Sediment transport in the coastal environment: Tech. Report 209, Ralph M. Parsons Laboratory for Water Resources and Hydrodynamics, Mass. Inst. of Technology, 105 p.

McManus, D. A., Kolla, V., Hopkins, D. M., and Nelson, C. H., 1974, Yukon River sediment of the northernmost Bering Sea shelf: Jour. Sed. Petrol., 44, p. 1052-1060.

McManus, D. A., Kolla, V., Hopkins, D. M., and Nelson, C. H., 1977, Distribution of bottom sediments on the continental shelf, northern Bering Sea: U.S. Geological Survey Prof. Paper 759-C, 31 p.

Muench, R. D., Charnell, R. L., and Coachman, L. K., 1977, Oceanography of Norton Sound, Alaska: September-October 1976: Tech. Report, Pacific Marine Environmental Lab., NOAA, Seattle, 18 p.

Nelson, C. H. and Creager, J. S., 1977, Displacement of Yukon-sediment from Bering Sea to Chukchi Sea during Holocene time: Geology, 5, p. 141-146.

Nelson, C. H., 1977, Faulting, sediment instability, erosion, and deposition hazards of the Norton Basin sea floor: Annual Report to NOAA/OCSEAP, Juneau, Alaska, 129 p.

Nelson, C. H., 1978, Faulting, sediment instability, erosion, and deposition hazards of the Norton Basin sea floor: Annual report to NOAA/OCSEAP, Juneau, Alaska (unpublished).

Smith, J. D. and Hopkins, T. S., 1972, Sediment transport on the continental shelf off of Washington and Oregon in the light of recent current measurements, in Swift, D. J. P., Duane, D. B., and Pilkey, O. H., eds., Shelf sediment transport; process and pattern: Stroudsburg, Pa., Dowden, Hutchinson and Ross, Inc., p. 143-180.

Smith, J. D. and McLean, S. R., 1977, Boundary layer adjustments to bottom topography and suspended sediment; in Nihoul, J. C. J., ed., Bottom turbulence: New York, Elsevier Scientific Publishing Company, 306 p.

Southard, J. B., 1977, Erosion and transport of fine cohesive marine sediments, (abs.): Trans. Amer. Geophys. Union, 58(12), p. 1161.

A P P E N D I X A

Cruise Data Summary

Norton Sound - July 7-12, 1977

CRUISE REPORT

OF THE
BRANCH OF MARINE GEOLOGY
U.S. GEOLOGICAL SURVEY, MENLO PARK, CA

FOR

CRUISE -S4-77-BS-

GENERAL CRUISE INFORMATION

AREA: BERING SEA NORTON SOUND, NORTHERN BERING

SHIP: R/V SEA SOUNDER

CHIEF SCIENTIST(S): DAVE CACCHIONE / DAVE DRAKE

TYPE OF DATA
COLLECTED: GEOPHYSICAL , GEOLOGICAL , HYDROGRAPHIC

CRUISE DATES:	LOCAL DATE/TIME*	TIME(JD/GMT)	PORT
START CRUISE:	7 JUL 7 0 HRS	188/18 0	LEAVE NOME AK, STRT CRUZ
END CRUISE:	12 JUL 14 2 HRS	194/ 1 2	AR NOME AK, END CRUISE

* EXPRESSED IN LOCAL STANDARD TIME.

	HOURS	DAYS & HOURS
TOTAL UNDERWAY TIME:	127	5 DAYS 7 HRS

PERSONNEL LIST

NAME	AFFIL	DUTIES	ABOARD	ASHORE
D. CACCHIONE ON BOARD	UGS	CHIEF SCIENTST	185/22 0	198/19 0
P. WIBERG ON BOARD	UGS	DAFE CURATOR	185/22 0	198/19 0
D. DRAKE ON	UGS	GEOLOGIST	185/22 0	
D. THOR	UGS	GEOLOGIST	185/22 0	
H. NELSON ON	UGS	GEOLOGIST	194/24 0	
M. FIELD ON	UGS	GEOLOGIST	194/24 0	
J. JOHNSON NOAA SEATTLE	UGS	GEOPHYSICIST	185/22 0	
B. MUENCH	UGS	OCEANOGRAPHER	187/22 0	194/23 0
J. SALADIN	UGS	ELECTRONICS T	185/22 0	
J. NICHOLSON	UGS	ELECTRONICS T	185/22 0	
J. HASLETT	UGS	ELECTRONICS T	187/22 0	194/23 0
B. WILSON	UGS	MECHANICAL T	185/22 0	
H. GIBBONS	UGS	WATCH STANDER	185/22 0	
G. TATE	UGS	WATCH STANDER	185/22 0	194/23 0

B. RICHMOND	UGS	WATCH STANDER	185/22 0	198/19 0
C. TOTMAN	UGS	WATCH STANDER	185/22 0	
J. WHITNEY ON	UGS	WATCH STANDER	194/24 0	
E. CLUKEY	UGS	UNSP INVESTIGATR	185/22 0	

EQUIPMENT SYSTEMS USED

NAVIGATIONAL	GEOPHYSICAL	GEOLOGICAL	HYDROGRAPHICAL
MINIRANGER	UNIBOOM	BOX(SHIP) CORE	VAN DORN BOTTLE
INTEGRATED NAV	SIDE SCAN SONAR	TELEVISION	TRANSMISSOMETER
	3.5KH BATHYMETRY		TEMP/SALINOMETER
	12KH BATHYMETRY		EXP BATHY THERMO
	SHIPBOARD GRAVTY		AND CURRENT METR
	DIGITRACK		HYD CURRENT METR
			MAR CURRENT METR
			BEN CURRENT METR
			GEOPROBE

DATA COLLECTED

GEOPHYSICAL

DATA TYPE OR SYSTEM	RECORDING MEDIUM	TRACKLINE KILOMETERS	TRACKLINE N. MILES	RECORDING TIME(HRS)	ROLL/REEL LIST QTY
UNIBOOM	ANL PAPER ROLL	70.4	38.0	4.2	2
SIDE SCAN SONAR	ANL PAPER ROLL	41.6	22.4	4.1	3
3.5KH BATHYMETRY	ANL PAPER ROLL	1039.8	561.5	62.9	5
12KH BATHYMETRY	ANL PAPER ROLL	1025.7	553.9	61.8	8
BATHYMETRY + NAV	DIGIT MAG TAPE	1055.2	569.7	134.3	2
	PRINTR LISTING	335.9	181.4	134.6	2
SHIPBOARD GRAVTY	DIGIT MAG TAPE	1090.8	589.0	83.3	5
	PRINTR LISTING	0.0	0.0	0.0	1
	ANL PAPER ROLL	1084.0	585.3	83.1	3

GEOLOGICAL/HYDROLOGICAL SAMPLES

SAMPLING DEVICE	SAMPLING ATTEMPTS	SAMPLES RECOVERED	NUMBER OF SAMPLES FROM A GIVEN WATER DEPTH INTERVAL 0-100M	100-3000M	≥3000M
BOX(SHIP) CORE	8	6	6	0	0
VAN DORN BOTTLE	26	26	26	0	0
WATER BUCKET	24	24	24	0	0
EXP BATHY THERMO	22	20	20	0	0
CTD METER	23	23	23	0	0

TOTALS	103	99	99	0	0

GEOLOGICAL/HYDROLOGICAL (ANALOG)

DATA TYPE OR SYSTEM	RECORDING MEDIUM	RECORDING TIME (HRS)	NUMBER OF TAPES, ROLLS, LISTS, ETC.
TELEVISION	ANLOG MAG TAPE	1.5	2
SEAFLOOR CAMERA	PHOTOGRAPH	0.0	2
TRANSMISSOMETER	DIGIT MAG TAPE	0.0	1
NEPHELOMETER	DIGIT MAG TAPE	0.0	1
BEN CURRENT METR	DIGIT MAG TAPE	0.0	1
MAR CURRENT METR	DIGIT MAG TAPE	0.0	1
TEMP/SALINOMETER	ANL PAPER ROLL	77.0	1
CTD METER	DIGIT MAG TAPE	0.0	1

NUMERICAL OBSERVATION

DATA TYPE OR SYSTEM	NUMBER OF READINGS	TAKEN OVER HOW MANY STATIONS
PENETROMETER	11	6
TRANSMISSOMETER	26	25
AND CURRENT METR	4	3
HYD CURRENT METR	26	24

NAVIGATIONAL

DATA TYPE OR SYSTEM	RECORDING MEDIUM	NUMBER OF TAPES, ROLLS, LISTS, ETC.
MINIRANGER	PRINTR LISTING	1

OPERATIONS INFORMATION

STATION DATA STATIONS OCCUPIED: 29, TOTAL TIME ON STATION: 60.0 HRS,

TRACKLINES TRACKLINES RUN: 28, TOTAL TRACKLINE TIME: 62.1 HRS,

CUMULATIVE TRACKLINE DISTANCE: 1051.8 KM / 567.9 N. MILES

DEPLOYMENTS

GEOPROBE 1

A P P E N D I X B

A P P E N D I X B

A NEW INSTRUMENT SYSTEM TO INVESTIGATE SEDIMENT DYNAMICS ON CONTINENTAL SHELVES

D. A. CACCHIONE and D. E. DRAKE
U.S. Geological Survey, Menlo Park, CA (U.S.A.)

ABSTRACT

A new instrumented tripod, the GEOPROBE system, has been constructed and used to collect time-series data on physical and geological parameters that are important in bottom sediment dynamics on continental shelves. Simultaneous in situ digital recording of pressure, temperature, light scattering, and light transmission, in combination with current velocity profiles measured with a near-bottom vertical array of electromagnetic current meters, is used to correlate bottom shear generated by a variety of oceanic processes (waves, tides, mean flow, etc.) with incipient movement and resuspension of bottom sediment. A bottom camera system that is activated when current speeds exceed preset threshold values provides a unique method to identify initial sediment motion and bed form development.

Data from a twenty day deployment of the GEOPROBE system in Norton Sound, Alaska, during the period September 24 - October 14, 1977 show that threshold conditions for sediment movement are commonly exceeded, even in calm weather periods, due to the additive effects of tidal currents, mean circulation, and surface waves.

INTRODUCTION

Our ability to understand and eventually to predict the initial and established movements of bottom sediments on continental margins depends largely on our knowledge of how sediments respond to fluid stresses. In shallow marine areas, these bottom stresses are generated by a variety of forcing mechanisms (e.g., tides, wind-driven and density-driven circulations, surface and internal waves, and longshore currents) which vary widely in time and space. The large variability of the stress field is matched by a similarly complex variety of substrate characteristics that directly influence the response of the local sediment to a particular set of stress conditions. As Komar (1976) points out, the simple combination of a mean current and surface waves can produce unexpected and poorly understood sediment transport phenomena.

The need to investigate boundary layer flow and sediment transport conditions concurrently on the shelf has fostered the development of rugged *in situ* measurement systems which can collect geological and oceanographic data for extended periods (Sternberg, et al., 1977; Butman, et al., 1977; and Lavelle et al., 1977). The present paper describes a new instrument system, the Geological Processes Bottom Environmental (GEOPROBE) station, designed for relatively long duration studies of ocean currents and sediment transport within 2 meters of the sea floor. The GEOPROBE system incorporates many of the major features of earlier systems, but has a more complex sampling and digital recording scheme. Preliminary results of our initial experiment in Norton Sound, Alaska are presented to illustrate the performance of the GEOPROBE system.

System Description

The GEOPROBE system is a self-contained, instrumented tripod that is designed to operate on the sea floor for periods of up to 3 months. The system provides *in situ* measurements of hydrodynamic and geological parameters that can be used to interpret the temporal relationships between flow and sediment conditions at bottom sites in water depths of 300 meters or less.

Other *in situ*, self-contained bottom systems (Sternberg, et al., 1973; Lescht, 1977) have been utilized in sediment transport investigations on continental shelves. In all of the previous and contemporary systems a single current meter is used to measure bottom velocity at a fixed location above the sea floor. The GEOPROBE system is unique in that horizontal water current speed and direction are measured simultaneously at four levels within 1 meter of the bottom. From these current data a time-dependent profile of horizontal water velocity can be derived for the flow field very near the sea floor. The temporal variability of bottom stress and the dynamics of the bottom boundary layer can be investigated with these results.

Physical configuration

The GEOPROBE tripod assembly consists of four main components: an upper instrument cage, three legs, three horizontal strength members which join each leg near the base, and three metal-plate footpads (Fig. 1). Stainless steel pipe and plate (Type 304) were used throughout for strength, durability and corrosion resistance. The frame is modular in that the tripod support structure (footpads, legs, and lower strength members) are fitted together and bolted with sleeve and end-butt connections. The entire system can be assembled on the working deck of a research ship at sea. When fully erected, the tripod stands 3 m high and measures about 3.2 m between the base of each

leg. Total weight of the structure in air is about 500 kilograms.

The cylindrical pressure cases and instrument housings are made from either aluminum or stainless steel metal. Sacrificial zinc bars and zinc collars are securely attached to the tripod frame and to the instrument pressure cases to retard corrosion. In addition, the aluminum components have been hard-anodized and coated with epoxy-type paint.

Instruments

The GEOPROBE system employs a variety of sensors that have been integrated into a complex oceanographic measurement system. The sampling scheme is controlled by a master electronics unit that is described in the next section. The individual sensors are summarized in Table 1.

The heart of the flow measurement system consists of four electromagnetic current meters mounted in a vertical array with the uppermost sensor located one meter above the seafloor (Fig. 1). The spacing between these sensors can be varied; however, flow and electromagnetic interference requires a minimum separation between probes of about 15 centimeters. The sensors are arranged in pairs; each pair is supported by three horizontal cables and turnbuckles that are attached to the tripod legs. This support allows for a sturdy, adjustable suspension of the sensors with a minimum of flow disturbance.

Each electromagnetic current sensor consists of a small diameter sphere (~4 cm) that has four protruding electrodes arranged orthogonally around the perimeter. Opposing electrodes sense one component of the flow speed. Current speed, q, is given by

$q = (u^2 + v^2)^{1/2}$ where u and v are the speed components sensed by each pair of opposing electrodes, respectively. Current direction, θ, is given by $\tan \theta = \frac{v}{u}$.

The orientation of the GEOPROBE tripod is obtained from photographs of a Benthos deep-sea compass mounted on the tripod frame. This allows for rotation of the speed components during data reduction to give directions referenced to the earth's magnetic field. The sensors have been calibrated in a recirculating water flume using a laser-doppler velocimeter as the standard. The results of this calibration and performance evaluation were excellent and will be reported elsewhere.

The rotor-vane current meter provides additional current speed and direction data at a level of 1.8 meters above the bottom. It serves as a back-up to the electromagnetic current sensors. The pressure sensor is capable of detecting sea surface fluctuations due to surface waves, tides and other events. The sensor is mounted 2 meters above the sea floor in the lower part of the instrument cage (Fig. 2). Up to two temperature sensors are used to identify local time-dependent water mass changes, as well as to provide information on the thermal gradient above the sea floor. Estimates of the mixing properties within the bottom boundary layer can be derived from these data and the velocity shear measured with the current sensors.

Temporal changes in local bottom and near-bottom suspended sediment behavior are detected with the bottom camera system and with the transmissometer/nephelometer, respectively (Fig. 2). The Benthos camera can be programmed to take pictures of the sea floor at fixed time intervals (typically once every two or four hours). Additionally, a low-power programmer in the camera permits a rapid succession of photographs to be taken at a preselected rate whenever certain speed thresholds are exceeded, as detected by the electromagnetic current meter that is located one meter above the sea floor. Up to 4 threshold current values, corresponding to voltage level adjustments in the master electronics circuitry, are set prior to each experiment. For

example, if incipient motion of the local sediment is expected to occur when the current speed at 1 meter above the bed exceeds values of between 20 cm/sec and 25 cm/sec, threshold values of 15, 20, 25 and 30 cm/sec can be preselected to initiate a rapid sequence of bottom photographs at each of these values. Each rapid sequence will expose up to 8 frames, taken at intervals of 16, 32, 64, or 128 seconds. This burst of bottom photography can be used to identify initial motion of the bottom sediment as well as the development and movement of bedforms. The bottom camera provides about 800 single exposures on a 100 foot roll of 35 mm film.

A single instrument containing a beam transmissometer and right-angle scattering nephelometer is used to measure temporal fluctuations in the suspended materials. The transmissometer is a folded light beam transmitted over a one meter path. Both it and the nephelometer sense only relative changes in the light intensity and scattering properties of the local water volume. The optical data are later converted to changes in suspended material concentrations by application of calibration values determined prior to each deployment.

Electronics System

A master electronics unit specially designed and manufactured by SEA DATA Corporation (data logger model 651-5) for the GEOPROBE system controls the sampling program, data formating, and data recording. This system utilizes a quartz crystal clock accurate to 6 min/yr to establish very precise timing control of the complex sampling and recording scheme. A 30 volt DC battery is the power supply for all sensors except the Benthos camera system and the electromagnetic current meters. The tape recorder is a low power unit that allows for acquisition of about 17×10^6 bits of digital information with a 450 foot tape.

The electronics assembly consists of 22 electronics cards, a digital cassette tape recorder, power supply, and sample control panel. All components are mounted in a vertical rack that fits into a cylindrical pressure case that is 1.2 meters long and has an inside diameter of 15.5 centimeters. The sample control panel contains switches for selecting the camera burst pattern and the data sampling program.

Two distinct types of sampling modes, basic and burst, are available. In the basic mode certain measurements are either averaged (rotor speed and pressure) or instantaneously sampled (vane direction, temperature, light transmission and light scattering) during a preselected basic time interval, I,

$$I = (2^n)\ 1.875 \text{ minutes}$$

where $n = 0,1,2....7.$

These data are digitized and recorded at the end of each interval.

In the burst mode a number of sequential samples of pressure and horizontal current speed are acquired at a rapid rate. Owing to the power requirements of the electromagnetic current sensors, they are sampled only in this mode. Each burst sample consists of a pressure value that is an average taken over the burst period (i.e. over the time interval between successive burst samples), and of instantaneous values of 8 horizontal components of current speed. The burst mode is initiated at the center time of each basic mode interval. Burst data samples are digitized and recorded at the completion of each burst sequence. Available burst rates are once every 1, 2, 4, or 8 seconds; up to 512 samples can be taken during each burst sequence.

The total duration of each experiment is limited by either tape capacity, or system power. Typically with a basic mode interval of 60 minutes and with a burst sequence of 60 samples taken at a rate of once per second, a continuous operation of about 90 days can be achieved.

Launch and recovery system

The present version of the GEOPROBE system is limited to water depths of about 300 meters; a depth restriction imposed principally by the recovery techniques. Future systems that are designed for deeper water will also require different pressure and transmissometer/nephelometer sensors, both of which are rated for 300 meters.

The normal launch technique involves lowering the GEOPROBE tripod to the sea floor using a winch and cable. The primary recovery system consists of an acoustic transponder - release unit and a PVC line bucket containing about 75 m of braided nylon line. Both release unit and line bucket are rigidly mounted on the instrument cage. Once the GEOPROBE system has been accurately located using shipboard navigation and the ranging mode of the acoustic transponder, upon command the acoustic release frees a buoyant glass float. The float pulls the nylon line out of the line bucket to the sea surface. The bitter end of the line is attached to the tripod lifting point. The back-up recovery system consists of a bottom anchor that is connected to the tripod with a long (about 150 m) bottom drag line. A surface buoy moored to the bottom anchor provides a convenient locator and back-up recovery device.

Results

The GEOPROBE system was initially field-tested in a water depth of 20 meters about one mile west of Mission Beach, California near the Naval Undersea Center oceanographic tower during July 1976 (Cacchione, et al., 1976). All sensor and electronics elements functioned satisfactorily except for water leakage into the electromagnetic current meter case. The current meter package was repaired and the system was deployed in Norton Sound, a large shallow arm of the Northern Bering Sea that indents the western coast of Alaska south of the Seward Peninsula.

The GEOPROBE system was launched on September 24, 1976 and successfully recovered 20 days later in a heavy snow fall on the R/V SEA SOUNDER. The entire system was intact and had operated satisfactorily except for the upper pair of electromagnetic current sensors. One of the horizontal cable supports for this pair of current meters had come free of its leg attachment, causing the sensors to lay over in some arbitrary manner.

Analysis of the data on the cassette tape and the bottom photographs shows that the near-bottom water at the GEOPROBE site was extremely turbid and moved in a general NW direction at about 12 cm/sec during the experimental period. This average condition represents the high volume flux of suspended materials emanating from the nearby Yukon River. Nelson and Creager (1977) have shown that most of the sediment discharge of the Yukon River is eventually deposited in the Chukchi Sea, with extremely low rates of modern accumulations in most parts of Norton Sound and other sections of the Northern Bering Sea.

The GEOPROBE sampling scheme for this experiment was set as follows: basic mode interval of 30 minutes, burst mode rate of once per second, burst mode length of 132 samples.

Bottom pressure, speed (rotor) and direction (vane) for the entire period are shown in Fig. 3 along with the tidal curve for Nome, Alaska. Both bottom pressure and bottom current have a distinct tidal signal. Although the tidal range is only about 0.3 meters, the tidal currents have peaks as high as 10 cm/sec.

Fig. 2 is a composite of some GEOPROBE system data plotted with the wind speed and direction data measured by the National Weather Service at Nome. Several striking events can be related in this data set:

(1) The occurrence of peak bottom current speeds on September 29 and October 2 are not correlated with high wind speeds.

(2) The peak current speed on September 29 is correlated with a rapid decrease in light transmission and sharp increase in light scattering values.

(3) The decrease in bottom temperature of nearly 1°C between October 7-9 is correlated with a change in the average bottom current direction (from northerly to southeasterly) and a gradual increase in light transmission.

(4) The wind direction and bottom current direction are not strongly correlated.

Table 2 contains the statistical measures of the basic mode data. The transmissometer and nephelometer values have been omitted because they are treated as relative variations only.

Except for the mechanical failure of the mount for the upper pair of current meters, the burst mode data (pressure and horizontal current components) provided 960 consecutive "bursts" of good quality information. Burst data are shown in Fig. 5 for the period of relatively high currents on September 29 (see Fig. 4). The apparent ragged, sharp changes in the curves are a result of the point-to-point computer plotting. In addition, since the dominant water wave period is about 6 seconds, relatively large differences in speed can occur between successive samples taken only one second apart. The average values for the upper and lower current meters, and pressure sensor for the entire burst sequence in Fig. 5 are 25 cm/sec, 14 cm/sec, and 17.5 m, respectively.

The maximum wave induced currents at the current meter mounted 50 cm above the bed are about 9 cm/sec. The maximum horizontal wave current, u_m, as given by linearized, small amplitude wave theory is

$$u_m = \frac{\pi H}{T \sinh kh} \qquad (1)$$

where H is wave height, T is wave period, k is wave number, h is water depth. Using values taken from the pressure data of $H \simeq 50$ cm and $T \simeq 6$ sec.

equation (1) yields $u_m \simeq 7$ cm/sec, about 25 percent below the measured values. This discrepancy is not excessive because of the limitations in using linearized, small amplitude wave solutions. The comparison of relative magnitudes is reasonably good.

Each burst of current data for the 3-day period, September 28-30, has been averaged and plotted in Fig. 6. Bottom shear velocity, u_*, is also plotted in the lower part of this figure:

$$u_* = \frac{q2-q1}{2.5 \ln (z2/z1)} \qquad (2)$$

where q2 and q1 are average burst current speeds at levels z2 and z1, respectively.

The value of u_* shown by the dashed line in Fig. 6 represents the critical shear velocity needed to initiate motion of bottom sediment whose mean grain size is 0.07 mm, the mean size which characterizes the bottom sediment at the GEOPROBE site. This critical value of u_* was derived from the modified Shields Diagram presented by Madsen and Grant (1976). Wherever the measured u_* exceeds the critical u_* value, i.e. where the solid line is above the dashed line in Fig. 6, initiation of bottom sediment movement is predicted. It must be emphasized that the values of q2, q1, and u_* in Fig. 6 are averages of the burst current speeds; wave-induced current motion has been essentially removed.

The calibration data for the electromagnetic current meters, mentioned earlier, were used to derive a maximum error in the u^* values. This maximum error of about 2 cm/sec is indicated by the vertical bar in Figure 6. The peak diurnal values of u^* are significantly above the threshold values of 1.75 cm/sec, and no values of u^* are less than zero.

Discussion and Conclusions

According to Madsen and Grant (1976) the critical value of u_* derived from the Shields Diagram is applicable to situations where both waves and

steady currents are affecting the bottom, as well as the more commonly applied case of undirectional, steady flow. The shear velocity values plotted in Fig. 6 represent the steady flow case. Based on a technique derived by Madsen and Grant (1976) for predicting the initiation of motion of bottom sediment by the combined action of waves and currents, the mean value of current speed for the entire period (12.1 cm/sec), when combined with the peak wave-induced speeds shown in Fig. 5 (about 9 cm/sec), produces a u_* of 1.5 cm/sec. This value exceeds the critical u_* of 1.3 cm/sec (Fig. 6), suggesting that the action of surface waves when combined with the mean flow conditions can initiate sediment movement.

The GEOPROBE system can provide valuable data on both the oceanographic factors that cause sediment movement and the detailed mechanics of this movement at specific sites on the continental shelf. Although the bottom currents had a relatively low mean (12.1 cm/sec), the added effects of tidal flow and surface wave-induced currents often produced enough bottom stress to exceed the threshold values necessary for incipient sediment movement. This high rate of occurrence of current-induced sediment disturbance is corroborated by the low visibility as determined from the bottom photographs and the low light transmission readings (0.3 v on a full scale of 5 volts). The high level of turbidity obscured the bottom in most of the photographs.

These results indicate that the threshold for sediment movement in the vicinity of the GEOPROBE site in western Norton Sound was frequently exceeded during the experiment, even during periods of relatively quiescent atmospheric conditions. These generally high values of bottom shear velocity, if typical of other ice-free periods, could account for the relatively low rates of sediment accumulation in this area.

ACKNOWLEDGMENTS

This study was supported by the U.S. Geological Survey and by the Bureau of Land Management through interagency agreement with the National Oceanic and Atmospheric Administration, under which a multi-year program responding to needs of petroleum development of the Alaskan continental shelf is managed by the Outer Continental Shelf Environmental Assessment Program (OCSEAP) Office. The authors also wish to thank Dr. Hans Nelson, USGS, for his assistance in the field.

REFERENCES

Butman, B., Noble, M., and Folger, D. W., 1977. Observations of bottom current and bottom sediment movement on the mid-Atlantic continental shelf. Trans. Am. Geophys. Union, 58(6).

Cacchione, D. A., Drake, D. E., Dingler, J. R., Winant, C. D., and Olson, J. R., 1977. Observations of sediment movement by surface and internal waves off San Diego, California. Trans. Am. Geophys. Union, 58(5).

Komar, P. D., 1976. The transport of cohesionless sediments on continental shelves. In: D. J. Stanley and D.J.P. Swift (eds.), Marine Sediment Transport and Environmental Management; John Wiley and Sons, New York, pp. 107-125.

Lavelle, J. W., Young, R. A., Swift, D.J.P., and Clarke, T. L., 1977. Temporal variability of inner shelf near-bottom fluid velocity and particulate concentration measurements. Trans. Am. Geophys. Union, 58(6).

Lescht, B. M., 1977. Frequency distribution of bottom shear stresses within a tidal cycle on the inner continental shelf. Trans. Am. Geophys. Union, 58(6).

Madsen, O. S., and Grant, W. D., 1976. Sediment transport in the coastal environment. Ralph M. Parsons Laboratory Rept. No. 209. Mass. Inst. of Technology, Cambridge, Mass., 105 p.

Nelson, C. H., and Creager, J. S., 1977. Displacement of Yukon-derived sediment from Bering Sea to Chukchi Sea during Holocene time. Geology, 5: 141-146.

Sternberg, R. W., Morrison, D. R., and Trimble, J. A., 1973. An instrumentation system to measure near-bottom conditions on the continental shelf; Marine Geology, 3:181-189.

Sternberg, R. W. Nittrouer, C. A., and Larsen, L. H., 1977. An integrated approach to the study of marine sedimentological processes: new instruments and methods; Trans. Am. Geophys. Union, 58(6).

TABLE I

GEOPROBE Instrumentation

Sensor (no.)	Type	Manufacturer	Model No.
current meters (4)	electromagnetic	Marsh-McBirney, Inc.	555 B
current meter (1)	Savonius rotor/vane	Bendix, Env. Sci. Div.	Q-9
pressure (1)	quartz crystal	Paroscientific, Inc.	4270
temperature (2)	thermistor	Yellow Springs Instr. Co.	-
transmissometer (1)	visible light	Montedoro-Whitney Corp.	TMU
nephelometer (1)	90 degree scatter	Montedoro-Whitney Corp.	TMU
camera/flash (1) w/ auxiliary power unit	35mm/strobe	Benthos, Inc.	372/383/391

TABLE II

Statistical values of GEOPROBE data -
Norton Sound, Alaska; Sept 24 - Oct 14, 1977

Type	Mean	Std. Deviation	Max.	Min.
current speed (cm/sec)	12.1	4.8	32.0	3.0
current direction (degrees/true)	280	-	-	-
pressure (m)	17.52	0.20	18.20	17.02
temperature (°C)	8.24	0.51	8.84	7.16

FIGURE CAPTIONS

Figure 1. The GEOPROBE system, an instrumented bottom tripod, is deployed from the R/V SEA SOUNDER in Norton Sound, Alaska on Sept. 24, 1976. Note the vertical array of small, spherical electromagnetic current meters tautly suspended within the tripod legs by horizontal cables.

Figure 2. The instrument cage on the GEOPROBE tripod contains the following items numbered in the picture: (1) - temperature sensor; (2) - camera; (3) - auxiliary power supply for camera/flash units; (4) - pressure housing for Sea Data electronics, tape recorder, and 30V-DC power supply; (5) - strobe flash unit; (6) - pressure sensor; (7) pressure housing for current meter electronics; (8) - transmissometer/nephelometer; (9) - acoustic release; and (10) - recovery float atop line bucket.

Figure 3. Basic mode pressure and current data taken with GEOPROBE system in Norton Sound, Alaska, in 1976. Data are actually discrete values that represent half-hourly averages of indicated parameters; solid lines are drawn through the points for simplicity. Current data were obtained with the rotor-vane current meter. Top curve is plotted from data published in the standard tide tables for Nome, Alaska.

Figure 4. As in Fig. 3, GEOPROBE system data shown are actually discrete values of half-hourly averages; solid lines are drawn through the points for simplicity. Current data were obtained with the rotor-vane current meter. Light transmission and light scattering values are uncalibrated, relative measures of voltage outputs. Top curves of hourly wind speed and wind direction were obtained from the National Weather Service office in Nome.

Figure 5. Burst mode data of current speed measured with the GEOPROBE electromagnetic current meters at levels 50 cm (q2) and 20 cm (q1) above the sea floor, respectively. Burst pressure (p) data were obtained simultaneously with the current measurements.

Figure 6. Average values of the burst current speed measurements obtained with two electromagnetic current meters at 50 cm (q2) and 20 cm (q1) above the sea floor, respectively. Each value is an average of the 132 samples in a burst, taken at a rate of once per second. u_* is the bottom shear velocity computed from equation (2). The estimated maximum error in u^* is indicated by the vertical bar.

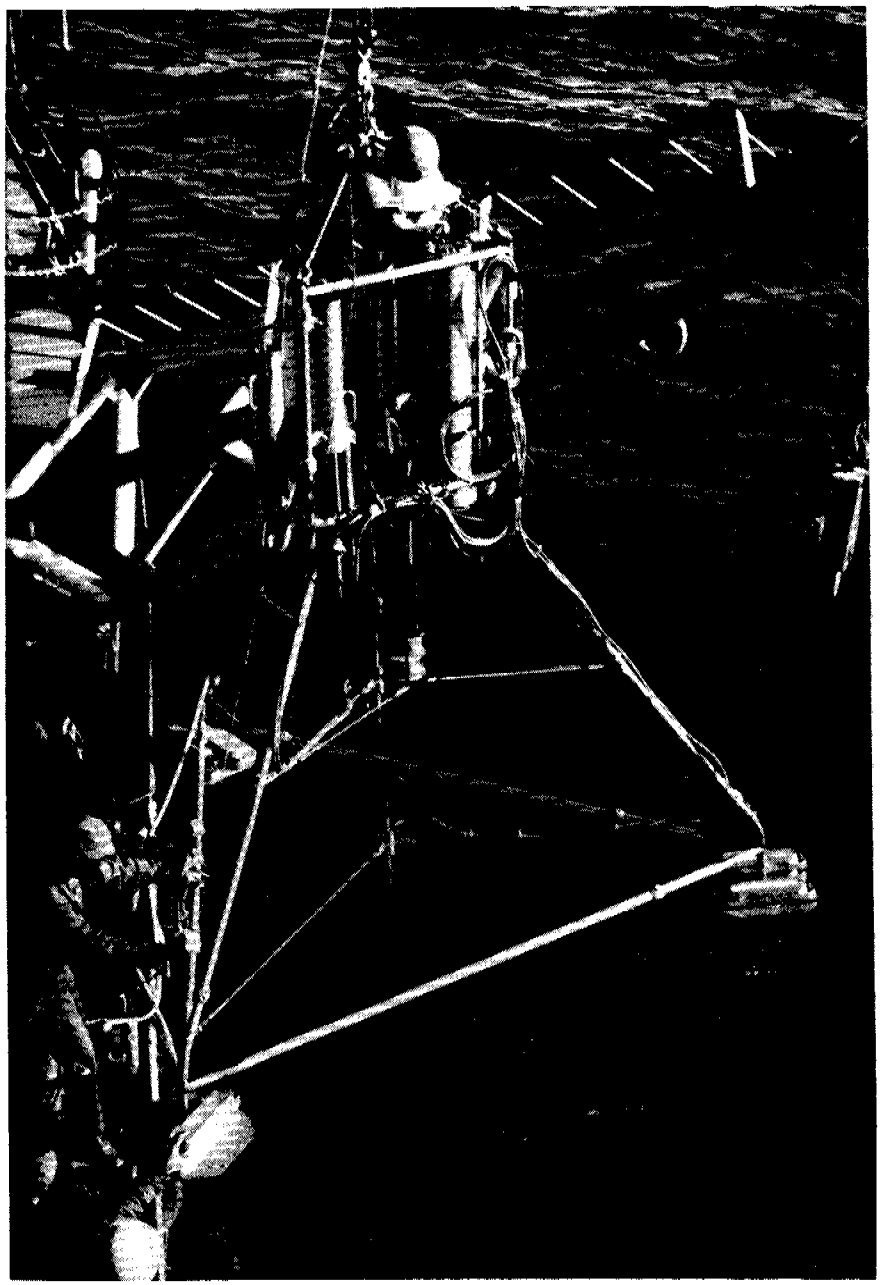

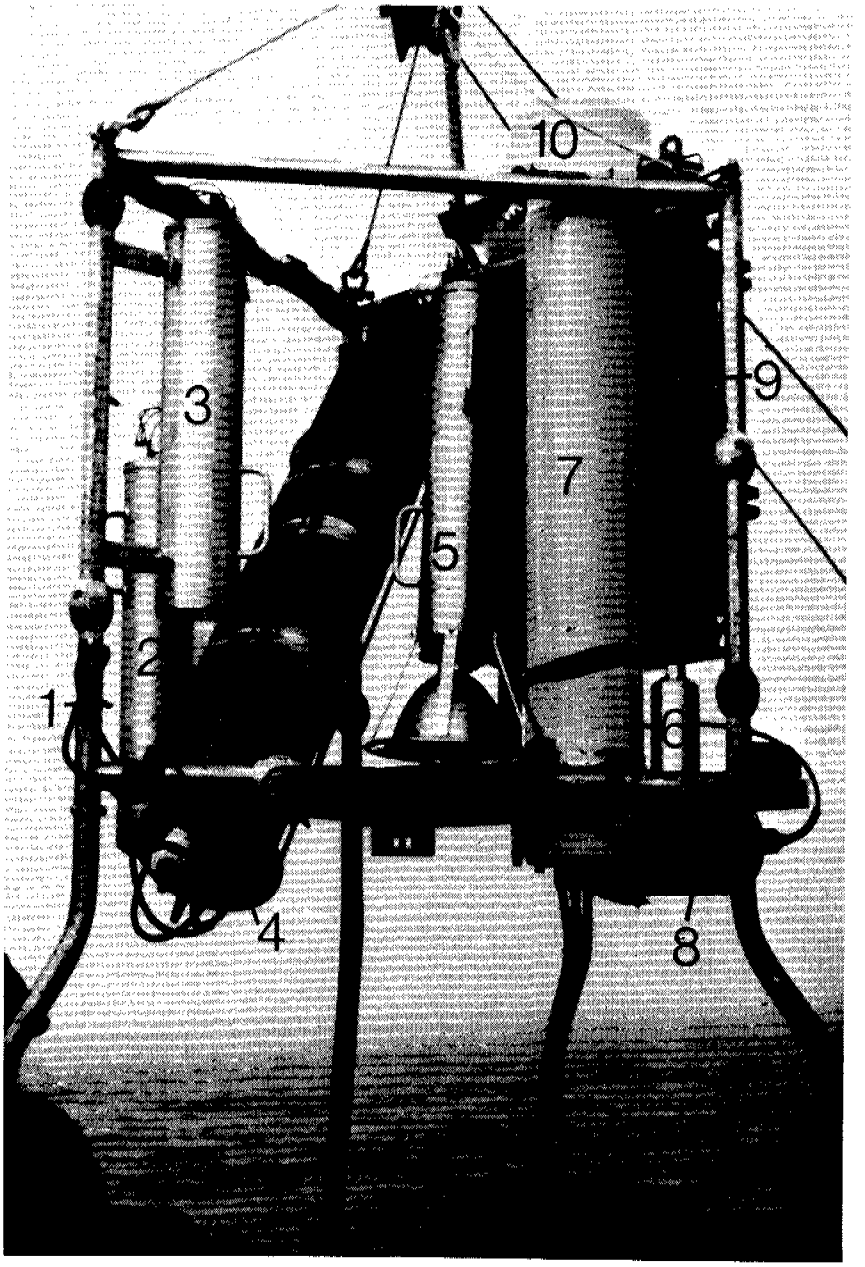
10
9
3
4
7
5
2
1
6
4
8

SEPTEMBER
25
27
29
OCTOBER
1
3
5
7
9
11
13
TIDAL HEIGHT
(meters)
0.2
0.1
0
-0.1
0.2
BOTTOM
PRESSURE
(meters)
18.0
17.5
17.0
CURRENT
SPEED
(cm/sec)
30
20
10
DIRECTION
(degrees)
360
270
180
090
000

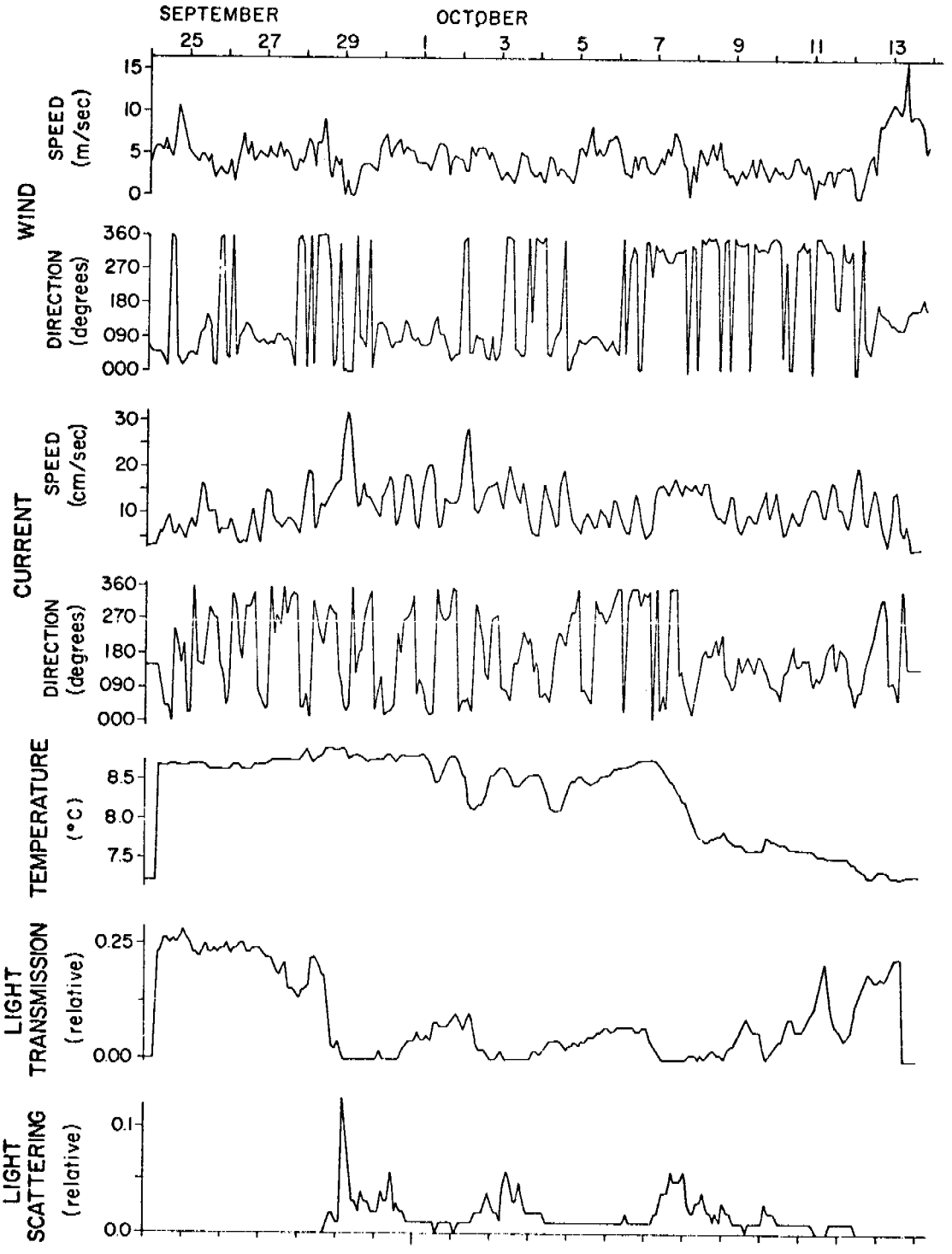
SEPTEMBER
OCTOBER
25
27
29
1
3
5
7
9
11
13
WIND
SPEED (m/sec)
15
10
5
0
DIRECTION (degrees)
360
270
180
090
000
CURRENT
SPEED (cm/sec)
30
20
10
DIRECTION (degrees)
360
270
180
090
000
TEMPERATURE (°C)
8.5
8.0
7.5
LIGHT TRANSMISSION (relative)
0.25
0.00
LIGHT SCATTERING (relative)
0.1
0.0

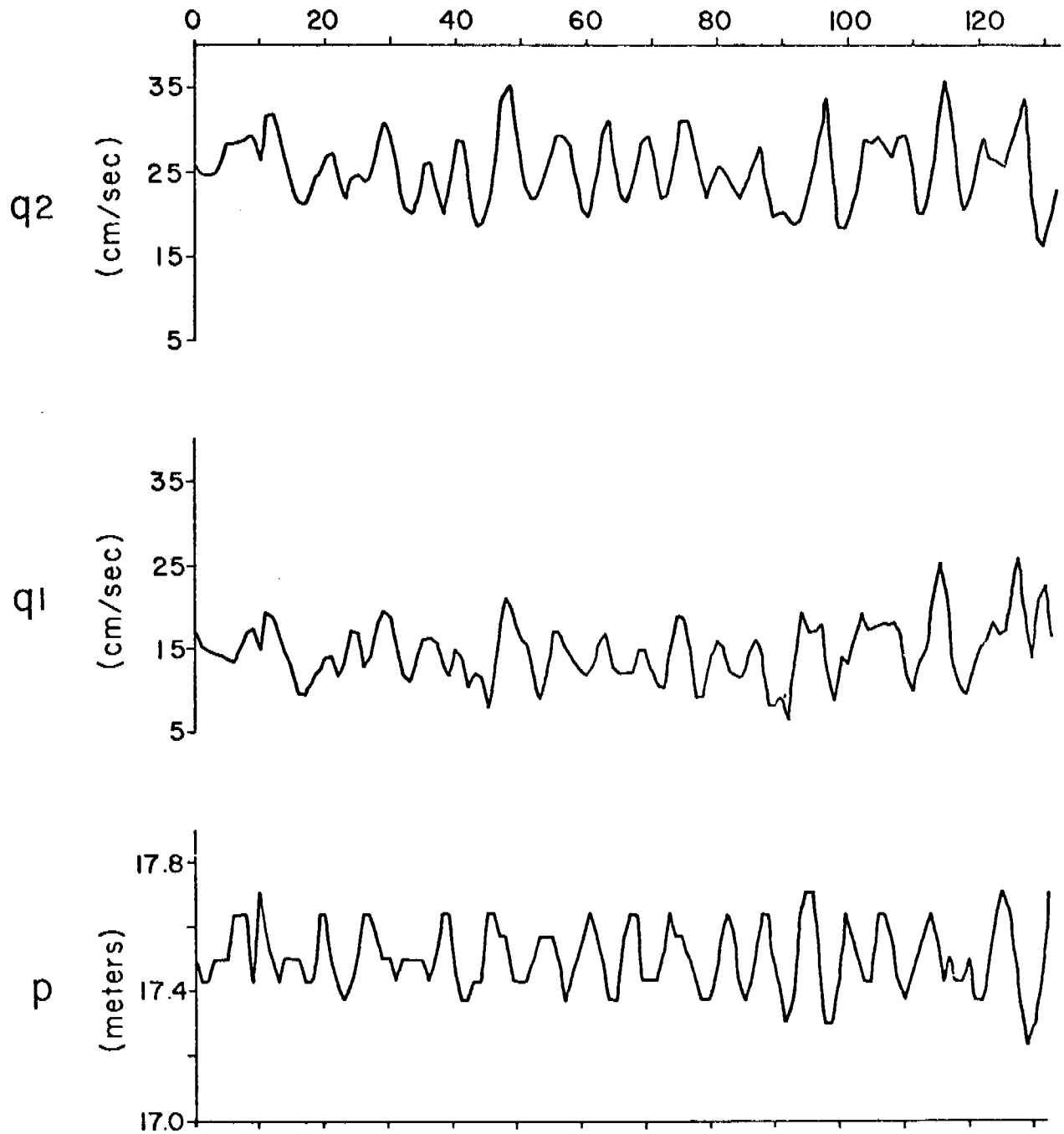
0
20
40
60
80
100
120
q2
35
25
15
5
(cm/sec)
q1
35
25
15
5
(cm/sec)
p
17.8
17.4
17.0
(meters)

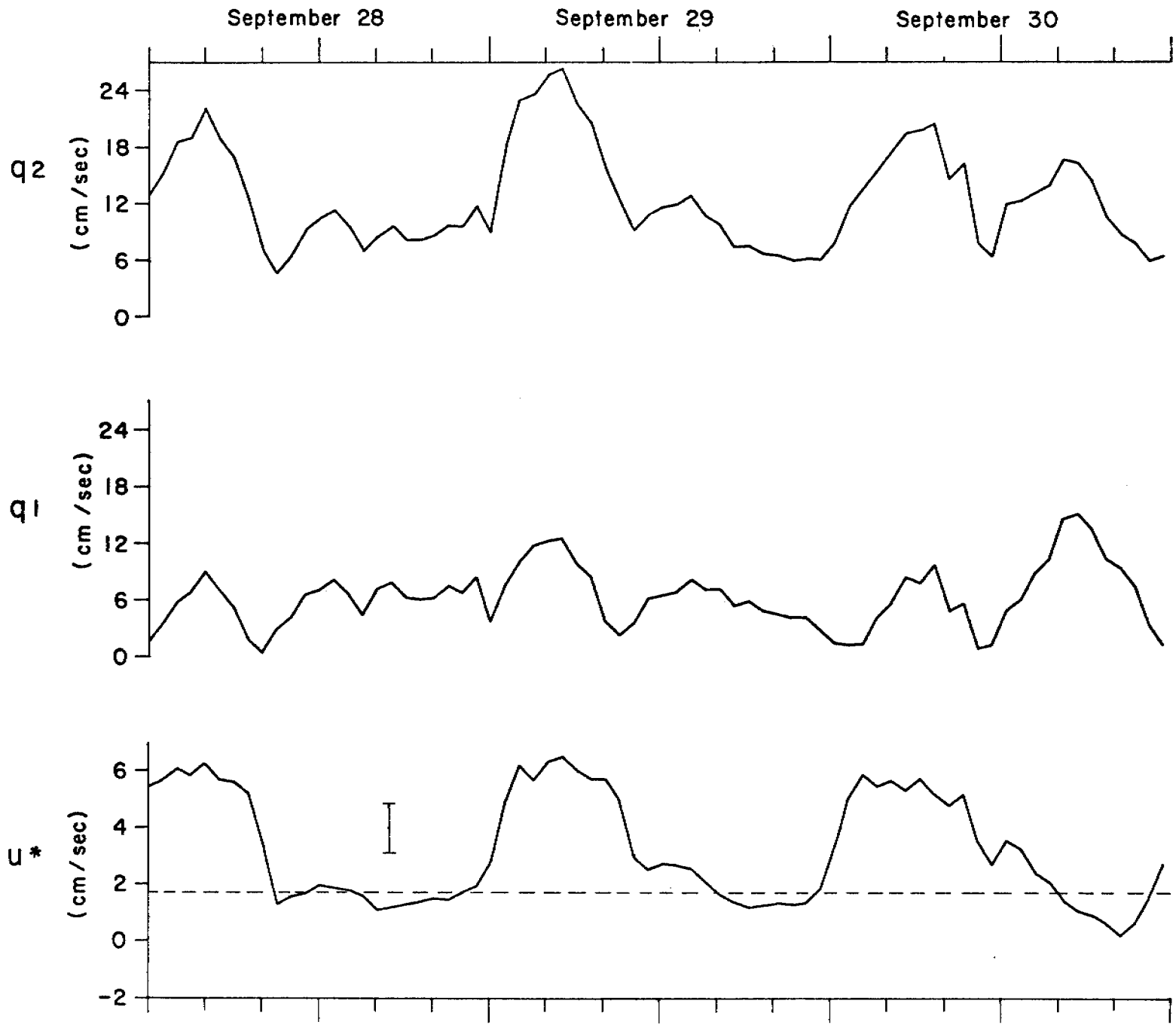
September 28
September 29
September 30
q2
(cm/sec)
24
18
12
6
0
q1
(cm/sec)
24
18
12
6
0
u*
(cm/sec)
6
4
2
0
-2

A P P E N D I X C

Current Meter Data for Norton Sound

GEOPROBE sensors

July 8 - September 27, 1977

STATISTICS AND HISTOGRAMS OF CURRENTS AT GEOPROBE, NOR SND 77
LOCATION = LAT 64 00N, LONG 165 00W, DEPTH = 17.5 METERS
OBSERVATION PERIOD = 0000 8 JUL 77 TO 2300 25 SEP 77 (80.0 DAYS)
N = 1920 DT = 1.00 HOURS, UNITS = (CM/SEC)

	MEAN	VARIANCE	ST-DEV	SKEW	KURT	MAX	MIN
S	10.63	44.73	6.69	0.662	2.778	32.28	0.00
U	0.50	96.76	9.84	0.375	3.201	30.63	-24.35
V	4.79	37.73	6.14	0.343	3.460	25.08	-17.16

S = SPEED
U = EAST-WEST COMPONENT OF VELOCITY, EAST =POSITIVE U
V = NORTH-SOUTH COMPONENT OF VELOCITY, NORTH = POSITIVE V

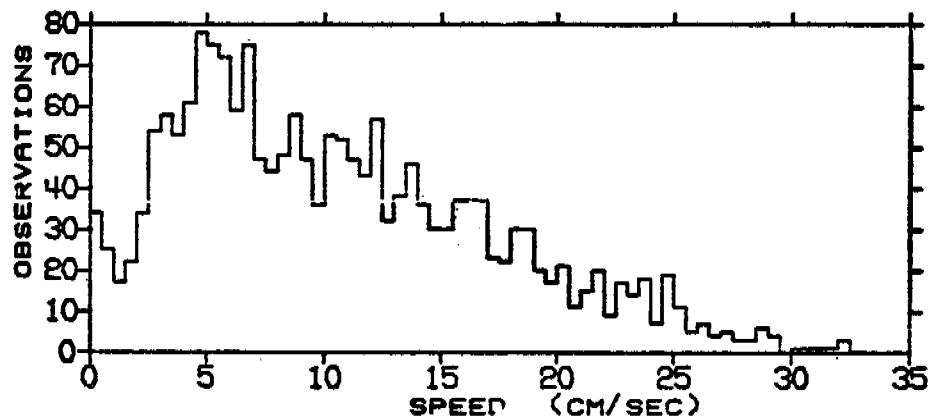

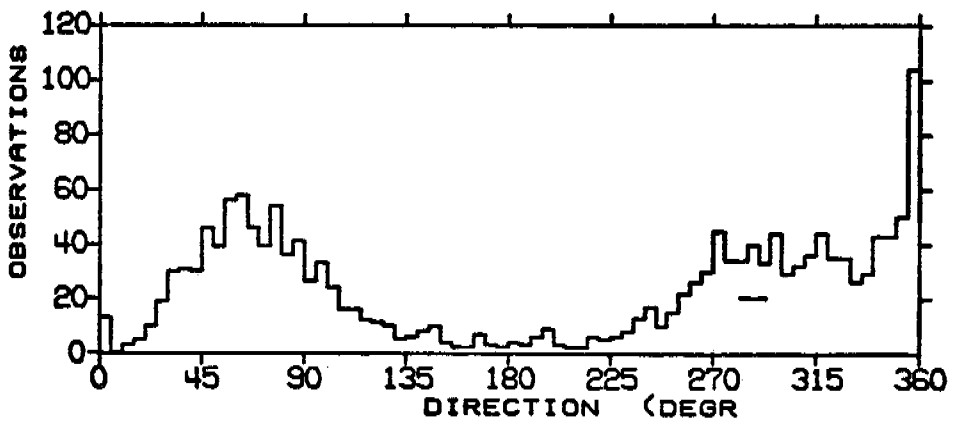

TIME SERIES OF VECTOR AVERAGED CURRENTS AT GPB-ROTOR/VANE, NS77
LOCATION = LAT 64 00N, LONG 165 00W, DEPTH = 17.5 METERS
OBSERVATION PERIOD = 0000 8 JUL 77 TO 2300 27 JUL 77 (20.0 DAYS)
AVERAGING INTERVAL = 1.0 HOURS (1 POINTS)

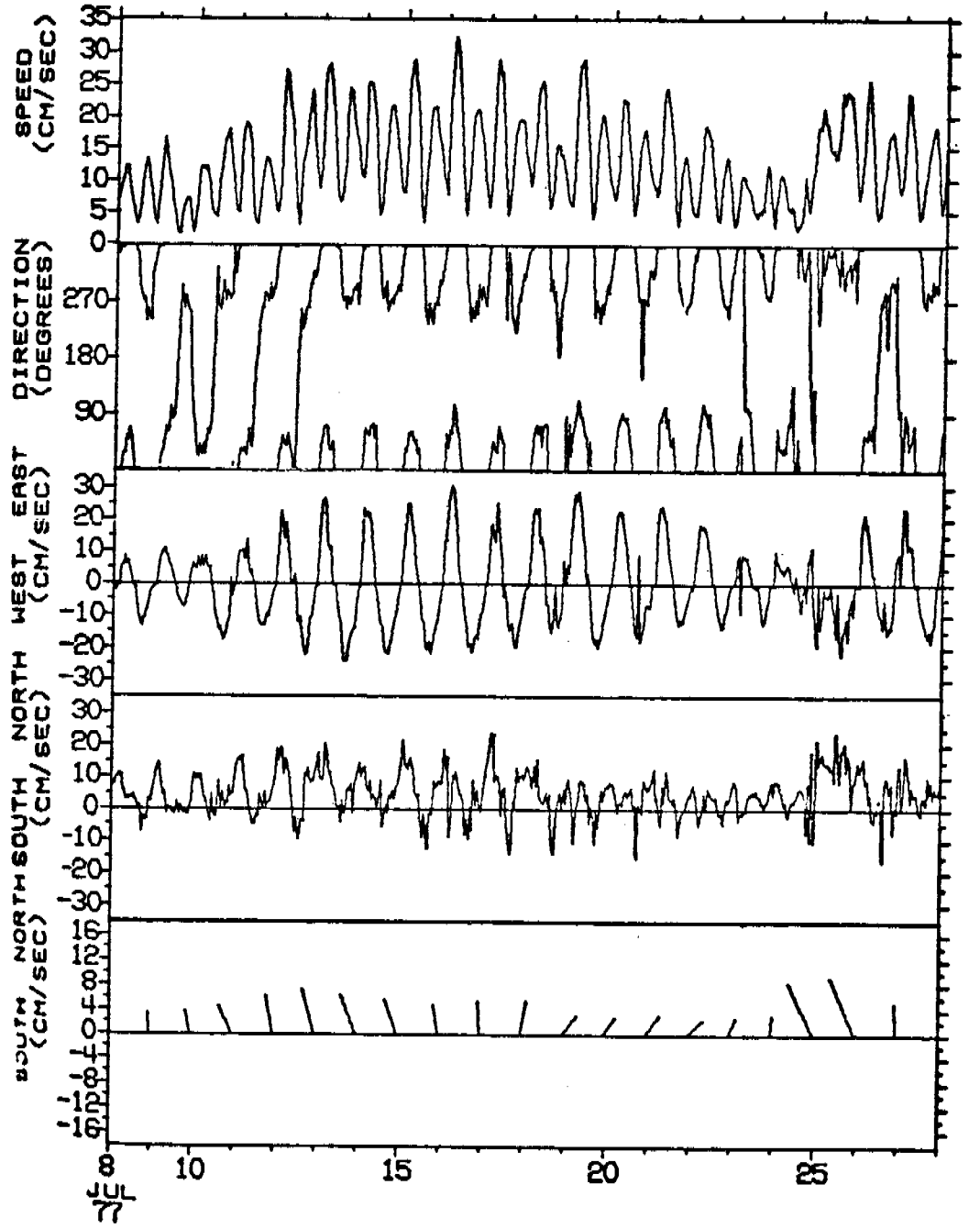

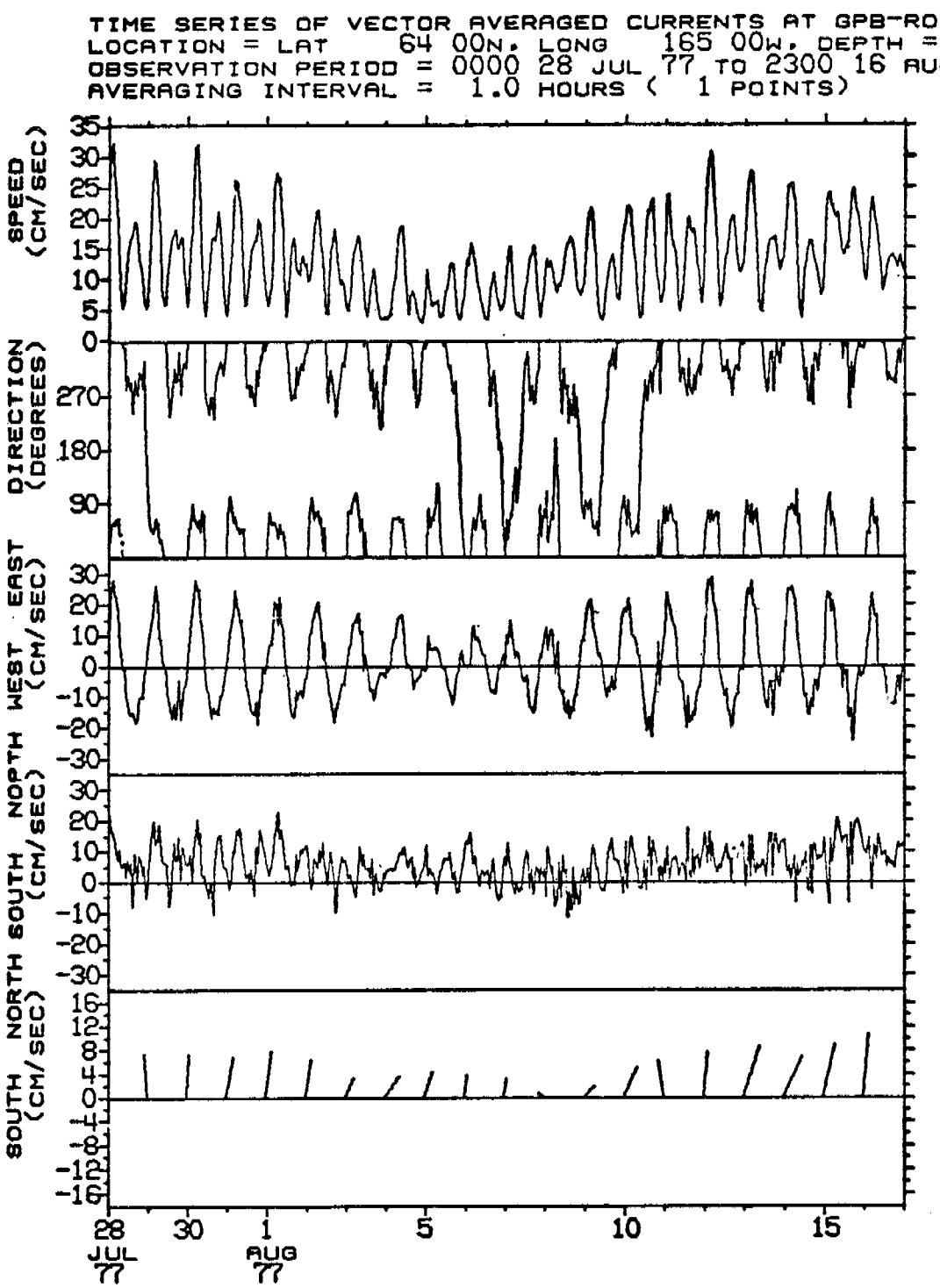
TIME SERIES OF VECTOR AVERAGED CURRENTS AT GPB-ROTOR/VANE. NS77
LOCATION = LAT 64 00N. LONG 165 00W. DEPTH = 17.5 METERS
OBSERVATION PERIOD = 0000 28 JUL 77 TO 2300 16 AUG 77 (20.0 DAYS)
AVERAGING INTERVAL = 1.0 HOURS (1 POINTS)
SPEED (CM/SEC)
DIRECTION (DEGREES)
WEST EAST (CM/SEC)
SOUTH NORTH (CM/SEC)
SOUTH NORTH (CM/SEC)
28 JUL 77
30
1 AUG 77
5
10
15

TIME SERIES OF VECTOR AVERAGED CURRENTS AT GPB-ROTOR/VANE. NS77
LOCATION = LAT 64 00N. LONG 165 00W. DEPTH = 17.5 METERS
OBSERVATION PERIOD = 0000 17 AUG 77 TO 2300 5 SEP 77 (20.0 DAYS
AVERAGING INTERVAL = 1.0 HOURS (1 POINTS)

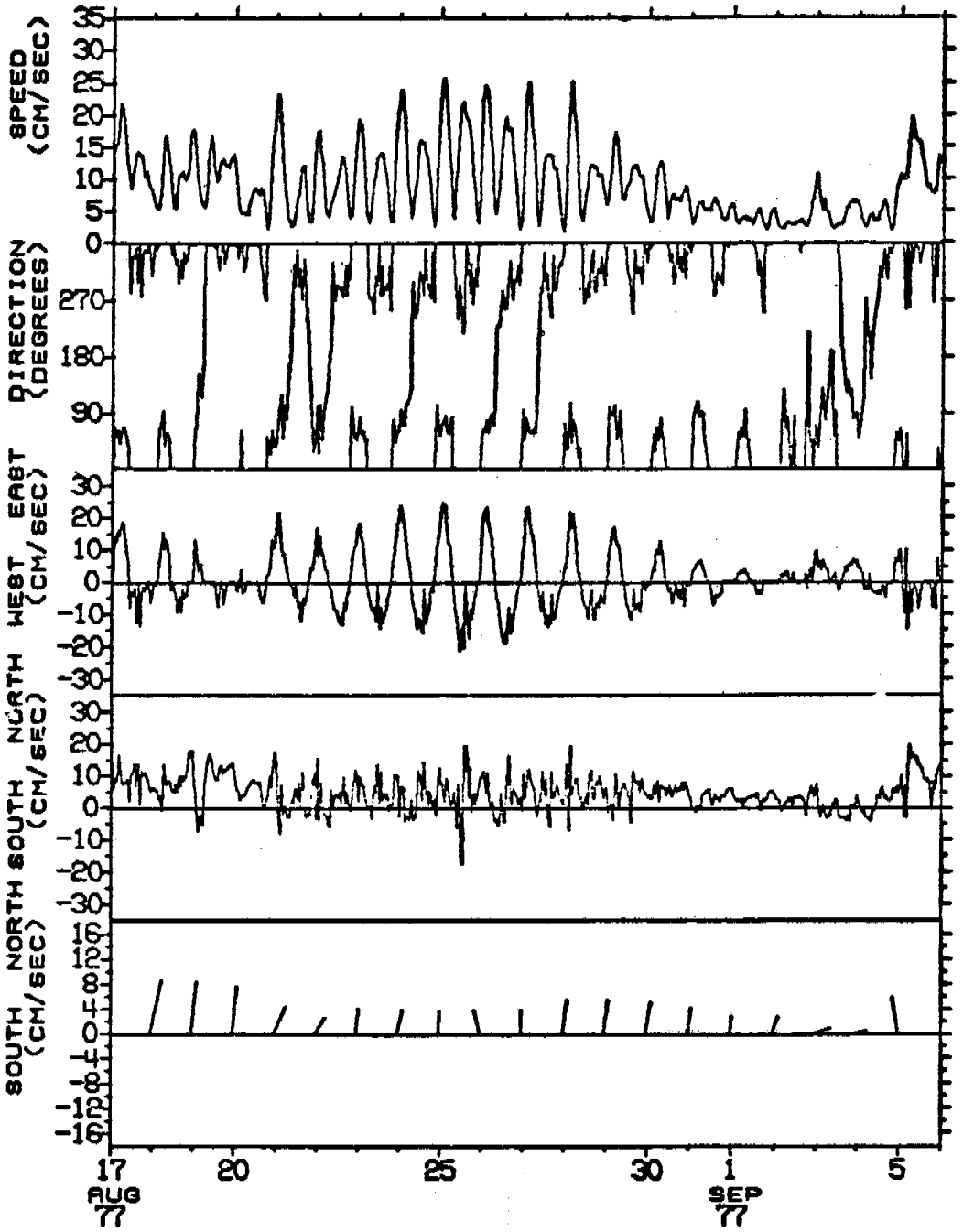

TIME SERIES OF VECTOR AVERAGED CURRENTS AT GPB-ROTOR/VANE. NS77
LOCATION = LAT 64 00N, LONG 165 00W, DEPTH = 17.5 METERS
OBSERVATION PERIOD = 0000 6 SEP 77 TO 2300 25 SEP 77 (20.0 DAYS)
AVERAGING INTERVAL = 1.0 HOURS (1 POINTS)

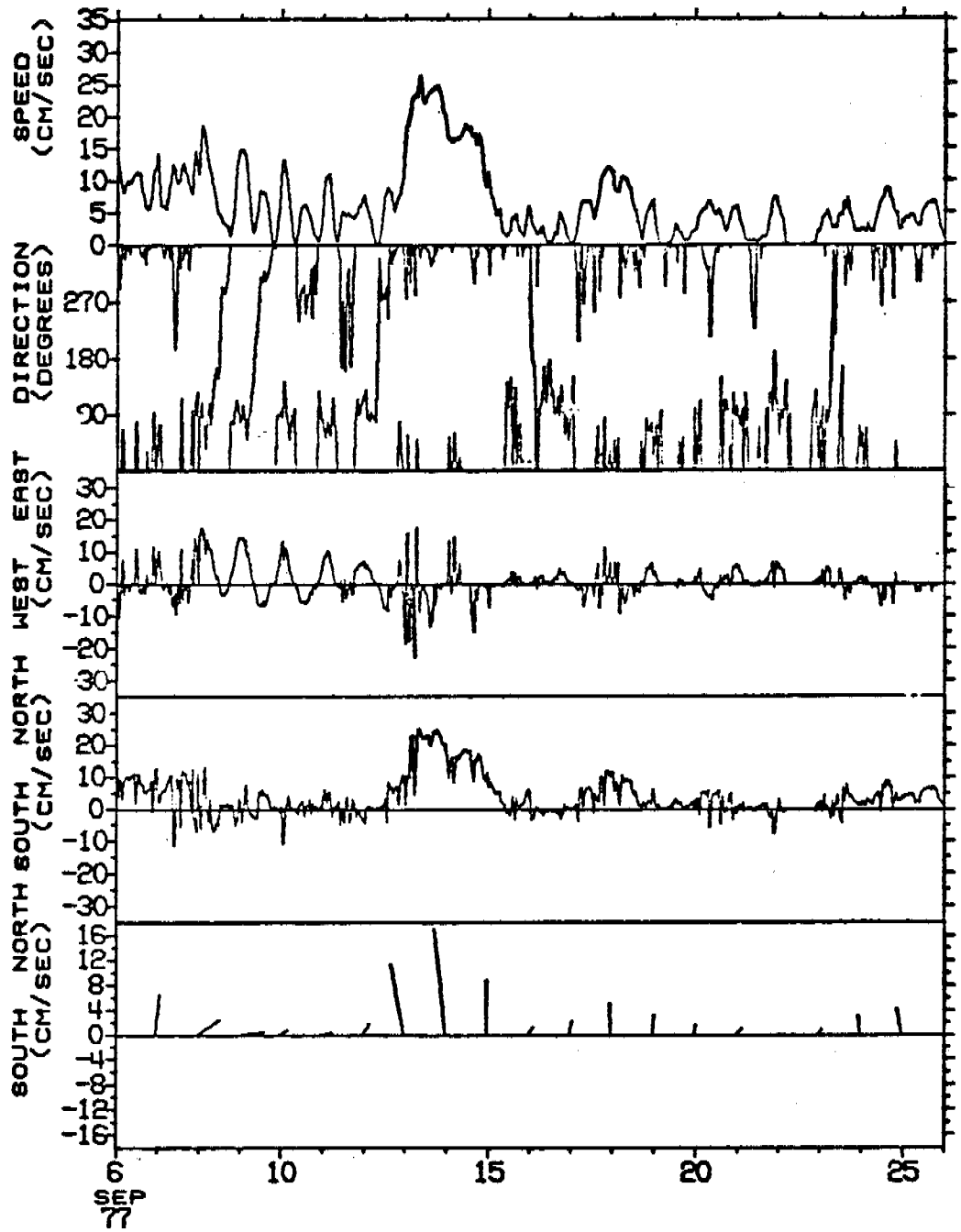

PROGRESSIVE VECTOR DIAGRAM OF CURRENTS AT GEOPROBE, NOR SND 77
LOCATION = LAT 64 00N, LONG 165 00W, DEPTH = 17.5 METERS
OBSERVATION PERIOD = 0000 8 JUL 77 TO 2300 25 SEP 77 (80.0 DAYS)
• EVERY 2.0 DAYS BEGINNING AT 0000 8 JUL 77

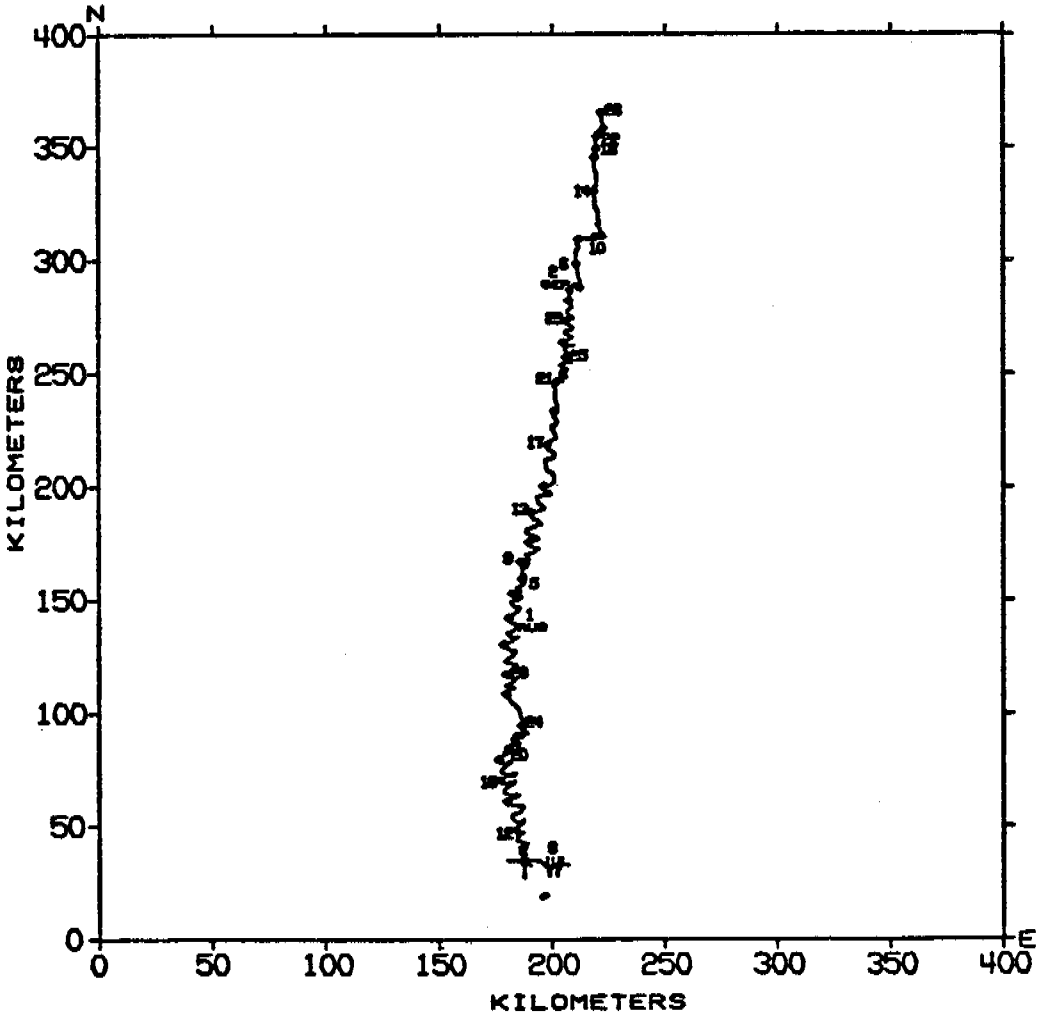

U, V AND ROTORY SPECTRA OF CURRENTS AT GEOPROBE, NOR SND 77
LOCATION = LAT 64 00N, LONG 165 00W, DEPTH = 17.5 METERS
OBSERVATION PERIOD = 0000 8 JUL 77 TO 2300 25 SEP 77 (80.0 DAYS)
N = 1920, DT = 1.0 HOURS, SMOOTHING - DANIELL WINDOW

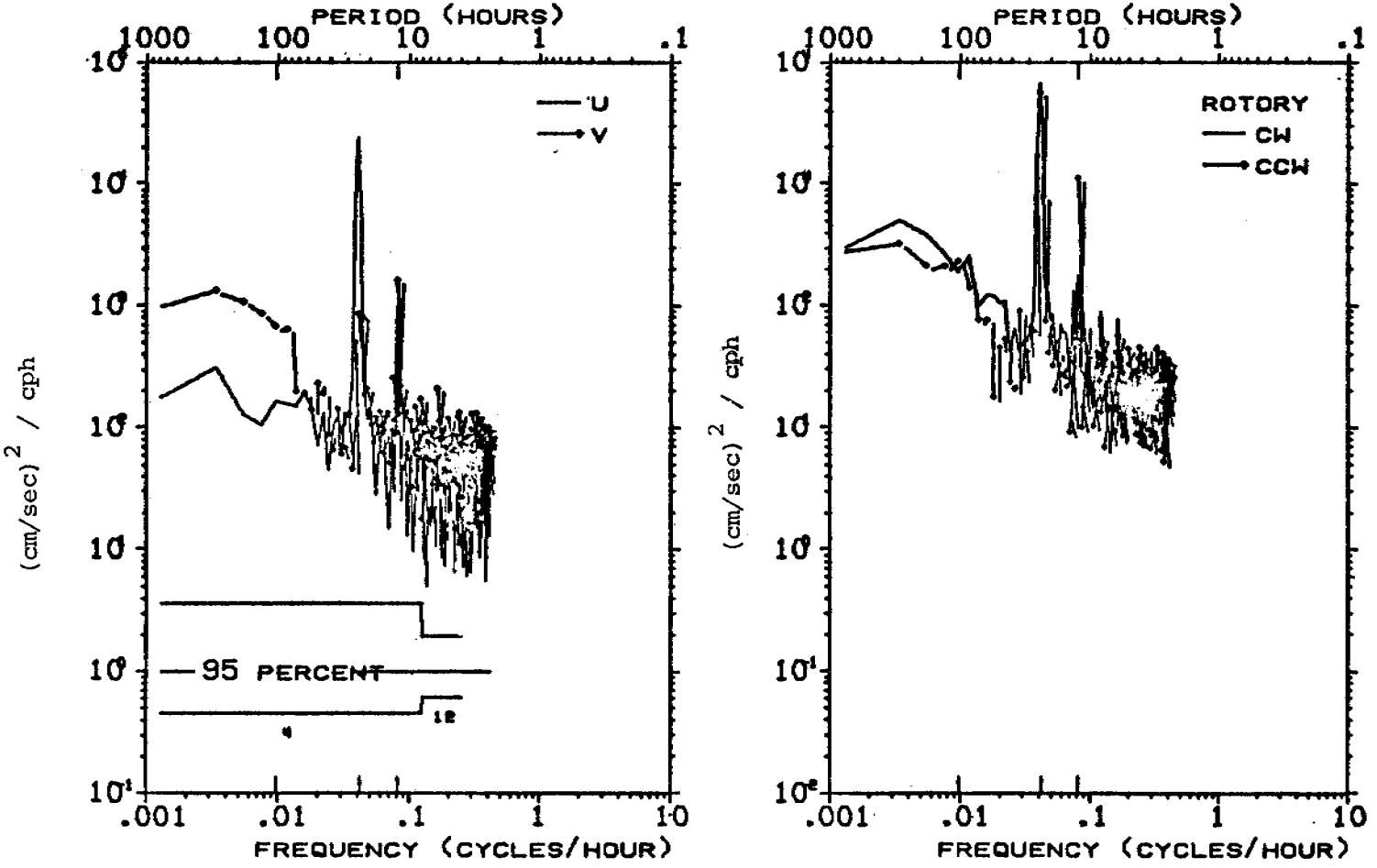

KINETIC ENERGY SPECTRUM OF CURRENTS AT GEOPROBE, NOR SND 77
LOCATION = LAT 64 00N, LONG 165 00W, DEPTH = 17.5 METERS
OBSERVATION PERIOD = 0000 8 JUL 77 TO 2300 25 SEP 77 (80.0 DAYS)
N = 1920, DT = 1.0 HOURS, SMOOTHING - DANIELL WINDOW

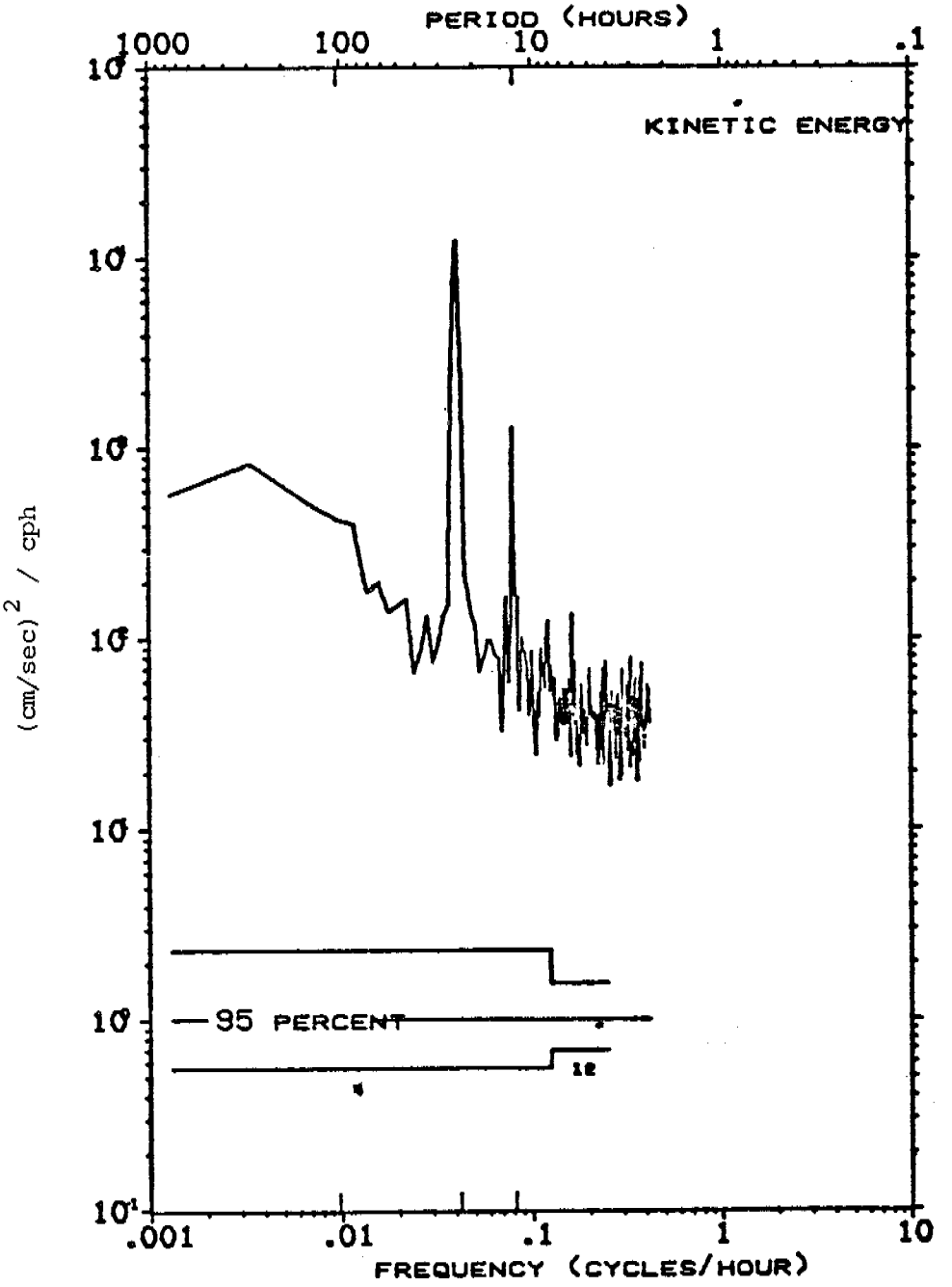

U, V AND ROTORY SPECTRA OF CURRENTS AT GEOPROBE, NOR SND 77
LOCATION = LAT 64 00N, LONG 165 00W, DEPTH = 17.5 METERS
OBSERVATION PERIOD = 0000 8 JUL 77 TO 2300 25 SEP 77 (80.0 DAYS)
N = 1920, DT = 1.0 HOURS, SMOOTHING - DANIELL WINDOW

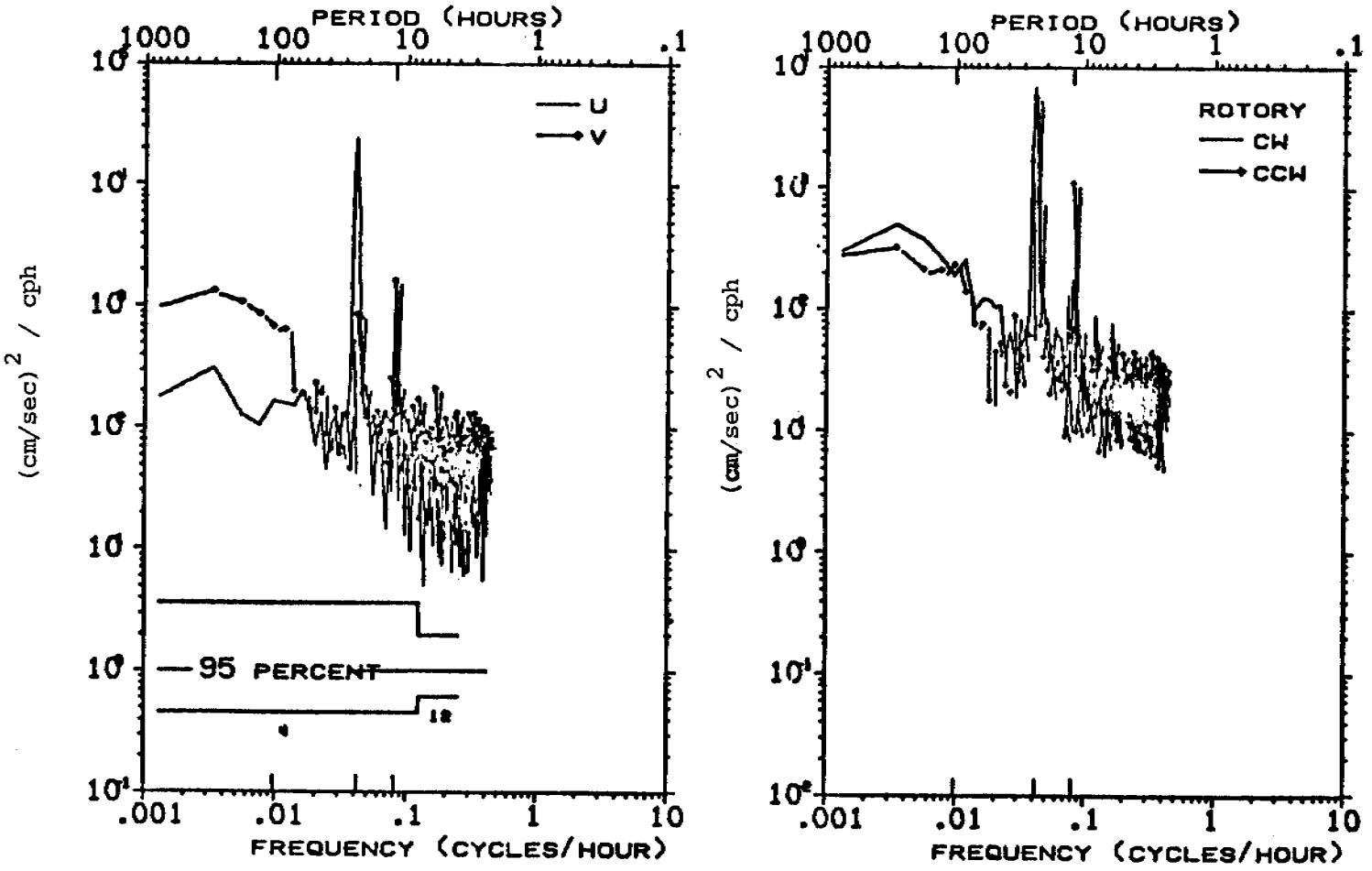

STATISTICS AND HISTOGRAMS OF CURRENTS AT CM1 - GEOPROBE, NS77
LOCATION = LAT 64 00N, LONG 165 00W, DEPTH = 17.5 METERS
OBSERVATION PERIOD = 0000 8 JUL 77 TO 2300 25 SEP 77 (80.0 DAYS)
N = 1920 DT = 1.00 HOURS, UNITS = (CM/SEC)

	MEAN	VARIANCE	ST-DEV	SKEW	KURT	MAX	MIN
S	8.93	25.96	5.10	0.622	2.862	28.18	0.03
U	2.14	78.95	8.89	0.279	2.281	28.01	-18.94
V	1.60	19.53	4.42	0.920	4.804	21.92	-16.12

S = SPEED
U = EAST-WEST COMPONENT OF VELOCITY, EAST =POSITIVE U
V = NORTH-SOUTH COMPONENT OF VELOCITY, NORTH = POSITIVE V

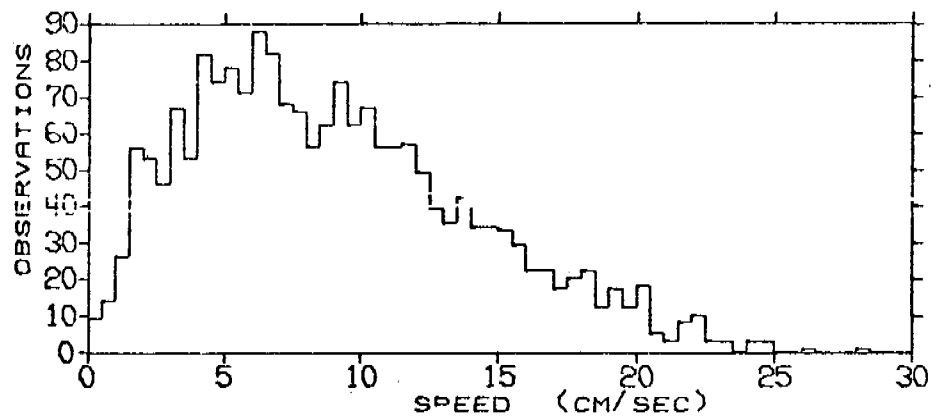

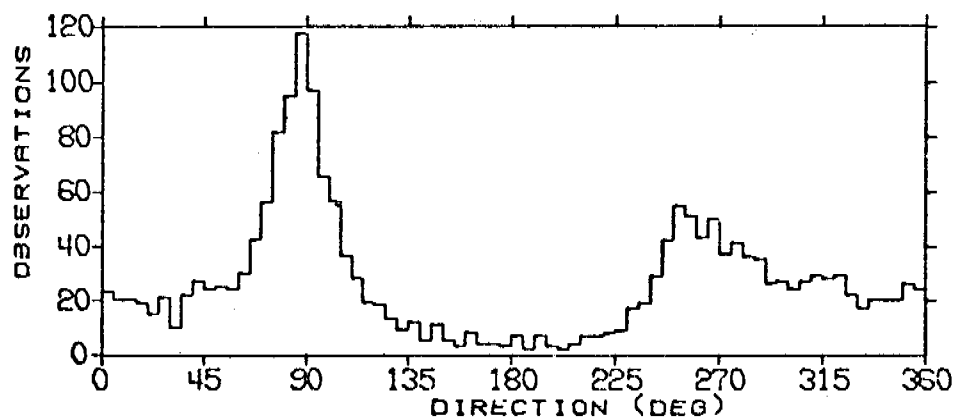

TIME SERIES OF VECTOR AVERAGED CURRENTS AT CM1 - GEOPROBE, NS77
LOCATION = LAT 64 00N, LONG 165 00W, DEPTH = 17.5 METERS
OBSERVATION PERIOD = 0000 8 JUL 77 TO 2300 27 JUL 77 (20.0 DAYS)
AVERAGING INTERVAL = 1.0 HOURS (1 POINTS)

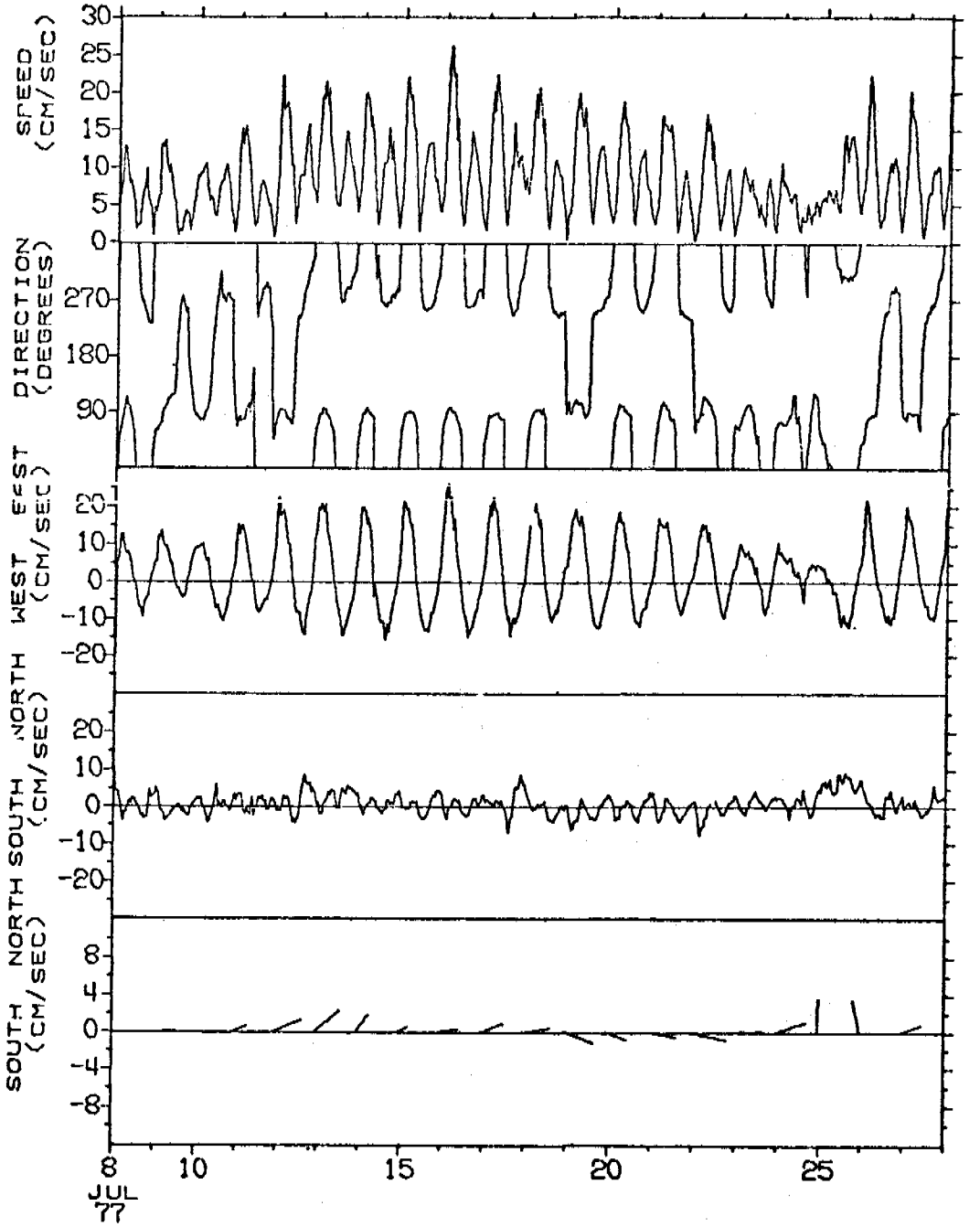

TIME SERIES OF VECTOR AVERAGED CURRENTS AT CM1 - GEOPROBE, NS77
LOCATION = LAT 64 00N, LONG 165 00W, DEPTH = 17.5 METERS
OBSERVATION PERIOD = 0000 28 JUL 77 TO 2300 16 AUG 77 (20.0 DAYS)
AVERAGING INTERVAL = 1.0 HOURS (1 POINTS)

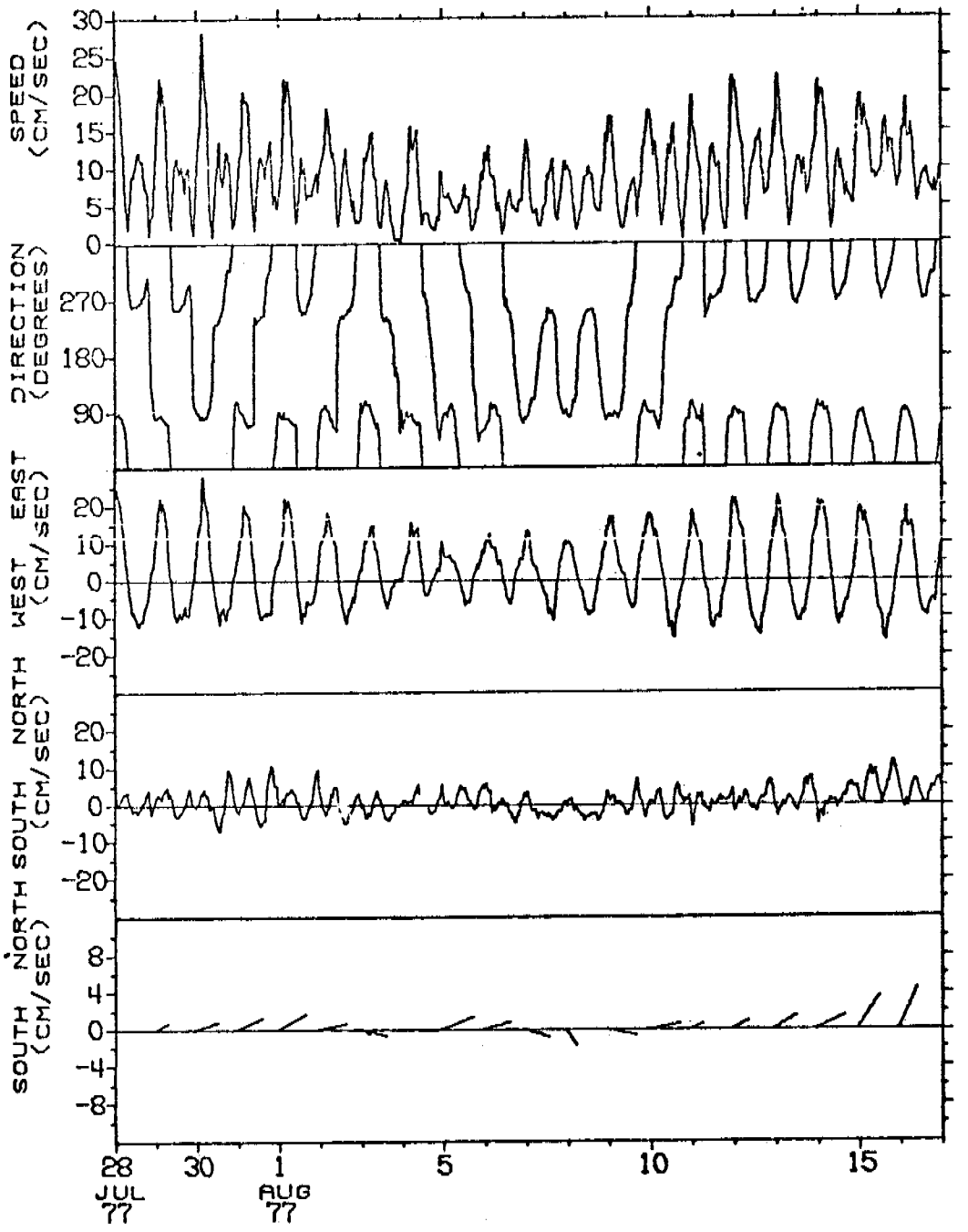

TIME SERIES OF VECTOR AVERAGED CURRENTS AT CM1 - GEOPROBE, NS77
LOCATION = LAT 64 00N, LONG 165 00W, DEPTH = 17.5 METERS
OBSERVATION PERIOD = 0000 17 AUG 77 TO 2300 5 SEP 77 (20.0 DAYS)
AVERAGING INTERVAL = 1.0 HOURS (1 POINTS)

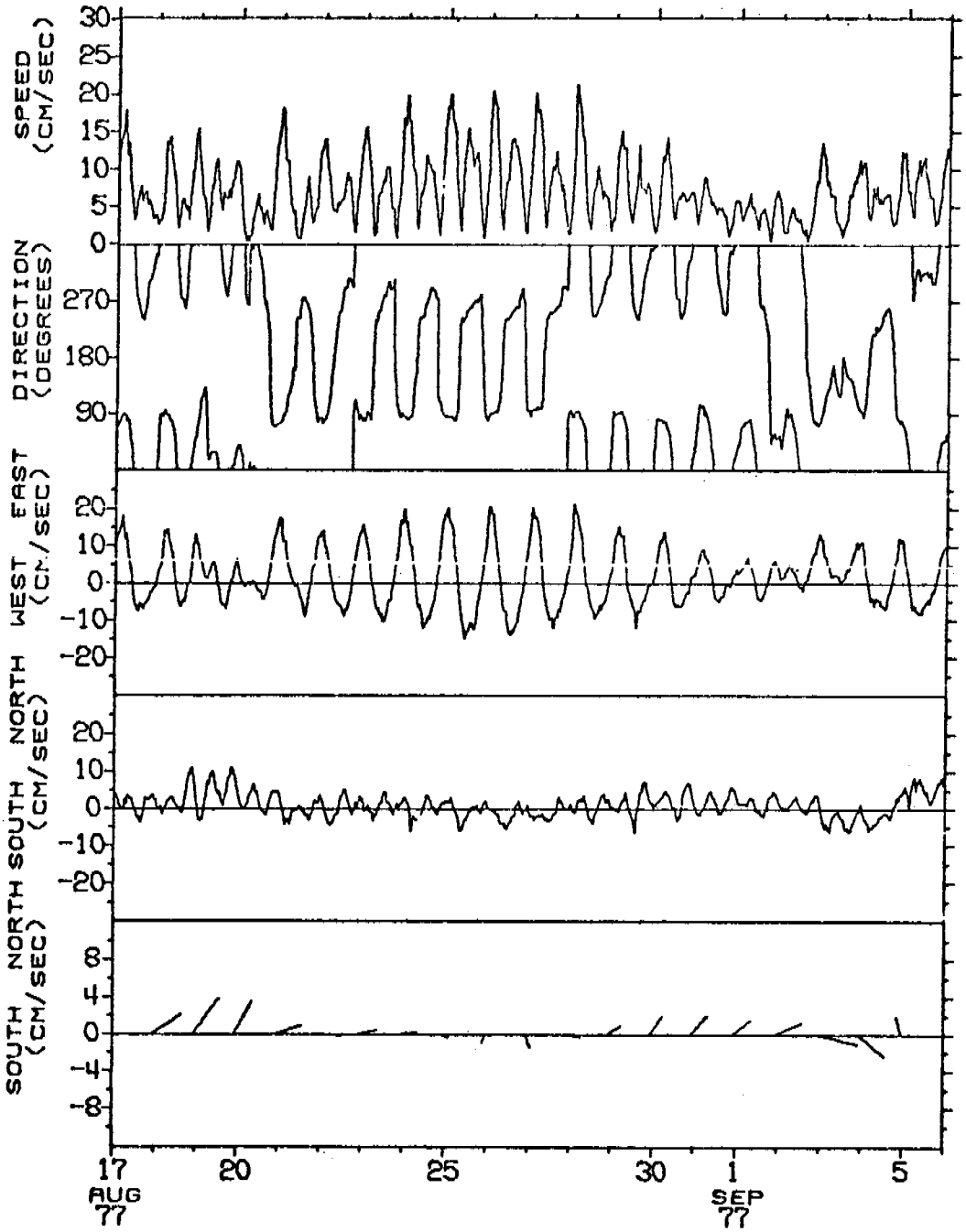

TIME SERIES OF VECTOR AVERAGED CURRENTS AT CM1 - GEOPROBE, NS77
LOCATION = LAT 64 00N, LONG 165 00W, DEPTH = 17.5 METERS
OBSERVATION PERIOD = 0000 6 SEP 77 TO 2300 25 SEP 77 (20.0 DAYS)
AVERAGING INTERVAL = 1.0 HOURS (1 POINTS)

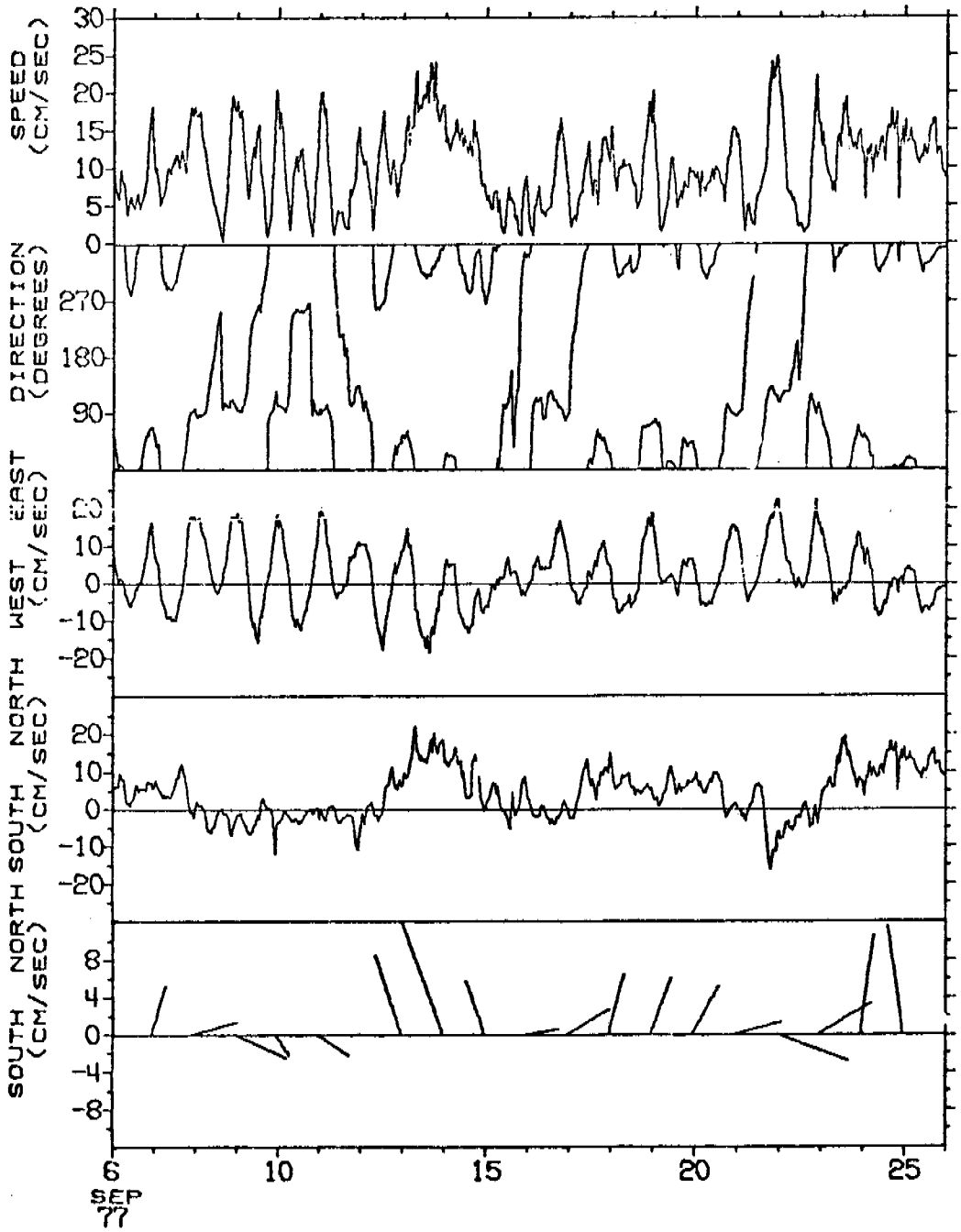

PROGRESSIVE VECTOR DIAGRAM OF CURRENTS AT CM1 - GEOPROBE, NS77
LOCATION = LAT 64 00N, LONG 165 00W, DEPTH = 17.5 METERS
OBSERVATION PERIOD = 0000 8 JUL 77 TO 2300 25 SEP 77 (80.0 DAYS)
* EVERY 2.0 DAYS BEGINNING AT 0000 8 JUL 77

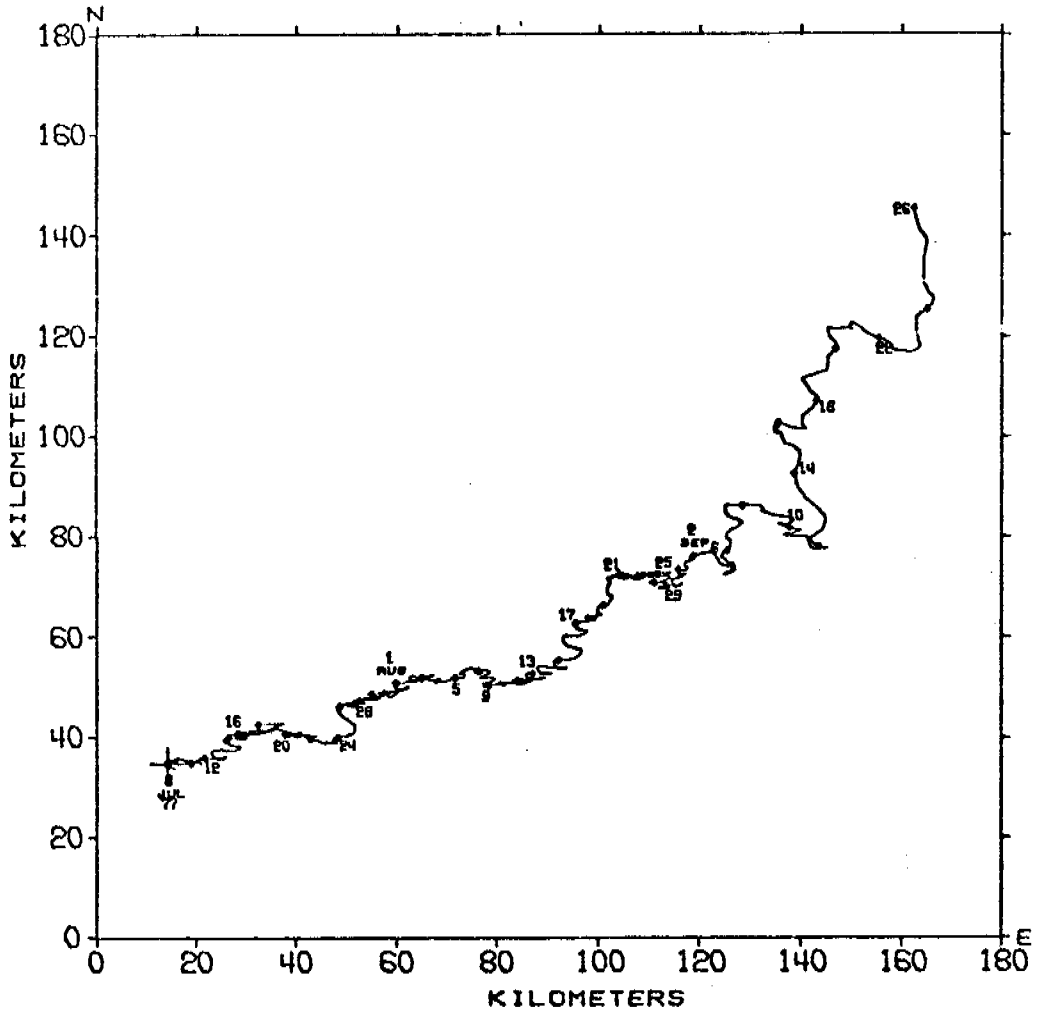

KINETIC ENERGY SPECTRUM OF CURRENTS AT CM1 - GEOPROBE, NS77
LOCATION = LAT 64 00N, LONG 165 00W, DEPTH = 17.5 METERS
OBSERVATION PERIOD = 0000 8 JUL 77 TO 2300 25 SEP 77 (80.0 DAYS)
N = 1920, DT = 1.0 HOURS, SMOOTHING - DANIELL WINDOW

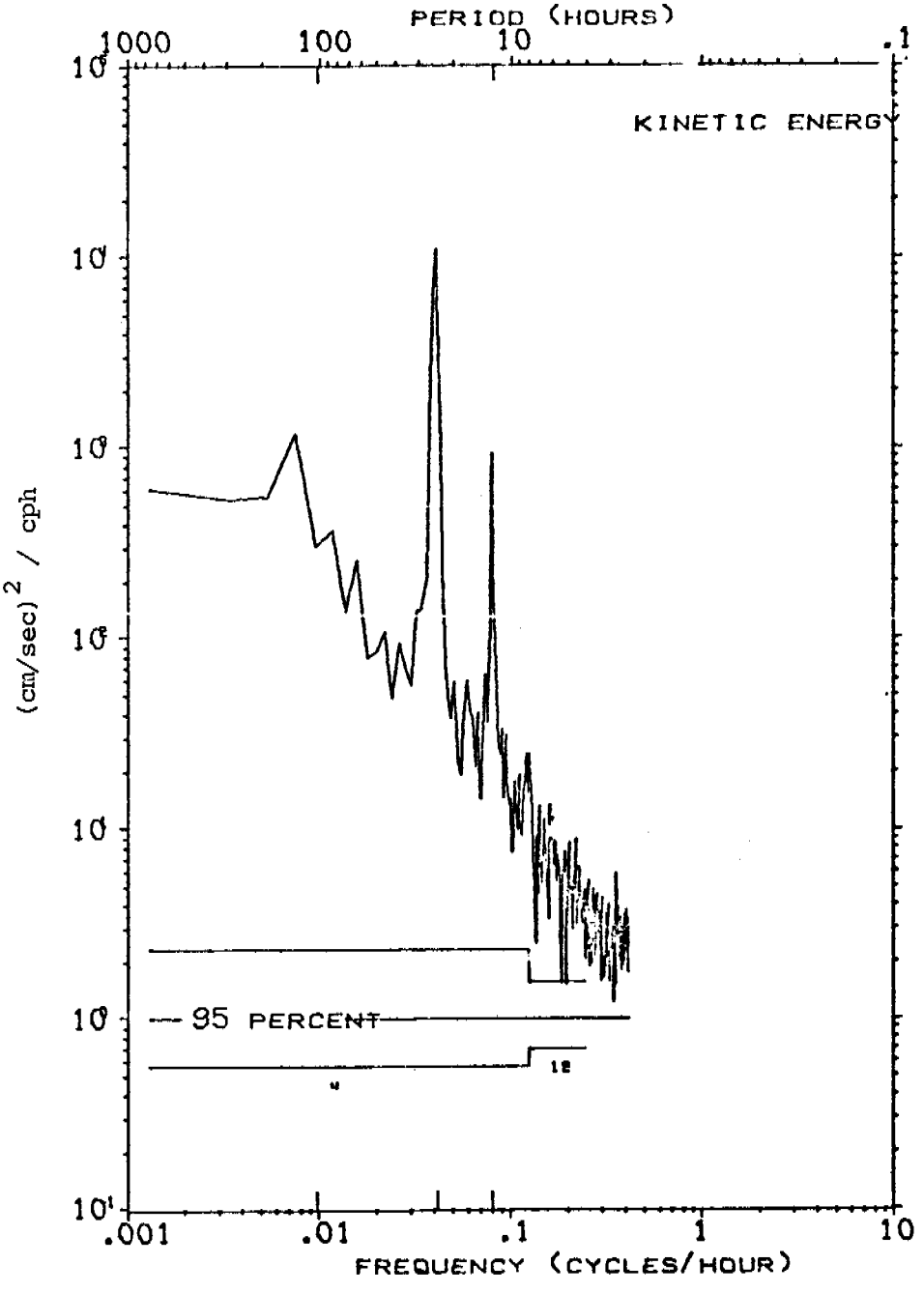

U, V AND ROTORY SPECTRA OF CURRENTS AT CM1 - GEOPROBE, NS77
LOCATION = LAT 64 00N, LONG 165 00W, DEPTH = 17.5 METERS
OBSERVATION PERIOD = 0000 8 JUL 77 TO 2300 25 SEP 77 (80.0 DAYS)
N = 1920, DT = 1.0 HOU S, SMOOTHING - DANIELL WINDOW

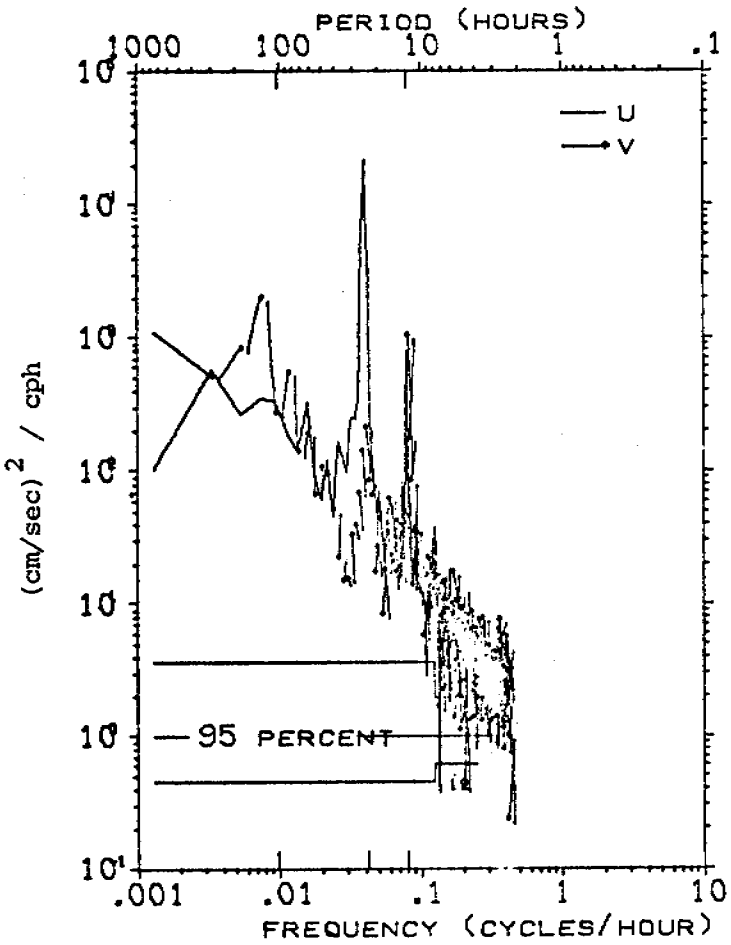

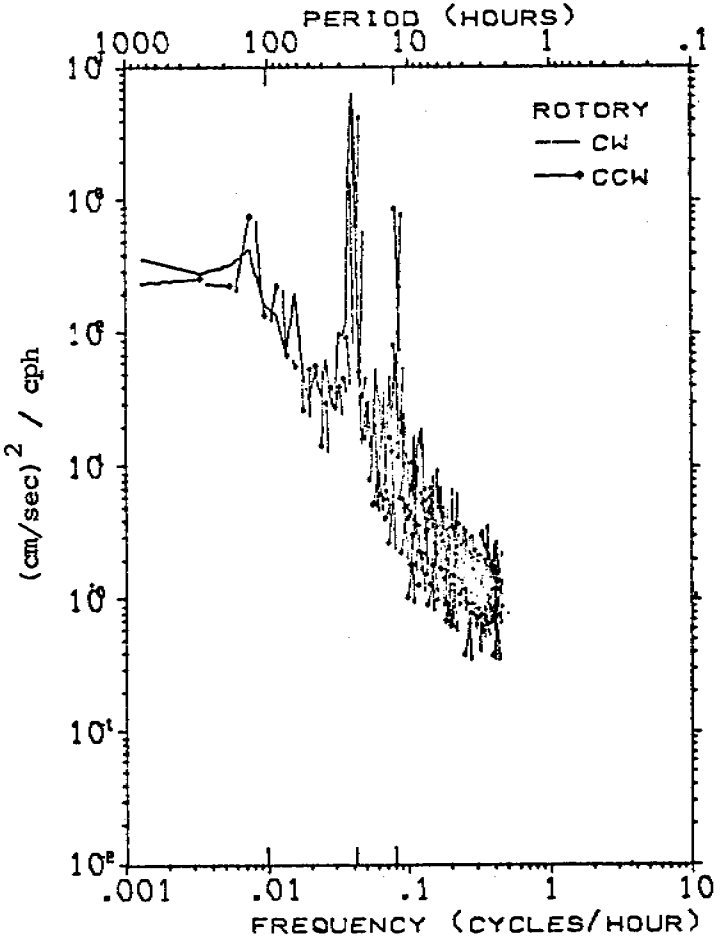

STATISTICS AND HISTOGRAMS OF CURRENTS AT CM2 - GEOPROBE, NS77
LOCATION = LAT 64 00N, LONG 165 00W, DEPTH = 17.5 METERS
OBSERVATION PERIOD = 0000 8 JUL 77 TO 2300 25 SEP 77 (80.0 DAYS)
N = 1920 DT = 1.00 HOURS, UNITS = (CM/SEC)

	MEAN	VARIANCE	ST-DEV	SKEW	KURT	MAX	MIN
S	12.11	40.29	6.35	0.465	2.896	36.99	0.23
U	0.96	122.97	11.09	0.173	2.144	32.11	-23.48
V	2.81	55.16	7.43	0.684	4.509	35.84	-27.62

S = SPEED
U = EAST-WEST COMPONENT OF VELOCITY, EAST =POSITIVE U
V = NORTH-SOUTH COMPONENT OF VELOCITY, NORTH = POSITIVE V

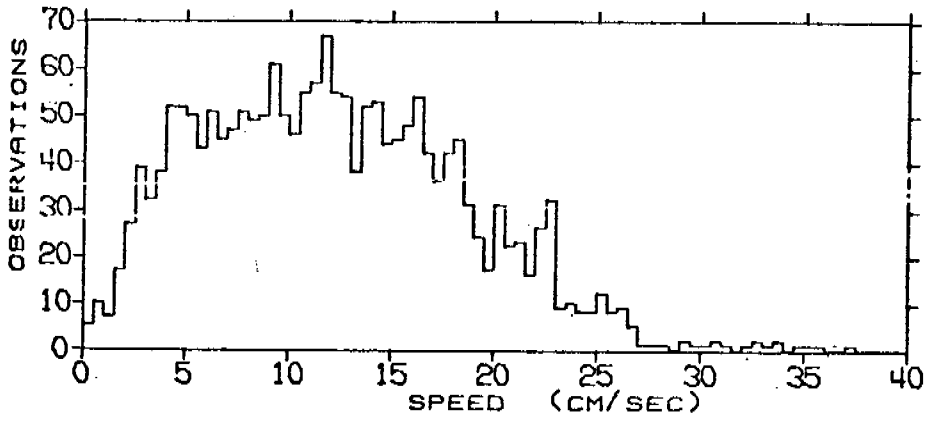

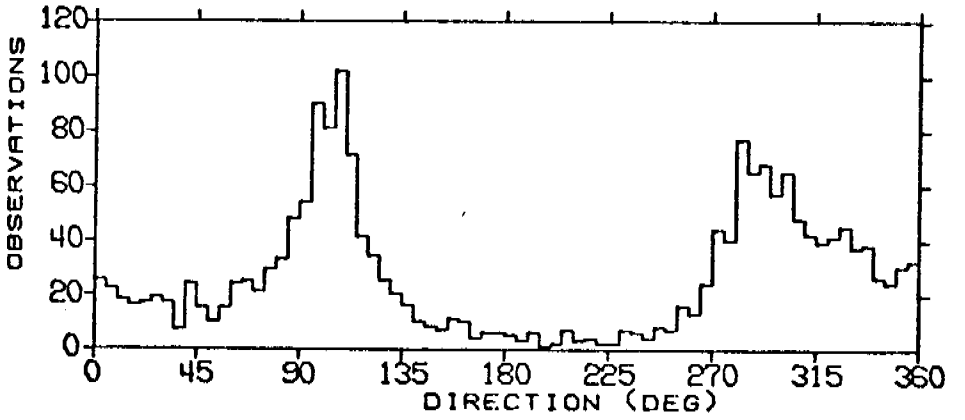

TIME SERIES OF VECTOR AVERAGED CURRENTS AT CM2 - GEOPROBE, NS77
LOCATION = LAT 64 00N, LONG 165 00W, DEPTH = 17.5 METERS
OBSERVATION PERIOD = 0000 8 JUL 77 TO 2300 27 JUL 77 (20.0 DAYS)
AVERAGING INTERVAL = 1.0 HOURS (1 POINTS)

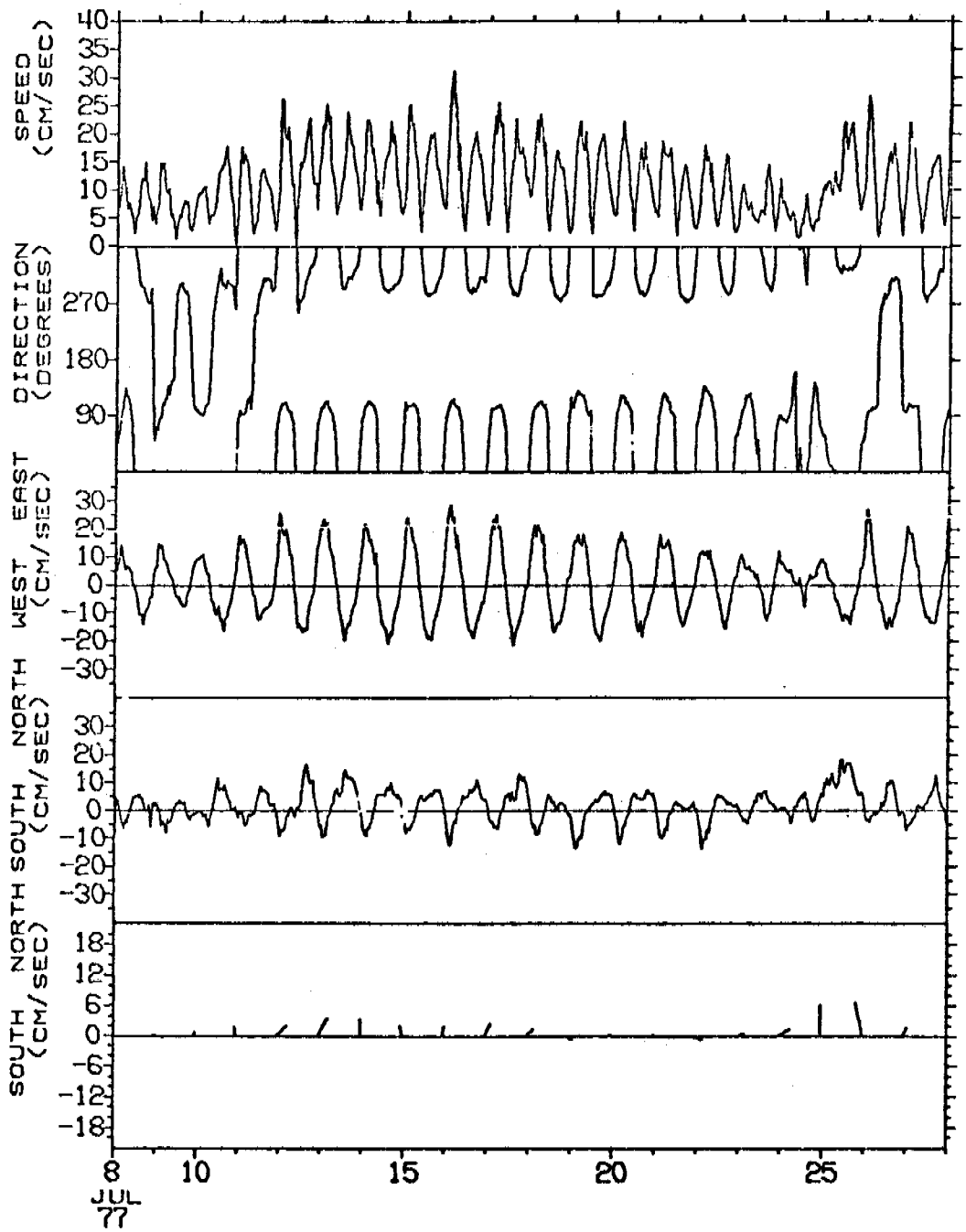

TIME SERIES OF VECTOR AVERAGED CURRENTS AT CM2 - GEOPROBE, NS77
LOCATION = LAT 64 00N, LONG 165 00W, DEPTH = 17.5 METERS
OBSERVATION PERIOD = 0000 28 JUL 77 TO 2300 16 AUG 77 (20.0 DAYS)
AVERAGING INTERVAL = 1.0 HOURS (1 POINTS)

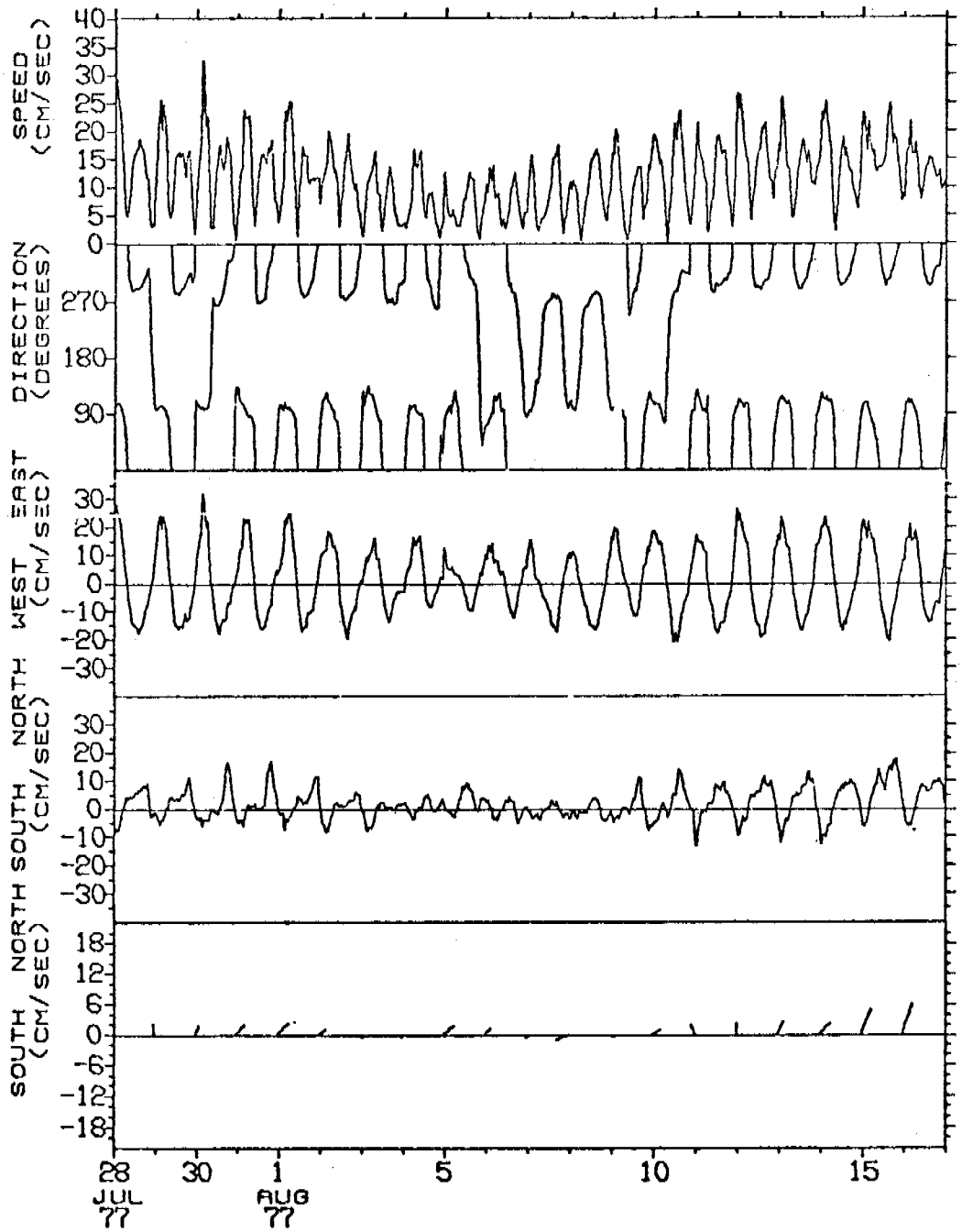

TIME SERIES OF VECTOR AVERAGED CURRENTS AT CM2 - GEOPROBE, NS77
LOCATION = LAT 64 00N, LONG 165 00W, DEPTH = 17.5 METERS
OBSERVATION PERIOD = 0000 17 AUG 77 TO 2300 5 SEP 77 (20.0 DAYS)
AVERAGING INTERVAL = 1.0 HOURS (1 POINTS)

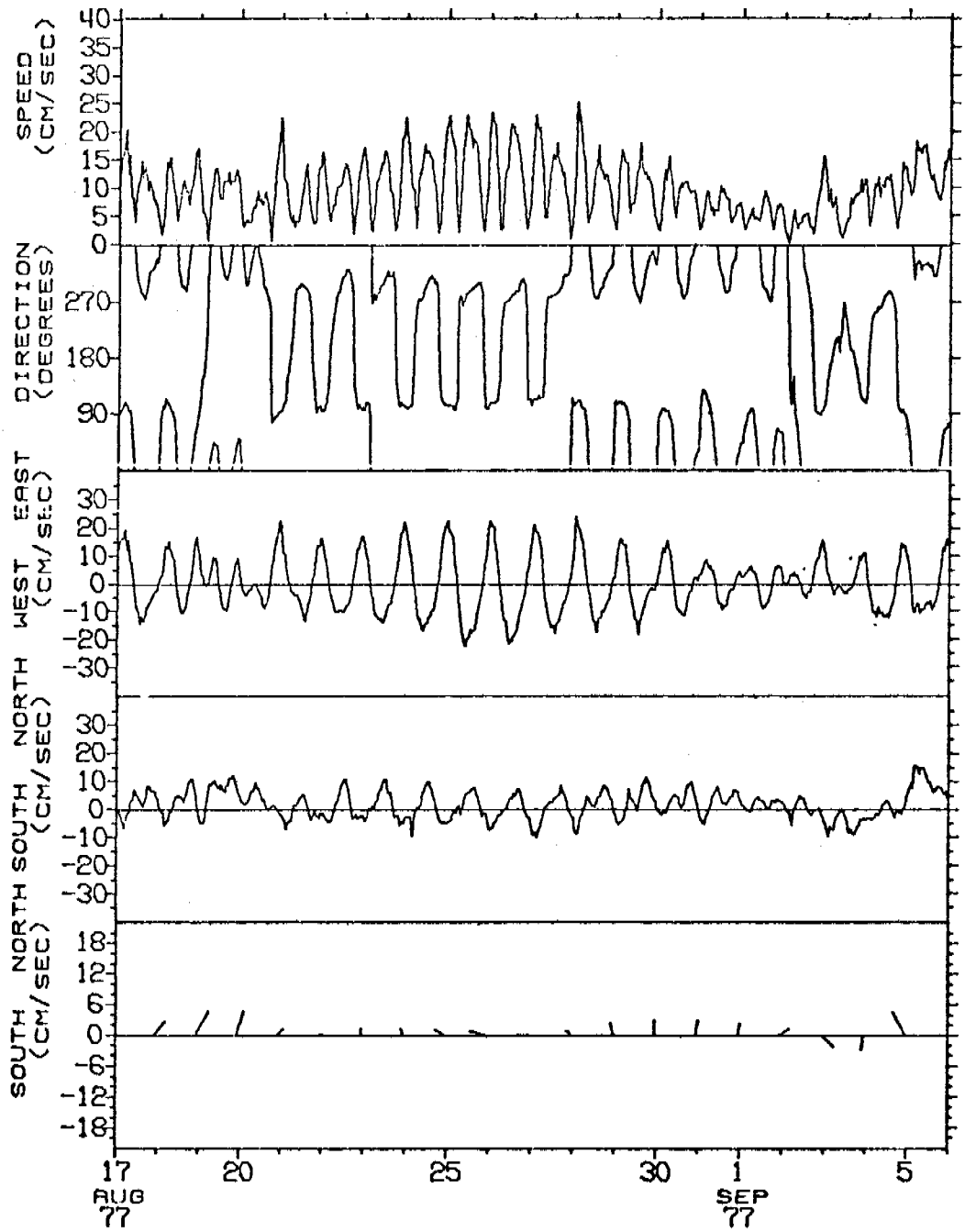

TIME SERIES OF VECTOR AVERAGED CURRENTS AT CM2 - GEOPROBE, NS77
LOCATION = LAT 64 00N, LONG 165 00W, DEPTH = 17.5 METERS
OBSERVATION PERIOD = 0000 6 SEP 77 TO 2300 25 SEP 77 (20.0 DAYS)
AVERAGING INTERVAL = 1.0 HOURS (1 POINTS)

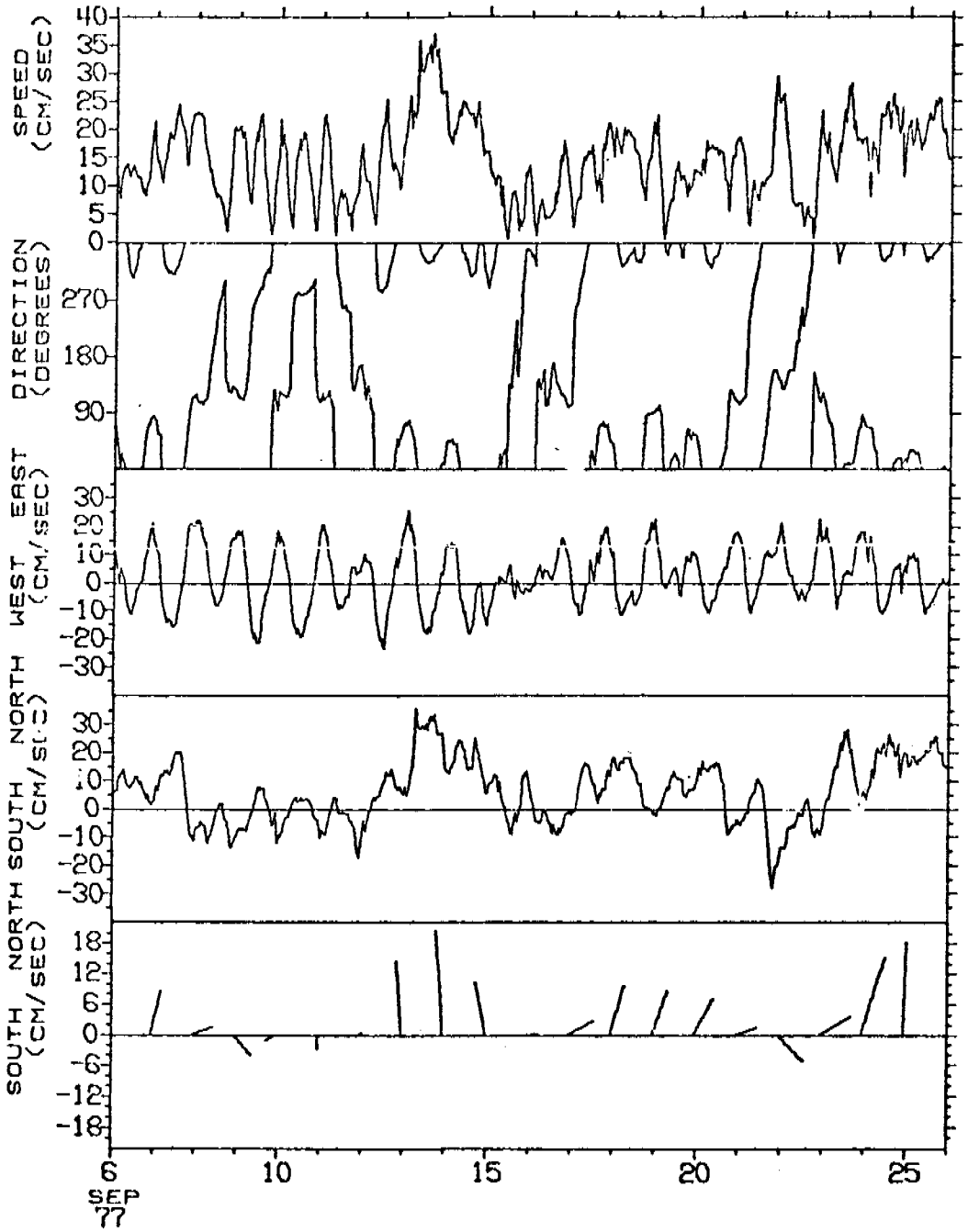

PROGRESSIVE VECTOR DIAGRAM OF CURRENTS AT CM2 - GEOPROBE, NS77
LOCATION = LAT 64 00N, LONG 165 00W, DEPTH = 17.5 METERS
OBSERVATION PERIOD = 0000 8 JUL 77 TO 2300 25 SEP 77 (80.0 DAYS)
* EVERY 2.0 DAYS BEGINNING AT 0000 8 JUL 77

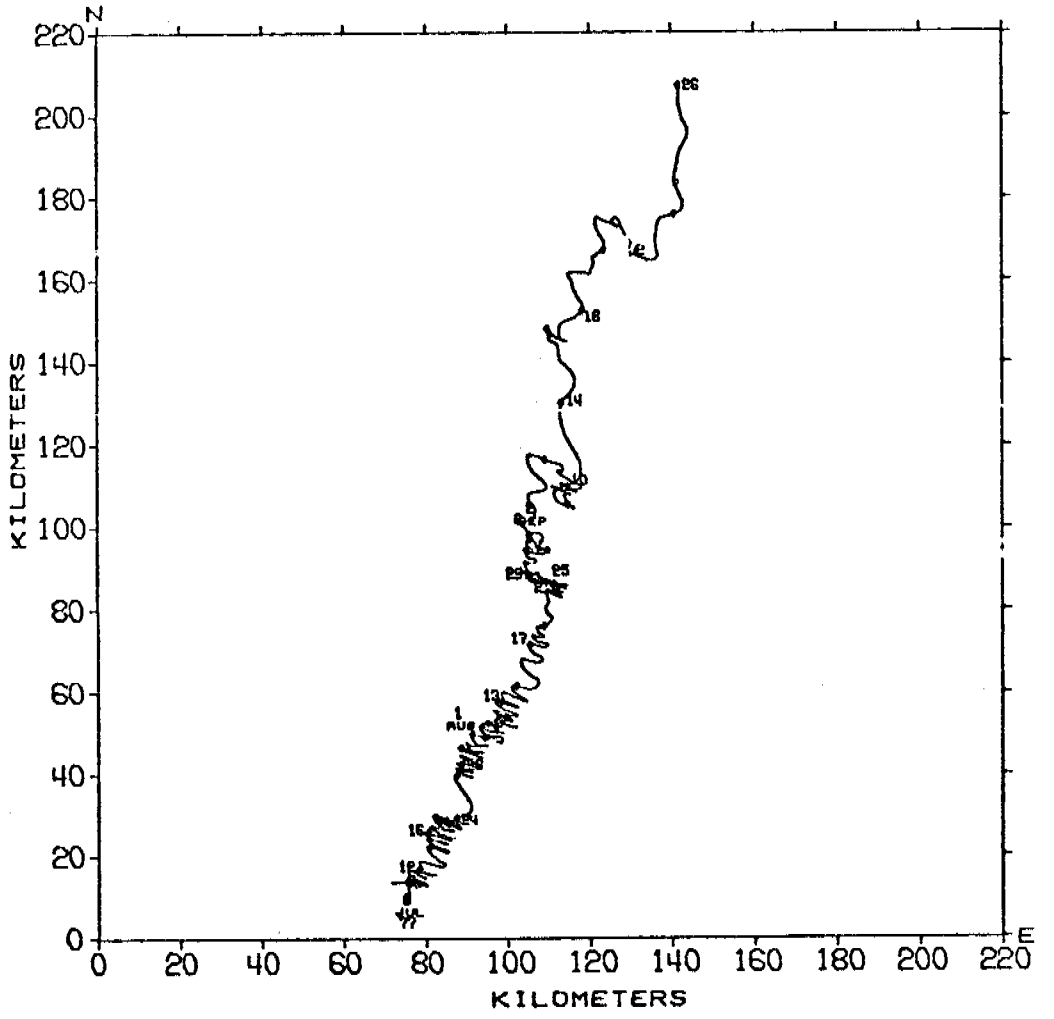

KINETIC ENERGY SPECTRUM OF CURRENTS AT CM2 - GEOPROBE, NS'77
LOCATION = LAT 64 00N, LONG 165 00W, DEPTH = 17.5 METERS
OBSERVATION PERIOD = 0000 8 JUL 77 TO 2300 25 SEP 77 (80.0 DAYS)
N = 1920, DT = 1.0 HOURS, SMOOTHING - DANIELL WINDOW

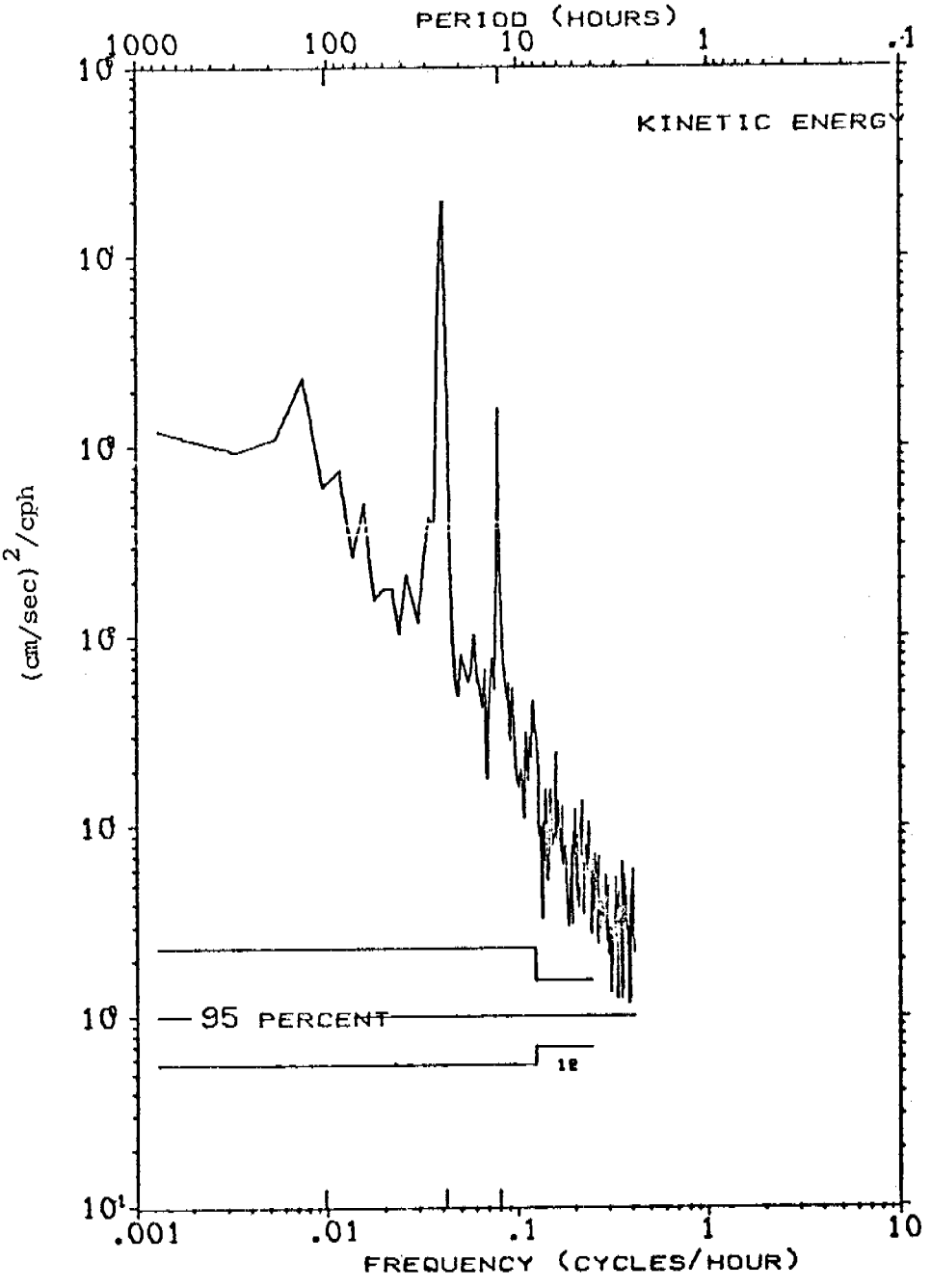

U, V AND ROTORY SPECTRA OF CURRENTS AT CM2 - GEOPROBE, NS77
LOCATION = LAT 64 00N, LONG 165 00W, DEPTH = 17.5 METERS
OBSERVATION PERIOD = 0000 8 JUL 77 TO 2300 25 SEP 77 (80.0 DAYS)
N = 1920, DT = 1.0 HOURS, SMOOTHING - DANIELL WINDOW

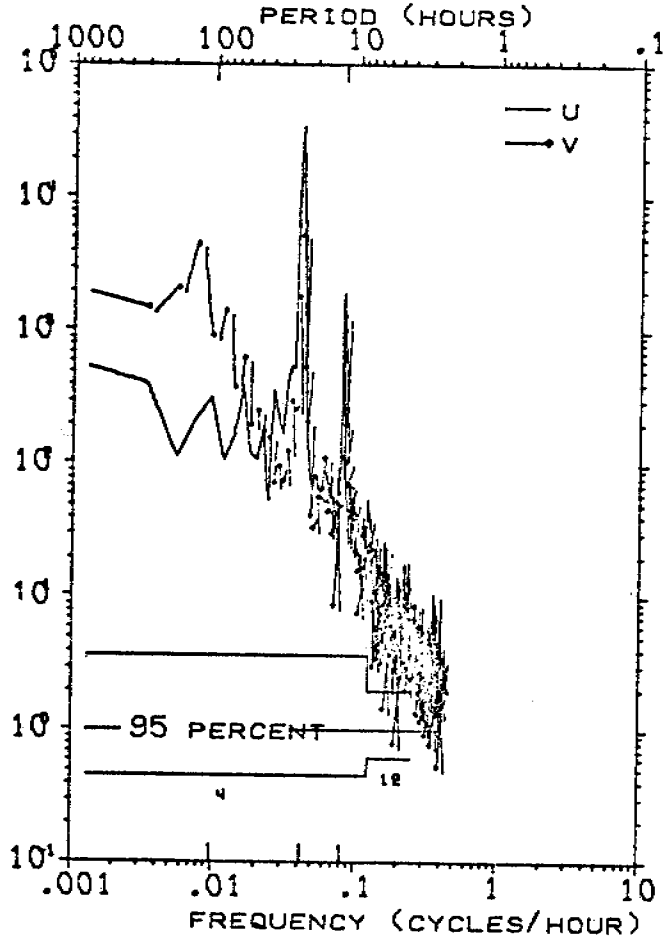

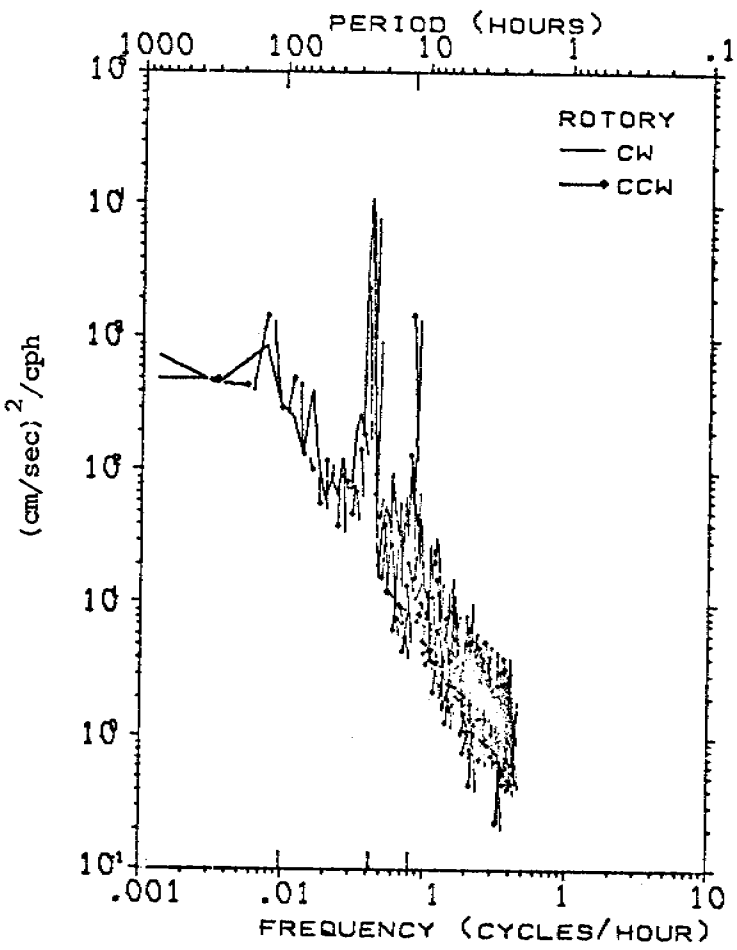

STATISTICS AND HISTOGRAMS OF CURRENTS AT CM3 - GEOPROBE, NS77
LOCATION = LAT 64 00N, LONG 165 00W, DEPTH = 17.5 METERS
OBSERVATION PERIOD = 0000 8 JUL 77 TO 2300 25 SEP 77 (80.0 DAYS)
N = 1920 DT = 1.00 HOURS, UNITS = (CM/SEC)

	MEAN	VARIANCE	ST-DEV	SKEW	KURT	MAX	MIN
S	13.00	47.84	6.92	0.558	3.020	39.68	0.66
U	1.42	155.17	12.46	0.209	2.107	34.77	-27.55
V	3.62	46.52	6.82	1.113	5.413	37.24	-23.09

S = SPEED
U = EAST-WEST COMPONENT OF VELOCITY, EAST =POSITIVE U
V = NORTH-SOUTH COMPONENT OF VELOCITY, NORTH = POSITIVE V

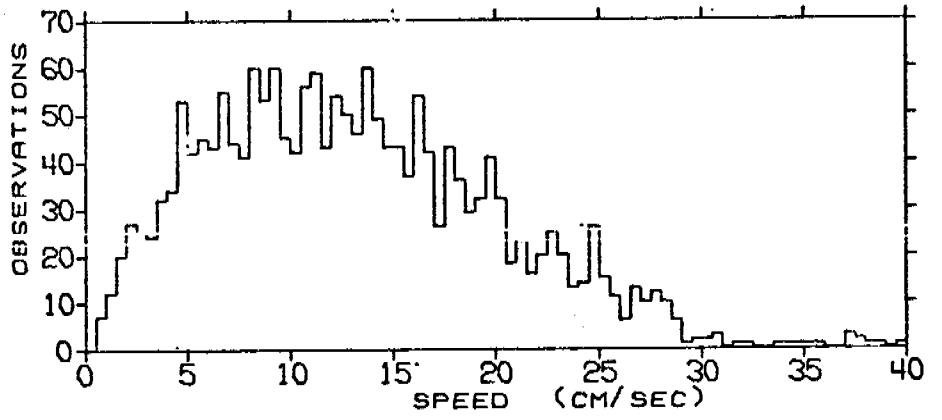

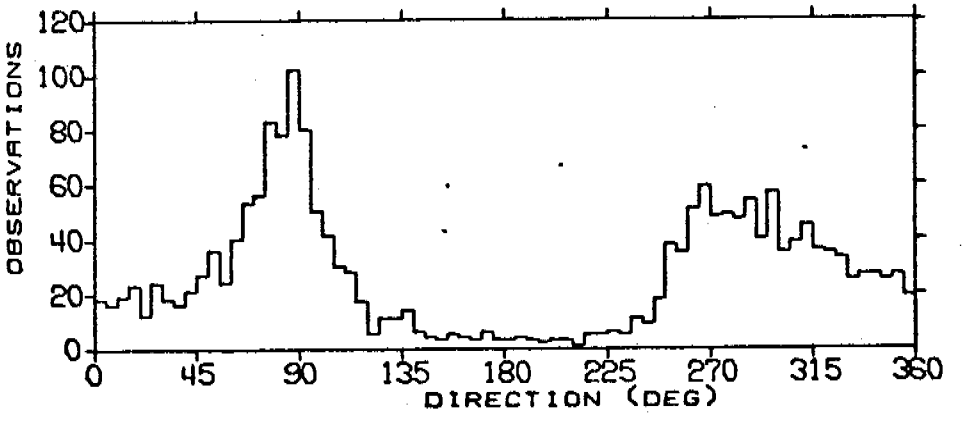

TIME SERIES OF VECTOR AVERAGED CURRENTS AT CM3 - GEOPROBE, NS77
LOCATION = LAT 64 00N, LONG 165 00W, DEPTH = 17.5 METERS
OBSERVATION PERIOD = 0000 8 JUL 77 TO 2300 27 JUL 77 (20.0 DAYS)
AVERAGING INTERVAL = 1.0 HOURS (1 POINTS)

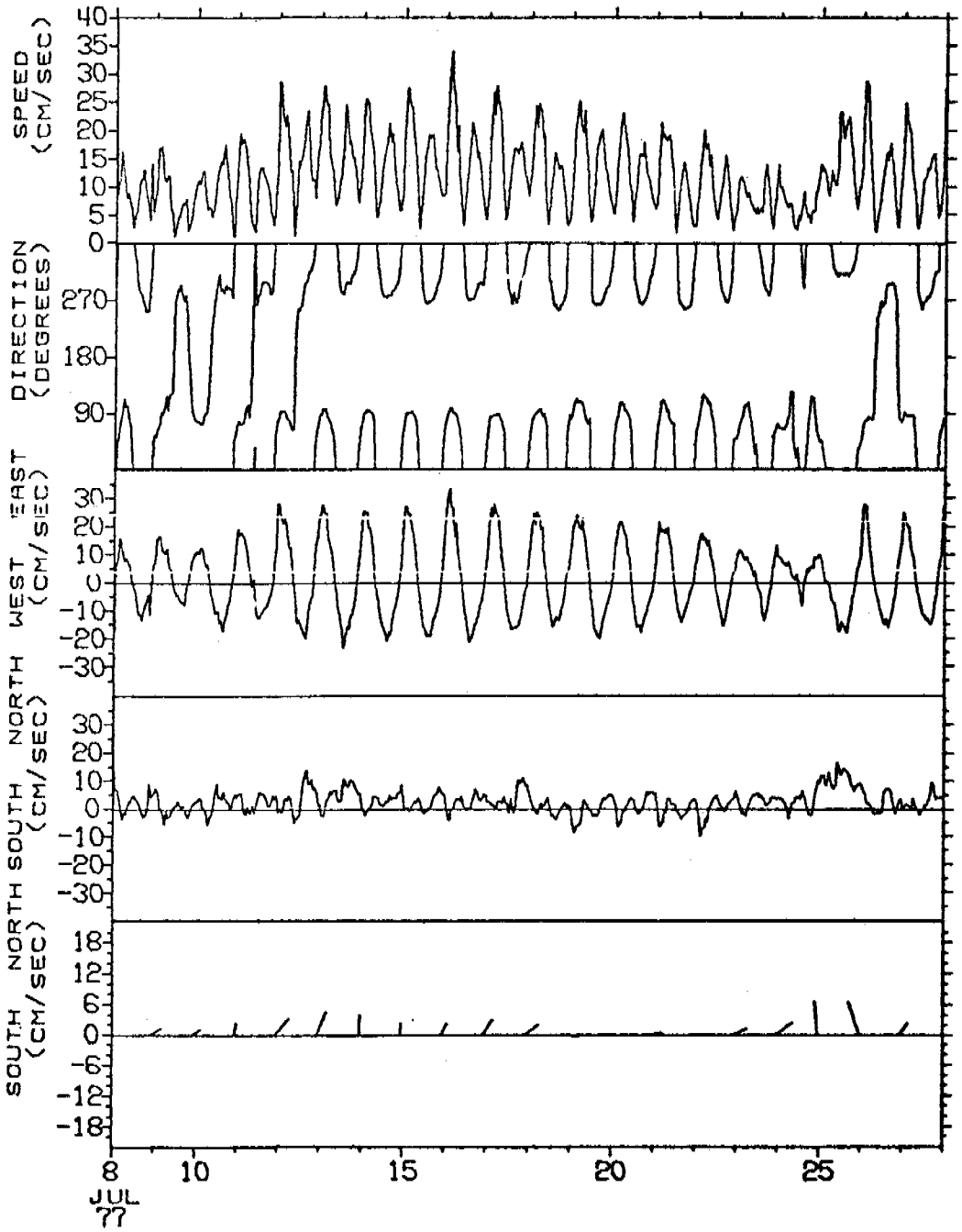

TIME SERIES OF VECTOR AVERAGED CURRENTS AT CM3 - GEOPROBE, NS77
LOCATION = LAT 64 00N, LONG 165 00W, DEPTH = 17.5 METERS
OBSERVATION PERIOD = 0000 28 JUL 77 TO 2300 16 AUG 77 (20.0 DAYS)
AVERAGING INTERVAL = 1.0 HOURS (1 POINTS)

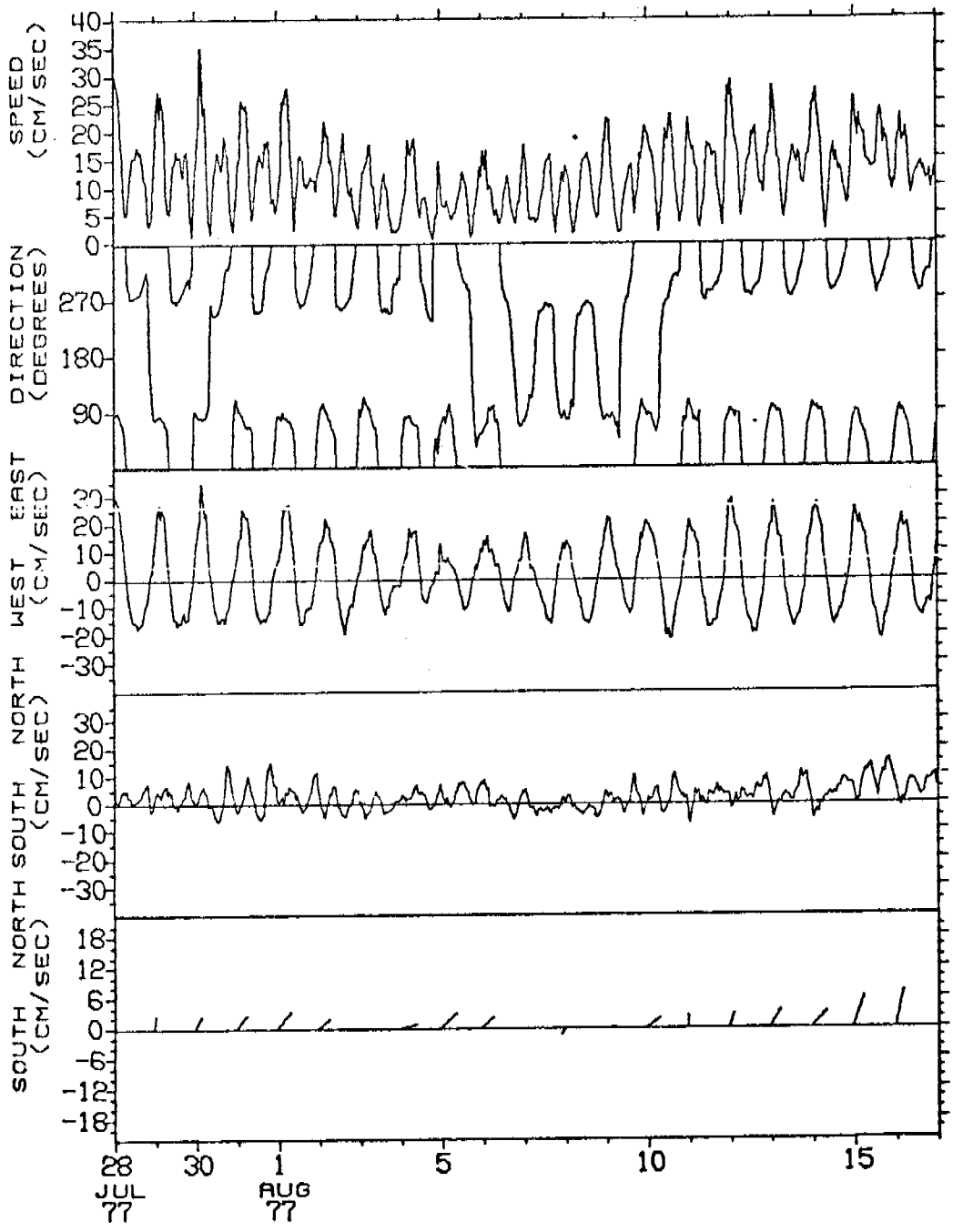

TIME SERIES OF VECTOR AVERAGED CURRENTS AT CM3 - GEOPROBE, NS77
LOCATION = LAT 64 00N, LONG 165 00W, DEPTH = 17.5 METERS
OBSERVATION PERIOD = 0000 17 AUG 77 TO 2300 5 SEP 77 (20.0 DAYS)
AVERAGING INTERVAL = 1.0 HOURS (1 POINTS)

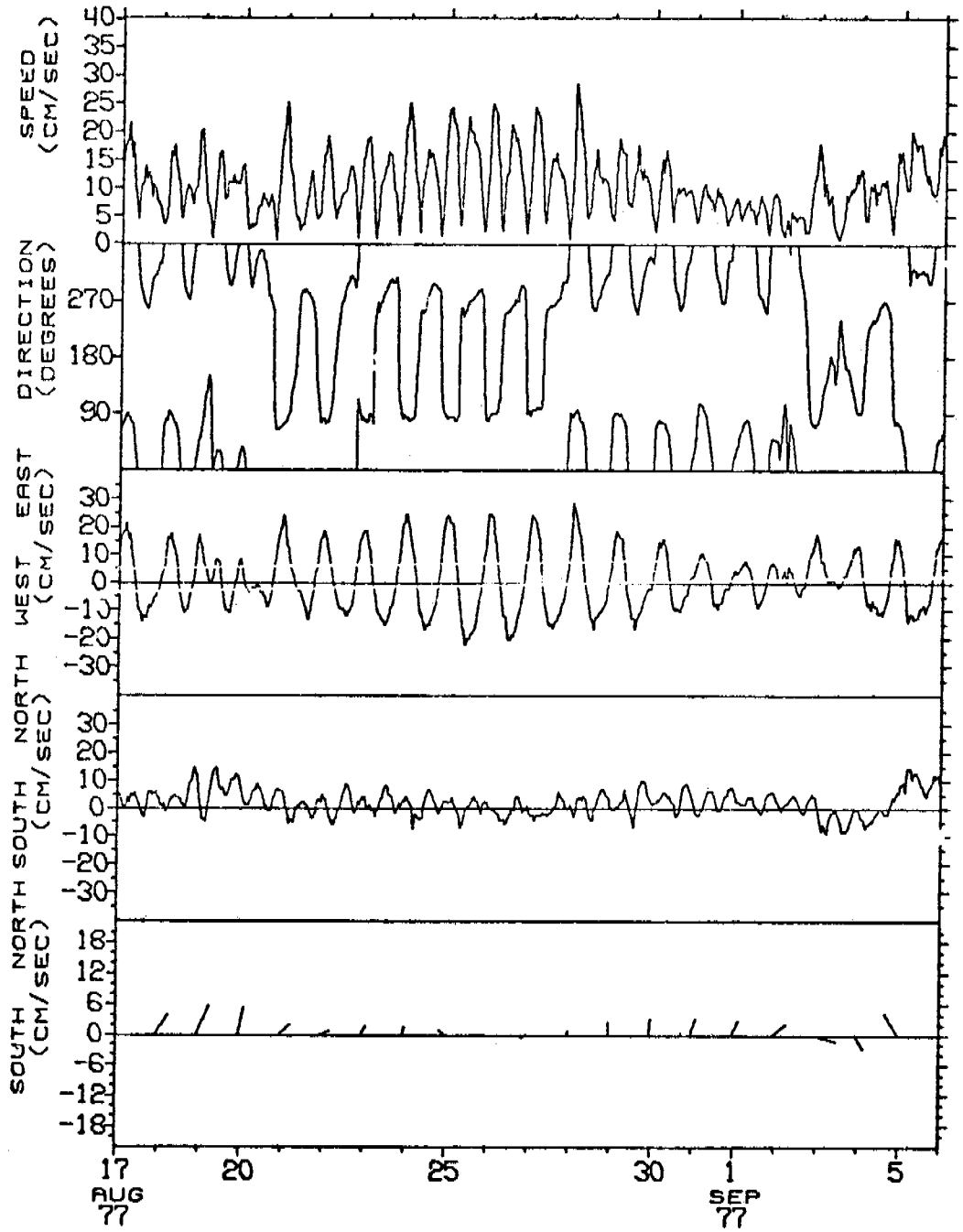

TIME SERIES OF VECTOR AVERAGED CURRENTS AT CM3 - GEOPROBE, NS77
LOCATION = LAT 64 00N, LONG 165 00W, DEPTH = 17.5 METERS
OBSERVATION PERIOD = 0000 6 SEP 77 TO 2300 25 SEP 77 (20.0 DAYS)
AVERAGING INTERVAL = 1.0 HOURS (1 POINTS)

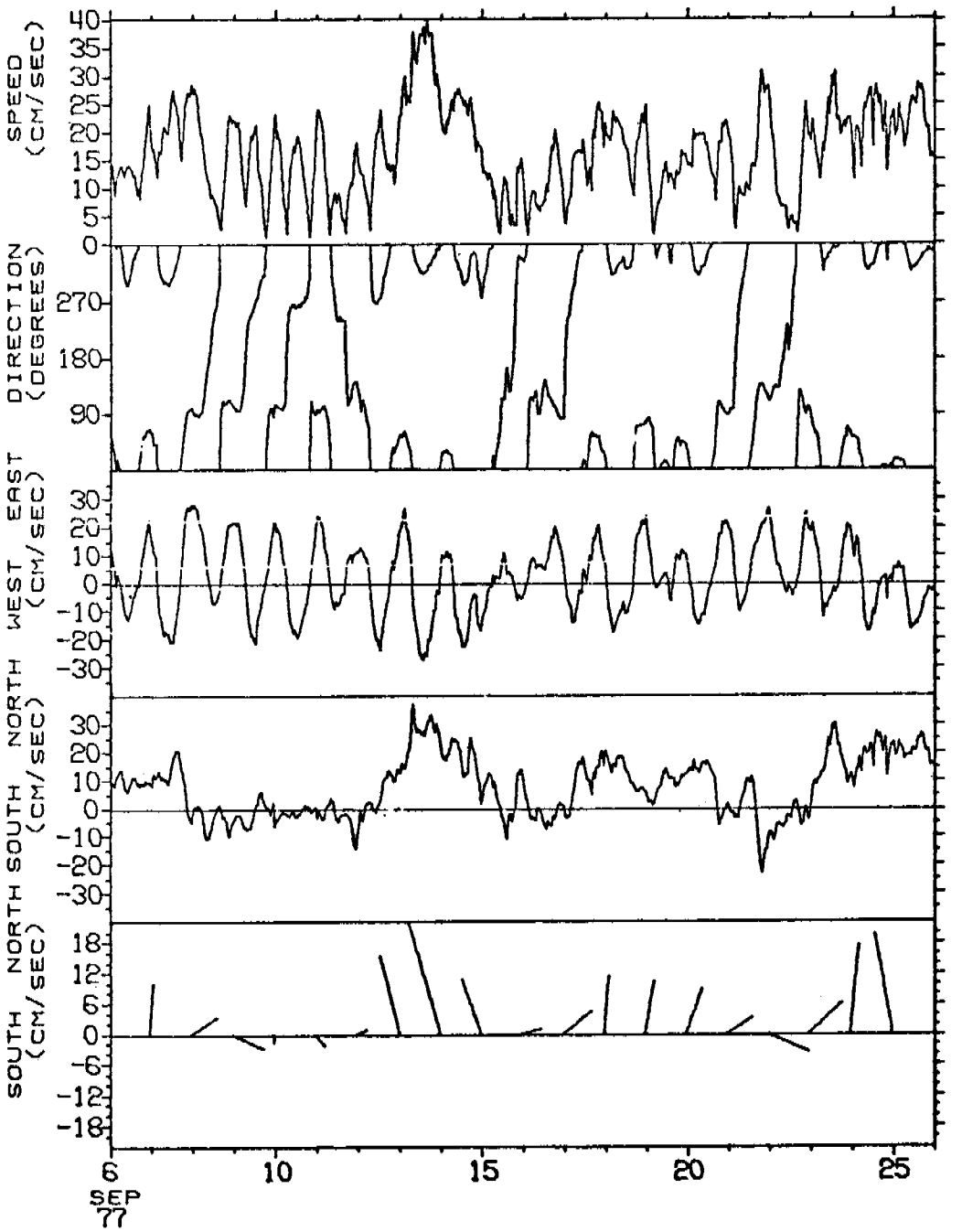

PROGRESSIVE VECTOR DIAGRAM OF CURRENTS AT CM3 - GEOPROBE, NS77
LOCATION = LAT 64 00N, LONG 165 00W, DEPTH = 17.5 METERS
OBSERVATION PERIOD = 0000 8 JUL 77 TO 2300 25 SEP 77 (80.0 DAYS
* EVERY 2.0 DAYS BEGINNING AT 0000 8 JUL 77

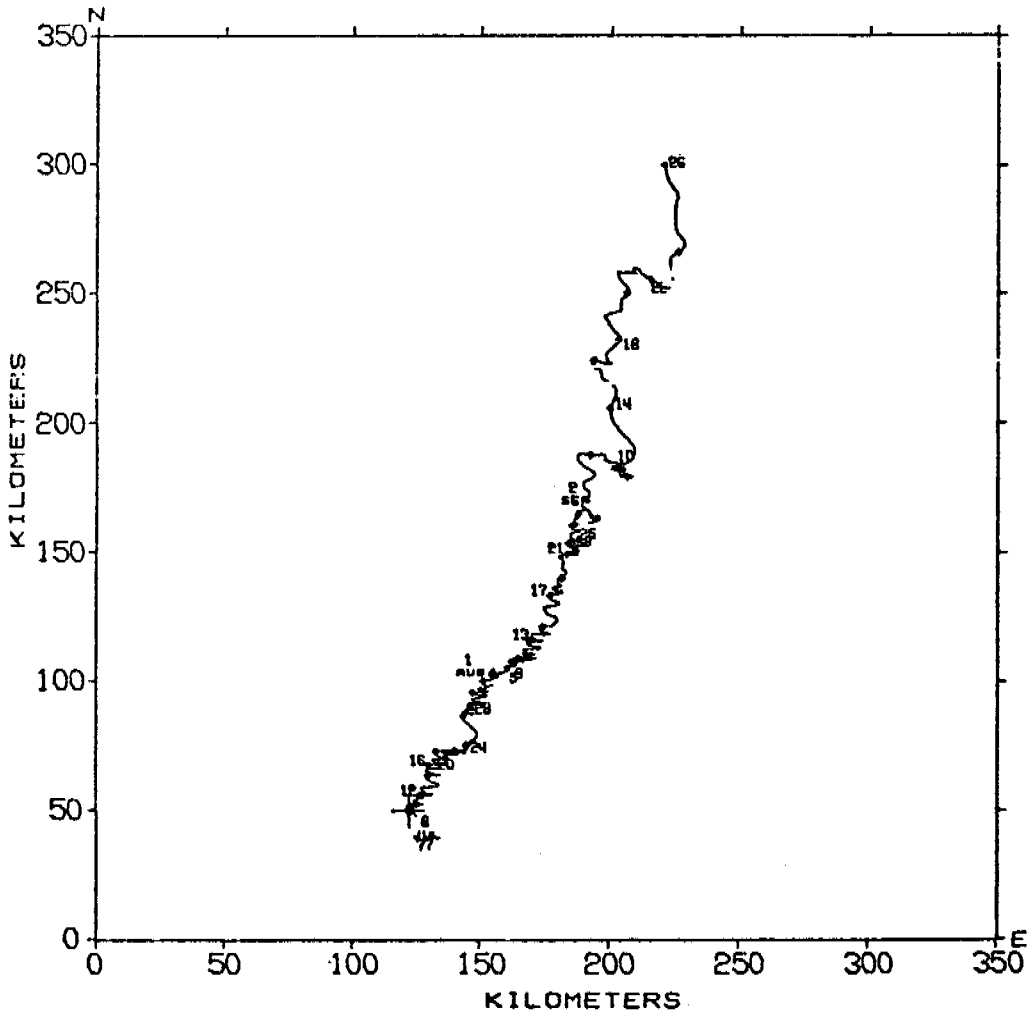

KINETIC ENERGY SPECTRUM OF CURRENTS AT CM3 - GEOPROBE, NS77
LOCATION = LAT 64 00N, LONG 165 00W, DEPTH = 17.5 METERS
OBSERVATION PERIOD = 0000 8 JUL 77 TO 2300 25 SEP 77 (80.0 DAYS)
N = 1920, DT = 1.0 HOURS, SMOOTHING - DANIELL WINDOW

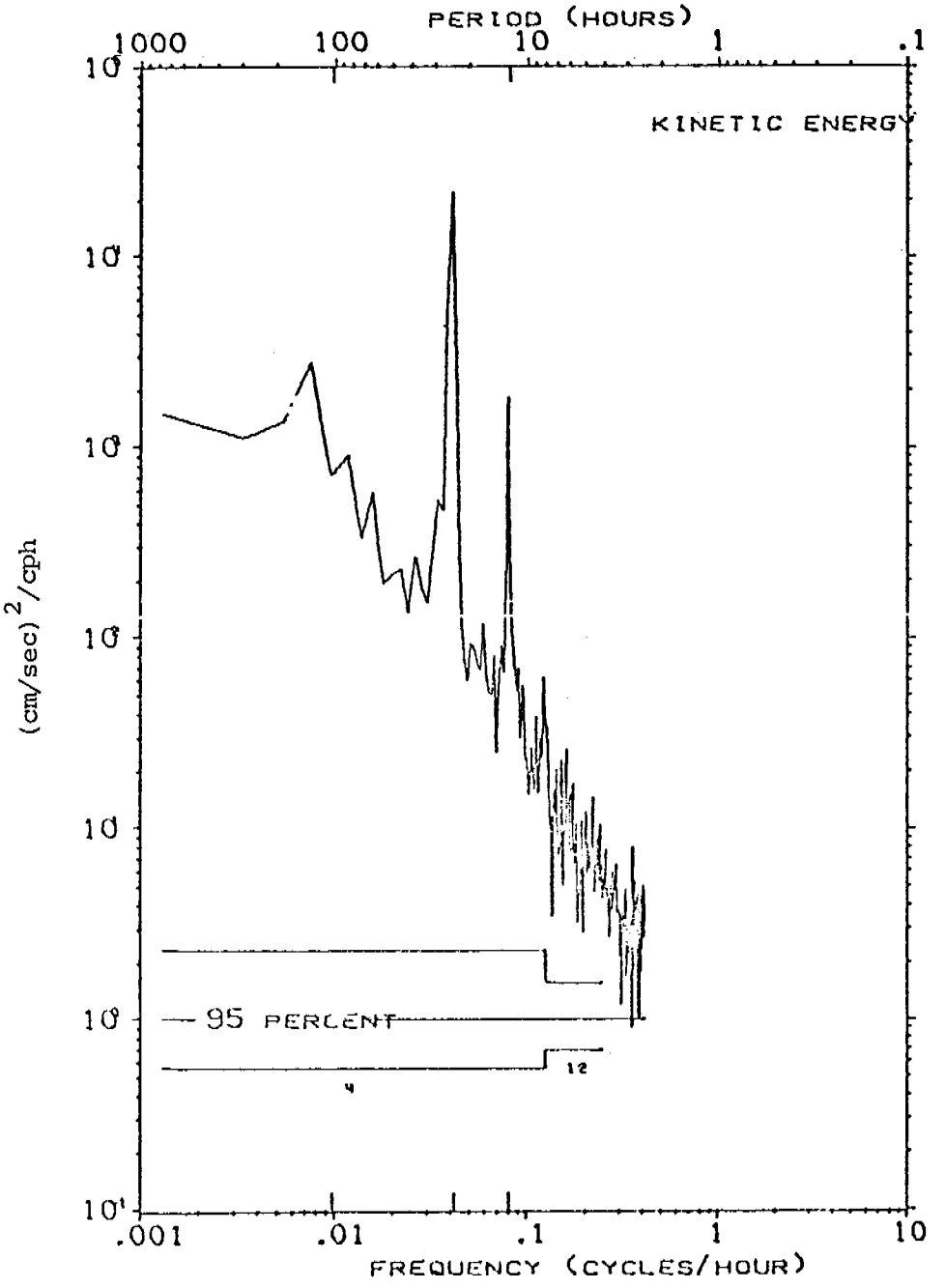

U, V AND ROTORY SPECTRA OF CURRENTS AT CM3 - GEOPROBE, NS77
LOCATION = LAT 64 C0N, LONG 165 00W, DEPTH = 17.5 METERS
OBSERVATION PERIOD = C000 8 JUL 77 TO 2300 25 SEP 77 (80.0 DAYS)
N = 1920, DT = 1.0 HOURS, SMOOTHING - DANIELL WINDOW

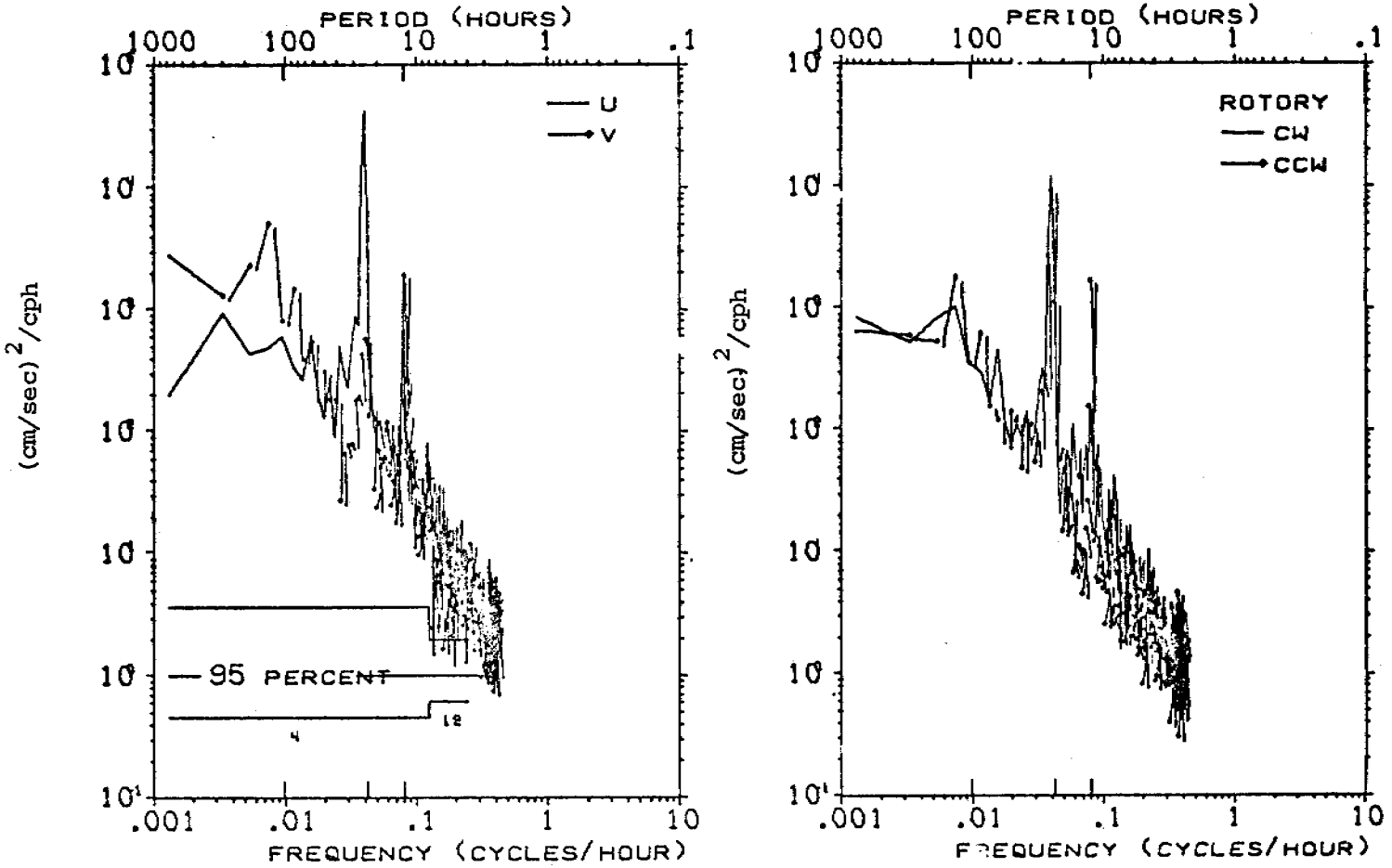

STATISTICS AND HISTOGRAMS OF CURRENTS AT CM4 - GEOPROBE, NS77
LOCATION = LAT 64 00N, LONG 165 00W, DEPTH = 17.5 METERS
OBSERVATION PERIOD = 0000 8 JUL 77 TO 2300 25 SEP 77 (80.0 DAYS)
N = 1920 DT = 1.00 HOURS, UNITS = (CM/SEC)

	MEAN	VARIANCE	ST-DEV	SKEW	KURT	MAX	MIN
S	14.05	56.05	7.49	0.543	2.966	43.10	0.16
U	2.43	159.37	12.62	0.135	2.099	36.86	-24.59
V	2.03	84.10	9.17	0.678	4.407	42.22	-32.04

S = SPEED
U = EAST-WEST COMPONENT OF VELOCITY, EAST =POSITIVE U
V = NORTH-SOUTH COMPONENT OF VELOCITY, NORTH = POSITIVE V

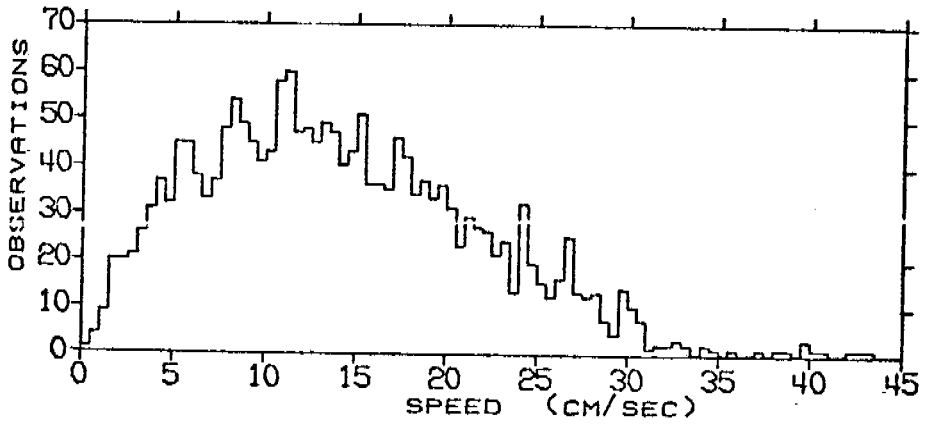

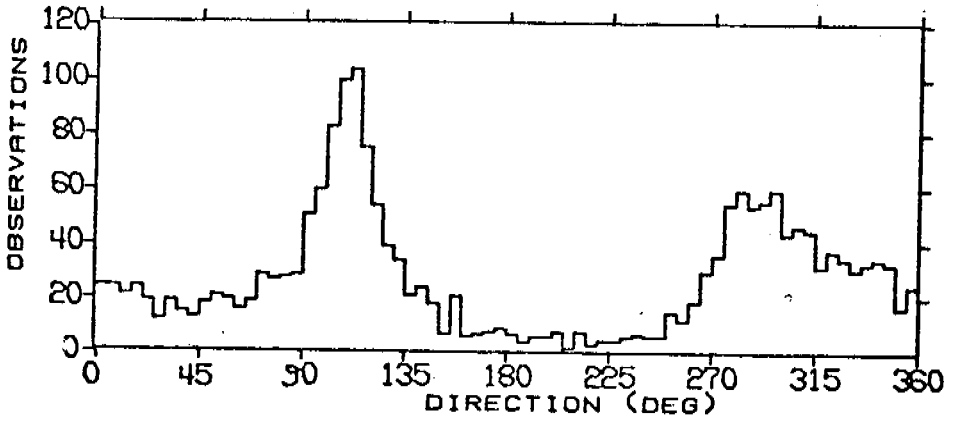

TIME SERIES OF VECTOR AVERAGED CURRENTS AT CM4 - GEOPROBE, NS77
LOCATION = LAT 64 00N, LONG 165 00W, DEPTH = 17.5 METERS
OBSERVATION PERIOD = 0000 8 JUL 77 TO 2300 27 JUL 77 (20.0 DAYS)
AVERAGING INTERVAL = 1.0 HOURS (1 POINTS)

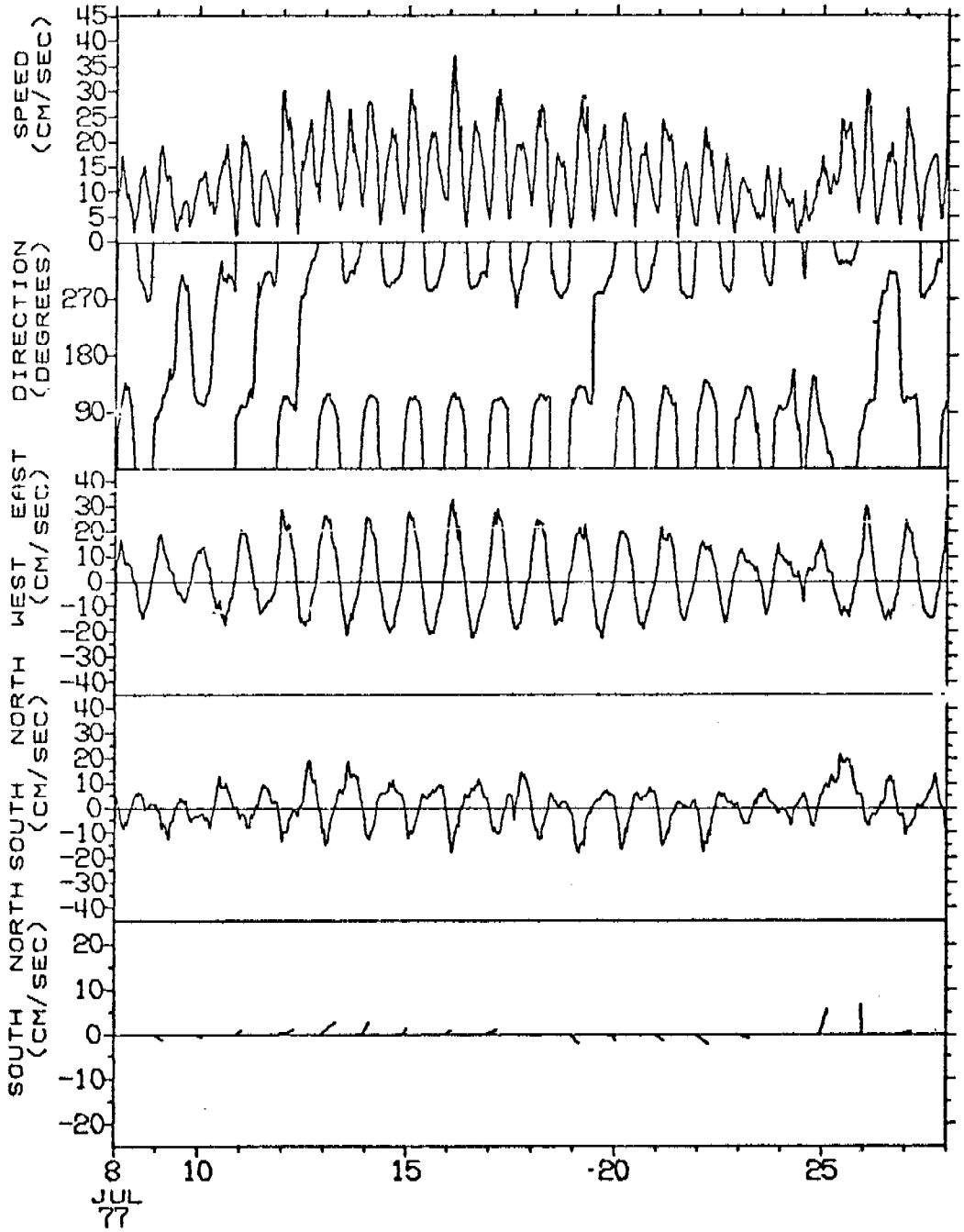

TIME SERIES OF VECTOR AVERAGED CURRENTS AT CM4 - GEOPROBE, NS77
LOCATION = LAT 64 00N, LONG 165 00W, DEPTH = 17.5 METERS
OBSERVATION PERIOD = 0000 28 JUL 77 TO 2300 16 AUG 77 (20.0 DAYS)
AVERAGING INTERVAL = 1.0 HOURS (1 POINTS)

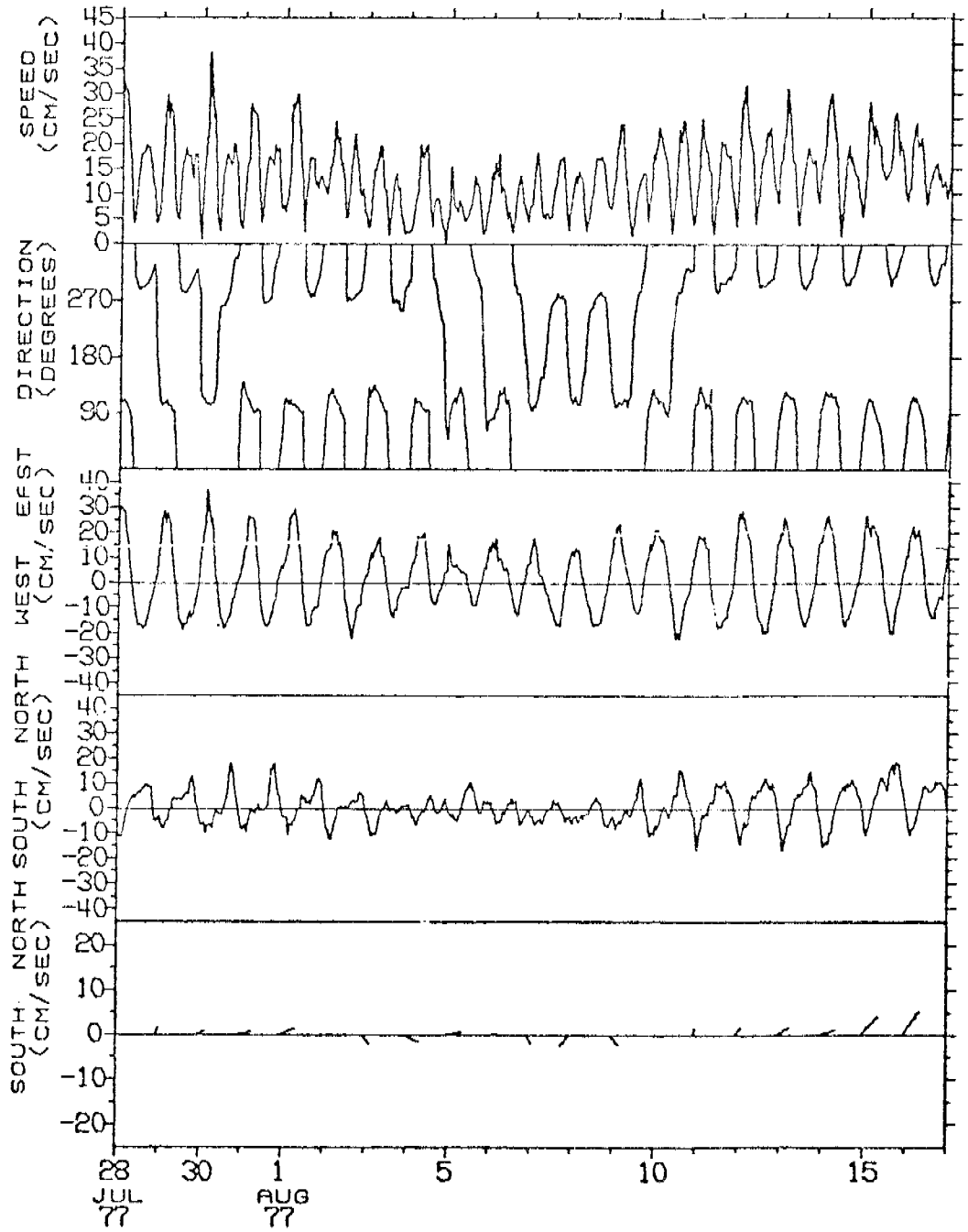

TIME SERIES OF VECTOR AVERAGED CURRENTS AT CM4 - GEOPROBE, NS77
LOCATION = LAT 64 00N, LONG 165 00W, DEPTH = 17.5 METERS
OBSERVATION PERIOD = 0000 17 AUG 77 TO 2300 5 SEP 77 (20.0 DAYS)
AVERAGING INTERVAL = 1.0 HOURS (1 POINTS)

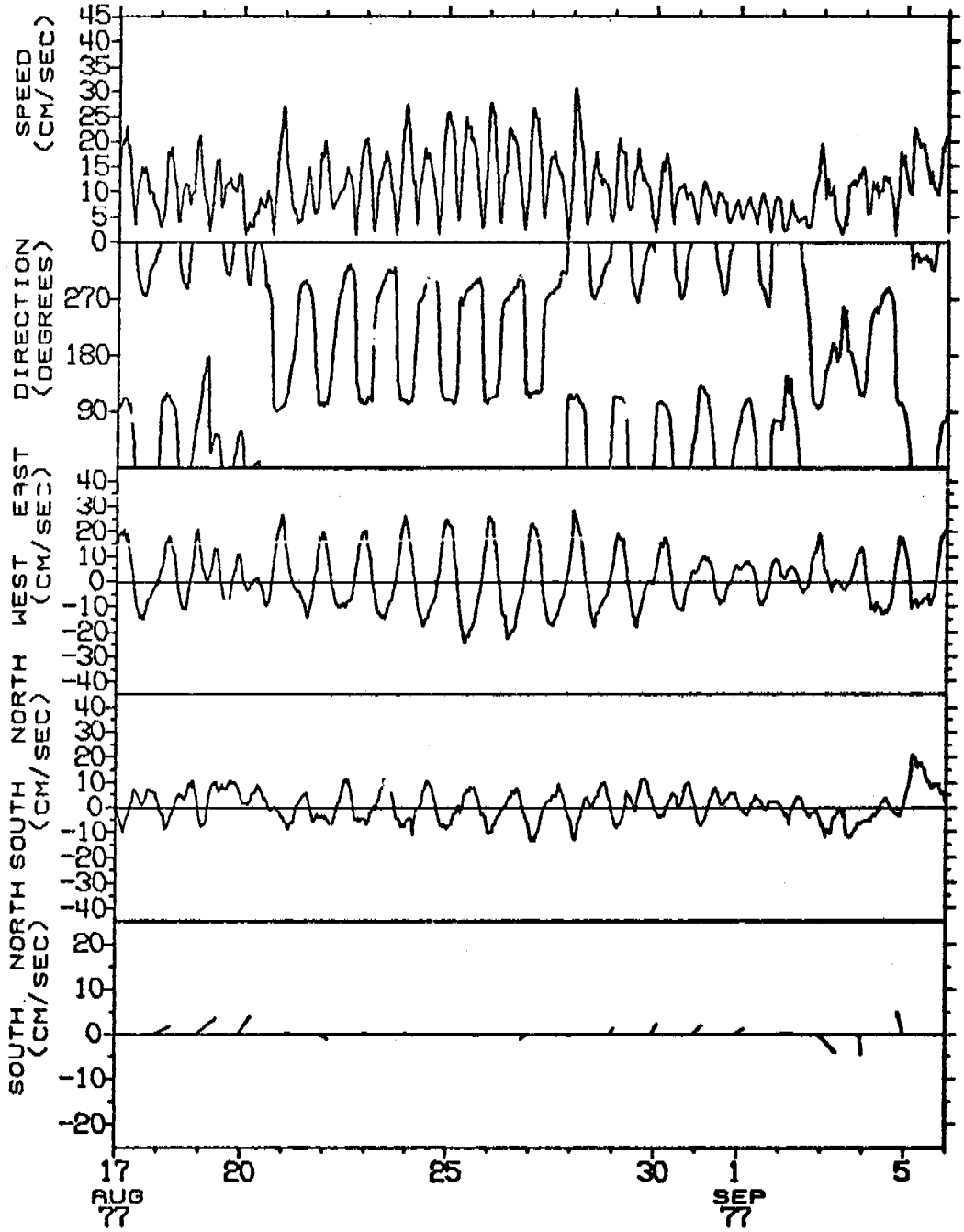

TIME SERIES OF VECTOR AVERAGED CURRENTS AT CM4 - GEOPROBE, NS77
LOCATION = LAT 64 00N, LONG 165 00W, DEPTH = 17.5 METERS
OBSERVATION PERIOD = 0000 6 SEP 77 TO 2300 25 SEP 77 (20.0 DAYS)
AVERAGING INTERVAL = 1.0 HOURS (1 POINTS)

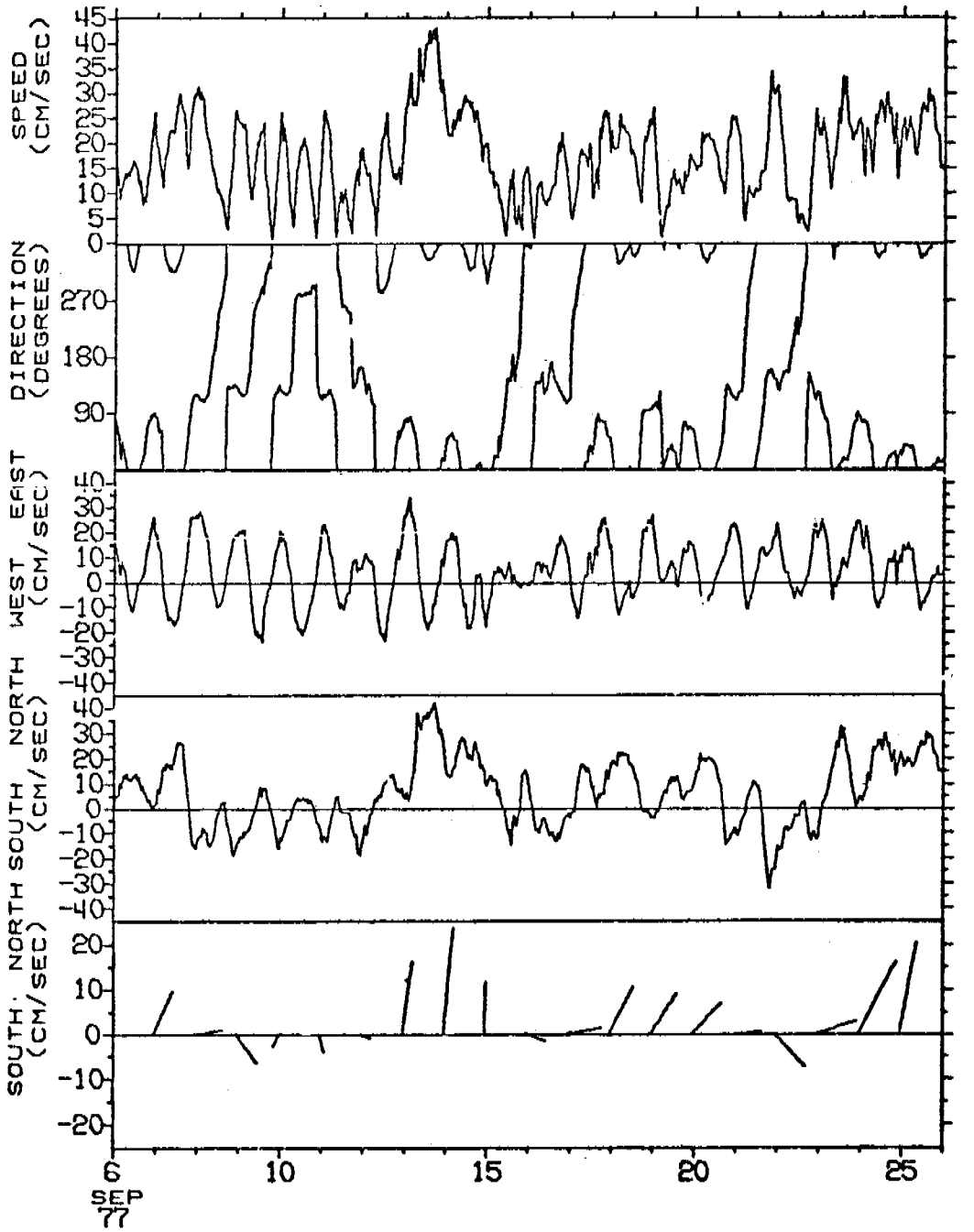

PROGRESSIVE VECTOR DIAGRAM OF CURRENTS AT CM4 - GEOPROBE, NS77
LOCATION = LAT 64 00N, LONG 165 00W, DEPTH = 17.5 METERS
OBSERVATION PERIOD = 0000 8 JUL 77 TO 2300 25 SEP 77 (80.0 DAYS)
* EVERY 2.0 DAYS BEGINNING AT 0000 8 JUL 77

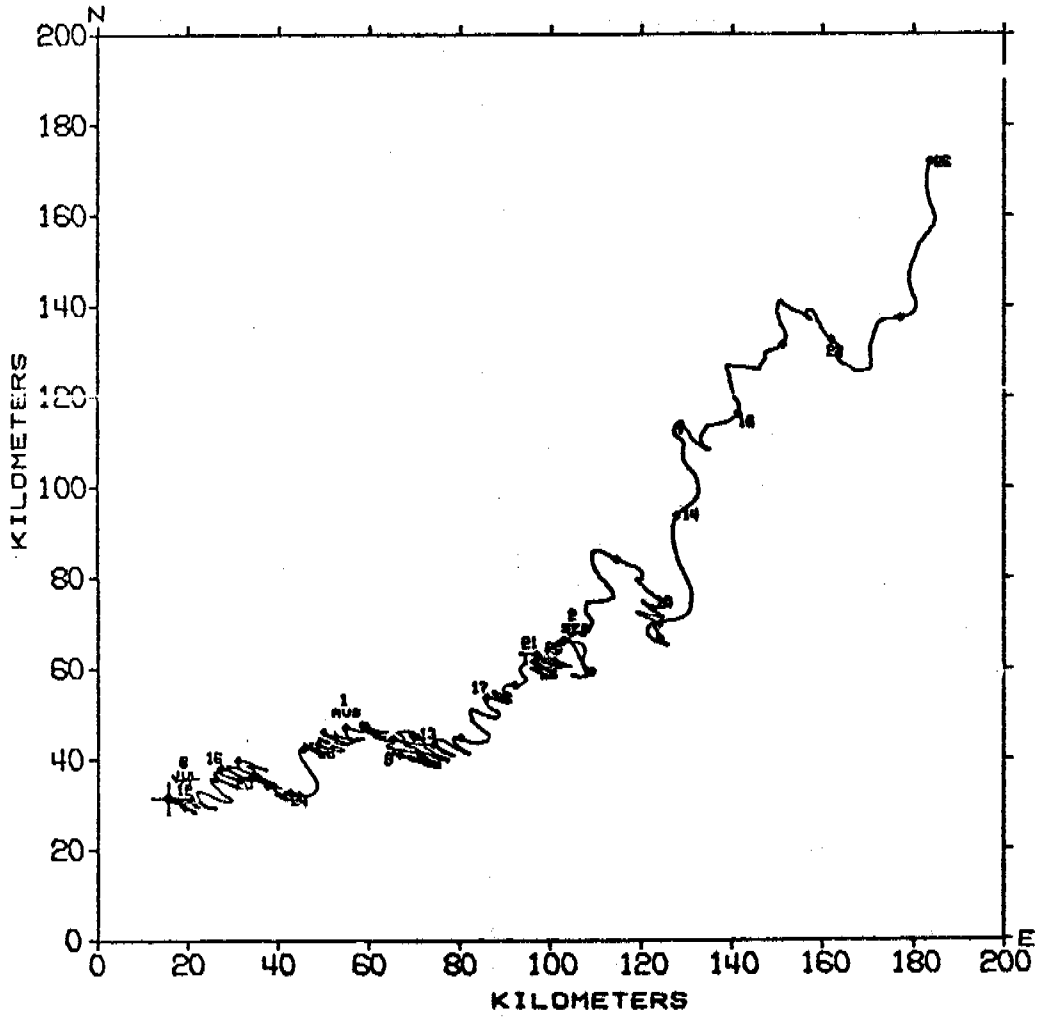

KINETIC ENERGY SPECTRUM OF CURRENTS AT CM4 - GEOPROBE, NS77
LOCATION = LAT 64 00N, LONG 165 00W, DEPTH = 17.5 METERS
OBSERVATION PERIOD = 0000 8 JUL 77 TO 2300 25 SEP 77 (80.0 DAY
N = 1920, DT = 1.0 HOURS, SMOOTHING - DANIELL WINDOW

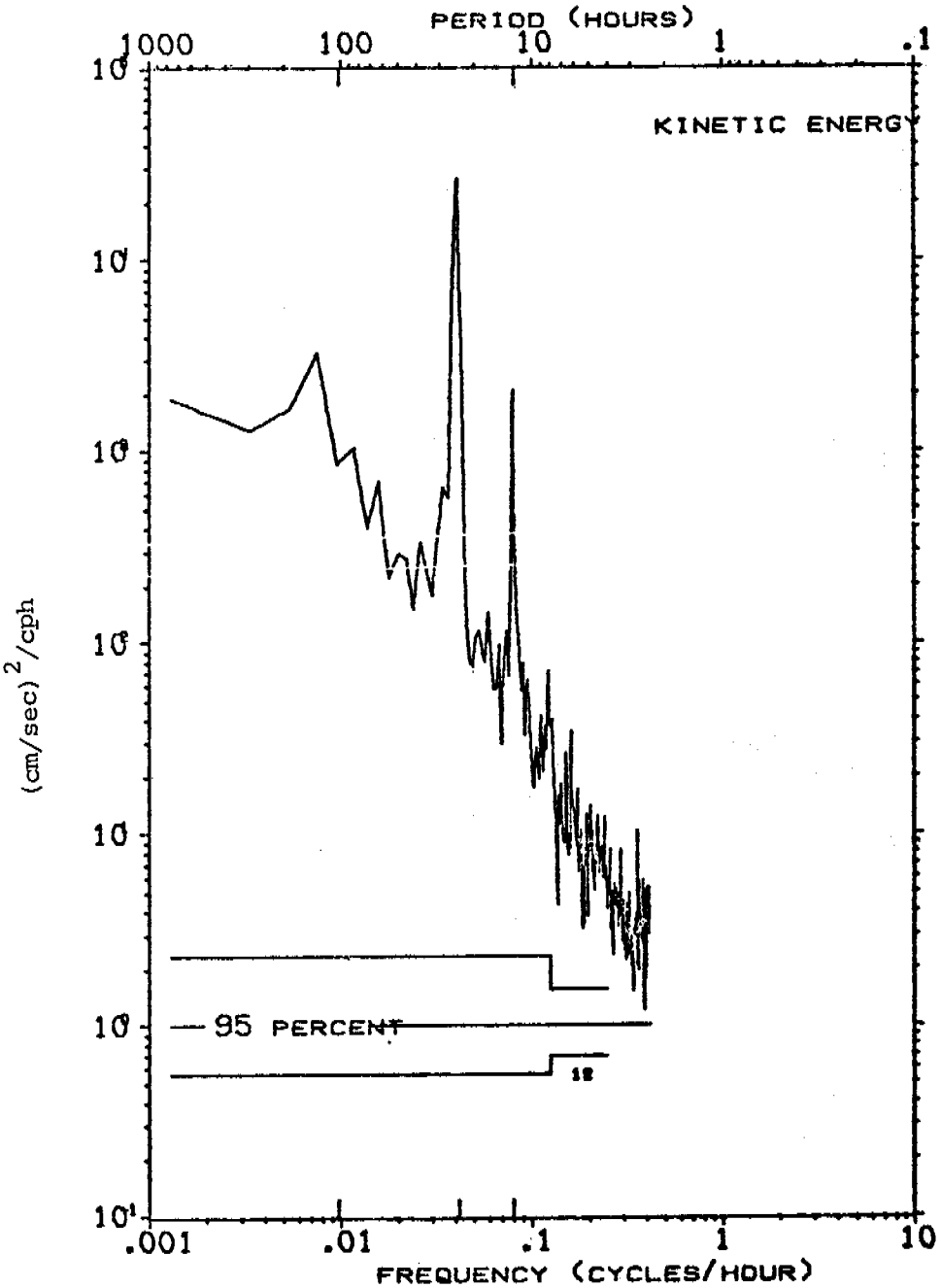

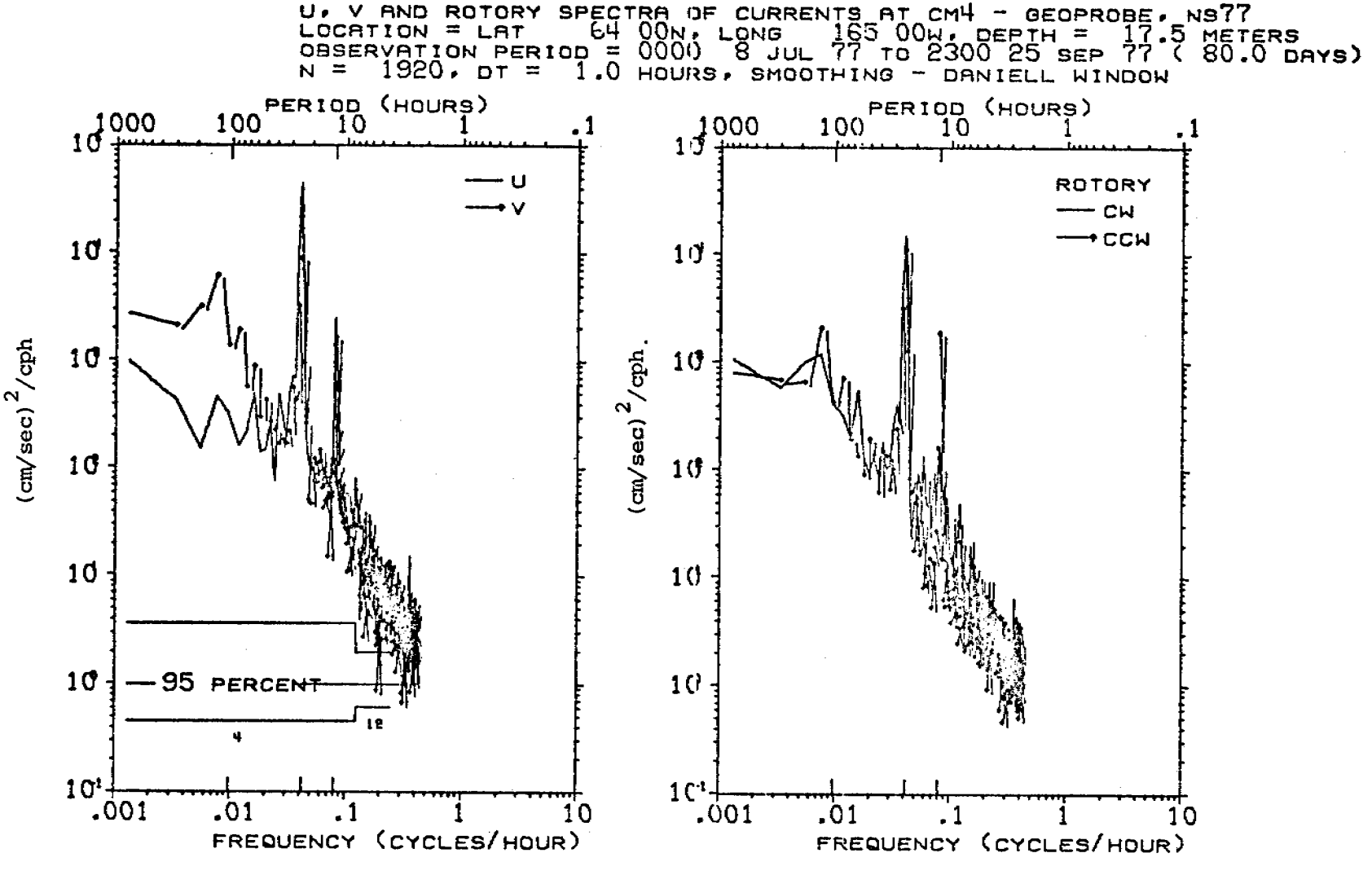
U, V AND ROTORY SPECTRA OF CURRENTS AT CM4 - GEOPROBE, NS77
LOCATION = LAT 64 00N, LONG 165 00W, DEPTH = 17.5 METERS
OBSERVATION PERIOD = 0000 8 JUL 77 TO 2300 25 SEP 77 (80.0 DAYS)
N = 1920, DT = 1.0 HOURS, SMOOTHING - DANIELL WINDOW
PERIOD (HOURS)
1000
100
10
1
.1
U
V
95 PERCENT
(cm/sec)^2/cph
FREQUENCY (CYCLES/HOUR)
.001
.01
.1
1
10
ROTORY
CW
CCW

ANNUAL REPORT

Research Unit No. 431
April 1, 1977 - March 31, 1978
53 Pages

COASTAL PROCESSES AND MORPHOLOGY OF THE BERING SEA COAST OF ALASKA

Asbury H. Sallenger, Jr.
John R. Dingler
Ralph Hunter

U.S. Geological Survey
Menlo Park, California 94025

I. SUMMARY OF OBJECTIVES, CONCLUSIONS AND IMPLICATIONS WITH RESPECT TO OCS OIL AND GAS DEVELOPMENTS

Storms pose major hazards to coastal developments along the Bering Sea coast of Alaska. During FY76, debris lines that resulted from the November, 1974 storm were found to be nearly 5 m above mean sea level in places along the northern Bering Sea coast of Alaska. Our study on the coastal effects of this major storm continued in FY77 with investigations on amounts of coastal change. Tundra bluffs in the vicinity of Nome were eroded as much as 45 m. This erosion was, however, irregular in plane view. Giant cusps with a longshore wavelength averaging 413 m were replaced during the storm by giant cusps spaced 863 m. The net effect of these changes was a relatively complex pattern of shoreline erosion and accretion. For example, the shoreline accreted 50 m at one location while 150 m away the shoreline eroded 10 m. Interestingly, the net change was accretional. Similar changes were measured for a storm that occurred in 1950, but in this case the net change was erosional as expected. The accretion observed for the 1974 storm may be related to freeze-up processes, but the mechanisms are unknown.

During the FY77 field season, beach and nearshore profiles were measured three times at locations along the northern Bering Sea coast of Alaska. A storm in September, 1977 caused a surge of nearly 2 m. Changes in beach and nearshore profiles that presumably resulted from this storm were again complex. One profile comparison indicated net accretion, whereas a profile located 50 m away showed evidence of both substantial accretion and erosion.

Coastal change is not, however, restricted to storm conditions. Giant cusps were observed to migrate along the coast at 5-6 m/day during the period 6/23/51 - 7/30/51. This migration caused as much as 50 m accretion at a given location over a period of several weeks.

One use of this kind of data is to establish a coastal development set-back line. That is, the appropriate government body would prohibit developments within areas subject to inundation by storm surge or undermining by coastal erosion. Additional input into this analysis must include the long-term rate of erosion. This question needs more study. For structures that must cross the coastline (e.g. pipelines) the maximum scour depth must be established for both storms and over the long-term. Our investigations of these problems had only begun.

The south coast of the Alaska Peninsula has numerous deep embayments which may one day be considered for deep water port facilities. These ports could service offshore petroleum exploitation in both the Bristol Bay area and areas offshore the Pacific coast of the Alaska Peninsula. In order to provide some baseline information, a reconnaissance of the physical coastal environment of Cold Bay and Pavlov Bay was undertaken. This included determination of net longshore transport directions, coastal morphology and beach sediment characteristics. The results can be used for preliminary siting studies, qualitative assessments of coastal stability and the long-term directions of transport of particulate pollutants in the littoral system.

II. INTRODUCTION

A. General Nature and Scope of Study

Prior to FY76, little information was available on the coastal processes of the Bering Sea coast of Alaska. This was a significant gap in our knowledge in view of anticipated coastal and nearshore developments in support of offshore petroleum exploitation.

During the first year of our study (FY76), much of our effort was involved with regional characterization of the physical environment of the coast. This included determination of net littoral drift directions (areas 1, 2 and 3 on Fig. 1), classification of coastal morphology (areas 1 and 3) and detailed reconnaissance of beach morphology and sediment characteristics (areas 1 and 3). From these studies preliminary assessments have been made on coastal stability, sediment sources and sinks and sediment transport pathways along the coast. These studies laid the groundwork for the more quantitative studies of coastal processes that followed.

During the second and final year of our study (FY77), detailed investigations on coastal processes commenced in the Norton Sound area (Fig. 1, area 1). These studies generally followed two directions. First, historical studies of the effect of storms on coastal change were initiated. These studies included measurements of coastal change from aerial photographs, debris-line elevations, and computer simulations of wave characteristics for the particularly severe November, 1974 storm. Second, direct measurements were made during the FY77 field season of the amounts of coastal change and of the nearshore wave charactistics. The wave measurement program was intended to be a field verification of the computer model. The direct measurement of coastal change was a first step toward relating amounts of coastal change with computed wave characteristics.

The ultimate objective of the study was to develop a quantitative understanding of those processes controlling coastal erosion and accretion for the diverse coastal types found along the Bering Sea coast of Alaska. Our work on the quantitative aspects of the problem, however, had only just begun when funding was terminated.

B. Specific Objectives

1. Measurement of amounts of coastal change in the Nome area that resulted from the November, 1974 storm.

2. Computer simulations of wave characteristics during the 1974 storm.

3. Remonitor beach/nearshore profile locations established during the 1976 field season in area 1 (Fig. 1) at the beginning and end of the field season.

4. In situ measurements of wave characteristics and sea level variations in the vicinity of Nome (area 1, Fig. 1).

5. Remonitor beach profiles established in the southern portion of the Bristol Bay coast of the Alaska Peninsula during the '76 field season. Additionally, a reconnaissance of the physical coastal environment of Pavlov and Cold Bays was undertaken.

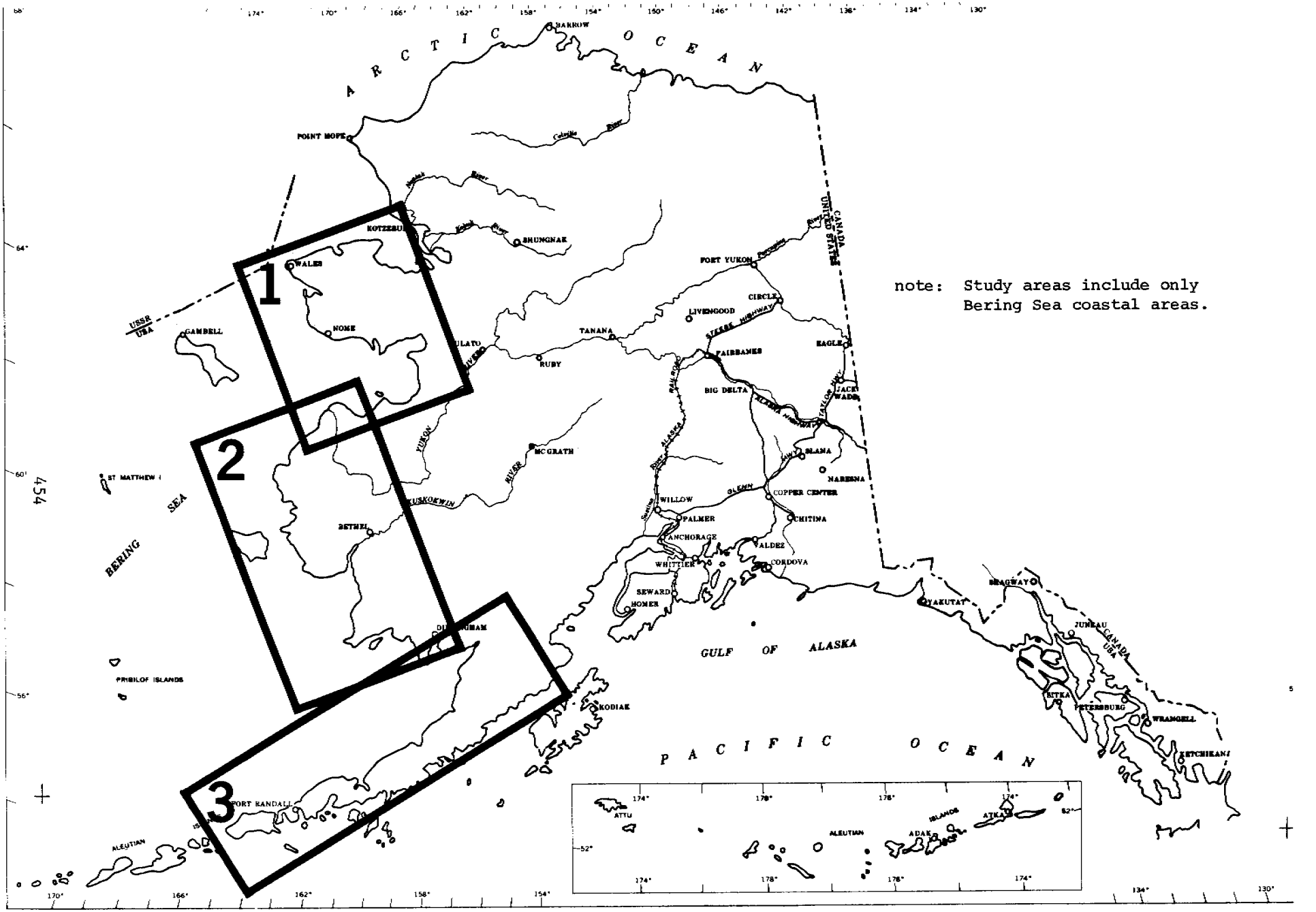

note: Study areas include only Bering Sea coastal areas.

FIG. 1

C. Relevance to Problems of Petroleum Development

Storms pose major hazards to coastal developments along the northeast Bering Sea coast. For example, the major 1974 storm resulted in debris line elevations as high as 4.75 m above MSL and caused wave heights reportedly in excess of 3 m at Nome. Comparisons of vertical aerial photography from before and after the storm show that tundra bluffs in the vicinity of Nome were eroded as much as 45 m landward. Shoreline changes were complex. Rhythmic shoreline topography with a longshore wavelength of 340 m was replaced during the storm by rhythmic topography with a wavelength of 590 m. This resulted in a complex pattern of shoreline erosion and accretion.

One use of this kind of data is to establish a coastal development set-back line. That is, the appropriate government body would prohibit developments within areas subject to inundation by storm surge, overwash, etc.. Additional input into this analysis must include the long-term rate of erosion of the coast. This is a question that needs more study. For structures that must cross the coastline (e.g. pipelines) the maximum scour depth must be established both for storms and over the long-term. Our investigations of these problems had only begun.

III. CURRENT STATE OF KNOWLEDGE

Our previous work in the area has been briefly summarized in section II of this report (see also Sallenger, et al., 1977). Relevant work prior to FY76 includes:

A. Greene (1970) observed longshore drift directions near Nome to be variable for June and July 1967, but predominately to the east. Wave heights were generally low ($\sim$30 cm), but storms during the late summer and fall were reported to produce high energy conditions.

B. The Draft E.I.S. for the Lost River Project reports that wave heights vary from approximately 30 cm in height up to 5 to 7 m with a theoretical maximum of 12 m off the mouth of the Lost River. Longshore transport is generally from west to east. Sediment transported during storm conditions greatly exceeds that transported under "normal" conditions.

C. The Corps of Engineers conducted several studies in the area including:

1. a report on flood protection and navigation improvement for Unalakleet.
2. National Shoreline Report which reports severe coastal erosion in Dillingham.

D. Several studies attempting to catagorize coastal morphology at very small scales have been conducted (e.g. Putnam, 1960 and Dolan, 1967).

E. Additional studies include work on Quaternary marine transgressions and old strand lines (i.e. Hopkins, 1967) and several studies on beach placer deposits near Nome (i.e. Greene, 1970) and along the south shores of Bristol Bay (i.e. Berryhill, 1963).

IV. STUDY AREA

The study area includes the Bering Sea coastal areas delineated in Fig. 1. Most of our work has been in area 1 (Fig. 1). Reconnaissance level studies have been conducted in Cold Bay and Pavlov Bay on the Pacific Coast of the Alaska Peninsula. See section II of this report for locations of specific studies.

V. METHODS

Methods used in achieving FY77 objectives are listed below. More detailed and additional methods are given in section VI of this report.

A. Wave Model. Computer simulations of the wave climate during the '74 storm utilized the refraction program developed by Dobson (1967) and modified by Thrall (1973) to include the effects of wind stress on wave growth. Using the meteorological characteristics during the storm and digitized depth data, the program propagated (hind cast) deepwater waves across the shelf to the shoreline.

B. Coastal change during the '74 storm. Shoreline positions derived from vertical aerial photography taken before and after the storm were compared.

C. Beach and nearshore profiles. Nearshore portions of a profile were monitored with a precision fathometer mounted in a 5.8 m inflatable boat powered by twin 40 h.p. engines. The electro-optical distance measuring capacity of the Total Station (Model 3810A; Hewlett-Packard) was used for positioning the boat on profile lines. The Total Station measured the horizontal distance to the boat as the boat moved shoreward along a profile line. The instrument has a range of 1.6 km under average conditions and an accuracy of ± (4.9 mm + 3 cm per 300 m) for slope distance and 30" for zenith angle. The horizontal distance is computed internally from slope distance and zenith angle. The onshore portions of the profile were measured using the vertical and horizontal distance capabilities of the Total Station.

D. Wave Monitoring. Wave conditions were obtained during the months of July and August (1977) in the form of repeated temporal observations of bottom pressure fluctuations. Four Transducer, Inc. 0-50 psia sensors were deployed in a 1-3-2 linear array of 7 m unit spacing. The deployment site was in 6 m of water approximately 1 km west of Nome (Fig. 1). The array was oriented approximately parallel to the adjacent coastline.

An unattended Shelf and Shore (SAS) system (Lowe, et al., 1972) was used to collect and record the data. The shelf system consisted of an articulated spar buoy with basal underwater connections to the sensors and an above-water PCM encoder and transmitter. The shore station, located in the Nome Federal Building, consisted of a receiving unit and slaved tape recorder.

Two hundred observations were made during the summer. Each observation lasted 10 minutes and observations were made every six hours. The sample interval was 8 per second. The data will be reduced by computer to obtain spectral estimates of wave height, period and directions.

VI. RESULTS, DISCUSSION AND CONCLUSIONS

Four separate reports have been prepared.

---

note: figure and table numbers begin with 1 for each report

A. COASTAL CHANGE ALONG THE NORTHERN BERING SEA COAST OF ALASKA

STORM CHANGES

NOVEMBER, 1974 STORM

Introduction

During the second week of November, 1974 a severe storm moved from southwest to northwest across the Bering Sea and caused extensive damage to communities along the northern Bering Sea coast of Alaska (Fig. 1). A detailed description of the meteorological characteristics of the storm is given in Fathauer (1975). At Nome, barometric pressure dropped 56 mb over a period of 26 hours and peak winds had a velocity of 111 km/hr. from the south. Nearshore waves were reportedly 3-4 m in height.

The southerly winds and shallow offshore depths (e.g. mean depth of Norton Sound is approximately 20 m) contributed to a storm surge of large magnitude along the coast. Elevations of debris lines that resulted from this surge were measured at 30 locations distributed around the study area. Debris line elevation provides a measure of storm sea level rise due predominately to the combined effects of drop in barometric pressure, wind set-up, wave set-up and run-up. Generally, the major proportion of storm sea level rise can be attributed to wind set-up. The storm surge was superimposed on a spring high tide, but this was of relatively minor significance since the astronomical tide range for the region is low (e.g. the diurnal range at Nome is .49 m). Debris line elevations ranged from 3.25 m above mean sea level north of Norton Sound to nearly 5 m along the eastern flank of Norton Sound (Fig. 2). The maximum value is probably a result of the geometry of the Sound and compares in magnitude to disastrous storm surges caused by hurricanes on the Gulf of Mexico coast. At Nome, storm surge and waves overtopped a sea wall and caused nearly 15 million dollars in damage.

The storm occurred during freeze-up. The northern Bering Sea generally has greater than 80% ice coverage between late November and mid-May. This led to some interesting consequences in regard to coastal change and movement of coastal sediments.

Bluff Erosion

In the vicinity of Nome, bluffs 2-5 m in height extend along the coast for 40 km. These are generally composed of muds and are overlain by tundra vegetation. Vertical aerial photography is available for this region for June 17, 1974 and July 23, 1976. Except for the November, 1974 storm, no storm of sufficient magnitude to erode the bluffs occurred during this period. Thus, comparisons of the relative positions of bluffs for these two times should yield the amount of change attributable to the 1974 storm. Using a zoom transfer scope, bluff positions were plotted for each time at a common scale of approximately 1:5700.

Bluffs were eroded as much as 45 m. The erosion was, however, irregular in plane view, ranging from 0 to 45 m east of Nome where bluffs are 1.5 to 2 m high and 0-18 m west of Nome where bluffs are 3-5 m high. An example of this irregular

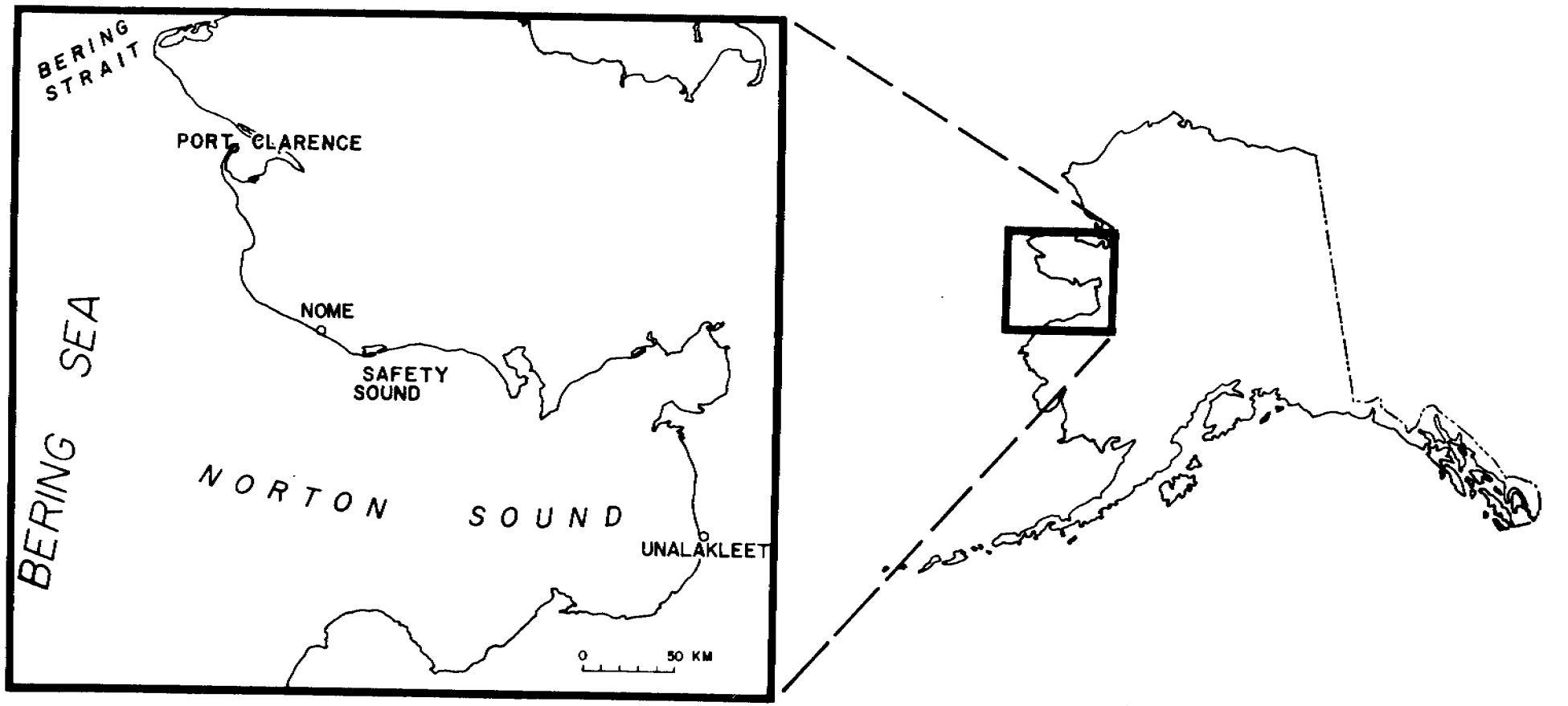

Fig. 1. Location of study area

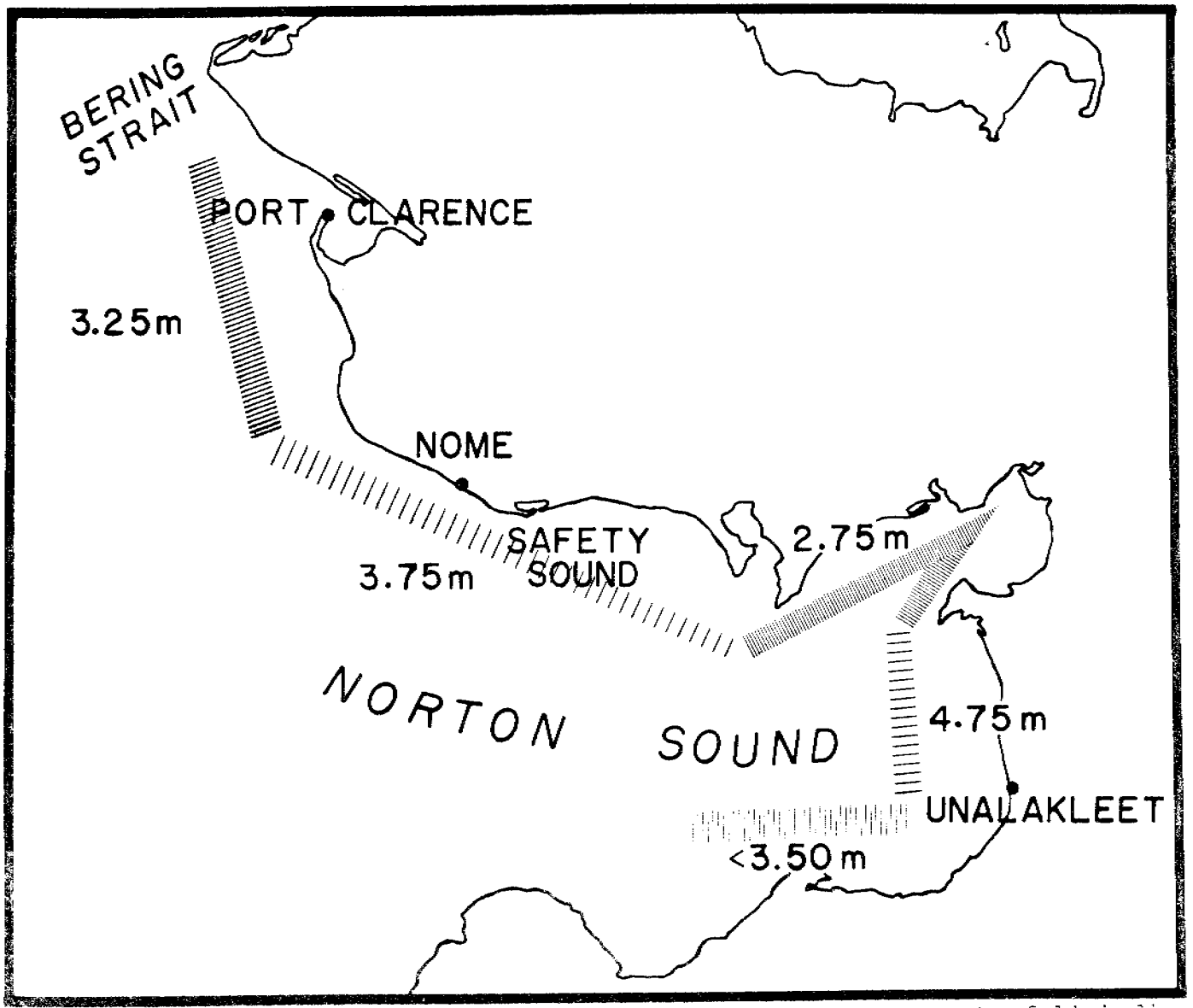

Fig. 2. Summary of measurements of debris line elevations. These are based on 30 measurements of debris line elevation distributed evenly around the study area. The elevations are referenced to observed sea level due to the paucity of predicted and measured tidal information for the area. This causes no large errors since the astronomical tide range for the region is relatively low. For example the diurnal range at Nome is .49 m. Consequently, to consider the measurements referenced to mean sea level would suggest maximum errors of approximately ±.25 cm.

pattern of erosion is shown in Fig. 3A where an embayment separated by two promontories was eroded into a once linear bluff. That the bluff was linear prior to the storm is confirmed by pre-storm photography. Depth to permafrost inland from the coast ranges from approximately .5 to .8 m depending on the composition of overlying material, but is much deeper near the coast and on the beaches (Greene, 1970). Variations in the lateral proximity of permafrost to the bluffs prior to the storm may have contributed to the observed non-uniform amount of erosion.

The surface of the platform to the left of the observer in Fig. 3B was presumably at or near the surface of permafrost prior to the storm. A .5-1.0 m thick layer of sediment and tundra that laid on top of the platform was stripped off by the storm waves whereas the frozen material below was resistant to modification. These platforms were best developed at the promontories discussed above. The photograph was taken in July, 1975 about one month of ice free conditions after the storm. No longer having the insolating protection of the overburden, the platform had eroded away by solifluction and other processes by the summer of 1976.

Shoreline Changes

Shoreline changes were complex. Along the barrier spit enclosing Safety Sound (Fig. 1), vertical aerial photography is available for June 17, 1974 and September 9, 1976. These were compared as before to yield shoreline changes.

Prior to the storm, giant cusps with a longshore wavelength averaging 413 m were observed (Fig. 4A). Giant cusps are crescentric and regularly spaced shoreline features similar in form to beach cusps, but are an order of magnitude or more larger and are generally associated with offshore bars. The pre-storm cusps observed, however, were not obviously associated with a bar. A bar was visible on aerial photographs through the sea surface, but it was sinuous and irregular in plane view with no apparent relation to the cusps. However, there may have been an inner bar present that was not visible in the photography. The pre-storm cusps were apparently destroyed by the storm and were replaced by much larger giant cusps spaced 863 m (Fig. 4A). Oblique bars that were obviously associated with the new cusps were observed on the post storm photography. The net effect of these changes was a relatively complex pattern of erosion and accretion. For example, the shoreline accreted 50 m at one location while 150 m away the shoreline eroded 10 m. Interestingly, the net change was accretional.

The giant cusps also controlled the location and extent of overwash; the overwash extending farther landward opposite embayments of the rhythmic shoreline topography (Fig. 5). In the same manner, giant cusps appeared to control the erosion of coastal vegetation. For example, in Fig. 5 it is seen that the beach grass closely parallels the form of the giant cusps. On the Outer Banks of North Carolina, Dolan (1971) made a similar observation. The regular spacing of breaches in a dune ridge following a storm matched the spacing of giant cusps.

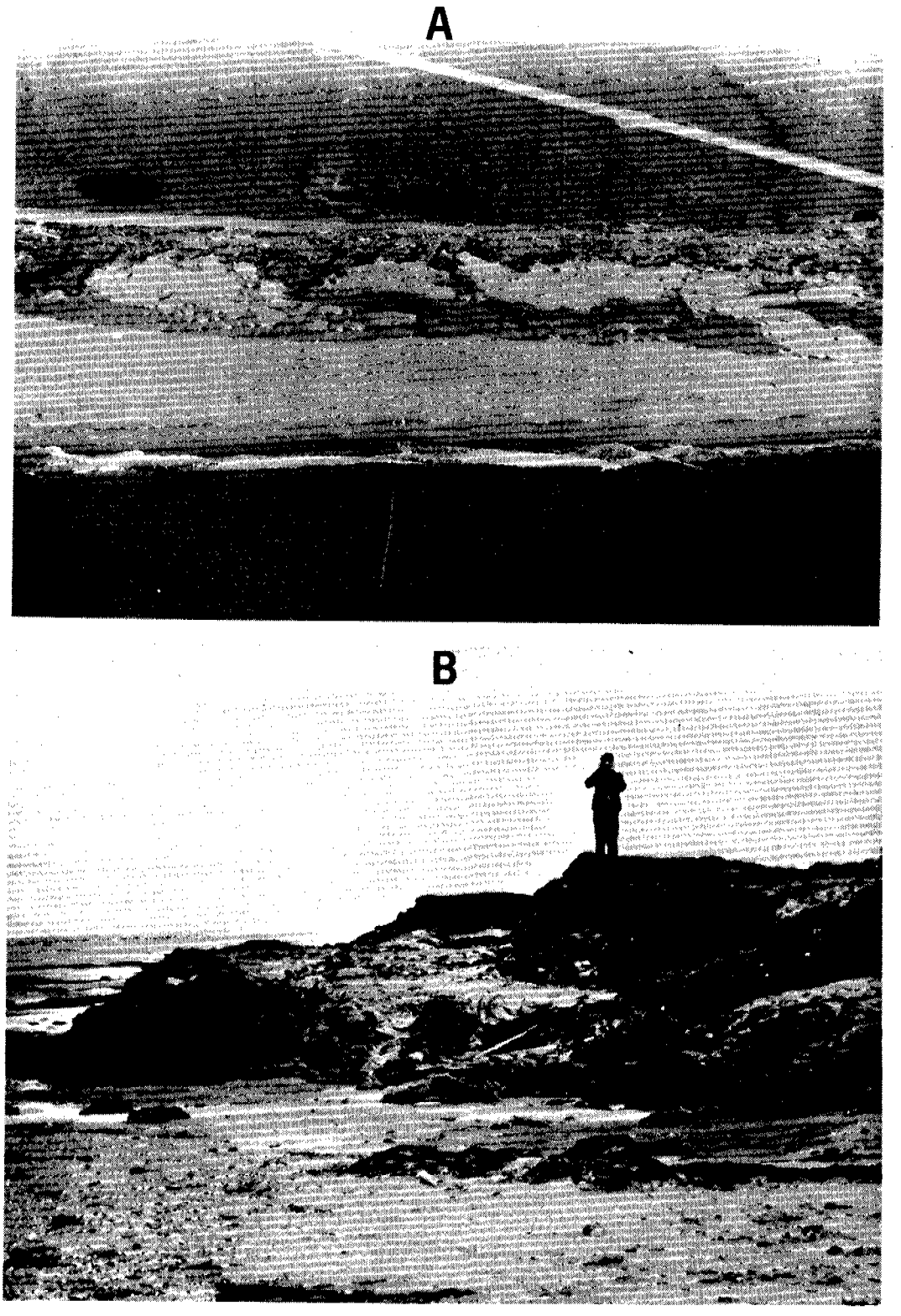

Fig. 3. A. Aerial view of the post-storm bluff. Note the embayment and two promontories on the left. This was a result of nonuniform erosion during the storm (see text). B. Ground view of one of the promontories shown in Fig. 3A. Note the platform to the left of the observer. Presumably, the surface of the platform was at the surface of permafrost prior to the storm. The unfrozen overburden was stripped off by storm waves.

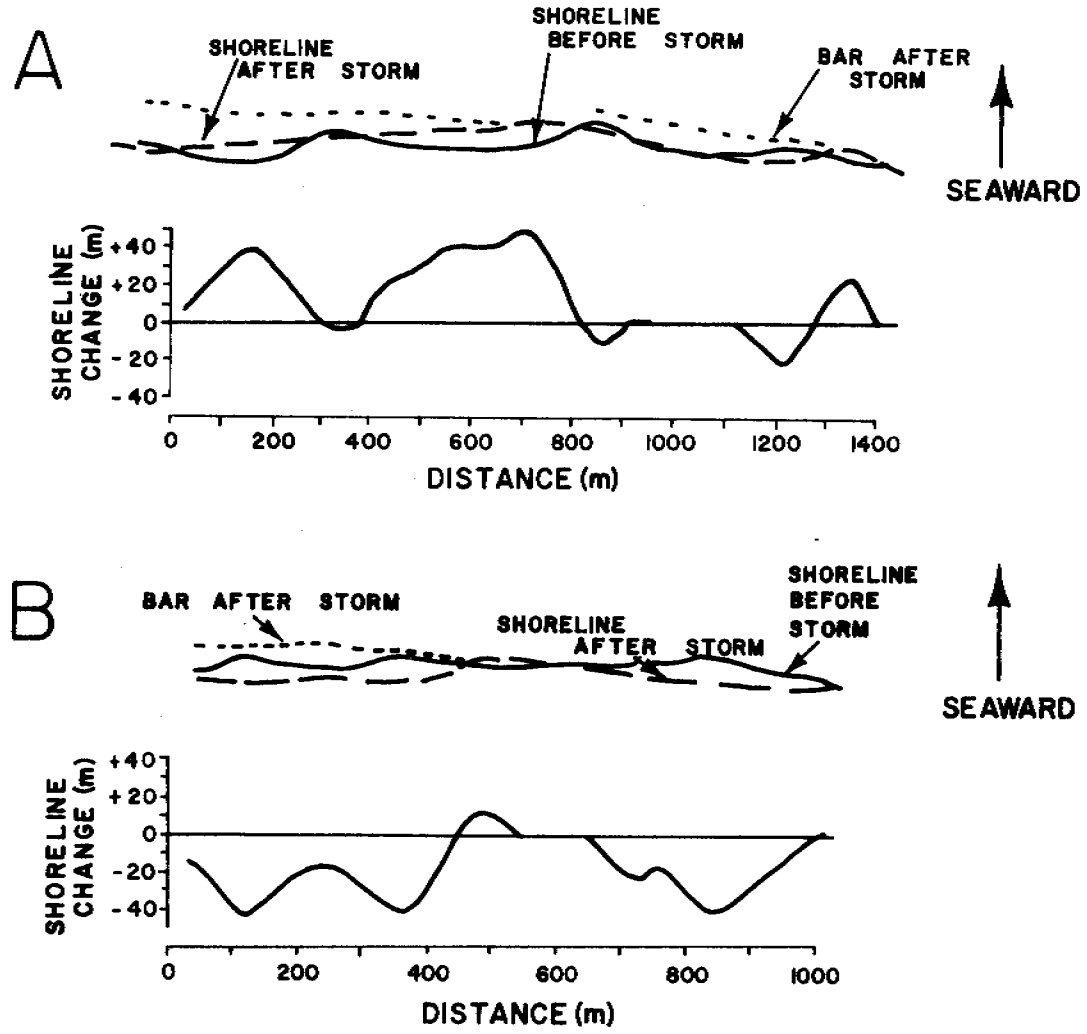

Fig. 4. A. An example of shoreline changes that resulted from the November, 1974 storm. Note the complex pattern of erosion and accretion and that the net change is accretional. B. An example of shoreline changes that resulted from the November, 1950 storm. Note again the complex pattern of changes, but that in this case the net change is erosional. Only one horn of the post-storm giant cusps is shown. The mean spacing of the post-storm features was 1.7 km.

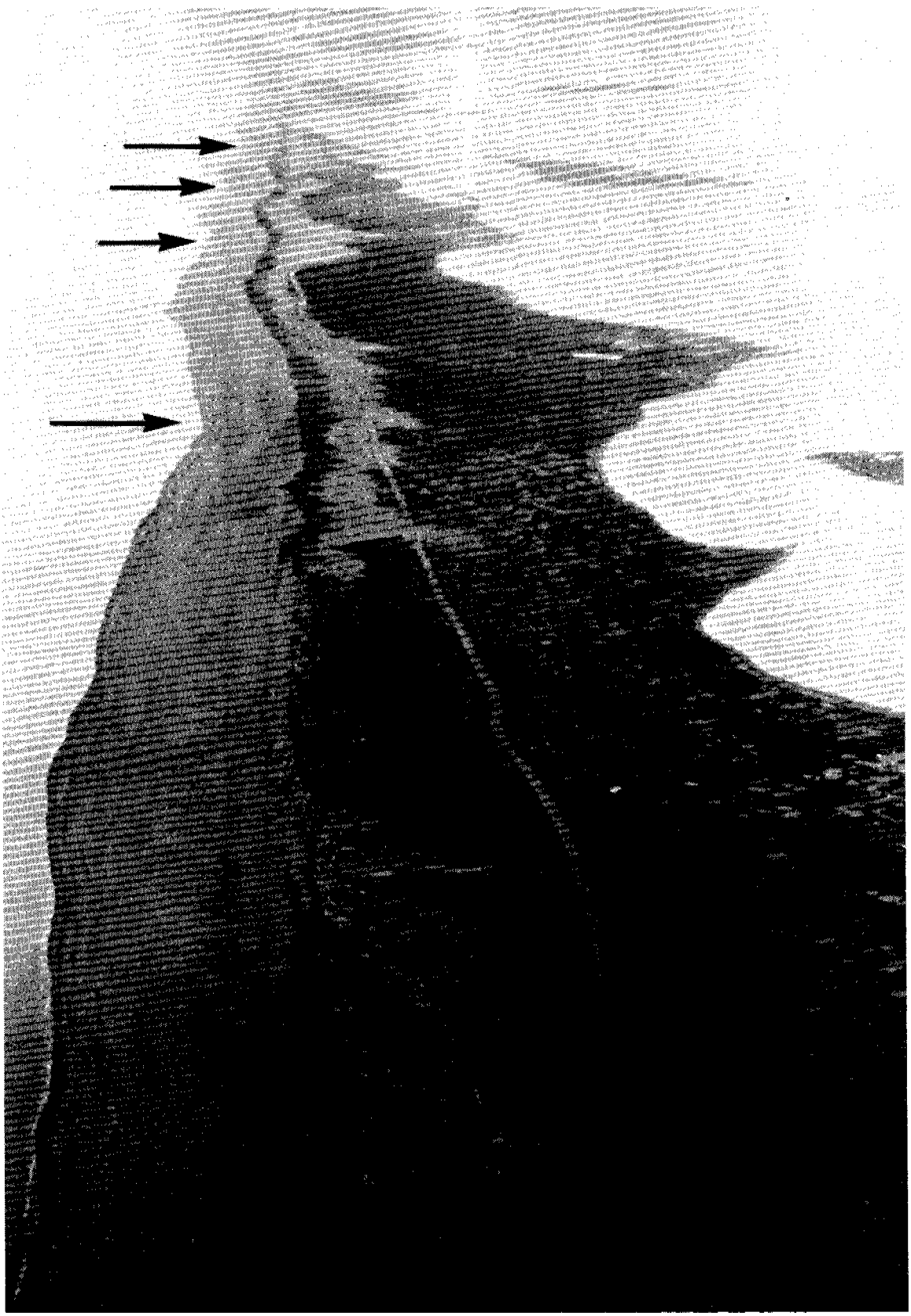

Fig. 5. Post-storm aerial view of the barrier spit enclosing Safety Sound. Note the maximum extent of overwash is opposite the embayments (arrows) of the rhythmic shoreline topography. Also, the beach grass line parallels the rhythmic shoreline.

COMPARISONS OF SHORELINE CHANGES BETWEEN THE 1974 AND NOVEMBER, 1950 STORMS

Shoreline comparisons based on photography from August 28, 1950 and June 22, 1951 showed similar changes in giant cusps. A relatively severe storm with southwesterly winds was recorded at Nome on November 10, 1950. On the pre-storm photography giant cusps spaced 363 m were observed (Fig. 4B). These were replaced by very large giant cusps spaced 1.7 km, presumably as a result of the storm. Again a complex pattern of erosion and accretion resulted where at one location the shoreline eroded 41 m while 140 m away the shoreline accreted 12 m. In contrast to the 1974 storm, however, the net change was erosional.

The net accretion associated with the 1974 storm is perplexing. The comparisons of photography for both the 1950 and 1974 storms had good control. Numerous stable irregularities on the lagoon shoreline were used to match scales and orientation. Also, the trends for each storm were generally evident on all photographs compared.

It is interesting that air temperatures preceding each storm were quite different. They remained well below 0°C on the five days preceding the 1974 storm with daily minimums as low as -23°C (Fig. 6). Preceding the 1950 storm air temperatures were much warmer and generally above 0°C. When sea water temperature falls below its freezing point, an ice foot will begin to develop along the shoreline. An ice foot can form by a number of mechanisms (see for example Joyce, 1950). One of these is the freezing of spray and swash on the foreshore. By this process a rampart is built composed of ice and sediment which protects the foreshore from modification by waves. During storms, an ice foot of large proportions can be formed (Rex, 1964). For the 1974 storm, however, the optimum temperatures for ice foot formation existed prior to the storm. There may have been a thin covering of sea ice present in Norton Sound prior to the storm. The southerly winds could have pushed this ice against the south facing beaches. Perhaps these freeze-up processes contributed in some manner to the shoreline accretion observed for the 1974 storm. The mechanism is, however, unclear. The source of sediment may have been from the wide storm surf zone, but it is difficult to perceive how sufficient sediment would be displaced landward to account for the observed large scale changes. Furthermore, it appears that these potential ice effects were not capable of preventing modification of the landward parts of the barrier by storm surge and waves (Fig. 5).

Perhaps post-storm accretion occurred prior to the post-storm photography. Nearshore ice generally protects the beaches until mid-June. Thus, there was approximately a three month interval between the storm and the post storm photography during which the shoreline could prograde. However, it is questionable that there would be up to 50 m of accretion beyond the pre-storm shoreline as a result of normal rebuilding processes following the storm. Post-storm accretion cannot, however, be ruled out.

SEPTEMBER, 1977 STORM

A moderately severe storm was recorded at Nome in early September, 1977. A debris line at Nome harbour that resulted from this storm was approximately 2 m above MSL. Beach and nearshore profiles were measured in the Nome area during the third week of August and were remonitored during the second week of October. Comparisons of

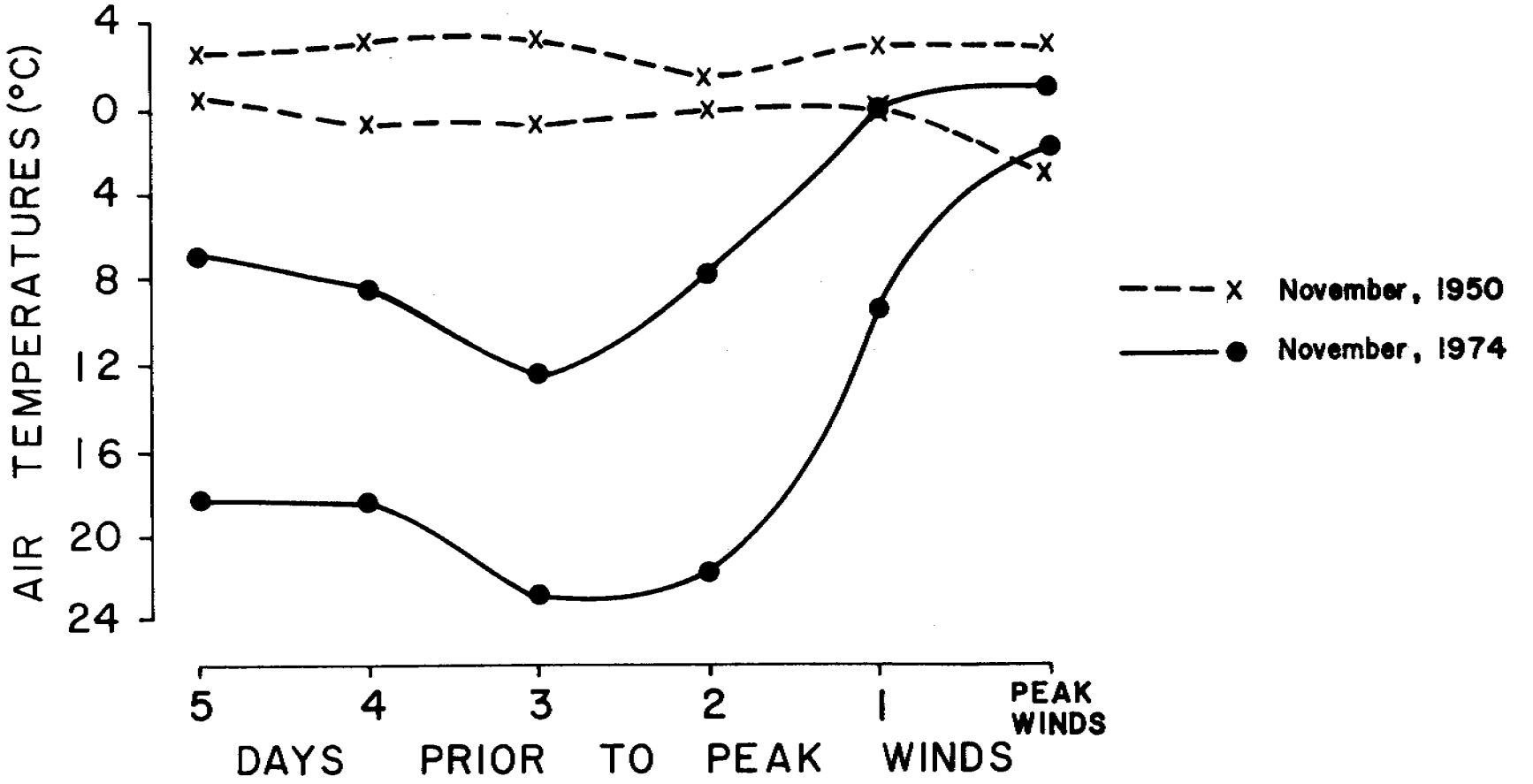

Fig. 6. Maximum and minimum daily air temperatures preceding the 1974 and 1950 storms.

these profiles show the amount and character of coastal change that occurred during this period. Presumably, much of the change can be attributed to the September storm.

Two of these comparisons from Safety Lagoon are shown in Figs. 7 and 8. These are located at Station B16 (see profile location sheet in Sallenger, et al., 1977). The profile lines are parallel and 50 m apart, and are oriented approximately normal to the shoreline trend.

The comparison shown in Fig. 7 indicates that the net change was accretional. A bar has formed approximately 250 m seaward of the normal shoreline. In contrast, Fig. 8 shows that only 50 m away there was both substantial erosion and accretion. Again, a bar has formed. The sediment may have been supplied from erosional areas both seaward and shoreward of the bar. The foreshore slope has been decreased as would be expected during a storm, yet this decrease in slope was the result of accretion.

Obviously, nearshore changes in this environment are quite complex. A detailed report on the changes that occurred during this storm will be included in our Final Report.

NON-STORM CHANGES

The wave climate of the northern Bering Sea is dominated by locally generated sea. Swell waves generated in the southern Bering Sea are greatly reduced in magnitude before reaching the coast by refraction and frictional dissipation over the wide continental shelf. Thus, in the absence of strong onshore winds, nearshore wave conditions can be quite low.

This is not to imply, however, that coastal change occurs only during severe storms. Vertical aerial photography is available for 6/23/51, 7/13/51 and 7/30/51 for a portion of Safety spit (Fig. 1). Giant cusps spaced 1.7 km were observed on the 6/23/51 photography. These cusps were apparently formed as a result of the severe November, 1950 storm as has been discussed earlier. A comparison of shoreline positions in the vicinity of the cusp horns is shown in Fig. 9. Winds were dominantly from the southwest during the period covered by the photography. Locally generated waves caused a net transport to the east along the coast. In response to this transport, the cusps migrated along the coast at 5-6 m/day. This migration caused as much as 50 m accretion at a given location over a period of several weeks. Studies by Dolan (1971) on the Outer Banks of North Carolina have shown that migration of these kinds of features undermined a groin and caused its failure.

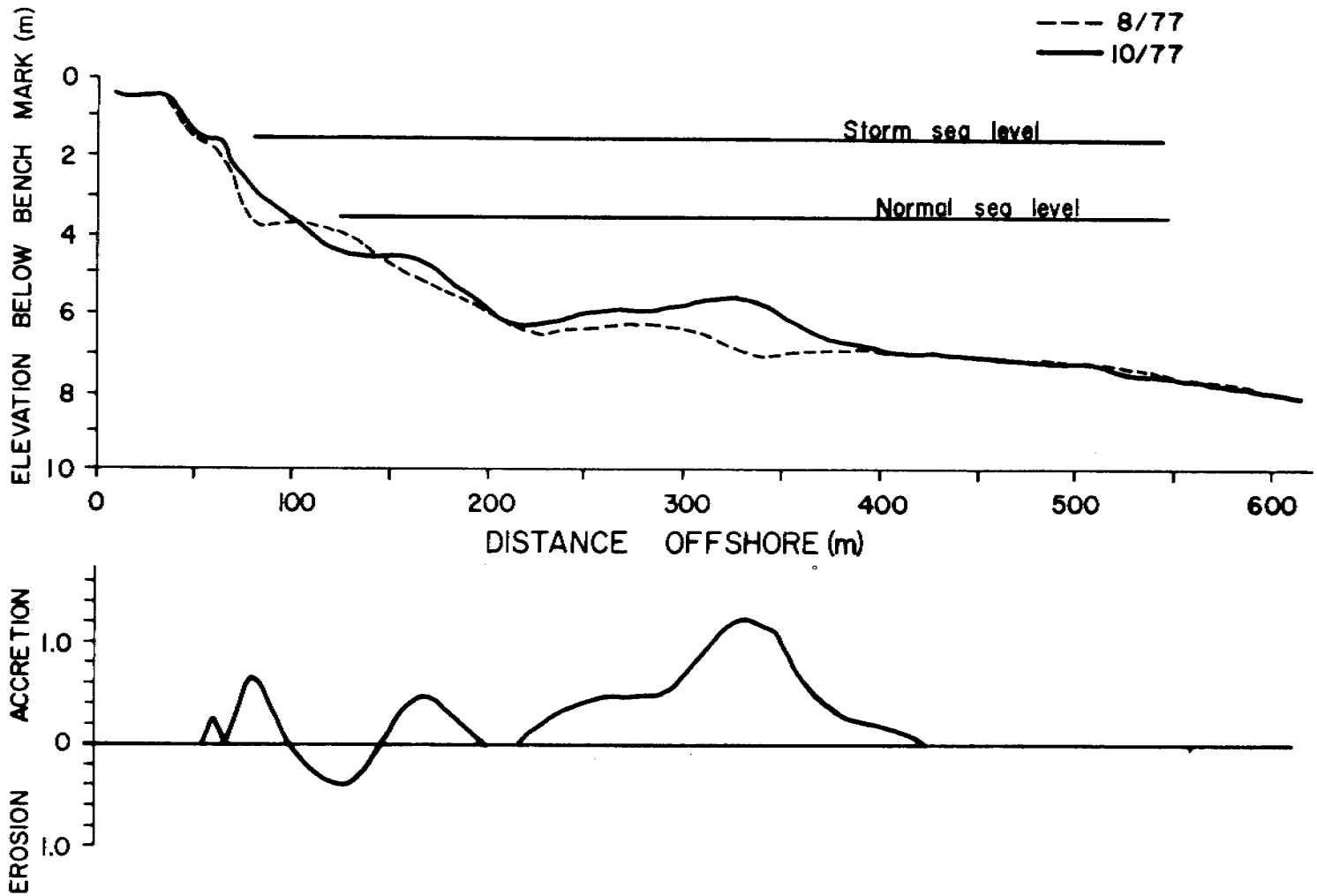

Fig. 7. Beach and nearshore profile comparison.

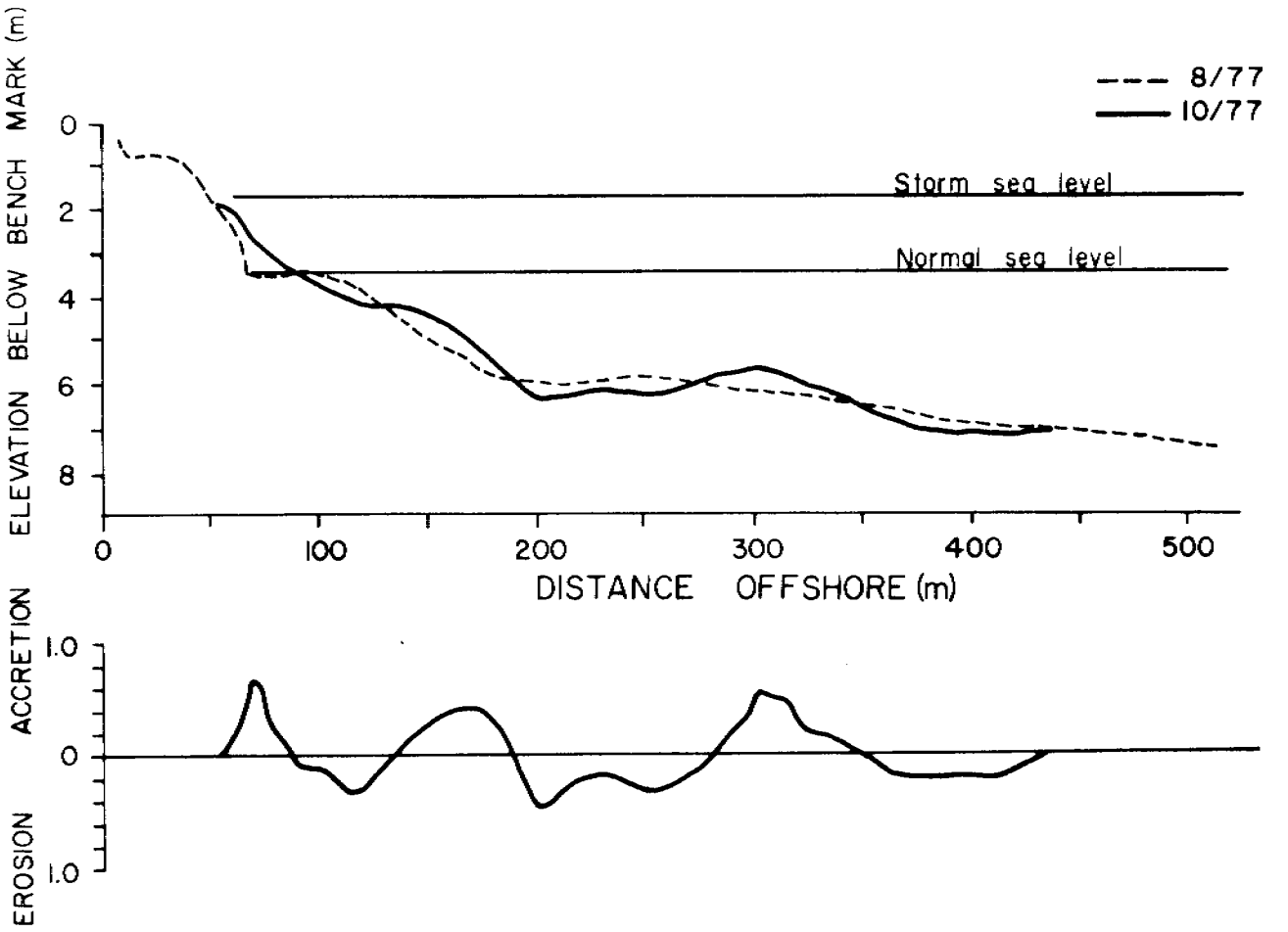

Fig. 8. Beach and nearshore profile comparison.

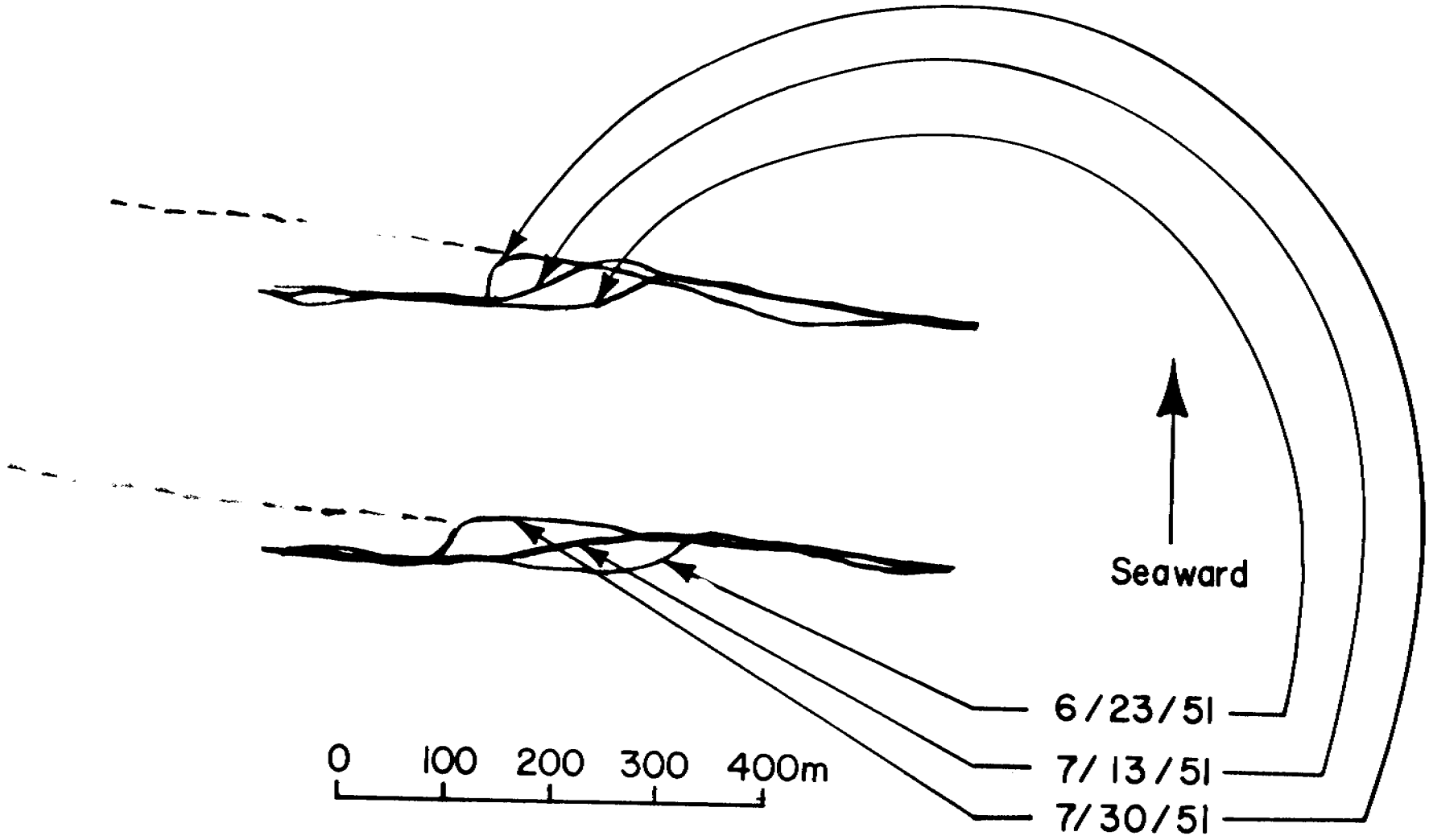

Fig. 9. Migration of giant cusps.

B. RECONNAISSANCE OF THE PHYSICAL COASTAL ENVIRONMENT OF COLD BAY AND PAVLOV BAY, ALASKA

INTRODUCTION

The south coast of the Alaska Peninsula has numerous deep embayments which may one day be considered for deep water port facilities. In order to provide some baseline information, a reconnaissance of the physical coastal environment of Cold Bay and Pavlov Bay was undertaken. This included determination of net longshore transport directions, coastal morphology and beach sediment characteristics. The results can be used for preliminary siting studies, qualitative assessments of coastal stability and the long term directions of transport of particulate pollutants along the coast.

NET LONGSHORE TRANSPORT DIRECTIONS: COLD BAY AND PAVLOV BAY, ALASKA

Net longshore transport directions for Cold Bay and Pavlov Bay, Alaska are given on Fig. 7. These interpretations are based on geomorphic criteria given in Sallenger, et al. (1977). Arrows refer to the net direction of wave induced sediment transport along the shoreline. Lengths of arrows are arbitrary.

Directions of transport for Cold Bay are generally into the Bay as expected. Convergences of transport occur at the head of the Bay west of Kinzarof Lagoon and at a spit enclosed lagoon south of the town of Cold Bay. On the east side of Cold Bay, there are few indications of transport direction.

Longshore transport directions for Pavlov Bay are somewhat more complex. Similar to Cold Bay, transport converges at the head of the Bay. There is a divergence point, however at Black Point. North of here sediment supplied to the coast by numerous braided streams is transported towards the head of Pavlov Bay. South of Black Point sediment is transported towards the mouth of the bay. Similar to Cold Bay, there are few indications of transport directions on the east side of the Bay.

COASTAL MORPHOLOGY: COLD BAY AND PAVLOV BAY, ALASKA

The coastlines for Pavlov and Cold Bays were divided in reaches (Fig. 8). where each reach has a relatively uniform coastal morphology. Descriptions of the coastal morphology within each reach are given in Tables 1 and 2. The locations of photographs in Figures 1-6 are shown on Fig. 8. A brief description of the general coastal morphology of the two bays follows. For details see Tables 1 and 2, Figures 1-6 and 8.

In general, the coastal morphology of Cold Bay and Pavlov Bay are quite similar. On the east sides of both bays the coast is composed primarily of beaches backed by cliffs and wave cut slopes. However, rocky headlands and the lack of beaches are locally common along the east coast of Pavlov Bay. At the heads of both bays coastal relief is generally low. For Pavlov Bay, beaches are backed by low coastal plain.

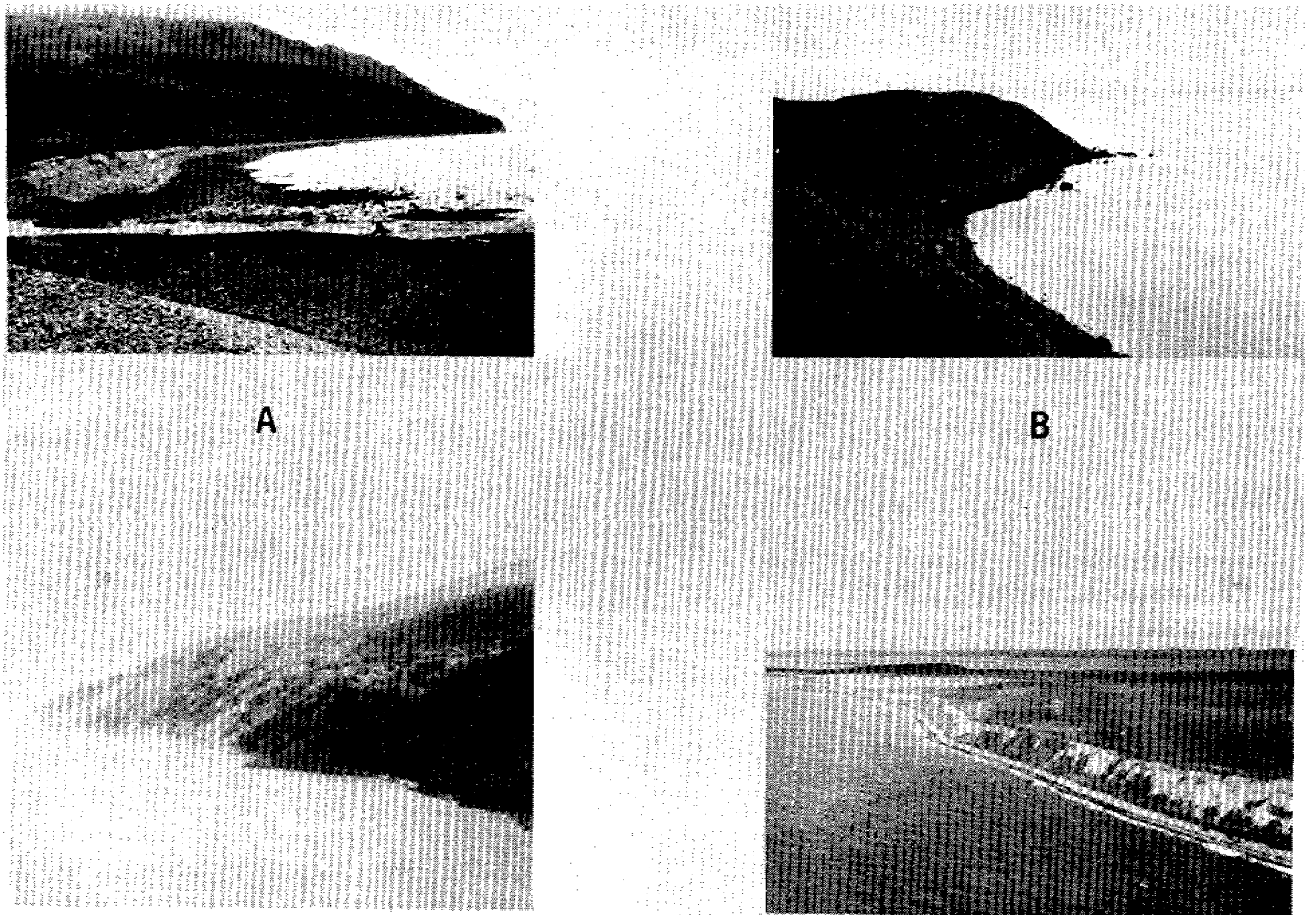

FIG 1

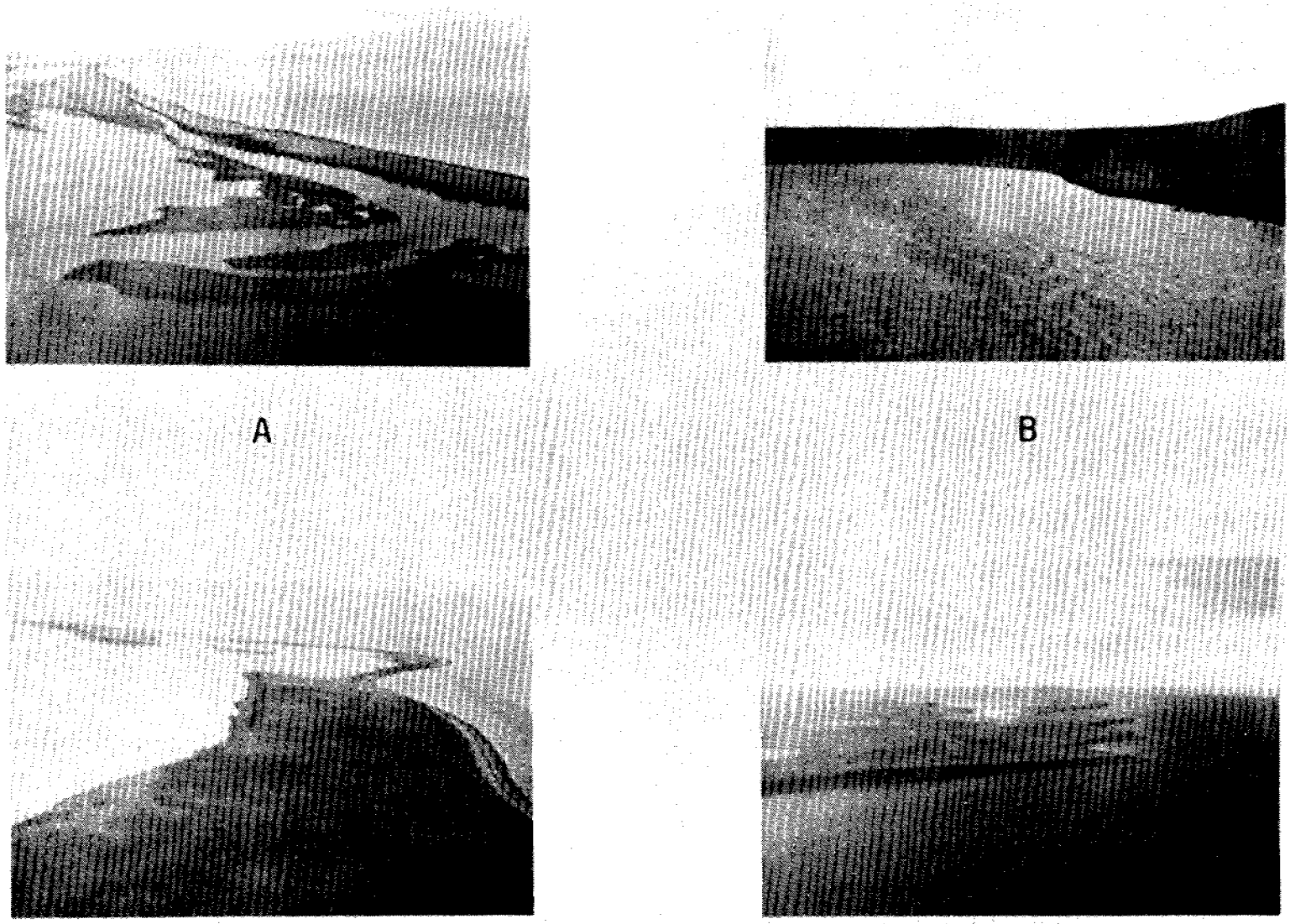

FIG 2

A

B

FIG 3

A

B

C

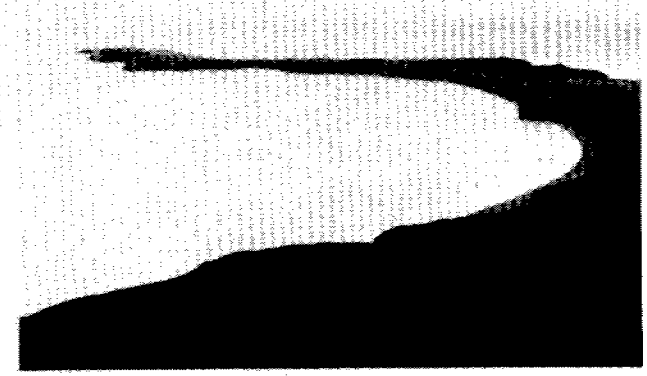

D

FIG 4

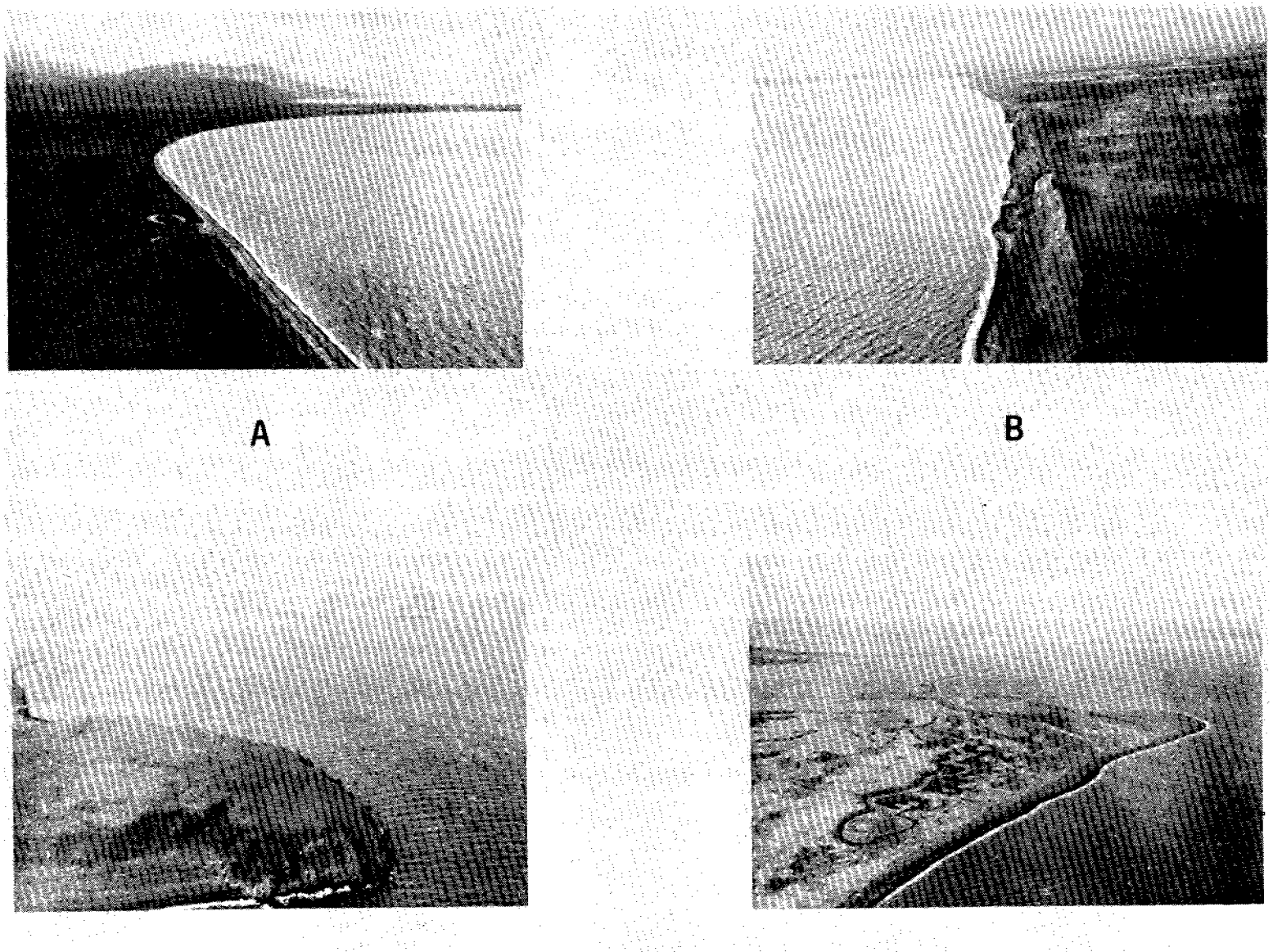

FIG 5

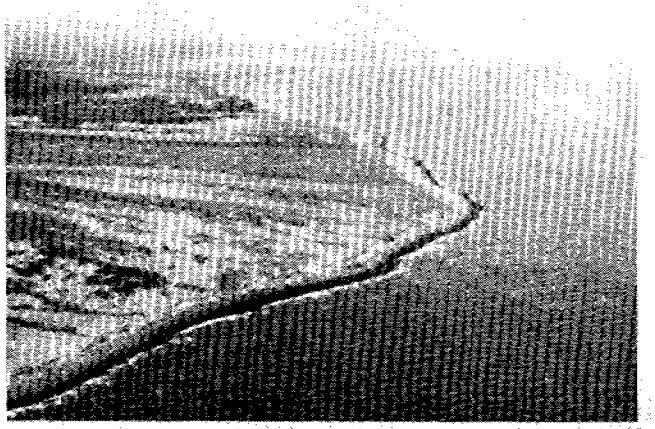

A

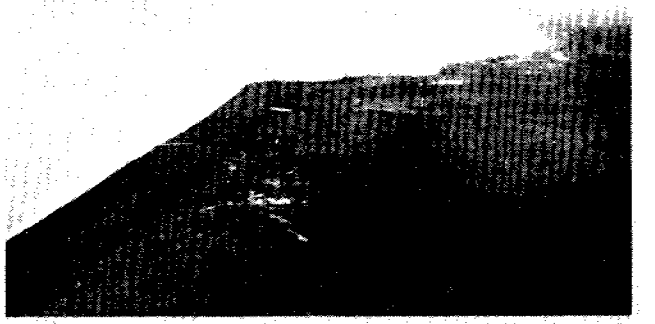

B

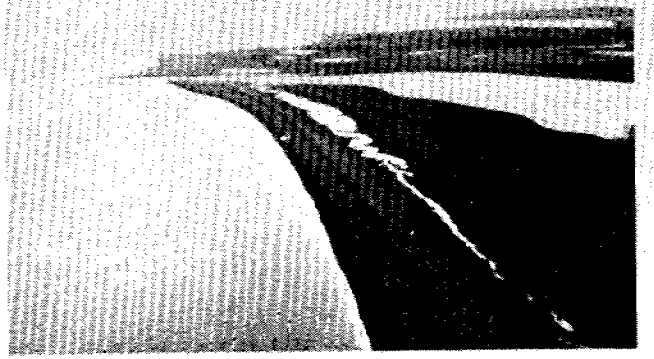

C

D

FIG 6

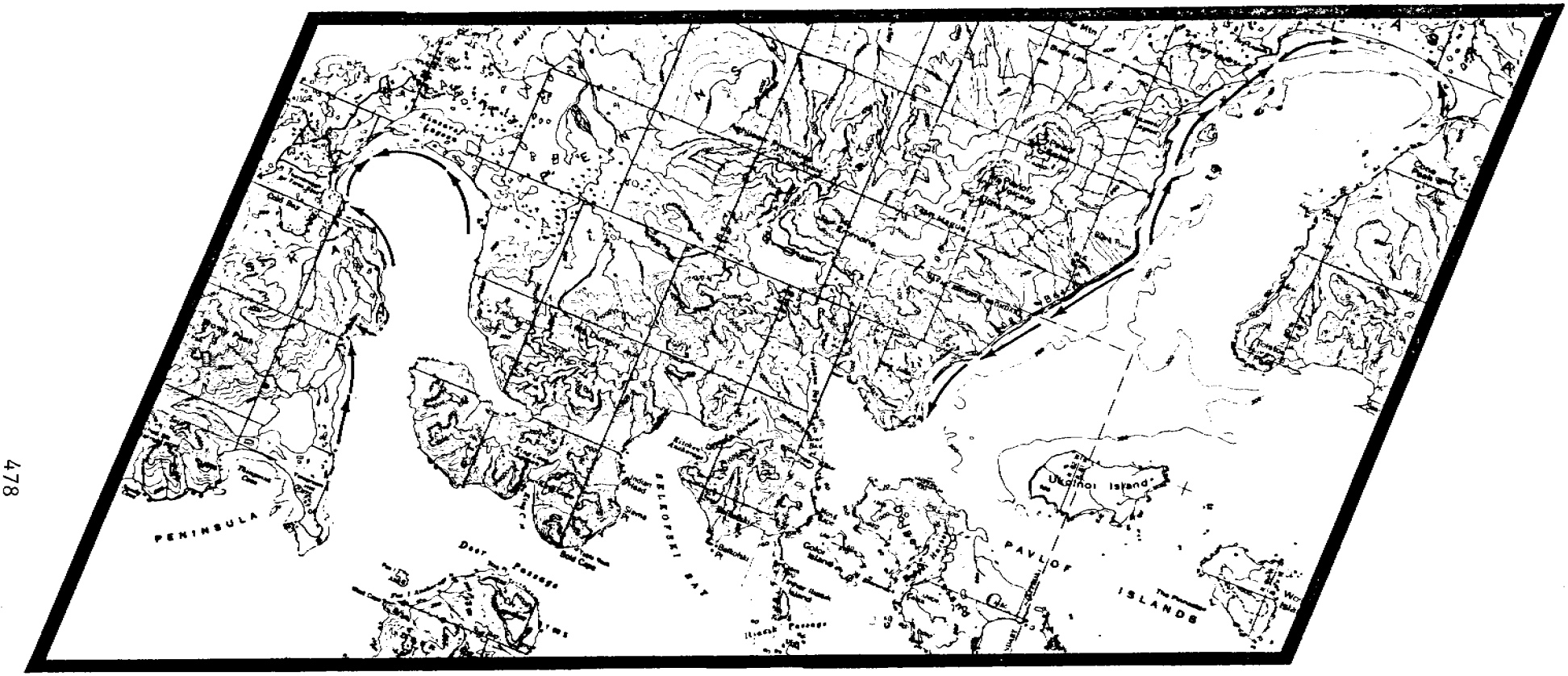

Fig. 7. Net longshore sediment transport directions. Cold Bay is on the left. Pavlov Bay is on the right.

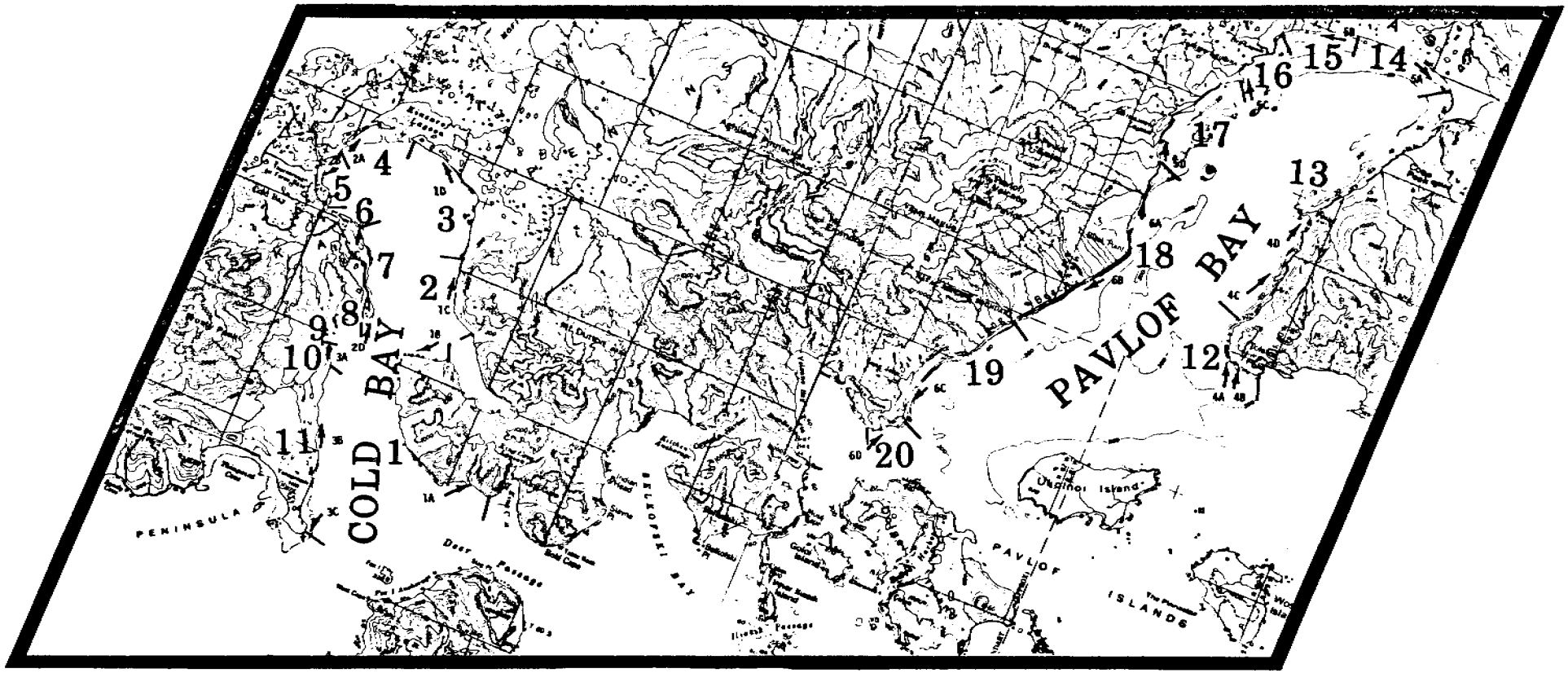

Fig. 8. Reach locations (large numbers) and photograph locations (small numbers and letters which refer to figure numbers).

Fig. 9. Station locations.

TABLE 1: COASTAL MORPHOLOGY OF COLD BAY, ALASKA

REACH	DESCRIPTION
1	mostly vegetated wave cut slopes, beaches locally absent at headlands (fig. 1A and 1B)
2	boulder/cobble beaches backed by relatively steep slopes; slopes are vegetated and do not appear to be wave cut (fig. 1C)
3	beaches backed by partly vegetated wave cut cliffs (fig. 1D)
4	mostly depositional features;(e.g. barrier spits and islands, beach ridge complexes) (fig. 2A)
5	beaches backed by partly vegetated wave cut cliffs (fig. 2B)
6	mostly depositional features; (e.g. barrier spits) (fig. 2C)
7	beaches backed by vegetated wave cut slopes (fig. 2D)
8	barrier spits
9	beaches backed by vegetated wave cut bluffs
10	barrier spit; beach ridge complex (fig. 3A)
11	beaches backed by vegetated wave cut slopes (fig. 3B and 3C)

TABLE 2: COASTAL MORPHOLOGY OF PAVLOV BAY, ALASKA

REACH	DESCRIPTION
12	rocky headland (fig. 4A); beaches are generally absent, but when present are composed predominantly of boulders (fig. 4B)
13	pocket beaches separated by rocky headlands (fig. 4C); cliffs occur at headlands and vegetated wave cut slopes occur in between headlands (fig. 4D)
14	beaches backed by low coastal plain; some dune ridge development (fig. 5A)
15	beaches backed by mostly vegetated wave cut slopes (fig. 5B)
16	rocky headlands separating spit enclosed lagoons (fig. 5C)
17	mostly depositional features (e.g. spits, beach ridge complexes) (fig. 5D)
18	beaches backed by gentle slopes leading to Pavlov and adjacent volcanoes; numerous braided streams that supply sediment to the littoral system (fig. 6A); scattered boulders on beaches and the slopes behind; in places boulders act as groins capturing sediment from the littoral system (fig. 6B)
19	mostly depositional features (e.g. spits at the mouths of streams, beach ridge complexes) (fig. 6C)
20	rocky outcrops; low cliffs; and pocket beaches (fig. 6D)

Depositional features such as barrier spits occur at the head of Cold Bay. These sediment sinks occur at the convergence of longshore transport for Cold Bay (Fig. 7). Sediment is supplied by eroding cliffs on either side (Table 1). On the west side of both bays depositional features are common. Braided streams flowing down the flanks of Pavlov and adjacent volcanoes apparently supply considerable sediment to the littoral system. Generally, sediment introduced to the coast north of Black Rock will be transported to the north and will contribute to the development of depositional features in reaches 16 and 17 (see Fig. 8 and littoral drift directions). Sediment introduced south of Black Rock will contribute to the development of depositional features in reach 19. On the west side of Cold Bay wave eroded slopes are common as well as depositional features. The pathways the sediment follows from these sources to sinks can be determined by comparing the longshore transport directions and coastal morphology.

GRAIN SIZES OF BEACH SEDIMENTS, COLD BAY AND PAVLOV BAY, ALASKA

METHODS

Because of the coarse gravelly nature of most of the beach sediments around Cold and Pavlov Bays, grain sizes were measured from photographs of the beach surface rather than by sieving. At each locality visited (referred to as "stations" in Tables 3 and 4), a series of photographs was taken along a line perpendicular to the shoreline. Each photograph of the beach surface was taken vertically downward from eye level, and a scale was included so that measurements could be made from the photograph. The first photograph at each station was taken at the waterline (referred to as "substation 1" in Tables 3 and 4), the second was taken 8 m landward (substation 2), and others were taken at equal intervals up to the back edge of the beach, as marked by vegetation or a scarp. Station locations are shown in Fig. 9.

Grain size parameters measured from the photographs include (1) percent gravel, as estimated from visual comparison charts (Note that the percent sand is simply 100 minus percent gravel and that the sand-gravel boundary is 2 mm), (2) the diameter of the grain that was judged visually to represent the mean grain diameter of the gravel fraction, and (3) the diameter of the largest grain in each 50 x 80 cm photographic frame. The measurements of percent gravel and mean grain diameter at all the substations of a given station were combined into a station average, and the largest grain at any of the substations was defined as the largest grain at the station.

RESULTS

Cold and Pavlov Bays have a striking similarity of form, as is to be expected from their similar origins. The similarity of the two bays was found to extend to the grain sizes of their beach sediments also. The similarity in grain size is due in part to the similarity in form of the two bays, in part to the similarity in wave forces, and in part to the similarity in source materials of the beach sediments.

The east sides of both Cold and Pavlov Bays are rugged, in places without beaches but more commonly with relatively narrow beaches composed mostly or entirely

TABLE 3: SIZE DATA FOR COLD BAY BEACHES

Sample number		Percent gravel		Mean diameter of gravel (cm.)		Maximum diameter of gravel (cm.)	
Station number	Substation number	at substation	station average	at substation	station average	at substation	at station
H1	1	100	100	4.5	3.9	9.5	20.0
	2	100		3.3		10.0	
	3	100		3.7		10.0	
	4	100		3.6		12.0	
	5	100		4.3		20.0	
H2	1	98	99	8.8	6.6	15.0	15.0
	2	100		5.4		12.0	
	3	100		5.5		11.7	
H3	1	100	100	3.8	3.5	12.6	12.6
	2	100		3.2		7.0	
H5	1	100	100	6.4	4.2	14.0	14.0
	2	100		1.9		4.3	
H6	1	100	58	1.7	1.6	7.0	7.0
	2	15		1.4		6.5	
H7	1	100	65	2.0	2.4	6.0	7.2
	2	30		2.8		7.2	
H8	1	3	4	1.5	1.4	2.6	3.2
	2	5		1.3		3.2	
H14	1	70	77	25.0	8.3	57.0	57.0
	2	100		7.5		19.5	
	3	100		5.0		15.5	
	4	100		1.5		17.5	
	5	15		2.4		7.5	
H9	1	100	80	1.9	2.2	12.0	12.0
	2	100		1.6		8.5	
	3	40		3.0		8.0	
H10	1	99	91	2.5	2.7	8.0	13.0
	2	75		2.0		11.0	
	3	100		3.5		13.0	
H11	1	100	100	6.0	3.6	27.0	27.0
	2	100		2.5		12.0	
	3	100		2.5		9.0	
H13	1	95	65	1.8	3.6	14.5	14.5
	2	20		4.0		11.5	
	3	80		5.0		14.0	
H12	1	100	100	7.0	5.8	19.0	19.0
	2	99		4.5		17.0	

TABLE 4: SIZE DATA FOR PAVLOV BAY BEACHES

Sample number		Percent gravel		Mean diameter of gravel (cm.)		Maximum diameter of gravel (cm.)	
Station number	Substation number	at substation	station average	at substation	station average	at substation	at station
H15	1	100	100	23.0	20.0	44.0	52.0
	2	100		23.0		52.0	
	3	100		14.0		26.0	
H16	1	99	100	1.3	1.2	3.0	3.5
	2	100		1.0		2.8	
	3	100		1.3		3.5	
H17	1	99	100	2.7	2.5	18.0	18.0
	2	100		1.4		3.8	
	3	100		3.5		14.0	
H18	1	95	88	0.9	1.6	3.5	5.4
	2	95		1.2		3.4	
	3	75		2.8		5.4	
H19	1	10	55	1.2	1.6	2.9	6.5
	2	100		2.0		6.5	
H20	1	100	100	1.0	1.4	3.5	4.8
	2	100		1.2		4.8	
	3	100		2.0		3.5	
H21	1	3	1	1.3	0.7	2.5	2.5
	2	1		0.7		1.5	
	3	0		--		--	
H22	1	100	67	0.5	1.2	2.0	6.0
	2	10		1.6		4.2	
	3	90		1.5		6.0	
H23	1	100	88	0.5	0.8	1.9	6.0
	2	75		1.0		6.0	
H24	1	65	34	0.5	1.0	2.7	4.0
	2	2		1.0		4.0	
H25	1	100	80	1.2	2.6	8.5	11.0
	2	100		1.2		6.0	
	3	100		1.6		5.9	
	4	20		6.5		11.0	
H26	1	5	37	4.5	9.2	15.5	22.5
	2	10		10.0		19.0	
	3	95		13.0		22.5	
H29	1	8	14	5.0	4.5	9.1	10.0
	2	20		3.9		10.0	
H28	1	2	44	1.2	9.6	2.9	3.8
	2	100		0.3		1.6	
	3	30		1.4		3.8	
H27	1	100	99	1.2	1.0	3.1	4.3
	2	100		0.9		4.3	
	3	97		0.9		2.5	

of gravel (Cold Bay stations H1-H6, Pavlov Bay stations H15-H18, Tables 3 and 4). The coarsest beaches occur near the entrances to the bays (Cold Bay station H1, Pavlov Bay station H15), probably because of the relatively great exposure to large waves from the Pacific Ocean.

The west sides of both Cold and Pavlov Bays are less rugged than the east sides, and the west-side beaches are generally finer than the east-side beaches (Cold Bay stations H9-H14, Pavlov Bay stations H22-H29). The relative fineness of the west-side beaches is especially evident in the low percentages of gravel and correspondingly high percentages of sand; the west-side gravel fractions are more comparable in grain size to the two sides of the bays. The beaches on the west side of Pavlov Bay are especially sandy due to the large amounts of volcanic sand carried by streams from Pavlov Volcano and its neighboring peaks.

The low northern ends of both Cold and Pavlov Bays have beaches composed of relatively fine-grained sediments. The finest beach sediments in both bays were found near the northwestern corners of the bays (Cold Bay station H8, Pavlov Bay station H21); these sediments are mostly sand, with little gravel, and the gravel that does occur is relatively fine. The sediments near the northeastern corners of the bays (Cold Bay station H7, Pavlov Bay station H20) are dominantly gravel, but the gravel is finer than at most places on the east sides of the bays.

SIGNIFICANCE

Most of the coarser grained gravelly beaches of Cold and Pavlov Bays have acquired their coarse nature by the winnowing of finer grained material during shoreline erosion. The occurrence of erosion in the past, however, does not necessarily mean that the beaches are still eroding, for the coarse material remaining on the beaches tends to act as "armor" against the wave forces that cause erosion. Even if the coarse material does not completely stop shoreline erosion, it must slow it down considerably.

The finer grained sandy beaches of Cold and Pavlov Bays represent depositional areas of several types. Those around the northern ends of the bays represent permanent "sinks" where material winnowed from eroding shorelines to the south is finally deposited after being transported northward along the bay shorelines. Some relatively fine-grained beaches elsewhere around the bays are deposits that tend to bridge minor bay indentations and thus serve as conveyer belts for the transport of sediment along the shorelines. Finally, the sandy beaches around the west side of Pavlov Bay are deposits that are present only because of the large amounts of sand supplied to the area by streams; if this supply were cut off, most of this sand would be eroded and transported alongshore to the northern end of the bay.

C. WAVE CLIMATE MODEL FOR THE NORTHEASTERN BERING SEA

A wave-climate model for the northeastern Bering Sea is presently nearing completion. Hind cast deep water wave characteristics are input into a computer program. The program refracts these waves across the shelf and accounts for wind stress on wave growth and bottom friction. More details on methodology are given in section V of this report.

Some preliminary results are shown in Fig. 1. Input waves have a height of 2 m and period of 5.4 seconds. Wind is from the south at 40 knots. The solid lines are wave orthogonals which are everywhere perpendicular to wave crests. Where orthogonals spread, wave heights become relatively low. Thus, waves entering Norton Sound for these conditions are lower in height than waves along the coast north of Norton Sound (Fig. 1). As wave orthogonals converge wave height becomes large. South of the Bering Strait wave orthogonals cross in places (Fig. 1). These caustics result in complex wave patterns and in some cases may be hazardous to navigation.

Output from the wave climate model is presently being checked for computational errors. Results from our study on the wave characteristics during the 1974 storm will be reported in our Final Report.

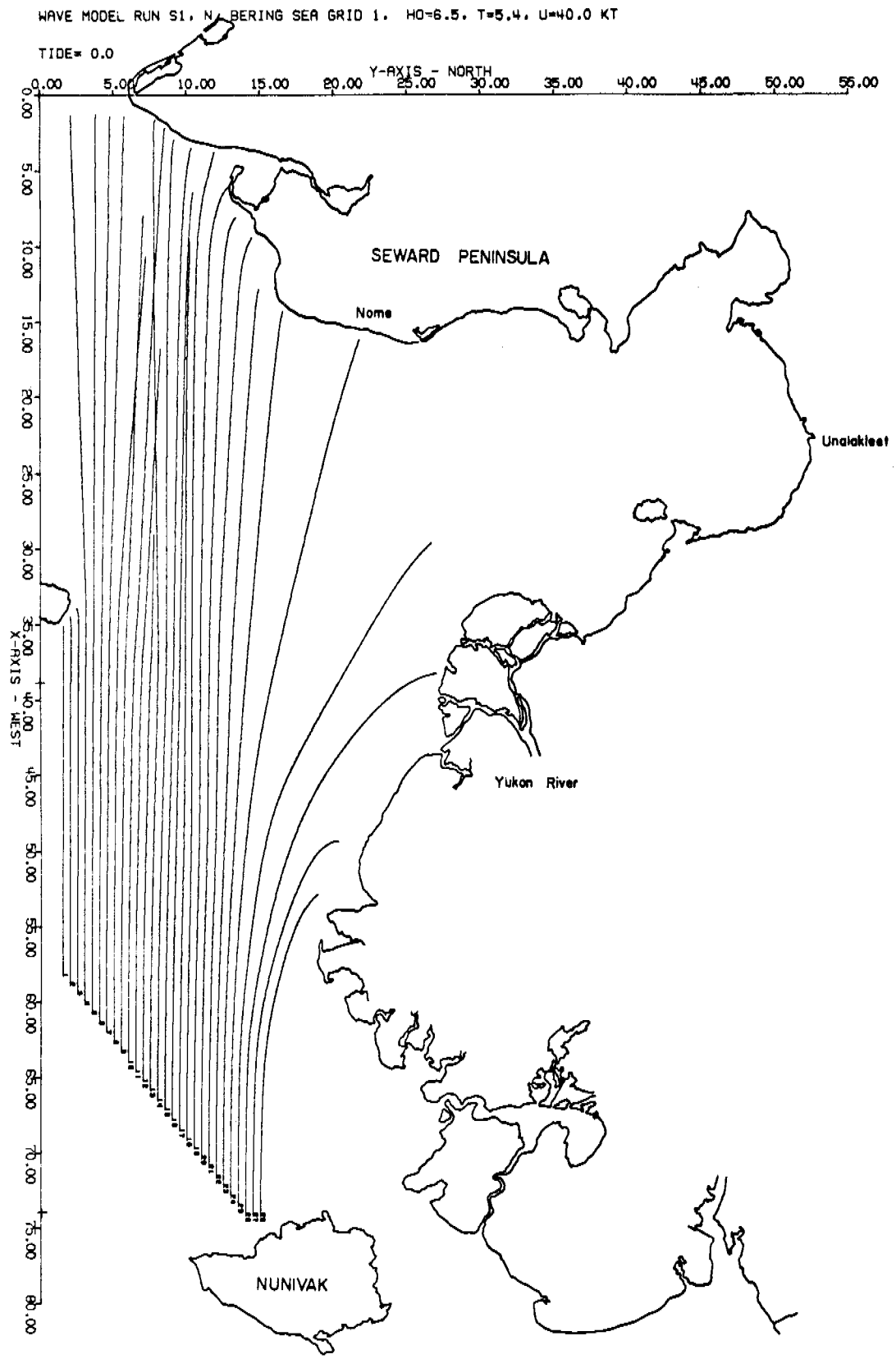

Fig. 1. Preliminary wave model output.

D. WAVE MEASUREMENTS; NOME, ALASKA

Introduction

The wave monitoring station sat on the bottom several hundred meters offshore at the western edge of Nome, Alaska (Figure 1). The station consisted of 4 pressure sensors and a data encoding/transmitting spar buoy (see Section V). The array configuration was selected along the guidelines of Pawka, et al. (1976) with a sensor unit spacing that would resolve directions for waves of greater than three second periods. The array orientation of S74°E approximately paralleled the adjacent shoreline.

The station was installed on 8-9 July 1977. Data transmission began on 9 July 1977 at 1630 BST. The transmitter failed to turn on for the 2230 BST transmission of 11 July 1977, was fixed and restarted on 16 July 1977 at 0040 BST. The transmitter operated on schedule from that time until 1 September 1977 when, due to low batteries, it failed to turn on for the 1840 BST transmission. The station was removed on 12-15 September 1977 after being unable to reactivate the transmitter. During the time the station was in operation, 200 ten minute observations were recorded. These were later plotted on strip chart for visual inspection. By the end of the final year of the contract appropriate wave records will be spectrally analysed on the U.S.G.S. Honeywell computer to obtain wave directions and size.

Analysis

In order to obtain wave direction following the technique of Pawka, et al. (1976) some number of blind sensors are placed in a line with known spacing between them. Wave spectra can be obtained from each pressure sensor separately and the values are averaged together to obtain the wave energy at the station.

A cross-spectra is calculated for each pair of sensors and these are combined for frequencies of interest, taking into account the spacings between the pairs, to obtain wave direction as a function of frequency. The unit spacing between sensors determines the minimum period for which a direction can be obtained. Maximum directional resolution occurs for periods near the minimum, and the reliability of the technique decreases as the period is further increased.

Based on fetch length and previous personal observation, we decided to "tune" the array for short period waves (3 to 10 seconds). Three seconds is definitely a lower limit because a three second wave is just starting to feel bottom in six meters of water. Waves of period greater than about 10 seconds were not expected because the fetch is too short for locally generated waves of greater period and distant, long period waves are blocked from the area by the Aleutians and certain other islands.

The wave spectra in this chapter are depth corrected using linear wave theory. Only wave periods greater than three seconds are corrected so that spectral noise at short periods is not mistaken for wave induced pressure fluxuations. The root-mean-square wave (rms) height can be directly calculated from the plots by multiplying the energy (area under the curve between any two frequencies) by eight and taking the square root.

Results

First, the strip chart records were inspected to get a gross feeling for the wave conditions over the summer. Wave records were grouped into three catagories based on wave amplitude (Figs. 2, 3, 4). Considering all 200 observations, "small" waves (Fig. 2) occurred 71.5% of the time. The breakdown on a monthly basis is shown in Table 1. It should be recognized that there is bound to be overlap between catagories, especially since the analog records are not depth corrected.

Looking at the analog records sequentially, it is seen that, for the most part, the "medium" and "large" waves occurred together during what must have been a small, 5 day summer storm.

One final point of interest -- Figs. 2 and 4 show wave conditions six hours apart. This indicates the rapidity in which the wave climate can change as stormy weather approaches the Nome area.

Wave spectra for Figs. 2 and 4 are shown in Figs. 5 and 6 respectively. Part a of each Figure shows the spectral estimates for sensors 1 to 4 and part b shows the average for all 4 sensors. Actually, all four sensors give essentially the same spectral values which means the average value is a very good estimate of the wave climate. The spectra in both cases are what one would expect for locally derived waves. Thus, in calm weather the locally derived waves are small in amplitude and short in period. When the storm arrives wave amplitudes grow and there is a shift toward longer periods. The short time between records means that there is still a contribution from the short wave periods since the wind duration is short. In both records there is a small peak in the curve at about 9 seconds. Since this peak does not change amplitude between the two records, it probably represents swell from outside the storm area. By the end of this period of larger waves (Fig. 7) the wave period had shifted to higher periods while the rms wave height remained about the same.

All the spectral results presented here are subject to minor modification. They were produced by newly written programs and these programs are now being compared with working programs at the Scripps Institution of Oceanography. This information will, therefore, be updated and expanded for the final project report.

TABLE 1: MONTHLY FREQUENCY OF OCCURRENCE OF WAVE AMPLITUDES

Month	"small"	"medium"	"large"	Total
July	43	22	2	67
Aug./Sept.	100	25	8	133
Total	143	47	10	200

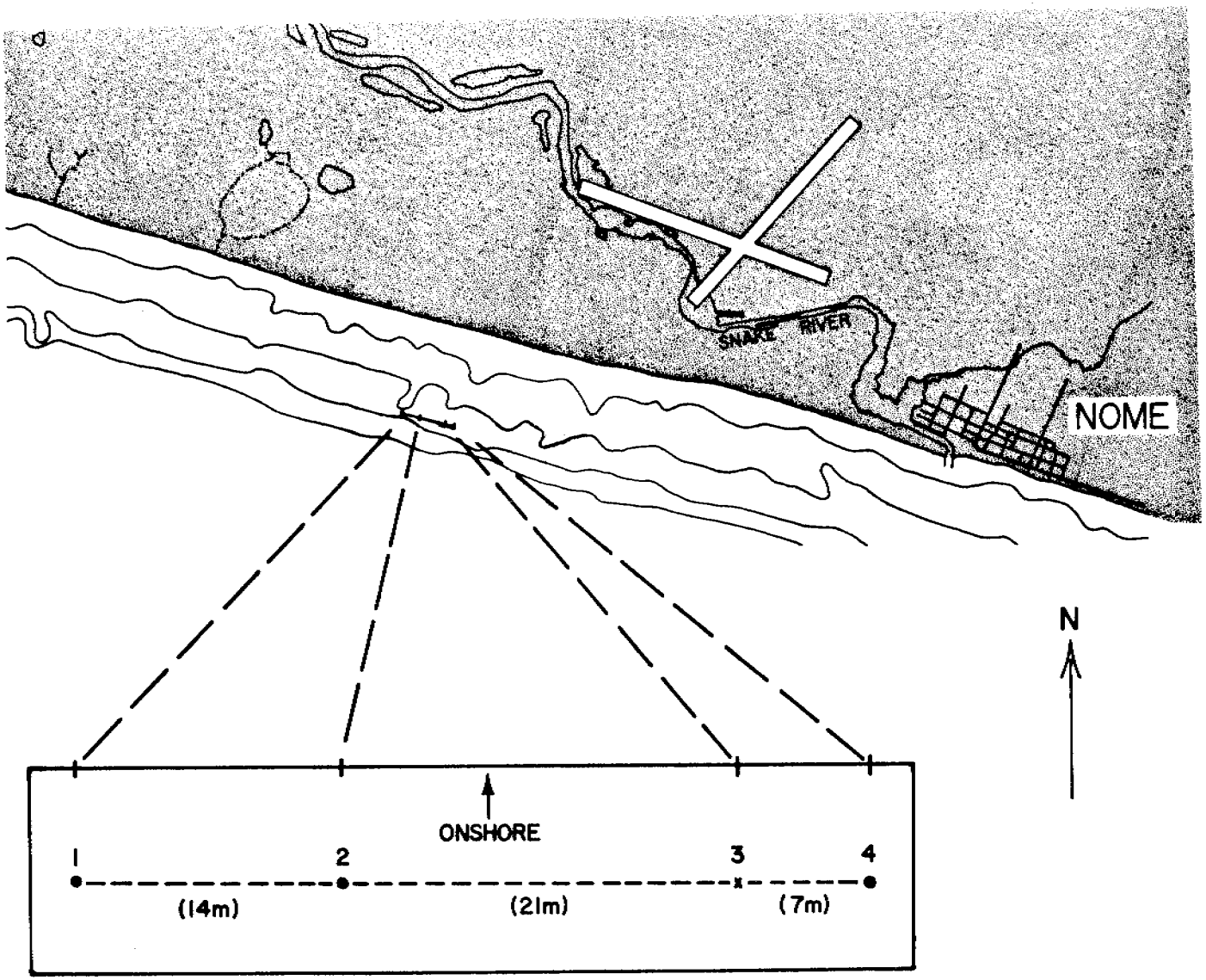

Fig. 1. Location map for shelf station including encoding/transmitting buoy (X) and four pressure sensors (●, X) in a linear array. Array is not drawn to scale on the chart.

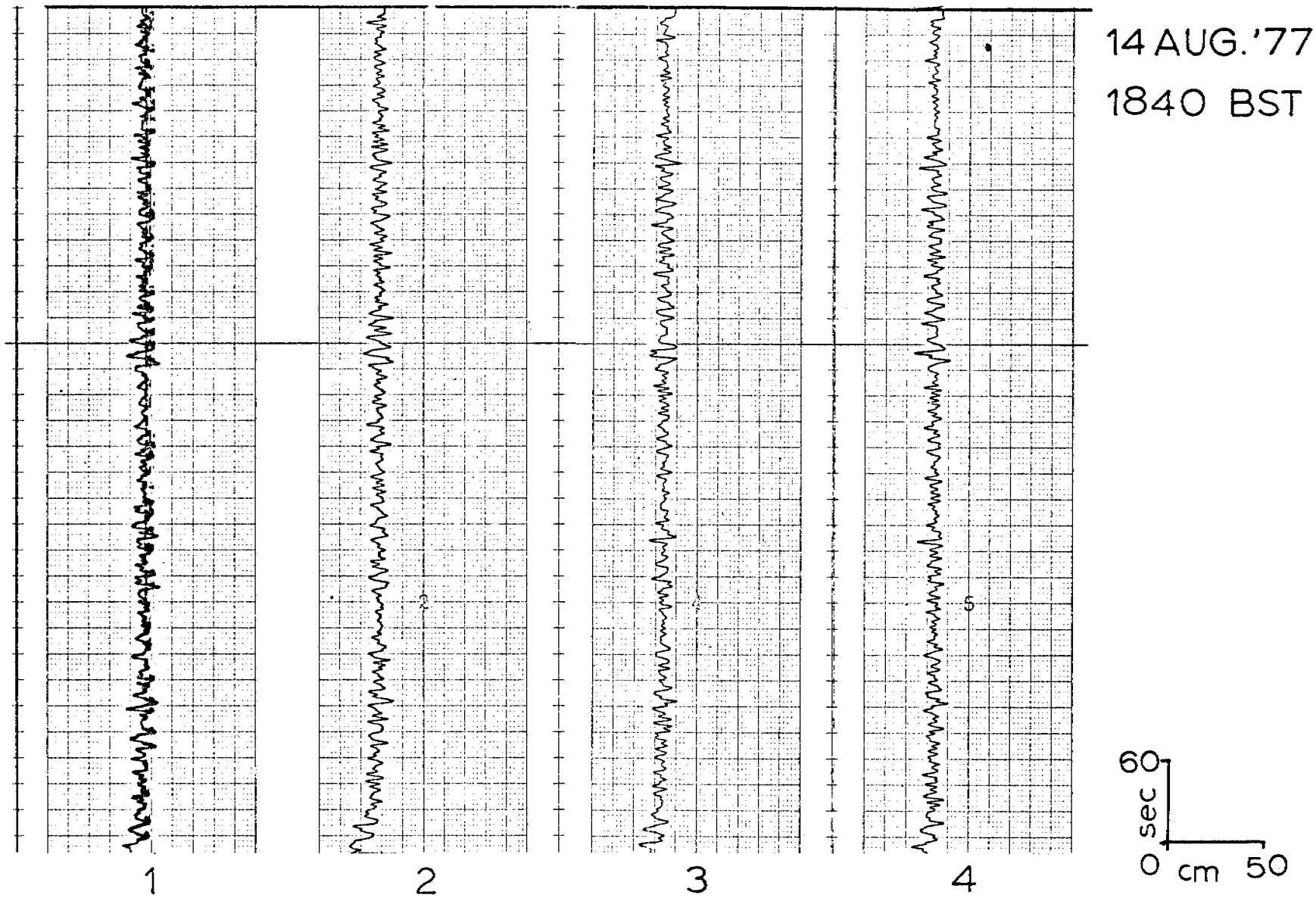

Fig. 2. Pressure record typical of usual summer wave conditions at the shelf station. These are the "small" waves referred to in the text.

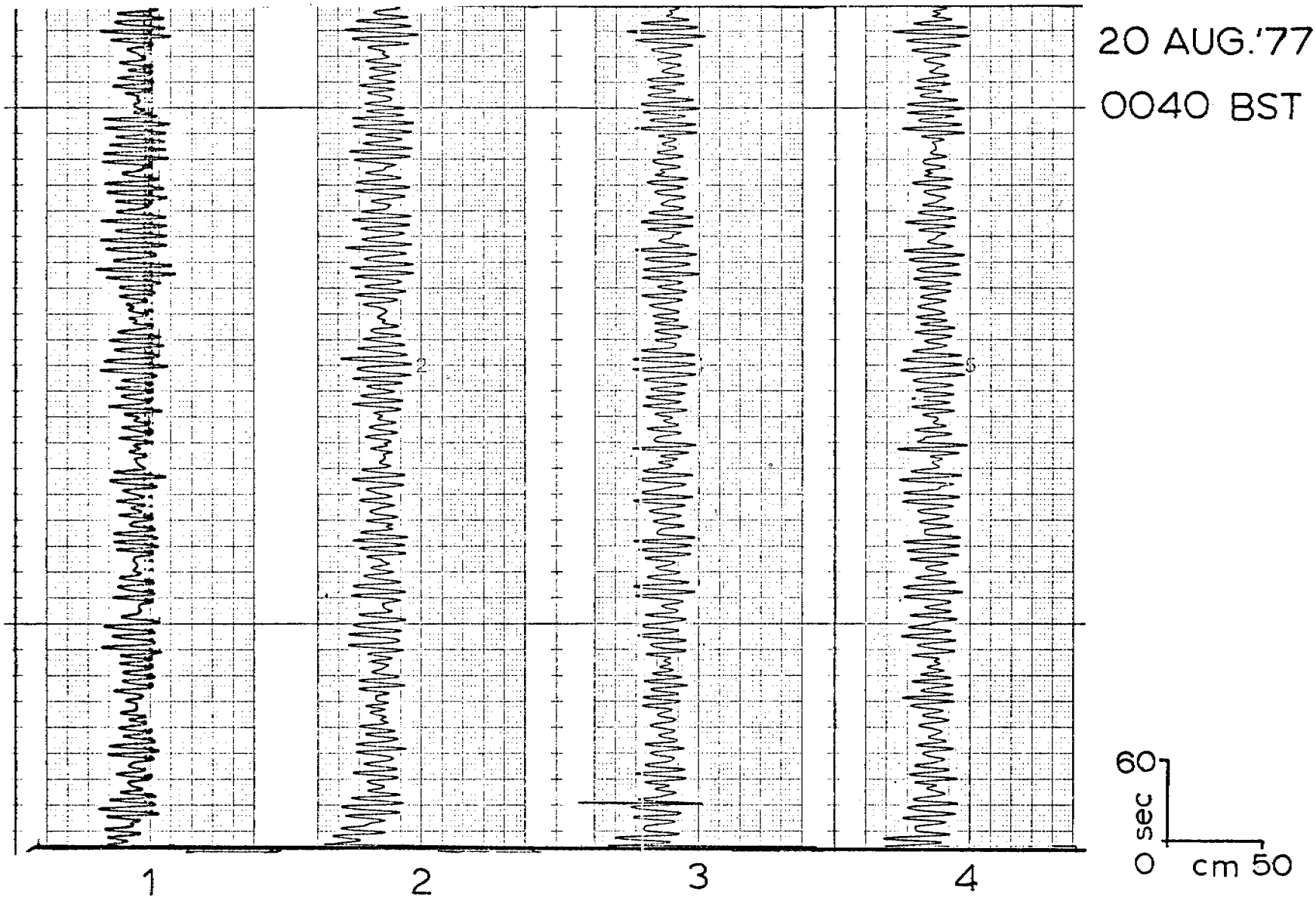

Fig. 3. Pressure record of less frequent wave conditions at the shelf station. These are the "medium" waves referred to in the text.

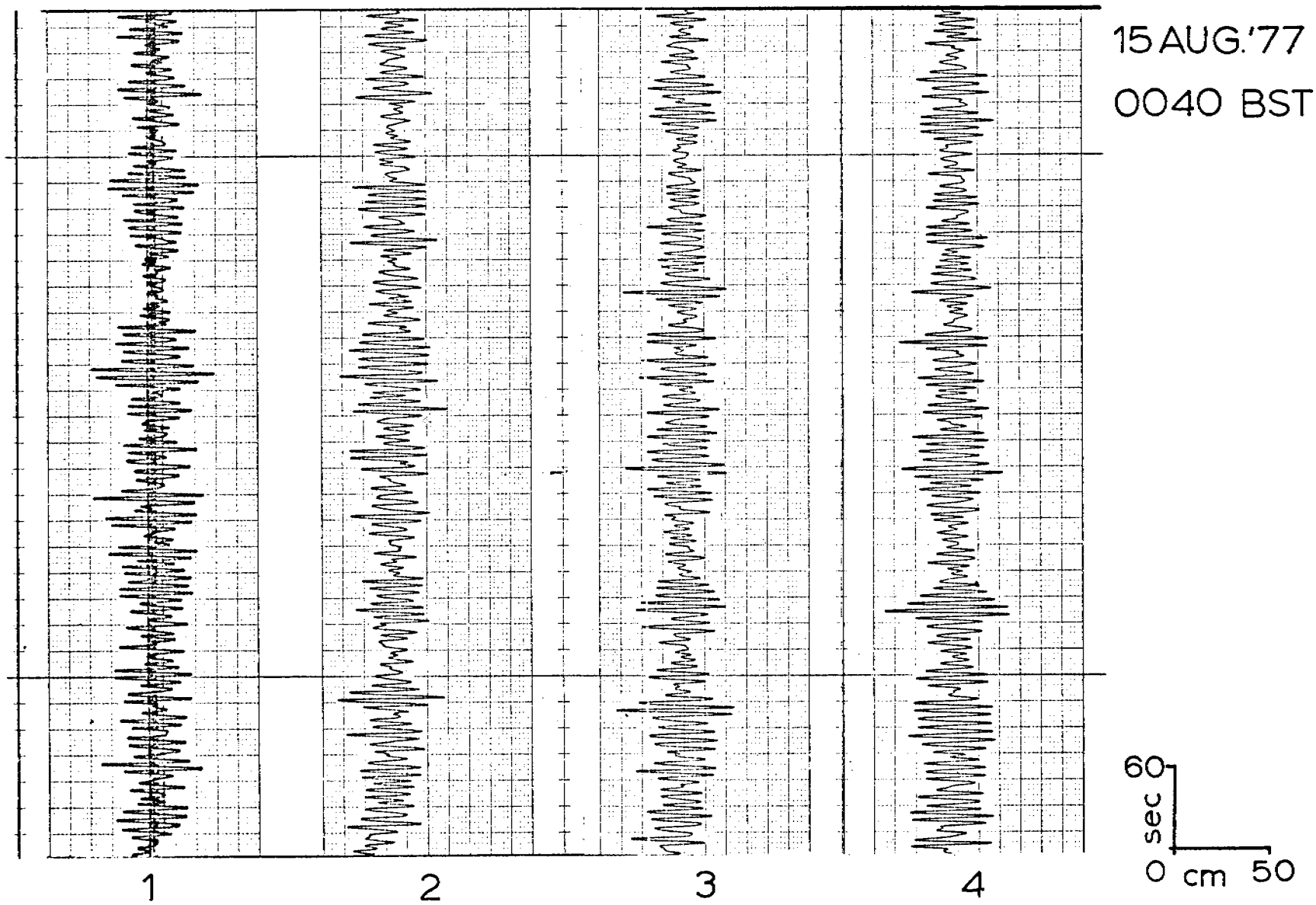

Fig. 4. Pressure record typical of the largest waves measured at the shelf station. These are the "large" waves referred to in the text.

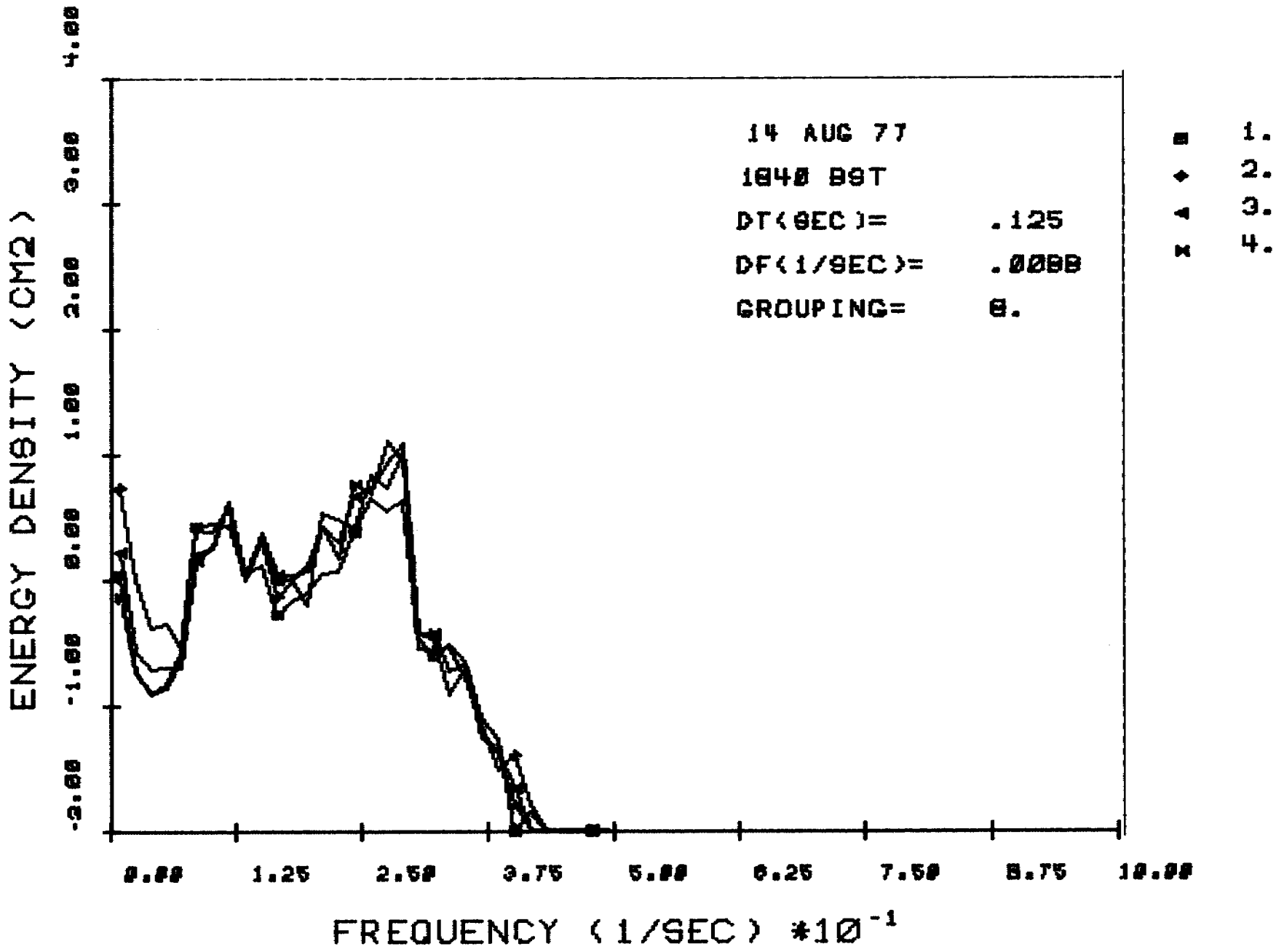

Fig. 5a. Wave spectrum for sensors 1 through 4.

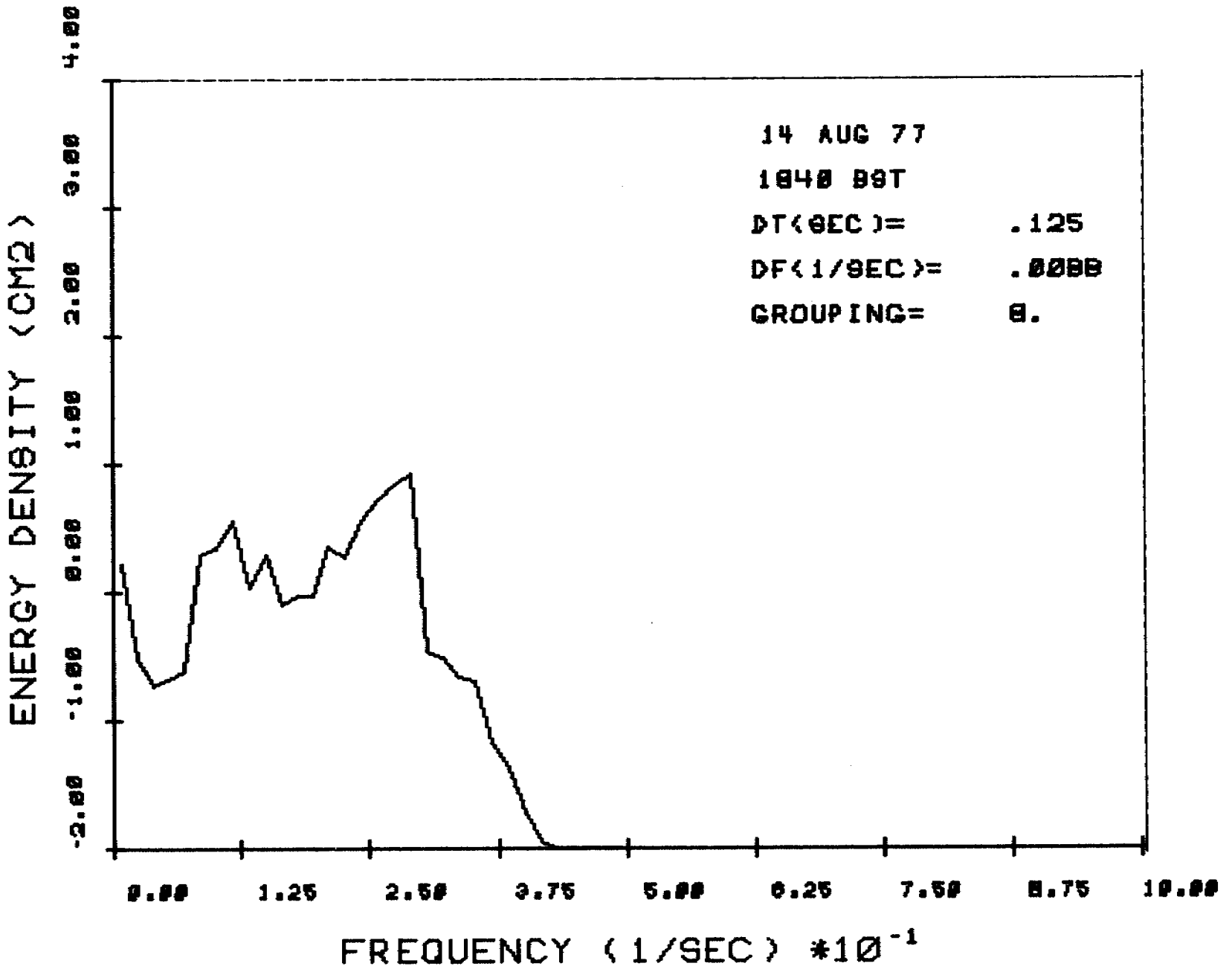

Fig. 5b. Wave spectrum based on an average of four sensors.

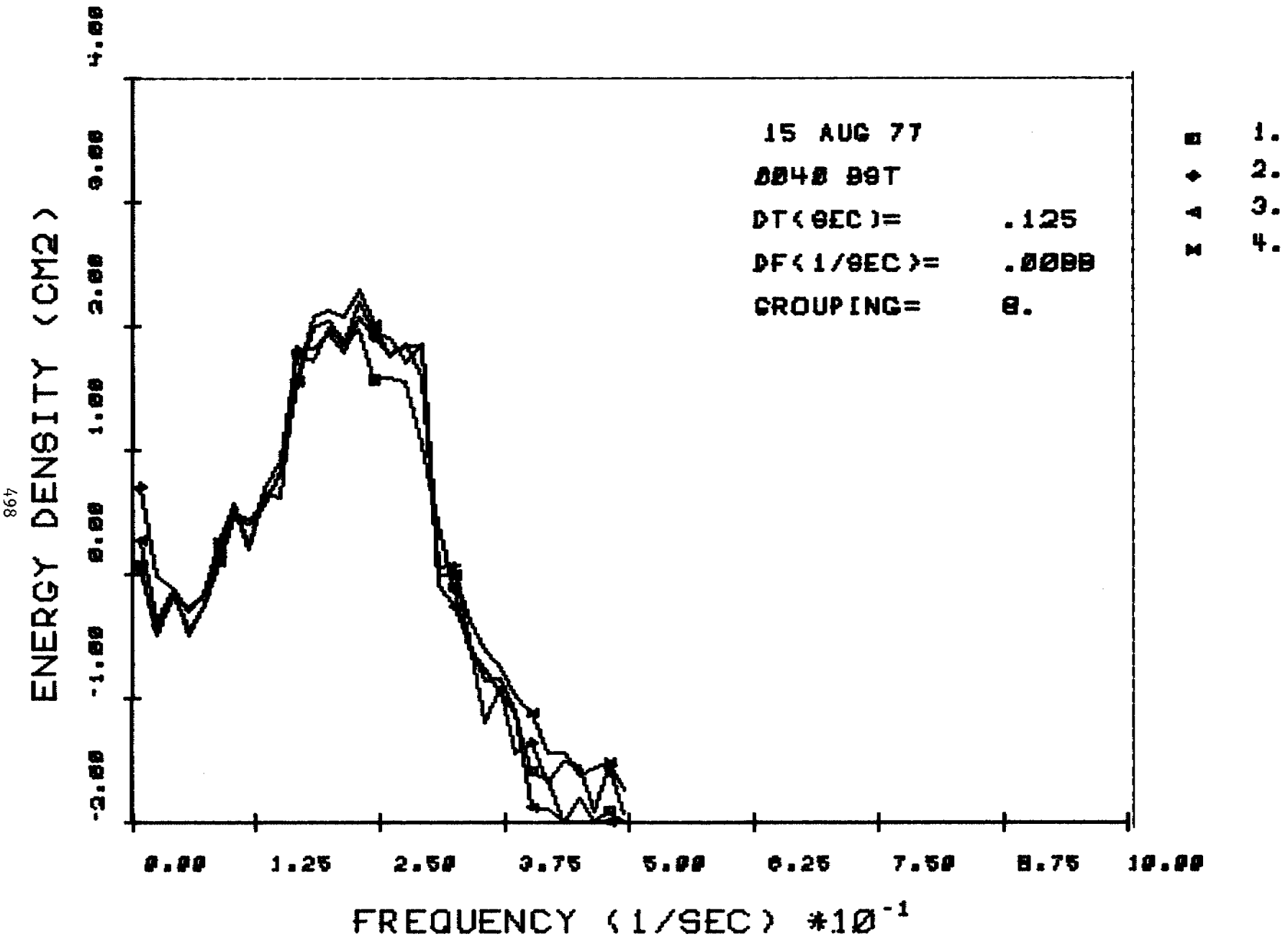

Fig. 6a. Wave spectrum for sensors 1 through 4.

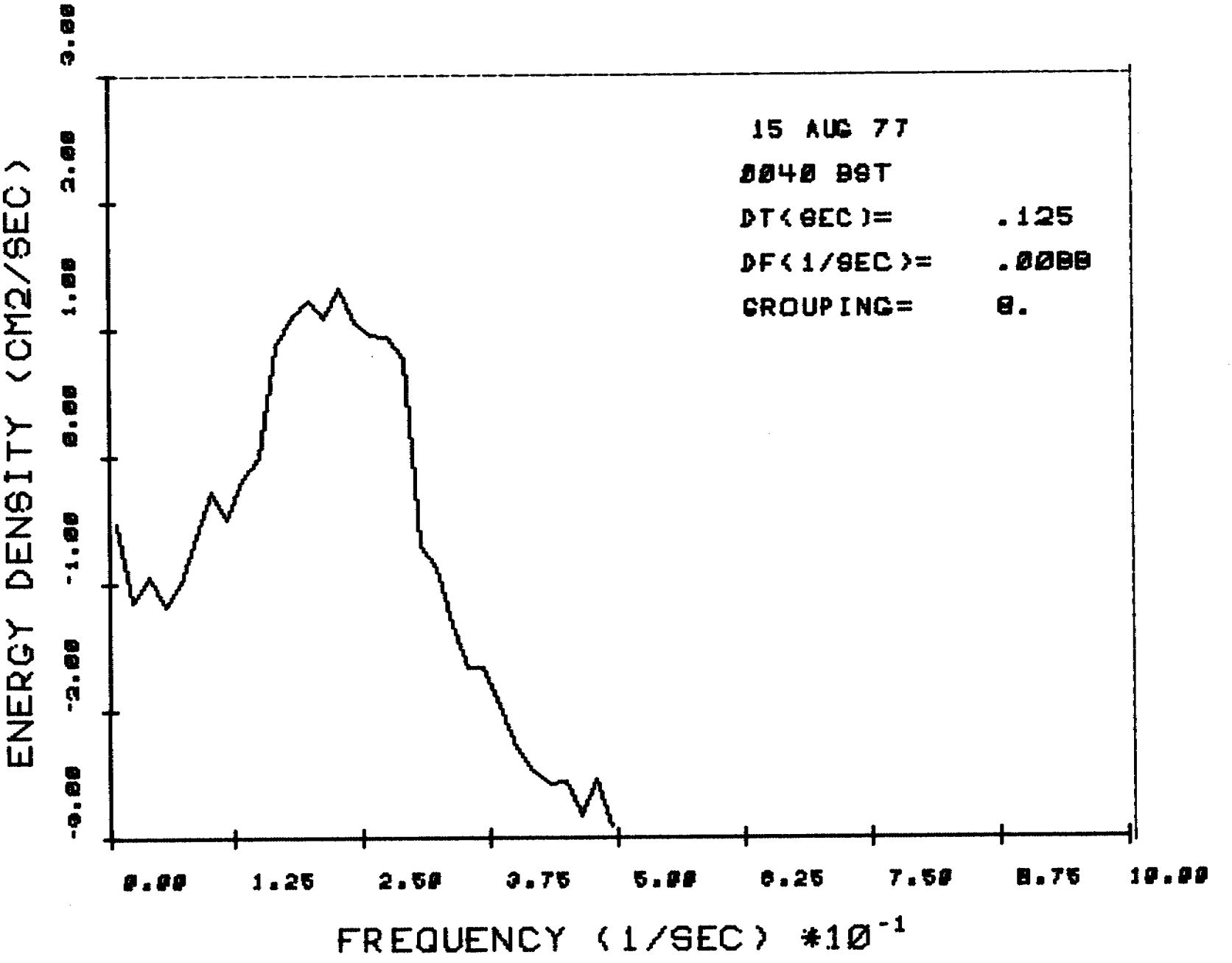

Fig. 6b. Wave spectrum based on average of four sensors.

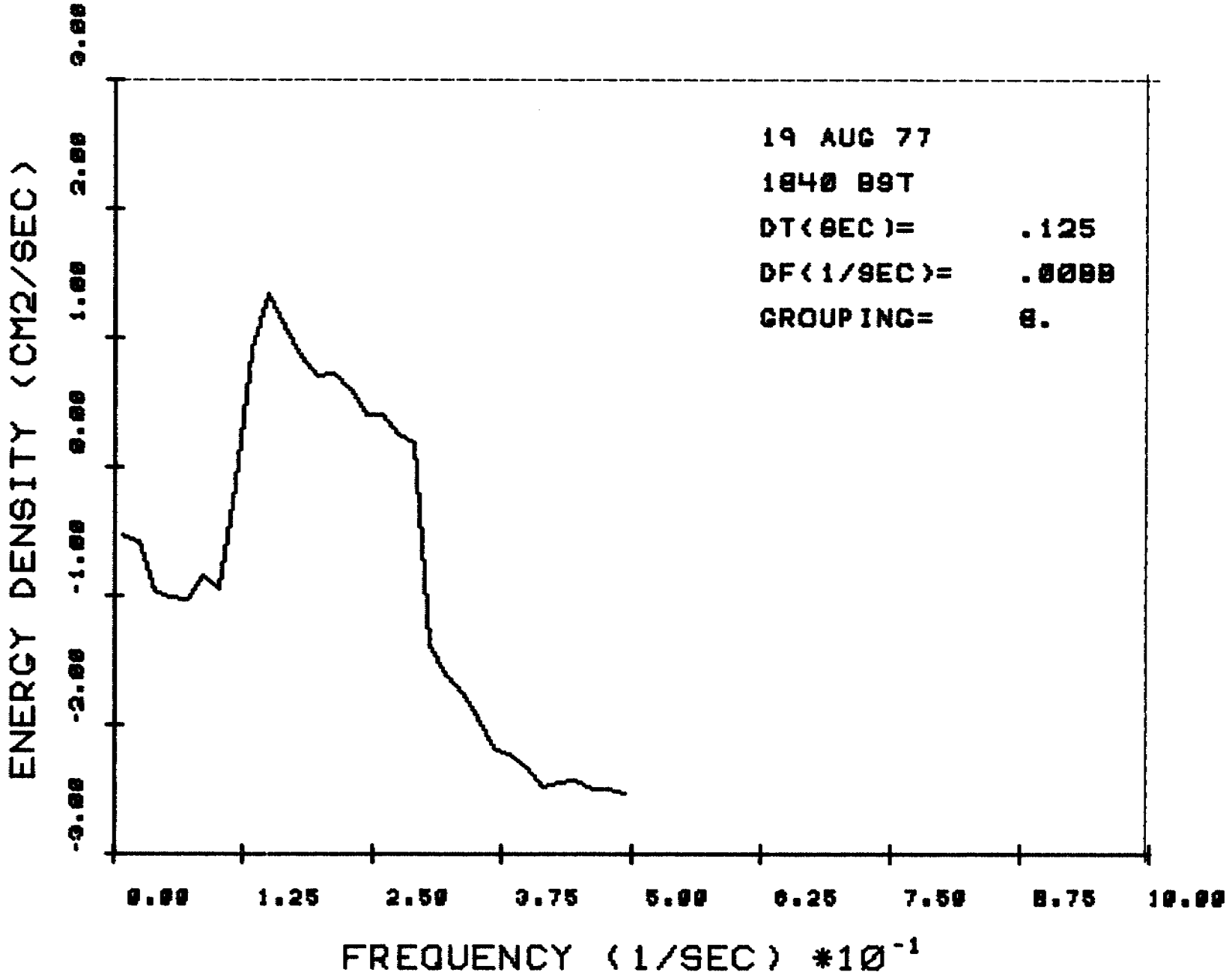

Fig. 7. Wave spectrum based on average of four sensors.

X. NEEDS FOR FURTHER STUDY

A. In order to properly evaluate the output of the wave model, we need direct measurement of a wide spectrum of wave energies. At least one more field season of wave measurement is necessary.

B. More detailed work on scour depths on the beach and nearshore are necessary. The results from one field season are not enough and cannot be interpreted as being representative.

C. OCSEAP should consider maintaining a medium-level study on coastal processes of the southern portion of the Bristol Bay coast of the Alaska Peninsula. This is a critical area in view of its high biological productivity (e.g. Izembek Lagoon) and its proximity to potential deep water ports on the south side of the Peninsula.

X. AUXILIARY MATERIAL

A. References Used

Berryhill, R. V., 1963, Reconnaissance of beach sands, Bristol Bay, Alaska. U.S. Bureau of Mines, Report Inv. 6214:48pp.

Dobson, R. S., 1967, Some applications of a digital computer to hydraulic engineering problems, Stanford Univ., Dept. of Civil Engineering, Tech. Report 80.

Dolan, R., 1971, Coastal landforms: crescentic and rhythmic, Geol. Soc. Am. Bull., 82:177-180.

Fathauer, T., 1975, The great Bering Sea storms of 9-12 November 1974, Weatherwise: 76-83.

Greene, H. G., 1970, Morphology, sedimentation and seismic characteristics of an arctic beach, Nome, Alaska -- with economic significances, M.S. thesis, San Jose State College, San Jose, CA: 139pp.

Hopkins, D. M., 1967, Quaternary marine transgressions in Alaska, in Hopkins, D. M., ed. The Bering Land Bridge, Stanford Univ. Press: 495 pp.

Joyce, J. R. F., 1950, Notes on ice-foot development, Nemy Fjord, Graham Land, Antarctica, J. Geol. 58:646-49.

Lowe, R. L., Inman, D. L., Brush, B. M., 1972, Simultaneous data system for instrumenting the shelf. Proc. Coastal Eng. Conf., 13:95-112.

Pawka, S. S., Inman, D. L., Lowe, R. L., Holmes, L., 1976, Wave climate at Torrey Pines Beach, California, U.S. Army Corps of Engineers, Coastal Eng. Research Center, Tech. Paper 76-5:372 pp.

Sallenger, A. H., Hunter, R., Dingler, J., 1977, Coastal processes and morphology of the Bering Sea coast of Alaska, FY76 Annual Report, OCSEAP, NOAA: 66 pp.

Thrall, D. E., 1973, Development of a computer program to simulate wind wave generation, refraction and shoaling in the Gulf of Maine, Engineering Design and Analysis Laboratory, Univ. of New Hampshire, EDAL Rep. 113:25 pp.

B. Papers in Preparation

Hunter, R., Sallenger, A., and Dupre, W., Directions of net longshore sediment transport for the Bering Sea coast of Alaska.

Sallenger, A. H., Coastal Effects of a major storm in a subarctic environment.

C. Oral Presentations

Sallenger, A. H., and Hunter, R. E., 1977, Coastal effects of a major storm in the northern Bering Sea, Abstracts with Programs, Geol. Soc. Am. Annual Mtg. (Seattle, Washington), v. 9, no. 7, p. 1152-3.

Annual Report Task D-9

Research Unit #473

April 1977 to March 1978

SHORELINE HISTORY OF CHUKCHI AND BEAUFORT SEAS AS AN AID TO PREDICTING OFFSHORE PERMAFROST CONDITIONS

D. M. Hopkins and R. W. Hartz
U. S. Geological Survey
345 Middlefield Road
Menlo Park, CA 94025

TABLE OF CONTENTS

SUMMARY

During the summer of 1977 we made a geologic reconnaissance of the coastal bluffs, beaches, and barrier islands between Point Barrow and Brownlow Point. In particular we concentrated on the problems of origin and renewability of the barrier islands, age and origin of the sediment comprising the coastal bluffs, the relationship between age of surface and ice content, and climatic history of the last 100,000 years.

We established that the barrier islands of the Beaufort Sea originated from numerous sources, but are mostly derived from hillocks of Pleistocene sediments that have been drowned and left as tundra-covered islands. We identified many areas along the mainland coast where gravel is now accumulating, and established that gravel is almost universally distributed at depths of 10 m or less in the subsurface of the coastal plain from the Kuparuk River to the Canning River. Ancient marine beach deposits which can be traced discontinuously from Barrow Village to Prudhoe Bay, were recognized as being an interglacial shoreline and an important source of sand and gravel for modern beaches and barrier islands. We confirmed that gravel from two sources of sharply contrasting lithology reaches the beaches and barrier island of the Beaufort Sea.

During the field season we collected data on high spindrift and the limits of the 1970 storm surge along the Chukchi and Beaufort Sea coasts. We also measured coastal retreat based on the relative position of C&GS benchmarks, and mapped coastal stratigraphy in detail.

This report presents detailed data on stratigraphy, lithology, pollen rain, longshore sediment transport, coastal erosion, coastal morphology, and shoreline history.

INTRODUCTION

Investigation of coastal geology and shoreline history of the Chukchi and Beaufort Seas was initiated in 1976. Many facets have been conducted in cooperation with federal and state agencies and universities. The primary objective of our study is to ascertain the relationship of coastal geology and geomorphology to shoreline history and offshore permafrost.

Exploration and production of offshore oil and gas reserves in the Beaufort Sea will require large amount of artificial fill for the construction of causeways, pipe lines, artificial islands, and support facilities. Gravel is the primary material used for artificial fill in the arctic, nearly 10,000,000 m^3 has been quarried in the Prudhoe Bay oilfield, and the location of potential quarry sites is essential to the development and production phases. The environmental impact of quarrying operations can be minimized by locating areas of thick gravel deposits or sites where gravel is now accumulating. Construction of onshore support facilities also requires knowledge of potential flooding hazards during storm surges and the possible effects of coastal erosion.

DATA GATHERING

Field operations were conducted during a six-week period from late July to early September, 1977. Utilizing N.A.R.L. air support we established various base camps along the Beaufort Sea coast between Point Barrow and Brownlow Point. Reconnaissance of the coastal bluffs, beaches, and barrier islands was then conducted on foot or from inflatable boats.

An important objective was to determine sources of gravel and directions of longshore sediment transport, paying special attention to the problems of origin and renewability. Each chain of barrier islands from Point Barrow to Brownlow Point was visited, island profiles were drawn and samples were collected for granulometric analyses and lithologic pebble counts. Mainland beaches and river bars were also sampled in order to establish the role of various sources of nourishment and direction of transport. The results are summarized in Appendices I and II.

Natural and excavated sections of the coastal bluffs and artificial gravel pits were examined and sampled in order to establish sedimentological and climatic history of the coastal plain (Appendix I).

Samples of the modern pollen rain were collected in order facilitate the interpretation of ancient pollen spectra (Appendix III).

The high spindrift line of the 1970 storm surge was mapped from Point Barrow to the Canning River, this data has been combined with data collected along the Chukchi Sea coast in 1976 in order to establish the zone of probable inundation during maximum storm surge conditions. Maps of the storm surge limits from Icy Cape to the Colville River are presented in Appendix IV.

Radiocarbon samples were collected from numerous localities along the coast, about 50 of these samples have been submitted for dating and the results should be forthcoming. Fossil mollusks were also collected from about 20 sites and they have been submitted for identification and possible amino-acid racemization studies.

In order to estimate rates of coastal retreat we measured the relative position of Coast and Geodetic Survey benchmarks and combined this data with the study of air photos and topographic maps to produce an erosional hazards map (Appendix V).

RESULTS

Material comprising the barrier island chains has been derived from multiple sources. Historical studies as well as analysis of island forms, and observation of directions in which sediments fine show that the individual islands act as single, coherent sediment cells; i.e., sand and gravel migrate from one island to another only within island groups.

Thus island groups such as the McClure, McGuire, and Stockton Islands now constitute mutually isolated sediment systems. Gravel quarried from these sites would not be replenished.

Gravel and sand, for use as artificial fill, is presently being quarried only beneath stream channels in the Prudhoe Bay oilfield. We conclude that all of the gently sloping region extending northward from the Brooks Range to the Beaufort Sea coast between the Canning River and the Kuparuk River appears to be underlain by glacial outwash and alluvium composed of sand and gravel with overburden probably no more than 10 meters thick.

A new map classifying coastal erosional hazards and a short text on the coastal morphology of NPR-A from Icy Cape to the Colville River has been completed. The map was presented and explained at a public meeting on environmental studies in NPR-A held in Anchorage during early December. It shows that the coast of the Beaufort Sea is retreating much more rapidly than the Chukchi Sea coast and that the entire Arctic coast, with the exception of a few prograding river deltas, is undergoing rapid retreat.

A new map of high spindrift and storm surge limits along the coast of NPR-A was completed and made available to B.L.M. for use in their environmental studies of NPR-A. It delineates the limits of the 1970 storm surge, the major surge of the past 100 years, and indicates areas likely to be inundated during future storms.

SUMMARY OF FOURTH QUARTER OPERATIONS

A. Ship and laboratory activities

1) No cruises
2) D. M. Hopkins, R. W. Hartz, R. E. Nelson, P. A. Smith
3) Laboratory activities: Hand-picked and submitted samples for radiocarbon dates.
Hand-picked samples for identifiable seeds and insects.
Mollusks submitted for amino-acid racemization.
Samples submitted for identification of fossil microfaunas.
4) Field activities: D. M. Hopkins and R. W. Hartz attended the Beaufort Sea synthesis meeting at Barrow in January 1978.

B. Estimate of funds expended: See Annual Report RU 204, 1977-1978.

APPENDIX I. COASTAL MORPHOLOGY, COASTAL EROSION, AND BARRIER ISLANDS

BY

D. M. HOPKINS AND R. W. HARTZ

COASTAL MORPHOLOGY, COASTAL EROSION, AND BARRIER ISLANDS

by

D. M. Hopkins and R. W. Hartz

Coastal regime--the seasonal round.--The Beaufort Sea (fig. 1) is ice-covered most of the year; the open-water season is variable in length and extends, at its longest, only from mid-July to early October (Wiseman and others, 1973). The Alaskan segment has a microtidal regime; astronomical tides amount to only about 15 cm (U.S. Dept. Commerce, 1978), and their effects are subordinate to changes in sea level due to changes in barometric pressure and onshore and offshore winds. Wave energy is limited. Even during the open season, the arctic ice-pack generally lies only a few tens of kilometers offshore, and consequently, potential fetch is small. However, the frequent northeast gales of late summer can have a fetch as great as 300 km and can generate a swell 2 m high (Wiseman and others, 1973). These late-summer storms and the barometric lows with which they are associated can result in storm surges reaching as much as 3 m above normal sea level (Hume and Schalk, 1967; E. Reimnitz, written commun., 1977).

In autumn, Beaufort Sea beaches become sheathed in ice and ice-cemented gravel and later in snow; during the remainder of winter and spring they are protected from further effects of waves or moving ice (Wiseman and others, 1973). When the ice breaks up in late June or July, however, the beaches and offshore islands are disrupted to varying degrees by moving ice pushing onshore. Furrows tens of meters long and ridges a meter or more high are created on some exposed outer beaches. At the same time, low coastal bluffs begin to thaw, creating mud flows which ooze down over adjoining beaches or over the snowbanks that continue to cover them.

Figure-1 Index Map

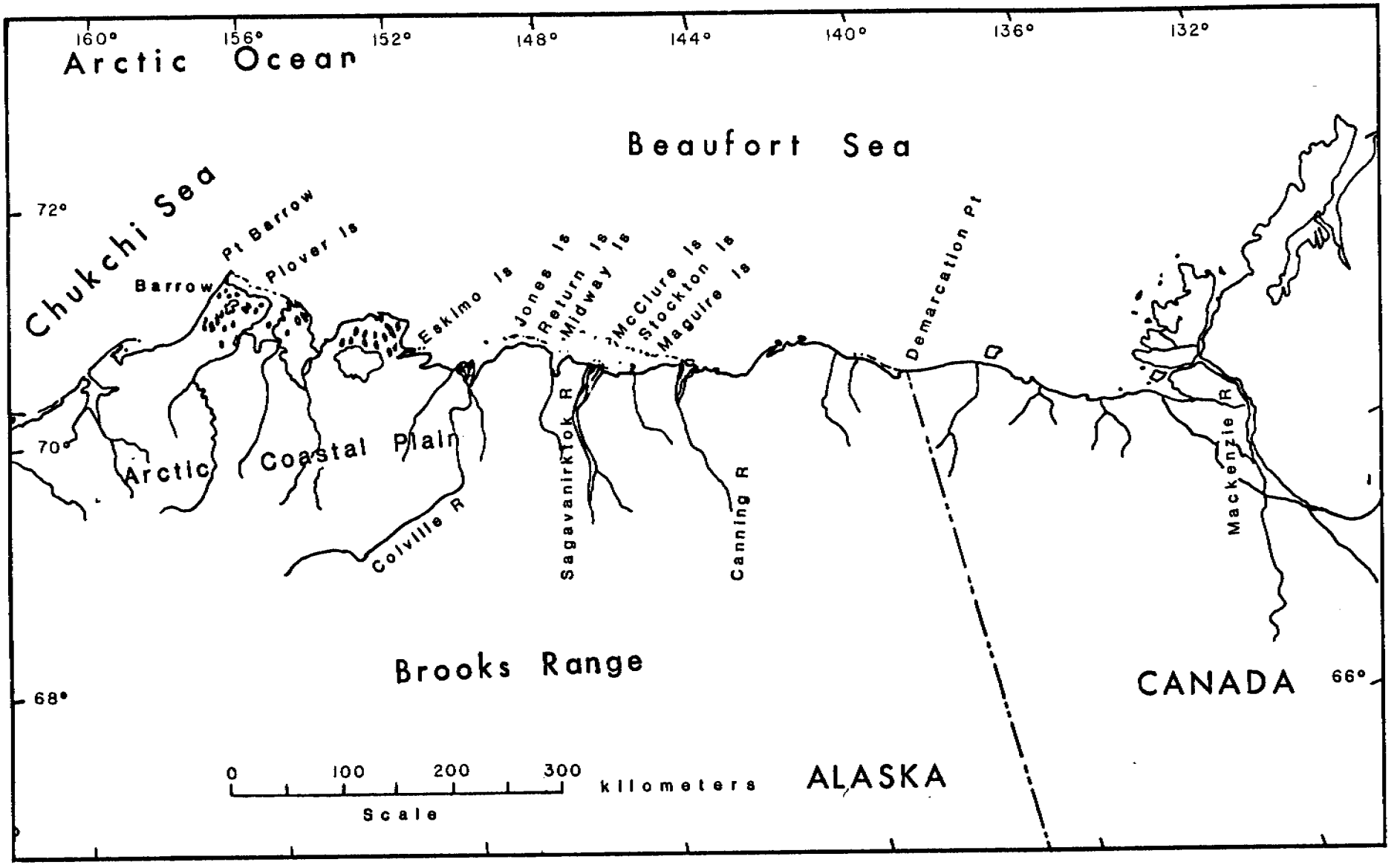

In late summer, beginning commonly in mid-August but sometimes as early as late July, the Arctic front in its northward migration reaches the Arctic coast, and Pacific storms begin to cross the region. The resulting lowered barometric pressure results in higher sea level. Wave energy is intensified, and sea ice may once again be driven onto the outer beaches. Most of the coastal changes--bluff retreat, spit elongation, and island migration-- and most of the sediment transport is accomplished during this late summer and early autumn period.

Coastal geology.--Recent studies of the Beaufort Sea coast by L. D. Carter, O. J. Ferrians, Jr., R. W. Hartz, D. M. Hopkins, and R. E. Nelson indicate that east of Oliktok Point, the Arctic coastal plain is underlain by a series of coalescing alluvial and glacial-outwash fans extending northward from the Brooks Range (Fig. 2C & D). They consist mostly of sandy gravel. The fans generally extend to the coast, but in some places, the immediate coastal area is occupied by the Flaxman Formation, a marine sandy mud of Pleistocene age which contains abundant glaciated pebbles, cobbles, and boulders foreign to Alaska and quite different in lithology from the gravel of Brooks Range origin in the alluvial fans (Leffingwell, 1919).

The Flaxman Formation contains a suite of pebble types almost completely different from the pebble types found in the alluvial and glaciofluvial deposits of streams draining the Brooks Range. Consequently, pebble-lithology counts can be used to identify the relative importance of Brooks Range alluvial deposits relative to the Flaxman Formation as sources of beach sediment (Rodeick, 1975). Gravel derived from alluvium and outwash of streams draining the Brooks Range consists largely of

Explanation: Figures 2a,b,c,d

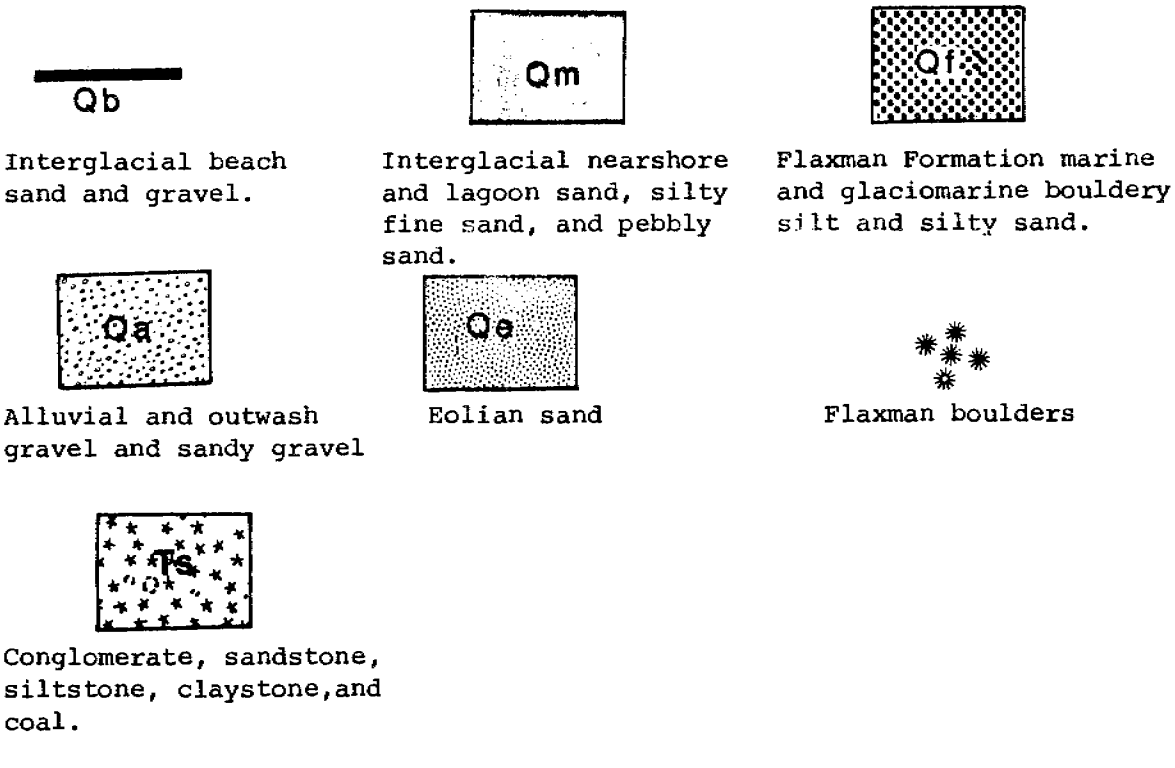

Figure-2a

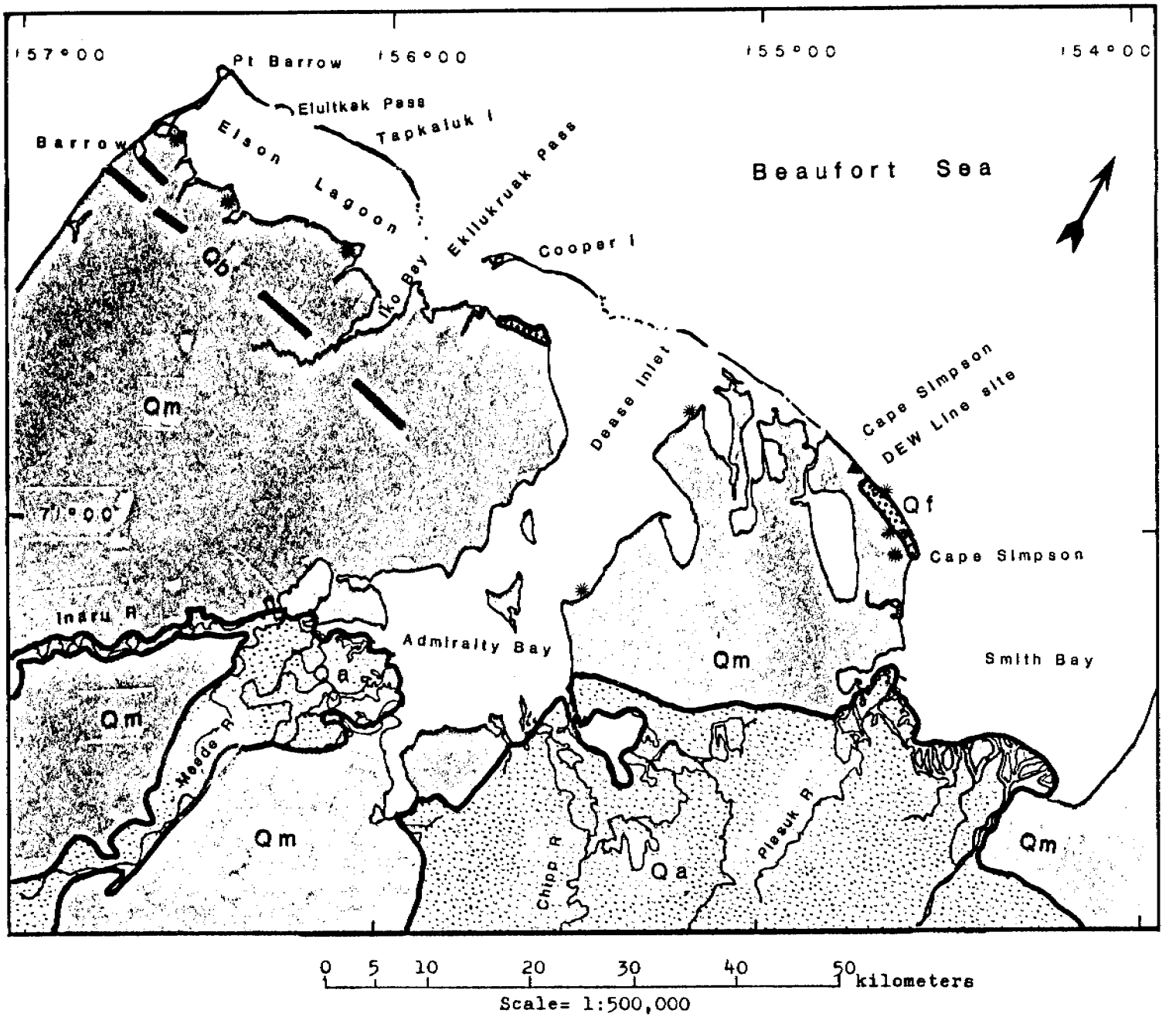
157°00
Pt Barrow
156°00
155°00
154°00
Elultkak Pass
Tapkaluk I
Barrow
Elson Lagoon
Beaufort Sea
Qb
Ikpikpuk R
Ekilukruak Pass
Cooper I
Qm
Dease Inlet
Cape Simpson
DEW Line site
71°00'
Qf
Cape Simpson
Inaru R
Admiralty Bay
Qm
Smith Bay
Qm
Meade R
Qm
Chipp R
Qa
Plasuk R
Qm
0 5 10 20 30 40 50 kilometers
Scale= 1:500,000

Figure-2b

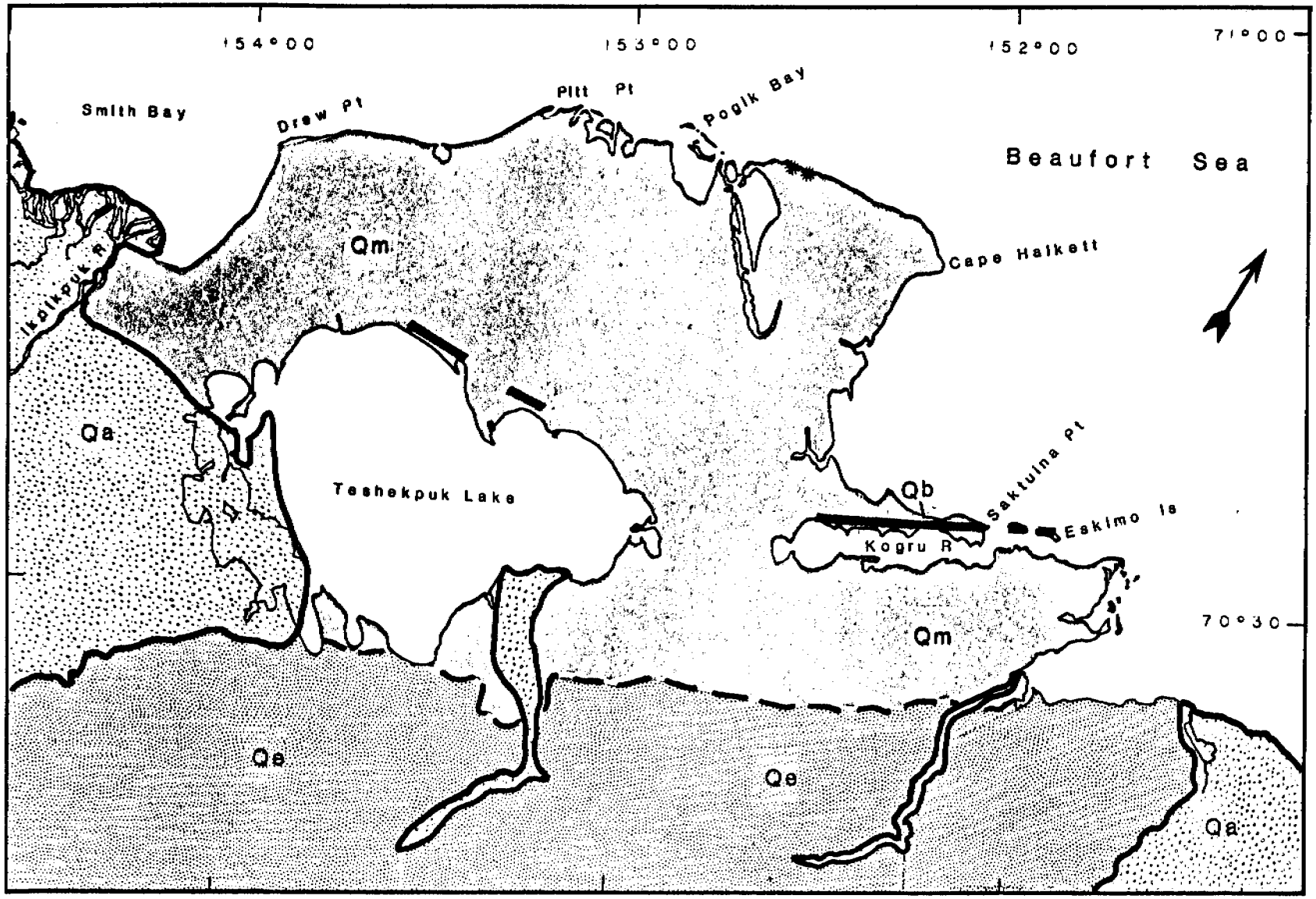
154°00
153°00
152°00
71°00
Smith Bay
Drew Pt
Pitt Pt
Pogik Bay
Beaufort Sea
Ikdlkpuk R
Qm
Cape Halkett
Qa
Teshekpuk Lake
Qb
Saktulina Pt
Eskimo Is
Kogru R
70°30
Qm
Qe
Qe
Qa
0 5 10 20 30 40 50 kilometers
Scale= 1:500,000

Figure-2c

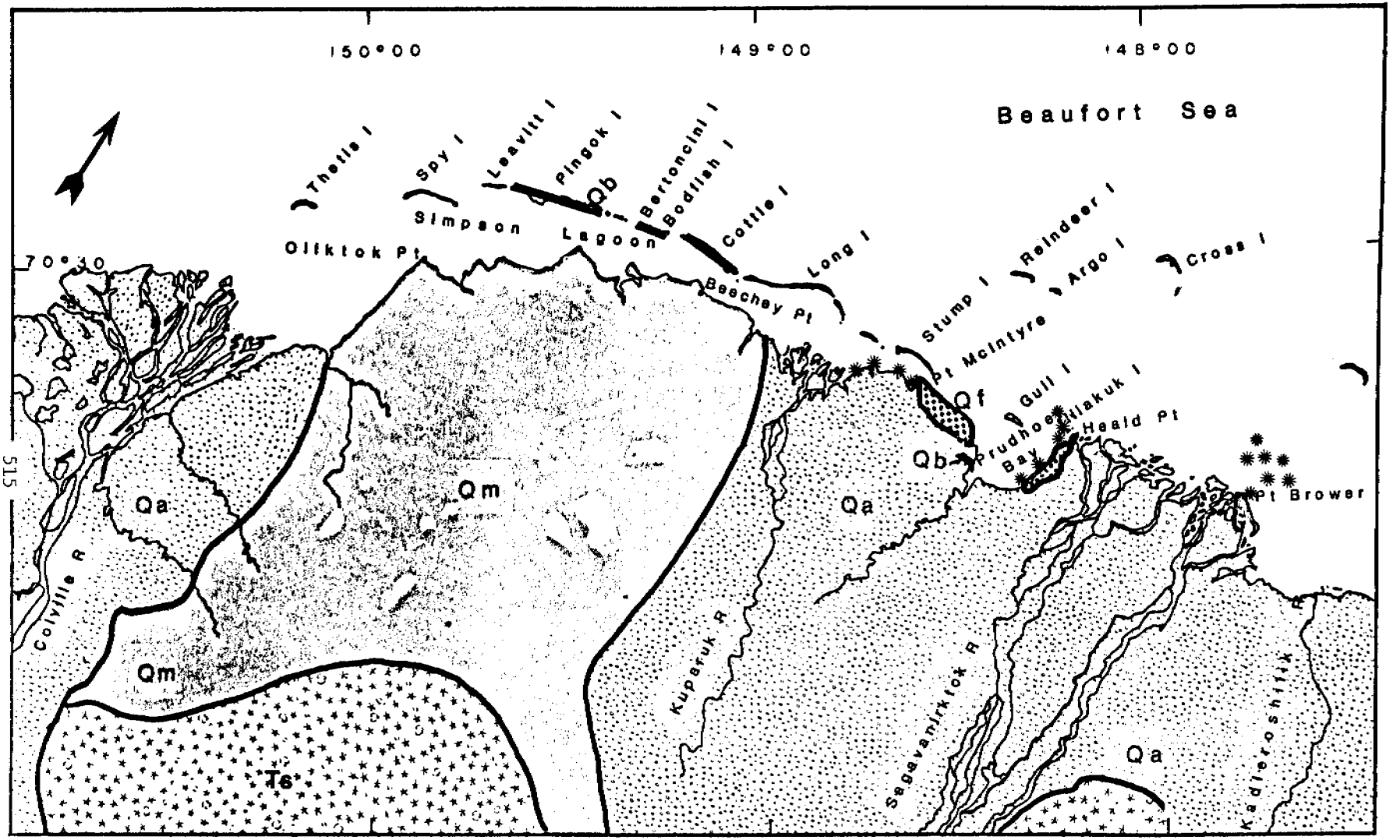

0 5 10 20 30 40 50 kilometers

Scale= 1:500,000

Figure-2d

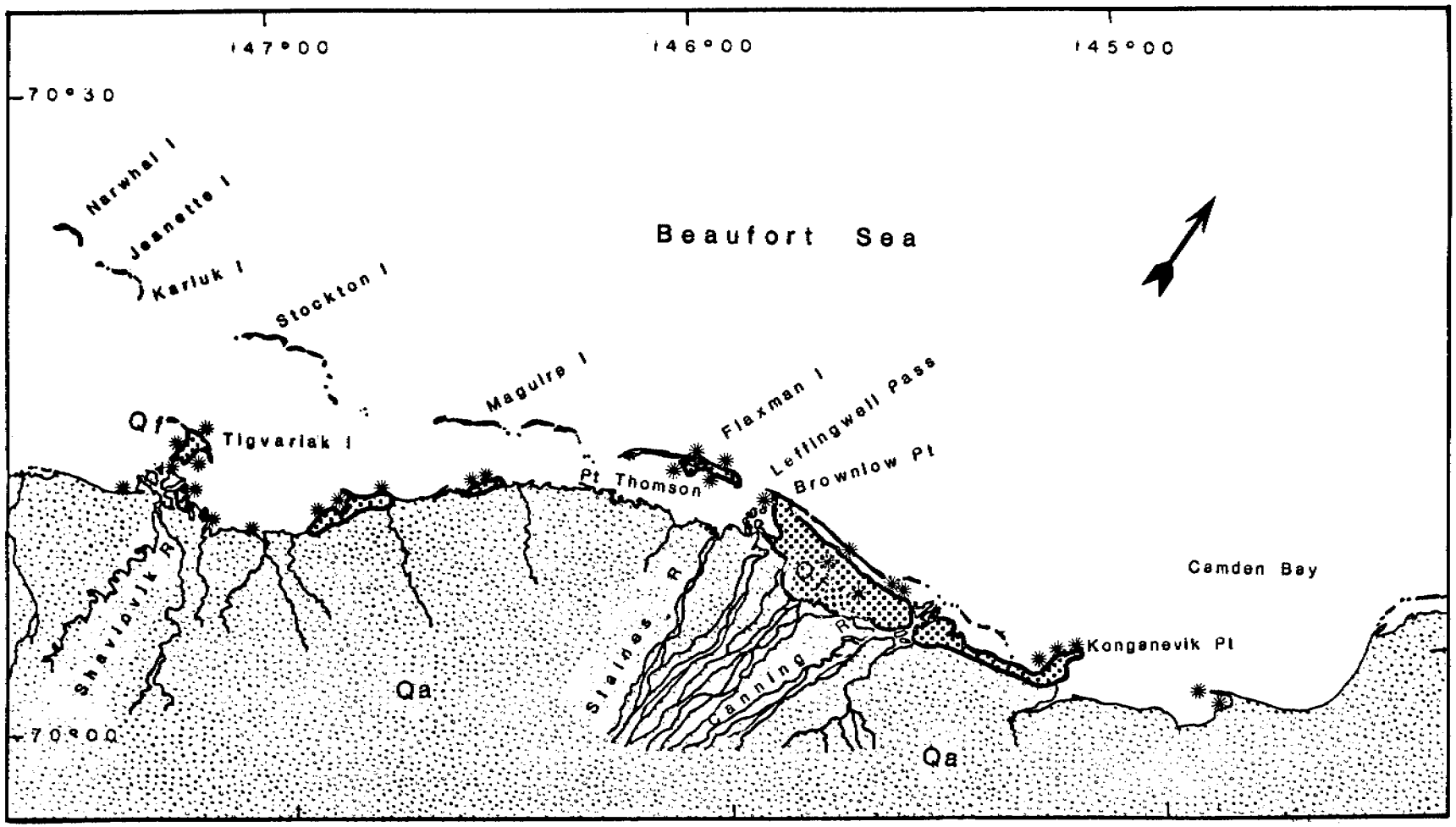
147°00
146°00
145°00
70°30
70°00
Narwhal I
Jeanette I
Karluk I
Stockton I
Maguire I
Flaxman I
Leffingwell Pass
Brownlow Pt
Pt Thomson
Tigvariak I
Qf
Beaufort Sea
Shaviovik R
Sagavanirktok R
Canning R
Qa
Qa
Camden Bay
Konganevik Pt
0 5 10 20 30 40 50 kilometers
Scale= 1:500,000

chert, graywacke, and grit, and includes notable quantities of vein quartz, while gravel derived from the Flaxman Formation consists largely of dolomite and also includes notable quantities of red quartz, red granite, pyroxenite, and diabase.

The Flaxman Formation underlies most of Tigvariak Island, Flaxman Island, and large mainland areas between and to the east of the distributaries of the Canning River, as well as smaller areas near Point McIntyre, Heald Point, and Point Brower and some still smaller coastal areas farther east (fig. 2). The Flaxman Formation also crops out extensively on the submerged continental shelf. Most of Pingok, Bertoncini, and Bodfish Islands and two small high-standing areas on Cottle Island are underlain by sandy pebble gravel interpreted here as representing remains of an ancient island chain formed during the last interglacial interval, about 120,000 years ago. This ancient beach gravel contains a mixture of Brooks Range and Flaxman pebbles.

The Arctic coastal plain west of Oliktok Point is divided into two belts separated by a line of low mounds and ridges generally less than 10 m in altitude. The inner Arctic coastal plain is a mosaic of areas underlain by Pleistocene marine pebbly sand of the Gubik Formation, of Pleistocene dune fields, and of Pleistocene and Holocene sandy alluvial plains and deltas (Williams and others, 1977; Carter and Robinson, in press). Gravel is found on the inner coastal plain only beneath the floodplain and terraces of the Colville River. The outer coastal plain and much of the sea floor to the north is underlain by compact stoney mud of the Flaxman Formation. The mounds and ridges that separate the inner from the outer coastal plain extend from Barrow southeastward along the

north side of Teshekpuk Lake through the peninsula north of Kogru River, to Saktuina Point and the Eskimo Islands (fig. 2A & B). This high ground is underlain by beach sand and fine gravel of the Gubik Formation, and contains a mixture of pebbles of Brooks Range and Flaxman origin, and represents, in our opinion, a westward continuation of the former Pleistocene island chain which forms the cores of modern Pingok, Bertoncini, Bodfish, and Cottle Islands.

Throughout the region, the Pleistocene marine, alluvial, and glaciofluvial sediments are mantled by 2 or 3 m of late Pleistocene and Holocene thaw-lake sediments consisting of peat and mud, commonly with a minor admixture of pebbles, cobbles, and boulders redeposited from the underlying Pleistocene sediments. Much of the Beaufort Sea coast is so low that the Pleistocene deposits lie below sea level, and only the mantle of Holocene peaty thaw-lake deposits can be seen in the coastal bluffs. Throughout the region, the Pleistocene and Holocene sediments are perennially frozen at depths greater than a few tens of centimeters, and the near-surface sediments contain variable but generally large quantities of ground ice.

Coastal geomorphology.--The mainland coast of the Beaufort Sea is crenulated and deeply embayed, especially in the segment west of the Canning River, the region to which our studies were confined. A series of en echelon island chains resembling barrier chains serve to provide a relatively straight outer coast in some regions, but other deeply embayed coastal segments, notably Harrison Bay and Smith Bay, lack protective island chains. Even where offshore islands are present, they may offer little shelter to the mainland coast, because they commonly

enclose lagoons so wide as to allow considerable wave fetch. Furthermore, the sheltered waters become freed of floating ice relatively early in the summer, and so the lagoon shores are exposed to wave action for longer periods.

Some details of the form of the Beaufort Sea coast are inherited from the coastal morphology created during the next previous high-sea-level episode, 120,000 years ago. Simpson Lagoon, Kogru River, Teshekpuk Lake, and perhaps Admiralty Bay all occupy the former positions of interglacial lagoons that lay behind the ridge of Gubik sand and gravel marking the position of an interglacial barrier chain. A few thousand years ago, the sites of these shallow water bodies were low-lying but dry; thermokarst collapse of ice-rich lagoonal sediments allowed the sea to invade.

Beaches and longshore transport.--The mainland shores are characterized by narrow, lowlying beaches backed by coastal bluffs generally less than 10 m and commonly only 2 or 3 m high. The beaches are rarely wider than 20 m and commonly are only a few tens of centimeters thick. Gravel predominates in beaches between the Canning River and Point McIntyre and sand in beaches farther east. Gravel sources are scarce, and in many places the mainland beaches are obviously starved. It is not uncommon to see beaches which consist of low ridges of sand and gravel perched on a seaside bluff 1.0 to 1.5 m high carved in peat and mud (fig. 3).

Most, if not all, of the coarse sediment comprising the beaches is derived from erosion of coastal bluffs. Rivers deliver no coarse material to the mainland or island beaches; they drop their load of

Figure-3 Showing beach deposition atop bluff.

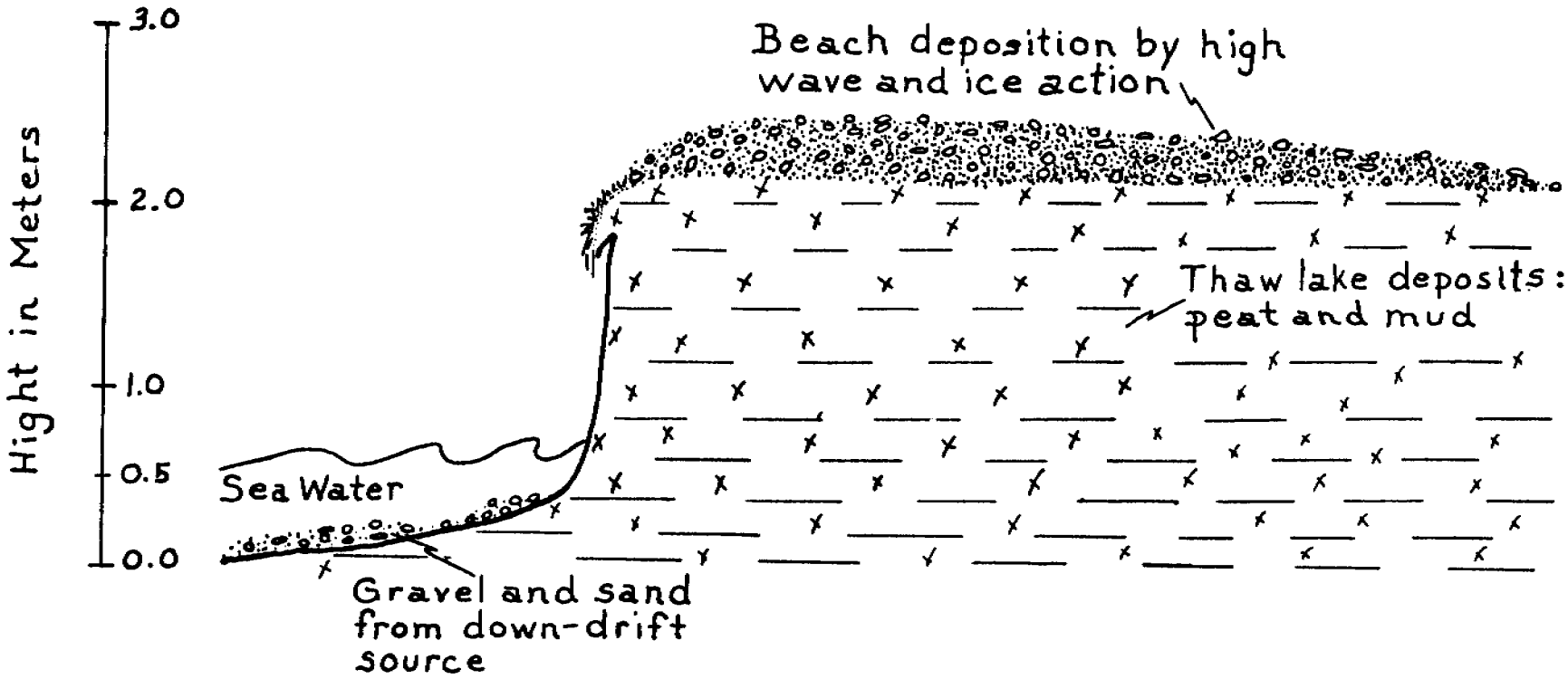

sand and gravel a few kilometers inland and only easily resuspended fine sand, silt, and clay reaches the lagoons and estuaries (Arnborg and others, 1966; Barnes and Reimnitz, 1974).

However, sand and gravel reaches the beach in small quantities from coastal bluffs carved in alluvial and glacial-outwash fans away from the immediate vicinities of the river mouths. Larger quantities of sand and gravel are delivered to beaches in areas where coastal bluffs are carved in the Flaxman Formation or into the pebbly sand of the hillocks and ridges marking the sites of the Pleistocene island chain. Nevertheless, large segments of the Beaufort Sea coast, especially in the stretch extending from northwestern Harrison Bay to Barrow village, are backed by coastal bluffs in which grave-sized particles are lacking, and sand-sized particles are scarce.

A minor amount of sand and gravel is provided to some beaches by ice push. Ice-plowed gravel ridges on Cross and Narwhal Island and along the lowlying coast near Cape Simpson DEWLine station, among other places, contain cobbles and boulders coarser than any that can be found onshore nearby, indicating that grounded ice is plowing gravel to the beach from a submerged nearshore source.

The direction of littoral sediment drift is generally westward, but wave refraction induces many local reversals along the crenulate mainland coast and also on the more arcuate offshore islands. The mainland coast is thus divided into many small littoral transport cells, mostly shorter than 10 km. Some of the island chains form slightly longer west-drifting transport cells, but others, as we shall show later, seem to consist of isolated slugs of gravel migrating southwestward without interchange with other islands or with the mainland coast.

Because wave energy is low and the open season short, total amounts of sediment transport along the beaches are small. The rate of longshore drift of sediment has not been estimated for points on the mainland coast, but Wiseman and others (1973) estimate longshore transport on the outer coast of Pingok Island at 10,000 m^3 during the summer and autumn of 1972. The observed rate of lengthening of western Pingok and Leavitt Islands between 1955 and 1972 (Wiseman and others, 1973) suggests that this rate has been sustained over a long period. A lower rate of mass transport is indicated for the Maguire Islands; however, the observed rate of island migration, there (Wiseman and others, 1973), indicates mass transport of slightly more than 5,000 m^3/yr. Mass transport is probably lower along most parts of the mainland coast.

Thermokarst collapse, thermal erosion, and coastal retreat.--Despite the short open season and the prevalence of a low wave-energy regime, the coast of the Beaufort Sea is retreating at a spectacular pace. Rates of coastal erosion observed there are, for example, an order of magnitude faster than those reported for the Chukchi Sea coast (MacCarthy, 1953; Hopkins, 1977). The rapid retreat of the Beaufort Sea coast is governed by the involvement of the distinctively Arctic processes of thermokarst collapse and thermal erosion[1/] acting

---

1/ Thermokarst collapse is defined here as collapse or loss of volume due to melting out of ground ice in excess of normal porosity of the sediment. Thermal erosion is defined here as lateral erosion resulting from melting out of ground and interstitial ice accompanied by lateral current-transport of resulting fine materials.

upon bluffs composed of perennially frozen and predominantly fine-grained sediment.

The arctic coastal plain and those Beaufort Sea islands that are composed of ice-rich Pleistocene sediments are affected by thermokarst collapse. Localized thawing in onshore areas results in subsidence due to the melting-out of excess ground ice, and the resulting subsidence basins become occupied by rapidly growing thaw lakes. On the higher or steeper parts of the arctic coastal plain, there is enough relief so that thaw lakes tend to break through and drain to lower ground before reaching diameters larger than 1 or 2 km. Near the coast, however, lakes can coalesce into shallow water bodies of scalloped outline, tens of kilometers across; Teshekpuk Lake is the largest example. Abrupt changes in the outline of the coast can result when the retreating shoreline breaks through into such a lake. Prudhoe Bay seems to have originated in this manner (Hopkins and others, 1977).

The sea coast and, to a lesser extent, lake shores, are also affected by thermal erosion. Thermal erosion is most rapid and effective along coastal segments where the bluffs are composed of ice-rich, frozen mud, silt, or fine sand containing few or no stones. Thawing and erosion of bluffs composed of pebbly sand or sandy gravel releases enough coarse sediment to thicken the beach and minimize undercutting. The fibrous, interlacing structure of arctic peat and turf makes these materials also somewhat resistant to wave attack; thick peat accumulations thus tend to persist as minor promontories on actively retreating coasts, and surficial turf drapes like a robe over the face of an actively retreating bluff cut in fine sediment.

Most of the bluff erosion takes place during late summer and autumn. Drifting snow accumulates in the lee of the shore bluffs during winter, and the resulting snow drifts tend to persist well into July. Where snow is lacking, mudflows and slumps regrade the coastal bluffs and partly cover the narrow beaches. During late summer and autumn, when the weather is dominated by the passage of cyclonic low-pressure systems, sea level rises above the tops of the low beaches. The remaining snow and much of the slumped material is quickly removed, and waves begin to attack the exposed bluffs. Even when the sea is nearly calm, the cold salt water thaws the frozen mud, releasing small particles to be carried away by longshore currents. Such bluffs can be quickly undercut to depths as great as 6 or 8 meters. When frost cracks extending along the axes of ice wedges are intersected, blocks as large as houses collapse onto the submerged beach. Destruction of the collapsed blocks by continued lapping of the waves may require several years (Leffingwell, 1919; Lewellen, 1977).

Rates of coastal retreat (Table I) differ in different sites, depending not only upon differences in the composition of the coastal bluffs, but also upon exposure and upon morphology of the adjoining sea bottom. The highest rates of coastal retreat are recorded on promontories and points, probably because these areas are affected by rapid coastal erosion from opposing directions. Nevertheless, many bays and estuaries have persistently cuspate outlines, evidently indicating that thermal erosion and thermokarst collapse tend to cause parallel retreat of the shoreline, regardless of coastal orientation. As Lewellen (1977) observes, promontories and points tend to persist in the same general

Table I

Section of Coastline	Composition of Bluffs	Average Yearly Rate of Retreat (M)	Source of Information
Point Barrow to Iko Bay	Quaternary marine silts and fine sand, overlain by thaw lake deposits (Williams and Carter, 1977).	2.1 3.3 2.2 2.5	MacCarthy, 1953 Hume & Schalk, 1972 Lewellen, 1977 Hartz, in press
Iko Bay to Admiralty Bay		3.1 3.0	Lewellen, 1977 Hartz, in press
Admiralty Bay to Cape Simpson		30.0 (Cape Simpson only) 4.6 4.3	Leffingwell, 1919 Lewellen, 1977 Hartz, in press
Cape Simpson to Pitt Point		30.0 (Drew Pt. only) 12.0 11.4	Leffingwell, 1919 Lewellen, 1977 Hartz, in press
Pitt Point to Cape Halkett		12.0 11.4	Lewellen, 1977 Hartz, in press
Cape Halkett to Kogru River		3.2	Hartz, in press
Kogru River to Oliktok Point	Quaternary marine silts and fine sands + Quaternary eolian sands + Quaternary alluvium, overlain by thaw lake deposits.	2.0	Hartz, unpub. data
Oliktok Point to Beechey Point		1.4 1.6	Dygas and others, 1972 Lewellen, 1977
	Quaternary marine silts and fine sands. Overlain by thaw lake deposits.		
Beechey Point to Point McIntyre	Quaternary marine silts and fine sands + Quaternary Flaxman Formation + Quaternary alluvium. Overlain by thaw lake deposits.	1.0 1.0	Barnes and Reimnitz, 1977 Lewellen, 1977
Point McIntyre to Heald Point	Quaternary alluvium and Quaternary Flaxman Formation. Overlain by thaw lake deposits.	2.0 1.7	Barnes & Reimnitz, 1977 Lewellen, 1977
Heald Point to Tigvariak Island		< 3.0	Hartz, unpub. data
Tigvariak Island to Point Thomson		2.0	Hartz, unpub. data

Table I (cont.)

Section of Coastline	Composition of Bluffs	Average Yearly Rate of Retreat (M)	Source of Information
Point Thomson to Brownlow Point	Quaternary alluvium and Quaternary Flaxman Formation. Overlain by thaw lake deposits.	9.0 (Brownlow Pt. only) 6.8 (2 data points) 3.5	Leffingwell, 1919 Lewellen, 1977 Hartz, unpub. data
Flaxman Island	Quaternary Flaxman Formation. Overlain by thaw lake deposits.	9.2 3.5	Leffingwell, 1919 Lewellen, 1970
Brownlow Point to Camden Bay	Quaternary alluvium and Quaternary Flaxman Formation. Overlain by thaw lake deposits.	1.6	Lewellen, 1977
Camden Bay to Demarcation Point		1.5	Lewellen, 1977
Demarcation Point to Mackenzie Bay	Quaternary alluvium silts, sands, and gravels.	$\pm$2.5	MacKay, 1963

areas, and the morphology of the coast tends to remain similar over periods of many decades, in spite of the observed rapid rates of erosion and apparent preferentially high rates of erosion on promontories.

Shorelines adjoined by narrow lagoons tend to retreat more slowly than do open coasts. However, as we have noted, many lagoons and embayments are so wide that the island chains afford little protection to the mainland coast. Furthermore, rates of retreat observed on the lagoon sides of some of the high-standing islands are as rapid as the retreat rates on the seaward coasts. It may be important that the protected waters of lagoons and bays warm up and become free of ice much earlier than waters adjoining the outer coast.

Coastal bluffs that are adjoined by water shallow enough to be exposed during the early summer low-water periods retreat much less rapidly than do coastal segments adjoined by deeper water. For this reason, high-standing remnants of Pleistocene sediments tend to be preserved in promontories adjoining the mouths of large rivers, being protected, there, by pro-delta shoals. Conspicuous examples are Heald Point and Point Brower on either side of the mouth of the Sagavanirktok River. Tigvariak Island seems to persist because pro-delta shoals of the Shaviovik River refract waves and reduce wave energy in the surrounding waters.

Rates of coastal retreat also vary dramatically from one year to another, depending upon the time of breakup of sea ice, variations in size of open-water areas, and timing and intensity of late summer and autumn storms.

Coastal retreat is so rapid as to pose a serious hazard in many areas to man-made structures near the coast. Rates of coastal retreat have consequently been measured in many places and on many occasions (Leffingwell, 1919; MacCarthy, 1953; MacKay, 1963; Hume and Schalk, 1967; Lewellen, 1970; Dygas and others, 1972; Hume and others, 1972; Wiseman and others, 1973; Lewis and Forbes, 1975; Barnes and others, 1977; Hartz, in press; Reimnitz and others, 1977; P. J. Cannon, unpub. rept. to OCSEAP, 1978).

Coastal retreat proceeds at the relatively modest average rate of about one meter per year along the Canadian Beaufort Sea coast between the MacKenzie River delta and Demarcation Point (Leffingwell, 1919; MacKay, 1963; Lewis and Forbes, 1975). Coastal retreat along the mainland coast between Demarcation Point and the Colville River averages about 1.6 m/yr, although local short-term rates may be much higher; at Oliktok Point, for example, shoreline retreat of 11 m was observed within a single two-week period (Dygas and others, 1972). Rates of shoreline retreat on the Pleistocene remnants of Pingok Island are also on the order of 1.5 m/yr, with lagoon shores reported to be retreating more rapidly than the seaward coast which is well protected by a wide sand beach (P. J. Cannon, unpub. rept. to OCSEAP, 1978).

The high-standing areas of Flaxman Island are disappearing much more rapidly. Lewellen (1977) reports that the seaward coast retreated about 3.5 m/yr between 1949 and 1968 and that the lagoon shore retreated almost as rapidly. Erosion evidently progressed at similar rates between 1911 and 1949 and possibly at a much greater rate between the visit by the Franklin Expedition in 1826 and Leffingwell's observations in 1911 (Leffingwell, 1919; Lewellen, 1977).

Average rates of coastal retreat are highest from Harrison Bay eastward to Barrow. Lewellen's (1977) 68 data points indicate an average retreat rate 4.7 m for this segment of the coast, and Leffingwell reported short-term erosion rates as great as 30 m/yr at Drew Point and Cape Simpson.

Areas of progradation are almost entirely restricted to the immediate vicinity of the mouths of the larger rivers. The Canning, Shaviovik, Sagavanirktok, Kuparuk, Colville, Ikpikpuk, Topagoruk, and Meade Rivers all have prograding deltas at their mouths, and actively prograding deltas are probably present at the mouths of the larger streams east of the Canning River, as well.

Offshore islands.--Several OCSEAP studies focused upon the description and origin of the Beaufort Sea islands west of the Canning River and upon the shoreline processes affecting them. The islands are obviously prime candidates for siting petroleum exploration and production facilities, or, alternately, prime candidates for gravel quarrying. On the other hand, they profoundly affect water circulation and sediment movement on the inner shelf, anchor sea ice and widen the zone of shorefast ice, offer shelter to large shorebird populations during the late summer molt, and, in a few exceptional areas, provide important nesting habitat. Thus, it has become important to obtain a clearer idea of their origin, sources of sediment, and probable future.

Low-lying islands off the mouths of major rivers are simply emergent depositional shoals of fine river sand representing the outer fringes of the deltas. Gull Island, at the mouth of Prudhoe Bay, may also be an emergent shoal of fine sand transported by currents a few kilometers westward from the mouth of the Sagavanirktok River.

Other islands are obviously erosional remnants that have been isolated from the mainland by thermokarst collapse and rapid thermal erosion. These islands lie near the mainland, generally stand 4 m or more above sea level, are more or less equidimensional, and have cuspate outlines. Tigvariak Island, composed mostly of Flaxman Formation, is a good example. The cuspate outlines of the Eskimo Islands shows that they, too, are erosional remnants--in this case, of Pleistocene beach sand and pebbly sand. Another erosional remnant, probably of late Pleistocene non-marine sediments lies at the mouth of Pogik Bay. The Niakuk Islands off Heald Point are low-lying lag deposits of Flaxman boulders on the site of former islets of Flaxman Formation (Leffingwell, 1919; Erk Reimnitz and P. W. Barnes, oral commun., 1977).

More conspicuous are three chains of curvilinear islands resembling barrier chains (fig. 2). The eastern chain extends from Brownlow Point through Flaxman Island to Reindeer Island; the central chain from Pt. McIntyre through Stump Island to Thetis Island; and the western chain from Cape Simpson DEWLine Station through the Plover Islands to Point Barrow. All three chains diverge northwestward from the mainland coast. The eastern and central chains are open westward so that both Reindeer and Thetis Islands lie about 14 km offshore. The Plover Island chain is closed on the west by Point Barrow spit which extends the Chukchi Sea coast 7 1/2 km northeastward from the mainland at the Naval Arctic Research Lab.

The islands are mostly recent constructional accumulations of sand and gravel, but Flaxman Island and several islands in the central part of the central chain (Cottle, Bodfish, Bertoncini, and Pingok) have cores of Pleistocene sediments. These erosional remnants stand 3 to 10 m

above sea level and support a continuous cover of non-halophytic tundra vegetation. All are disappearing rapidly by wave erosion and thermokarst collapse.

The constructional parts of the islands may be as long as 9 km and are nowhere higher than 3 m. They generally range from 90 to 110 m in width but may be as wide as 460 m in the rare areas of accretionary beach ridges and spits. The island chains consist of broadly arcuate or bow-shaped groups of islands separated from one another by major passes. The passes differ greatly in width and depth; most are several kilometers wide but only 2.5 or 3 m deep; a few are only a few hundred meters wide, and these may be 10 m or more in depth. The passes are sites of strong currents and major water exchange. Leffingwell Pass has deepened steadily and dramatically during the past 150 years (Leffingwell, 1919; Lewellen, 1977), and in 1976 had reached a depth of 10.5 m (Reimnitz and Toimil, 1977). Other passes may be undergoing similar dynamic changes.

The bow or arcuate shape of the island groups is caused by deflections as much as 2 or 3 km landward at eastern and western ends. Within the groups, individual islands are sinuous and are separated by ephemeral passes generally only a few hundred meters wide and only one to two meters deep. Migration of islands, filling of old passes, and development of new ones (Wiseman and others, 1973) results in such rapid changes in morphology that maps and air photos 20 years old are almost useless for locating oneself during an overflight.

Typical profiles across the islands show a central depression that may contain a small pond adjoined by a high berm about 20 m wide and 1 or

2 m high on the ocean side and by a low berm 10 or 15 m wide and less than 1.5 m high on the lagoon side (fig. 4). A more complex morphology may be seen at the western termini of island groups; there, successions of storms have commonly built recurved accretionary spits consisting of small areas of ridge and swale topography. Exceptional storms occasionally extend the western terminus of an island group southwestward past previously formed recurved spits, and the old spits then persist as claw-like spurs on the lagoon sides of the islands. These bypassed spits are the most persistent and commonly the highest parts of the constructional islands. Some spurlike protuberances mapped by Leffingwell in 1912 could still be recognized in 1977, although they had been truncated, and their relative positions had changed because of the continuing westward migration of more active parts of the islands.

The constructional islands are extensively inundated, every few years, during autumn storm surges. The most extreme storm events, such as the storm surge of 1970, can inundate the islands almost completely (Erk Reimnitz, oral commun., 1977).

Ice-push affects different islands to different degrees. Most affected are Cross and Narwhal Islands in the eastern chain. These islands lie far offshore, near the shear zone between shorefast ice and the Arctic ice pack. Narwhal and Cross Islands feature belts of ice-push ridges as much as 2.5 m high extending as much as 300 m inland from the ocean beach. Three separate generations of ice-push ridges could be recognized during our visit to the island in 1977. Well preserved ridges at least a year old could be distinguished by the presence

Figure-4 Barrier island profiles

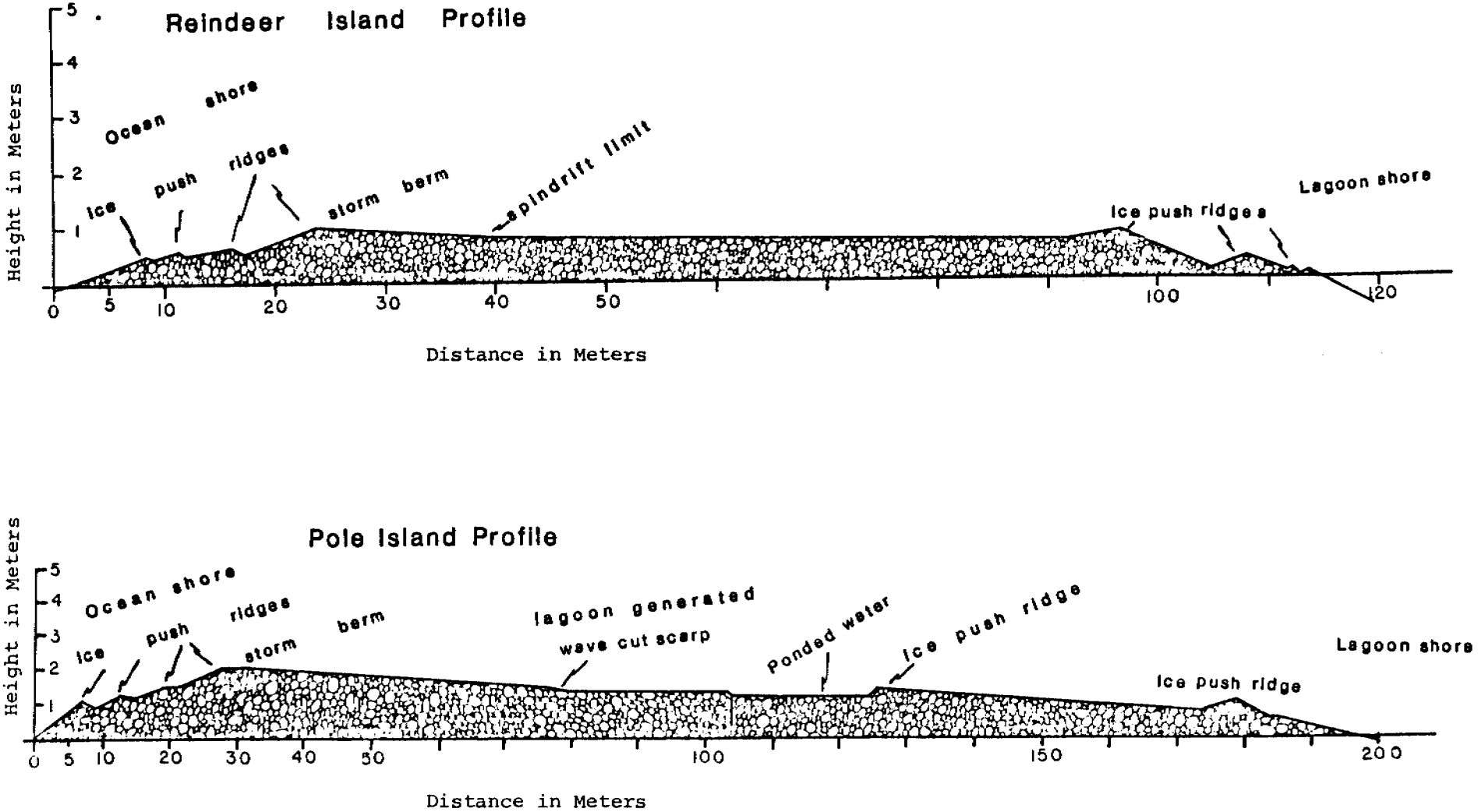

of vehicle tracks left by researchers camped on the island during the winter of 1976-77.

The constructional islands are migrating westward and landward at a rapid pace. Migration rates westward ranging from 19 to 30 m/yr and landward ranging from 3 to 7 m/yr have been established for various islands in the eastern and central chains (Lewellen, 1970; Wiseman and others, 1973). The more arcuate and isolated islands, such as Narwhal, Cross, Spy, and Thetis Islands appear to be migrating southwestward en masse at rates of 4 to 7 m/yr (Reimnitz and others, 1977). Stump Island is exceptional in that, between 1950 and 1976, it seems to have moved due south and directly landward at a rate of 4 m/yr without any lateral migration (Barnes and others, 1977). The pace of landward or southwestward migration is such that most parts of the contructional islands require only 30 or 40 years to cross a given point on the sea floor

The constructional islands are mostly devoid of vegetation of any kind, reflecting their short history, but a sparse cover of halophytic plants is present in those few constructional areas that are older than 30 or 40 years. Because vegetation is generally lacking, the constructional portions of the islands typically lack dunes. However, dunes are extensive on the rear of beaches and adjoining tundra of Pingok, Bertoncini, and Bodfish Islands. Small dunes are also present in an area of sparse halophytic vegetation at the west end of Cooper Island, and they probably can be found in the sparsely vegetated areas that are present on a few of the other constructional islands.

Firmly ice-bonded permafrost is present beneath the older, sparsely vegetated recurved spits and spurs (Rogers and Morack, 1977). These areas can be recognized by the presence of frost cracks extending across ancient wave-

constructed ridges and swale. Most areas in the constructional parts of the islands, however, lack firmly bonded permafrost (Rogers and Morack, 1977), although interstitial ice was found in the sediment in a borehole on Reindeer Island; the interstices in the sediment beneath the younger parts of the islands must be filled with a two-phase mixture of brine and ice. Evidently 40 or 50 years are required for freezing to progress to a point where brine is either excluded or frozen and the sediment becomes bonded firmly enough to crack when subjected to the extremely cold winter temperatures.

Pebble lithology differs from one island group to another, reflecting differences in the sources of material making up the islands (fig. 5). The sand and gravel in all island groups within the eastern chain is entirely derived from the Flaxman Formation. In this island chain, however, coarse gravel with large cobbles is found on Flaxman Island and also on westernmost Jeanette, Narwhal, and Cross Islands, while the islands between Flaxman and Jeanette Islands and also Reindeer and Argo Islands at the western end of the chain are composed of much finer material. It is notable that the core of Flaxman Island consists of Flaxman Formation and that Flaxman Formation also crops out on the sea floor from Cross through Narwhal and Jeanette to Karluk Island (Rodeick, 1975; Reimnitz and Toimil, 1977).

Gravel in the central island chain consists mostly of Brooks Range pebble types with a 10 to 25% admixture of Flaxman lithologies. The Pleistocene beach gravel that forms the cores of several islands in the central part of the chain is a similar mixture. There is little

difference in coarseness of gravel from one island group to another, but the coarsest gravel on strongly arcuate Spy and Thetis Islands is found at the northern, leading edges of these islands.

Gravel lithology in the western chain differs from one island group to another, as a consequence of a series of step-wise changes at Ekilikruak and Eluitkak Passes (fig. 5). East of Ekilikruak Pass, Flaxman lithologies comprise more than 90% of the gravel; between Ekilikruak and Elnitkak Passes, the gravel contains a 30% admixture of Brooks Range lithologies; and west of Elnitkak Pass, Brooks Range lithologies makeup more than 60% of the gravel.

It is clear that the major passes within the Beaufort Sea island chains are barriers to sediment transport and serve to isolate the different island groups from one another. Reimnitz and others (1977) concluded, for example, that "various types of evidence indicate that Cross Island is not receiving gravel from an outside source". The arc- or bow-shape of the island groups and their frequent terminations in compound recurved spits confirms that the passes are sediment sinks, not sediment transmission belts. Confirmation comes from the observation by Reimnitz and Toimil (1977) that the deepest part of Leffingwell Channel is floored with compact, current-scoured mud, not sand and gravel, and that Flaxman boulders litter the bottom of the pass east of Karluk Island. Further confirmation comes from our observation that relative proportions of Brooks Range and Flaxman pebble types change in stepwise fashion across two passes in the western island chain. Some of these observations come from passes that seem to be nowhere deeper than 2.5 m, indicating that sediment cannot bypass a trough deeper than 2.5 m in this low-energy sea.

Several lines of evidence demonstrate that the island chains are not unified sediment-transport system, but rather that many of the island groups have or once had their own sediment sources. The presence of gravel on Jeanette, Narwhal, and Cross Islands much coarser than the gravel comprising islands that lie eastward and updrift establishes beyond doubt that a source of sediment lies or once lay somewhere seaward on the continental shelf. The eastern islands within the Plover chain are or once were fed from the bluffs east of Cape Simpson DEWLine Station, while the peninsula leading from Eluitkak Pass to Point Barrow may be fed by sediment moving northward up the Chukchi Sea coast and eastward around Point Barrow, but the islands between Eluikrak and Eluitkak Pass differ enough to indicate that they originated from a sediment source that has now disappeared. Leavitt Island, in the central part of the central chain, is obviously fed by the erosion of Pingok Island and other Pleistocene remnants that lie eastward and updrift, but Long, Egg, and Stump Islands lie still further updrift and must have originated from a different source. Thetis and Spy Islands, like Cross Island, seem to "represent the dying phase of the barrier island system off northern Alaska" (Reimnitz and others, 1977) and to be drifting southwestward from sources that have long-since disappeared.

The island passes themselves seem to be of diverse origin. Our (D. M. Hopkins and R. W. Hartz) study of Flaxman Island establishes that the Leffingwell Channel is the site of a former distributary of the Canning River which was drowned by rising sea level at some time within the last few thousand years. Other passes have probably originated

in similar manner. Still others may originally have simply been low areas between Pleistocene hillocks. Some of the deep passes, however, may have originated much more recently as breaches formed in a low-lying barrier bar during a storm surge which were subsequently deepened by tidal scour to the point where sand and gravel could no longer bypass them.

We conclude that the constructional area of Flaxman Island is fed by coastal drift of sediment eroded from the Pleistocene remnants that form the island core. The Maguire Islands and possibly the Stockton Islands may originally have been westward continuations of this barrier chain which became isolated as a result of storm-breaching and tidal deepening of intervening channels; if this speculation is correct, then Flaxman Island would have once been a much larger and more adequate source of sediment.

Karluk, Jeanette, and Narwhal Islands are evidently lag deposits resulting from the erosion and eventual destruction of hillocks of Flaxman Formation that are now preserved only as outcrops of Pleistocene sediment on the sea floor. Ice-push may continue to add new coarse material to the seaward beaches of these islands. Cross Island originated from another hillock of Flaxman Formation, as did Reindeer and Argo Islands, but Reindeer and Argo Islands have now migrated a kilometer or more landward from the site of the former hillock of Flaxman Formation.

The central chain of islands originated by erosion of a row of hillocks representing a Pleistocene island chain. Erosion has completely destroyed the original hillocks that were the source of the

eastern islands and western islands in the chain. The source hillocks for Spy and Thetis Island disappeared many centuries ago and these two islands have subsequently moved several kilometers seaward from their initial positions.

Long term comparisons seem to indicate that the islands are migrating with little loss of area and mass. Wave overwash during storm surges helps to move sand and gravel from the nearshore zone onto the body of the island, and ice-push rakes the lagging coarser particles from deep water and returns them to the island surface. However, the islands will eventually disappear. The Dinkum Sands seem to be an example of a member of the chain that eventually lost mass and became completely submerged.

Because the islands in the Beaufort Sea island chains are mostly lag deposits derived from sand and gravel sources that have now disappeared, they must be regarded as irreplaceable. If they were removed, they would not be replaced by natural processes, and the local oceanographic and biological regime would be irreversibly perturbed.

References cited

Arnborg, L., Walker, H. J., and Peippo, J., 1966, Suspended load in the Colville River, Alaska, 1962: Geog. Annaler, v. 49, ser. A, p. 131-144.

Barnes, P. W., and Reimnitz, E., 1974, Sedimentary processes on Arctic shelves off the northern coast of Alaska, in Reed, J. C., and Sater, J. E., eds., The coast and shelf of the Beaufort Sea: Arctic Inst. North America, p. 439-476.

Barnes, P. W., Reimnitz, E., Smith, G., and Melchior, J., 1977, Bathymetric and shoreline changes, northwestern Prudhoe Bay, Alaska: U.S. Geol. Survey open-file rept. 77-161, 10 p.

Carter, L. D., and Robinson, S. W., in press, Aeolian sand and interbedded organic horizons at Kaoluk Creek; regional implications: U.S. Geol. Survey open-file rept.

Dygas, J. A., Tucker, R., and Burrell, D. C., 1972, Geologic report of the heavy minerals, sediment transport, and shoreline changes of the barrier islands and coast between Oliktok Point and Beechey Point, in Kinney, P. J., and others, eds., Baseline data study of the Alaskan Arctic aquatic environment: Univ. Alaska Inst. Marine Sci. Rept. R-72-3, p. 62-121.

Hartz, R. W., in press, Erosional hazards along the Arctic coast of the National Petroleum Reserve-Alaska: U.S. Geol. Survey open-file rept., 7 p.

Hopkins, D. M., 1977, Coastal processes and coastal erosional hazards to the Cape Krusenstern archaeological site: U.S. Geol. Survey open-file rept. 77-32, 15 p.

Hopkins, D. M., and others, 1977, Offshore permafrost studies, Beaufort Sea: U.S. Natl. Oceanog. and Atmospheric Adm., Environmental Assessment of Alaskan Continental Shelf, Principal Investigator's Repts. for Year Ending March 1977, v. 16, p. 396-518.

Hume, J. D., and Schalk, M., 1967, Shoreline processes near Barrow, Alaska; a comparison of the normal and the catastrophic: Arctic, v. 20, p. 86-103.

Hume, J. D., Schalk, M., and Hume, P. W., 1972, Short-term climate changes and coastal erosion, Barrow, Alaska: Arctic, v. 25, p. 272-278.

Leffingwell, E. DeK., 1919, The Canning River region, northern Alaska: U.S. Geol. Survey Prof. Paper 109, 251 p.

Lewellen, R. I., 1970, Permafrost erosion along the Beaufort Sea coast: Pub. by the author (P.O. Box 2435, Littleton, CO 80161), 25 p.

_____1977, A study of Beaufort Sea coastal erosion, northern Alaska: U.S. Natl. Oceanic and Atmospheric Adm., Environmental Assessment of the Alaskan Continental Shelf, Ann. Repts., Principal Investigators for the year ending March 1977, v. 15, p. 491-527.

Lewis, C. P., and Forbes, D. L., 1975, Coastal sedimentary processes and sediments, southern Canadian Beaufort Sea: Beaufort Sea Proj. Tech. Rept. no. 24, Victoria, B.C., 68 p.

MacCarthy, G. R., 1953, Recent changes in the shoreline near Point Barrow, Alaska: Arctic, v. 6, p. 44-51.

MacKay, J. R., 1963, Notes on the shoreline recession along the coast of the Yukon Territory: Arctic, v. 16, p. 195-197.

Reimnitz, E., Barnes, P. W., and Melchior, J., 1977, Changes in barrier island morphology--1949 to 1979, Cross Island, Beaufort Sea, Alaska: U.S. Geol. Survey open-file rept. 77-477, p. F1-F14.

Reimnitz, E., and Toimil, L. J., 1977, Diving notes from three Beaufort Sea sites, in Barnes, P. W., and others, eds., Marine environmental problems in the ice-covered Beaufort Sea shelf and coastal regime: Natl. Oceanog. and Atmospheric Adm., Environmental Assessment of Alaskan Continental Shelf, Principal Investigator's Repts. for year ending March 1977, v. 17, p. J1-J7.

Rodeick, C. A., 1975, The origin, distribution, and depositional history of gravel deposits on the Beaufort Sea continental shelf, Alaska: San Jose State Univ., M.S. thesis, 76 p.

Rogers, J., and Morack, J., 1977, Beaufort Sea coast permafrost studies: U.S. Natl. Oceanic and Atmospheric Adm., Environmental Assessment of the Alaskan Continental Shelf, Ann. Repts., Principal Investigators for the year ending March 1977, v. 17, p. 467-510.

U.S. Department of Commerce, 1978, Tide tables, 1978; high and low water predictions; west coast of North America and South America, including Hawaii: Dept. Commerce, 222 p.

Williams, J. R., Yeend, W. E., Carter, L. D., and Hamilton, T. D., 1977, Preliminary surficial deposits map of National Petroleum Reserve Alaska: U.S. Geol. Survey open-file rept. 77-868, scale 1:500,000.

Wiseman, W. J., Jr., Coleman, J. M., Gregory, A., Hsu, S. A., Short, A. D., Suhayda, J. N., Walters, C. D., Jr., and Wright, L. D., 1973, Alaskan Arctic coastal processes and morphology: Louisiana State Univ., Coastal Studies Inst., Tech. Rept. no. 149, 171 p.

APPENDIX II. PEBBLE LITHOLOGIES OF BARRIER ISLANDS AND MAINLAND BEACHES

PEBBLE LITHOLOGIES OF BARRIER ISLANDS AND MAINLAND BEACHES

In order to ascertain sources of nourishment of beaches and barrier islands and to determine directions of sediment transport we collected random samples of 100 pebbles at various points along the Beaufort Sea coast. Pebble lithology counts were then conducted and the results are graphically presented on the following maps.

The maps clearly display that mainland beaches and barrier islands receive sediment from multiple sources. Present outcrops of Flaxman Formation on the mainland coast are insufficient to account for the high percentage of Flaxman material on many of the barrier island groups, indicating that many of the original source areas have been completely eroded away, leaving only the coarse sediment as a lag deposit. The movement of sediment along shore is an important process on the Beaufort Sea coast and most of the lag deposits, which are the core materials of many island groups, have migrated westward from the original sites of deposition.

The reader is referred to Appendix I which contains a thorough discussion of the Flaxman and Brooks Range lithologies, and Appendix IX in Annual Report RU-204, 1978.

EXPLANATION OF MAP SYMBOLS

Flaxman Formation Lithology: Dolomite

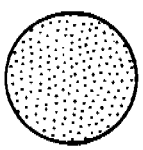

Other

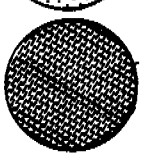

Brooks Range Lithology:

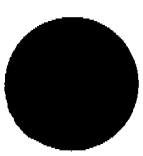

Unknown Source:

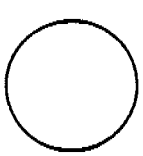

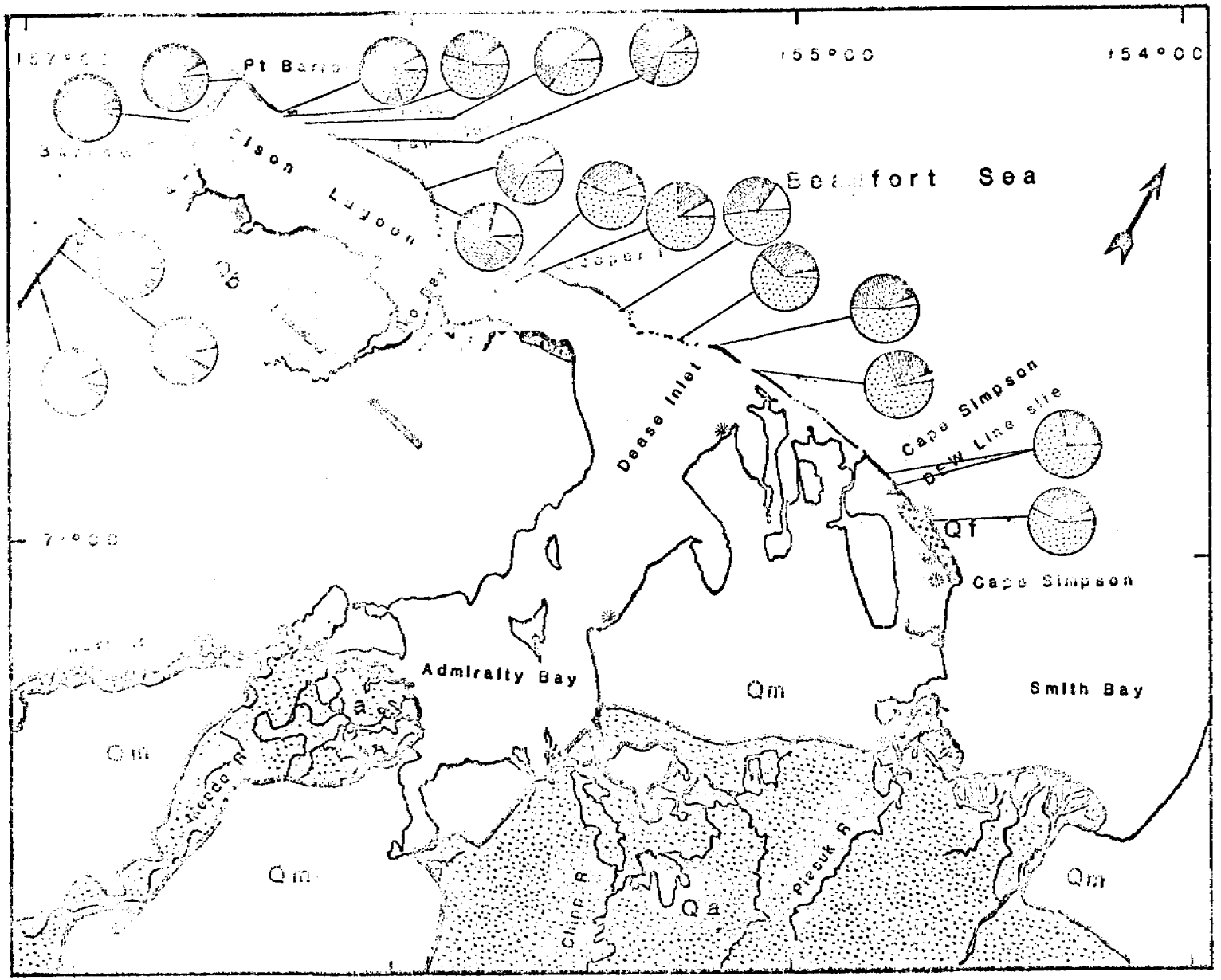
157°00
Pt Barrow
155°00
154°00
Elson Lagoon
Beaufort Sea
Dease Inlet
Cape Simpson
DEW Line site
Qf
Cape Simpson
Admiralty Bay
Qm
Smith Bay
Qm
Qm
Qa
Qm
0 5 10 20 30 40 50 kilometers
Scale= 1:500,000

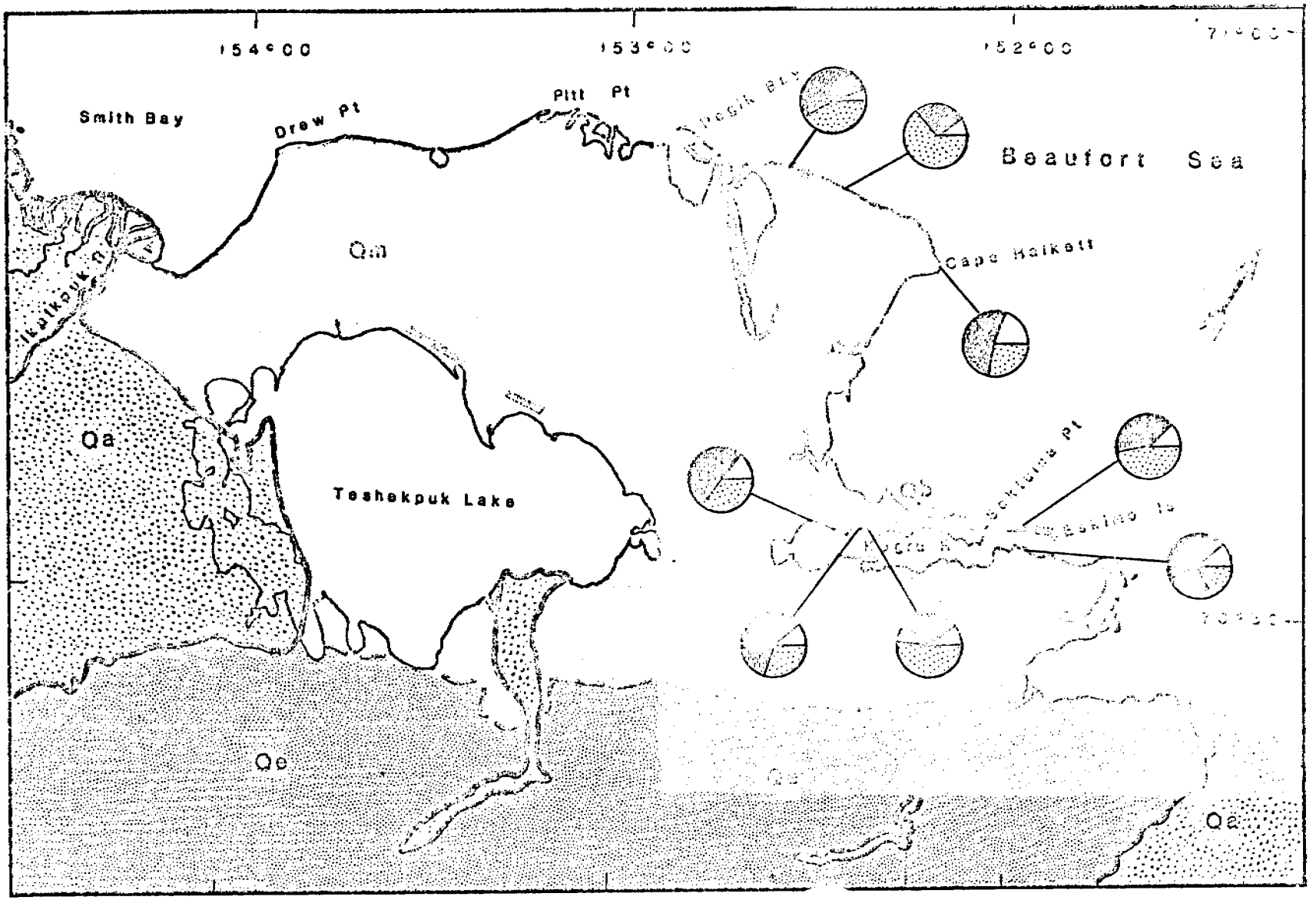
154°00
153°00
152°00
Smith Bay
Drew Pt
Pitt Pt
Beaufort Sea
Cape Halkett
Qm
Qa
Teshekpuk Lake
Qb
Qe
Qe
Qe
0 5 10 20 30 40 50 kilometers
Scale= 1:500,000

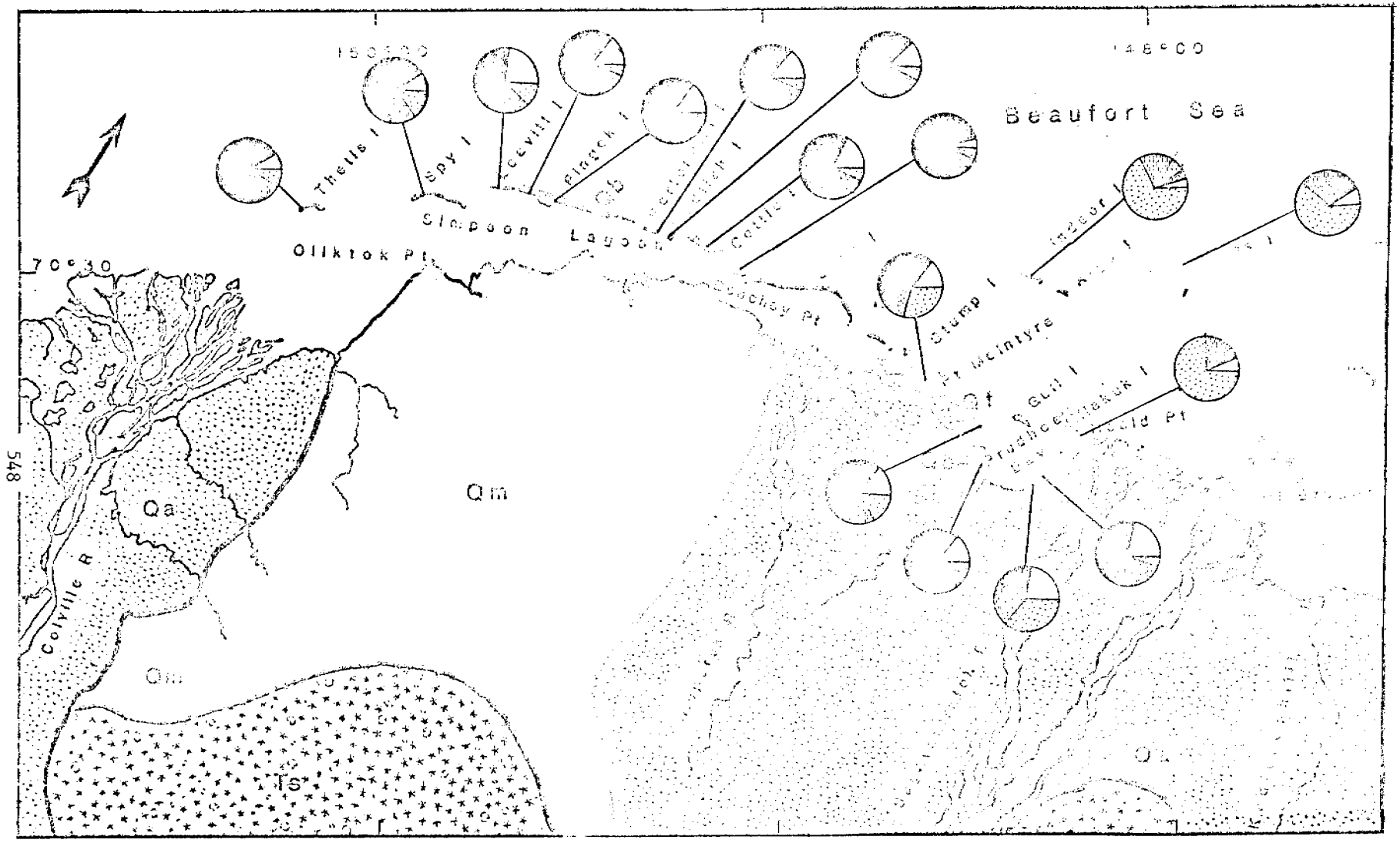

0 5 10 20 30 40 50 kilometers

Scale= 1:500,000

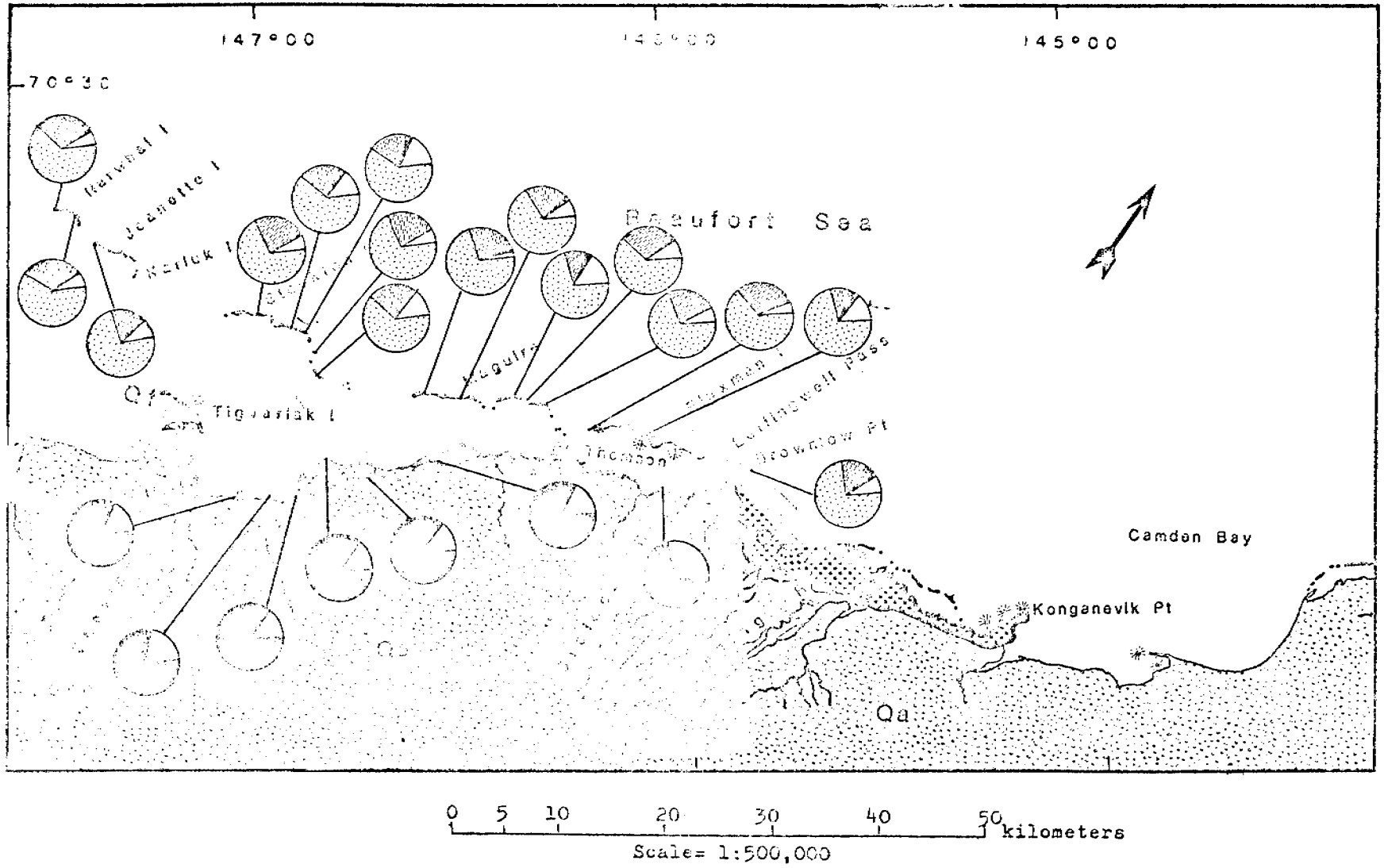
147°00
145°00
70°30
Beaufort Sea
Kadleroshilik R
Camden Bay
Konganevik Pt
Qa
0 5 10 20 30 40 50 kilometers
Scale= 1:500,000

APPENDIX III. MODERN POLLEN RAIN ON THE CHUKCHI AND BEAUFORT SEA COASTS, ALASKA

BY

R. E. NELSON

MODERN POLLEN RAIN ON THE CHUKCHI AND BEAUFORT SEA COASTS, ALASKA

by

Robert E. Nelson
Branch of Alaskan Geology
U. S. Geological Survey
345 Middlefield Road
Menlo Park, California 94025

and
Dept. of Geological Sciences
University of Washington
Seattle, Washington 98195 *

INTRODUCTION

Little has been done in the line of Quaternary palynology on the Arctic Coastal Plain of Alaska since the early studies of Livingstone (1955; 1957) and Colinvaux (1964). Even less has been done with regard to modern pollen studies, which are a necessary prerequisite to understanding fossil pollen spectra.

This study is the initial product of an attempt to gather together sufficient modern pollen data from the Arctic Coastal Plain to give depth and meaning to studies of fossil pollen floras in this region. While the sampling of coastal environments is neither ecologically nor geographically exhaustive, it is hoped that this preliminary report may provide both some insight into modern pollen rain here as well as impetus for further work.

Most of the samples used in this study were collected from coastal bluffs underlain by sandy or gravelly deposits of the last (Sangamon) interglacial high sea level stand. This porous substrate, compounded by the topographic relief of the coastal bluffs, has resulted in more xeric conditions along the coast than probably exist even one kilometer inland. Whether this significantly affects the pollen rain can only be determined by further sampling inland from the coast.

SAMPLE COLLECTION AND PROCESSING

The samples utilized in this study were collected during the course of

---

* Please use this address for any correspondence.

geological field investigations along the Chukchi and Beaufort Sea coasts of northern Alaska during the summers of 1976 and 1977. Moss polsters were collected by hand and then sealed in sterile plastic sample bags; surficial algal muds from dry pond bottoms were scraped from the upper 5 mm of sediment, placed in sterile sample bags and sealed.

In the laboratory, about 5 ml of each sample was placed in a plastic 15 ml centrifuge tube and covered with a 5% solution of KOH. Samples were then placed in a boiling water bath for 15 minutes, after which they were mixed to within 1 cm of the top of the centrifuge tube with distilled water. The samples were then centrifuged at approximately 5000 rpm for one minute, and the supernatants decanted and discarded. Samples were washed once with distilled water, then filtered through a 180-micron or 250-micron sieve in order to remove coarse debris. The fine residue was washed with 10% HCl to remove carbonates, then treated with 48% HF in a hot water bath for 30 minutes to remove silicates. Residues remaining after the HF treatment were washed with glacial acetic acid and then acetolysed 3 to 4 minutes. Final residues were mounted in glycerine jelly beneath 22 x 30 mm coverslips, and counted at a magnification of 200x.

In general, one entire slide was counted to obtain a satisfactory count of pollen grains, although it was occasionally necessary to count a second slide. The number of grains counted in each sample is shown in Table I. Percentages of total pollen (exclusive of spores) for Picea (spruce), Alnus (alder), Betula (birch), Gramineae (grasses), Cyperaceae (sedges), and Salix (willow) are shown in Figure 1; percentages for other taxa accounting for more than 1% of the total pollen (included in "others" in Figure 1) are enumerated in Table I.

DISCUSSION

Extraordinarily high spruce pollen content makes two samples stand out immediately in Figure 1, samples 77-ANr-1 and 77-ANr-2d, from the Prudhoe Bay area. Moriya (1976) also detected a surprisingly high (7.5%) percentage of spruce in his

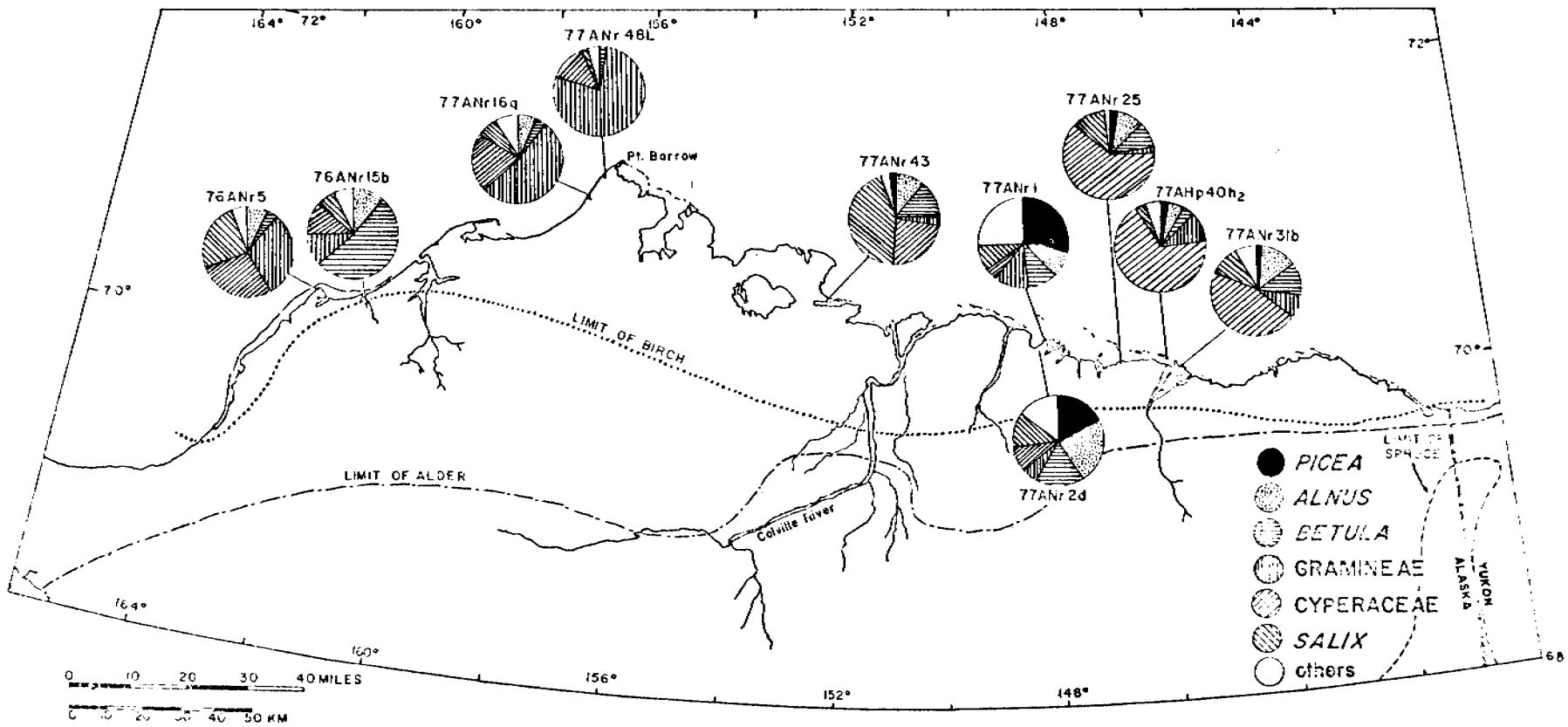

Figure 1

Index map showing location and major pollen taxa of samples reported in this study. Also shown are modern distributional limits for spruce (Picea glauca), alder (Alnus crispa) and birch (Betula nana). Distribution limits taken from Hulten (1968) and Viereck and Little (1972), modified for birch to include plants growing at sample site 76ANr15b.

TABLE I

Sample No.	Grains Counted	Sample Type	Dominant Surrounding Vegetation	Other taxa*
76 ANr 5	423	moss polster	sedges locally dominant, some grasses and prostrate willows	Ericaceae (2.4%) Saxifragaceae (1.2%)
76 ANr 15b	322	moss polster	Dryas, grasses, Eriophorum; prostrate willows common to locally abundant; Betula nana uncommon but not rare	Ericaceae (2.2%)
77 ANr 16q	250	moss polster	Carex-Eriophorum meadow with admixed Gramineae, prostrate willows and Petasites frigidus	Ericaceae (1.6%) Oxyria-type (2.4%) (Polygonaceae)
77 ANr 48L	399	moss polster	dry tundra, moss from the bottom of a dry depression, surrounded by grasses with some Salix, sedges, Saxifraga and Caryophyllaceae	Ericaceae (1.7%)
77 ANr 43	351	surface mud, dry pond	Carex-Eriophorum meadow with some grasses; abundant prostrate willows beyond 5 meters	Ericaceae (1.4%)
77 ANr 1	192	moss polster	Ground only about 50% covered by vegetation. In order of abundance, Dryas, Gramineae, Artemisia arctica. About 10% other herbs	Pinus (5.2%) Ericaceae (7.8%) Artemisia (4.2%) other Compositae (1.6%) Saxifragaceae (1.6%) Rosaceae (3.1%)
77 ANr 2d	346	moss polster	moist tundra dom. by Carex and Eriophorum, with grasses and prostrate willows, Pedicularis and other herbs	Pinus (1.4%) Ericaceae (2.6%) Rosaceae (3.2%) Polygonum bistorta type (2.6%) Scrophulariaceae (1.2%)
77 ANr 25	186	surface mud, dry pond	drained thaw lake basin, wet tundra dominated by Carex and Eriophorum, some prostrate willows	none
77 ANr 31b	245	surface mud, dry pond	sedges, some grasses and occasional prostrate willows	Artemisia (2.0%)
77 AHp 40h$_2$	179	moss polster	dry tundra, dominated by very short Carex, Eriophorum, some Cladonia and short grass. Cardamine, Papaver, and Taraxacum on bluff faces	Artemisia (1.7%)

* Taxa present in amounts exceeding 1% of total pollen, in addition to taxa shown in Figure 1.

Table showing additional data for samples reported in this study.

sample from a polygon fill at Prudhoe Bay. That pine should constitute over 5% of sample 77-ANr-1 is even more surprising, since the nearest pines to Prudhoe Bay are jack pine (Pinus banksiana) in the central Yukon Territory, and lodgepole pine (P. contorta) in southeastern Alaska, both over 1,000 km distant. The nearest spruce to Prudhoe Bay lies some 150 km to the south.

Both samples 77-ANr-1 and 77-ANr-2d were taken from areas near the Sagavanirktok River main channel, however, and it is possible that some of the conifer pollen in them may be redeposited from older deposits or areas with higher percentages of modern conifer pollen further to the south. Pollen of Sequoia type was found in both samples, in addition to a few primitive trilete spores probably derived from Tertiary or Cretaceous strata over which the river flows upstream from my sample sites. Moriya's sample (1976, p. 345) was collected from a depth of 5 cm and thus may not reflect represent modern pollen rain, but rather that of some time in the recent past (probably since 1900).

The high spruce content in the Prudhoe Bay samples is also interesting from another standpoint: is pollen production in the Prudhoe Bay area really lower (by as much as an order of magnitude) than elsewhere along the Beaufort Sea coast, or is some strange circumstance of atmospheric circulation concentrating the southerly storm winds, with their content of forest-zone pollen, such that they are directed directly over the Prudhoe Bay area ?

It would seem most likely that a combination of these two factors is involved, but absolute pollen influx studies, using pollen traps monitored over a number of years in numerous localities, would be necessary to determine the relative importance of each factor. Such a detailed study is beyond the scope of our work, but may well provide an interesting project for future work.

Also worthy of note with regard to spruce pollen is its failure to account for as much as 1% of the total pollen in any of the samples from Barrow southwards along the Chukchi coast, as far as Icy Cape, including the two spectra Livingstone

(1955) published for the Barrow area. Only five grains were found in the four samples I have counted along this coastal stretch, out of a total of 1,396 pollen grains. It would seem to follow, then, that fossil spectra from this same area that show significant amounts of spruce would imply either northward movement of the spruce treeline or a shift in the southerly storm winds.

Sample 76-ANr-15b, taken several miles inland from the Chukchi coast along the Nokotlek River, represents pollen rain at the geographical distribution limit for dwarf birch (Betula nana). Although neither Hulten (1968) nor Viereck and Little (1972) show dward birch extending this far towards the coast in this area, I found a number of individuals growing at or near the site where this sample was collected. The high (53.7%) percentage of birch in this sample is thus understandable.

The relatively high percentages of grass pollen in samples 77-ANr-16q and 77-ANr-48L (53.6% and 79.2%, respectively) are consistent with values reported by Livingstone (1955) for two samples from near Barrow (41% and 49%), although it is most probably overrepresented in my sample 48L. Livingstone's samples also showed 5% and 10% alder at Barrow, whereas sample 77-ANr-48L contains less than 1% alder. This is at least in part a product of the overrepresentation of grass pollen in this sample.

The three easternmost samples analysed, 77-ANr-25, 77-AHp-40h$_2$, and 77-ANr-31b, are dominated by sedge pollen, even though this area is where both dwarf birch and alder distribution limits most closely approach the sample sites. Local pollen production in this area might therefore be relatively high compared to the other sited studied.

SUMMARY

Spruce pollen is found in abnormally high concentrations in modern pollen samples from the Prudhoe Bay area, although some of this may be due to reworking

of extralocal and/or fossil pollen by flooding of the Sagavanirktok River. Spruce pollen is present in only minute traces in coastal samples between Icy Cape and Point Barrow.

Birch pollen can represent more than half the total pollen present in samples taken at its distribution limit, yet drops to no more than 10% a few tens of kilometers beyond its distribution limit. Grass seems to be slightly more important than sedge along the Chukchi coast, whereas the opposite tends to be true along the Beaufort Sea coast of Alaska. Alder pollen is variable, but tends to decrease in importance with greater distance beyond its distribution limit. Sedge is particularly important along the eastern part of the Beaufort coast, at least as far as the mouth of the Canning River, the furthest east that samples have been taken.

Sphagnum does not account for more than 2% of total pollen and spores in any of the samples studied, except for the two Prudhoe Bay samples. Implications of this are discussed in the section regarding spruce content in those two samples.

ACKNOWLEDGMENTS

This work could not have been done without the tactical support of the United States Naval Arctic Research Laboratory (NARL) at Barrow, Alaska, and their assistance is gratefully acknowledged. Peggy A. Smith aided greatly in collection of materials in the field, and Mia La Londe processed some of the samples in the laboratory. Dr. Matsuo Tsukada brought the Moriya book to my attention, and Yorko Tsukada assisted with translation of the passage relating to the Prudhoe Bay sample.

REFERENCES CITED

Colinvaux, Paul A., 1964: Origin of Ice Ages: Pollen evidence from Arctic Alaska. Science, vol. 145, No. 3633, p. 707-708; August 14, 1964

Hulten, Eric, 1968: Flora of Alaska and Neighboring Territories. Stanford, California: Stanford University Press, 1008 pages

Livingstone, D. A., 1955: Some pollen profiles from Arctic Alaska. Ecology, vol. 36, no. 4, p. 587-600; October, 1955

Livingstone, D. A., 1957: Pollen analysis of a valley fill near Umiat, Alaska. American Journal of Science, vol. 255, p. 254-260; April, 1957

Moriya, Kikuo, 1976: Flora and Palynomorphs of Alaska. Tokyo: Kodansha Company; 366 pages (in Japanese)

Viereck, Leslie A., and Elbert L. Little, Jr., 1972: Alaska Trees and Shrubs. Washington, D. C.: Forest Service, U. S. Department of Agriculture: Agriculture Handbook No. 410; 265 pages

APPENDIX IV. HIGH SPINDRIFT AND STORM SURGE LIMITS , ICY CAPE TO THE COLVILLE RIVER

BY

R. W. HARTZ

HIGH SPINDRIFT AND STORM SURGE LIMITS: ICY CAPE TO THE COLVILLE RIVER

In order to gain a more thorough understanding of the potential hazards to coastal development we need to know the horizontal and vertical limits of inundation during storm surges. Many investigators have studied the beach and near shore environment along the coasts of the Beaufort and Chukchi Seas, the results of these studies show that the action of storm surges significantly increases the rate of coastal erosion and sediment transport. However, little information is available on the extent of salt water intrusion under storm surge conditions.

Barnes and Reimnitz' Annual Report (RU 205) contains an excellent discussion of the events during the 1970 storm surge, so I will not belabor the issue. Briefly, during the late summer of 1970 an intense southwesterly storm combined with unusual open-water conditions to produce a severe storm surge that raised sea level as much as 3 meters. As a result of this storm a high spindrift line of wood and debris was deposited along most of the Chukchi and Beaufort Sea coasts.

The map is based on field studies conducted along the Chukchi Sea coast in 1976 and along the Beaufort Sea cosst in 1977. In areas not covered by personal observations I have estimated the position of the high spindrift line on the basis of examination of coastal morphology and topography. The dashed line on the map indicates the relative position of the high spindrift line.

CHUKCHI SEA
Wainwright
Tapkaluk
KUK RIVER
Kungok
Kuk River
Nuiqsut
Nigliq Channel
Nechelik Channel
Apikuaruk Creek
Colville River
Nigliq
Pukakruk
Omalik
RESERVE
NOA
Ivisaruk
Oumalik
Kogosukruk River
NAVAL PETROLEUM
Atakkiuk
Tunalik

UNITED STATES
MENT OF THE INTERIOR
EOLOGICAL SURVEY

MEADE RIVER

ALAS
TOPOGRAPH

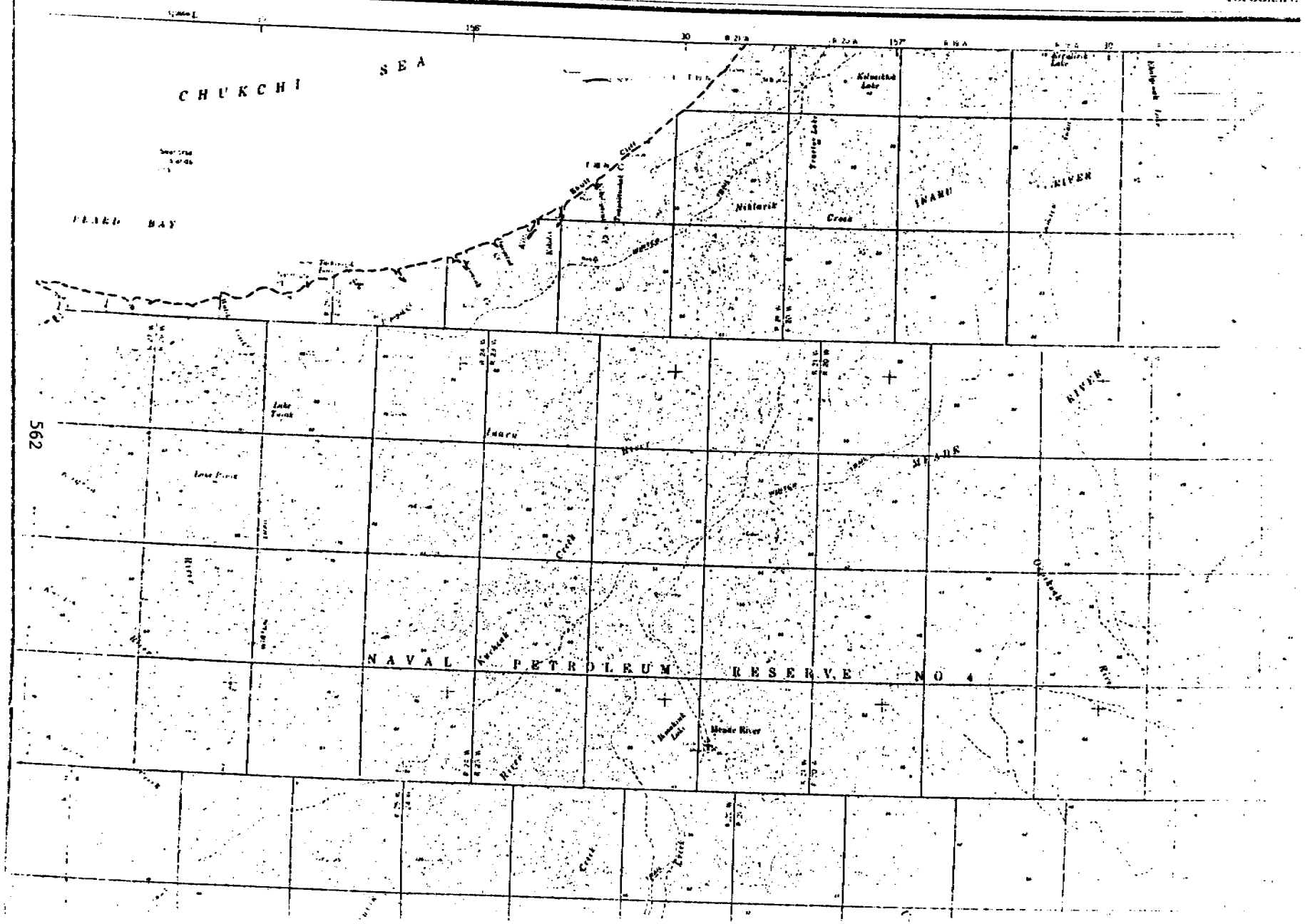

CHUKCHI SEA
Pt Barrow
Plover Pt
Deadmans Island
Brant Pt
Telegakrok Pt
ELSON LAGOON
PLOVER ISLANDS
BEAUFORT SEA
Eluktak Entrance
Scott Pt
Cooper Island
Ross Pt
Tuligeak Pt
Ike Bay
Christie Pt
Sanigaruak Island
Igalik Island
Tangent Pt
Kugurak Island
Tuhmanik Island
Martin Island
Lake Sangoonak
Lake Tuzikoak
DEASE INLET
Black Head
Tiny Island

UNITED STATES
DEPARTMENT OF THE INTERIOR
GEOLOGICAL SURVEY

TESHEKPUK

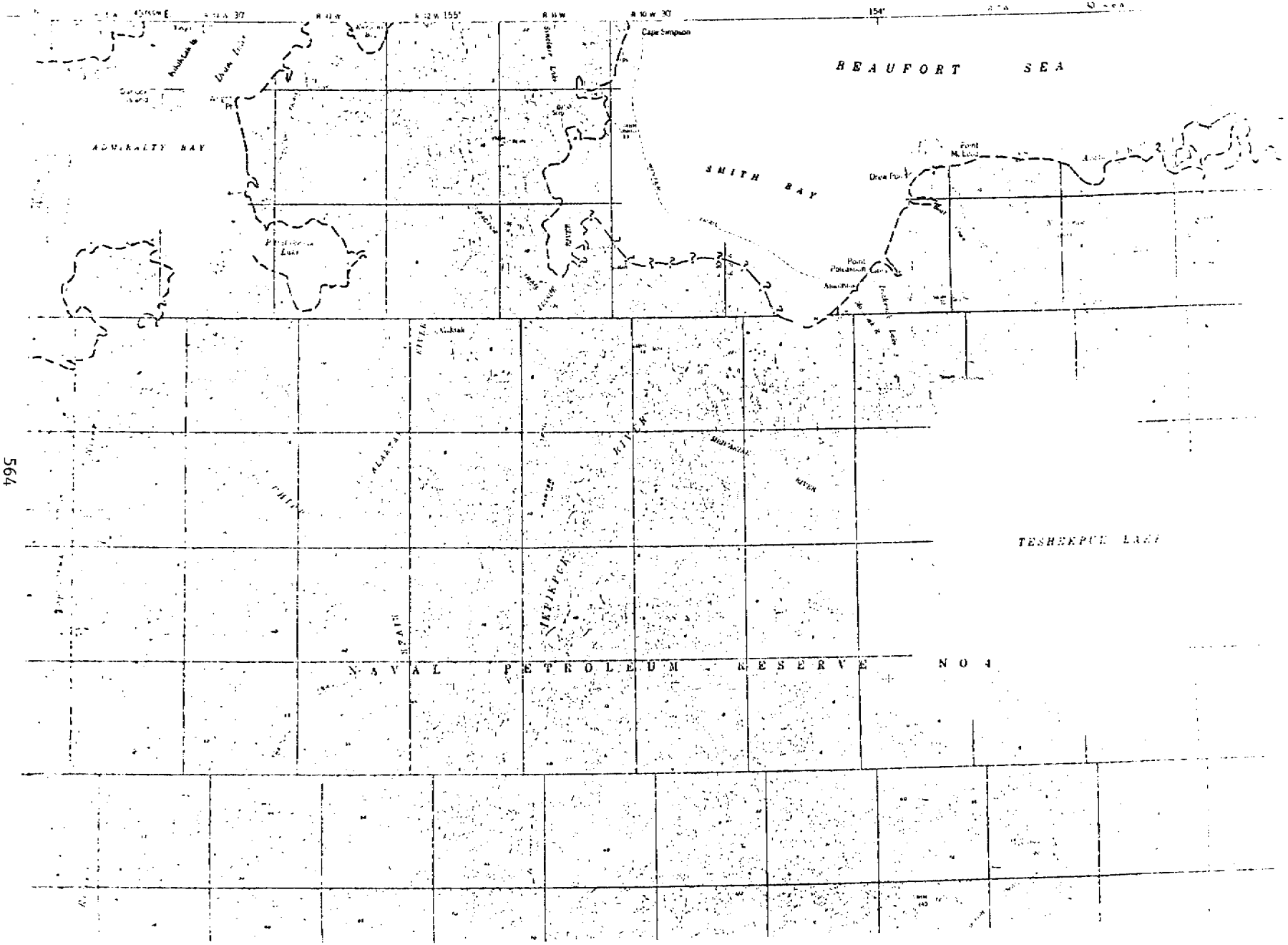

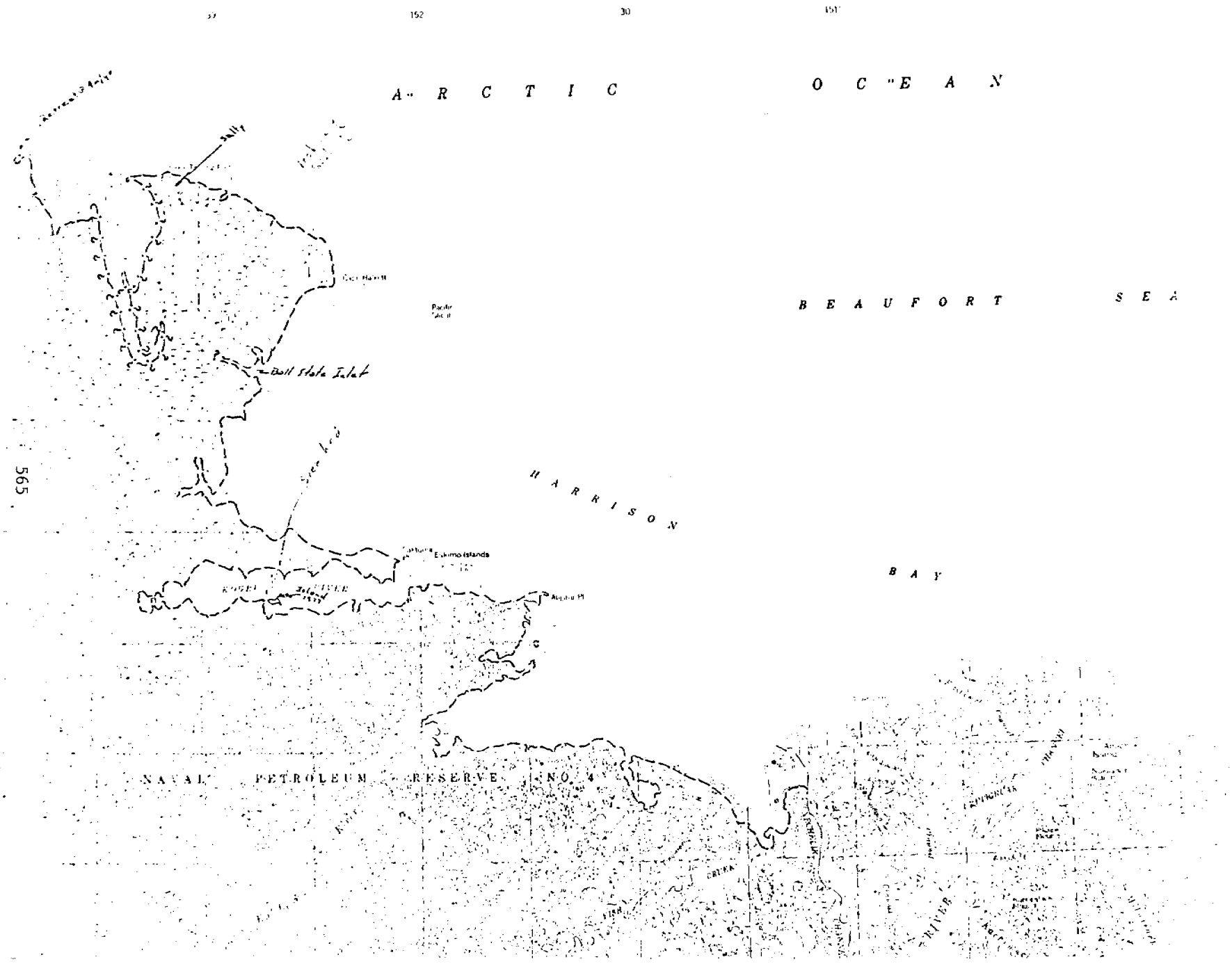
A R C T I C O C E A N
B E A U F O R T S E A
H A R R I S O N B a y
Bell State Island
Eskimo Islands
NAVAL PETROLEUM RESERVE NO. 4
565

APPENDIX V. EROSIONAL HAZARDS MAP OF THE ARCTIC COAST OF THE NATIONAL PETROLEUM RESERVE - ALASKA

BY

R. W. HARTZ

EROSIONAL HAZARDS MAP OF THE ARCTIC COAST OF THE NATIONAL PETROLEUM RESERVE-ALASKA

by

R. W. Hartz

This erosional hazards map evaluates rates of change in coastal morphology and on this basis categorizes land-use hazards along the Chukchi and Beaufort Sea coastal segments of NPR-A. The evaluation and the discussion that follows draw heavily upon the reports listed in the bibliography. A synthesis of these works has been combined with personal field observations made during the summers of 1976 and 1977. In areas that were not covered by previous reports or by personal observations, rates of coastal retreat have been estimated by examining single nonsequential sets of air photos and topographic maps.

This study was supported jointly by the U.S. Geological Survey and the Bureau of Land Management through interagency agreement with the National Oceanic and Atmospheric Administration as part of the Outer Continental Shelf Environmental Assessment Program (OCSEAP). David M. Hopkins participated in the study and reviewed the manuscript.

Most coastal erosion takes place during late summer and autumn. Drifting snow accumulates in the lee of beach bluffs during winter and the resulting snow drifts tend to persist on the beaches through June and into July. Where snow is lacking, mud slumps and flows, caused by thawing permafrost, regrade the coastal bluffs and partly cover the narrow mainland beaches. Lunar tides are small, persisting sea ice minimizes wave fetch, and the barometric high pressure systems of early summer keep sea level low, so that the small waves of June and July wash only the lowest part of the

beach. During late summer and autumn, however, the weather is dominated by the passage of cyclonic low pressure systems, permitting sea level to rise. The remaining snow and much of the slumped material is quickly removed from the beach. The rise of sea level in response to low barometric pressure may be augmented by a setup due to onshore winds, resulting in storm surges 3 to 3.5 m above normal sea level (Hume and Schalk, 1967; Reimnitz, personal commun., 1977). Yearly rates of coastal retreat and longshore sediment transport are (in some cases) greatly accelerated during such storm surges.

In general, the entire coastline of NPR-A from Icy Cape to the Colville River delta may be characterized as thermoerosional, although localized accretionary segments are found on certain spits, bars, and river deltas such as the spit at Point Franklin and the Meade River delta. The Chukchi Sea and Beaufort Sea coastlines have contrasting erosional regimes.

The Chukchi Sea erosional regime extends from Icy Cape to Point Barrow. It forms a linear, northeast-southwest trending coast with few large embayments. The coastline of the Chukchi regime is controlled by longshore sediment transport to the northeast with localized reversals to the southwest occurring from Icy Cape to Pingorarok Hill and from Point Franklin to Peard Bay. Longshore transport is the dynamic force responsible for the construction of the barrier island which form Kasegaluk Lagoon and the offshore bar system that extends from Icy Cape to Skull Cliff. Littoral drift may be augmented by southwest to westerly storm surges that can move as much sediment in one event as is moved during the entire open-water season under normal conditions. These

barriers and offshore bars tend to dampen wave attack on the mainland coastal bluffs that are as high as 25 m, but most bluffs are in the 7 to 8 m range. The coastal bluffs are predominantly composed of sand and pebbly sand of the Gubik Formation, in places underlain by Cretaceous bedrock. Bedrock outcrops, where present, are relatively resistant to wave attack and tend to form a straight coastline. Coastal segments lacking bedrock outcrops erode readily when subjected to wave action and they provide the clastic sediments necessary for the construction of barrier islands offshore bars, and mainland beaches.

The Beaufort Sea erosional regime extends from Point Barrow to the Colville River delta and produces a deeply embayed coastline that trends northwest-southeast. Longshore sediment transport is generally to the northwest with localized reversals in littoral drift occurring in association with some embayments such as Smith Bay and Pogik Bay. A large portion of the Beaufort Sea coast is exposed to direct wave attack due to its orientation (i.e., the angle at which it receives incoming waves) and the absence of barrier islands and extensive offshore bar systems. Where barrier islands are present they afford little protection for the mainland coast because they enclose lagoons wide enough to permit considerable wave fetch. The mainland bluffs are as high as 10 m, but most are in the 2 to 4 m range. They consist of silt, fine sand, and peat of the Gubik Formation; bedrock is not exposed along the Beaufort Sea coast. The fine grained, ice-rich sediments of these coastal bluffs erode rapidly but provide little sediment coarse enough to remain on the beach.

Rates of coastal retreat are particularly rapid along the Beaufort Sea coast. During the ice free period from July to October even small waves erode a large portion of the coastal bluffs. Retreat of the Chukchi Sea coast, though fairly rapid, tends to be limited to major storms in the ice-free season and is moderated by the considerable supply of sand and gravel furnished by erosion of the coastal bluffs and made available for beach nourishment. Where present, bedrock outcrops also tend to retard bluff retreat along the Chukchi Sea coast. The Beaufort Sea beaches are much narrower and erosion of the coastal bluffs yields little sand and gravel; thus beaches tend to be thin and undernourished. During periods of low barometric pressure, sea level commonly rises above the beaches and even small waves can vigorously assault the coastal bluffs. The exposed frozen silt and fine sand is quickly thawed, eroded, and removed, commonly forming a thermal niche which can undercut the bluffs for a distance of several meters. When frost cracks, along the axes of the ice wedges, are intersected by the thermal niche huge blocks of tundra up to 6 m wide may collapse into the swash zone. In exposed areas such as Cape Halkett, Drew Point, and Cape Simpson, where wave attack can come from any one of several directions, this process accounts for phenomenal rates of coastal retreat, as much as 25 m per year (Leffingwell, 1919).

When considering coastal construction sites, careful evaluation of the erosional hazards under normal and catastrophic conditions must be made in order to avoid costly repairs or relocations. Storm surges along the Chukchi Sea coast have raised sea level 3 m or more, inundating and undermining the foundations of two 5,000-gallon

oil tanks that were installed during the mid-50's as part of the now abandoned Icy Cape DEW-Line site. These oil tanks now lie on the active beach only a few meters from the swash zone and serve as a grim reminder of inadequate considerations of erosional hazards.

Bibliography

Hayes, M. O., and Nummedal, Dag, 1977, Tentative morphologic classification of Barrier Islands along the Arctic coast of Alaska: Chukchi-Beaufort Sea OCSEAP Mtg., Barrow, Informal Rept. RY-59, Task-DY, 47 p.

Hume, J. D., and Schalk, M., 1967, Shoreline processes near Barrow, Alaska; a comparison of the normal and the catastrophic: Arctic, v. 20, no. 2, p. 86-103.

Hume, J. D., Schalk, M., and Hume, P. W., 1972, Short term climate changes and coastal erosion, Barrow, Alaska: Arctic, v. 25, no. 4, p. 272-278.

Leffingwell, E. DeK., 1919, The Canning River region northern Alaska: U.S. Geol. Survey Prof. Paper 109.

Lewellen, R. I., 1970, Permafrost erosion along the Beaufort Sea coast: [Pub. of the author] P.O. Box 1068, Littleton, CO, 25 p.

_____1973, The occurrence and characteristics of nearshore permafrost in northern Alaska, p. 131-136, in Permafrost, the North American Contribution to the Second International Conference: Washington, DC, Natl. Acad. Sci.

_____1974, Offshore permafrost of Beaufort Sea, Alaska, in Reed, J. C., and Sater, J. E., eds., Arctic: Arctic Inst. North America.

_____1977, A study of Beaufort Sea coastal erosion in northern Alaska: Arctic Inst. North America, RU-407, Final Rept., 24 p.

McCarthy, G. R., 1953, Recent changes in shoreline near Point Barrow, Alaska: Arctic, v. 6, p. 45-51.

Moore, D. G., 1964, Acoustic-reflection reconnaissance of continental shelves; eastern Bering and Chukchi Seas, in Miller, R. L., ed., Papers in Marine Geology, Shepard Commemorative Volume: New York, MacMillan Co.

Rex, R. W., 1964, Arctic beaches, Barrow, Alaska, p. 384-400, in Miller, R. L., ed., Papers in Marine Geology: New York, MacMillan Co.

Wiseman, W. J., Jr., Short, A. D., and others, 1973, Alaskan Arctic coastal processes and morphology: Louisiana State Univ., Coastal Studies Inst., Tech. Rept. No. 149.

ANNUAL REPORT

Contract # 03-5-022-55
Research Unit # 483
Reporting Period 1 April 1977 -
31 March 1978
Number of pages: 45

Seismotectonic Studies of Northeast and Western Alaska

Principal Investigators

N. N. Biswas
L. Gedney

Geophysical Institute
University of Alaska
Fairbanks, Alaska 99701

Prepared Jointly for the

National Oceanic and Atmospheric Administration
Under Contract No. 03-5-022-55

and the

U. S. Geological Survey
Under Contract No. 14-08-0001-16688

PREFACE

This report describes the seismicity studies of the following two widely separated areas in Alaska: (a) northeast seismic zone and (b) seismic zone around Norton and Kotzebue Sounds. The study for the first zone is primarily supported by the U. S. Geologic Survey Contract No. 14-08-0001-1668. Since the objectives under this grant is to a large extent complementary to those of NOAA, and as logistic support to service the seismographic network around Barter Island was derived from NOAA, the results obtained for the northeast part of Alaska have been described simultaneously with those obtained for the western area.

TABLE OF CONTENTS

LIST OF FIGURES

LIST OF TABLES

I. SUMMARY: OBJECTIVES, CONCLUSIONS AND IMPLICATIONS FOR OIL AND GAS DEVELOPMENTS

The objectives under the present study are to evaluate the extent of seismic hazards posed by earthquakes in northeast and western Alaska. The analysis of the seismic data gathered to date shows that, on the eastern part of Beaufort Sea shelf, the area north of Barter Island is subject to earthquakes in the magnitude range of from 5 to 6.

During the exploration and development phases of the proven hydrocarbon reserves in this area, one of the design criteria for structures should be to withstand ground vibrations corresponding to those from a shallow earthquake (less than 20 km) of at least magnitude 6.0. Linear structures, like pipelines, used for transportation of oil or gas through the eastern part of the Brooks Range and the Chandalar and Yukon River basins should take into account the possibility of ground dislocations, perhaps by a significant amount over a period of time, at points of major mapped fault crossings.

In the western part of Alaska, around the Seward Peninsula, analysis of the data gathered to date indicates a higher level of seismisity than was recognized prior to this study. This phenomenon appears to be common to both offshore and onshore areas. Further, consideration of the magnitudes of larger earthquakes indicates that this area is seismically more active than northeast Alaska.

Some efforts during this study were directed to investigate icequakes. The results show that fracturing of landfast ice sheets under meteorological instability can be effectively detected by seismic methods. The

seismic waves generated by these sources are different from those generated by tectonic processes. A proper understanding of the mechanism of propagation of seismic waves through ice sheets and adjoining media (air and water) appears to be a viable tool to investigate the various elastic properties of ice sheets.

II. INTRODUCTION

A. General Nature and Scope of Study

This report describes the seismicity studies being undertaken in two widely separated areas of Alaska. Because the objectives of the two studies are virtually the same, we will discuss them simulataneously.

The first area of study lies in northeast Alaska. It extends from the eastern part of the Beaufort Sea Shelf in the north, to 66°N latitude on the south. This area was seismically instrumented for the first time during the end of 1975. Later in 1976, the second area in western Alaska was instrumented. This included the Seward Peninsula, and provided coverage of the surrounding offshore areas including Norton and Kotzebue Sounds.

Data products from a number of agencies, foreign and domestic, have noted a seismic zone near Barter Island on the eastern part of the Beaufort Sea during the years prior to 1968. This has appeared to be separated from the central Alaska seismic zone by an aseismic zone trending approximately through the eastern Brooks Range. In addition, past data show a virtual absence of seismic activity west of approximately 152°W in the northern latitudes of the state.

As for the Seward Peninsula area, several concentrations of earthquakes have been documented from past observations, particularly west of 156°W longitude. It was the intent of the present study to more closely define the characteristics of the seismicity of northeast and western Alaska by the operation of carefully spaced seismographic networks.

B. Scientific Objectives

The specific objectives of the seismological studies for both the areas are the following:

(i). To determine the spatial and temporal characteristics of the seismicity, and its relationship to mapped tectonic features.

(ii). To determine the predominant failure mechanisms associated with the earthquakes located along or near the known geological features or trends.

(iii). To determine magnitudes, and if possible, strain release patterns associated with the larger earthquakes in the respective areas, for use in projections as to possible activity in the future.

(iv). To determine characteristics of seismic energy attenuation as functions of epicentral distances.

C. Relevance to Problems of Petroleum Development

It has been well established that hydrocarbons in commercial quantities occur in onshore and offshore areas of the Beaufort Sea. Large scale exploration programs for hydrocarbon concentrations, and their eventual development in areas adjoining the proven reserves, are a certainty in the near future. Consequently, the evaluation of the level of seismicity for these areas is a logical undertaking to assist in the planning and design of future construction projects.

Similar development planning and construction in the potentially oil-rich areas of the western Alaska continental shelf is not as far advanced as that in the northeast. Results obtained thus far in this part of the state, however, indicate that the level of seismicity is much higher than previously thought. To establish this finding within desirable bounds of precision will require a data base which can only be obtained by the operaion of a localized, high-resolution seismographic network for a reasonable length of time.

III. CURRENT STATE OF KNOWLEDGE

A. Northeast Alaska

As mentioned earlier, it has appeared from past data that the seismic zone around Barter Island is isolated. However, results obtained since the inception of the present study have shown (Gedney et al., 1977; Biswas et al., 1977) that this zone is actually on a northward extension of the central Alaska zone of shallow seismicity. Earthquakes in the latter zone are felt to be a direct consequence of plate subduction, where the north Pacific lithospheric plate underthrusts Alaska, a phenomenon traceable as far north from the coast as the area around McKinley National Park. It is difficult, however, to invoke this phenomenon as being the immediate cause of earthquakes in northeast and western Alaska, both of which are more than 400 km distant from the Alaskan subduction zone. It thus appears that a more indirect association must be at work relating the activity of the three seismic regimes which are generally contiguous in extent and contemporaneous in time.

The largest earthquake reliabily recorded in northeast Alaska during the past decade had a magnitude (M_L) of 5.3 and was located about 30 km north of Barter Island on the Beaufort Sea shelf. Since the emplacement of the local seismographic network, however, we have found that a great many more earthquakes over a wider magnitude range occur here than earlier data have revealed. During a two-year recording period (1976-77), locatable events ranged approximately in magnitude from 1.0 to 4.0, and many others occurred which were non-locatable due to equipment outages or low magnitude.

B. Western Alaska

The largest earthquake to have been instrumentally documented in western Alaska occurred about 30 km inland from the northern coast of Norton Sound in 1950, and was of magnitude 6.5. Since then, teleseismic data have failed to reveal any further significant seismic activity in this area. However, the present study with the localized network demonstrates clearly that the area is still active, and points out a north-south distribution of epicenters passing through the area of the 1950 earthquake. In addition, earthquakes located during 1977 occur widely throughout the entire area, including both Norton and Kozebue Sounds. Most significantly, there are a number of instances, particularly on the Seward Peninsula, where earthquake clusters are found to lie along, or parallel to mapped faults or lineal structural trends. Earthquakes recorded during the year ranged in magnitude from 1.0 to 4.5.

IV. STUDY AREA, SOURCES, METHODS AND RATIONALE OF DATA COLLECTION

The study area in northeast Alaska is bounded by meridians 140° and 150° W, and parallels 66° and 72° N. This includes the eastern part of the Beaufort Sea shelf and coastal plane, the Romanzof Mountains, the eastern Brooks Range, and the Chandalar and Yukon River basins. The layout of the seismographic stations installed in the study area is shown in Figure 1.

The western study area is bounded by meridians 156° and 172°W, and latitudes 62° and 68° N. This includes the Seward Peninsula and Norton and Kotzebue Sounds. The station layout is shown in Figure 2. It can be seen in Figures 1 and 2 that major portions of the areas covered by the networks are inland. Aside from the obvious impracticality of employing ocean-bottom seismometers, there are other reasons for utilizing land-based seismographic networks in what is largely meant to be an assessment of offshore seismic hazards.

Crustal earthquakes commonly migrate with time along a fault or fault system. This means that if a given section of an active fault yields (resulting in an earthquake), then at a later time a somewhat distant point of the same fault may yield to accumulated stresses. Thus, for an assessment of seismic hazards for an area, it is essential to consider the seismic activity for the adjoining areas also. In view of this, the stations of the networks were distributed on a near-regional scale, with the capability to locate earthquakes of magnitude as low as 1.0 occurring within the area of interest. It may be noted, as discussed in later sections, that both the study areas are characterized by crustal earthquakes.

Details of the stations, the equipment used at the field and recording sites, and the mode of data telemetry to the Geophysical Institute at Fairbanks are discussed in detail elsewhere (Biswas et al., 1977) and will not be repeated here. However, it should be stressed that about 90 percent of the budget allocated, particularly for the study area in western Alaska, is consumed by leasing the microwave channels for data telemetry to Fairbanks. From our past experience of seismic data gathering in Alaska, we have favored the central recording system over local recording to minimize data gaps. These are usually caused by unreliable local power (110V) supplies, more frequent personnel turnover, and maladjustment or failure of individual local precision timing systems.

V. RESULTS

A. Northeast Alaska

It is apparent, on examining the available epicentral data for northeast Alaska prior to 1968, that these are incomplete and poorly representative of the area. The following section will therefore deal only with the accumulated data from 1968 through 1977.

For the period from 1968 to 1973, the best available data for the study area are those collected by the Canadian networks. This information has been compiled from eight Canadian annual catalogs (Stevens et al., 1976; Horner et al., 1974, 1975, and 1976; Bashman et al., 1977a; Wetmiller, 1976 and 1977). Locations are numerical solutions computed by a least-squares method utilizing a one-layer crustal model 36 km in thickness, and hypocentral depths were constrained to mid-layer

(18 km). In some cases, the Canadians supplemented their network data with central Alaskan data in the location process. The Canadian catalogs list ten earthquakes located in northeast Alaska during 1974 and 1975. One of the 1975 events was also located by the University of Alaska central Alaskan network, and the latter solution indicated a smaller error than that obtained by the Canadian network. Not counting this earthquake, focal parameters of the remainder in the Canadian list are given in Table 1 of Appendix I. A general estimate of errors in location of these epicenters is on the order of $\pm$ 100 km (Bashman et al., 1977b).

From Table 1 it can be seen that the majority of the listed earthquakes fall in the magnitude range from 3 to 4. This indicates the detection threshhold for earthquakes in northeast Alaska by the Canadian network. It is also noted that the standard deviations (σ) of the traveltime residuals generally run greater than 1.0 sec. The epicentral plot in Table 1 on an overlay of the study area including station locations is shown in Figure 1. In this and in other figures discussed later of epicenter plots, we have have not distinguished the individual earthquakes according to their magnitudes.

During 1974 and 1975, routine data reduction procedures utilizing the basic central Alaskan network located a number of earthquakes on the southern edge of the study area (Table, 2 Appendix I). A plot of the data in Table 2 is shown in Figure 3. None were located north of 68°N. This, plus the factors mentioned above, indicate the limitations of locating earthquakes in northeast Alaska by the central Alaskan network or Canadian network or a combination of both. These limitations are due to the inherent network configuration and their distances ($\approx$ 200 km) from the source area.

Since the installation of the northeast net in late 1975, many earthquakes in the area have been identified, and details of these are given in Tables 3 (1976) and 4 (1977) of Appendix I. All solutions in Tables 2, 3, and 4 are based on a weighted least-squares method. The details of the computer program used are given by Lee and Lahr (1975); the velocity structure used is given elsewhere (Biswas et al., 1977). Plots of the epicenters in Tables 3 and 4 are shown in Figures 4 and 5, respectively.

The symbols NO, GAP, DMIN, RMS and ERH in Table 2, 3 and 4 refer, respectively, to the number of station readings used to locate each earthquake, largest azimuthal difference between stations with respect to the epicenters, distance of the epicenter from the nearest station, the root mean square of travel time residuals (σ), and the standard error in epicenter location.

In the initial computer runs, all focal parameters were allowed to vary. The results indicated that focal depths ranged between the surface and about 20 km. In subsequent computer runs, focal depths were constrained to 10 km to eliminate 1 degree of freedom in the location problem.

Comparison between Tables 3 and 4 shows that more earthquakes were located by the local network during 1977 than during 1976. This should not be construed as being due to an actual increase in activity, but rather to increased station reliability after the experience gained during the first year of operation. In any event, it is clear that local seismic coverage under the present project has led to the detection of many earthquakes which would otherwise have gone unrecorded and unverified.

B. Western Alaska

Again, for comparison, we demonstrate the difference in detection capability which can be achieved by a localized seismographic network over purely teleseismic recording (an obvious point, but one which should be emphasized). A plot of all the epicenters found in the records available to us prior to 1977 in the western study area including station locations is shown in Figure 2. In contrast, we list in Table 5 of Appendix I, the earthquakes which we have documented in a period of only slightly more than 12 months (1977). The symbols used for the heading of each column represents the same quantities as mentioned before.

As was done for the northeast sector, the scaled data were initially processed for free solutions (all focal parameters allowed to vary). The results showed similar characteristics, so in subsequent runs we constrained the focal depths here, also, to 10 km. The velocity structure used was also the same. The resulting plot is shown in Figure 6.

In Tables 2, 3, 4, and 5, it can be seen that the values of σ are generally less than 1.0 second, with the exception of some isolated events. However, despite fixing the focal depths to 10 km, a number of earthquakes show significant uncertainties in location. It is anticipated that the errors associated with the locations of these events can be reduced by rescaling the raw data. This is anticipated for the near future.

VI. DISCUSSION

A. Northeast Alaska

To relate the epicentral locations determined in this study to known tectonic elements, all earthquakes listed in Tables 1, 2,3, and 4 are plotted on an overlay of structural trends (Figure 3, Grantz et al., 1976) of the study area in Figure 7. The offshore traces of these structures were mapped by the above authors using marine geophysical methods.

The eastern section of Figure 3 of Grantz et al., was enlarged photographically by a factor of about 10, and the structural traces were digitized at close intervals. These data were then converted to the same projection and linear scale as was used to plot the epicenters to compile Figure 7. This figure should not be used to correlate individual earthquakes with particular structures, since all locatable earthquakes (1968-1977), regardless of the order of error in their epicentral locations, have been retained in this figure. However, it illustrates the relationships between the general trends of seismicity and structures.

In the offshore area, the primary epicentral concentration is that resulting from a magnitude 5.3 earthquake in 1968 and its aftershocks. The onshore distribution illustrates the extent of the active seismic zone, and how it merges smoothly with that of central Alaska.

Despite significant location uncertainties as mentioned above, a general northeast-southwest trend can be discerned, particularly north of 68° latitude. In the offshore area, these earthquakes tend to concentrate along the axes of synclines and anticlines. This apparent causal relationship between folded structures and earthquakes must remain a

matter of conjecture for the present. Between 68° and 70° the primary concentration parallels, approximately, the interface between the Colville geosyncline and the Romanzof Mountains. In these areas of known large-scale faulting, such as those in the Romanzof Mountains and the Brooks Range, the occurrences of earthquakes can be more readily interpreted.

For an earthquake in the eastern part of the study area (Yukon Territory, Canada), Leblanc and Wetmiller (1974) presented fault plane solution which showed a principal horizontal compressive stress in a WNW-ESE direction. This is probably representative of the general direction of compressive stress in the North American plate in that area. West of here, in central Alaska, results of various studies as summarized by Bhattacharya and Biswas (1978) indicate a predominant northwest-southeast direction to this axis. Translating these two principal stress directions into the study area, it may be suggested that the area is under continuous compressive stress in an approximate WNW-ESE direction. The very orientation of the structural elements in northeast Alaska seems to substantiate this interpretation. Currently, the primary sources of stress release in the area appear to be associated with the mapped thrust faults along topographic highs, and along strike-slip faults, particularly the Porcupine fault and the Kobuk trench in low lands on the south of the Brooks Range.

In order to study the presence of any correlation of individual earthquakes or cluster so far located in northeast Alaska (1968-1977) with the mapped traces of tectonic features, all earthquakes in Tables 2, 3, and 4 having $\sigma \leq 1.5$ sec have been collected into a separate group. The plot of these together with the 1968 series located north of 70° N latitude is shown in Figure 8. It must be mentioned that there

are a number of earthquakes in the latter group which have $\sigma \geq 1.5$ sec. However, these have been retained in this plot as they are indicative of the offshore trend of seismicity.

North of 70° N latitude, any change in the spatial distribution of earthquakes from those shown in Figure 7 is not expected. Between 68° and 70° N latitudes, the epicenters scatter considerably with some lying on structural traces. The overall distribution is so diffused that it is not possible with the available data to identify which fault or faults are active at present. In the southwest corner, however, the epicentral concentration relatively increases and tends to concentrate on and around the Procupine fault and Kobuk trench which appears to indicate that these two structures are quite active at present. In passing we note that the Trans-Alaska oil pipeline crosses these two structures in the southwest corner of the study area.

B. Western Alaska

A number of shallow and deep faults and structural trends in Norton Sound have been identified by Johnson and Holmes (1977) from marine geophysical studies. Eittreim et al. (in press) have shown the offshore and onshore trends of the Kotzebue arch and associated structures. The structural map of the Seward Peninsula reproduced in Figure 9 was compiled by Hudson (1977).

The consolidation of the above three maps into a single one compatible to that used for plotting epicenters of earthquakes is in progress. In the interim, we make the following general observations regarding the trends of the epicenters and their spatial relationships with the mapped structures.

A plot of all the past data (Figure 2) reveals a clear linear trend ($\sim$ 100 km long) of epicenters in a NW-SE direction near the

intersection of 156° W longitude and 66° N latitude. Elsewhere, epicentral distribution does not exhibit any such characteristic. The epicentral plot of earthquakes recorded during 1977 by the local network, on the other hand, shows a number of important trends (Figure 6).

The cluster labelled A closely follows the onshore mapped trace of the Kaltag fault (not shown in Figure 9). This fault is known to extend several hundred kilometers offshore (Nelson et al., 1974), although the earthquake data so far analyzed do not resolve this segment.

The cluster marked B_2 coincides with that of B_1 of Figure 2. The cluster C_2 traverses the epicentral area of the 1950 (M_L = 6.5) earthquake in a north-south direction. Also, this cluster closely follows the trace of the fault system through the center of the block marked C_1 in Figure 9. The fourth cluster D_2 falls within block D_1 of Figure 9 which also includes a well defined fault system. Further west, a number of earthquakes were located both offshore and onshore during 1977 on and around the site of the 1964 earthquake (M_L = 6.0) near Port Clarence.

On the northern side of the study area, a number of epicenters are seen to parallel the coast of the Seward Peninsula. In and around Kotzebue Sound the epicenters scatter so widely that no correlation with the mapped structures is possible at this stage of the study.

During the winter months of 1977, a series of tremors were recorded by the seismographic station at Kotzebue. The frequency of occurrence of the tremors appeared similar to those observed during for earthquake swarms. However, the studies of the recorded wave trains for the tremors revealed that their source was nontectonic in nature.

Subsequent analyses of the data showed that the tremors are due to the formation of fractures in the landfast ice sheet around Kotzebue Sound. These were caused by the concentration of excessive stresses in ice sheets by meteorological instability. For brevity, we called these phenomena icequakes, which have been discussed in some detail for two of the 1977 episodes elsewhere (Biswas et al., 1977).

We have completed the qualitative part of the analysis for the entire 1977 data for icequakes; the results are summarized in Figure 10. The third swarm not reported earlier is found to be very similar in nature as the first two.

VII. CONCLUSION

The analyses of the past and currently acquired seismic data revealed the following important trends of seismicity for the northeast and western Alaska:

A. Northeast Alaska

(i). The active seismic zone around Barter Island appeared to be isolated from the past data. The results from the present study, on the other hand, show that this seismic zone is an intregral part of the central Alaska seismic zone.

(ii). Within the last 10 years, the largest earthquake (M_L = 5.3) occurred in an area located about 30 km offshore from Barter Island. It was recorded by 94 stations around the world; the main shock was followed by a series of aftershocks, the locations of which show a ENE-WSW seismic trend along the axial traces of the offshore folded structures.

(iii). The available data represent too short a time interval for the determination of recurrence rates for earthquakes of magnitude greater than 5.0 in the study area. However, the data are indicative of the design need for man-made structures to withstand ground vibrations from a shallow earthquake of at least magnitude 6.0.

(iv). The remainder of the earthquakes located in northeast Alaska are smaller than 5.0 magnitude and tend to be distributed on the eastern side of the interface between the Colville geosyncline and the Romanzov Mountains. A notable concentration of epicenters occur on and around the Porcupine fault and the Kobuk trench on the south side of the Brooks Range. Linear structures, like the pipelines, should have appropriate design provisions for periodic displacements of small extent at the crossings of these two seismically active geological structures. It seems retional to assume that episodic motions of small magnitude may eventually add up to a significant ground displacement over a length of time.

B. Western Alaska

(i). Within the last 27 years, the largest earthquake instrumentally recorded in the study area was of magnitude 6.5; it was located about 30 km inland from the northern boundary of Norton Sound. This was followed by earthquakes of magnitudes 6.0 (1964), 6.0 and 5.8 (1965), and 5.2 (1966), located about 60 km, 40 km and 15 km inland from Port Clarence, Norton Bay and Hotham Inlet (Kotzebue Sound), respectively. Since the areas around the epicenters of these earthquakes are thinly populated, their seismic impact passed largely undocumented.

(ii). The local network recorded a large number of earthquakes in the magnitude range of $1.0 \leq M_L \leq 4.5$ during a period of slightly more than 12 months (1977). The epicenters of these earthquakes are found to be distributed on and around the inland trace of the Kaltag fault, and around the 1950 and 1964 earthquakes. An epicentral concentration is found to extend in the north-south direction along a fault system about 150 km east of Cape Nome. A diffused distribution of epicenters are seen in Norton and Kotzebue Sounds with some scatter around the 1966 earthquake to the immediate west of Hotham Inlet.

(iii). No attempt has been made at this stage of our study to interpret the tectonic significance and the associated seismic hazards posed by the features mentioned above.

VIII. SUMMARY: FOURTH QUARTER OPERATIONS

A. Task Objectives:

(i). To reinstall the two horizontal component seismometers at Kotzebue.

(ii). To maintain and continue to improve signal-to-noise ratio of the daily recorded data.

(iii). To continue scaling and processing of daily recorded data.

B. Field and Laboratory Activities:

(i). The two horizontal component seismometers installed during the last field season to supplement the vertical component seismometer at Kotzebue failed to respond to ground vibrations. This was attributed to the shift in lavel of the seismometer bases during ground freeze up; it should be noted that the permafrost lies at shallow depths around the station site. Since the seismometers were buried under about 1.5 feet of ground, they became inaccessible after ground freeze up. Thus, to record icequakes according to original plan, two additional horizontal seismometers were installed over frozen ground during the early part of the reporting period.

(ii). The daily data (160 ft.) in form of 16-mm film recorded during a part of the fourth quarter, have been scaled and punched on computer cards for processing.

(iii). Two swarms of icequakes have been recorded by the three-component system at Kotzebue. However, due to the poor coupling between the ground and the horizontal sensors, their recordings of icequakes appear relatively inferior in quality compared to those recorded by the vertical component seismometer.

ACKNOWLEDGEMENTS

We thank Drs. O. Ferrians and R. A. Page of the U.S. Geological Survey and Drs. G. Weller and N. Harding of the Arctic Project Office (OCSEAP) for their continuous support and encouragement during the study period. We express appreciation to Drs. D. Hopkins, A. Grantz, W. Patton and S. Eittreim of the U. S. Geological Survey for stimulating discussions on the tectonic elements of northeast and western Alaska. We also express appreciation to Mr. T. R. Flesher of OCEAP for logistic support in time. We are indebted to R. Siegrist, W. Gregory and R. Foster for the maintenance of the seismographic networks. We are grateful to Mr. R. Eppley and other members of the Alaska Tsunami Warning Center for making available the seismic recrods gathered by the center. We are also grateful to Drs. W. H. K. Lee and J. C. Lahr of the U.S.G.S., for providing a copy of their computer program for the location of earthquakes, and for participating in helpful discussion for its adoption on the University of Alaska computer.

This research was supported by the U.S. Geological Survey Contract No. 14-08-000.-16688, NOAA Contract No. 03-5-022-55, Task #12, and by the State of Alaska.

REFERENCES

Bashman, P. W., R. B. Horner, R. J. Wetmiller, A. E. Stevens and G. Lebanc, 1977. Canadian earthquakes-1972, Seismological Series, No. 76, Ottawa Canada.

Bashman, P. W., D. A. Forsyth and R. J. Wetmiller, 1977B. The seismicity of northern Canada, Can. J. Earth Sci., 14, 1646-1667.

Bhattacharya, B., and N. N. Biswas, 1978. Implications of North Pacific plate tectonics in central Alaska: Focal mechanisms of earthquakes, to appear in Tectonophysics.

Biswas, N. N., L. Gedney and P. Huang, 1977. Seismicity Studies: (A) Northeast Alaska and (B) Norton and Kotzebue Sounds, Environmental assessment of the Alaskan Continental Shelf: Hazard and data management, NOAA Report XVIII, 269-315.

Eittreim, S., A. Grantz and O. T. Whitney, (in press). Cenozoic sedimentation and tectonics of the Hope Basins and southern Chukchi Sea.

Gedney, L., N. N. Biswas, P. Huang, S. Estes and C. Pearson. 1977. Seismicity of northeast Alaska, Geophys. Res. Letters, 4, 175-177.

Grantz, A., M. L. Holmes and B. K. Kososki, 1976. Geologic framework of the Alaskan continental terrace in the Chukchi and Beaufort Seas, C.S.P.G. Memoir No. 4, Canadian Continental Mergin.

Hornor, R. B., W. G. Milne and G. A. McMechan, 1976. Canadian earthquakes-1971, Seismological Series, No. 74, Ottawa, Canada.

_____, 1975. Canadian earthquakes-1970, Seismological Series, No. 69, Ottawa, Canada.

_____, 1974. Canadian earthquakes-1969, Seismological Series, No. 67, Ottawa, Canada.

Hudson, T., 1977. Geologic map of Seward Peninsula, Alaska, U. S. Geological Survey: Open File Report No. 77-796A.

Johnson, J. L. and M. L. Holmes, 1977. Preliminary report on surface and subsurface faulting in Norton and northeastern Chirikov Basin, Alaska, Environmental assessment of the Alaskan Continental Shelf: Hazards and data management, NOAA, Report XVIII, 14-41.

Leblanc, G. and R. J. Wetmiller, 1974. An evaluation of seismological data available for the Yukon Territory and Mackenzie Valley, Can. J. Earth Sci., 71, 1635-1656.

Lee, W. H. K. and J. C. Lahr, 1975. A computer program for determining hypocenter, magnitude, and first motion patterns of local earthquakes: U. S. Geological Survey Open-file Report No. 75-311.

Nelson, C. H., D. M. Hopkins and D. W. School, 1974. Tectonic setting and Cenozoic sedimentary history of the Bering Sea, in Herman, Y. , Marine Geology and Oceanography of the Arctic Seas, New York, Springer-Verlag, 119-140.

Stevens, A. E., W. G. Milne, R. B. Horner, R. J. Wetmiller, G. Leblanc and G. A. McMechan, 1976. Canadian earthquakes-1968, Seismological Series, No. 71, Ottawa, Canada.

Wetmiller, R. J., 1977. Canadian earthquakes-1975. Seismological Series, No. 77, Ottawa, Canada.

_____, 1976. Canadian earthquakes-1974. Seismological Series, No. 73, Ottawa, Canada.

_____, 1976. Canadian earthquakes-1973. Seismological Series, No. 72, Ottawa, Canada.

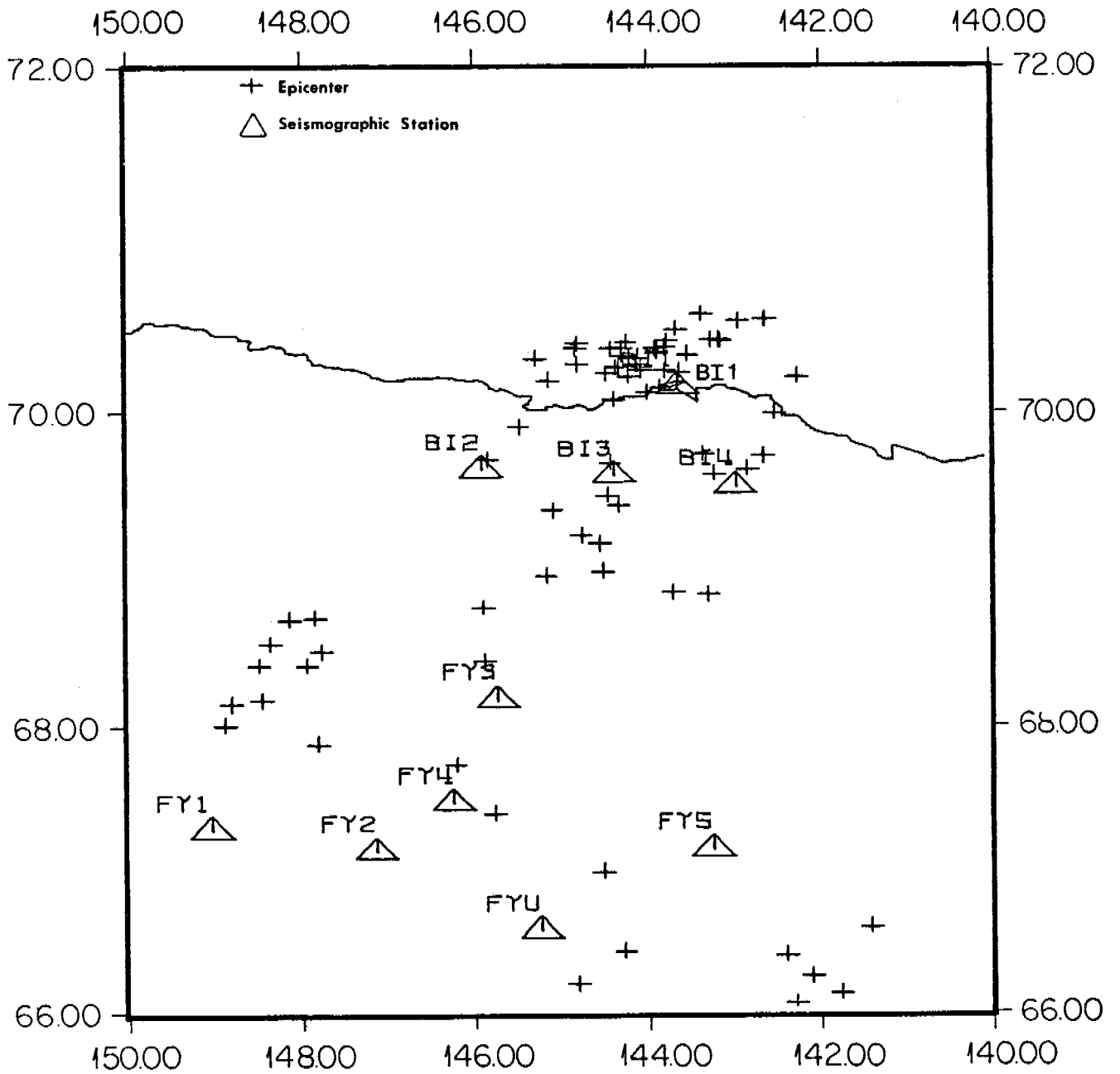

Figure 1. Map indicating locations of seismographic stations in northeast Alaska and epicenters of earthquakes (1968-1975) located by Canadian seismographic network.

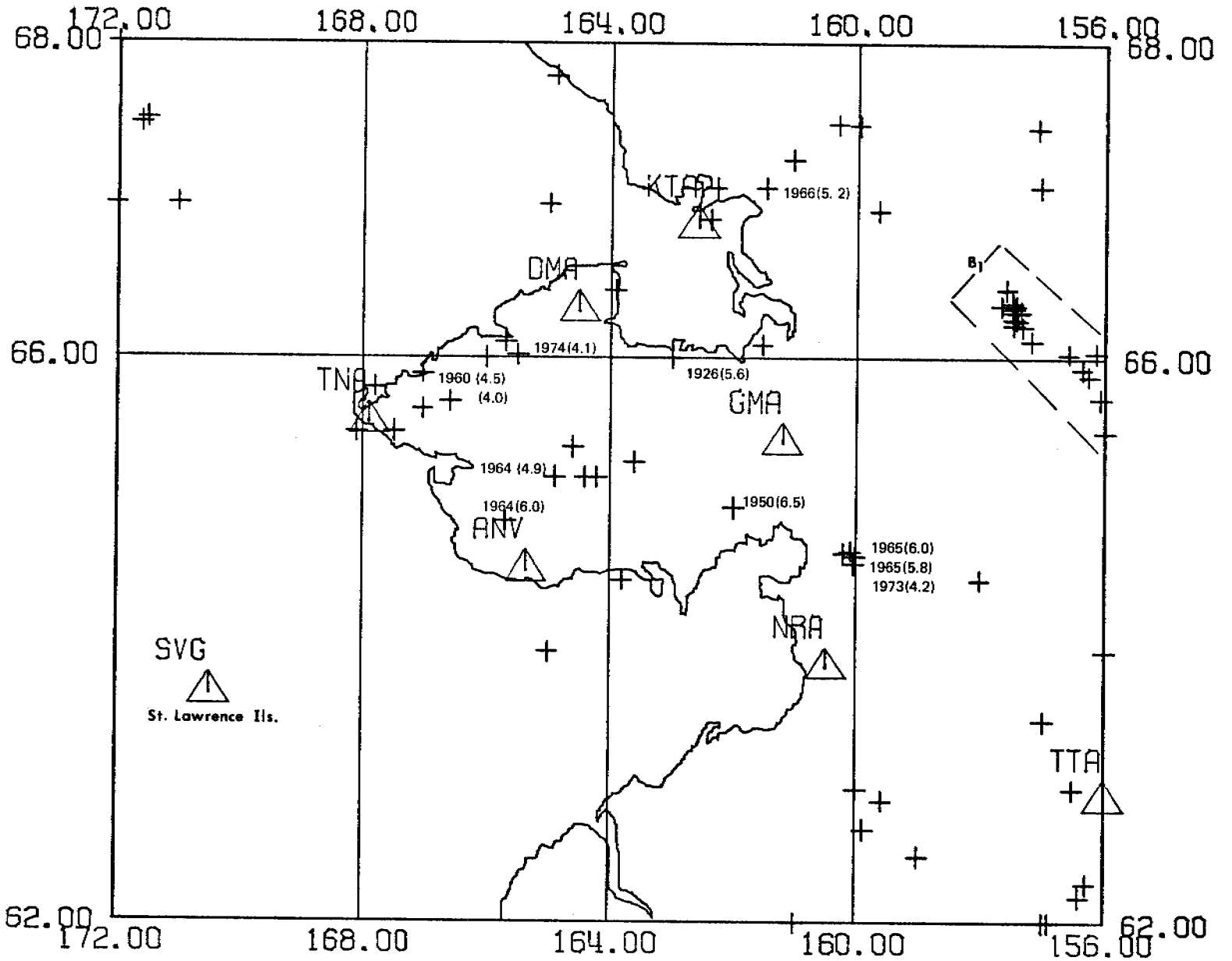

Figure 2. Map indicating locations of seismographic stations in western Alaska (hollow triangle) and epicenters of all earthquakes located prior to this study by nonlocal-seismographic networks.

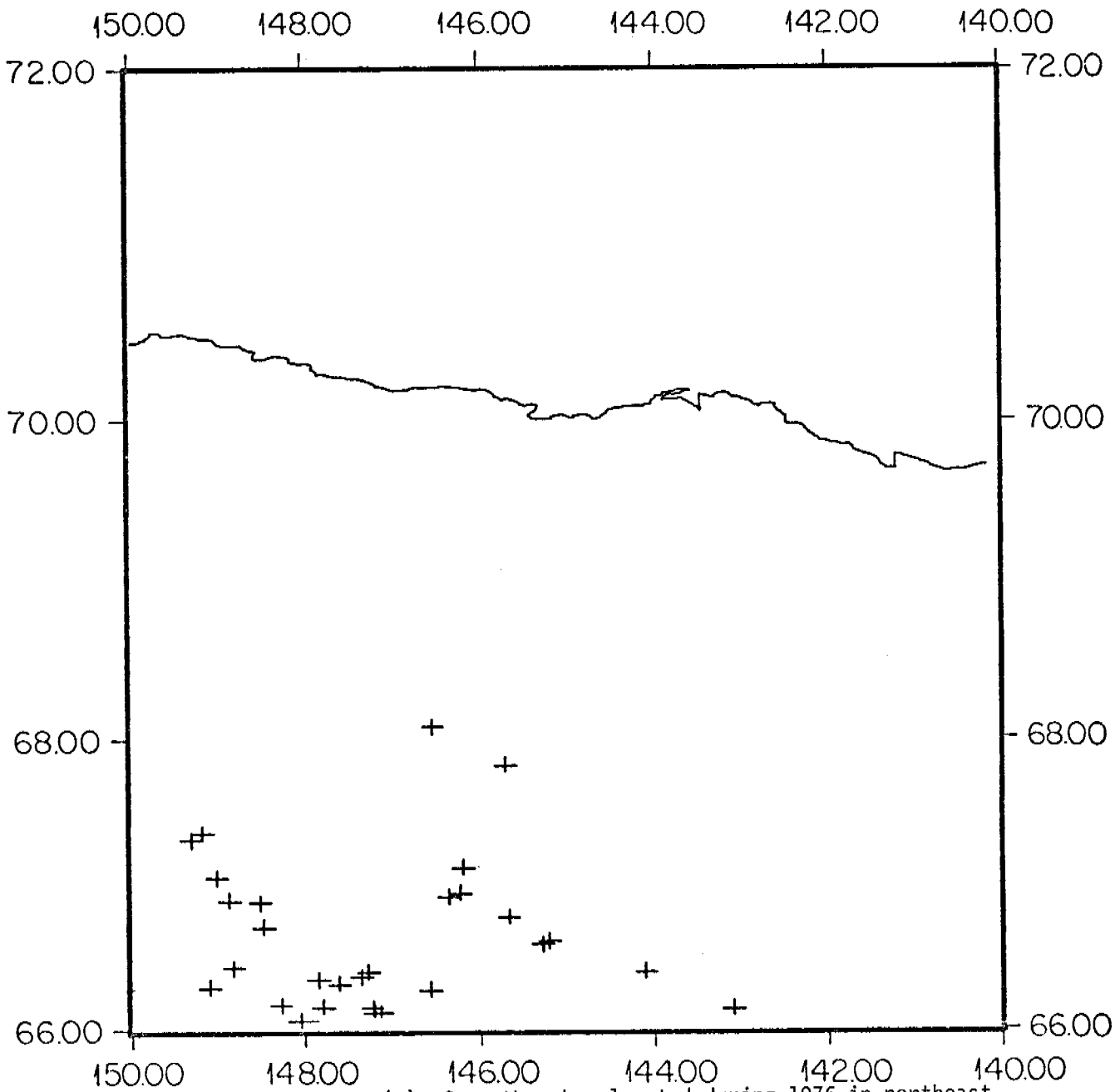

Figure 3. Epicenters (+) of earthquakes located during 1976 in northeast Alaska by the local seismographic network.

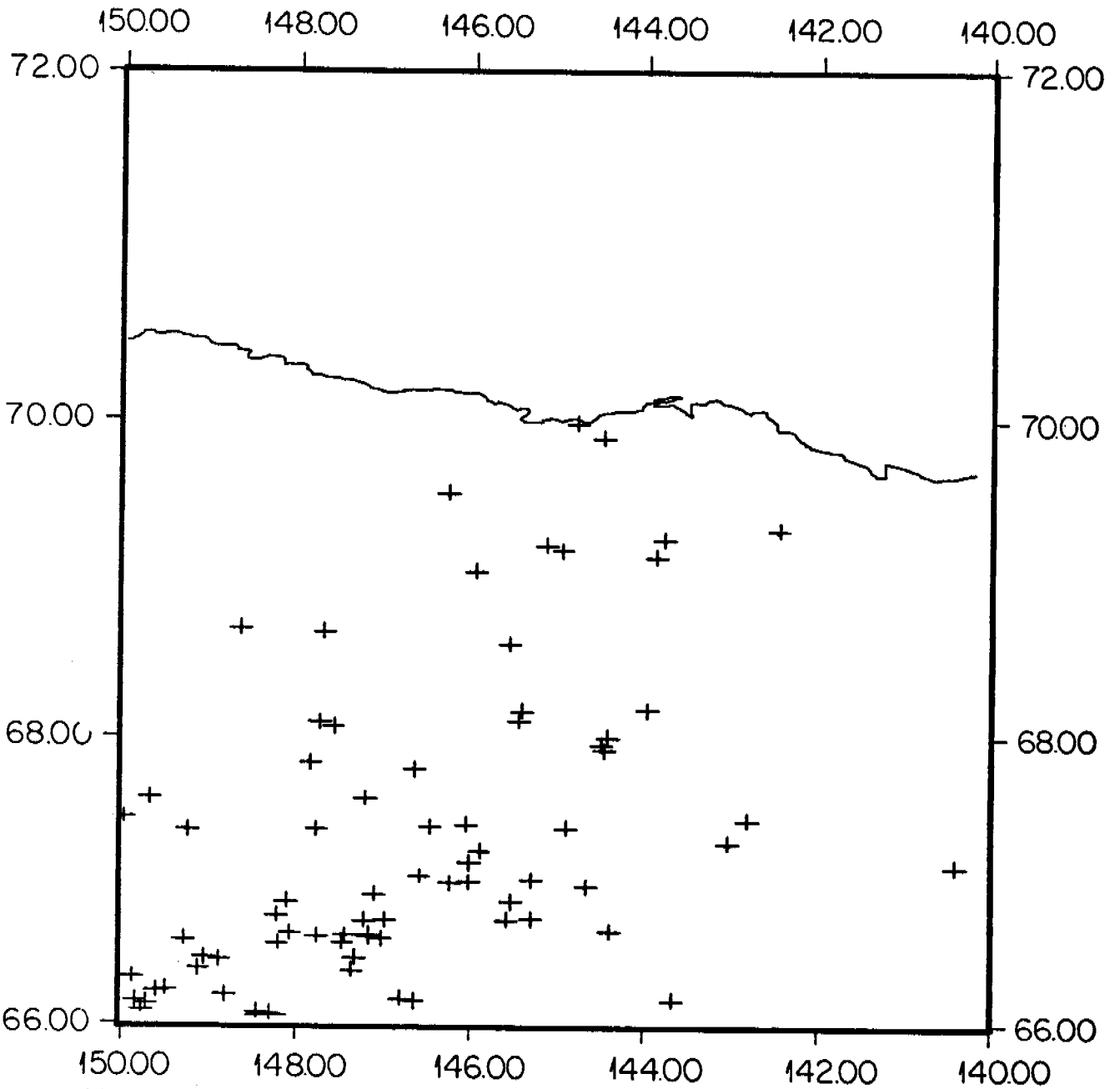

Figure 4. Epicenters (+) of earthquakes located during 1976 in northeast Alaska by the local seismographic network.

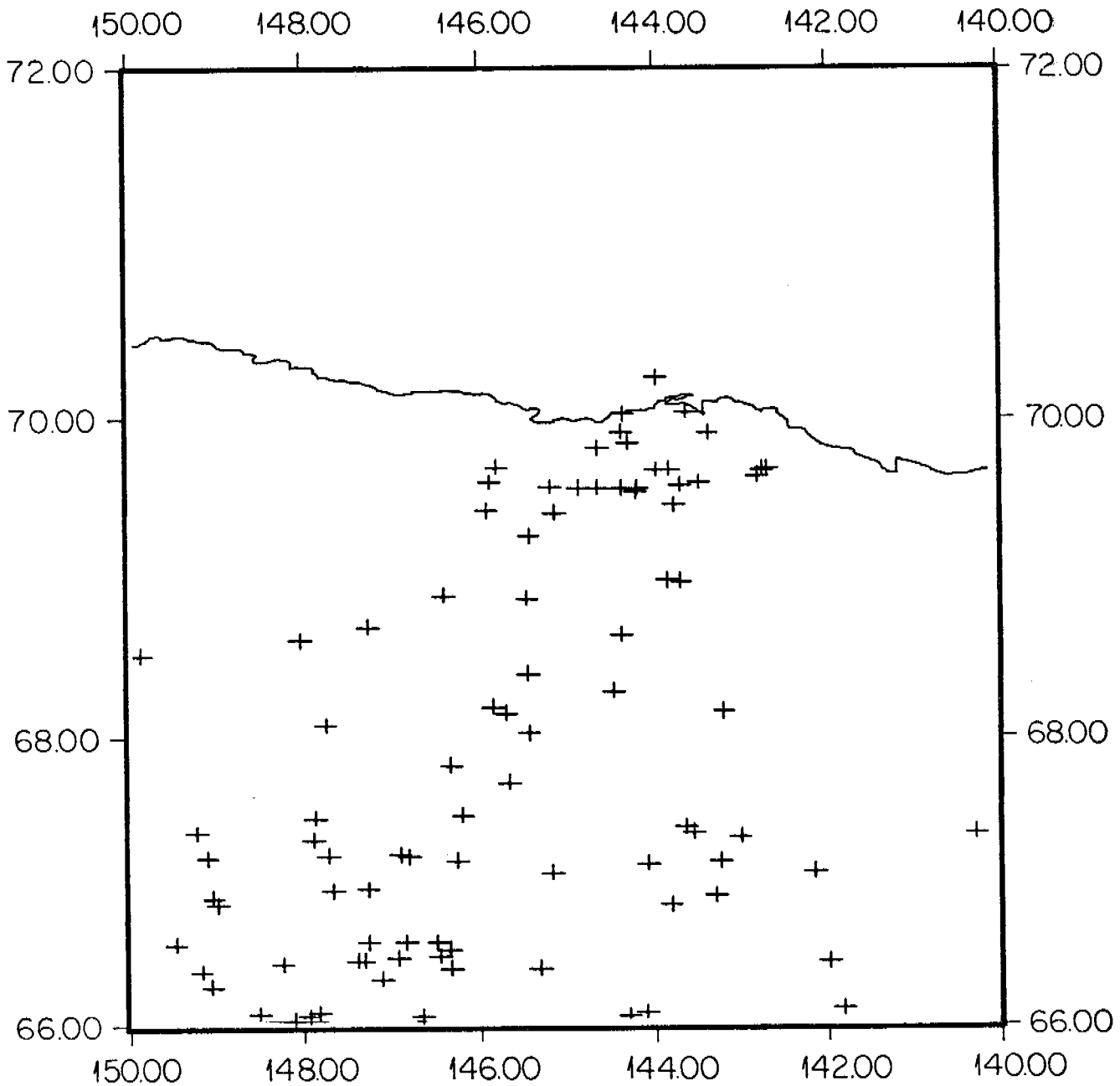

Figure 5. Epicenters (+) of earthquakes located during 1977 in northeast Alaska by the local seismographic network.

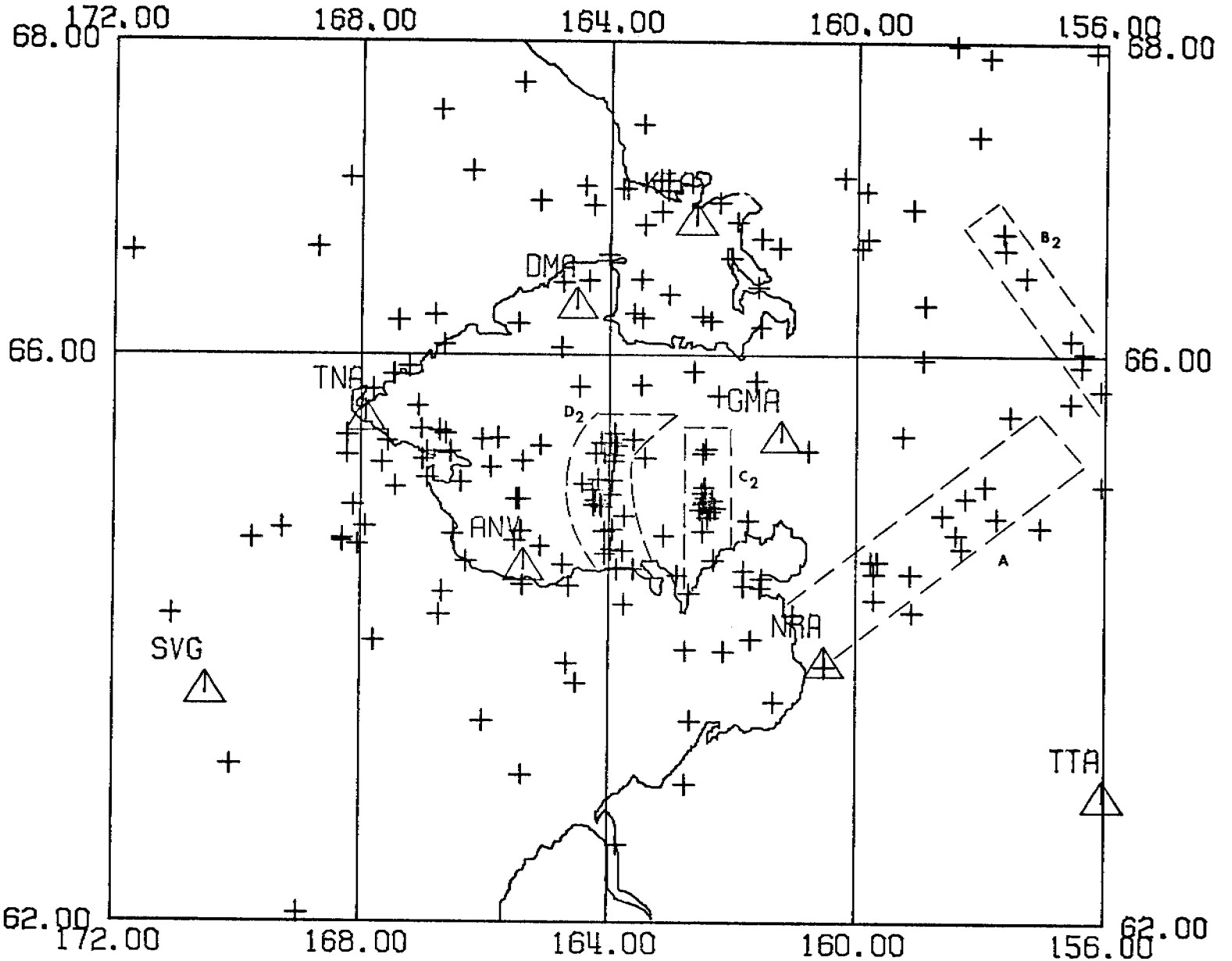

Figure 6. Epicenters (+) of earthquakes located during 1977 in western Alaska by the local seismographic network.

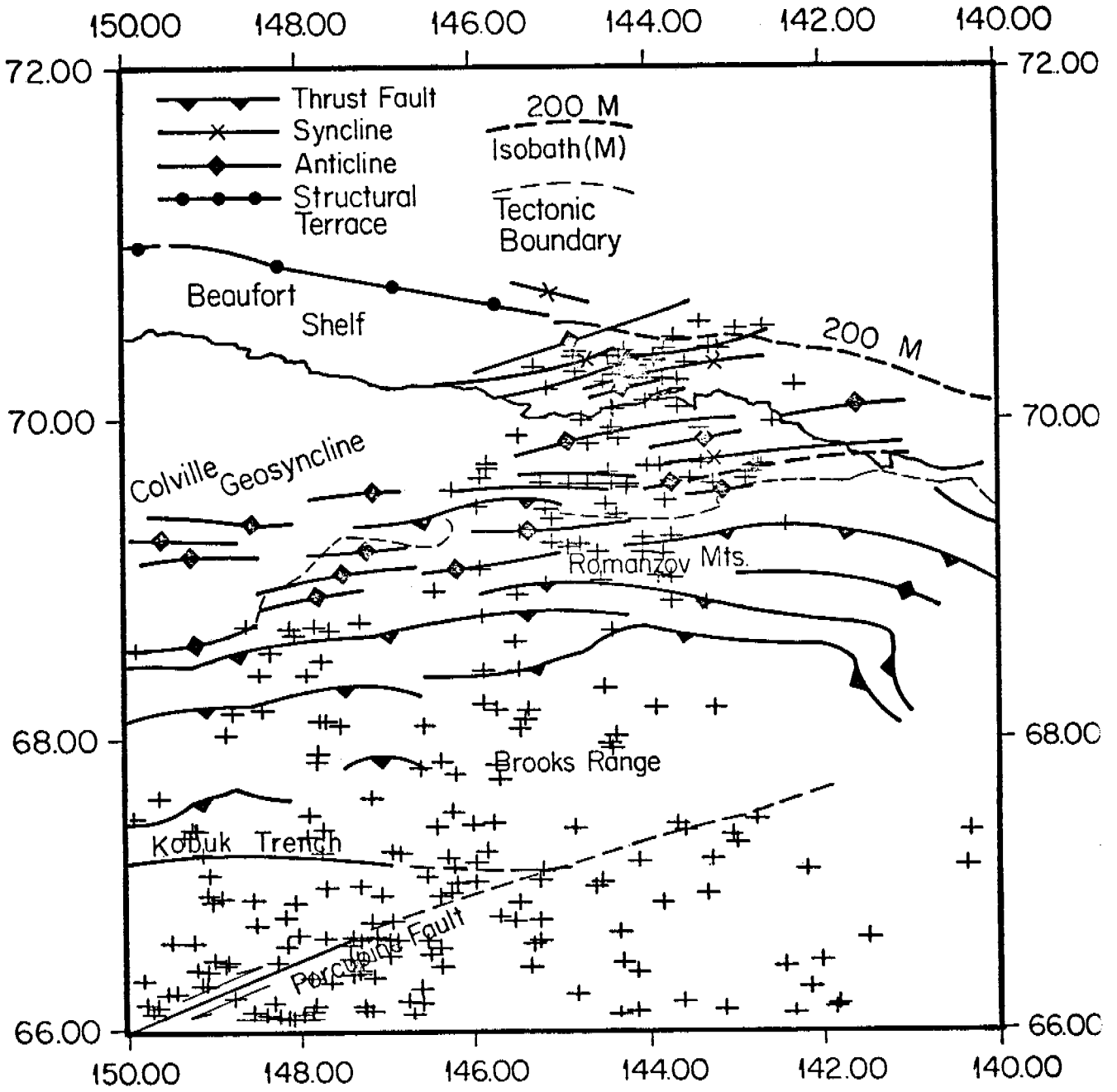

Figure 7. Epicenters (+) of earthquakes located during 1968 through 1977 plotted on an overlay of the structural traces in northeast Alaska.

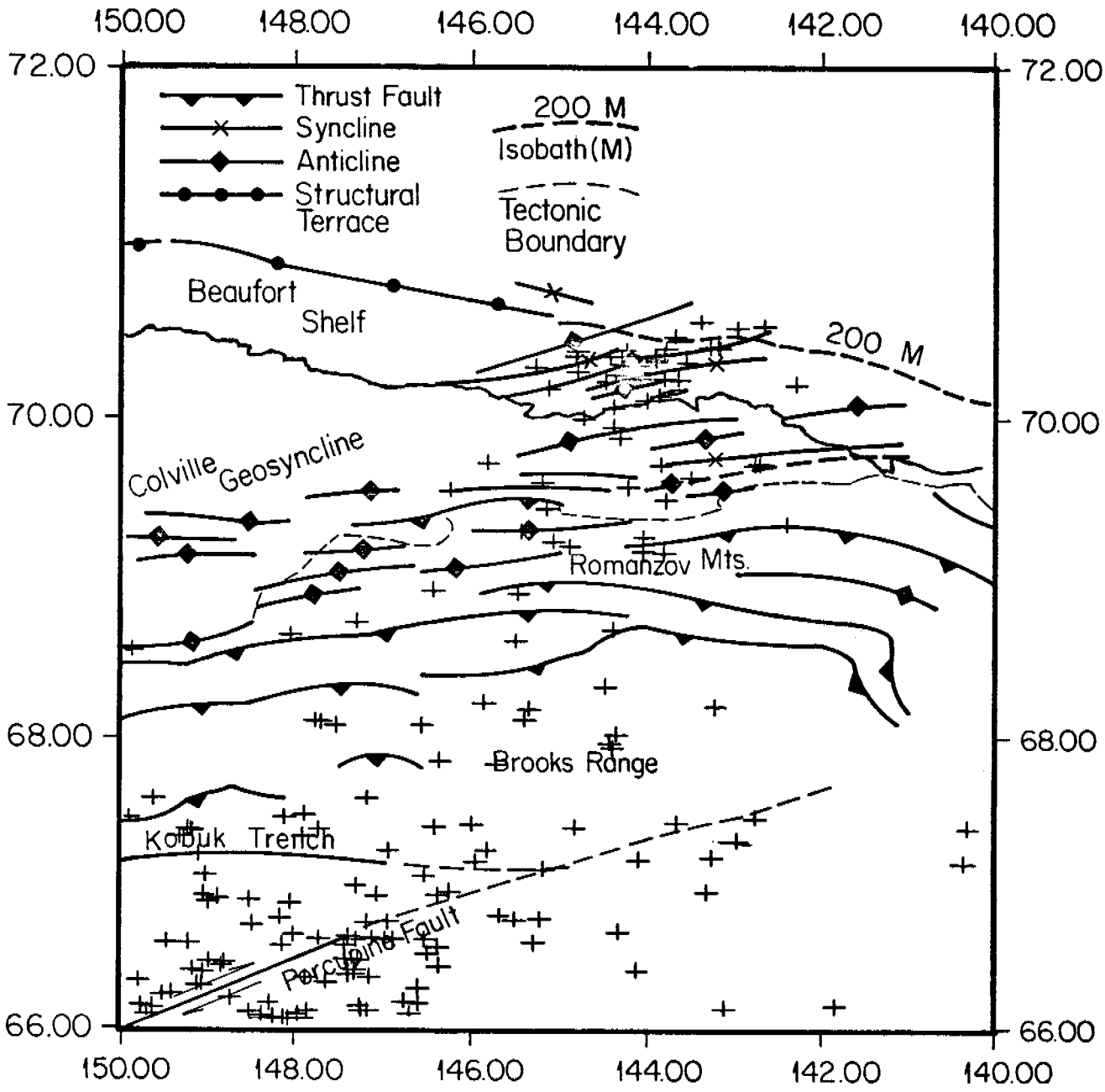

Figure 8. Epicenters (+) of earthquakes located during 1976 and 1977 by the local seismographic network having $\sigma \leq 1.5$ sec plotted on an overlay of the structural traces in northeast Alaska. The epicenters shown north of 70° N latitude are from Canadian catalog.

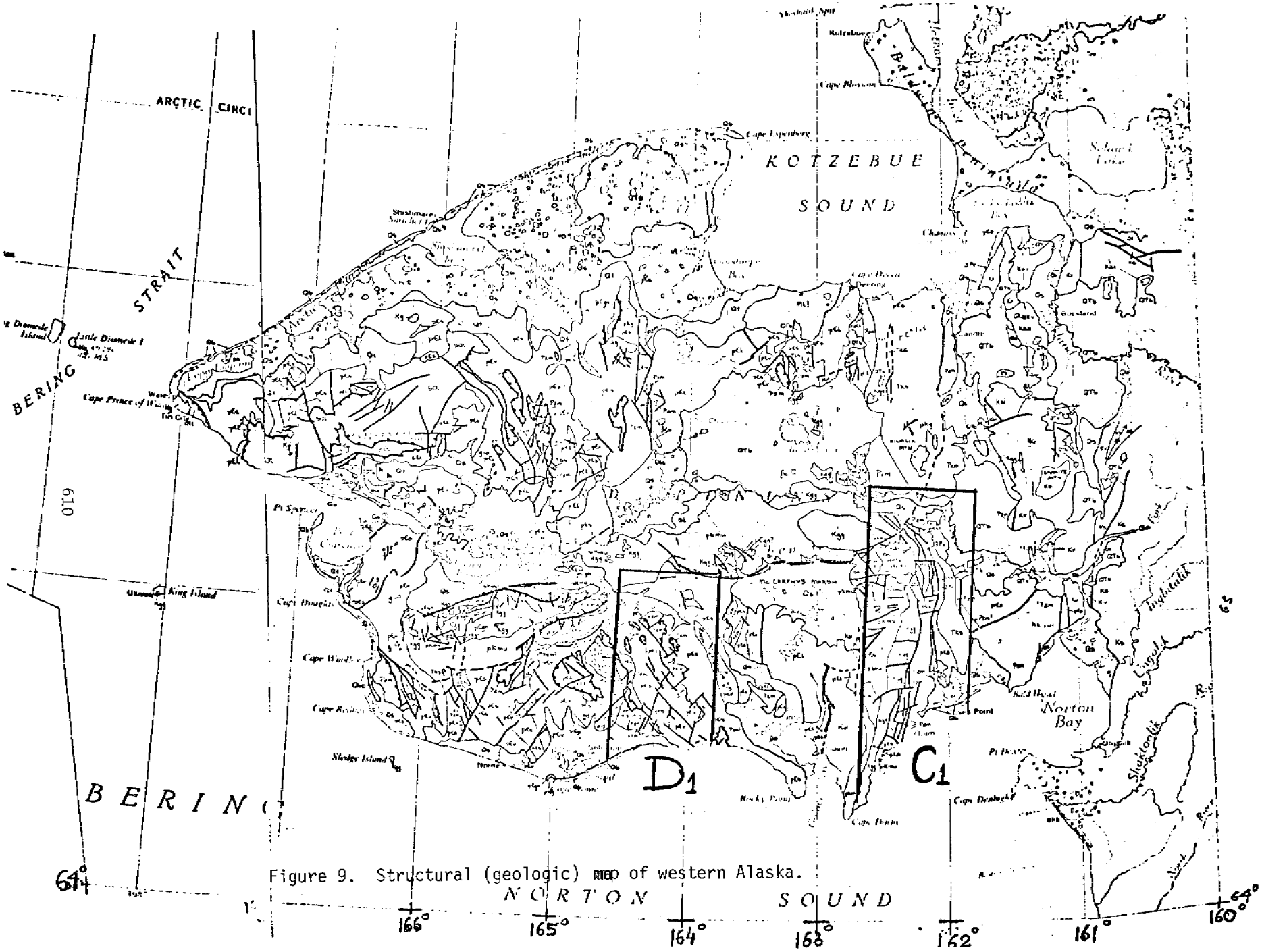

Figure 9. Structural (geologic) map of western Alaska.

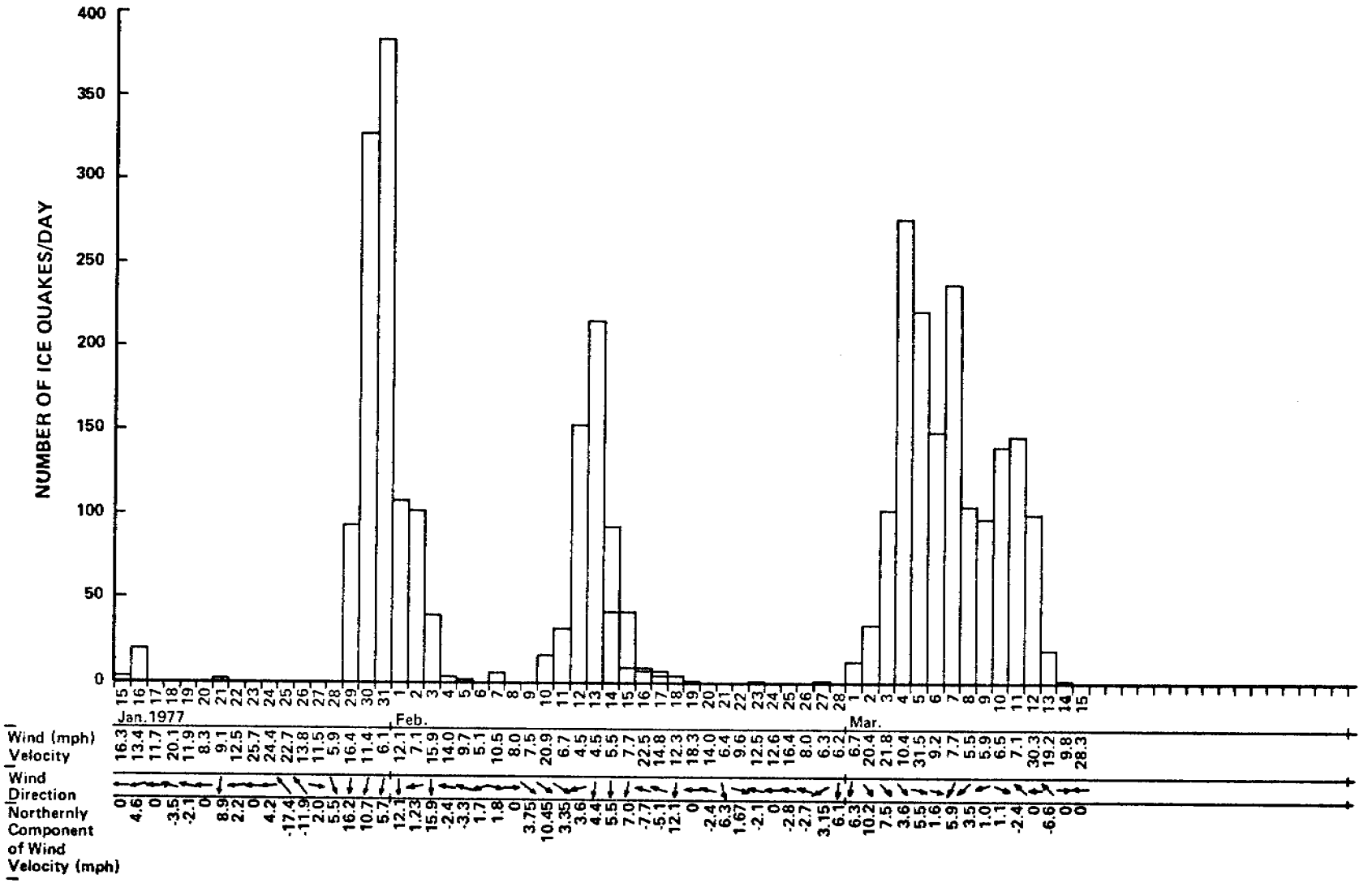

Figure 10. Number of icequakes/day (1977) versus meteorological data gathered by the Kotzebue weather station during the same period.

APPENDIX

TABLE 1

Date	Origin	Lat(N)	Lon(W)	Depth	Mag	No	Rms
680122	0949 04.5	70 31.8	142 57.6	18.0	2.9	2	1.4
680122	0951 24.2	70 12.0	142 16.8	18.0	3.8	4	0.8
680122	1404 52.1	70 21.0	143 52.8	18.0	4.3	17	2.5
680122	2344 34.1	70 24.6	143 46.2	18.0	5.3	32	2.3
680123	0013 25.0	70 13.8	143 48.0	18.0	3.2	3	0.1
680123	0031 28.3	70 34.2	143 22.8	18.0	3.3	2	0.7
680123	0223 10.1	70 12.0	144 12.6	18.0	3.2	2	0.3
680123	0235 26.3	70 22.2	143 48.0	18.0	3.6	3	1.1
680123	0236 52.3	70 03.6	144 22.8	18.0	3.6	4	1.3
680123	0800 54.1	70 18.6	144 11.4	18.0	3.6	3	0.4
680123	0830 45.1	70 24.0	144 14.4	18.0	4.1	12	1.9
680123	2057 52.1	70 21.6	144 17.4	18.0	4.3	15	2.2
680124	1053 31.4	70 10.2	145 07.2	18.0	3.7	4	2.0
680125	1656 37.4	70 21.6	144 49.2	18.0	3.6	3	1.8
680126	0456 16.3	70 28.8	143 39.6	18.0	3.6	3	1.2
680130	0928 33.2	70 15.0	144 19.2	18.0	3.8	4	1.0
680130	0930 18.0	70 15.0	144 21.0	18.0	3.5	3	0.0
680201	2047 28.2	70 19.2	144 17.4	18.0	3.4	4	0.8
680205	0407 21.3	70 19.2	144 17.4	18.0	3.9	4	1.7
680206	1636 22.1	70 21.6	143 54.6	18.0	4.5	15	2.3
680206	1842 54.2	70 23.4	144 47.8	18.0	3.9	5	1.3
680210	1729 00.1	70 20.4	143 53.4	18.0	4.3	11	2.1
680210	1729 19.2	70 13.6	143 37.8	18.0	4.3	10	3.0
680210	1736 12.5	70 15.0	144 03.6	18.0	3.5	4	2.4
680210	1739 50.4	70 32.4	142 39.0	18.0	3.9	5	2.7
680212	2105 09.2	70 16.2	144 47.4	18.0	3.6	4	0.9
680213	0059 02.2	70 25.2	143 16.2	18.0	4.1	9	2.7
680218	2114 51.4	70 18.6	144 06.6	18.0	3.2	4	2.2
680221	2158 08.2	70 18.0	145 16.2	18.0	3.7	4	1.4
680221	2306 39.3	70 19.8	143 31.8	18.0	3.3	4	1.4
680228	0619 32.4	70 06.0	143 59.4	18.0	3.3	4	2.3
680228	0836 16.2	70 24.6	143 09.6	18.0	4.1	7	2.4
680228	2257 56.4	70 07.8	143 50.4	18.0	3.3	3	1.8
680309	1355 37.1	70 16.2	144 06.0	18.0	4.2	4	0.7
680324	1625 21.2	69 12.6	144 45.0	18.0	3.5	4	1.4
680425	1033 50.1	70 12.6	144 27.6	18.0	4.4	6	0.5
680716	1802 27.0	67 51.0	147 46.2	18.0	4.5	2	0.0
681124	2209 53.3	70 16.2	144 07.8	18.0	3.7	3	1.2
681226	1054 55.1	68 59.4	144 30.0	18.0	3.6	2	0.3
690669	1524 43.2	69 24.0	144 19.2	18.0	3.4	3	0.7
691107	0610 37.2	68 40.2	148 05.4	18.0	2.6	3	0.8
691107	0622 24.3	68 40.8	147 48.6	18.0	3.0	3	1.2
691211	1154 12.2	69 43.2	143 21.6	18.0	3.0	3	0.7
691214	1459 13.2	66 58.8	144 30.0	18.0	3.6	3	0.3
691214	2240 41.2	71 53.4	148 29.4	18.0	3.5	2	0.5
700204	0921 16.2	69 40.8	145 48.6	18.0	3.6	4	1.7
700710	0335 21.1	70 21.6	144 25.2	18.0	2.9	3	0.6
700812	1221 23.3	68 45.0	145 52.2	18.0	3.5	4	2.4
700825	0319 25.2	69 09.6	144 32.4	18.0	3.2	3	1.2
700912	1334 26.2	67 22.8	145 44.4	18.0	3.2	3	1.3
710115	2147 03.1	68 50.4	143 18.0	18.0	3.7	6	1.3
710128	0506 44.1	66 35.4	141 26.4	18.0	4.2	14	2.5
710302	0032 05.3	70 13.8	144 04.2	18.0	4.3	6	2.3
710328	1918 11.2	67 49.2	161 15.0	18.0	3.8	3	0.6
710416	1346 18.5	66 07.2	141 47.4	18.0	3.4	2	2.2
710430	0210 28.2	67 42.6	146 11.4	18.0	3.0	3	1.1
710601	0834 47.3	69 40.2	144 25.2	18.0	2.9	3	1.7
710618	0154 42.4	68 27.6	147 43.8	18.0	3.1	2	1.4
710629	1452 58.0	68 07.2	148 45.0	18.0	3.4	2	0.0
710701	0158 02.1	68 30.6	148 18.6	18.0	4.3	9	2.0
710704	1301 11.0	68 22.2	148 26.4	18.0	2.8	2	0.0
710704	2117 03.6	68 08.4	148 24.6	18.0	3.7	2	1.5
710705	0310 47.2	72 15.0	149 01.2	18.0	3.6	2	0.5
710705	1149 32.0	67 58.8	148 49.2	18.0	3.0	2	0.0
710705	1253 38.0	68 22.2	147 54.0	18.0	2.5	2	0.0
720101	1127 3802	66 24.6	144 15.6	18.0	2.1	6	2.1
720118	1836 23.2	66 03.0	142 18.0	18.0	3.6	3	1.0
720416	2351 19.3	68 24.0	145 51.0	18.0	3.3	3	1.3
721123	1639 57.2	69 22.2	145 04.2	18.0	4.0	3	1.1
730206	1414 11.0	66 14.4	142 07.2	18.0	3.1	12	0.5
730406	1754 32.0	69 27.6	144 27.0	5.0	3.7	16	0.9
740321	1141 37.0	66 10.8	144 47.4	18.0	3.4	14	1.2
740331	0507 44.2	68 51.0	143 42.0	18.0	2.4	3	1.6
740515	1617 21.0	66 23.4	142 24.6	18.0	0.0	7	1.0
740521	0137 45.0	70 25.2	143 10.8	18.0	3.2	2	0.0
740720	0422 55.0	69 53.4	145 27.6	18.0	0.0	7	0.7
750329	1546 34.1	69 42.6	142 39.6	18.0	3.3	4	0.8
750330	1133 34.2	69 36.0	143 13.8	18.0	3.9	3	0.9
750331	1253 03.0	69 58.8	142 32.4	18.0	3.8	15	0.6
750808	1144 39.0	68 57.6	145 09.0	18.0	4.5	18	1.2

TABLE 2

DATE	ORIGIN	LAT (N)	LONG (W)	DEPTH	MAG	NO	GAP	DMIN	RMS	ERH
740609	9 5 30.36	66-18.90	147-21.69	10.00*	1.64	4	254	100.0	0.47	
740614	1555 8.26	66-32.23	145-17.37	10.00*	1.22	4	205	4.4	0.21	
740616	658 39.54	66-51.52	148-52.62	10.00*	2.29	5	244	165.3	0.43	6.2
740619	1843 31.06	64-38.44	149- 6.18	10.00*	1.72	4	255	7.2	0.06	
740629	714 58.50	66-16.04	147-37.65	10.00*	1.75	4	193	112.9	0.69	
740825	841 2.35	66- 6.93	148-17.09	10.00*	2.29	4	190	146.6	0.58	
740901	1844 14.26	67-16.76	149-19.20	10.00*	3.52	5	239	197.1	0.36	22.2
741022	424 24.35	67-46.53	145-42.41	10.00*	3.67	5	306	137.2	0.52	93.7
741031	546 15.82	67-19.42	149-11.72	10.00*	2.48	4	241	194.2	0.49	
741120	158 54.36	66-14.65	149- 6.90	10.00*		7	174	161.2	0.10	1.2
741204	1254 23.64	67- 1.29	149- 1.75	10.00*	2.75	4	278	232.7	0.05	
741208	553 31.01	65-59.14	149-48.05	10.00*	2.39	4	265	126.8	1.03	
741224	158 0.43	66-13.30	146-35.31	10.00*	1.82	4	221	72.3	0.33	
741226	533 15.52	66-52.48	146-22.22	10.00*	2.05	4	290	62.1	0.62	
750104	444 27.02	65-59.04	146-54.58	10.00*	2.30	5	197	99.8	0.65	36.5
750109	2313 25.06	66- 3.42	147- 8.84	10.00*	2.06	4	222	103.5	0.52	
750111	1554 15.61	66- 3.84	147-13.42	10.00*	2.29	4	225	106.0	0.62	
750209	355 13.06	64-44.21	147- 2.86	10.00*	0.42	4	187	0.2	1.68	
750211	1824 54.85	66-50.41	148-31.18	10.00*	2.82	4	241	149.5	0.43	
750211	2250 56.28	66-33.73	145-12.70	10.00*	2.70	4	257	0.2	1.87	
750212	1515 9.28	66-54.33	146-14.19	10.00*	1.84	4	292	59.5	0.23	
750219	1417 7.62	66- 0.09	148- 3.91	10.00*	1.95	4	179	117.3	0.52	
750228	1541 6.83	66-20.60	144- 5.81	10.00*	2.10	4	281	55.2	0.55	
750309	355 55.69	66-43.95	145-40.75	10.00*	2.72	4	234	28.3	0.82	
750323	1451 21.40	66-17.47	147-51.77	10.00*	1.86	4	254	122.3	0.27	
750329	1439 33.94	69- 9.82	144- 2.19	10.00*	3.72	8	315	294.5	0.16	26.3
750329	1547 16.94	67- 4.66	146-12.18	10.00*	2.96	5	271	72.3	1.56	5.2
750503	1048 48.64	68- 2.39	146-32.32	10.00*	2.09	6	303	174.6	0.97	322.9
750511	439 24.25	64-48.16	147-31.90	10.00*	0.44	3	158	20.4	0.00	
750528	228 37.98	66-40.17	148-28.91	10.00*	2.03	5	201	145.6	1.38	35.9
750630	037 46.10	66- 5.52	147-14.72	10.00*	1.68	4	237	105.2	0.74	
751201	1533 50.29	66- 4.61	143- 5.70	10.00*	3.10	6	265	109.2	0.35	10.4
751201	2148 42.91	66-23.10	148-50.13	10.00*		5	255	169.4	0.58	111.4
751231	1721 48.91	66-20.84	147-17.34	10.00*	2.59	5	195	95.6	0.73	140.2

TABLE 3

DATE	ORIGIN	LAT(N)	LONG(W)	DEPTH	MAG	NO	GAP	DMIN	RMS	ERH
760110	1310 33.05	66-30.59	146-21.63	10.00*	2.61	4	203	51.5	0.26	
760115	712 30.93	66-33.73	146-30.15	10.00*	1.45	5	190	57.3	1.36	40.7
760118	1521 40.84	67- 9.60	149- 6.28	10.00*	2.15	6	232	183.2	1.36	34.9
760120	226 44.51	66-52.73	149- 2.06	10.00*	3.01	6	215	172.6	0.64	29.2
760121	738 11.90	66- 0.63	148- 7.03	10.00*	2.15	5	180	119.0	0.23	4.8
760125	2223 44.21	65-50.30	147-40.66	10.00*	2.37	8	162	95.8	1.97	13.7
760131	855 16.73	66-56.62	147-17.04	10.00*	3.03	6	224	100.7	0.37	14.7
760207	2329 4.41	66- 3.37	147-50.26	10.00*	2.32	4	281	121.0	0.07	
760210	1614 24.90	67- 8.64	146-16.39	10.00*	3.20	3	274	80.0	1.54	
760214	1319 41.37	67-25.99	147-52.83	10.00*	2.72	4	273	151.8	0.51	
760214	2357 7.34	67-47.93	146-20.32	10.00*	3.28	4	299	146.5	0.47	
760216	17 3 1.36	66-55.96	147-40.71	10.00*	2.05	6	221	116.6	1.54	34.1
760217	2317 26.45	66- 2.80	148-31.18	10.00*		5	188	129.2	0.23	5.0
760225	1815 36.74	65-33.43	142-11.35	10.00*	3.64	6	268	176.6	0.40	64.5
760308	721 50.72	67- 3.57	145-10.90	10.00*	2.90	3	249	62.4	0.50	
760309	148 7.54	67-19.84	149-13.65	10.00*	2.84	5	242	195.8	0.19	79.9
760309	1154 52.83	67-10.85	146-55.09	10.00*	2.53	5	245	101.9	0.36	134.6
760317	2337 3.02	66- 2.06	144-17.99	10.00*		6	204	71.5	1.82	31.1
760318	0 1 6.95	66- 5.63	141-49.57	10.00*		5	281	160.5	0.94	6.2
760322	540 7.79	66-32.61	149-28.22	10.00*	2.48	5	232	181.6	1.31	8.8
760403	6 6 12.23	66-33.73	147-16.96	10.00*	2.73	6	191	91.9	0.70	20.7
760411	2030 24.62	65-36.18	144-53.09	10.00*	3.55	5	199	107.8	0.59	82.8
760412	723 59.56	69-42.89	145-48.56	10.00*	0.70	4	267	10.6	0.16	
760413	745 15.20	66-17.92	147- 8.03	10.00*	2.24	4	189	90.8	0.37	
760426	1255 47.03	66-14.72	149- 3.28	10.00*	2.41	4	209	159.9	0.66	
760427	2221 19.12	66-49.80	148-59.52	10.00*	2.83	5	212	169.7	0.42	0.1
760430	622 35.00	68-53.95	145-27.73	10.00*	2.75	5	134	82.6	0.85	10.9
760505	023 30.65	67-20.24	140-17.21	10.00*		4	273	232.4	1.28	
760505	223 10.41	68- 4.33	147-45.37	10.00*	3.33	4	218	201.1	1.03	
760506	224 41.59	68-39.72	144-22.36	10.00*	3.16	4	162	103.2	0.58	
760507	539 19.78	66-26.92	146-56.66	10.00*	3.08	6	179	78.2	1.70	245.9
760508	610 33.83	67-17.14	147-53.62	10.00*	3.00	5	171	142.7	0.03	0.1
760509	1249 50.29	66-33.73	146-51.65	10.00*	1.70	3	262	73.2	0.56	
760513	1832 50.08	69-36.59	143-42.20	10.00*	0.94	4	205	26.1	0.02	
760519	1624 36.15	69-29.13	143-46.75	10.00*	0.85	6	198	25.8	0.10	14.9
760527	743 6.56	67- 7.48	144- 5.22	10.00*	2.75	5	202	80.0	0.89	17.9
760530	16 1 55.32	69-37.54	143-29.41	10.00*	0.87	4	218	23.1	0.02	
760602	1551 16.80	67- 4.06	142- 9.00	10.00*	2.25	5	233	146.0	1.77	63.7
760602	2122 58.11	67-18.36	143- 1.01	10.00*	3.55	4	230	127.1	2.04	
760608	1936 38.37	66-21.15	149-10.66	10.00*	2.85	5	217	173.0	0.65	16.3
760613	23 0 28.61	66- 2.26	146-40.64	10.00*	3.55	6	158	87.9	0.79	27.6
760616	1727 30.79	65-58.23	149- 2.52	10.00*	2.65	4	266	133.7	0.73	
760621	837 35.79	69-42.58	142-41.83	10.00*	2.53	4	234	23.8	0.02	
760623	1156 0.35	69-42.40	142-45.16	10.00*	2.75	4	232	22.6	0.04	
760623	16 2 35.62	66-56.08	136-27.52	10.00*		6	293	388.7	0.31	9.9
760624	1243 38.82	66-27.85	146-28.42	10.00*		7	112	57.3	1.46	15.5
760624	1318 28.07	66-22.75	146-20.35	10.00*	3.05	6	164	54.2	0.25	7.4
760628	212 41.72	66- 2.12	147-57.49	10.00*		5	154	136.5	0.41	9.0
760702	013 5.07	67- 8.42	143-15.07	10.00*	2.00	4	202	0.2	0.34	
760722	1940 6.18	67-22.45	143-39.22	10.00*	2.20	4	191	31.5	0.15	
760728	856 9.47	69-33.87	144-12.86	10.00*	1.72	4	196	6.6	0.19	
760809	16 0 0.	69-56.69	144-22.36	10.00*	1.94	6	233	34.9	0.	0.0
760811	1632 29.13	70- 3.07	144-21.72	10.00*	2.18	4	318	51.8	1.98	
760819	1130 44.82	68-42.80	147-16.36	10.00*	3.73	9	206	90.4	0.51	6.5
760823	9 9 4.30	66-25.88	147-24.47	10.00*	2.84	7	136	78.5	0.36	3.3
760826	313 48.79	69-42.33	143-49.78	10.00*	1.31	5	131	24.9	1.06	4.7
760829	1916 4.80	68- 9.82	143-12.22	10.00*	2.35	6	178	103.5	0.61	11.4
760923	2245 30.59	68-11.29	145-51.23	10.00*	2.21	8	155	7.8	0.42	4.3
761004	4 1 25.76	67-40.91	145-39.94	10.00*	3.59	6	122	34.4	2.24	23.1
761022	1613 37.59	68-17.40	144-27.95	10.00*	2.22	6	135	118.6	0.78	11.8
761030	14 2 50.76	69-35.76	145-11.67	10.00*	1.82	4	181	27.4	0.11	
761105	9 4 51.73	69-17.41	145-26.50	10.00*	2.05	4	259	41.2	0.28	
761125	2244 44.00	68-37.59	148- 2.73	10.00*	2.79	5	231	140.5	0.10	4.6
761206	1357 18.87	66-24.47	148-15.00	10.00*	3.38	6	198	94.7	2.42	44.7
761207	17 8 10.42	69-25.86	145- 8.54	10.00*	2.09	5	131	34.8	1.25	42.5
761226	256 25.96	66-53.76	143-17.76	10.00*	2.23	5	255	92.4	0.34	24.4
761227	0 0 56.67	66-25.93	147-20.33	10.00*	2.71	5	191	95.8	0.46	54.4
761228	643 23.09	69-52.33	144-18.07	10.00*	1.84	4	299	32.0	1.13	
761230	18 6 36.61	68-55.11	146-24.73	10.00*	2.61	6	186	81.3	0.85	14.3

TABLE 4

DATE	ORIGIN	LAT (N)	LONG (W)	DEPTH	MAG	NO	GAP	DMIN	RMS	ERH
770111	957 10.15	66- 7.88	143-34.11	10.00*		5	272	87.8	3.64	44.7
770112	615 37.13	65-51.25	142-48.87	10.00*		6	235	133.6	2.31	72.1
770119	839 15.25	69- 9.45	143-47.79	10.00*		5	176	51.7	0.25	3.5
770208	724 11.70	69-11.56	144-52.79	10.00*	2.40	4	171	48.3	0.53	
770210	7 8 11.08	69-59.51	144-43.78	10.00*	2.08	4	295	47.3	0.10	
770217	2053 45.63	66-49.39	148- 2.79	10.00*	2.86	7	218	53.3	1.07	12.7
770301	14 4 34.30	65-59.37	148-27.61	10.00*	3.19	6	144	122.2	2.65	21.1
770311	3 6 36.16	67-11.29	145-49.46	10.00*	3.32	6	172	255.4	0.58	31.7
770313	556 13.88	69-13.65	145- 4.39	10.00*	2.54	5	157	48.6	0.69	12.6
770320	17 5 23.93	65- 4.79	149- 2.05	10.00*	2.43	4	179	60.3	0.01	
770326	2028 1.55	69-54.16	144-25.13	10.00*	2.24	4	296	35.3	1.56	
770406	250 59.33	68- 2.20	147-31.15	10.00*	2.54	5	231	76.8	0.46	3.1
770422	1748 9.01	67-44.93	146-34.83	10.00*	2.90	8	125	36.5	2.21	17.4
770424	245 26.43	66-35.80	147-59.79	10.00*	2.81	5	238	70.8	1.16	23.1
770424	334 0.91	66-59.27	145-12.70	10.00*	2.06	5	162	47.7	2.23	9.3
770424	7 2 18.31	66-42.39	145-12.70	10.00*	2.42	7	163	16.3	1.00	47.6
770501	128 10.94	66-42.27	145-30.41	10.00*	2.21	6	199	20.8	0.44	38.8
770518	1 0 16.11	69-16.04	143-42.53	10.00*	2.39	9	130	40.2	2.47	91.1
770525	1811 16.07	63-42.35	149-40.07	10.00*	3.19	12	145	36.4	1.46	6.0
770604	1956 11.14	66-25.50	147-15.14	10.00*	2.35	6	134	78.3	0.55	8.3
770607	1523 27.23	66-26.21	152-35.89	10.00*	2.95	6	190	63.5	0.31	10.4
770607	21 1 59.49	64-33.08	143-42.23	10.00*	2.62	4	239	157.1	0.46	
770617	827 23.50	65-25.47	147-38.31	10.00*	4.20	9	298	168.0	1.77	70.2
770618	1117 55.34	66-57.74	146- 9.46	10.00*	1.78	6	91	44.8	2.55	13.4
770624	17 4 55.16	67-15.09	142-57.02	10.00*	2.05	5	307	18.0	0.96	241.3
770625	2232 12.70	67-47.61	147-46.58	10.00*	3.20	9	171	76.7	3.14	25.2
770701	2017 56.02	67-19.25	149-10.54	10.00*	1.15	3	319	10.7	0.07	
770707	754 36.99	66-24.34	148-47.93	10.00*	2.14	8	127	96.3	0.30	1.8
770709	359 17.07	66-35.20	147-21.60	10.00*	2.51	4	225	61.1	0.16	
770709	1925 39.37	66- 8.73	148-44.00	10.00*	2.77	9	119	125.5	0.39	2.6
770712	325 9.83	66-10.48	149-31.35	10.00*	2.37	7	144	124.2	0.77	5.8
770712	318 10.27	66-11.13	149-24.61	10.00*	2.90	6	210	122.1	0.71	15.3
770712	1522 53.87	66-34.37	147- 5.93	10.00*	2.09	4	222	61.5	0.17	
770713	432 26.51	67-24.57	149-53.63	10.00*	2.70	5	260	42.9	0.12	6.8
770729	727 54.94	68- 8.93	145-20.70	10.00*	2.38	7	123	14.8	0.73	8.0
770729	1538 32.52	67- 6.33	145-56.73	10.00*		6	120	40.4	0.37	2.1
770729	1553 16.25	67- 6.50	145-56.33	10.00*	1.50	6	120	40.2	0.19	1.7
770802	16 2 44.37	67-58.86	144-20.68	10.00*	2.83	8	136	59.4	0.09	0.6
770804	1150 34.90	66- 1.86	148-22.31	10.00*	2.70	8	107	125.0	0.81	6.1
770806	053 28.91	69-20.02	142-23.84	10.00*	2.95	6	249	30.9	0.14	14.7
770807	12 2 29.23	66-16.43	149-47.73	10.00*	2.34	5	282	149.1	0.63	68.2
770825	1851 37.24	67- 0.72	146-31.05	10.00*	2.41	8	79	28.1	0.31	2.0
770825	2233 0.76	67-20.01	147-42.28	10.00*	1.99	4	229	35.1	0.53	
770826	1022 49.74	66-31.29	148- 8.36	10.00*	2.12	5	156	81.4	0.15	3.5
770828	638 25.73	66-33.59	146-57.24	10.00*	2.18	6	117	63.3	0.75	42.2
770829	11 8 49.59	68-35.15	145-28.96	10.00*	2.58	8	157	49.7	0.60	6.8
770831	230 26.02	66- 5.15	149-37.47	10.00*	2.15	4	271	140.0	0.51	
770903	319 6.06	67- 6.03	140-19.55	10.00*	3.07	5	276	223.1	0.50	49.0
770906	1149 33.69	67-20.91	144-48.54	10.00*	2.17	4	214	61.2	0.38	
770909	242 29.61	68-39.64	147-37.87	10.00*	3.18	9	204	97.9	2.84	40.8
770909	16 0 1.83	66-49.71	145-27.18	10.00*	2.73	8	127	31.8	1.64	11.2
770910	1729 52.25	67-22.30	145-59.14	10.00*	1.97	6	94	13.2	0.12	1.3
770916	20 0 5.09	66-56.41	144-34.44	10.00*	1.67	6	144	50.8	2.57	16.5
770916	2118 58.60	68-40.80	148-34.92	10.00*	3.02	9	224	132.5	2.59	40.7
770917	1827 27.10	64-57.60	148-37.61	10.00*	4.07	9	311	237.3	0.88	73.5
'17	2125 26.67	65- 9.78	147-11.28	10.00*	3.78	8	302	180.0	0.39	28.3
770919	839 40.60	66- 6.33	149-44.96	10.00*	2.40	4	272	137.2	0.57	
770919	9 0 20.18	66-58.46	145-56.91	10.00*	2.14	5	139	52.8	2.65	37.5
770919	2035 40.51	67-24.84	142-44.50	10.00*	2.33	6	272	37.7	1.25	70.9
771007	630 34.91	67-32.70	149-36.69	10.00*	2.69	6	273	41.5	0.79	46.2
771007	2045 42.51	66-19.84	147-17.20	10.00*	2.28	4	172	88.9	0.08	
771009	1115 43.94	66- 1.14	148-13.64	10.00*	2.42	9	95	121.4	0.85	6.2
771013	22 2 54.64	66-35.50	147- 5.93	10.00*	2.30	5	166	59.4	2.26	38.7
771020	1058 9.81	65-58.67	147-57.44	10.00*	2.35	6	104	113.5	0.22	2.4
771027	2154 38.89	64-45.65	147-50.45	10.00*	0.94	4	113	16.2	2.06	
771028	1450 33.99	64-44.40	147-51.14	10.00*	1.04	4	121	16.9	2.04	
771029	213 9.55	64-59.34	148- 3.04	10.00*	0.94	4	257	18.7	2.11	
771029	2124 9.94	64-52.36	147-46.51	10.00*	0.90	4	161	18.3	1.72	
771030	1053 33.68	66-37.41	144-18.39	10.00*	2.05	5	221	40.7	0.56	22.3
771031	312 14.27	67-32.93	147- 8.66	10.00*	2.36	5	217	41.3	0.60	1.5
771102	455 57.04	66-32.00	147-23.67	10.00*	2.55	10	87	67.2	1.13	6.0
771102	15 0 33.71	68- 9.69	143-53.09	10.00*	1.86	4	184	125.9	2.80	
771104	2320 15.27	67-23.92	155-27.52	10.00*	3.23	7	220	167.9	0.53	9.7
771105	040 42.48	66-20.52	150-16.10	10.00*	2.50	6	239	117.9	0.64	26.6
771106	2049 38.54	67-55.60	144-24.92	10.00*	2.88	7	132	59.1	0.89	7.2
771106	2145 50.07	67-53.34	144-22.27	10.00*	3.00	9	133	91.8	1.25	11.0
771109	712 51.11	66-32.74	149-12.35	10.00*	2.24	6	192	145.3	0.83	3.8
771109	729 46.35	66-25.13	148-58.27	10.00*	2.82	10	100	94.6	0.67	4.7
771115	141 45.80	66-41.61	147- 9.14	10.00*	2.35	4	126	87.4	0.44	
771116	1445 31.00	68- 4.94	145-22.96	10.00*	3.22	7	239	15.1	0.48	7.8
771117	554 37.53	66- 5.86	150-50.60	10.00*	3.12	8	124	105.8	0.46	3.7
771120	1854 27.52	64-36.76	149- 7.82	10.00*	4.08	7	322	282.6	0.61	130.6
771122	712 44.90	69- 3.41	145-53.67	10.00*	2.35	4	176	63.2	2.40	
771203	1734 42.94	66-34.59	147-41.39	10.00*	2.32	5	142	95.2	1.07	9.3
771205	1858 22.77	66-41.87	146-54.90	10.00*	2.14	4	190	77.1	0.60	
771210	2318 2.60	68- 4.23	147-40.83	10.00*	2.94	6	171	105.0	0.47	29.9
771215	254 30.26	66- 2.30	149-40.87	10.00*	2.61	7	163	152.8	1.31	9.6
771217	719 19.83	67-21.22	146-23.77	10.00*	2.40	4	125	39.7	0.63	
771217	719 59.40	66-52.95	147- 2.37	10.00*	2.69	3	183	27.1	0.06	
771218	715 9.46	66- 6.78	146-34.30	10.00*	2.46	5	146	78.9	0.28	22.1
771226	1313 35.61	69-33.07	146-13.25	10.00*	1.89	4	325	15.1	0.58	
771226	1643 9.73	66-20.22	149- 2.06	10.00*	2.14	5	237	168.4	0.68	7.9
771227	13 7 32.33	66- 7.81	146-43.82	10.00*	2.36	5	139	83.4	0.39	7.1
771231	826 20.54	66-43.59	148- 9.25	10.00*	2.34	3	231	70.0	0.04	

TABLE 5

DATE	ORIGIN	LAT (N)	LONG (W)	DEPTH	MAG	NO	GAP	DMIN	RMS	ERH
770115	012 44.96	68-22.30	158-51.96	10.00*	3.84	5	334	232.8	0.31	
770118	1328 5.49	66-55.23	162-16.90	10.00*	1.77	4	283	16.4	0.60	
770228	2120 18.27	65-57.59	155-55.31	10.00*	3.25	8	187	102.6	1.24	20.6
770226	1953 54.76	67- 8.99	160-25.08	10.00*	2.58	4	300	101.3	0.76	
770224	1928 1.44	64-47.33	167-50.57	10.00*	3.43	7	300	120.7	0.86	60.0
770212	2050 3.61	67-45.96	165-20.46	10.00*	2.92	6	311	155.8	1.29	349.8
770207	533 54.59	65- 1.36	162-28.79	10.00*	2.41	6	163	73.9	0.16	2.3
770205	2233 58.40	66-21.90	161-57.24	10.00*	2.61	4	191	61.4	0.28	
770302	1110 8.96	63-11.21	165-22.30	10.00*	3.75	7	288	153.1	2.68	82.7
770311	212 46.09	67- 6.91	160- 2.02	10.00*	2.64	6	301	116.2	2.24	132.2
770313	111 53.91	65-26.69	165-51.67	10.00*	2.96	3	357	81.6	7.58	
770319	1 2 17.66	64-58.48	162-22.12	10.00*	3.27	3	154	73.5	0.07	
770320	524 1.78	64-59.08	162-18.80	10.00*	2.17	4	154	70.8	0.00	
770320	1220 19.94	64-53.34	163-37.79	10.00*	2.69	6	126	90.8	1.32	25.6
770321	8 6 2.77	62-13.67	166- 6.18	10.00*	4.49	5	311	262.5	3.76	672.4
770402	427 40.72	65-44.74	156-32.51	10.00*	2.76	4	212	135.4	0.47	
770402	5 0 46.15	65-18.31	158-45.93	10.00*	2.83	4	222	178.5	7.49	
770403	1433 9.68	66-37.95	162- 4.55	10.00*	2.69	6	214	290.1	1.70	20.9
770407	19 8 24.32	64-54.62	157-45.76	10.00*	2.55	6	174	172.4	0.48	4.6
770408	12 2 45.70	65-10.29	167-13.03	10.00*	2.35	5	195	54.3	0.17	9.8
770409	910 55.96	65-13.40	167- 7.57	10.00*	2.82	5	184	52.6	0.10	12.7
770409	18 9 37.60	63-55.62	164-45.74	10.00*	2.12	4	246	76.5	0.29	
770409	2240 39.91	66-57.45	163- 6.89	10.00*	3.42	5	244	25.2	0.07	6.4
770410	044 18.45	65- 4.54	167-29.55	10.00*		5	220	57.6	1.30	88.7
770410	1640 46.64	64-54.17	162-24.49	10.00*	1.70	5	148	80.4	0.28	0.0
770411	950 10.38	64-47.69	164- 5.57	10.00*	4.01	7	127	66.3	0.42	3.5
770411	1826 11.88	64-57.20	164- 6.05	10.00*	2.69	5	166	74.6	0.34	12.2
770412	028 6.84	65- 5.19	167-15.88	10.00*	3.45	5	207	61.0	1.00	62.0
770412	043 34.76	65-13.47	166-59.66	10.00*		4	183	57.0	0.37	
770412	641 32.55	64-40.12	168-16.05	10.00*		4	274	100.7	2.83	
770413	535 16.37	65- 0.67	164-18.22	10.00*	3.17	6	101	71.4	0.79	8.3
770413	648 10.54	65-19.89	163-24.57	10.00*	2.16	5	143	87.6	0.72	8.9
770413	650 37.58	65-21.33	163-48.09	10.00*	2.33	4	134	75.3	0.41	
770414	320 28.47	66-51.10	164-35.08	10.00*	2.79	3	270	86.5	0.11	
770414	347 46.09	66-59.64	165- 4.21	10.00*	3.38	6	240	109.0	0.49	23.9
770414	543 41.94	65-28.69	163-51.66	10.00*	2.26	4	125	62.1	0.85	
770414	1858 52.74	64-49.00	162-28.04	10.00*	3.10	4	121	89.6	0.13	
770414	1955 5.19	65-54.94	162-35.70	10.00*	3.25	6	131	82.9	0.64	5.7
770415	13 0 42.64	65-23.42	163-59.15	10.00*		5	127	68.1	0.97	40.3
770416	1854 32.89	66-11.46	161-36.21	10.00*	2.75	5	200	86.1	0.29	2.8
770417	1920 4.74	65-15.33	167-37.24	10.00*		5	212	36.7	0.46	52.3
770418	13 2 40.03	65-48.01	167- 9.70	10.00*		4	209	43.9	0.58	
770419	1245 22.15	65-27.58	166-34.85	10.00*		6	139	63.0	1.82	76.0
770419	2126 12.97	65- 9.10	166-54.24	10.00*	3.26	5	182	65.6	1.38	71.1
770420	1049 38.80	67- 2.94	163-13.49	10.00*	2.89	3	283	34.9	0.54	
770423	3 9 24.55	65-22.20	164- 2.40	10.00*	2.60	5	124	69.3	1.49	35.8
770423	1552 21.12	65-11.10	164-11.26	10.00*	2.45	6	90	87.2	0.79	6.0
770426	959 27.56	64-24.01	164-38.99	10.00*	3.95	5	191	38.9	1.25	11.0
770427	1126 33.10	65-27.53	166-28.32	10.00*		4	265	102.9	0.30	
770427	1752 7.72	64-16.28	160-54.88	10.00*	2.90	5	162	46.9	0.96	60.2
770428	1828 7.51	64-57.69	167-56.33	10.00*		4	305	130.1	0.23	
770428	1045 50.17	65- 3.58	165-36.67	10.00*	2.88	5	217	56.9	1.23	36.8
770429	13 2 44.78	65- 5.25	164-13.51	10.00*	2.23	4	148	80.1	1.46	
770429	1310 6.28	65- 5.19	164-13.28	10.00*	2.24	4	148	80.2	1.41	
770429	1353 30.44	65- 3.95	165-35.29	10.00*	2.63	5	127	57.3	1.10	7.8
770429	2220 46.24	64-59.97	162-14.68	10.00*	2.58	5	207	67.4	1.66	73.9
770430	19 0 8.67	65-21.41	166-32.17	10.00*		6	141	68.0	0.56	0.3
770501	558 43.92	66-51.82	164- 7.21	10.00*	1.72	3	222	66.2	0.11	
770501	739 31.10	67- 0.27	164-17.20	10.00*	2.00	3	238	75.4	0.03	
770505	1110 26.70	64-40.33	164- 5.93	10.00*	2.45	4	200	62.1	0.32	
770505	1912 13.42	66-58.14	163- 4.98	10.00*	0.63	3	272	24.6	0.20	
770507	15 6 9.50	65-11.59	164- 7.16	10.00*	3.43	6	90	87.1	2.94	29.0
770508	19 5 5.86	64-53.79	169-19.75	10.00*		5	300	99.1	2.56	34.9
770511	1932 37.69	65-57.13	163-47.00	10.00*	3.52	5	207	36.1	2.16	2.3
770511	1953 26.74	67-25.82	164- 7.14	10.00*	2.65	3	308	92.1	0.87	
770511	22 0 19.86	64-25.38	158-50.85	10.00*		3	291	100.3	0.14	
770512	532 37.51	64-15.91	171- 8.48	10.00*		5	323	210.0	1.48	434.6
770514	1033 30.12	66-15.64	162-30.82	10.00*	3.42	5	151	65.9	0.23	3.4
770516	1735 38.25	65- 2.05	164-10.29	10.00*		4	136	77.7	0.74	
770519	1242 55.04	65- 9.12	164-30.53	10.00*	2.49	7	146	77.6	0.94	13.8
770520	728 21.88	65-22.13	165-43.04	10.00*		4	229	83.4	0.85	
770523	14 3 23.96	65-47.65	163-24.41	10.00*	2.61	5	141	56.2	1.22	8.2
770523	1829 13.65	64- 5.91	167-37.62	10.00*		4	290	120.8	1.02	
770529	823 7.60	65-16.23	165-22.30	10.00*		3	206	79.2	0.21	
770529	2143 23.39	65-25.35	165-22.30	10.00*		3	212	69.3	2.77	

TABLE 5 (Cont'd)

DATE	ORIGIN	LAT (N)	LONG (W)	DEPTH	MAG	NO	GAP	DMIN	RMS	ERH
770601	841 4.34	64-38.66	159-42.43	10.00*	3.36	5	244	92.6	0.86	1.9
770603	1345 41.25	65-52.42	167-27.27	10.00*		4	235	41.0	0.50	
770604	2222 24.51	66-13.65	166-41.27	10.00*	3.00	4	212	93.3	1.92	
770609	1450 15.69	63-52.29	160-30.70	10.00*	1.77	3	347	2.1	0.19	
770611	1620 51.44	65-57.13	166-34.18	10.00*	3.18	3	215	75.7	2.62	
770612	7 5 44.77	65-19.44	163-57.23	10.00*	2.66	5	133	75.6	0.30	11.9
770613	1625 25.42	66-17.44	162-11.63	10.00*	2.41	3	265	105.7	0.45	
770613	1626 7.75	64-42.48	164-43.51	10.00*	3.15	5	238	138.7	2.83	12.5
770616	16 4 23.54	64-59.41	162-31.34	10.00*	2.36	6	109	77.7	0.12	1.1
770625	1552 5.54	64-57.52	162-20.36	10.00*	3.52	6	109	73.7	1.11	14.6
770625	1948 53.56	65-15.33	165-54.52	10.00*		3	128	81.6	0.00	
770630	1222 42.04	65-20.34	163-50.49	10.00*	3.26	4	142	76.2	0.05	
770630	1656 44.55	65-20.84	164-13.95	10.00*	2.78	4	214	69.1	1.31	
770701	130 11.01	64- 1.29	161-56.43	10.00*	2.29	3	270	71.5	0.49	
770707	1929 47.91	65-47.22	167-55.30	10.00*	3.33	5	263	25.3	2.15	24.3
770712	2323 33.22	66-38.08	161-14.49	10.00*	3.31	3	297	134.5	0.03	
770714	1822 14.22	66-32.24	157-33.46	10.00*	2.84	4	233	181.7	1.17	
770715	1436 44.78	66-38.92	157- 9.40	10.00*	3.06	6	226	284.3	3.09	19.0
770716	1236 40.71	66-54.84	162-58.42	10.00*	1.27	3	260	17.5	0.57	
770718	2315 54.80	64- 0.68	161-59.24	10.00*	2.72	4	272	73.5	0.28	
770723	1751 48.75	65- 3.12	162-27.84	10.00*	2.99	6	104	71.4	0.80	6.9
770725	1521 3.80	65-50.20	161-42.30	10.00*	2.62	4	250	131.6	0.94	
770726	2323 20.31	64-49.68	163- 0.39	10.00*	2.84	6	199	107.0	2.26	26.5
770810	729 11.56	64-42.99	163-54.61	10.00*	2.59	8	137	72.0	2.87	17.1
770814	1212 10.53	64-33.92	159-35.42	10.00*	3.44	5	133	87.6	0.24	9.9
770814	1429 53.31	67-14.11	163-20.14	10.00*	3.10	7	297	53.4	3.74	63.0
770903	2234 47.62	65-26.21	155-22.47	10.00*	2.87	3	187	104.8	1.49	
770910	1511 36.56	64-30.38	160-58.72	10.00*	3.06	4	192	72.4	0.06	
770910	2318 17.35	66- 2.34	156-23.48	10.00*	3.25	4	195	122.7	0.35	
770914	1546 21.06	64-45.05	165-35.44	10.00*	3.31	5	156	23.7	0.53	10.6
770920	352 2.82	64-20.38	162-43.89	10.00*	2.74	5	166	119.4	0.24	0.7
771008	2250 2.11	64-43.32	156- 3.55	10.00*	3.50	6	174	186.5	0.68	38.9
771014	524 58.01	66-19.26	156-32.76	10.00*	3.25	4	217	132.2	0.31	
771021	1423 39.58	65-24.62	167-37.47	10.00*	4.07	6	189	21.6	0.17	39.3
771027	853 12.36	64-33.70	166-21.19	10.00*	3.66	7	222	47.1	2.88	53.4
771029	737 32.66	65-18.01	168-19.36	10.00*	3.74	7	272	34.5	2.45	60.7
771102	1918 22.16	65-45.19	162-11.63	10.00*	2.19	7	142	57.3	0.50	3.2
771107	934 33.82	67-44.43	156-13.83	10.00*	3.43	5	255	217.4	0.36	19.8
771107	513 56.36	65-51.74	159-29.95	10.00*	3.18	6	137	93.4	1.35	10.9
771113	2226 39.99	66-46.81	157-42.22	10.00*	3.39	4	211	215.9	0.11	
771122	1115 10.01	64-39.64	169-41.61	10.00*		4	254	114.8	0.22	
771123	2138 15.12	64- 0.25	162-32.19	10.00*	2.37	4	284	100.3	0.19	
771126	132 45.73	64-25.04	161-52.47	10.00*	2.23	3	244	88.6	0.36	
771126	1651 4.76	65-20.76	154-56.34	10.00*	3.55	7	203	99.2	1.90	52.5
771128	227 3.61	63- 1.12	162-45.38	10.00*	2.80	6	274	148.2	1.02	14.0
771201	619 16.10	64-33.95	160-53.56	10.00*	2.42	4	184	77.6	0.10	
771201	649 51.47	65-23.08	162-26.03	10.00*	1.83	8	128	56.1	0.69	4.8
771201	18 0 46.86	64-35.19	161-27.05	10.00*	1.81	4	217	90.1	0.09	
771202	344 4.94	64-15.06	159-12.78	10.00*	2.74	4	186	75.0	0.21	
771205	614 45.26	65- 3.66	162-25.60	10.00*	2.59	7	103	69.4	0.64	5.9
771205	11 3 2.67	65- 7.11	162-26.97	10.00*	2.15	7	100	66.5	0.61	5.5
771205	1143 8.99	65- 5.49	162-28.85	10.00*	2.27	8	102	69.3	0.54	2.2
771206	1155 42.28	62-41.06	163-43.11	10.00*	3.35	8	288	209.7	2.51	144.5
771209	051 38.57	64-48.21	165-28.31	10.00*	2.97	5	137	27.6	0.58	6.3
771210	18 1 20.35	63-23.02	162-36.88	10.00*	3.46	7	252	118.7	0.39	13.3
771211	840 28.18	64-12.79	166-49.13	10.00*	3.32	7	278	79.9	1.40	18.4
771212	955 9.82	66- 1.26	164-31.30	10.00*	3.44	5	113	32.2	2.29	19.2
771214	1442 0.21	63-29.53	166- 1.81	10.00*	2.87	4	326	276.6	0.17	
771215	1944 39.45	66- 8.52	156-27.57	10.00*	3.12	6	204	126.0	0.51	11.0
771216	447 14.65	66-59.86	168-52.89	10.00*	3.90	5	307	166.0	0.72	304.7
771220	732 23.43	65-25.82	163-45.52	10.00*	2.89	4	232	117.4	2.90	
771221	1349 40.97	64-33.70	164-13.03	10.00*	3.02	6	157	55.2	2.60	15.8
771222	12 8 8.05	65-25.82	162-55.34	10.00*	2.10	3	220	78.6	3.08	
771225	12 9 4.11	65-21.15	162-29.44	10.00*	2.13	6	123	59.1	1.19	11.0
771226	622 23.33	64-33.70	163-36.94	10.00*	2.71	7	153	84.0	0.75	8.8
771226	639 10.31	64-38.78	159-13.70	10.00*	3.04	6	264	104.7	2.06	107.8
771227	1550 35.12	64-33.70	163-52.57	10.00*	2.46	5	155	71.5	0.37	11.8
771231	2051 47.26	64-31.03	162-50.68	10.00*	2.88	5	151	121.5	0.21	2.7
771231	837 49.77	65-21.13	164-17.35	10.00*	2.76	5	144	102.0	0.30	11.0
780101	518 30.02	66-28.81	163-14.59	10.00*	1.97	6	143	49.8	3.15	56.5
780102	1958 38.25	65-50.29	164-38.62	10.00*	2.88	8	206	145.1	1.95	15.8
780104	1110 21.70	66-51.10	161-25.86	10.00*	2.23	4	267	51.6	1.81	

MILESTONE CHART

RU #: 483 PI: N. N. Biswas, L. Gedney

Major Milestones: Reporting, data management and other significant contractual requirements; periods of field work; workshops; etc.

MAJOR MILESTONES	1977			1978													
	O	N	D	J	F	M	A	M	J	J	A	S	O	N	D		
Servicing of field sites completed	X	X	X	X													
Data scaled and processed	X	X	X	X													
Data scaled and punched on computer cards for processing					X	X											
Checking of replacement of existing equipment at field sites is in progress							X	X	X								
Field season begins										X	X	X	X				

△ Planned Completion Date

▲ Actual Completion Date